Faculty of Textile Engineering
Technical University of Liberec

STRUTEX

Structure and Structural Mechanics of Textile Fabrics

Struktura a strukturní mechanika textilií

23rd international conference
23. mezinárodní konference

2022

CONFERENCE BOOK

SBORNÍK TEXTŮ

PARTNERS / SPONSORS

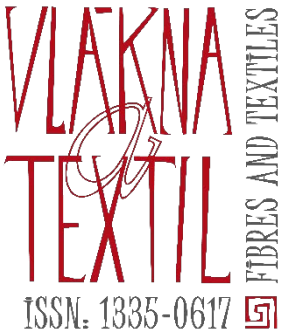

The most beloved sights of ^Liberec

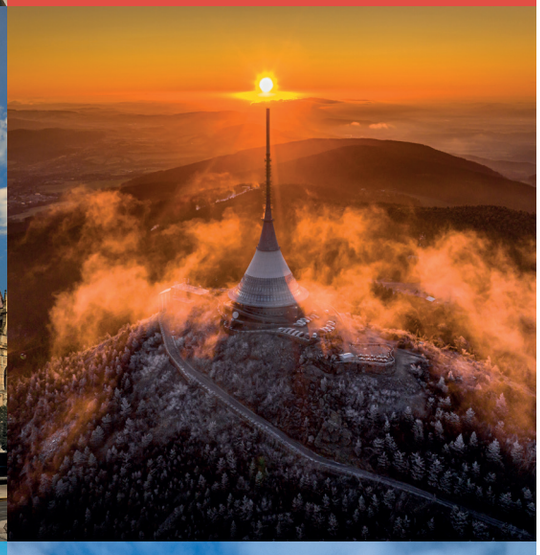

Visit^Liberec

City Information Centre
nám. Dr. E. Beneše 23, Liberec
phone: +420 485 101 709
e-mail: info@visitliberec.eu
www.visitliberec.eu, www.liberec.cz
www.facebook.com/visitliberec
#visitliberec

We greatly appreciate Technical University of Liberec for education of students in the field of textile. Without next generation textile experts we can not keep working and would be not able to develop new products.

with thanks

Caledon textile

KORDÁRNA
KORDÁRNA PLUS A.S.
An Indorama Ventures Company

Velká nad Veličkou 890
+420 518 312 224
kordarna@kordarna.cz

WE ARE KORDARNA:

EUROPEAN CENTRE OF TECHNICAL TEXTILES

by Indorama Ventures

One of the largest manufacturers of technical fabrics in Europe

With seventy years of experience and seven hundred professionally trained employees, we supply fabrics to more than fifteen countries in Europe, North America, South America and Asia.

Supplier of major world's tire and conveyor belt manufacturers

Our cord and conveyor belt fabrics serve as reinforcements of products by world-class manufacturers such as Continental, Pirelli, Nokian, Bridgestone, Contitech, Fenner Dunlop or Sempertrans.

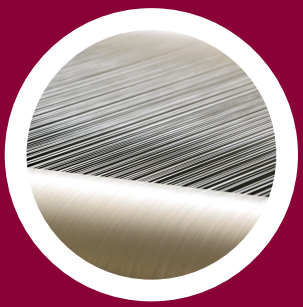

Integrated production from fibre to fabric

We integrate the whole manufacturing process from the output of our polyester fibre to the impregnated technical fabric that serves as the backbone of tires and conveyor belts.

WWW.KORDARNA.CZ

People.Health.Care.

The Lohmann & Rauscher Company
is an international company
with a long history.
It has over 160 years
of experience in making
dressing materials
and medical devices
and it has always focused
on the needs of its
customers and patients.

The company is a world-leading supplier of medical devices and hygiene products of the highest quality. It develops individual solutions to the problems of patients and healthcare workers worldwide, from classic dressing materials, to modern therapy systems.

Plant in Nová Paka
Lohmann & Rauscher s.r.o.
Legií 265
509 01 Nová Paka
Czech Republic

Plant in Slavkov
Lohmann & Rauscher s.r.o.
Bučovická 256
684 01 Slavkov u Brna
Czech Republic

Headquarters • General inquiries
Telephone: +420 544 425 601
Fax: +420 544 227 331
E-mail: info.slavkov@cz.LRmed.com
https://www.lohmann-rauscher.com

Rieter CZ s.r.o.

Ústí nad Orlicí

Rieter CZ s.r.o. is part of the Swiss Group, Rieter, that is a leading world producer of textile machinery and complete textile systems. Rieter CZ s.r.o. is characterised by a strong emphasis on innovations that are developed in the company development centre. Other features include precision production of textile machines and components for modern technologies and processes.

Rieter • Make the Difference
www.rieter.cz, www.rieter.com

RIETER

ADFORS
People are our strength

2 production plants - in Litomyšl and Hodonice

more than **2000** employees

turnover **7.8 bn CZK**

120 k tons of glass fibre per year

6 brands of unique glass fibre production

PEOPLE ARE OUR STRENGTH SO THEY ARE OUR FIRST PRIORITY.

Thanks to this approach, we already have been certified as a Top Employer for the last few years.

top EMPLOYER CZECH REPUBLIC 2018
CERTIFIED EXCELLENCE IN EMPLOYEE CONDITIONS

We are still growing and investing in both our employees and our technology too.

Working for us is very fulfilling. Come and join us!

CONTACTS

HEADQUARTERS AND LITOMYŠL PLANT

SAINT-GOBAIN
ADFORS CZ s.r.o.
Sokolovská 106
570 01 Litomyšl
+420 461 651 111

HODONICE PLANT

SAINT-GOBAIN
ADFORS CZ s.r.o.
Zahradní 256
671 25 Hodonice
+420 515 207 111

HR department
kariera.adfors@saint-gobain.com
www.adfors.cz

SAINT-GOBAIN

ADFORS
silný díky lidem

2 výrobní závody – v Litomyšli a v Hodonicích

přes **2000** zaměstnanců

roční obrat **7.8 mld. Kč**

120 tisíc tun skleněného vlákna ročně

6 značek unikátních výrobků ze skleněného vlákna

LIDÉ JSOU PRO NÁS NA PRVNÍM MÍSTĚ, JSME TOTIŽ SILNÍ PRÁVĚ DÍKY NIM.

I díky tomuto přístupu jsme už několik let oceněni jako Top employer.

top EMPLOYER CZECH REPUBLIC 2018
CERTIFIED EXCELLENCE IN EMPLOYEE CONDITIONS

Rosteme a investujeme do rozvoje, jak naší technologie, tak našich ADFORSáků.

Pracovat pro nás prostě stojí za to, přidej se k nám.

KONTAKTY

SÍDLO SPOLEČNOSTI A ZÁVOD LITOMYŠL

Sokolovská 106
570 01 Litomyšl
+420 461 651 111

ZÁVOD HODONICE

Zahradní 256
671 25 Hodonice
+420 515 207 111

Personální oddělení
kariera.adfors@saint-gobain.com
www.adfors.cz

SAINT-GOBAIN

STAP a.s. – Narrow Fabrics Manufacturer from Czech Republic

Our products are tailored to meet exacting specifications established by a number of NATO military forces. STAP a.s. is a major webbing manufacturer of military webbings, bindings and elastics to meet specifications in both IRR webbings and non-IRR webbings.

We are one of the few webbing suppliers who can offer our own in-house dying facilities to colour match to forces exacting shade requirements.

Our Multi Colour Camo printed webbing (up to 5 colours) is widely used on a variety of PLCE (Personal Load Carrying Equipment), MTP Webbing Systems & Pouches, Molle Webbing along our latest IRR Camo printed binding, designed to be used in conjunction with The Multi-Terrain Pattern (MTP) camouflage print.

We can offer bespoke custom printed webbing to match your military camouflage textile pattern.

Special treatments can be applied to the webbing straps including anti-bacterial, rotproof, water-repellent and flame-retardant finishes.

Webbings are cut to length and heat-sealed using our automatic machines and we are also able to offer a cutting and holing service using our ultrasonic facility.

Here we are able to create a wide range of made-up units, sewn webbing straps also with buckles.

We can also offer wide range of comercial products, like webbings, elastics, binding tapes, zippers, woven labels, braids, jacquard ribbons…

www.stap.cz

Schoeller Křešice s.r.o.

je významným výrobcem česaných vlněných, směsových a technických přízí.

Historie tohoto výrobního závodu, se datuje již od roku 1907, taktéž od tohoto data se zde nepřetržitě vyrábí česané příze. Od roku 1995 spadá naše společnost pod rakouskou skupinu

Schoeller Spinning Group,

která patří mezi největší evropské dodavatele česané příze. Na trhu je tato skupina známá především díky svému širokému portfoliu v České republice vyráběných přízí a úzkou spoluprací s orientací na zákazníka, pro kterého se snaží vyvíjet nebo přizpůsobovat výrobky, dle jeho specifických potřeb.

Největší částí výrobního portfolia tak tvoří příze, které jsou díky svým funkčním vlastnostem využívány na výrobu hasičských zásahových obleků (PBI), vlněných potahů do elektro aut (BMW, Volvo), letadel či vlaků, dále příze aramidové pro armádu, směsové na outdoorové oblečení, pro ponožkový průmysl, ale také vodivé (Inox kovová vlákna) a jádrové Dref 3.

Od roku 2018 je skupina Schoeller Spinning Group součástí nadnárodní společnosti

Indorama Ventures Company.

Schoeller Křešice s.r.o.

is a major producer of combed wool, mixed and technical yarns.

The history of this factory dates back to 1907, and since then, worsted yarns have been continuously produced here. Since 1995, our company has been part of an Austrian group

Schoeller Spinning Group,

which is among the largest European suppliers of worsted yarn. This group is known on the market mainly due to its wide portfolio of yarns produced in the Czech Republic and close cooperation and customer orientation, for whom it strives to develop and adapt products according to their specific needs.

The largest part of the production portfolio consists of yarns that, thanks to their functional properties, are used for the production of firefighting suits (PBI), wool covers for electric cars (BMW, Volvo), airplanes or trains, as well as aramid yarns for the army, mixed for outdoor clothing, for the sock industry, but also conductive (Inox metal fibers) and core Dref 3.

Since 2018, the Schoeller Spinning Group has been part of a multinational company

Indorama Ventures Company.

Faculty of Textile Engineering
Technical University of Liberec

23rd international conference
23. mezinárodní konference

STRUTEX

Structure and Structural Mechanics of Textile Fabrics

Struktura a strukturní mechanika textilií

CONFERENCE BOOK

SBORNÍK TEXTŮ

December / Prosinec 2022
Faculty of Textile Engineering
Technical University of Liberec

President of the conference

prof. Ing. Bohuslav Neckář, DrSc.
Technical University of Liberec

Scientific committee

prof. Luboš HES	Technical University of Liberec, Czech Republic
prof. S. M. ISHTIAQUE	Indian Institute of Technology Delhi, India
prof. Oldřich JIRSÁK	Technical University of Liberec, Czech Republic
prof. Yordan KYOSEV	Technische Universität Dresden, Germany
prof. Jiří MILITKÝ	Technical University of Liberec, Czech Republic
prof. Bohuslav NECKÁŘ	Technical University of Liberec, Czech Republic
dr. Vincent PLACET	University of Franche-Comté, France
prof. Jakub WIENER	Technical University of Liberec, Czech Republic
assoc. prof. Lukáš ČAPEK	Technical University of Liberec, Czech Republic
assoc. prof. Marcin BARBURSKI	Lodz University of Technology, Poland
assoc. prof. Brigita KOLČAVOVÁ SIRKOVÁ	Technical University of Liberec, Czech Republic
assoc. prof. Maroš TUNÁK	Technical University of Liberec, Czech Republic

ISBN 978-80-7494-621-9

CONTENTS

Dr. Hab. Alain BOURMAUD

Institution

University of South Brittany, Dupuy de Lôme Research Institute (IRDL), UMR CNRS 6027

Research Interest

Multiscale characterization of plant fibres; Link between ultrastructure and mechanical properties of plant fibres; Processing and recycling of plant fibres composites; Impact of growing conditions and environmental stress on flax and plant fibres properties. Cultural Heritage: Ultrastructural study of ancient flax fibres.

Keynote Lecture

MULTI-SCALE IMPACT OF FLAX FIBRES SPECIFICITY ON TEXTILE PREFORMS AND BIOCOMPOSITE PROPERTIES

Short biography

Alain Bourmaud is Researcher at the University of South Brittany since Sept. 2001. He received a master degree in polymer engineering in 1993 (Laboratory of Rheology of Saint-Etienne, France), and a PhD in Materials Science and Engineering, about the multi scale characterization of biocomposites in 2011 (University of South Brittany). Finally, he obtained the French habilitation to manage research (HDR) in 2017 (University of South Brittany). He published around 170 papers in international journals on biocomposite processing or plant fibre structure and properties; he supervised 18 PhD students and 4 post-doc (currently 5 PhD students and 1 post-doc). Alain is also the scientific coordinator of the FLOWER project (INTERREG Cross-Channel, 8 partners, 4.6M€, 2018-2023) and scientific leader of of a French Research Project dedicated to the study of old Egyptian flax fibres (ANUBIS, 2021-2025, 1.2 M€). Alain is involved in many research collaborations at the national (FEMTO, INRA, ENIT, CIMAP, PBS, ICUBE, Centrale Supelec….) and international (UoKazan, Bremen, UoPortsmouth, UoCambridge, Scion NZ…) scale. He has also built research links with a number of industrial partners in the field of biocomposites and plant fibres (PSA group, APM, Zodiac, Dedienne, Depestele, Ecotechnilin, Kaïros, Addiplast...). Finally Alain is expert for Horizon Europe projects, MSC fellowships or other French scientific calls.

Assoc. prof. Yiska GOLDFELD

Institution

Faculty of Civil and Environmental Engineering
TECHNION – Israel Institute of Technology

Research Interest

Textile reinforced concrete structures, structural health monitoring and development of smart self-sensory concrete structures, stability of shell structures.

Keynote Lecture

SMART SELF-SENSORY TEXTILE REINFORCED CONCRETE STRUCTURES - ACHIEVEMENTS & CHALLENGES

Short biography

Yiska Goldfeld is an Associate Professor in the Faculty of Civil and Environmental Engineering at the Technion – Israel Institute of Technology. She is the head of the Intelligent Structures Laboratory (ISLab) at the National Building Research Institute at the Technion. Her research interests are in the fields of textile reinforced concrete (TRC) structures, structural health monitoring, smart self-sensory concrete and TRC structures, and stability of shell structures.

Dr. Goldfeld obtained both her B.Sc. degree (1995, summa cum laude) and her Ph.D. (2002, direct Ph.D. track) from the Faculty of Civil and Environmental at the Technion. She also obtained an M.B.A degree (1999) from Ben Gurion University of the Negev. Before joining the Technion in 2004, she was a post-doctoral fellow in the Faculty of Aerospace Engineering at TUDelft, The Netherlands.

EFFECT OF TENSILE FATIGUE CYCLIC LOADING ON PERFORMANCE OF TEXTILE-BASED STRAIN SENSORS

Saba Sajjadieh*[1], Fateme Safari*, Bahare Ghalebi*, Mohsen Shanbeh*

*Department of Textile Engineering, Isfahan University of Technology, Isfahan8415683111, Iran.

[1]corresponding author e-mail: s.sajadieh@tx.iut.ac.ir

Abstract:

Textile-based strain sensors are a potential platform used in wearable devices for sensing and. 8 sensors containing monitoring the human body. These sensors not only have all the conventional sensors benefits but also, they are low-cost, flexible, light-weight, and easily adopted with three-dimensional shape of the body. Moreover, recent research has shown they are the best candidates for monitoring human's body motion. In this study, the effect of tensile fatigue cyclic loads on performance and sensitivity of textile-based strain sensors was investigated polyester/stainless steel staple fiber blend yarn as a conductive part with different structures were produced. The sensors varied in weft and warp density, percentage of stainless steel in conductive yarn, the number of conductive yarns, and weave pattern. The sensors were subjected to 500 cyclic loads operations and their tensile properties and sensitivity were investigated and compared before and after applying tensile fatigue cyclic loads. The results showed the textile-based strain sensors containing less percentage of stainless-steel fiber, lower number of conductive yarns, twill weave pattern and lower density in warp and weft direction have shown better performance after tensile fatigue cyclic loads.

Key words:

Tensile fatigue cyclic loading, strain sensor, smart textile, conductive yarn, woven fabric, sensitivity.

1. Introduction

In the last decade, the products of the textile industry have found especial applications in the field of intelligent textiles, so the use of electrical fibers, yarns, and textiles is growing rapidly [16]. Electronic textiles (e-textiles) known as smart textiles are structures with conductive properties that can be used in a variety of applications such as sensors, communication, health care, computation, thermal purposes, protective clothing, wearable electronics, and fashion [7]. Electronic textiles can be produced by different methods such as weaving, knitting, embroidery and printing [10]. Sensors convert non-electrical physical or chemical quantities into electrical signals or other recognized electronic outputs [18]. Textile-based sensors especially strain sensors are desired because of their flexibility, ease of deformation, elastic recovery and fatigue resistance [18]. Strain deformation in e-textiles can be sensed in different mechanisms such as piezoelectricity, optical diffraction or interferometry, capacitance and piezoresistance. The must usual strain sensors in smart textiles are piezoresistive because of their manufacturing process and ease of use [11,19]. The "piezoresistive" term refers to materials that change their electrical resistance by applying mechanical force due to microstructure change in conductive materials [3]. As mechanical force is applied to piezoresistive material, a mechanical deformation occurs. These deformations may change the electronic properties; therefore, the resistance will change [4]. As the force is removed, the electrical resistance regains regard to re-establishing structures [2]. The resistance can be evaluated by equation (1) which R is electrical resistance, ρ is the resistivity of

material and A and L are the area and pathway length which the current flows respectively [12]. To evaluate the performance of a strain sensor, required information about the key parameters such as sensitivity, limit of detection (LOD), linearity, response time, and stability is needed [19].

$$R = \rho \frac{L}{A} \quad (1)$$

Fatigue is defined as the failure of a structure or component due to repetition and a load cycle which is less than a load to cause failure of the structure in a single application [14]. The failure occurs due to the cyclic nature of the load which causes microscopic material imperfections to grow into a macroscopic crack [6]. Fabrics are subjected to tensile cyclic loads in different applications. Therefore, the study of the fatigue behavior of textiles in some applications such as sportswear is very important [17]. The fatigue failure in textiles usually is due to a reduction of elasticity during textile consumption. Fabric properties such as fabric density, weave design, yarn type and structure and material may affect the fatigue behavior of fabric [6].

There are many research work related textile-based strain sensors and their application. Shanbeh et al. produced woven strain sensors with different electrical conductivity and weft densities. They analyzed the effect of two different percentages of stainless-steel fibers in staple blend yarns that used in purpose-built strain sensors. They compared the sensitivity of strain sensors during 5 times cyclic loading. Their study showed that sensors containing less stainless-steel fiber have better performance. Moreover, the textile base strain sensor behavior during tensile cyclic loading wasn't stable. They claimed the electromechanical behavior of sensors under tensile loading is due to crimp, fiber migration, conductive fibers contact points and yarn diameter variation. [13]. Guo et al. presented four different textile-based strain sensors; two of them were conducted by coating and others by using conductive yarns in weaving process. Linear range of the sensor's work was reported [8]. Fen et al. developed a polyaniline (PANI)-coated polyurethane (PU) fiber with conductivity of $10^{-2}\Omega/cm$. They used fibers as a piezoresistive strain sensor which were subjected to 1500% strain deformation. The results showed that the resistivity was increased by applying strain but there were 3 different intensities. Furthermore, the fibers were under tensile cyclic loads on maximum 50% of strain level which results revealed the reversible response on the sensor. However, the reversibility wasn't absolute due to the hysteresis [5]. Liang et al. analyzed 16 knitted strain sensors' performance parameters such as sensitivity, linearity, hysteresis, responsiveness and fatigue during dynamic and static process. The sensors were made of three different materials consisting of a fabric coated with a conductive polymer, spun stainless steel yarn and silver-plated with different material composites. The sensors were tested at 10% strain and 100 times load-unload cycles. The results showed that sensors made of silver-plated yarn performed the best among other sensors. Moreover, sensors made of stainless-steel yarn performed the worst, because of knitted fabric properties [9]. Teyeme et al. developed a piezoresistive strain sensor from conductive fabric. The sensor had a stable dynamic response after 30 seconds, therefor they reported this sensor was suitable for slow-moving applications. They also found that the sensor wasn't sweat independent. Thus, they conclude the sensor was not acceptable for sports applications [15].

In this work, we study effect of tensile fatigue cyclic loading on performance of textile-based strain sensors. Moreover, effect of different structural parameters of textile-based strain sensors on their performance during tensile fatigue cyclic loading was evaluated.

2. Experimental

2.1. Materials

Eight different textile-based strain sensors were woven by using two different conductive yarns produced by Xiamen JL-fiber Science and Technology Co. Ltd., Xiamen, China. The conductive yarn was polyester/stainless steel staple fiber blend. The fineness of stainless-steel fiber was 12μm. Tensile

properties of yarns were measured by Zwick tensile tester, which works based on constant rate of elongation. In Table 1, the properties of yarns are shown.

Table 1. Mechanical and electrical properties of conductive yarns.

Yarn code	Percentage of stainless steel (%)	Nominal Count of yarn (Ne)	Breaking elongation (mm)	Breaking strength (cN)	Resistance (Ω/m)	Yarn diameter (μm)
A	28	20	3.080	31.604	2982	248.25 μm
B	40	20	3.246	28.228	2307	249.46 μm

The sensors were produced by polyester filament yarn (75 den) as warp with two different densities (23 and 40 per cm). The conductive yarns were used as weft in combination with polyester filament/spandex yarns in two different densities (15 and 25 per cm). In designated textile-based strain sensors two different numbers of conductive yarns i.e. 9 and 20 was inserted. In Figure 1, the picture of one produced sample is illustrated. Moreover, the samples were produced with Plain and Twill (2/1) patterns. Optimax rapier weaving machine with 180 width and 450 PPM speed was used to produce all samples.

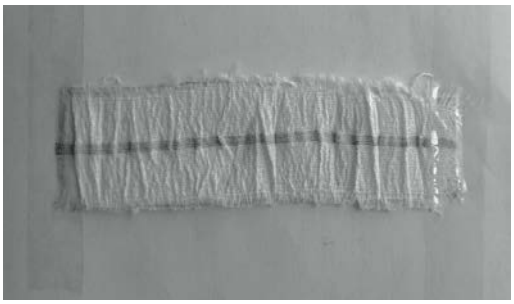

Figure 1. Textile-based strain sensor

2.2. Methods

For measuring sensors' sensitivity and resistance variation of textile-based strain sensors during tensile test an electronic circuit was used which the strain sensor was one of the resistors series with other reference resistors as proposed by Guo et al. [8]. A purposed-built instrument was used for applying cyclic loads on sensors which is shown in Figure 2 [1]. The details operating method of instrument was explained in reference 1.

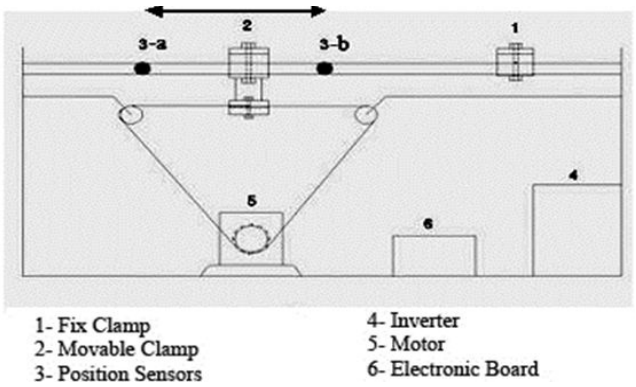

Figure 2. The schematic of equipment used for cyclic load [1]

The dimension of textile-based strain sensors was 25 × 200 mm. The samples were then subjected to wet relaxing process. Samples were immersed in 90° water for 10 minutes. Then, they were dried in ambient temperature and the shrinkage percentage was calculated by equation 2 which l_1 is the initial length of sample and l_2 is the length of sample after wet relaxation.

$$shrinkage(\%) = \frac{l_1 - l_2}{l_1} \times 100 \quad (2)$$

Tensile properties of samples were tested in weft direction based on ASTM-D5034 (2007) using Zwick tensile tester. In Table 2, the specifications of samples are shown.
The samples were tested in 10 cyclic loading at 50% of breaking strain level in weft direction. The resistance variation was recorded during cyclic test. The sampling rate was set at 10 per second similar to 10 Hz in frequency.
The sensitivity of each sensor was calculated using equation 3, which G is sensitivity of the sensor, V_{max} and V_{min} are the maximum and minimum voltage that has been recorded in each tensile cyclic load from beginning to end and ε is strain. The average sensitivity of 10 cycles was considered as sensor's sensitivity.

$$G = \frac{(V_{max} - V_{min})/V_{min}}{\varepsilon} \quad (3)$$

Table 2. Specifications of samples

Sample code	Conductive yarn code	Number of conductive yarns	Weave pattern	Warp density (1/cm)	Weft density (1/cm)	Shrinkage (%)	Test speed (mm/min)	Breaking Strength (N)	Breaking Elongation (%)
1	A	9	Plain	40	15	32.4	230	56.20	174.76
2	A	20	Plain	40	15	24.2	230	78.04	129.26
3	B	9	Plain	40	15	29.5	230	55.63	154.87
4	B	20	Plain	40	15	21.3	230	61.00	128.30
5	A	9	Plain	40	25	29.6	140	175.02	89.70
6	B	9	Plain	40	25	15.7	130	187.49	82.56
7	B	9	Twill	40	25	15.7	210	143.10	251.07
8	B	9	Plain	23	25	16.5	140	146.22	152.08

Each sample was subjected to 500 tensile fatigue cyclic loads. They were loaded up to 50% of its breaking elongation and 3.4 Hz cyclic loading frequency was set, based on average running speed of a normal person.
The microtomy technique was used to evaluate the width cross-section of conductive yarns before and after tensile fatigue cyclic loads. The sensitivity of each sensor was also measured 24 hours after tensile fatigue cyclic loads test using mentioned methods.

3. Results and discussion

In Figures 3a and 3b, the voltage variation of textile-based strain sensors before and after tensile fatigue cyclic loading of two samples is shown. By applying tension to the fabric, the yarns are subjected to compressive forces at interchange points. This pressure may cause the variation of yarns' cross-section and the more possibility of contact between the stainless-steel fibers into the yarn. Although, the electro-mechanical properties of all samples during tensile cyclic loads revealed the same trend but the effect of structural parameters of samples on voltage variation was observed. The electro-mechanical variation of samples during tensile cyclic loads may be influenced by woven fabric shrinkage after wet relaxation. Figure 4 displays the sensitivity of textile-based strain sensors before and after tensile fatigue cyclic loading. The increase of contact pressure between yarns into fabric structure during tensile force could be the reason for compactness of yarns and therefore more possibility of conductive fiber contacts into yarn structure. This phenomenon may cause the decrease of sensitivity of samples during tensile cyclic loading.

As shown in Figure 4 the sensitivity of sample 2 after tensile fatigue cyclic loads decreased from 0.695 to 0.370 during 1st to 10th cyclic loading. Moreover, the sensitivity of sample 5 during tensile cyclic loading increased. The sensitivity (G) of eight textile-based strain sensors is shown in Table 3.

As can be seen in Table 3, the sensitivity of samples after tensile fatigue cyclic loading confirmed the structural variation of samples. It seems that the tensile fatigue cyclic loads in predetermined elongation may cause shrinkage removal of samples which cause the electro-mechanical variation of textile-based strain sensors.

It was observed that the sensitivity has a direct relation with conductivity of yarns before tensile fatigue cyclic loading, but this trend was not observed after tensile fatigue loading. The cross-section of conductive yarns (as shown in Figure 6) confirmed the fiber displacement in yarn cross-section which could be the reason for this phenomenon.

The textile-based strain sensor woven with plain pattern showed higher sensitivity compare with Twill 2/1 woven fabric before and after tensile fatigue cyclic loading. However, the sensitivity sample 7 woven with Twill pattern is more stable than plain ones (sample 6) that is maybe because of yarn float in fabric structure.

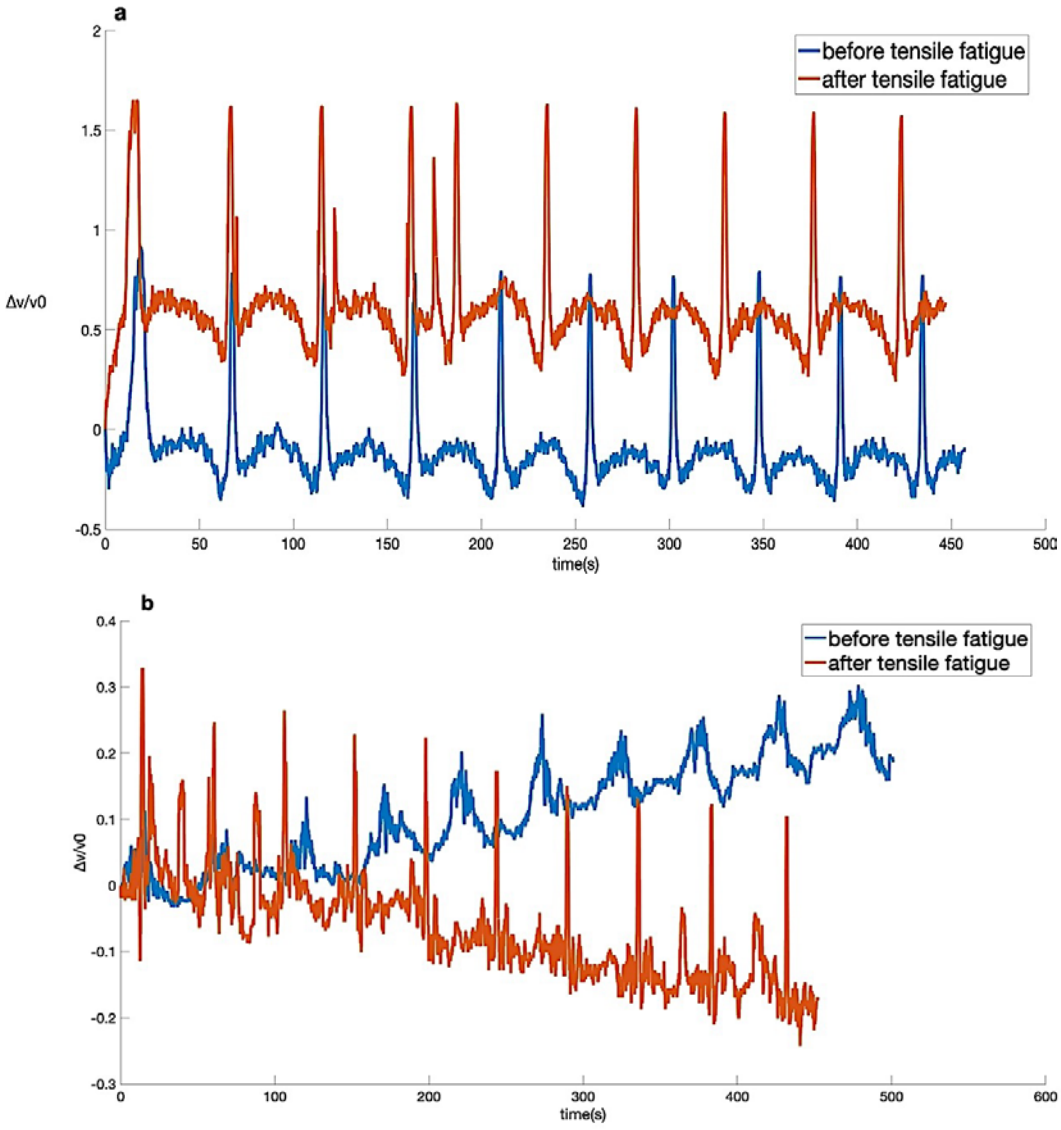

Figure 3. Voltage variation of two textile-based strain sensor during tensile cyclic loading before and after tensile fatigue cyclic loading. a) sample 5, b) sample 2. (The blue curve is before tensile fatigue cyclic loads and red curve after tensile fatigue cyclic loads.)

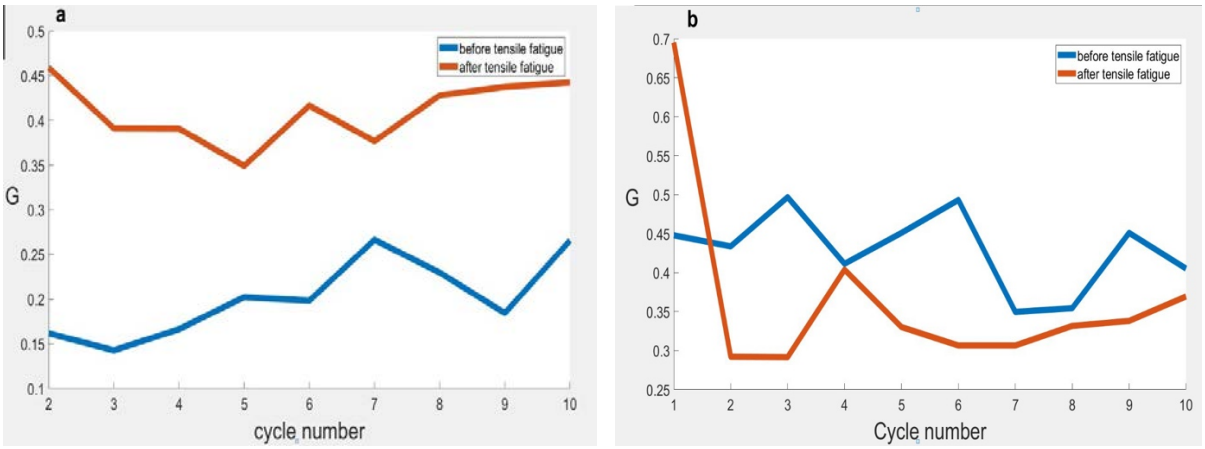

Figure 4. sensitivity (G) variation of two textile-based strain sensors during tensile cyclic loads before and after 500 tensile fatigue cyclic loading a) sample 5, b) sample 2. (The blue curve is before tensile fatigue cyclic loads and red curve after tensile fatigue cyclic loads.)

Table 3. The sensitivity (G) of textile-based strain sensors before and after tensile fatigue cyclic loads.

Sample code	Sensitivity of samples before tensile fatigue	Sensitivity of samples after tensile fatigue
1	0.156	2.29
2	0.131	0.409
3	0.138	0.171
4	0.273	5.22
5	0.205	0.420
6	0.131	0.409
7	0.409	0.402
8	0.838	0.358

It was found that by increasing the weft density, the sensitivity of textile-based strain sensors increased (As shown in Table 3). This trend can be because of lower shrinkage of woven fabrics with higher value of weft density. Moreover, by increasing the number of conductive yarns, the sensitivity or the voltage variation during tensile cyclic loading was increased. This observation could be explained by lower shrinkage values of samples produced by higher number of conductive yarns. It seems that the structural variation of these samples was prominent because of tensile fatigue cyclic loading.

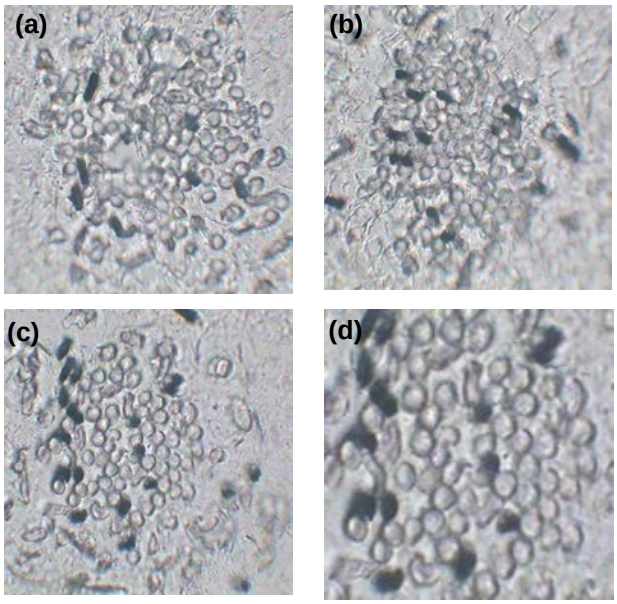

Figure 6. Conductive yarn cross-sections (a) before tensile fatigue cyclic loads of yarn A pulled out from sample 2, (b) after tensile fatigue cyclic loads of yarn A pulled out from sample 2, (c) before tensile fatigue cyclic loads of yarn B pulled out from sample 2, (d) after tensile fatigue cyclic loads of yarn B pulled out from sample 8

4. CONCLUSIONS

In this study, 8 different textile-based strain sensors were produced by using weaving method. The sensitivity and electro-mechanical properties of samples during tensile cyclic loading showed the effectiveness of tensile fatigue cyclic loading. Moreover, the evaluation of cross-section of conductive yarns before and after tensile fatigue cyclic loading showed displacement of conductive fibers in yarn structure. Our finding confirmed the effect of percentage of conductive fibers in the yarn, weft and warp density, number of weft yarn, weave pattern on sensitivity and electro-mechanical properties of textile-based strain sensors after tensile fatigue cyclic loading. The minimum and maximum values of sensitivity before tensile fatigue loading was 0.131 and 0.409, respectively, but after tensile fatigue loading was 0.171 and 5.22. In future, we aim to work on effect of tensile fatigue cyclic loading parameters on sensitivity of textile-based strain sensors in different testing conditions.

References

1. *Adeli, B., Ghareaghaji, A. A., & Shanbeh, M. (2011). Structural evaluation of elastic core-spun yarns and fabrics under tensile fatigue loading. Textile Research Journal, 81(2), 137-147.*
2. *Amjadi, M., Kyung, K.-U., Park, I. and Sitti, M. (2016), Stretchable, Skin-Mountable, and Wearable Strain Sensors and Their Potential Applications: A Review. Adv. Funct. Mater., 26: 1678-1698.*
3. *Eaton, W. P., & Smith, J. H. (1997). Micromachined pressure sensors: review and recent developments. Smart Materials and Structures, 6(5), 530.*
4. *Eldessouki, M., Aysha, T., Ratičáková, M., Šašková, J., Padil, V. V., Ibrahim, M., & Černík, M. (2017). Structural parameters of functional membranes for integration in smart wearable materials. Fibres & Textiles in Eastern Europe.*
5. *Fan, Q., Zhang, X., & Qin, Z. (2012). Preparation of polyaniline/polyurethane fibers and their piezoresistive property. Journal of Macromolecular Science, Part B, 51(4), 736-746.*
6. *Flamm, M., Spreckels, J., Steinweger, T., & Weltin, U. (2011). Effects of very high loads on fatigue life of NR elastomer materials. International Journal of Fatigue, 33(9), 1189-1198.*

7. *Grancarić, A. M., Jerković, I., Koncar, V., Cochrane, C., Kelly, F. M., Soulat, D., & Legrand, X. (2018). Conductive polymers for smart textile applications. Journal of Industrial Textiles, 48(3), 612–642*
8. *Guo, L., Berglin, L., & Mattila, H. (2010). Textile strain sensors characterization-sensitivity, linearity, stability and hysteresis. Nordic Textile Journal, (2), 51-63.*
9. *Liang, A., Stewart, R., & Bryan-Kinns, N. (2019). Analysis of sensitivity, linearity, hysteresis, responsiveness, and fatigue of textile knit stretch sensors. Sensors, 19(16), 3618.*
10. *Oatley, Giles, Tanveer Choudhury, and Paul Buckman. 2021. "Smart Textiles for Improved Quality of Life and Cognitive Assessment"* Sensors *21, no. 23: 8008.*
11. *Raji, R. K., Miao, X., Zhang, S., Li, Y., & Wan, A. (2018). Influence of rib structure and elastic yarn type variations on textile piezoresistive strain sensor characteristics. Fibres & Textiles in Eastern Europe.*
12. *Seyedin, S., Zhang, P., Naebe, M., Qin, S., Chen, J., Wang, X., & Razal, J. M. (2019). Textile strain sensors: a review of the fabrication technologies, performance evaluation and applications. Materials Horizons, 6(2), 219-249.*
13. *Shanbeh, M., & Emadi, M. (2016). Effect of weft density and/ percentage of stainless steel fiber content of weft yarn on electrical properties of woven fabric strain sensors. The Journal of The Textile Institute, 107(8), 958-966.*
14. *Shanbeh, M., Hasani, H., & Manesh, F. Y. (2012). An investigation into the fatigue behavior of core-spun yarns under cyclic tensile loading. Journal of Engineered Fibers and Fabrics, 7(4), 155892501200700406.*
15. *Teyeme, Y., Malengier, B., Tesfaye, T., & Van Langenhove, L. (2020). A Fabric-Based Textile Stretch Sensor for Optimized Measurement of Strain in Clothing. Sensors, 20(24), 7323.*
16. *Voyce, J., Dafniotis, P., & Towlson, S. (2005). Elastic textiles. In Textiles in sport (pp. 204-230). Woodhead Publishing.*
17. *V. Šafárová, K. Malachová and J. Militký (2014). "Electromechanical analysis of textile structures designed for wearable sensors," Proceedings of the 16th International Conference on Mechatronics - Mechatronika 2014, pp.416-422*
18. *Xiamoning, T., (2008). Electrical textile sensors for repeated large deformation. International conference on experimental mechanics 2008, 73754H*
19. *Zang, Y., Zhang, F., Di, C. A., & Zhu, D. (2015). Advances of flexible pressure sensors toward artificial intelligence and health care applications. Materials Horizons, 2(2), 140-156.*

INVESTIGATION OF THE USAGE OF ALTERNATIVE NEW GENERATION ECO-FRIENDLY FIBER BLENDS IN SYNTHETIC BASED DENIM FABRICS

Dilek Şarapnal [1]

Çalık Denim Tekstil AŞ. R&D Department, Yeşilyurt/Malatya, Turkey,

Osman Babaarslan [2]

Engineering Faculty, Textile Engineering Department, Cukurova University, Adana, Turkey

Corresponding Author email : dilek.sarapnal@calikdenim.com

Abstract

Polyester yarn is made from post-consumer waste such as bottles, fabrics, etc., in the composition of polyester ethylene terephthalate (PET). Polyester (mainly polyethylene terephthalate, PET) is the most commonly employed textile fibre with over 50% share in total production of textile fibres. Pla is a biobased and biodegradable polymer produced from renewable resources. PLA is also a thermoplastic aliphatic compostable polyester. In this study, 75% Cotton - 25% PLA, 75% Lyocell - 25% PLA and 75% Cotton - 25% PET blended yarns were produced as rigid, corespun and dualcore in the ring spinning system .The fabrics were weaved with produced yarn. In the finishing processes, some of the fabrics were treated with caustic and some of the fabrics were only washed. Fabrics containing PLA and PET were compared with each other. Fabrics containing PLA and PET fiber were evaluated in terms of strength, elasticity, abrasion and pilling performances. Although the weft tensile and tear properties of Cotton-PLA blended fabrics are lower than Lyocell-PLA and Cotton-PET blends, it has been indicated that PLA blended yarns can be used as an alternative to PET based yarns and fabrics

Key words:

Pla, Polyester, Lyocell, Blend Yarn and Fabrics, Fabric Performance

1. Introduction

One of the most common raw materials used in the global textile industry is Polyethylene terephthalate (PET) fiber, cotton fiber and their blends. Cotton and polyester staple fibers constitute 58% and 28% of staple yarns, respectively. [1] Polyester (mainly polyethylene terephthalate, PET). The most widely used textile fiber in total textile fiber production. In general, it has excellent performance properties. In addition to this feature, it is a non-biodegradable fiber that consumes fossil fuels {2] Polylactic acid (pla) has been recognized as one of the solutions for the disposal of plastics, as it is produced from renewable resources and completely biodegrades at the end of its life [3] In addition to offering advantages in the use of pet and cotton fiber blends, pet-cotton production has negative effects on the environment. Fabrics made using pla offer good moisture management properties for underwear, sportswear, active wear and fashion wear due to their excellent wicking ability, rapid moisture spreading and drying properties [4] The dry tensile strength of lyocell fiber is greater than that of other man-made cellulosic staples, not only its physical, mechanical and chemical properties are better than viscose fiber, but also environmentally friendly because the lyocell process uses non-toxic NMMO solvent [5].

The current study aims to comparison of eco-friendly pla fiber to cotton-pes blended fabrics, as well as the physical properties of pla fiber in lyocell-pla and cotton-pla blended fabrics will be compared.

2. Experimental

2.1. Materials

Pla, cotton, polyester and lyocell fibers were used in the production of the yarns used in this study. Polylactic acid (PLA, Palmetto Synthetics LLC), lyocell (TencelRB , Lenzing AG), PET and cotton fibres were sourced. The properties of selected fibres are given in Table 1 and characteristic strength-elongation curves are plotted in Table 1.

Table 1. Fiber details

Parameters	Pla	Lyocell	Polyester	Cotton
Fineness (dtex)	1,66	1,7	1.53	0.11 (4.7mic)
Fibre length (mm)	38	38	38	29.3
Tenacity (cN.tex–1)	25	33	57.4	29.8
Elongation (%)	52	13	18	7.3

18 Ne ring-spun rigid, core and dual core-spun yarn has been produced. 78dtex lycra® and 55dtex T400® (PET/PTT) are used in the production of core-spun and dual core-spun yarns.
The details of yarns are given in Table 2 .

Table 2. Yarn type and compositions

Yarn Code	Yarn Types	Sheath *fiber* composition	Yarn description
A1	Rigid	25% Pla+75% Lyocell	Ne 18/1 RK
A2	Corespun	Sheath fiber-25% Pla+75% Lyocell	Ne 18/1 RK 78 LYC
A3	Dualcore	Sheath fiber-25% Pla+75% Lyocell	Ne 18/1 55 dtex T400 78 LYC
B1	Rigid	25% Pla+75% Cotton	Ne18/1 RK
B2	Corespun	Sheath fiber-25% Pla+75% Cotton	Ne 18/1 RK 78 LYC
B3	Dualcore	Sheath fiber-25% Pla+75% Cotton	Ne 18/1 55 dtex T400 78 LYC
C1	Rigid	25% Pes+75% Cotton	Ne18/1 RK
C2	Corespun	Sheath fiber-25% Pes+75% Cotton	Ne 18/1 RK 78 LYC
C3	Dualcore	Sheath fiber-25% Pes+75% Cotton	Ne 18/1 55 dtex T400 78 LYC

2.2. Methods

Rigid, core-spun and dual-core yarns were produced in the ring-spinning process. The weaving process was completed on Picanol type machines.
Finishing processes of the woven fabrics have been completed. In addition to comparing the use of Pla and the use of Pes, the effect of the pre-treatment step on the fabric performance was also investigated. Fabric weaving details are given in Table 3.
The codes and explanations given to the fabrics according to the pre-processing steps are given in Table 4.

Table 3. Fabric details

	CTPLA B1	**CTPLA B2**	**CTPLA B3**	**CLYPLA A1**	**CLYPLA A2**	**CLYPLA A3**	**CTPES C1**	**CTPES C2**	**CTPES C3**
Warp Yarn	14/1 RK Slub	14/1 RK Slub	14/1 RK Slub	14/1 RK Slub	14/1 RK Slub	14/1 RK Slub	14/1 RK Slub	14/1 RK Slub	14/1 RK Slub
Weft Yarn	B1 (Rigid)	B2 (Core-spun)	B3 (Dual core-spun)	A1 (Rigid)	A2 (Core-spun)	A3 (Dual core-spun)	C1 (Rigid)	C2 (Core-spun)	C3 (Dual core-spun)
Comb	70	70	70	70	70	70	70	70	70
Weft Density	21	21	21	21	21	21	21	21	21
Weave Types	3/1Z	3/1Z	3/1Z	3/1Z	3/1Z	3/1Z	3/1Z	3/1Z	3/1Z

Table 4. Pre-processing steps

Fabric Code	**Sheath fiber composition**	***Treatment Process***
CTPLA B1-W	%25 Pla +% 75 Cotton	Washed
CTPLA B1-C	%25 Pla +% 75 Cotton	10 Be' Caustic
CTPLA B2-W	%25 Pla +% 75 Cotton	Washed
CTPLA B2-C	%25 Pla +% 75 Cotton	10 Be' Caustic
CTPLA B3-W	%25 Pla +% 75 Cotton	Washed
CTPLA B3-C	%25 Pla +% 75 Cotton	10 Be' Caustic
CLYPLA A1-W	%25 Pla+%75 Lyocell	Washed
CLYPLA A1-C	%25 Pla+%75 Lyocell	10 Be' Caustic
CLYPLA A2-W	%25 Pla+%75 Lyocell	Washed
CLYPLA A2-C	%25 Pla+%75 Lyocell	10 Be' Caustic
CLYPLA A3-W	%25 Pla+%75 Lyocell	Washed
CLYPLA A3-C	%25 Pla+%75 Lyocell	10 Be' Caustic
CTPES C1-W	%25 Pes +% 75 Cotton	Washed
CTPES C1-C	%25 Pes +% 75 Cotton	10 Be' Caustic
CTPES C2-W	%25 Pes +% 75 Cotton	Washed
CTPES C2-C	%25 Pes +% 75 Cotton	10 Be' Caustic
CTPES C3-W	%25 Pes +% 75 Cotton	Washed
CTPES C3-C	%25 Pes +% 75 Cotton	10 Be' Caustic

After conditioning the fabrics according to ASTM D 1776 for 24 hours (21ºC±1 temperature, 65±2 % relative humidity), all tests were carried out.
For this study, tensile strength,tear strength,elasticity&growth ,abrasion test results were evaluated. ASTM D5034, ASTM D1424, ASTM D 3107, TS EN ISO 12947-2 standard methods were used to determine the performance of the fabric, respectively.

3. Results and discussion

Tensile properties of fabric

Strength values are important for denim fabrics. Warp tensile values in all Cotton/Pla, Tensile/Pla and Cotton/Pes groups were found to be lower in fabrics made with rigid weft compared to the experiments made with core-spun and dual core-spun weft.

The increase in the warp tensile values of the fabrics using core-spun and dual core-spun weft was due to the increase in the warp yarn density.

The lowest weft tensile values were observed in the Cotton/Pla group. The increase in tensile values of the Tencel/Pla group compared to the Cotton/Pla group is due to the fact that the Tencel fiber is more durable than cotton.

It is possible that the Cotton/Pla group has less strength than the Cotton/Pes group, possibly because the Pla fiber is less durable than the polyester fiber.
Pla fiber is sensitive to alkaline treatments, but it has been determined that it does not significantly affect the tensile values between washing and 10 Be'causticizing processes as a finishing process. Tensile warp and weft test results are given in Figure 1 and Figure 2

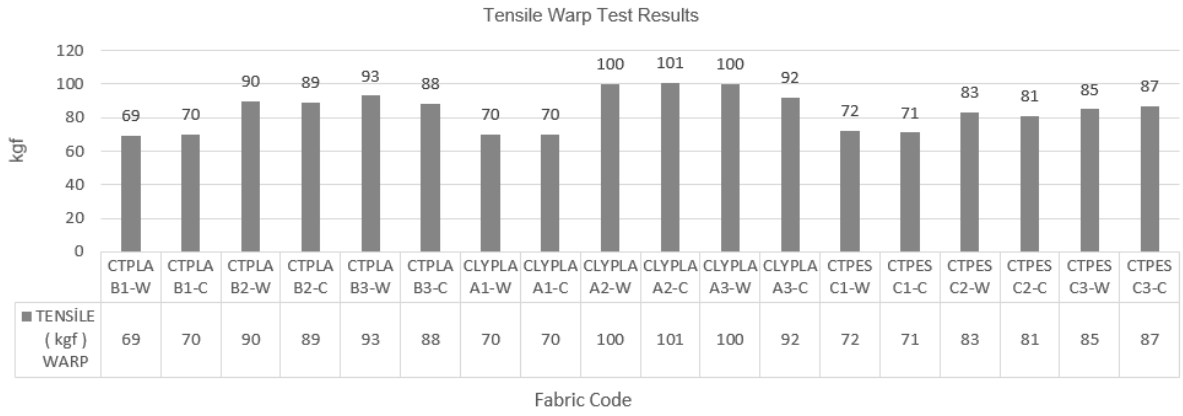

Figure 1. Warp tensile test results

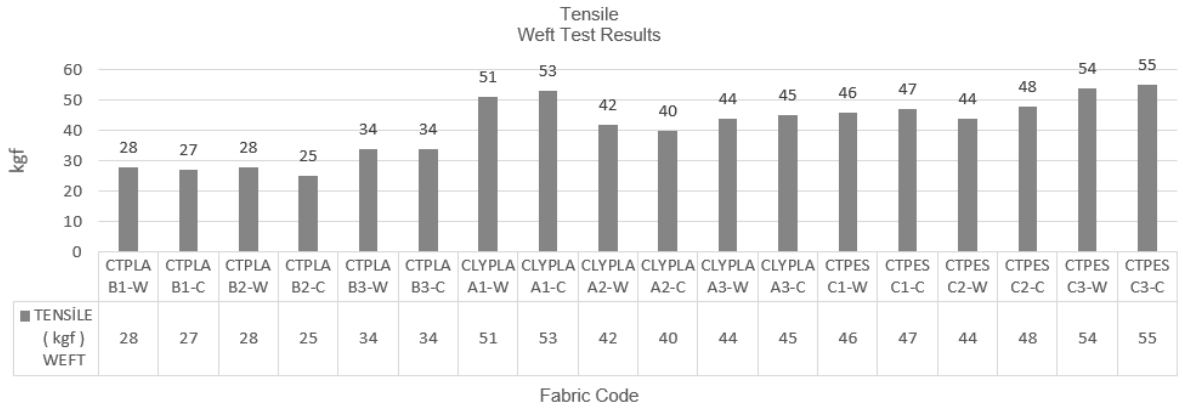

Figure 2. Weft tensile test results

It has been determined that the Warp and Weft Tear test results are in line with the interpretations obtained in the tensile values. Tear warp and weft test results are given in Figure 3 and Figure 4.

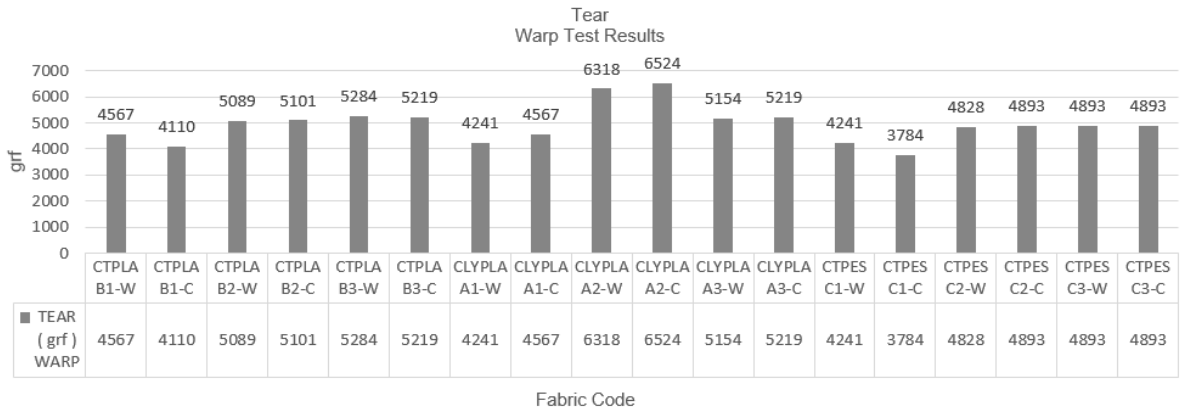

Figure 3. Warp tear test results

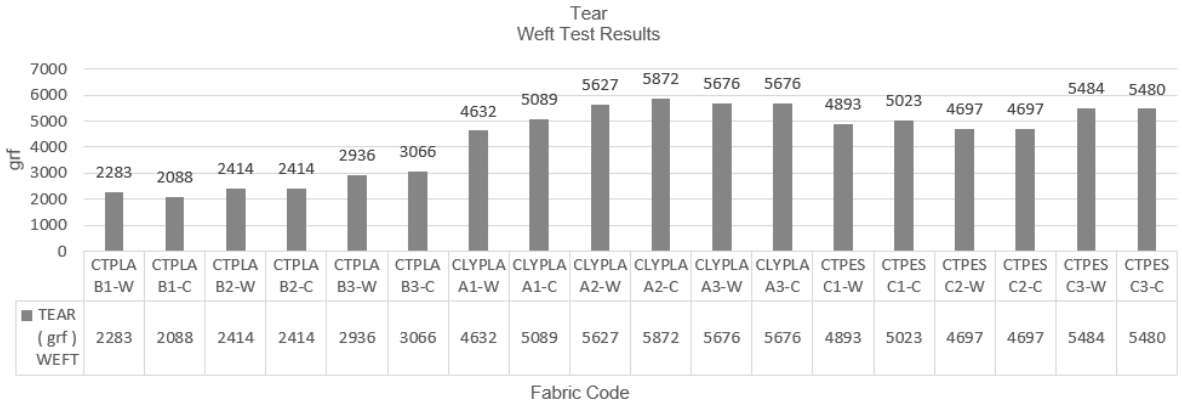

Figure 4. Weft tear test results

Elasticity and Growth results of fabrics

The elasticity values of the rigid fabrics are shown as zero. The elasticity value of the core-spun yarns of the cotton/Pla group and the Tencel/Pla group were higher than the elasticity value of the dualcore-spun yarns.In the Cotton/Pes group, elasticity the values of core-spun and dualcore-spun yarns were found to be close to each other.

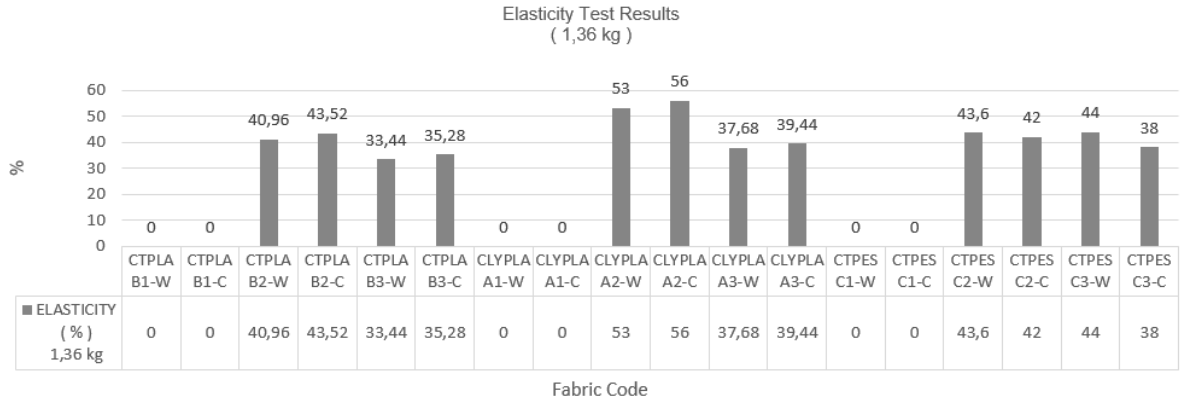

Figure 5. Elasticity test results

It was seen that the lowest growth value was in the group with Cotton/Pla, the highest in the group containing Tencel/Pla fiber.

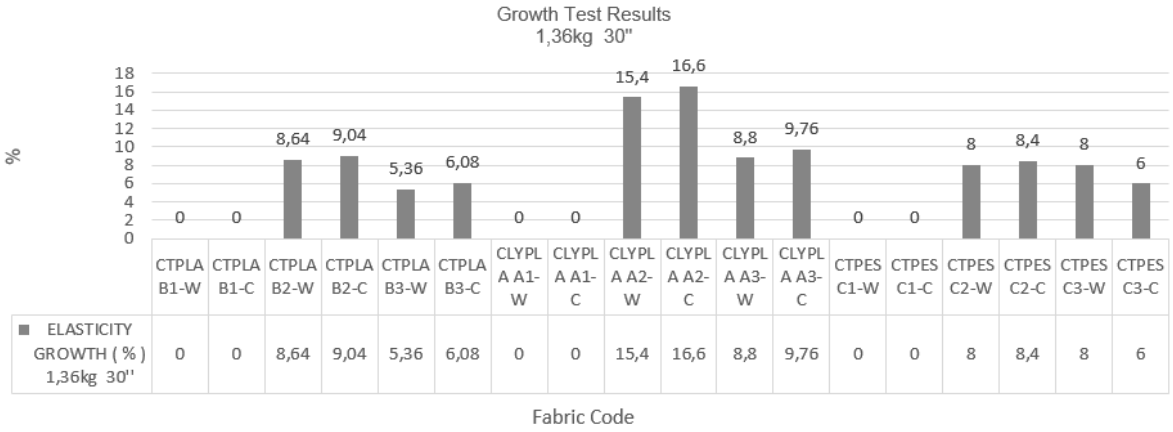

Figure 6. Growth test results

Abrasion results of fabrics

The abrasion test was performed on the back side of the fabrics and up to 25000 cycles. No breakage was detected in the yarns until 25000 cycles. There was no difference between 10 Be'causticization and washing processes.

Table 5. Abrasion test results

Fabric Code	Sheath fiber composition	Treatment Process	Abrasion	Fabric Face
CTPLA B1-W	%25 Pla +% 75 Cotton	Washed	>25000	Back
CTPLA B1-C	%25 Pla +% 75 Cotton	10 Be' Caustic	>25000	Back
CTPLA B2-W	%25 Pla +% 75 Cotton	Washed	>25000	Back
CTPLA B2-C	%25 Pla +% 75 Cotton	10 Be' Caustic	>25000	Back
CTPLA B3-W	%25 Pla +% 75 Cotton	Washed	>25000	Back
CTPLA B3-C	%25 Pla +% 75 Cotton	10 Be' Caustic	>25000	Back
CLYPLA A1-W	%25 Pla+%75 Lyocell	Washed	>25000	Back
CLYPLA A1-C	%25 Pla+%75 Lyocell	10 Be' Caustic	>25000	Back
CLYPLA A2-W	%25 Pla+%75 Lyocell	Washed	>25000	Back
CLYPLA A2-C	%25 Pla+%75 Lyocell	10 Be' Caustic	>25000	Back
CLYPLA A3-W	%25 Pla+%75 Lyocell	Washed	>25000	Back
CLYPLA A3-C	%25 Pla+%75 Lyocell	10 Be' Caustic	>25000	Back
CTPES C1-W	%25 Pes +% 75 Cotton	Washed	>25000	Back
CTPES C1-C	%25 Pes +% 75 Cotton	10 Be' Caustic	>25000	Back
CTPES C2-W	%25 Pes +% 75 Cotton	Washed	>25000	Back
CTPES C2-C	%25 Pes +% 75 Cotton	10 Be' Caustic	>25000	Back
CTPES C3-W	%25 Pes +% 75 Cotton	Washed	>25000	Back
CTPES C3-C	%25 Pla +% 75 Cotton	10 Be' Caustic	>25000	Back

Figure 7 show the abrasion test results of treated 10 Be' denim samples. Washed fabrics also have a similar backside appearance.

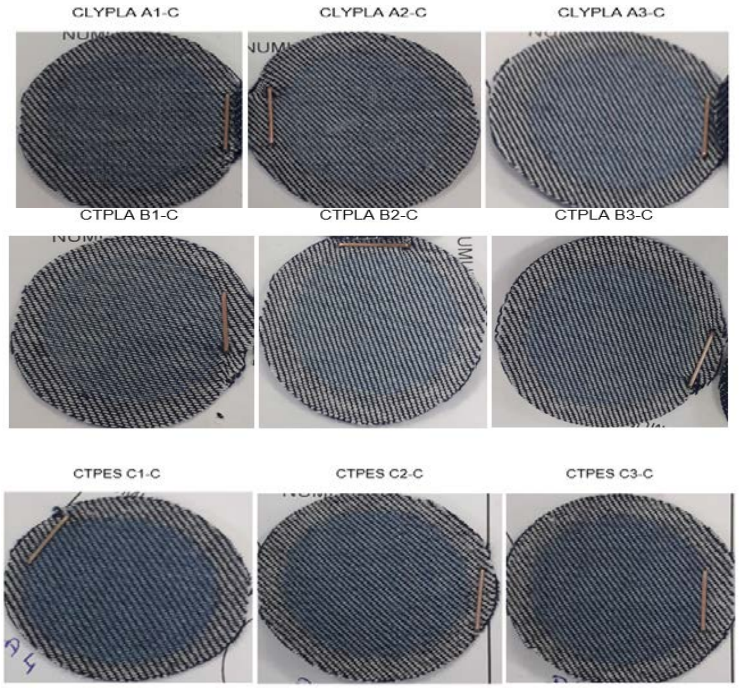

Figure 7. Abrasion test results of treated 10 Be' denim fabrics

Pilling Test results of fabrics

When the pilling test results for the Cotton/Pla and Tencel/Pla groups were evaluated over the washing and caustic treatments, results were close to each other. The pilling test results of the Cotton/Pes groups were found to be the lowest. There was no significant difference between 10 Be'Caustic and washing processes.

Table 6. Pilling test results

Fabric Code	Sheath fiber composition	Treatment Process	Pilling	Fabric Face
CTPLA B1-W	%25 Pla +% 75 Cotton	Washed	4	Back
CTPLA B1-C	%25 Pla +% 75 Cotton	10 Be' Caustic	4	Back
CTPLA B2-W	%25 Pla +% 75 Cotton	Washed	4-5	Back
CTPLA B2-C	%25 Pla +% 75 Cotton	10 Be' Caustic	4-5	Back
CTPLA B3-W	%25 Pla +% 75 Cotton	Washed	4	Back
CTPLA B3-C	%25 Pla +% 75 Cotton	10 Be' Caustic	4	Back
CLYPLA A1-W	%25 Pla+%75 Lyocell	Washed	4-5	Back
CLYPLA A1-C	%25 Pla+%75 Lyocell	10 Be' Caustic	4	Back
CLYPLA A2-W	%25 Pla+%75 Lyocell	Washed	4-5	Back
CLYPLA A2-C	%25 Pla+%75 Lyocell	10 Be' Caustic	4-5	Back
CLYPLA A3-W	%25 Pla+%75 Lyocell	Washed	4-5	Back
CLYPLA A3-C	%25 Pla+%75 Lyocell	10 Be' Caustic	4-5	Back
CTPES C1-W	%25 Pes +% 75 Cotton	Washed	2-3	Back
CTPES C1-C	%25 Pes +% 75 Cotton	10 Be' Caustic	2-3	Back
CTPES C2-W	%25 Pes +% 75 Cotton	Washed	3	Back
CTPES C2-C	%25 Pes +% 75 Cotton	10 Be' Caustic	3	Back
CTPES C3-W	%25 Pes +% 75 Cotton	Washed	3	Back
CTPES C3-C	%25 Pes +% 75 Cotton	10 Be' Caustic	2-3	Back

4. CONCLUSIONS

The use of Pla fiber instead of Pes fiber was investigated by applying different pretreatment processes. The strength values of Pla fiber blended fabrics and Pes fiber blended fabrics were compared. It has been observed that fabrics containing Pla fiber blend have lower strength than Pes fiber blended fabrics. When the 10 Be'causticizing process is compared with the fabrics that have only been washed, it has been observed that the 10 Be'causticizing process does not have a serious effect on the fabric strength values. When its physical properties are evaluated on the fabric, it has been determined that it can be used as an alternative to pes fiber because it is a biodegradable fiber. When Cotton/Pla blended yarns are evaluated in terms of strength, elasticity, pilling and abrasion test results, it is thought that Pla can be used to reduce the amount of cotton in the yarn. In this respect, it also contributes to sustainability.

References

1. *Chapman, A., Hollins, O., et al. (2010). Mistra future fashion review of life cycle assessments of clothing. Oakdene Hollins Research & Consulting, Stockholm, X(X), xxx-xxx.*
2. *Blackburn, R. S. (2005). Biodegradable and sustainable fibres. Chicago, IL: Taylor & Francis US*
3. *Yang,Y.,Zhang,M.,Ju,Z.,(2020). Poly(lactic acid) fibers, yarns and fabrics: Manufacturing, properties and applications, Textile Research Journal 0(0) 1–29*
4. *Prakash, C., Ramakrishnan, G., & Koushik, C. (2012). Effect of blend ratio of quality characteristics of bamboo/cotton blended ring spun yarn. Daffodil International University Journal of Science and Technology, 7(1), 34–37.*
5. *Shishoo,R.,(2012). The Global Textile and Clothing Industry: Technological Advances and Future Challenges*

WEAVEABILITY OF SPACER/DISTANCE FABRICS WITH HIGH PERFORMANCE FIBERS ON A TECHNICAL DOUBLE RAPIER JACQUARD WEAVING LOOM USING LANCETS

Recep Türkay Kocaman, Enrico Putzke, Frank Ficker

Hochschule Hof - University of Applied Sciences, Institute for Materials Science
Kulmbacher Straße 76, 95213, Münchberg, Germany
Phone +49 9281 409-8627
Fax +49 9281 409-55 8627
recep.kocaman@hof-university.de

Abstract:

In this study, a technical double rapier weaving loom was used for the weaving of spacer/distance fabrics with a polyester multifilament based ground warp, binding yarns and with polyester and basalt weft yarns. The spacing of the distance fabrics was achieved by using lancets. Four different bindings were developed and three different lancet heights have been used for the spacing. Thus developed spacer/distance fabrics showed uniform spacing between layers with a total thickness from 11.1 mm to 18.5 mm and were characterized according to their compressive resistance and energy absorption properties.

Key words:

woven spacer fabrics, distance fabrics, double rapier, jacquard, lancet

1. Introduction

Woven spacer fabrics are three dimensional textile structures consisting of two separate outer layers that are combined using binding yarns - keeping a space between two outer layers. Woven spacer fabrics are produced mainly by means of face-to-face weaving technique. Two surfaces of ground warp yarns are connected with pile yarns and for a carpet weaving, two layers are separated with a cutting mechanism within this technique [1]. Distance fabrics can also be woven using lancets. Two or more weft yarns can be inserted simultaneously into two different sheds. The distance warp yarn interlaces through the top and bottom fabric and the distance between the layers can be adjusted using appropriate lancet height. False picks or catching wefts can also be used to define the distance between layers [2]. Woven spacer fabrics can also be produced with modified double rapier weaving looms in order to weave semi-finished lightweight woven constructions [1, 3, 4]. Different geometries for the integration of foam between adjacent layers can also be realized using double rapier weaving technology with lancet systems [5]. This study summarizes the findings of the basic research for the weaveability of spacer/distance fabrics with high performance fibers using lancet systems with double rapier weaving technology, their compressive stress and energy absorption properties.

2. Experimental

2.1. Materials

Polyester multifilament yarns (167 Tex) purchased from Zwirnerei Nikol Weber GmbH were used as ground warp yarns, binding yarns and also as weft yarns. Basalt multifilament yarns (1200 Tex and 2400 Tex, MeltRock) were used as weft yarns for the weaving of spacer fabrics.

2.2. Methods

Four types of weave patterns were used for the study. The weave patterns were developed using the software EAT Scope Design (EAT GmbH). With this software it is possible to develop the bindings also

for double rapier weaving looms. Figure 1 shows the three-dimensional models of developed weave patterns independent of yarn count and their weft cross sections. Weaves differ from each other by weave pattern within top and bottom layer and number of binding yarn group. Weave number 1, 2 and 3 have two groups of binding yarns which have the same yarn count with the ground warp yarns, whereas weave number 4 has one group of binding yarn. Weave number 1 and 4 have one-up one-down weave with a step number 1 and have reinforcement yarns between in both layers. Weave number 3 has two-up two-down weave with a step number 2 and has one-up one-down reinforcement yarns between in both layers. Weave number 2 has one-up one-down weave without stepping and also reinforcement yarns between.

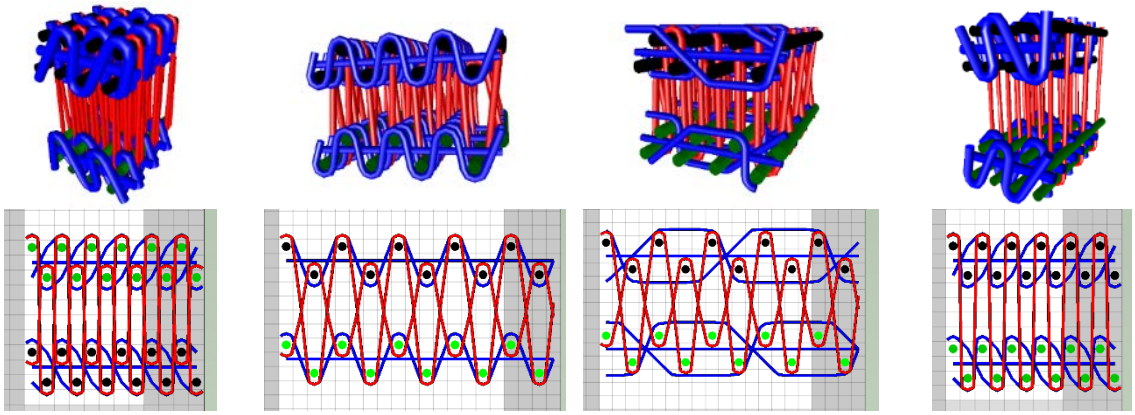

Figure 1. 3D models of developed weave patterns and their weft cross sections

A technical double rapier weaving machine (TF 20, Stäubli GmbH, Germany) was used for the weaving of spacer/distance fabrics. This machine has a UNIVAL 100 jacquard system which makes it possible to control each harness via servo motors. Every harness can be controlled independently. It also includes special rapiers for the insertion of high performance fibers like carbon, aramid, basalt and ceramic fibers. Levelled metal lancets were used for the spacing of distance fabrics. Lancets with three different levels, respectively 10 mm, 14 mm and 18 mm were chosen for the design of experiment. For an effective shed geometry adjustment and in order to assist the weaving of outer layers, two front weaving tables were adjusted with 2 mm distance from the top and from below for every lancet height. Basalt multifilament yarns with two different yarn counts and polyester multifilament yarn were used as weft yarns whereas polyester multifilament yarn was also used as ground warp yarn and binding yarn. Machine speed was adjusted between 40 and 45 rpm during weaving. The double rapier weaving loom has a continuous and discontinuous linear take-up system. Weft densities of the woven patterns were defined during the weaving for an optimum fabric tension and these density values were noted. After each row of inserted weft yarns, distance fabrics were taken up discontinuously with a defined length. Figure 2 shows the used lancet system and the examples of woven distance fabrics.

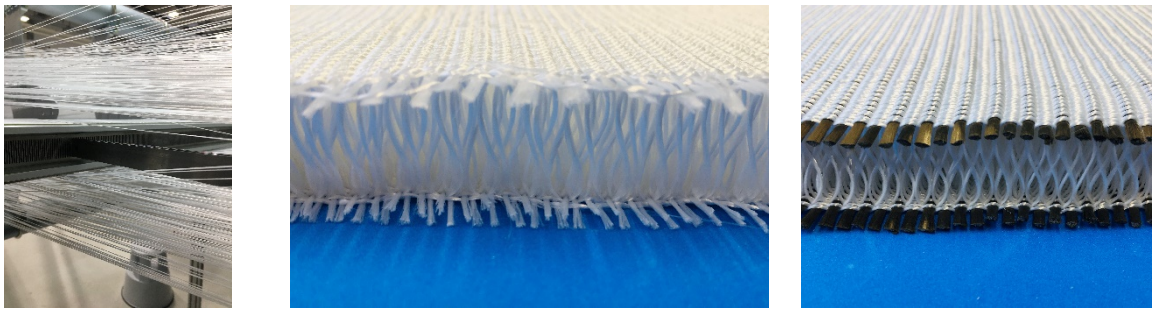

Lancet system

Distance fabric with polyester weft yarn

Distance fabric with basalt weft yarn

Figure 2. Lancet system and examples of woven distance fabrics

Compressive stresses of the chosen distance fabric samples were measured according to the test method DIN-EN-ISO 3386-I. Therefore, 70 mm x 70 mm, samples were prepared and 3 samples were measured from each woven spacer fabric type. The samples were loaded 3 times up to 70% of its thickness and then unloaded, and at the fourth time loaded up to 70%. First loading cycle was taken into account for calculation of energy absorptions and efficiencies.

3. Results and discussion

3.1. General findings

A uniform spacing was achieved in all of the woven distance fabrics. Weave pattern 3 with basalt weft yarn (2400 Tex) could not be woven because of insufficient binding which showed up during weaving. In general, weave patterns 3 and 4 showed visually looser structures with basalt weft yarns. Adjusted discontinuous take-up distances for each inserted weft row and measured thickness values of the woven samples are summarized in Table 1. According to the results, weave pattern 2 showed less fabric thickness values than the 18 mm lancet height. This could be because of the type of binding which leads to a compact structure after the release of the woven sample from the lancet zone. Weave pattern 1 and weave pattern 2 showed sufficient binding and compact structures compared to pattern 3 and pattern 4. Generally, total fabric thickness values were up to 2 mm higher than the used lancet heights.

Table 1. Summary of the findings

Weave pattern	Lancet height	Take-up [mm/weft row]	Distance fabric thickness [mm]
Weave 1	18 mm	1.4 – 3.0	18.2 – 18.4
	14 mm	1.2 – 2.8	15.4 – 16.1
	10 mm	1.1 – 2.6	11.1 – 12.1
Weave 2	18 mm	1.8 – 3.4	15.2 – 16.7
	14 mm	1.4 – 3.1	15.1 – 15.4
	10 mm	1.4 – 2.8	11.5 – 12.7
Weave 3	18 mm	1.2 – 2.2	16.1 – 18.2
	14 mm	1.1 – 1.6	15.7 – 16.1
	10 mm	0.9 – 1.4	11.9 – 13.0
Weave 4	18 mm	1.2 – 3.0	17.0 – 18.5
	14 mm	1.0 – 2.8	14.6 – 15.3
	10 mm	1.0 – 2.2	11.7 – 12.4

3.2. Compressive resistance properties

Compressive resistance properties of chosen woven distance fabrics were characterized according to the weave pattern, used weft yarn and lancet height. Figure 3 shows the comparison of measured compressive stress values of chosen samples.

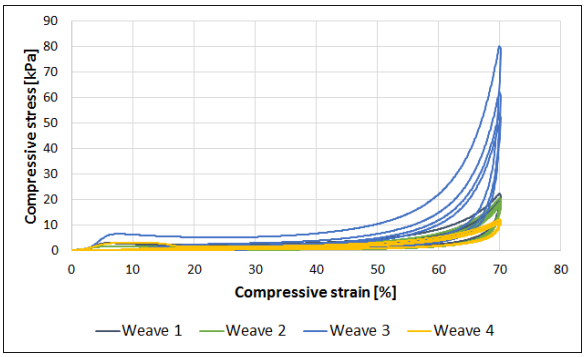

a) Weft yarn: Polyester 167 Tex
Lancet height: 18 mm

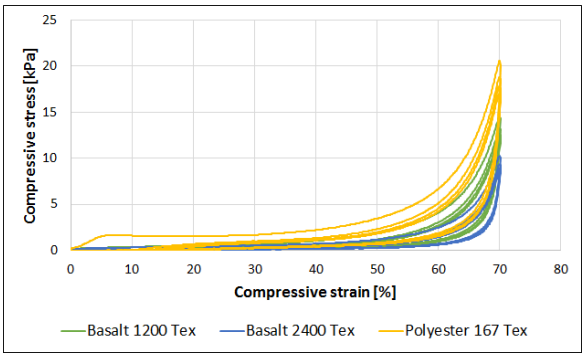

b) Weave pattern: Weave 2
Lancet height: 18 mm

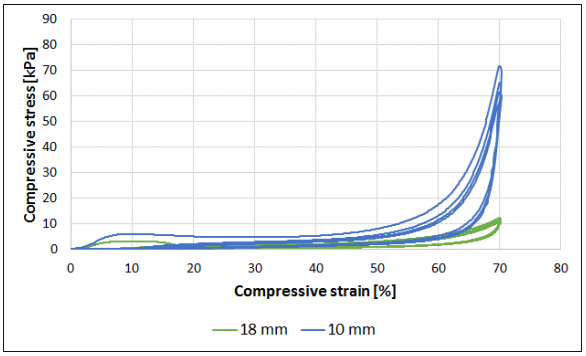

c) Weave pattern: Weave 4
Weft yarn: Polyester 167 Tex

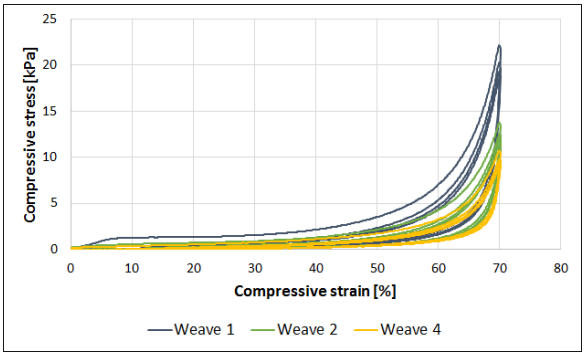

d) Weft yarn: Basalt 1200 Tex
Lancet height: 18 mm

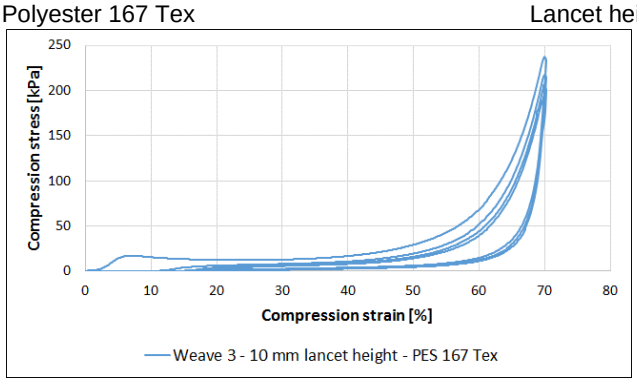

e) Weave pattern : Weave 3, Weft yarn: Polyester 167 Tex, Lancet height: 10 mm

Figure 3. Comparison of compressive resistance values of chosen woven spacer fabrics

Test results show generally lower compressive stress values, because there is not a monofilament binding yarn in these structures. Binding yarns were also multifilament yarns and their yarn counts correspond to the ground warp yarns. All of the samples showed a long plateau stage, approximately up to 50 % of the total thickness. According to the results, weave pattern 3 showed the best compressive stress value when the weave patterns were compared (Figure 3-a). Comparison of the samples with different weft yarn counts showed that the best compressive stress values were measured with the finest weft yarn; Polyester 167 tex, when the lancet height was 18 mm (Figure 3-b). This could be due to a higher compact structure, using the finer weft yarns. Lower inner fabric thicknesses (lancet height: 10 mm, fabric thickness: 11.5 mm) showed better compressive stress values within the same weave pattern and weft yarn type (lancet height: 18 mm, fabric thickness: 18.5 mm) as shown in Figure 3-c. Weave pattern 1 with two groups of binding yarns showed better compressive stress values compared to weave pattern 4 with only one group of binding yarn as expected (Figure 3-d). The best compressive resistance value was achieved within the weave pattern 3 with a polyester weft yarn and a fabric thickness of 11.6 mm (Lancet height: 10 mm) as shown in Figure 3-e.

3.3. Energy absorption properties

Calculation of the energy absorbed by a spacer/distance fabric under compression has a great importance. Compressive stress – strain diagrams can also show the energy absorption behavior, but using the energy absorption diagram will clearly show the absorbed energy per unit volume in order to understand the energy absorption property of a spacer fabric in a better way[6]. An energy absorption diagram shows the absorbed energy per unit volume as a function of the compressive stress and these kinds of diagrams were used in previous studies to show the energy absorption properties of foams, honeycomb structures and spacer fabrics [6, 7, 8]. Efficiency – compressive stress diagrams were also used to see energy absorption efficiency and the plateau stress [6, 7, 8]. A dramatic increase in the absorbed energy can be seen when the stress is towards the plateau stress in the efficiency – compressive stress diagrams and the stress maintains constant. Figure 4 shows the energy absorption diagrams of chosen samples (left) and their efficiency-compressive stress diagrams (right) which are calculated from the data of the first loading cycle.

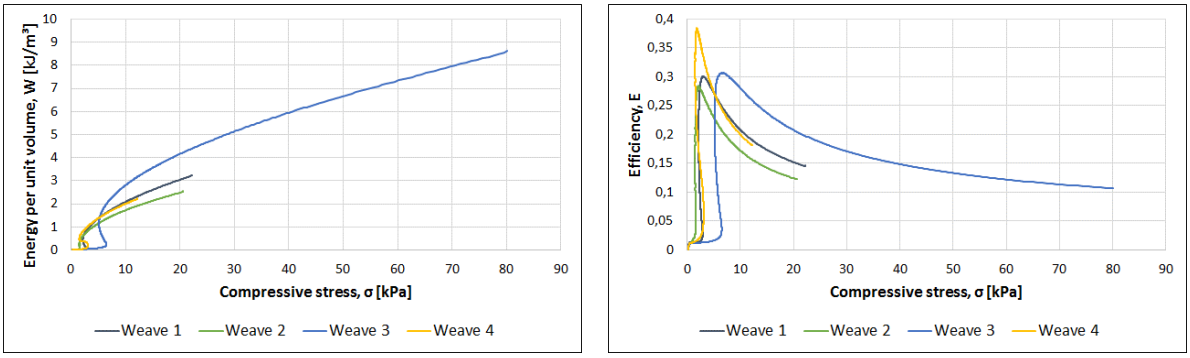

a) Weft yarn: Polyester 167 Tex, Lancet height: 18 mm

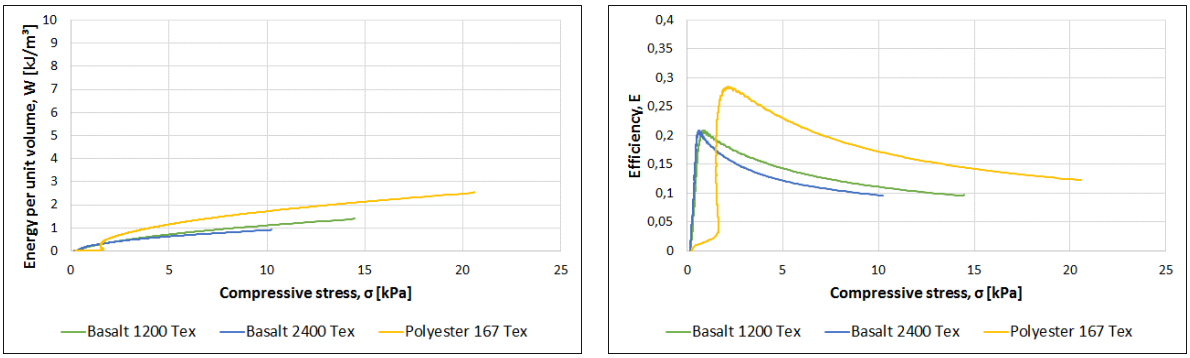

b) Weave pattern: Weave 2, Lancet height: 18 mm

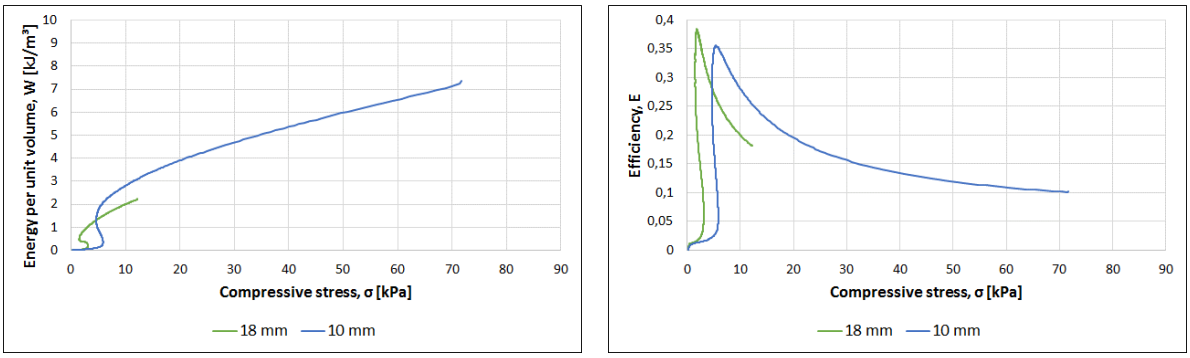

c) Weave pattern: Weave 4, Weft yarn: Polyester 167 Tex

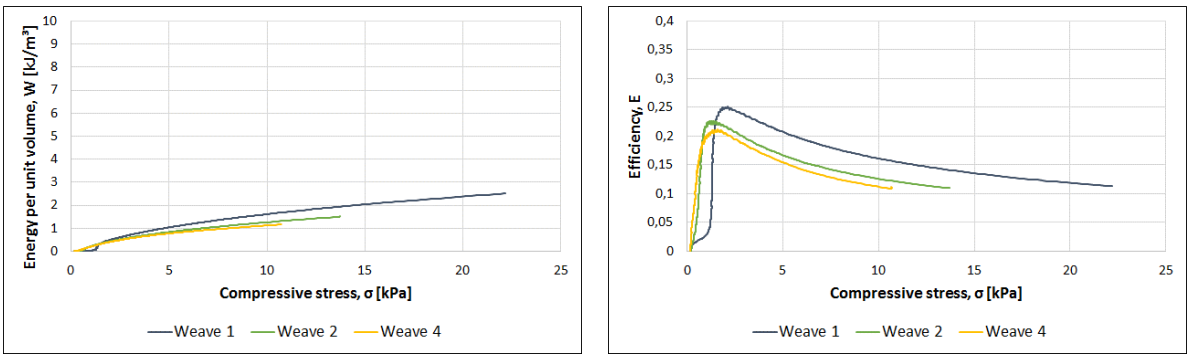

d) Weft yarn: Basalt 1200 Tex, Lancet height: 18 mm

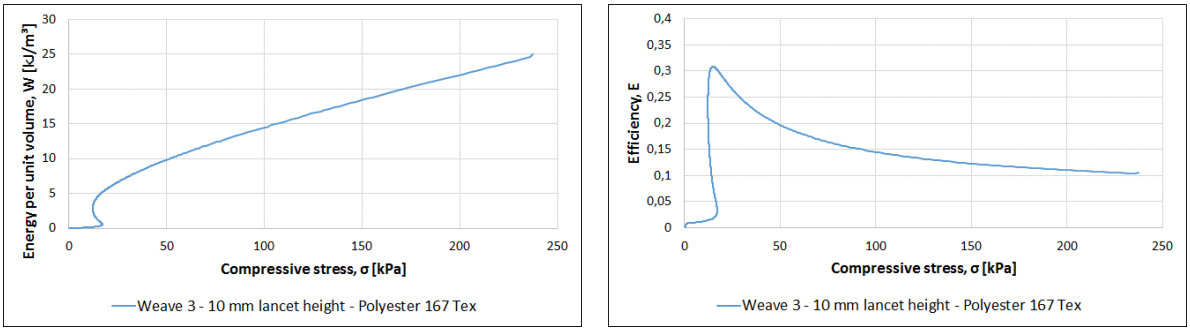

e) Weave 3, Weft yarn: Polyester 167 Tex, Lancet height: 10 mm

Figure 4. Energy absorption (left) and efficiency (right) diagrams of chosen woven spacer fabrics

The best energy absorption property was achieved within the weave pattern 3 with a polyester weft yarn in comparison of the weave pattern (Figure 4-a). The plateau stress of this weave was approx. 7 kPa. Up to approx. 2 kPa, weave patterns 2 and 4 showed higher energy absorption efficiencies. On the other hand, woven spacer fabric with polyester weft yarn showed a higher plague stress compared to basalt weft yarns (Figure 4-b). Thicker woven spacer fabric showed a longer plateau zone and a lower plateau stress (Figure 4-c). Thicker woven spacer fabric can absorb a defined amount of energy at lower stress. That means, thicker woven spacer fabric reaches its maximum efficiency point at a lower stress and energy level, which are approx. 1.71 kPa and 0.66 kJ/m³. Whereas the thinner woven spacer fabric reaches its maximum efficiency point at much higher stress and energy level, which are approx. 5.36 kPa and 1.9 kJ/m³. For this reason, both of these spacer fabrics have different working ranges. Comparison of weave pattern 1 with weave pattern 4 showed that the woven spacer fabric with two groups of binding yarns showed higher compressive stress and energy level and a higher efficiency, which is due to the effect of additional binding yarn system (Figure 4-d). Weave pattern 3 with an 11.6 mm thickness (10 mm lancet height) and polyester weft yarn showed the highest plague stress of approx. 15 kPa and the highest energy level of approx. 4.6 kJ/m³ all among the woven spacer fabrics.

4. CONCLUSIONS

In this study the weaveability of distance fabrics with high performance fibers like basalt yarns and polyester yarns on a technical double rapier weaving machine was discussed. Different woven fabric samples were compared according to their thicknesses and bindings. Important findings were summarized. Compressive resistance properties of chosen fabrics were compared according to their weave pattern type, weft yarn type and lancet height. Energy absorption properties of chosen samples were analyzed and compared according to the material, process and fabric parameters.

ACKNOWLEDGEMENTS

This research received no specific grant from any funding agency in the public, commercial, or not-for-profit sectors. The authors are grateful to Mr. Uwe Schwittai and Mr. Harald Ott for the weaving of spacer/distance fabrics and Ms. Susanne Schödel-Guthke for the testing of the fabric samples. The responsibility for the content of this publication lies with the author(s).

References

1. *Torun, A.R. (2011). Advanced manufacturing technology for 3D profiled woven preforms. PhD Study. Dresden University of Technology (Dresden)*
2. *Maes, D. (2009). Applications of distance fabrics and multiple layer weaves in technical textiles. http://www.technicaltextile.net*
3. *Mountasir, A. (2016). Entwicklung einer flexiblen Webtechnologie zur Fertigung integral gewebter 3D Halbzeuge für Faserkunststoffbauteile komplexer Geometrie. PhD Study. Dresden University of Technology (Dresden)*
4. *Großman, K., Mühl, A., Löser, M., Cherif, C., Hoffmann, G., Torun, A.R. (2010). New solutions for the manufacturing of spacer preforms for thermoplastic textile-reinforced lightweight structures. Prod. Eng. Res. Devel. 4:589-597*
5. *Lüling, C., Rucker-Gramm, P., Weilandt, A., Beuscher, J., Nagel, J., Schneider, J., Maier, A., Bauder, H., Weimer, T. (2021). Advanced 3D Textile Applications for the Building Envelope. Applied Composite Materials. 29:343-356*
6. *Liu, Y., Hu, H., Zhao, L., Long, H. (2011). Compression behavior of warp-knitted spacer fabrics for cushioning applications. Textile Research Journal. 82(I):11-20*
7. *Bates, S., Farrow, I., Trask, R. (2016). 3D printed elastic honeycombs with graded density for tailorable energy absorption. Proc. SPIE 9799, Active and Passive Smart Structures and Integrated Systems*
8. *Avalle, M., Belingardi, G., Montanini, R. (2001). Characterization of polymeric structural foams under compressive impact loading by means of energy-absorption diagram. International Journal of Impact Engineering 25:455-472*

SIMULATION OF THE SEGMENT FILLING INSERTION FABRICS AT THE YARN LEVEL

Jiahui Fang[1,2], Yordan Kostadinov Kyosev[2], Yuling Li[1], Yanxue Ma[1]

1. College of Textiles, Donghua University, Shanghai, 201620, China;
2.Technische Universität Dresden, Dresden, 01069, Germany;
corresponding author e-mail: fangjiahuizfh@163.com

Abstract:

Fabrics with segment filling insertion are finding application in several traditional luxurious textiles, clothing, and in the latest time as well for smart textiles. Segment filling allows the integration of conductive yarns for contacting areas, keeping the textile character of the structures. This work presents a method for 3D modeling woven structures with segment filling at the yarn level. The pattern image is analyzed by an image processing tool, written in Python, and used to create the initial weaving information. After that, the different regions are filled with suitable preselected weave types, such as plain, twill, or others. Finally, this data is used to compute the 3D coordinates of the weft and warp yarns, and saved in a suitable format. The 3D visualization is done by the TexMind Viewer, which allows its advanced version export in various formats for FEM, CFD, and other computations.

Keywords:

segment filling insertion fabrics; yarn level; product development; 3D simulation;

1. Introduction

According to the filling insertion method[1], weaving looms can be divided into shuttle looms and shuttleless looms, the weaving looms were all based on the normal filling method until 2019. As shown in Figure 1, every weft is filled from one side to the other with one single yarn in fabrics with a plain weave. Meanwhile, many researchers have taken numerous approaches in yarn-level woven fabric modeling[2]- [4] based on the normal filling method[5]- [7].

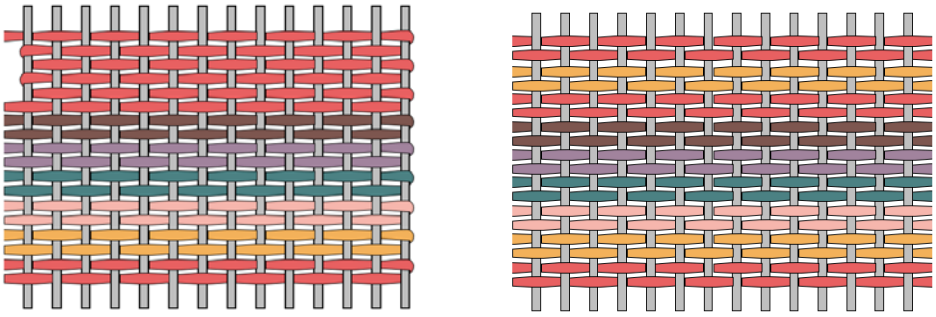

(a) Fabrics woven by shuttle loom (b) Fabrics woven by shuttleless loom

Figure 1. Normal filling insertion fabrics

With the improvement of automatic techniques, segment filling insertion fabrics (see Figure 2) can be weaved by a modified dobby loom in 2019[8]. The segment filling insertion fabrics are pretty complex, different from the normal woven fabrics, where the fabrics are composed of yarn-level patterns based on repeated sections[9-10]. As each row is composed of several yarns of different colors, which can be turned back at any position.

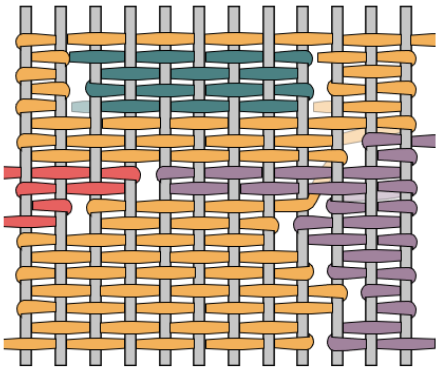

Figure 2. Segment filling insertion fabrics

The method for 3D simulation of woven structures with segment filling at the yarn level is systematically proposed in this work. Characterization of yarns in the segment filling insertion fabric as is shown in Fig.2, For the simulation of segmental filling insertion fabrics, the challenge is that the trajectory of the weft yarn is flexible, i.e., it can start and end at any position, in addition, it is continuous between different rows, the connection between the end of one row and the start of the next row is also much more complicated compared with normal woven fabrics.

2. Experimental

The simulation parameters are obtained through imaging analysis, area division, weave filling, and orientation property marks of key positions along the yarn trajectory. A topology based model, similar to those reported for braided structures[11] or in the general case for any textile architecture[12] was developed as a parametric mathematical model and then implemented in a Python program.

In the past years, a matrix of '0' and '1' is generally applied to describe the structure of a fabric[13]. In simulation analysis as well as 3D modeling of fabrics[14-15], this matrix describes the position relationship of warp and weft yarns, that is, the Z coordinate in the 3D coordinate system. Taking plain weave fabric as an example, as shown in Figure 3, its basic organizational structure matrix is shown in Figure 3(b). For other parameters[16-17], such as yarn geometry (e.g. yarn length, fineness, yarn spacing, etc.), yarn mechanics (e.g. initial modulus, strength, elongation, etc.), yarn color parameters, etc. The common feature of the above simulation as well as the modeling of woven fabrics is that the normal weft yarns are continuous in the row as well as disconnected at both ends. For the calculation of the key coordinates of the yarn trajectory, it is not necessary to consider the relationship between wefts. More realistic methods for the representation of the yarns at the fiber level can be implemented in the future, as reported by Liu et. al[18], but in the current work, the specific areas of the weft yarn transition have to be considered and modeled more detailed.

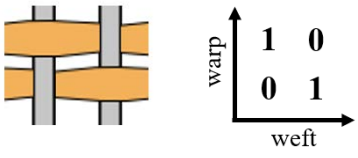

(a) Schematic diagram of plain weave (b) Matrix code for organization chart

Figure 3. Plain weave and its corresponding matrix

2.1. Methods

In this study, the initial pattern (noted as matrix $Z0_{ij}$, as shown in Figure 4 (a)) is first processed by the algorithm to divide the color minimum region, and the color information of each part of the region can

be extracted separately as well as saved in a new matrix of size i*j, noted as matrices $Z1_{ij}$, $Z2_{ij}$, ... Zn_{ij} (as shown in Fig. 4(b)), where each part of the divided region is composed of one single continuous weft yarn. (For the segment filling insertion fabric, its area division standards mainly follow the shortest floating line, as well as the principle of the shortest entanglement, which involves a complex process issue, not discussed in detail in this paper.)

The original pattern image is analyzed by algorithms written in python, in this paper, the simulation model of the segment filling insertion fabric is mainly obtained by connecting the key points with Cubic Hermite spline, so the calculation of the key points in the 3D coordinate system is the core of this study.

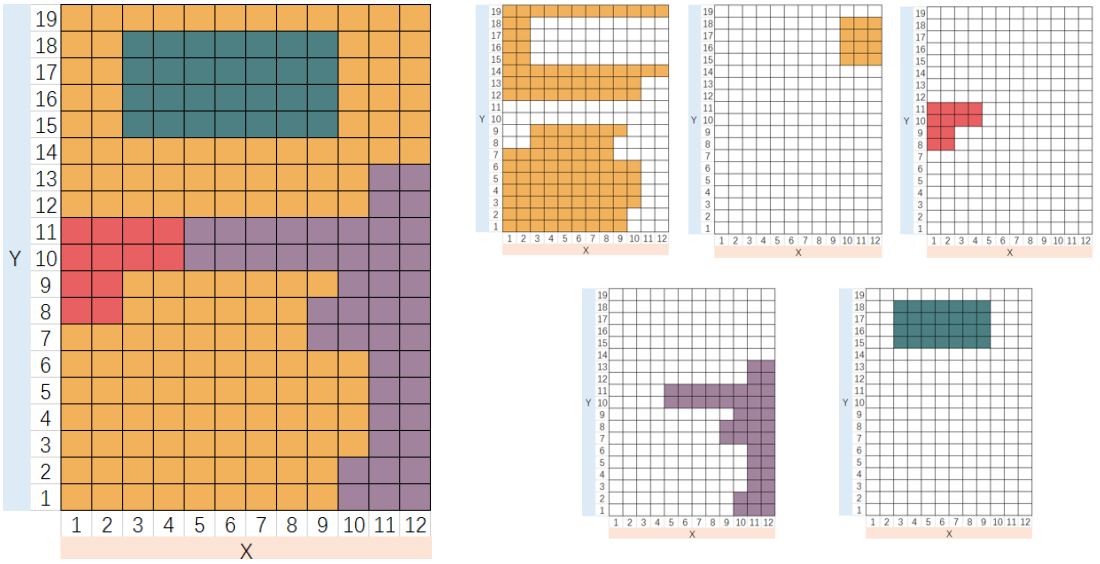

(a) Original Pattern (b) Extract the same color block area and divide it into suitable zones

Figure 4. Original Pattern and the divided zones

The new matrix obtained by the algorithm fills the divided area with plain organization, noted as $Y1_{ij}$, $Y2_{ij}$, …, Yn_{ij}, the matrix indicates the corresponding relationship between warp and weft in each row, the figure '△' is '1' in the matrix, i.e., the weft is on top; '○' corresponds to the matrix '-1', i.e., the weft is at the bottom; the blank is '0', i.e., the weft does not pass through the region, as shown in Figure 5, this matrix represents the topological information.

$Y1_{11}$ = 1, $Y1_{21}$ = -1, …, the non-zero region of this matrix is the range covered by the weft, i.e., a continuous yarn coverage, moreover, the key points of the yarn are recorded in the matrix Weft1[P()], where the coordinates of the key point $P(X_P, Y_P, Z_P)$ = (i, j, Yn_{ij}). The weave diagram is produced.

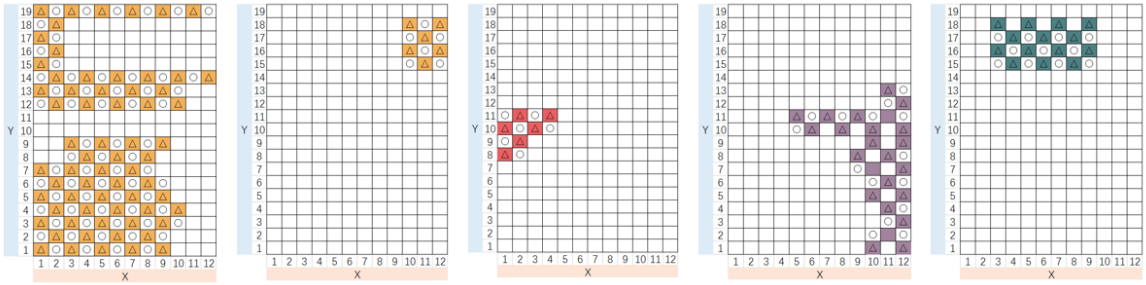

(a) Weft Yarn I(Y1) (b) Weft Yarn II(Y2) (c) Weft Yarn III (Y3) (d) Weft Yarn IV (Y4) (e)Weft Yarn I V(Y5)

Figure 5. The weave diagram of each weft

The coordinates of the weft at the last point of the previous row are marked as P(X_P, Y_P, Z_P), the adjacent row of wefts (as shown in Figure 6(a)), or the non-adjacent row of wefts (as shown in Figure 6(b)). The starting point is Q.

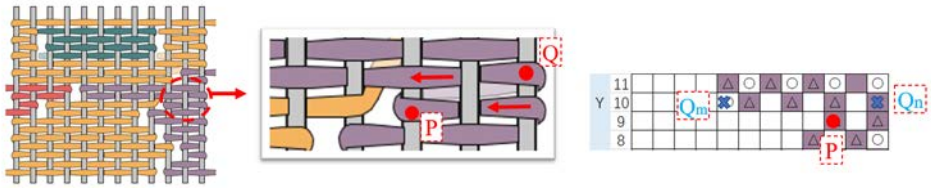

(a) Two points are on adjacent rows

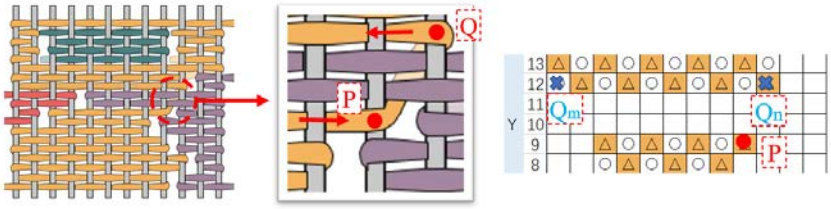

(b) Two points are not on adjacent rows

Figure 6. Connection of P and Q

The correct order of the key points is obtained by judging from Eq. 1. As shown in Figure 7.

$$Q=\begin{cases} Q_m, X_P \le X_{Qm} \\ Q_m, X_{Qm} < X_P < X_{Qn} \ \cup \left(X_p - X_{Qm}\right)^2 - \left(X_p - X_{Qn}\right)^2 \le 0 \\ Q_n, X_{Qm} < X_P < X_{Qn} \ \cup \left(X_p - X_{Qm}\right)^2 - \left(X_p - X_{Qn}\right)^2 > \ 0 \\ Q_n, X_{Qn} \le X_p \end{cases} \quad (1)$$

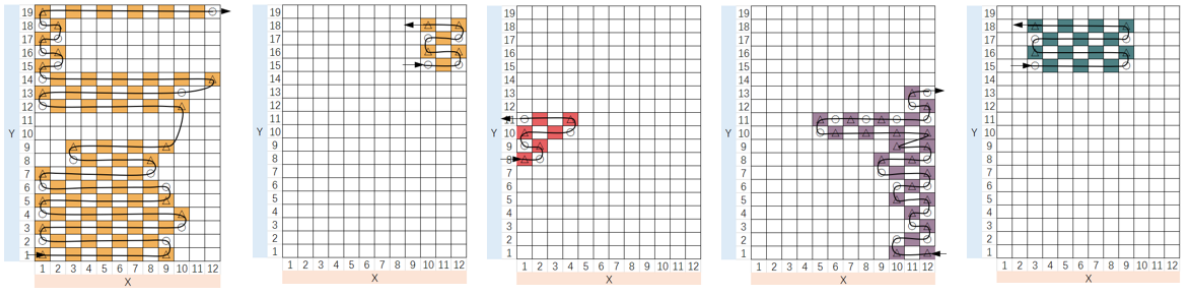

(a) Weft Yarn I(Y1) (b) Weft Yarn II(Y2) (c) Weft Yarn III (Y3) (d) Weft Yarn IV (Y4) (e)Weft Yarn I V(Y5)

Figure 7. Determine the weft trajectory

The weft yarn is continuously between rows, so the weft returned from the edge of the fabric. or create a floating line from one point(at the end of the previous row) to another point(the connection of the next row), which is another unique feature of the segmental filling insertion fabric. In the case of the weft return from the edge of the fabric, it is assumed that the next point is Q_n, i.e., a new control point N(X_N, Y_N, Z_N) needs to be inserted between the points P(X_P, Y_P, Z_P) and Q(X_Q, Y_Q, Z_Q) (as shown in Fig. 8). Thereby ensuring the trajectory variation of the yarn in the z-axis direction.

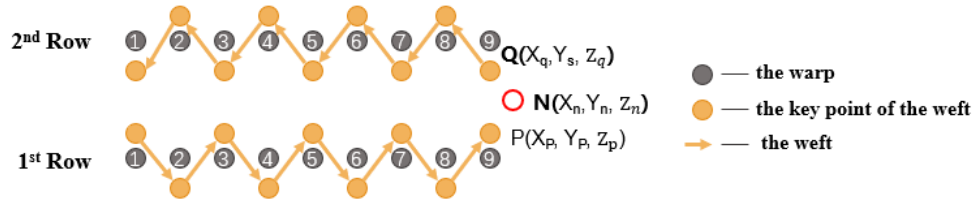

(a) Weft key points for the first and second row

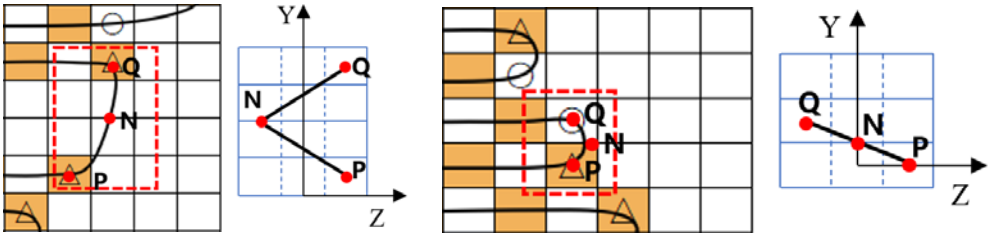

(b) Weft insertion across rows (c) Weft insertion does not across rows

Figure 8. Insert a new control point N based on Points P and Q

If the floating line is generated, i.e., a new control point N needs to be inserted between points P and Q, meanwhile, the Z coordinates of points P and Q are also to be compared, then the coordinates of the N point can be calculated.

$$\begin{cases} X_N = \frac{X_P + X_Q}{2} \\ Y_N = \frac{Y_P + Y_Q}{2} \\ Z_N = \begin{cases} \frac{Y_P + Y_Q}{2}, Z_P * Z_Q < 0 \\ -\frac{Y_P + Y_Q}{2}, Z_P * Z_Q > 0 \end{cases} \end{cases} \quad (2)$$

Meanwhile, the next weft is determined by calculating the relative position in the X-axis, followed the Eq. 2, starting from the left or right.

Finally, we got the key points of the yarn recorded in the matrix, suppose the yarn starts from (m,n) and ends at (w,v), the points through the yarn was saved in order in the matrix Weft1 = [P1(X_m, Y_n, Z_P), P2(X_{m+1}, Y_n, Z_P),…, Pi(X_i, Y_n, Z_P), N($\frac{X_P+X_Q}{2}$, $\frac{Y_P+Y_Q}{2}$, Z_N), P(X_Q, Y_Q, Z_Q),…, P(X_w, Y_v, Z_P)]. Moreover, all the simulation information is saved in the fabric matrix as follows, Fab = [Wefts[P1(),P2(),…, Pm()], Warps[P1(),P2(),…, Pn()],yarn parameters map].

2.2. Simulation Parameters

In addition to some parameters[19-20] that need to be analyzed from the original pattern, some additional parameters have to be input by the designer to simulate the fabric, as shown in Table 1.

Table 1. Specifications of 3D fabric.

	Input parameters	Output
Yarn parameters	Color map Warp radius r1 Weft radius r2 …	Simulation file
Fabric parameters	Warp density/ Warp gap Weft density/ Weft gap	

The number of warp and weft can be obtained after analysis the pattern. Meanwhile, the matrix information can be gained by further calculations. Many parameters can be caculated, such as, the warp length can be calculated from the yarn fineness and the size of the pattern. Integration of parameters in python to complete the simulation of the fabric as shown in Fig. 9.

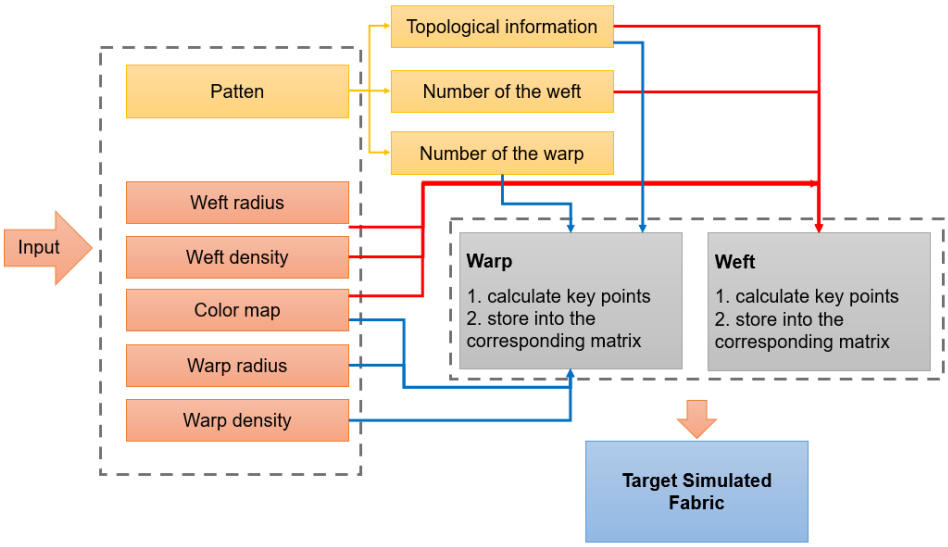

Figure 9. Calling and handling of parameters

3. Results and discussion

In this study, parameters are collected mainly by analyzing pattern as well as the input from the designer, then the Z-axis coordinates are obtained by filling the segmented area with unit matrix organization, besides, the different rows are connected by inserting auxiliary points; the weft trajectories are obtained from the key point sequence. Finally, yarn parameters are added to complete the simulation of the segmented filling insertion fabric.

The simulated segment filling insertion fabric is displayed by the TexMind Viewer, as shown in Figure 10. The floating yarns are generated between non-adjacent areas in the back view. Two simulated fabrics with the same warp density but different weft densities are named F1 and F2.

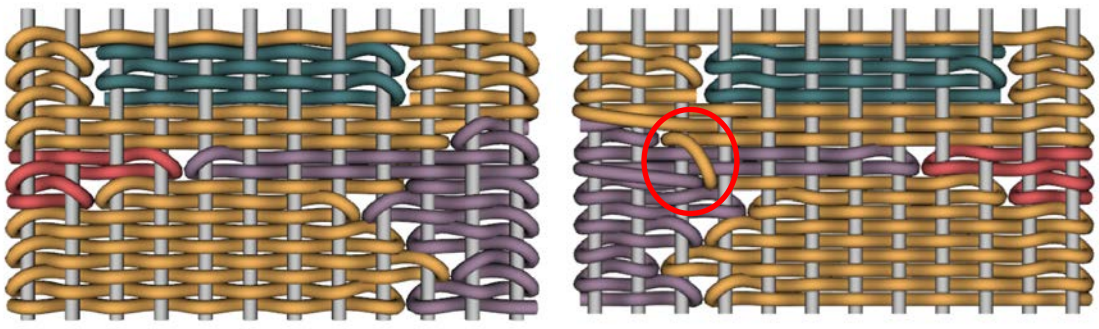

(a) The front view of the simulated fabric (F1) (b) The back view of the simulated fabric (F1)

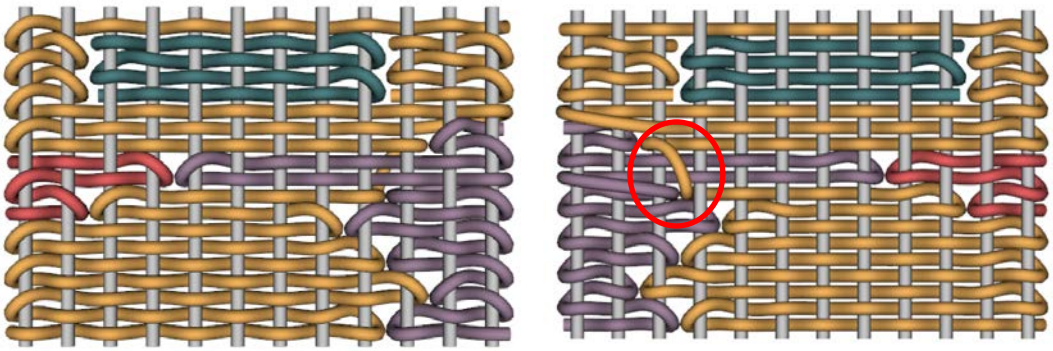

(c) The front view of the simulated fabric (F2) (d) The back view of the simulated fabric (F2)

Figure 10. The front view and the back view of the two simulated fabrics

The method proposed in this study, the simulation not only reflected the characteristics of the segment filling insertion fabric but also can be a guide for the fabric design and rationality check of the weaving process. This work solves the following problems in the simulation process: Determination of the sequence point Q in the process of weft yarn transferred to another row; Calculation of the correct auxiliary points by P and Q; The combination of yarn parameters as well as topological information matrix to obtain the simulated fabric.

However, the work still has some shortcomings, the bending of warp yarn is not considered in the simulation process and there are details that can continue to be optimized subsequently. More parameters can be added to improve the accuracy of the simulation.

4. CONCLUSIONS

Yarn-level simulation can assist in the design and weaving of the fabric, converting the original 2D weave diagram into a 3D intuitive visual effect, which is very significant for fabric-assisted design. Modeling in 3D visualization at the yarn level is more friendly for the designers, because they can make reasonable modifications to the design by the 3D model. Besides, yarn-level modeling can be also used to simulate the physical properties of textiles.

The structure of the segment filling insertion fabric has infinite possibilities, which can make the fabric more diverse, as different color areas can be woven with different functional yarns.

ACKNOWLEDGEMENTS

This research stay in Germany of Jiahui Fang for study was supported by 'the Fundamental Research Funds for the Central Universities' (Grant No.: 2232020E-10) and 'China Scholarship Council'

References

1. Mao X.H, Bao M.(2005) Weaving Volume II. China Textile Publishing House (Beijing).
2. Dong, Z., & Sun, C. T. (2009). Testing and modeling of yarn pull-out in plain woven Kevlar fabrics. Composites Part A: Applied science and manufacturing, 40(12), 1863-1869.
3. Leaf, J., Wu, R., Schweickart, E., James, D. L., & Marschner, S. (2018). Interactive design of periodic yarn-level cloth patterns. ACM Transactions on Graphics (TOG), 37(6), 1-15.
4. Jauffrès, D., Sherwood, J. A., Morris, C. D., & Chen, J. (2010). Discrete mesoscopic modeling for the simulation of woven-fabric reinforcement forming. International journal of material forming, 3(2), 1205-1216.
5. Tripathi, L., Chowdhury, S., & Behera, B. K. (2022). Modeling and simulation of impact behavior of 3D woven solid structure for ballistic application. Journal of Industrial Textiles, 51(4_suppl), 6065S-6086S.
6. Özdemir, H., & Başer, G. (2008). Computer simulation of woven fabric appearances based on digital video camera recordings of moving yarns. Textile Research Journal, 78(2), 148-157.
7. Özdemir, H., & Başer, G. (2009). Computer simulation of plain woven fabric appearance from yarn photographs. The Journal of The Textile Institute, 100(3), 282-292.
8. Fang, J., Ma, Y., Li, Y., et al. (2021). Design and development of urban cultural and creative products with segment filling insertion. In Journal of Physics: Conference Series: 1790(1): 012032.
9. Nilakantan, G., Keefe, M., Bogetti, T. A., Adkinson, R., & Gillespie Jr, J. W. (2010). On the finite element analysis of woven fabric impact using multiscale modeling techniques. International Journal of Solids and Structures, 47(17), 2300-2315.
10. Rief, S., Glatt, E., Laourine, E., Aibibu, D., Cherif, C., & Wiegmann, A. (2011). Modeling and CFD-simulation of woven textiles to determine permeability and retention properties. AUTEX Research Journal, 11(3), 78-83.
11. Kyosev Y. Generalized geometric modeling of tubular and flat braided structures with arbitrary floating length and multiple filaments. Textile Research Journal. 2016;86(12):1270-1279. doi:10.1177/0040517515609261
12. Kyosev, Y., Topology-Based Modeling of Textile Structures and Their Joint Assemblies, Springer Nature Switzerlang AG, 2019, 238 p,
13. Dash, B. P., Behera, B. K., Mishra, R., & Militky, J. (2013). Modeling of internal geometry of 3D woven fabrics by computation method. Journal of the Textile Institute, 104(3), 312-321.
14. Wielhorski, Y., Mendoza, A., Rubino, M., & Roux, S. (2022). Numerical modeling of 3D woven composite reinforcements: A review. Composites Part A: Applied Science and Manufacturing, 154, 106729.
15. Manjunath, R. N., & Behera, B. K. (2017). Modelling the geometry of the unit cell of woven fabrics with integrated stiffener sections. The Journal of The Textile Institute, 108(11), 2006-2012.
16. Lee, S. K., Byun, J. H., & Hong, S. H. (2003). Effect of fiber geometry on the elastic constants of the plain woven fabric reinforced aluminum matrix composites. Materials Science and Engineering: A, 347(1-2), 346-358.
17. Daelemans, L., Faes, J., Allaoui, S., Hivet, G., Dierick, M., Van Hoorebeke, L., & Van Paepegem, W. (2016). Finite element simulation of the woven geometry and mechanical behaviour of a 3D woven dry fabric under tensile and shear loading using the digital element method. Composites Science and Technology, 137, 177-187.
18. Liu, H., Kyosev, Y., & Jiang, G. (2022). Yarn level simulation of warp-knitted clothing elements – first results and challenges. Communications in Development and Assembling of Textile Products, 3(2), 115-126. https://doi.org/10.25367/cdatp.2022.3.p115-126
19. Cirio, G., Lopez-Moreno, J., Miraut, D., & Otaduy, M. A. (2014). Yarn-level simulation of woven cloth. ACM Transactions on Graphics (TOG), 33(6), 1-11.
20. Nilakantan, G., & Gillespie Jr, J. W. (2012). Ballistic impact modeling of woven fabrics considering yarn strength, friction, projectile impact location, and fabric boundary condition effects. Composite Structures, 94(12), 3624-3634.

NUMERICAL MODELLING OF TEXTILE STRUCTURES: POTENTIAL AND LIMITS

Karolína Boňková

Department of Textiles and Structures, Textile Faculty, Technical University of Liberec, Studentská 2, 461 17 Liberec, Czech Republic, e-mail: karolina.bonkova@tul.cz

Abstract:

Numerical modelling, namely finite element modelling, is a standardised tool in many branches of engineering. In textile engineering, due to the complexity of the structure, many limitations occur in using this approach. Despite the limitations the finite element modelling of textiles has huge potential for the future. This contribution deals with FE modelling of tensile test in wale and course direction of single jersey knitted fabric. The meso level of the structure was chosen for the model, so it could be possible to track the behaviour of yarn interlacement during the simulated deformation. The virtual model was created according to parameters of single jersey knitted fabric sample, which was produced from polyester monofilament. By using monofilament instead of staple yarn, contacts between fibres in yarn could be excluded in FE model preparation. Two different computational programs were used for simulations – MSC Marc Metant for implicit computing approach and ANSYS LS-DYNA for explicit computing approach. The results from implicit and explicit solver were compared and discussed. Validation of models was done and results were included in the discussion. Due to big deformations of textiles, explicit solver appears to be more suitable for finite element modelling in textile engineering.

Key words:

Finite element method, implicit and explicit solver, textile structures, modelling, tensile test, knitted fabric

1. Introduction

Textile structures are extremely variable which is one of the reasons why it is possible to find them in nearly every industrial sector from clothing industry, automotive to biomechanics etc. Modelling of textiles is a challenging topic for many reasons and one of them is their multi-scale structure character [1, 2]. Textile structures can be divided into three main groups – linear, planar and 3D shaped textiles. Each group can be further described on three levels – macro, meso and micro scale. Macro-scale describes overall shape of the textile, so for example if it is yarn, woven fabric or some 3D braided structure. Meso-scale investigates the core structure of the textile, how yarns are interlaced so basically it describes pattern of the yarn arrangement. Micro-scale model tracks how individual fibres are arranged around each other.

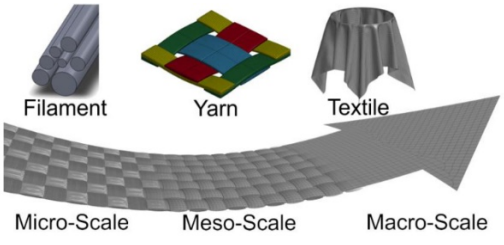

Figure 1. Representation of micro, meso and macroscale of textiles [1]

Textiles have inhomogeneous character and their mechanical behavior can be described mainly as viscoelastic. Thaks to these attributes the general geometry depiction of textile structures is complicated to desribe, because of its changeability. For example a shape of an individual staple yarn is different than the same yarn which is weaved in fabric. Many studies have beed done about this topic and in conclusion, geometry models of textile structures are always simplified at some level in comparism with the real geometry. By using computer tomography data and reconstruction of textile structure it is possible to create virtual textile model with exact geometry [3], but this method is time consuming and ususally only small part of the textile is modelled. Another aspect is, that even though we have high performance computational technology, it still is not efficient enough to capture all scales of the structure at the same time. Such model would be extremely demanding for the data and processing memory. Because of that we are able to model textiles usually on one or maximally two structural levels at the same time.

Creating virtual 3D model of textiles is first step for finite element modelling in which even more limitations occur such as description of material models, types of used elements, number of elements, contacts and more. Complex multicsale simulations are used in FE modelling of textiles, when results from one scale simulation are used as input data for another scale simulation [3]. According to work [4], the most important aspects for quality simulation on one scale with good corresponding results are:

- a realistic geometric model of textile structure,
- realistic boundary conditions,
- a realistic contact surface between yarns without penetration,
- physically measured yarn mechanical data used as input for material model.

Most of the studies which include FE modelling of textiles are oriented on woven fabrics which are commonly used as a reinforcement in textile composites [5]. Work of [6] studied optimization of geometrical model of knitted structures designated as an input for FE modelling. Similarly work [5] investigated mechanical behavior of knitted textiles and their geometrical modifications. Unfortunately neither of these works have FE models validated by experiment.

2. Experimental

2.1. Materials and methods

PERLON Polyester monofilament of diameter 0.1 mm was used to produce single jersey knitted fabric. Tensile test of monofilament was done to obtain information about its mechanical properties (Instron 4411, testing length 250 mm, testing speed 500 mm/min, 10 tested samples). Average tensile strength was 734 MPa and average modulus was 1950 MPa.

Single jersey knitted fabric was manufactured using Shima Seiki SRY 123LP machine with gauge G14. Relaxed fabric had 32 loops/50 mm in course direction and 98 loops/100 mm in wale direction so geometry of a single loop could be described by width 1.56 mm and height 1.02 mm.

2.2. Preparation of FE models

Two computational solvers were used – MSC Marc Metant (implicit solver) and ANSYS LS-DYNA (explicit solver). Two models were prepared, tensile test of virtual sample in course and tensile test of virtual sample in wale direction. In both softwares the same input geometry, material properties, boundary conditions, computational method and job results were set. Since programs offer different settings, models differed a little bit in used element and contact description but both were chosen as similar as possible.

a) Geometry

The geometry of the single jersey fabric was prepared in program TexMind WeftKnitting3D. Two models were prepared – one as a sample for tensile test in course direction and second as a sample for tensile test in wale direction. As an input information for the program, parameters shown in Table 1 were used.

Table 1. Parameters used for generating of geometry – models of single jersey knitted fabric samples

	Model for wale direction	Model for course direction
Number of courses	49	15
Number of wales	10	32
Loop width [mm]	1.56	
Loop height [mm]	1.02	
Monofile diameter [mm]	0.1	
Element length for export [mm]	0.2	

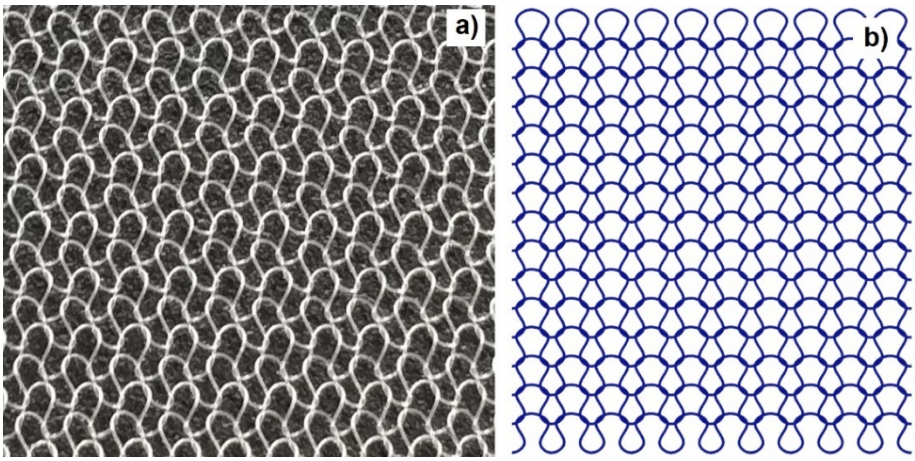

Figure 2. a) Single jersey knitted fabric from polyester monofilament, b) 3D virtual model of the textile

b) Meshing, material and contact

Beam elements were used. Beam had circular cross-section with diameter 0.1 mm. Average element length was 0.2 mm. In MSC Marc Metant element type 52 (Euler-Bernoulli beam) was used and in ANSYS LS-DYNA beam formulation 1 (Hughes-Liu) was chosen.

Linear elastic material model was chosen and described with values of modulus E = 1950 MPa, Poisson's ratio $\mu = 0.3$ and density $\rho = 1365$ kg/m^3.

In MSC Marc Metant, beam to beam touching contact was chosen. Friction coefficient was set to value 0.1.

In ANSYS LS-DYNA, automatic general contact was chosen. Static and dynamic friction coefficient were set to value 0.1.

c) Boundary conditions and job results

In both tensile tests edge nodes were disabled in every degree of freedom on one side (symbolized by cross) – this side represented static clamp of tensile testing machine. Other edge nodes were allowed in every rotational degree of freedom, one sliding degree of freedom in one direction and two remaining directions were disabled (symbolized by arrow). This side of model represented the edge of sample fixed in moving clamps of tensile testing machine. In LS-DYNA boundary conditions were applied directly on the nodes, in MCS Marc nodes were connected to one Rigid body element on each side.

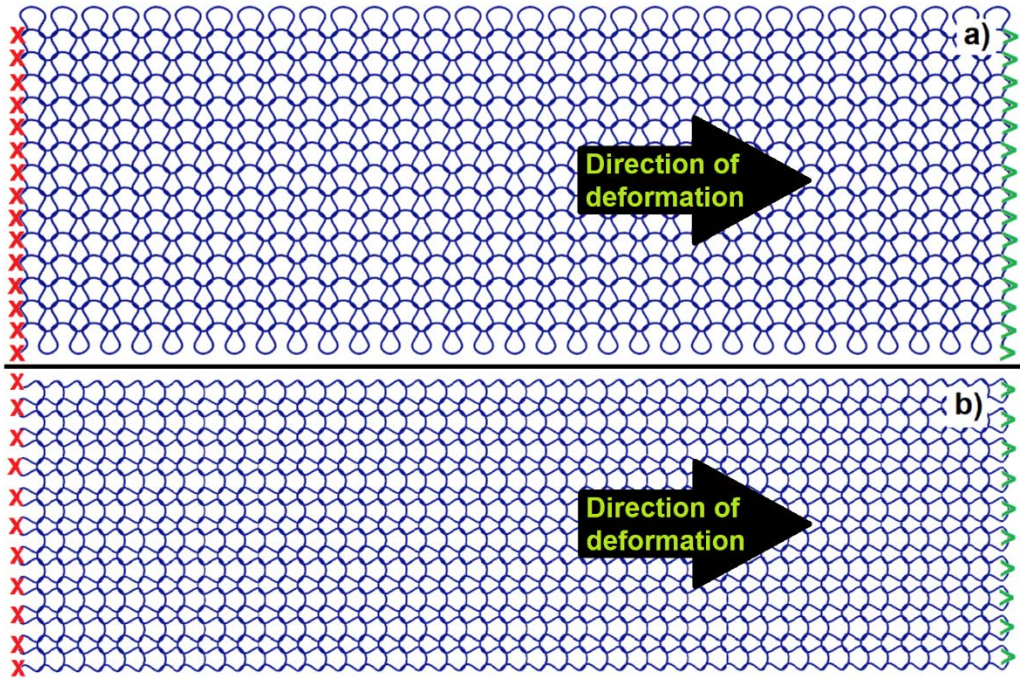

Figure 3. Boundary conditions a) course direction, b) wale direction

In both tests (tensile test in course and wale direction) models were elongated by 15 mm. Tests were controlled by displacement of destined nodes.

Displacement and reaction force were monitored as results of simulations.

2.3. Validation

For validation ADMET MTESTQuattro (TM) machine with 10lb head was used. For each direction (course, wale) 10 samples were prepared and tested. One sample had 90x15 mm dimensions for comfortable fixation to the clamps. The machine set up and sample can be seen in Figure 4. Clamps had coarse surface, so during testing there was no problem with slipping of the sample from the clamps. Testing length was 50 mm and testing speed was 40 mm/min.

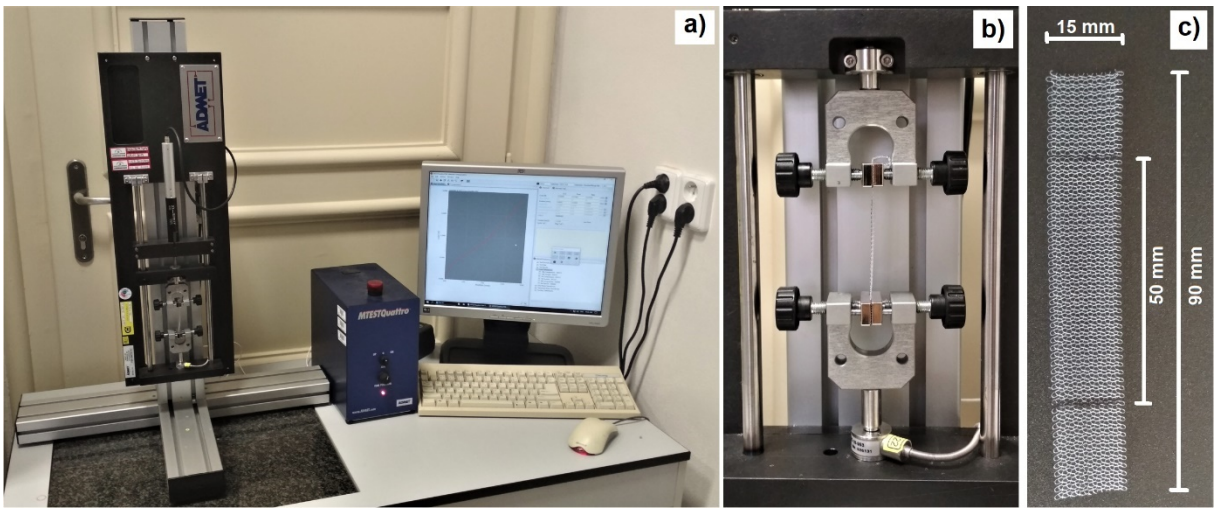

Figure 4. a) Testing machine setup, b) fixed sample in clamps, c) sample dimensions

3. Results and discussion

Table 2. Results of tensile tests – validation experiment and simulations

	Tensile test in wale direction		Tensile test in course direction	
	Displacement [mm]	Force [N]	Displacement [mm]	Force [N]
Validation Experiment	15	0.57	15	0.37
			7.83	0.67
MSC Marc Metant	15	2.96	15	0.04
ANSYS LS-DYNA	15	1.09	15	0.38
			29.5	0.65

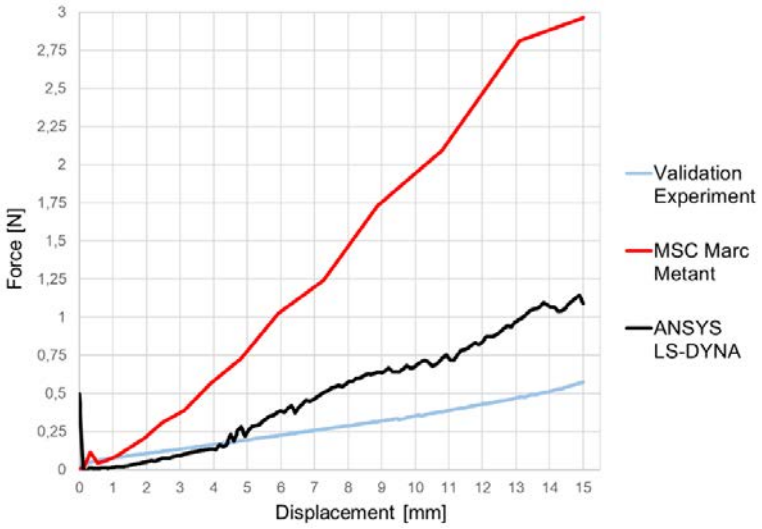

Figure 5. Comparison of tensile curves computed in MSC Marc, LS-DYNA and from validation experiment – testing in wale direction

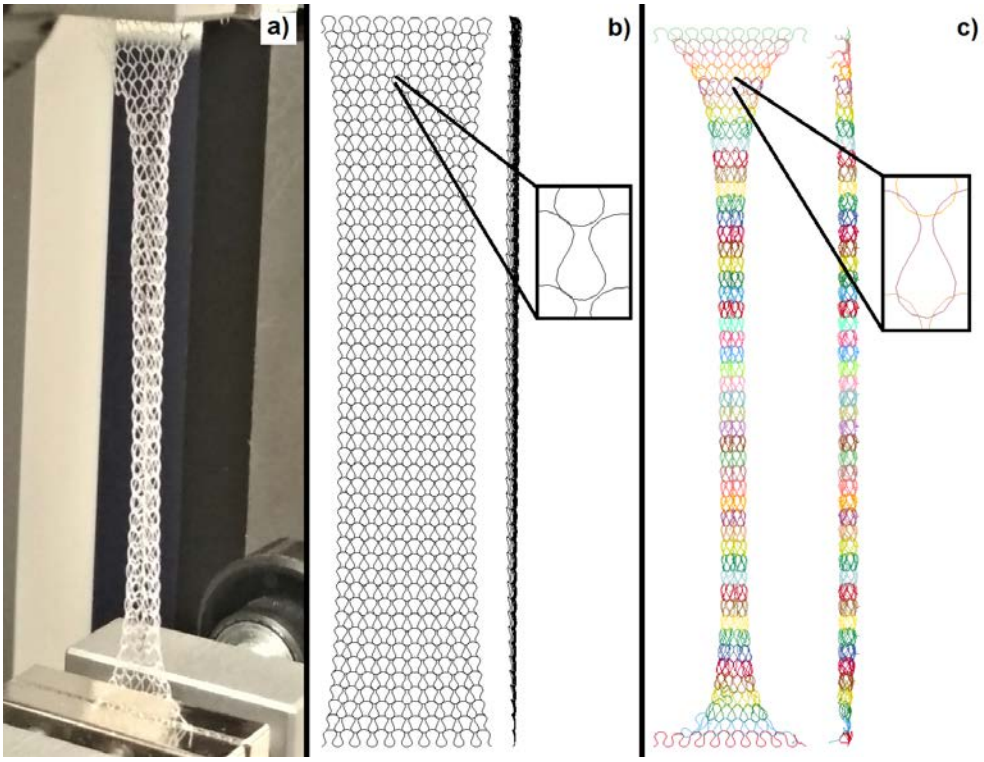

Figure 6. Visual comparison of deformed samples: a) validation experiment, b) MSC Marc simulation, c) LS-DYNA simulation – testing in wale direction

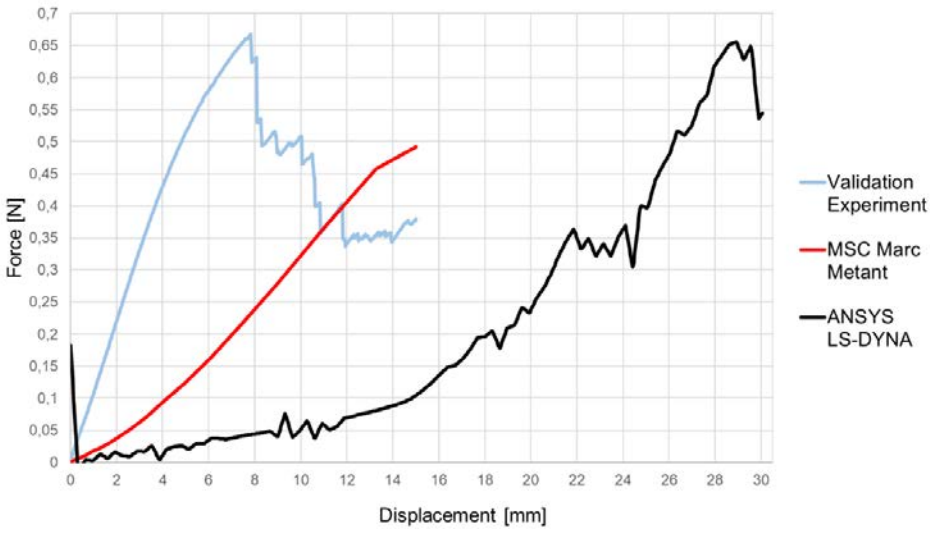

Figure 7. Comparison of tensile curves computed in MSC Marc, LS-DYNA and from validation experiment – testing in course direction

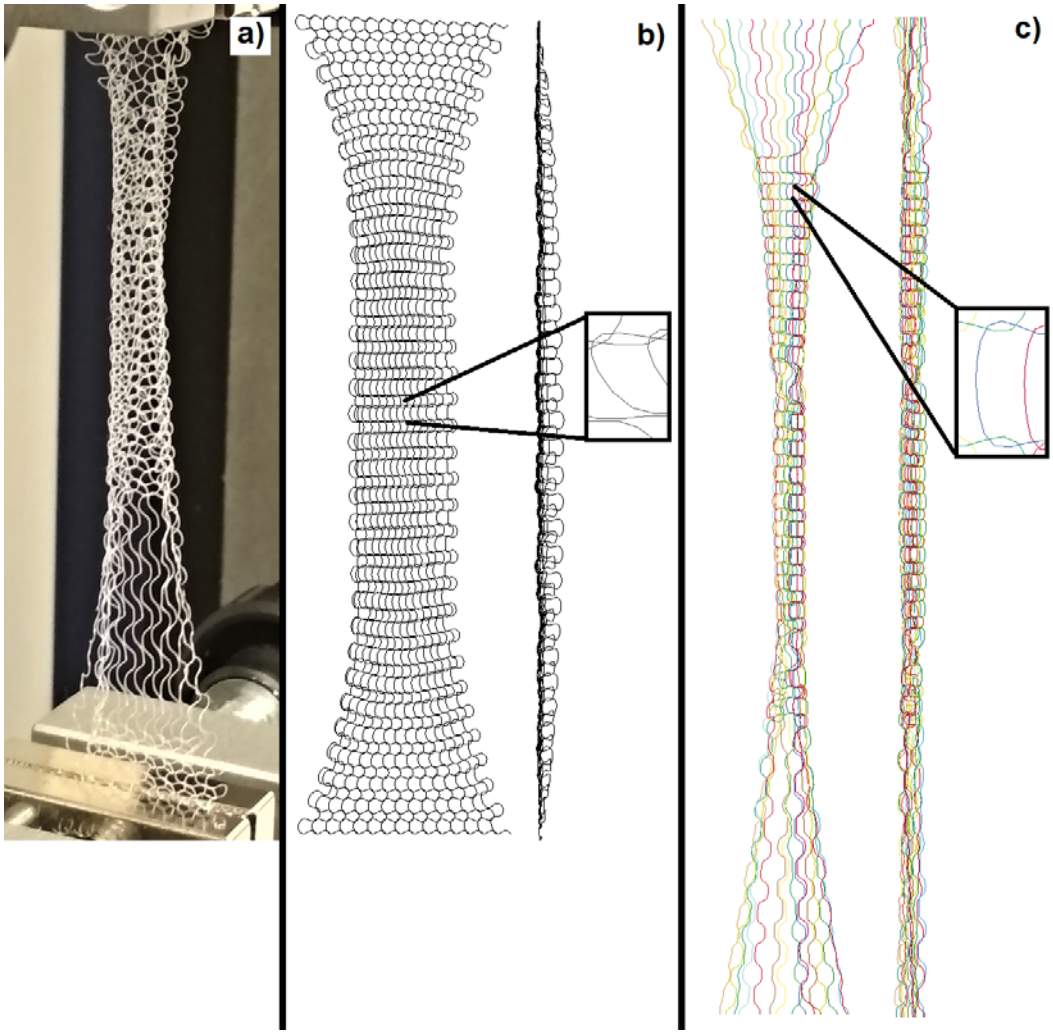

Figure 8. Visual comparison of deformed samples: a) validation experiment, b) MSC Marc simulation, c) LS-DYNA simulation – testing in course direction

Tensile test in wale direction: In Figure 6 c) it can be seen, that LS-DYNA visual representation of deformed sample corresponds with the real deformed sample very well. The elongated model sample is curled, narrow only in area of boundary conditions (same as nearby clamps) and some of the edge loops are pulled out. In LS-Dyna model no penetration of beams occurred. On the other hand, MSC Marc model after deformation is mainly narrow, minimally curled on the edges and the edge loops mostly remained in the initial shape. During the simulation there were even problems with penetration of the beams thorough all settings which supposed to prohibit that. From results we can see, that the MSC Marc model is not applicable and that the implicit solver with mentioned settings is not usable. In Figure 5 comparison of tensile curves in wale direction is shown. MSC Marc's result curve is extremely up dimensioned in comparison with the validation experiment. LS-DYNA's result curve is more accurate but the predicted value of the reaction force is still nearly twice bigger than the experimental value.

Tensile test in course direction: As it can be seen in Figure 8 a), the real sample at elongation of 15 mm is damaged by many pulled out loops. Neither model was able to simulate this at 15 mm elongation. Both models were visually compact and none of the loops were pulled out. Due to this, both simulations were repeated but with the elongation of 30 mm. The MSC Marc model was not able to simulate the slippage of the loops even with the higher deformation and plus beam penetrations occurred again. On the other hand, LS-DYNA model accurately predicted the slippage of loops during the higher deformation, even with the curled edges of the model which are appearing also in the real specimen. Again, the model did not have any penetrations of beams. In Figure 7 comparison of tensile curves in course direction is shown. Both simulated result curves are under dimensioned in comparison with the experimental curve, however the LS-DYNA's result curve with the 15 mm offset from the origin of the coordinate system, with some instabilities, is getting closer to the experimental curve and at its end it has nearly the same value of reaction force. LS-DYNA's value of reaction force is 0.65 N and the experimental value is 0.67 N.

Usually single jersey fabric is more elastic in course direction. Ratio of number of loops in a course is 1.5 times bigger than in a wale of the manufactured fabric. Due to that, experimental results from tensile tests show that the fabric is more rigid in course direction and more elastic in wale direction. After relaxation of the fabric, original width of the loop 1.81 mm shrank to 1.56 mm. Inner forces of the monofilament are certainly influenced by the shrinkage and FE model is not capable to predict these forces just from the input geometry model, which affects the results. As it can be seen in Figure 2, due to the bending stiffness of the monofilament, knitted fabric loops are not in a narrow position as it is in the case of the generated geometry model. There is also a difference between loop length even though that the geometry model was generated according to real parameters of the fabric. Average measured loop length is 4.62 mm and the modelled loop length is 3.93 mm. These geometric differences have influence on the results. Also simplified material model and friction model affect the simulated results.

4. CONCLUSIONS

Two finite element models of single jersey knitted fabric were prepared in computational software MSC Marc Metant with implicit solver and in computational software ANSYS LS-DYNA with explicit solver. Tensile test in a course and in a wale direction were simulated in both programs with as similar settings as possible. Validation of the models was done using ADMET MTESTQuattro machine which has great sensitivity so the experimental results have good accuracy. It appears that MSC Marc was not able to provide good results even with complex settings and penetrations of beams occurred during the simulations. ANSYS LS-DYNA performed great visual simulations of deformations of modelled samples which corresponded very well with real deformation of the specimen during the validation experiment. Simulated tensile curves were less corresponding with the experiments however that is influenced by the simplified geometry of the knitted fabric and simplified material model. In this case it can be said that the explicit solver is more suitable for modelling of textile mechanical deformations. For future simulations, more accurate input geometry, more complex material model as for example linear

piecewise material should be used and analyzed. Also, inner forces of the yarn after the relaxation of the knitted fabric should be considered and incorporated in FE simulations. Finite element modelling of mechanical behavior of textile structures is possible but experimental validation is necessary. FE simulations can be highly inaccurate without validation and models like that can be very misleading for the research.

ACKNOWLEDGEMENTS

This contribution was written at the Technical University of Liberec, Textile Faculty with the support of Student Grant Competition (project SGS-2022-6062 "Textile replacements designated for the chest wall reinforcement after bone defects"), which financially supported finite element course in computing program ANSYS LS-DYNA.

References

1. *Döbrich, O., Gereke, T., Cherif, Ch. (2015). Textile and Composite Modelling on a nearMicro-scale: Possibilities and Benefits. 10th European LS-DYNA Conference 2015, Würzburg, Germany [online 17.10.2022] https://www.dynalook.com/conferences/10th-european-ls-dyna-conference/4%20Materials%20II%20-%20Endless%20Fibers/01-Doebrich-TechnicalUnivDresden-P.pdf*
2. *Komeili, M., & Milani, A. S. (2011). Finite Element Modeling of Woven Fabric Composites at Meso-Level under Combined Loading Modes. In (Ed.), Advances in Modern Woven Fabrics Technology. IntechOpen. https://doi.org/10.5772/17333*
3. *Sodhani, D., Reese, S., Jockenhövel, S., Mela, P., Stapleton, S. E. (2018) Multi-scale modelling and simulation of a highly deformable embedded biomedical textile mesh composite, Composites Part B: Engineering, 143. 113-131. https://doi.org/10.1016/j.compositesb.2018.01.010.*
4. *Lin, H., Clifford, M., Long, A., Lee, K., Guo, N. (2012). A finite element approach to the modelling of fabric mechanics and its application to virtual fabric design and testing. Journal of The Textile Institute, 103. 1-14. DOI:10.1080/00405000.2012.660755.*
5. *Liu, D., Christe, D., Shakibajahromi, B., Knittel, Ch., Castaneda, N., Breen, D., Dion, G., Kontsos, A. (2017) On the role of material architecture in the mechanical behavior of knitted textiles, International Journal of Solids and Structures, 109.101-111.https://doi.org/10.1016/j.ijsolstr.2017.01.011.*
6. *Wadekar, P., Perumal, V., Dion, G., Kontsos, A., Breen, D. (2020). An optimized yarn-level geometric model for Finite Element Analysis of weft-knitted fabrics. Computer Aided Geometric Design, vol. 80, https://doi.org/10.1016/j.cagd.2020.101883.*

COMFORTABLE AND PROTECTIVE HYBRID WEFT-KNIT PLATED FABRIC FROM GLASS AND WOOL/ACRYLIC YARNS

Mehmet Erdem İnce[1], Sevgi İnanır, Esra Kumsal Erdoğan

Gaziantep University, Textile Engineering Department, 27310, Şehitkamil, Gaziantep, Türkiye.
[1]meince@ncsu.edu, eince@gantep.edu.tr; Tel: +90 342 317 27 30 Fax: +90 342 317 27 06

Abstract:

In this study, hybrid weft-knit plated fabrics were produced by co-feeding glass and wool/acrylic blend yarns. While the wool/acrylic yarn in contact with skin is expected to provide comfort, the glass yarn next to the environment is to provide protection. The physical, structural, air permeability, bursting strength, and the protection against flame properties of glass plus wool/acrylic plated fabric were compared with the reference fabrics consisting completely of glass or wool/acrylic blend yarn. Two factors: the yarn composition and the cam setting of the knitting machine were considered. Two-ply of glass yarn was fed to the each face of the reference glass fabric, and a single-ply of wool/acrylic yarn was fed to the each face of the reference wool/acrylic fabric. On the other hand, while the hybrid plated fabric's back face accommodated two-ply of glass yarn, its front face involved a single-ply of wool/acrylic yarn. Two different cam settings, loose and tight, were selected. The physical and the structural properties of the fabrics were measured. Then, air permeability, bursting strength, and the protection against flame tests were performed. Test results were subjected to detailed statistical data analysis and how they were affected by the yarn composition and the cam setting was presented with visual and self-explanatory graphs.

Key words:

Glass yarn, weft knit fabric, plated fabric, protective fabric, air permeability

1. Introduction

While textile fabrics only provided covering when they first appeared, now this expectation evolved into functionality. By functionality, it is understood that the fabric not only covers and comforts the individual, plus protects him against dangers from the outside. This expectation has increased the need for the hybrid fabrics where the natural yarns that provide comfort and the synthetic yarns that offer protection are used together. The wool fiber stands out with its comfort and insulation feature. On the other hand – as a result of its affordable price, moderate mechanical properties, high protection against flame and chemicals – glass fiber is widely used in technical textile applications. However, due to its hard and brittle structure, the glass fiber experiences high level of breakage in the fabric formation processes [4, 7, 8, 11]. The contact of broken fiber ends with the skin causes itching and discomfort. In addition, the moisture absorption performance of glass fiber is very low, which significantly lowers its comfort feeling. On the other hand, its compatibility with human skin, moisture absorption capacity, and thermal insulation capability renders the wool fiber very valuable in comfortable clothing.

Woven fabrics require laborious weaving preparation processes such as weft yarn preparation, warping, sizing, tying and drawing-in. However, these pre-processes are not required for weft knitted fabrics. Therefore, the production cost of weft knitted fabric is considerably lower than that of woven fabric. Woven and weft knitted fabrics are also quite different from each other in terms of fabric

structure and performance. The weft knitted fabric, which consists of meshed loops, easily stretches when exposed to any in-plane or out-of-plane load and easily takes the desired three-dimensional shape. This makes it possible to produce comfortable clothing from weft knitted fabric that drapes the body without any folding, and wrinkling [3, 6, 12-15].

The fabric pattern is one of the critical features that determine the performance of the fabric. The pattern of the weft-knit fabric is determined by the number and the position of different types of stitches inside the knit repeat, and the cam setting. Besides, the cam setting controls the fabric tightness through determining the size of the loops. Therefore, it is possible to produce weft knitted fabrics in numerous architectures by playing with the fabric pattern and the cam settings [1-2, 5, 9-10].

In this study, it was planned to produce protective and comfortable weft knitted fabric with different tightness using glass and wool/acrylic yarns. Due to the disturbing effect of the glass fiber in contact with the skin, the plated weft-knit fabric structure was selected. In the plated fabric structure, the wool/acrylic yarn was used on the surface of the fabric in contact with the body, while glass yarn was used on the other side (outer) of the fabric. It was anticipated that glass yarn provides protection against dangers from outside, while wool/acrylic yarn in contact with the skin is thought to provide comfort by establishing the desired micro-climate between the body and the fabric.

2. Experimental

2.1. Materials

In this study, E-glass multifilament yarn with a single-ply yarn count of 136 tex, and individual fiber diameter of 9 microns was used. Nm 7 count, high bulk, 50/50% wool/acrylic blend yarn was used as the yarn that would provide wearability and comfort to the fabric. Plated weft-knit fabrics were produced by Brother KH-864, hand-operated, 5E gauge knitting machine. The plating yarn feeder used in the production of all fabrics and the different yarn compositions fed to the feeder are given in Figure 1.

Figure 1. The plating yarn feeder and different yarn compositions fed to the feeder

We focused on two factors. The first one is the yarn composition, and the other is the cam setting of the knitting machine. While the yarn composition had three sublevels (completely glass yarn, completely wool/acrylic blend yarn, and the combination of glass and wool/acrylic blend yarn), the cam setting had only two sublevels (loose and tight cam settings). In the production of completely glass yarn fabric, 2-ply of glass yarn was fed into both the front and rear eyes of the plating yarn feeder (Figure 1). In glass plus wool/acrylic yarn (hybrid) fabric; while a single-ply of wool/acrylic yarn was fed to the rear eye of the feeder, 2-ply of glass yarn was fed to the front eye. Finally, in the fabric consisting completely of wool/acrylic yarn, a single-ply of wool/acrylic yarn was fed to both the front and rear eyes of the feeder. The yarn composition was coded as given below:

WA: single-ply wool/acrylic yarn, G: single-ply glass yarn;

GG/GG: 4-ply of glass yarn fabric (2-ply of glass yarn on both the front and back faces of the fabric).

WA/GG: The front face is a single-ply of wool/acrylic yarn, while the back face is 2-ply of glass yarn fabric.

WA/WA: 2-ply of wool/acrylic yarn fabric (a single-ply of wool/acrylic yarn on both the front and back faces of the fabric).

Two fabric tightness levels, 4 (tight fabric) and 8 (loose fabric) were selected as the cam setting. Thus, a total of 6 (3x2) different weft-knit plated fabrics were produced. The images of the fabrics are given in Figure 2.

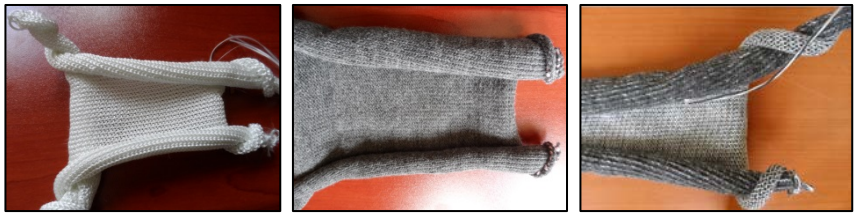

a b c

Figure 2. The completely glass yarn GG/GG fabric (a), the completely wool/acrylic yarn WA/WA (b), the hybrid WA/GG fabric (c)

2.2. Methods

A digital thickness gauge device with a presser foot diameter of 21.15 mm and a compression pressure of 2 kPa was used to measure the fabric thickness. BS 5441 standard was followed for length measurement. ASTM D737 was followed and the SDL ATLAS M021A test device was used in the air permeability tests. The circular fabric test area was taken as 20 cm^2 and the pressure drop was chosen as 200 Pa. Bursting strength test was performed on the knitted fabrics according to BS EN ISO 13938-1. A dome with an internal diameter of 30.5 mm and a corresponding internal area of 7.3 cm^2 was selected. The "Surface Ignition" test procedure was performed on the knitted fabrics via following the BS EN ISO 15025 standard. A specified flame with an application time of 10-second was performed on the back (purl loop) face of the all fabrics, thus the glass yarn surface of the wool/acrylic plus glass yarn (hybrid WA/GG) fabric sample was exposed to the flame.

3. Results and discussion

Yarn composition changed the fabric thickness at a statistically significant level (Figure 3 and Table 1). While the bulky structure of the wool/acrylic yarn increased the fabric thickness, the thin and regular structure of the glass yarn decreased the fabric thickness. The addition of wool/acrylic yarn to the fabric structure also increased the fabric thickness variation (standard deviation).

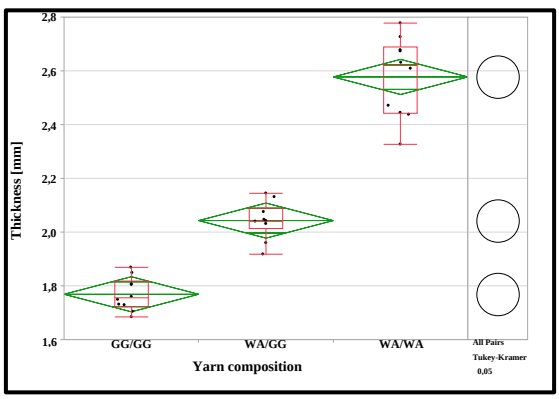

Figure 3. The effect of yarn composition on thickness

Note: The horizontal green line dividing the green diamond corresponds to the mean, while the distance between the lower and upper corners of the green diamond shows the confidence interval based on the 95% confidence level. One comparison circle for the mean calculated at each sublevel level is given in the right-hand column. The circles representing means that differ significantly from each other (α = 0.05) either do not intersect or intersect slightly.

Table 1. The effect of yarn composition on thickness

Property	Yarn composition				n	mean	sd	LL	UL	p-value
Thickness [mm]	WA/WA	A			10	2.58	0.15	2.51	2.64	<0.0001
	WA/GG		B		10	2.04	0.07	1.98	2.11	
	GG/GG			C	10	1.77	0.06	1.70	1.83	

Note: Levels that are not combined with the same alphabetic capital letter differ significantly from each other (α = 0.05). **n**: number of measurements, **sd**: standard deviation, **LL**: lower limit, **UL**: upper limit. The limits were established according to the 95% confidence level. A p-value less than 0.05 is an indication that the difference between at least two levels is statistically significant and is colored red.

The addition of glass yarn to the weft knitted fabric decreased the loop length (Figure 4 and Table 2). This is attributed to the thin and low-volume nature of the glass yarn. In other words; the addition of wool/acrylic blend yarn, which has a voluminous structure, to the fabric increased the loop length.

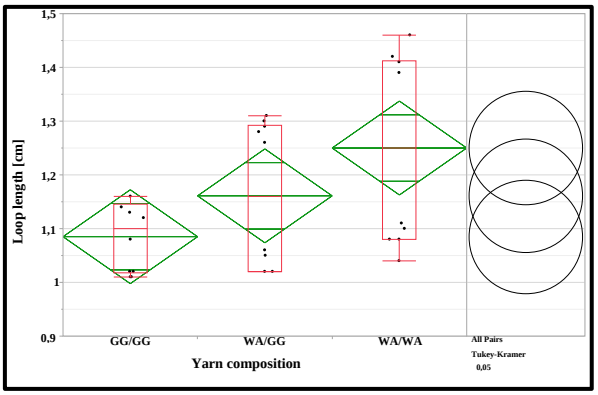

Figure 4. The effect of yarn composition on loop length

Table 2. The effect of yarn composition on loop length

Property	Yarn composition			n	mean	sd	LL	UL	p-value
Loop length [mm]	WA/WA	A		10	1.25	0.18	1.16	1.34	0.0362
	WA/GG	A	B	10	1.16	0.14	1.07	1.25	
	GG/GG		B	10	1.08	0.06	1.00	1.17	

The addition of wool/acrylic yarn, which is more voluminous and thicker than glass yarn, to the fabric structure closed the pores of the fabric and reduced air permeability (Figure 5 and Table 3). However, no statistically significant difference was observed between the air permeability of the purely wool/acrylic yarn (YA/YA) fabric and the wool/acrylic yarn plus glass yarn (YA/CC) fabric. Moreover, the addition of glass yarn to the fabric structure increased the air permeability variation of the fabric.

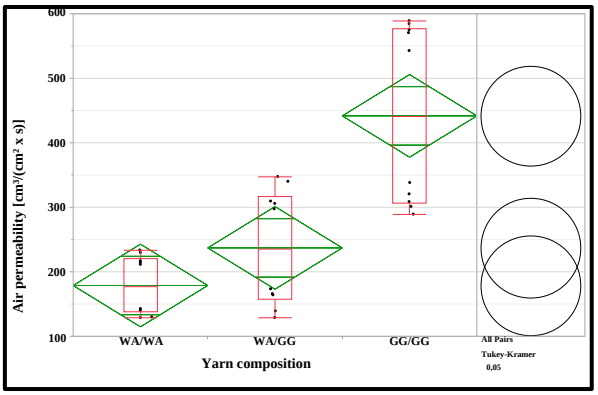

Figure 5. The effect of yarn composition on air permeability

Table 3. The effect of yarn composition on air permeability

Property	Yarn composition			n	mean	sd	LL	UL	p-value
Air permeability [$cm^3/(cm^2xs)$]	GG/GG	A		10	441,70	138,64	377,61	505,79	<0,0001
	WA/GG		B	10	237,00	89,44	172,91	301,09	
	WA/WA		B	10	178,70	45,28	114,61	242,79	

Figure 6 and Table 4 show the effect of yarn composition on fabric bursting strength (pressure). Hybrid plated (WA/GG) fabric with 2-ply of glass yarn on the back face and a single-ply of wool/acrylic yarn on the front face showed the highest bursting pressure. The hybrid plated fabric also exhibited the lowest bursting pressure variation, demonstrating a stable bursting performance. On the other hand, completely glass yarn (GG/GG) fabric and completely wool/acrylic yarn (WA/WA) fabric exhibited the lowest bursting pressure. The interaction of the glass yarn with the knitting elements while the yarn was being forced to take the loop form had resulted in fiber breakage, which showed itself as a decrease in bursting strength of the fabric. It is promising that the hybrid plated (WA/GG) fabric, consisting of a single-ply of wool/acrylic plus two-ply of glass yarn, exhibited the highest (statistically significant level higher than the other fabrics) and the most stable (lowest variation) bursting pressure.

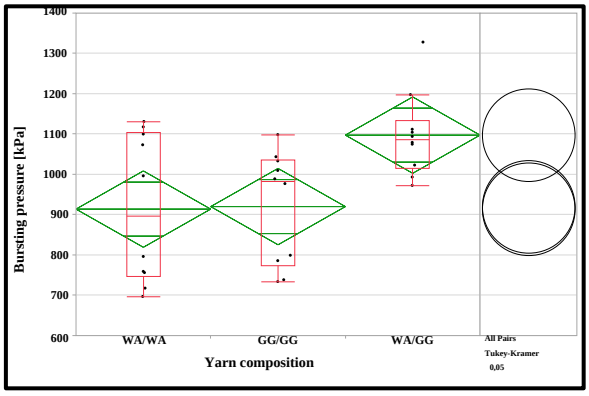

Figure 6. The effect of yarn composition on the bursting pressure

Table 4. The effect of yarn composition on bursting pressure

Property	Yarn composition			n	mean	sd	LL	UL	p-value
Bursting pressure [kPa]	WA/GG	A		10	1097.28	103.40	1002.50	1192.00	0.0133
	GG/GG		B	10	919.97	139.85	825.20	1014.70	
	WA/WA		B	10	913.74	183.58	819.00	1008.50	

The yarn composition affected the afterflame time at a statistically significant level (Figure 7 and Table 5). Completely wool/acrylic yarn (WA/WA) fabrics exhibited an average afterflame time of 123 seconds, while completely glass yarn (GG/GG) fabrics exhibited an average of zero afterflame time, that is, GG/GG fabrics did not ignite. While WA/WA fabrics burned completely, GG/GG fabrics preserved their integrity. The promising result here is that the hybrid (WA/GG) fabric and the completely glass yarn (GG/GG) fabric exhibited statistically the same average afterflame time. This is because that tightly knitted hybrid (WA/GG) fabric at the 4 cam setting did exhibit lack of flaming after the flame removal (i.e. afterflame time of zero second). Therefore, the tightly knitted (at 4 cam setting level) hybrid plated (WA/GG) fabric behaved similar with the completely glass yarn (GG/GG) fabric and did not exhibit flaming (i.e. not ignited) after the flame was removed at the end of 10 seconds.

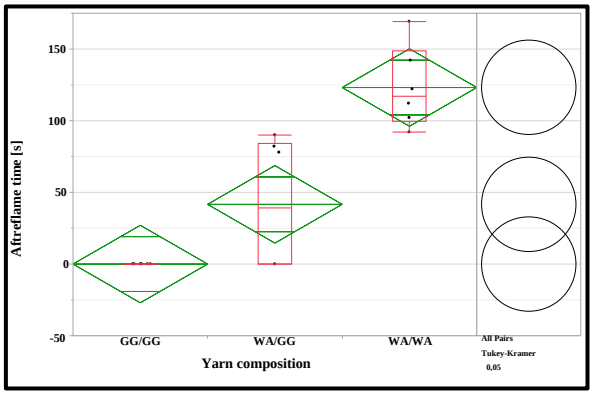

Figure 7. The effect of yarn composition on afterflame time

Table 5. The effect of yarn composition on afterflame time

Property	Yarn composition			n	mean	sd	LL	UL	p-value
Afterflame time [s]	WA/WA	A		10	123.17	28.29	96.12	150.21	<0.0001
	WA/GG		B	10	41.67	45.81	14.62	68.71	
	GG/GG		B	10	0.00	0.00	-27.05	27.05	

Figure 8 shows the burned images of completely glass yarn GG/GG fabrics knitted at 4 cam settings. Glass fibers that turned into black at the flame application point but kept their integrity exhibited a decreasing yellowing with distance from the flame point.

Figure 8. Pictures taken after the burning test of completely glass yarn GG/GG fabric knitted at 4 cam settings

Figure 9 shows the photos of the burned WA/GG fabric knitted at 4 cam setting. Flame propagation in WA/GG hybrid fabric remained within a limited area. The tight fabric structure and the presence of 2-ply of glass yarn on the surface where the flame is applied stopped the flame propagation. While the wool/acrylic yarn became charred at the flame application point, this charring decreased as moved away from the application point.

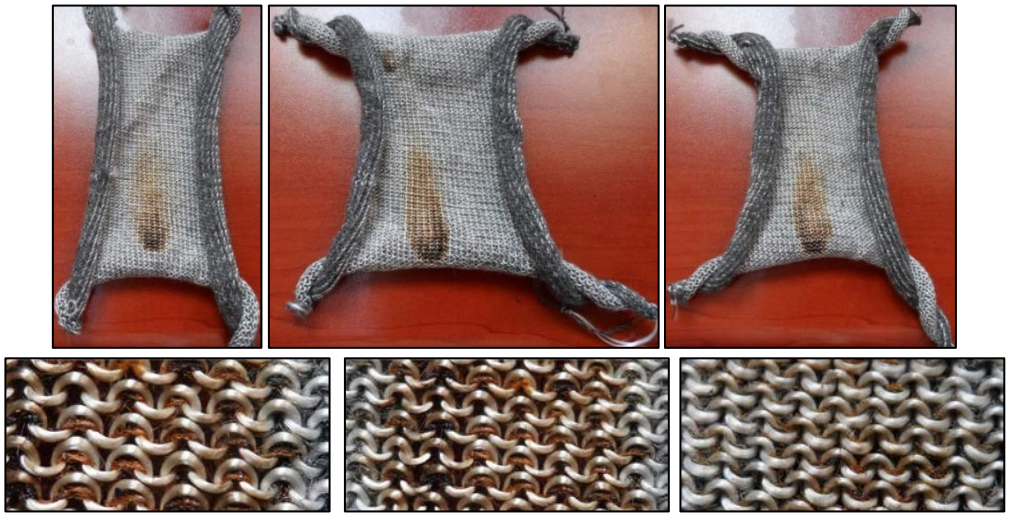

Figure 9. The photos of the burned WA/GG hybrid fabric knitted at 4 cam setting

4. CONCLUSIONS

In this study, weft-knit plated hybrid fabrics with different tightness were produced from glass and wool/acrylic yarns. In the hybrid plated fabric, while front face of the fabric formed from single-ply of wool/acrylic yarn, the back face formed from 2-ply of glass yarn. The physical, structural, air permeability, bursting strength, and protection against flame properties of the hybrid fabric were compared with the reference fabrics those consisted of only 4-ply of glass or only 2-ply of wool/acrylic yarn. The hybrid fabric exhibited comparable air permeability performance with the fabric from completely wool/acrylic yarn, while it demonstrated statistically significantly better bursting pressure than the reference fabrics from completely glass or wool/acrylic yarns. The hybrid fabric with tight cam setting also showed the similar flame resistance with the fabric from completely glass yarns.

ACKNOWLEDGEMENTS

We would like to thank Scientific Research Projects Management Unit (BAPYB) of Gaziantep University for their financial support to this study under the project number of MF.ÖKAP.21.11. This study was supported in the category of research project with undergraduate student participation. The second and third authors are the current undergraduate students of Textile Engineering Department of Gaziantep University.

References

1. *Abounaim, Md., Hoffmann, G., Diestel, O., Cherif, C. (2010), Thermoplastic composite from innovative flat knitted 3D multi-layer spacer fabric using hybrid yarn and the study of 2D mechanical properties. Composites Science and Technology, 70(2), 363-370.*
2. *Alpyildiz, T., İçten, B. M., Karakuzu, R., Kurbak, A. (2009). The effect of tuck stitches on the mechanical performance of knitted fabric reinforced composites. Composite Structure, 89(3), 391-398.*
3. *Ciobanu, L. (2011). Development of 3D Knitted Fabrics for Advanced Composite Materials. In Advances in Composite Materials – Ecodesign and Analysis. Brahim Attaf (Editor), InTech. 161-192.*
4. *Hu, H., Zhu, M. (2005). A study of the degree of breakage of glass filament yarns during the weft knitting process. AUTEX Research Journal, 5(3), 141-148.*
5. *Kane, C. D., Patil, U. J., Sudhakar, P. (2007). Studies on the influence of knit structure and stitch length on ring and compact yarn single jersey fabric properties. Textile Research Journal, 77(8), 572-582.*
6. *Ko, F. K. (2000). 3-D textile reinforcements in composite materials. In 3-D textile reinforcements in composite materials. Antonio Miravete (Editor), Boca Raton: CRC Press, 9-42.*
7. *Lau, K. W., Dias, T. (1994). Knittability of high-modulus yarns. The Journal of the Textile Institute, 85(2), 173-190.*
8. *Liu, X-M., Chen, N-L., Feng, X-W. (2009). Investigation on the knittability of glass yarn. The Journal of The Textile Institute, 100(5), 440-550.*
9. *Marmaralı, A. B. (2004). Atkı Örmeciliğine Giriş. E.Ü. Tekstil ve Konfeksiyon Araştırma – Uygulama Merkezi (İzmir).*
10. *Marmaralı, A., Kretzschmar, S. D. (2004). Örme Terimleri ve Tanımlamaları. E.Ü. Tekstil ve Konfeksiyon Araştırma – Uygulama Merkezi (İzmir).*
11. *Savci, S., Curiskis, J. I., Pailthorpe, M. T. (2001). Knittability of glass fiber weft-knitted preforms for composites. Textile Research Journal, 71(1), 15-21.*
12. *Savci, S., Curiskis, J. I., Pailthorpe, M. T. (2000). A study of the deformation of weft-knit preforms for advanced composite structures Part 1: Dry preforms properties. Composites Science and Technology, 60(10), 1931-1942.*
13. *Savci, S., Curiskis, J. I., Pailthorpe, M. T. (2000). A study of the deformation of weft-knit preforms for advanced composite structures Part 2: The resultant composite. Composites Science and Technology, 60(10), 1943-1951.*
14. *Savci, S., Curiskis, J. I., Pailthorpe, M. T. (1999). Formability of weft knitted preforms. International Committee on Composite Material (ICCM) 12 Conference, paper 841.*
15. *Zhong, T., Hu, Hong. (2007). Formability of weft-knitted fabrics on hemisphere. AUTEX Research Journal, 8(4). 245-251.*

PATTERN RELATED ISSUES IN THE MODELLING OF DEFORMED OVER SURFACE WARP KNITTED STRUCTURES WITH LONGER UNDERLAPS

Haisang Liu[1,2], Yordan Kyosev[2], Gaoming Jiang[1]

1. Jiangnan University, College of Textile Science and Engineering, Wuxi, Jiangsu, Lihu Ave. 1800, Binhu, 214122 China

2. TU Dresden, Institute of Textile Machinery and High Performance Material Technology, Chair of Development and Assembly of Textile Products, Dresden, Sachsen, Hohe Str. 6, 01069, Germany

sophie@stu.jiangnan.edu.cn

Abstract:

The yarn level modelling of warp knitted structures is a complex process. For structures placed on the plane, it is well investigated and there are a few software solutions and papers reported. This paper considers the simulation of warp knitted structure, deformed in the 3D space. Especially the modelling of the areas of high curvature are detailed observed. Underlaps with longer lengths makes an unreal visualization for simulation results. Different pattern with different length of the underlaps are modelled with original algorithm developed by the authors. Modelling and visualization problems in the areas with long underlaps are discussed and possible solutions are proposed.

Key words:

3D simulation, modelling, curved surface, high curvature, visualization, fabric structure

1. Introduction

In the era of continuous development of digital textiles, more and more scholars have focused on the simulation of fabrics. In the course of fabric simulation, 3-dimensional(3D) simulation has made a great progress in the recent years, which has become increasingly important in numerous application areas in production. 3D simulation is commonly used in fabric design, apparel design, etc., which is convenient for designers and consumers to obtain visualization results, helping us better understand the shape and structure of fabrics.

There are many softwares on the market for clothing design with fabric display, such as *Clo3D*, *Marvelous Designer*, *Revobit*, etc. All of them use texture mapping methods to add textures to clothing. Similarly, many scholars used texture mapping, transferring the flat patterns to complex models[1-3]. But the detailed textile structure was not well represented.

Yarn-level 3D simulation solved this problem well. Researchers conducted studies on flat fabrics. Peng et al.[4] simulated the weft knitted pattern and proposed the loop deformation. The structures of various types of flat warp-knitted fabrics were well demonstrated by 3D simulation[5]. Based on this, Liu et al.[6] added the jacquard parameters to simulate more complex warp knitting patterns. The above simulation research on flat fabrics had laid a good foundation for warp knitting simulation.

For knitted products with complex shapes, Yuksel et al.[7] meshed the existing models. Different shapes of meshes corresponded to different knitting structures. Wu et al.[8] labeled those meshes with knitting direction, filling the meshes with similar matching loops. Also loop force deformation were well analyzed to reach a more detailed result [9,10]. These 3D simulation above focused on weft knitted fabrics, which was a good reference for our research of warp knitted fabric simulation.

The authors also paid attention to the warp knitted fabric simulation. Renkens et al.[11] modelled the double needle-bed warp knitted fabrics using a mathematical method. Liu et al.[12] spread out a double-layer fabric and then rolled it into a tube with geometry calculation. They mainly discussed the fabric tube shape rather than the stitch details. Many flat models with stitch shape details were mentioned in the Kyosev's book[5,14]. Also, warp knitting stitch size was measured and the stitch model was established[14]. But only stitch main body was sized and underlaps were out of consideration.

During the simulation development and the practical experience with model simulation by ourselves, we find that some pattern related issues need to be improved when we establish the fabric models according to different knitting parameters for patterns.

2. Experimental

2.1. Modelling basis

In this paper, we develop our research based on our previous works[12,15]. The tubular fabric was spread out into a plane. And a spatial relationship of the stitch grids between the tube mesh and the plane mesh was derived to mapping the stitch coordinate on the tube. Then geometry tubes in Three.js, a lightweight cross-browser JavaScript library, were used to realize the fabric simulation.

2.2. Pattern related issues

Although the simulation results are good, we find some patterns related issues need to be improved. Figure 1 shows an example from our previous work[15], As we all know, the stitches in the warp knitted fabrics are connected with underlaps. But different patterns are made of different chain notation. Some underlaps is short, like the structure 1-0/1-2//. Some underlaps are longer like 1-0/2-3// and 1-0/4-5//, whose underlaps span several wales. There are high curvature areas at when fabrics are rolled into a tube in Figure 1.a. Stitches are simulated well with the 8-points model. But the underlap is lying in an unusual place, especially for longer underlaps.

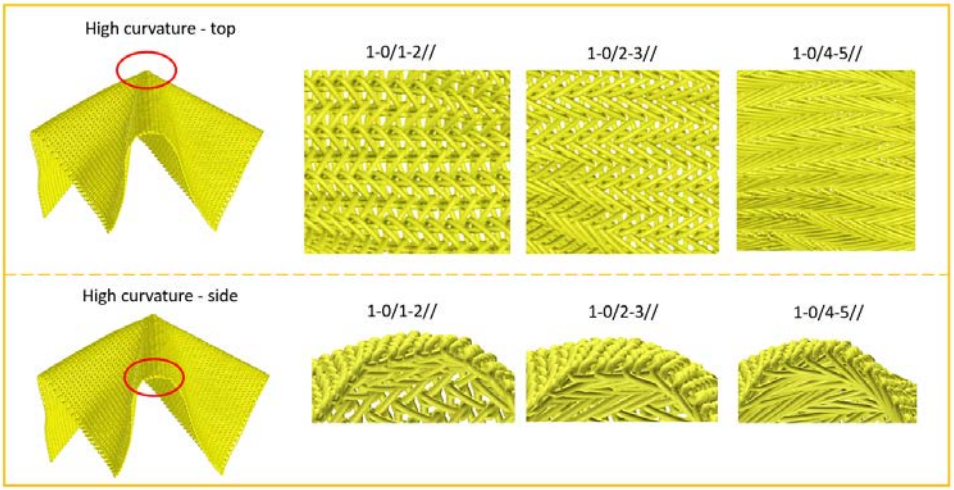

(a)

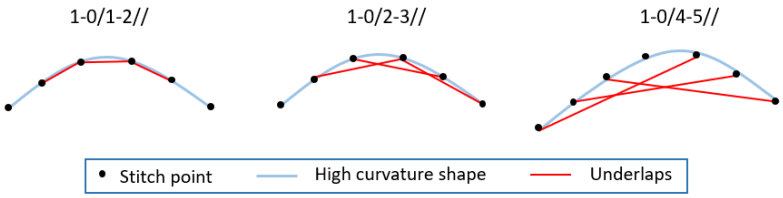

(b)

Figure 1. Pattern related issues with high curvature and long underlaps in 3D simulation.(a)simulation results with different underlap length[15];(b) Statement of underlaps with different lengths on the high curvature shape.

For a better visualization, we extract the underlap paths from a side view in Figure 1.b. In the structure 1-0/1-2//, the underlap is short so that they fit tightly to the deformed surface. But as the underlaps get longer in 1-0/2-3// and 1-0/4-5//, whose underlaps cross over several wales, the space become larger between underlaps and deformed surface. It is because the connecting yarns between two stitches are simulated by a straight line with two points. Actually, stitches on a real-world fabric fit well to the surface within the common underlap lengths. For a more realistic simulation results, some improvements need to be made.

2.3. Methods

The stitch grids not always in the same plane as mentioned in section 2.2. The long underlaps are overhang from the deformed surface. But the number of points on the underlap is changed to avoid unnecessary calculations.

Figure 2 is a schematic from the top view, where the fabric is bent into a curved surface. Figure 2(a) shows two stitches on a plane fabric, the straight underlap is exactly on the fabric surface. Figure 2(b) shows stitches on the same curvature surface. The vertical vectors of stitch grid that toward the outside of the model surface is represented as green lines. When the vector angle of two connected stitches is larger, the underlap is father away from the fabric surface. In Figure 2(c), the deformed surfaces have different curvature with two stitch vertical vector remains the same. The higher the curvature is, the more inaccurate the simulated underlap is.

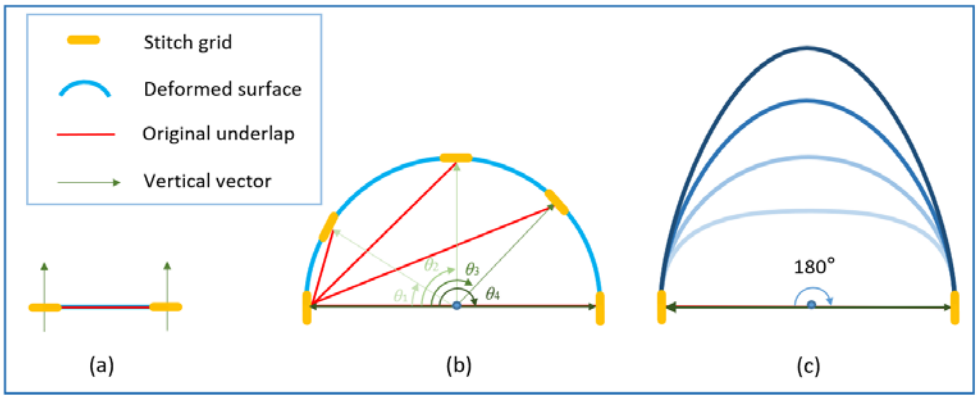

Figure 2. Stitch statement and the underlap positions. (a)Plane fabric; (b)Stitches on the same curvature surface; (c)The same stitches with different curvature surfaces.

In order to solve this problem, some control points are added to the underlap model, modifying the stitch model as shown in Figure 3. The points connecting the underlaps is very near to the stitch bottom center that can almost be ignored, so the underlap is regarded as an edge of the underlap triangle when calculating the added points. The underlap is divided into several segments. Because the triangles including the underlap segments are similar triangles, added points can be calculated by Eq.1 according to the wale distance ratio. Thus, the underlap can be pulled from the original shape, fitting the deformed surface well. In this example, the distance ratio $e = \frac{w}{4w} = 0.25$.

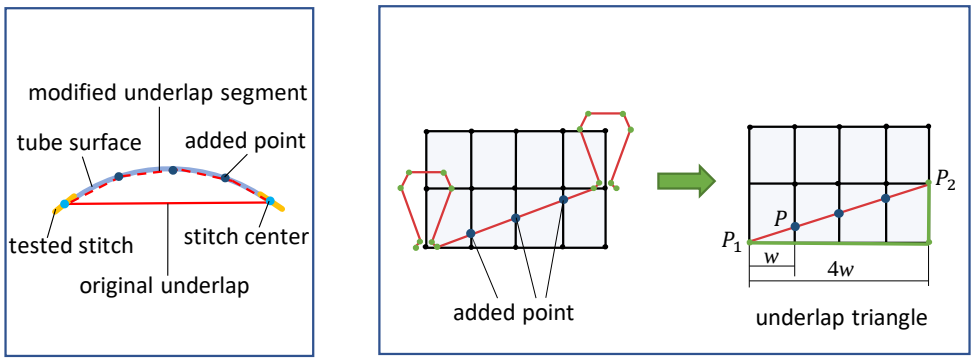

Figure 3. The modified stitch models with added control points on the underlap.

$$\begin{cases} P = e \times (P_2 - P_1) + P_1 \\ e = (P - P_1)/(P_2 - P_1) \end{cases} \quad (1)$$

Where, P is the added point, P_1 and P_2 are stitch points connecting underlap, e is the distance ratio.

In the other case, the stitches are on the bent fabric, not on the regular tube. There is an example for fabrics knitted by 1-0/4-5// in Figure 4. Different from the round fabric, the added points depend on the normal vectors of stitches. All the normal vectors are towards the same side of the fabric.

Seeing the Figure 4- Vector relationship, bent I is the occasion where the normal vector angle α is less than 180° . $\boldsymbol{V}_1$, $\boldsymbol{V}_2$ and $\boldsymbol{V}_3$ are the normal vectors of stitches. When the vector angle α_1 is larger than the value β, added points are put on the underlap lapping pass these two stitches. β is a specified angle value. The details of a tested yarn are shown in underlap triangle. And $\boldsymbol{V}_2$ becomes the first vector to compose the vector angle with the normal vector of the next stitch. For $\boldsymbol{V}_2$ and $\boldsymbol{V}_3$, the angle α_2 is less than the value β, so there is no added point at this position. Then it continues combining with the next stitch vector. When calculating the added points on the plane fabric, the underlap is also regarded as an edge of a triangle according to Eq.1. In bent II, when the angle α_2 of two normal vectors $\boldsymbol{V}_4$ and $\boldsymbol{V}_5$ is larger than 180° , the underlap is at the other side of the fabric. The added points are directly added on the underlap. Then $\boldsymbol{V}_5$ Then it continues combining with the next stitch vector.

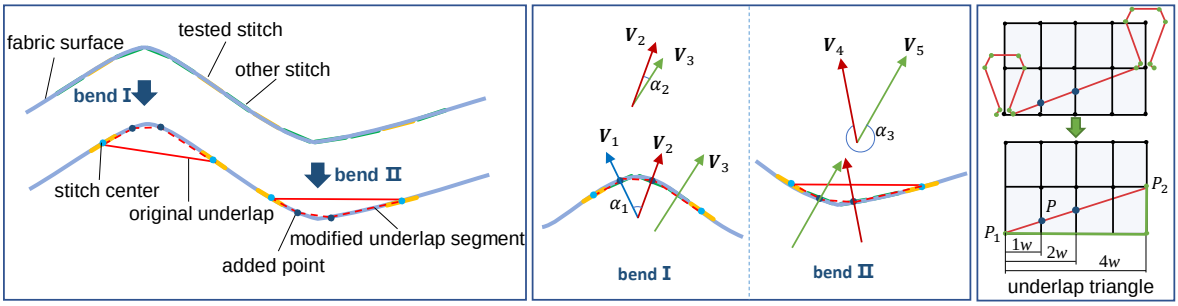

Figure 4. The modified stitch models on the bent fabric.

3. Results and discussion

3.1. Tubes

Figure 5 shows some simulation results for different underlaps on the same curvature of the regular tubes. The structure 1-0/1-2// is special because there is no added point on the underlap. The green triangles mark the red stitch position in the tested yarns. The maximum vertical distances from underlaps

to stitches are listed in Table 1. This measurement size for the modified group is the average of each underlap segments. The modified models seem thinner than the original ones, which means underlaps are closer to the surface. Each structure saves 48~79% distance. The longer the underlap, the more efficient improvement the modified model shows. For a fabric in the size of 15 wales × 10 courses (150 stitches), the time efficiency is recorded in Table 1. Although underlaps with added points takes longer calculation time, the differences are within an acceptable range of 10%. From the side view of these tubes in Figure 5, they look similar for one single yarn. But yarns in the modified simulation result are more neatly arranged.

Table 1. Size and time efficiency comparison for the tube models

	Thickness			Calculation time/15 wales ×10 courses		
Structure	**Original/*px***	**Modified/*px***	**Differences/%**	**Original/ms**	**Modified/ms**	**Differences/%**
1-0/2-3//	0.257	0.132	48.64	12.867	13.559	5.39
1-0/3-4//	0.366	0.134	63.39	13.856	14.709	6.15
1-0/4-5//	0.413	0.140	66.10	15.560	16.468	5.83
1-0/5-6//	0.525	0.144	72.57	14.636	15.660	7.00
1-0/6-7//	0.703	0.147	79.09	15.474	16.993	9.82

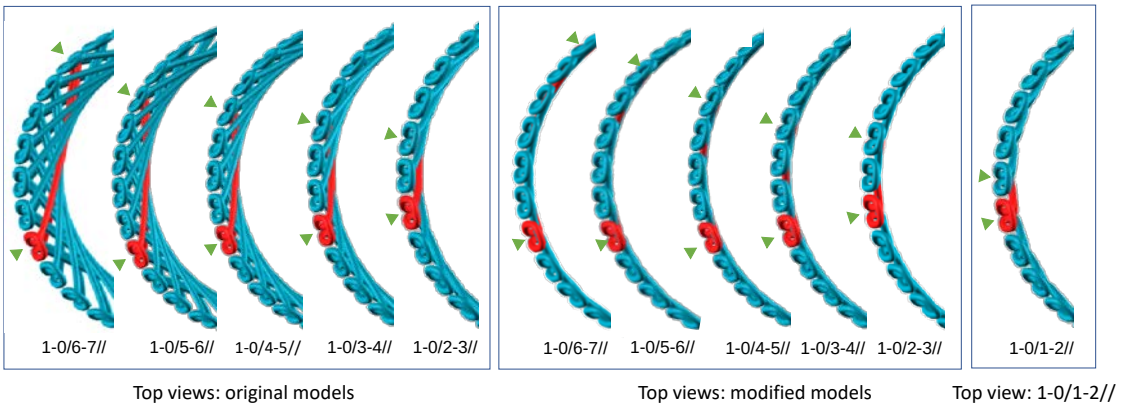

Figure 5. Simulation results of the original model and the modified model for regular tubes. (a) from top views; (b) from side views.

3.2. Bent fabric

In order to get the specified angle value β, fabrics are bent at certain angles. Figure 6 shows a group of fabrics with the bent angle of 60° before modified. The fabrics are bent at between the 7th and the 8th wales. The fabrics becomes thicker as the underlaps become longer. Both top views and side views of a structure 1-0/4-5// are also shown in Figure 6 as a visual example.

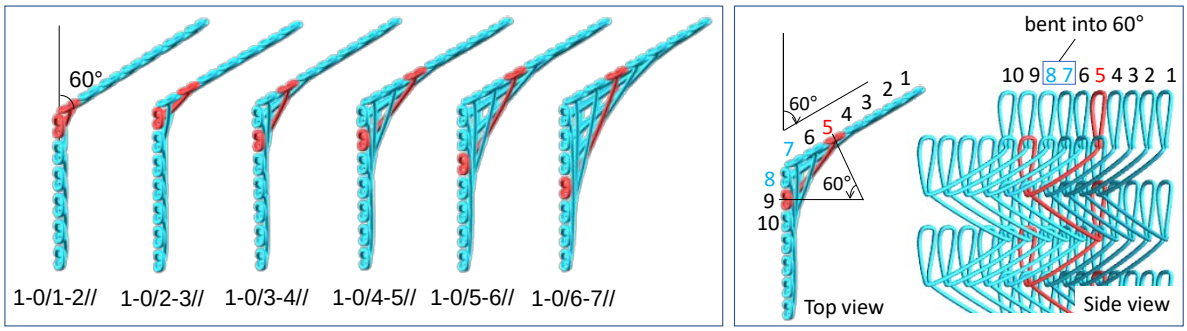

Figure 6. Bent fabrics at 60° before modified

Figure 7(a) is the vertical length (the maximum thickness of the fabric) from the underlaps to the fabric faces at several angles from 0° to 165° with the tested angle step 15°. For the short underlap structures 1-0/1-2// and 1-0/2-3//, the underlap become away from the fabric before the angle 75°. And then the underlap becomes closer to the fabric surface. This decrease is more obvious in the longer underlap structures. But for these structures, the turning angle is 90°. Take the structure 1-0/6-7// for example in Figure 7(b), when the bend angle becomes larger, the underlap triangle becomes smaller, resulting in a shorter distance trend to the fabric. It is because when the bend angle is larger, two fabric pieces get closer to each other. That is why the turning angle exists at 75° and 90°.
The added points can be omitted when the distance short enough. The differences are listed in Table 2 comparing with the flat fabric (0°). Structures are named from 0 to 5, which is relating to the stitch interval number the underlap passes. The differences under 10% are regarded as an acceptable range for the underlap simulation. The underlaps at the angle differences lager than 10% need added points to pull them back. Thus, the specified angle value β is obtained in Table 3.

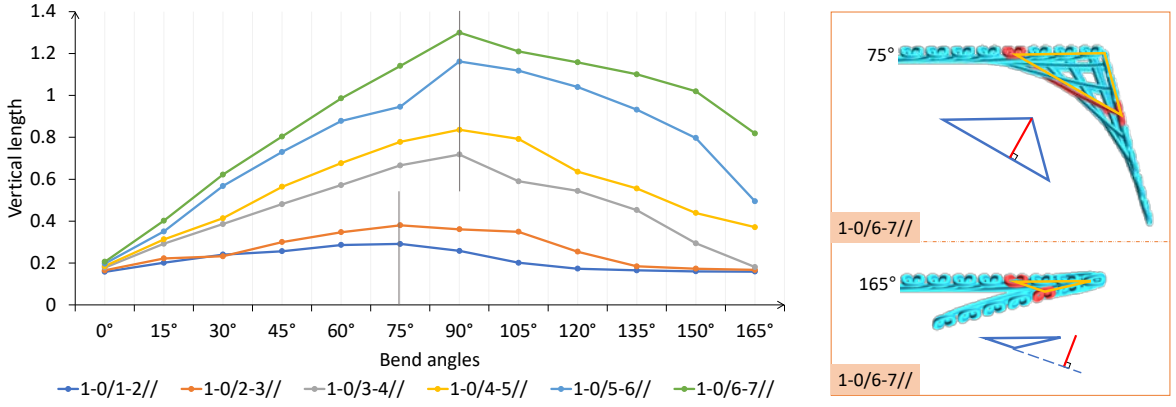

(a) (b)

Figure 7. Vertical length measurement results. Vertical length of bent fabrics at different angles

Table 2. Vertical distance differences comparing with the flat fabric

Stitch interval number	15°	30°	45°	60°	75°	90°	105°	120°	135°	150°	165°
0	27.22	51.90	62.03	81.01	84.18	63.29	27.22	9.49	4.43	1.27	0.63
1	34.55	40.61	81.82	110.30	130.30	118.79	111.52	53.94	11.52	4.85	1.21
2	64.04	116.85	170.22	221.35	274.16	303.37	231.46	205.62	154.49	65.17	1.69
3	69.19	123.78	204.86	265.95	320.54	351.89	328.11	243.78	200.54	137.30	100.54
4	78.17	188.32	270.56	345.69	380.20	489.85	467.51	427.92	373.10	304.57	151.27
5	95.15	201.94	290.29	378.64	453.88	531.07	487.38	462.14	434.47	395.15	297.57

Table 3. β ranges

Stitch interval number	β
0	$\begin{cases}\beta = 0° \text{ or } \beta > 120°, \text{no added pointss} \\ \text{else, added points}\end{cases}$
1	$\begin{cases}\beta = 0° \text{ or } \beta > 150°, \text{no added pointss} \\ \text{else, added points}\end{cases}$
2	$\begin{cases}\beta = 0° \text{ or } \beta > 165°, \text{no added pointss} \\ \text{else, added points}\end{cases}$
3	$\begin{cases}\beta = 0°, \text{no added pointss} \\ \text{else, added points}\end{cases}$
4	
5	

Figure 8 shows another example of the bent fabric at the bend angle of 45°. The added points are calculated according to the above regulars. All underlaps are pulled closer to the fabrics after modifying the models, which proves the method proposed in this paper is effective for a better visualization.

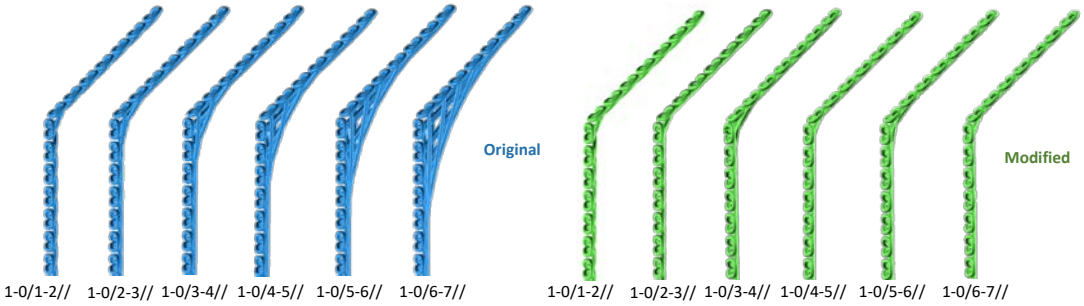

Figure 8. Comparison between original models and modified models at the bend angle of 45°

4. CONCLUSIONS

During our 3D simulation for warp knitted fabrics, a pattern related issues with underlaps on deformed surface is discussed. The longer the underlap will get an inaccurate simulation result. Thus, the vertical vectors of stitch grids on the deformed surface are analyzed. And the original stitch model is modified with additional control points on the underlaps. For the tube fabric, points are added at each wale that the underlaps pass. For the bent fabric, the points are added according to the vertical normal vector angles of stitches. Fabrics with several angles of normal vectors are analyzed. Relationships between points and stitch interval number are established and demarcation angles β are obtained. The size comparison results declare that underlaps are pulled back to the fabric well. The results show this method has a positive effectiveness in visualization.

ACKNOWLEDGEMENTS

The authors thank TU Dresden and Jiangnan University for supporting this work for their laboratories and advanced apparatus. This work was supported by National Science Foundation of China (61902150), Taishan Industry Leading Talents (tscy20180224) and China Scholarship Council (No.202106790059).

References

1. *Yuksel, C., Lefebvre, S., & Tarini, M. (2019). Rethinking texture mapping. Computer Graphics Forum, 38(2), 535-551.*
2. *Xu, Y., Yang, S., Sun, W., Tan, L., Li, K., et al. (2019). 3d virtual garment modeling from rgb images. In 2019 IEEE International Symposium on Mixed and Augmented Reality (ISMAR),37-45.*
3. *Mir, A., Alldieck, T., & Pons-Moll, G. (2020). Learning to transfer texture from clothing images to 3D humans. 2020 IEEE/CVF Conference on Computer Vision and Pattern Recognition (CVPR), 7021-7032.*
4. *Peng, J., Jiang, G., Xia, F., Cong, H., & Dong, Z. (2020). Deformation and geometric modeling in three-dimensional simulation of fancy weft-knitted fabric. Textile Research Journal, 90(13-14), 1527-1536.*
5. *Kyosev, Y. (2019). Warp knitted fabrics construction. (1 ed.). CRC Press(Boca Raton).*
6. *Liu, H., Jiang, G., & Dong, Z. (2020). Lapping modeling of looped warp knitted jacquard fabrics based on web. Journal of Engineered Fibers and Fabrics, 15(43), 1-13.*
7. *Yuksel, C., Kaldor, J. M., James, D. L., & Marschner, S. (2012). Stitch meshes for modeling knitted clothing with yarn-level detail. ACM Transactions on Graphics (TOG), 31(4), 1-12.*
8. *Wu, K., Gao, X., Ferguson, Z., Panozzo, D., & Yuksel C. (2018). Stitch meshing. ACM Transactions on Graphics (TOG), 37(4): No. 130, 1-14.*
9. *Weeger, O., Sakhaei, A. H., Tan, Y. Y., Quek, Y. H., Lee, T. L., et al. (2018). Nonlinear multi-scale modelling, simulation and validation of 3D knitted textiles. Applied Composite Materials, 25(4), 797-810.*
10. *Ielina, T., Galavska, L., Ausheva, N., & Dzikovich, T. (2021). 3d modelling of untwisted multifilament threads, curved in a knitted loop. Deutsche Internationale Zeitschrift für zeitgenössische Wissenschaft, (22), 74-79.*
11. *Renkens, W., & Kyosev, Y. (2011). Geometry modelling of warp knitted fabrics with 3D form. Textile Research Journal, 81(4), 437-443.*
12. *Liu, H., Jiang, G., & Dong, Z. (2022). Mesh modeling and simulation for three-dimensional warp-knitted tubular fabrics. The Journal of The Textile Institute, 113(2), 303-313.*
13. *Kyosev, Y. (2019). Topology-based modeling of textile structures and their joint assemblies. (1 ed.). Springer International Publishing(Switzerland).*
14. *Liu, H., Jiang, G., & Dong, Z. (2021). A shortened development process method for warp-knitted yarn-dyed shirt fabric. Textile Research Journal, 91(3-4), 443-455.*
15. *Liu, H., Kyosev, Y., & Jiang, G. (2022). Yarn level simulation of warp-knitted clothing elements–first results and challenges. Communications in Development and Assembling of Textile Products, 3(2), 115-126.*

NEW SOLUTIONS IN THE PRODUCTION OF COMPOSITES - MECHANICAL PROPERTIES OF COMPOSITES REINFORCED WITH TECHNICAL EMBROIDERY AND WOVEN FABRIC MADE OF FLAX FIBERS

Agata Poniecka[a], Marcin Barburski[a], David Ranz[b], Jesús Cuartero[c], Ramon Miralbes[b]

[a] Lodz University of Technology, Faculty of Material Technologies and Textile Design, Institute of Architecture of Textiles, Zeromskiego 116, Post code: 90-924 Lodz, Poland

[b] University of Zaragoza, Department of Design and Manufacture Engineering, C/María de Luna, Post code: 50018 Zaragoza, Spain

[c] University of Zaragoza, Department of Mechanical Engineering, C/María de Luna, Post code: 50018 Zaragoza, Spain

* Corresponding author: marcin.barburski@.p.lodz.pl

Abstract:

The main purpose of the article is to present the new possibilities of producing natural fiber composite reinforcement. In this case, a computer embroidery machine by ZSK type JCZA 0109-550 was used. A technical embroidery with a stitch length of 2 mm was made on the machine. The embroidery was made of flax roving with a linear density of 400 tex. The woven fabric was made of the same flax roving as the embroidery, with a surface mass of 400 g/m^2. Composites were then produced from the technical embroidery and woven fabric using the infusion method with epoxy resin. The individual configurations differed from each other in the orientation of the roving in the embroidery samples. Samples for tensile strength and tensile elongation tests consisted of 4 layers, while samples for the DCB test consisted of 6 layers, with the addition of a separating foil between the 3rd and 4th layer. Composites were then subjected to strength tests - tensile strength, tensile elongation and DCB test (Double Cantilever Beam test), on the INSTRON machine. During the action of force along the direction of the fibers, composites containing technical embroidery as reinforcement were characterized by higher strength than composites containing woven fabric as reinforcement. Additionally, embroidery is a barrier to the formation of interlayer cracks. Technical embroidery is made on the basis of Tailored Fiber Placement (TFP) technology. This technology allows optimizing the mechanical values of the composite reinforcement.

Key words:

Technical embroidery, flax fibres, composites, mechanical properties, tailored fiber placement

1. Introduction

The composite production technology is faced with the challenge of minimizing the resulting production waste. This idea is reflected in the Tailored Fiber Placement (TFP) method, which includes technical embroidery. It consists in placing the medium on the surface of a flat textile product in any direction of the X and Y axes. The embroidery can also reach a certain dimension in the direction of the Z axis by overlapping embroidery layers. The height of the stacking sequence can be up to 8 mm. The amount of production waste in this kind of preforms is minimized thanks to the production of a precisely designed pattern, without the need to cut an element from a larger surface. The main waste generated during the production of technical embroidery is non-woven fabric or other types of backing on which the embroidery was made. The amount of this waste can be reduced by using an appropriate hoop size [1].

Electric wires, optics, glass or carbon fibers, electrically conductive yarns and others are used to perform technical embroidery increasing the performances of the final application [2].

Technical embroidery is now mainly used in textronics, to create heating mats (e.g., in car seats), connecting sensors, shielding, conductive interconnections and interfaces. Technical embroidery can be also used to create antennas or as an alternative to solid copper to make a coil for unilateral nuclear magnetic resonance systems. [3–7].

In the case of the following tests, linen roving was used to make the samples. The use of this material in the production of composites has increased significantly since 2012 [8]. Composites containing natural fibers exhibit a high level of vibration damping and a low weight [9-10].

The characteristics of the reinforcement itself, used for the production of composites, i.e. the arrangement of the fibers, the type of weave, the linear density of the yarn, the density of the yarn arrangement in the fabric, have an impact on the out-plane fracture toughness of the composite. Z-pinning, fiber stitching and the use of 3D fabrics can enhance these properties. The disadvantage of these methods is a reduction in tensile strength, a reduction in the modulus of elasticity and fatigue performance [11-18]. The answer to these disadvantages is the use of technical embroidery technology. As proven in previous studies, the use of technical embroidery for the production of composite reinforcements improves strength of composites, compared to ones containing woven fabric as reinforcement. [19-20].

2. Experimental

2.1. Materials

The GiS BasePack version 10 program was used to make the embroidery pattern. The embroidery were made on a ZSK embroidery machine, type JCZA 0109-550 (Figure 1a). This machine is equipped with a W-type head designed for technical embroidery. The rule of the operation of this head is shown in Figure 1b.

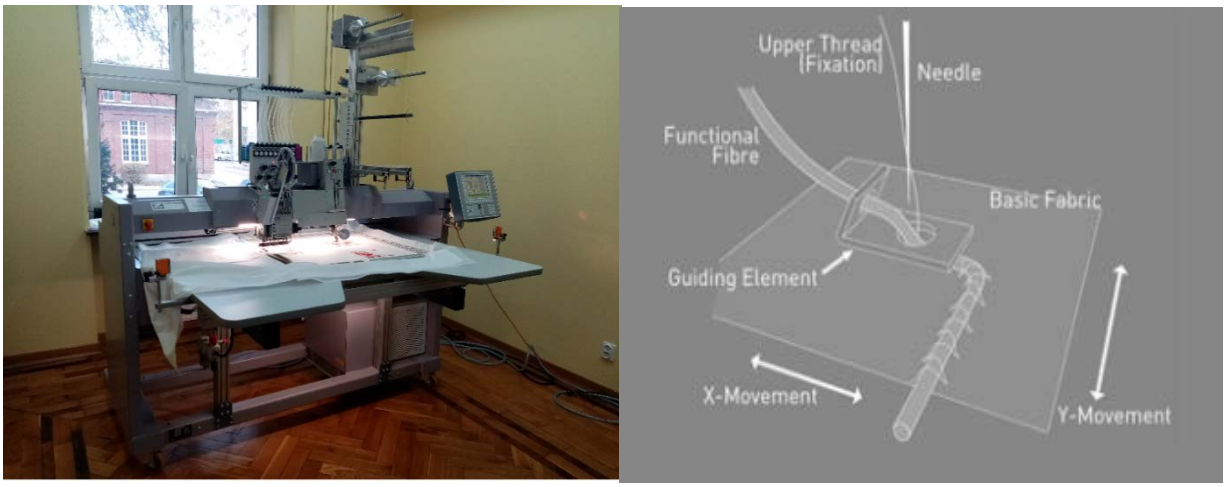

Figure 1a and 1b. 1a - ZSK embroidery machine, type JCZA 0109-550 [own source]; 1b - Scheme of laying the medium on the base [21]

The subject of the research was composites containing two types of flax fiber reinforcements: technical embroidery and woven fabric. The embroidery was made with the use of Safilin linen roving with a linear weight of 400 tex. Gunold monofilament with a linear weight of 11 tex was used to make the fastening zig-zag stitch. The length of the zig-zag stitch was 2 mm and the width was 1.2 mm. In the case of manufacturing samples for the DCB test, an induced crack was created, leaving an area without stitching yarns and placing a plastic foil after making three layers of embroidery, and then three more layers of embroidery were placed. The tensile strength of the flax roving was 7,37 cN/tex and the tensile

elongation was 1,69 %. Embroidery was made on a base of cotton fabric with an area weight of 280 g/m2 and non-woven fabric with an area weight of 35 g/m^2.The flax woven fabric was made from the same roving used for the embroidery. The surface mass of the fabric was 400 g/m^2. All reinforcement samples were then impregnated with the following resin system: SR GreenPoxy 33 epoxy resin and SD4772 hardener at a ratio of 100:32. Composite samples were made using the infusion method.

In total, the following variants for tensile strength and tensile elongation tests were prepared:

Table 1. Configurations for tensile strength and tensile elongation tests

Reinforcement	technical embroidery	technical embroidery	technical embroidery	woven fabric	woven fabric
Fiber orientation	0°	±45°	90°	0/90°	±45°

For interlaminar fracture toughness test, the following variants were prepared:

Table 2. Configurations for interlaminar fracture toughness test

Reinforcement	technical embroidery	woven fabric
Fiber orientation	0°	0/90°

2.2. Methods

The tensile strength and tensile elongation tests were performed according to the PN-EN ISO 527-4 standard [22]. The samples were stretched at a constant speed until the breakage was attained. The relative elongation at maximum force, maximum force, breaking force and relative elongation at break values were collected during the testing. The tests were carried out using a 100 kN load cell on an INSTRON universal testing machine, model 8032. A 50 mm gauge length extensometer was used to measure the specimens' elongation. The test parameters were as follows: grips distance: 100 mm; speed of testing: 1 mm/min; sample size 250×25×3.5 mm; number of samples: 5 of each variant. The test findings are presented in the graph of tensile stress as a function of elongation.

Mode I interlaminar fracture toughness test (DCB - Double Cantilever Beam Test) was carried out based on the ASTM D 5528-01 standard [23]. The test consisted of opening by the crosshead movement, until the samples broke. During stretching, the values of the load (P) and delamination length (δ) were recorded. The test was stopped when the delaminating crack spreads to at least 45 mm from the apex of the initial fracture or when the crack growth at delamination was from 3 to 5 mm. The tests were conducted on a INSTRON universal testing machine with a 50 kN load cell. The velocity of the test was 5 mm/min. The test parameters were as follows: grips distance 0 mm; speed of testing: 5 mm/min; sample size: 160×25×5 mm; number of samples: 5 of each variant.

Both tests were made on the INSTRON universal testing machine, presented in Figure 2a and 2b.

Figure 2a and 2b. 2a - Tensile strength and tensile elongation test; 2b - Interlaminar fracture toughness test [own source]

3. Results and discussion

3.1. Tensile strength and tensile elongation tests

Tensile strength and tensile elongation values are presented on the Figure 3.

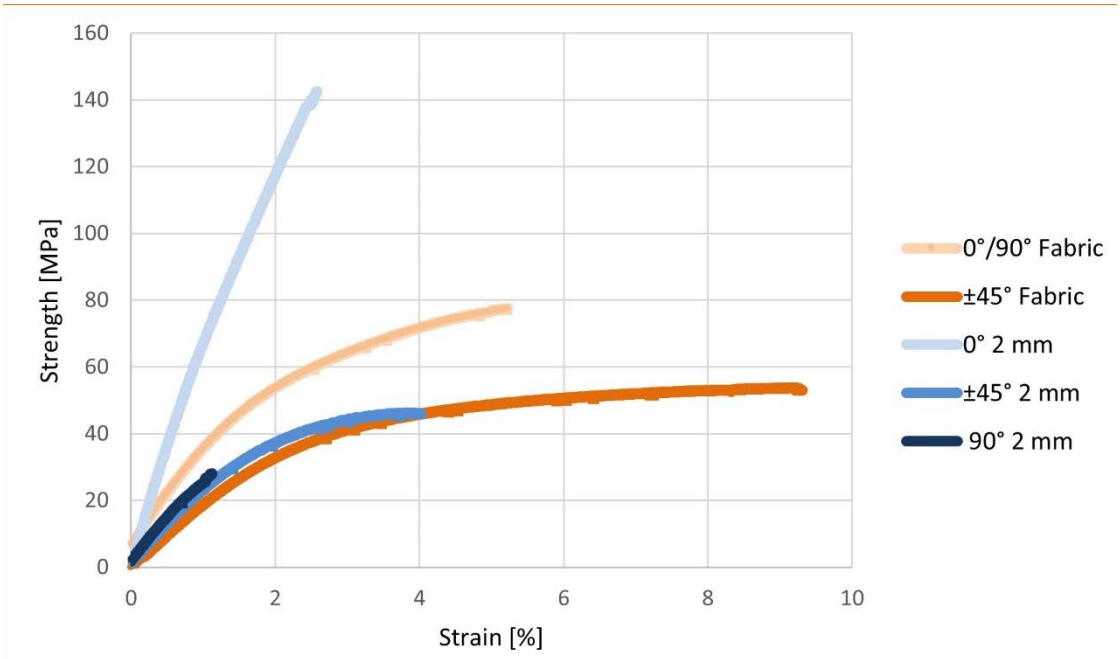

Figure 3. Tensile strength and tensile elongation of produced samples

As shown in Figure 3, based on performed tests, it can be concluded that the tensile strength is greatest when a force is applied along the fibers (0° variant). In these variants, most fibers are involved in the

stretching process. The composite with technical embroidery placed at an angle of 0° to the acting force showed by far the highest tensile strength (142 MPa). Its strength was almost twice as high as that of a composite containing woven fabric as reinforcement, although the woven fabric contains two systems of threads in its structure - weft and warp. The strength of the composite with embroidery placed at an angle of 90° to the acting force as reinforcement turned out to be by far the smallest. In this case, none of the roving fibers is involved in the stretching process. Only the resin and the base on which the embroidery was made is responsible for the strength of the sample. In the case of samples ±45°, the strength of the embroidery variants and the woven fabric were on a similar level.

However the failure strain in ±45° woven samples is twice than in ±45° embroidery samples.. This is due to the fact that the roving in the woven fabric structure has a significant crimp, which increases the elongation. In addition, when a tensile force is applied, shear and bending forces first act in the composite. The fibers in the composite first have to travel from the ±45° direction to the 0° direction - then they are subjected to a tensile force. In the case of composites containing embroidery as reinforcement, the 0° system showed a greater elongation than the 90° system. This is due to the tensile force along the axis of the fibers.

3.2. Interlaminar fracture toughness

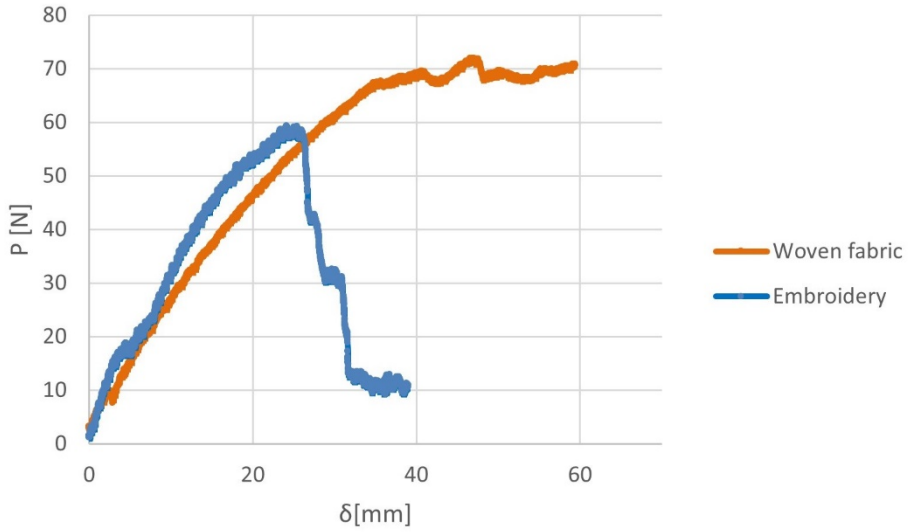

Figure 4. Interlaminar fracture toughness of produced samples

In Figure 4 it can be clearly seen that the composite containing woven fabric as reinforcement showed a greater degree of delamination. For about the first 2 millimeters of opening the sample, both variants showed almost identical characteristics. On the other hand, at about 4 mm opening, the composite containing embroidery as reinforcement cracks. The embroidery is therefore a barrier to delamination of the sample. The composite containing the fabric as reinforcement was delaminated - it broke when it opened about 35 mm.

In the case of samples containing embroidery as reinforcement, the type of the crack formed was also influenced by the sample manufacturing technology itself. The roving layers themselves could be divided in half, while one of the parts always contained fabric, fleece and a backing thread - which increased the strength of this layer. The crack always occurred in the layer not containing these systems.

4. CONCLUSIONS

The use of embroidery as a reinforcement of a composite increases its tensile strength in the direction of fiber stretching, compared to a composite containing woven fabric as reinforcement. Whereas composites containing woven fabric as reinforcement, in each variant of fiber arrangement, showed higher strain.

As a result of the conducted tests, it can be concluded that the vertical stitching of embroidery prevents the delamination of the composite, because the composite with technical embroidery as reinforcement does not undergo the opening process during the test.

It is possible to adjust the strength properties of the composite, containing technical embroidery as reinforcement, to the expected loads affecting the finished product. This fact should be considered when designing finished products with embroidered patterns as reinforcement. In the case of beam systems, it is recommended to arrange the strengthening medium in the direction of the acting tensile forces.

References

1. *Poniecka, A., Barburski, M., Urbaniak, M. (2021). Mechanical properties of composites reinforced with technical embroidery made of flax fibers. AUTEX Research Journal, https,//doi.org/10.2478/aut-2021-0025*
2. *Mecnika, V., Hoerr, M., Krievins, I., Jockenhoevel, S., Gries T. (2014). Technical Embroidery for Smart Textiles, Review. Materials Science Textile and Clothing Technology, 9, 56-63.*
3. *Abbas, B., Khamas, S.K., Ismail, A., Sali, A. (2019). Full Embroidery Designed Electro-Textile Wearable Tag Antenna for WBAN Application. Sensors, 19(11), 2470.*
4. *Linz, T., Vieroth, R., Dils, Ch., Koch, M., Braun, T., Friedrich Becker, K., et al. (2008). Embroidered Interconnections and Encapsulation for Electronics in Textiles for Wearable Electronics Applications. Advances in Science and Technology, 60, 85–94.*
5. *Shafti, A., Ribas Manero, R.B., Borg, A.M., Althoefer, K., Howard, M.J. (2017). Embroidered Electromyography, A Systematic Design Guide. IEEE Transactions on Neural Systems and Rehabilitation Engineering, 25 (9), 1472–1480.*
6. *Morris, R.H., McHale, G., Dias, T., Newton, M.I. (2013). Embroidered coils for magnetic resonance sensors. Electronics, 2(2), 168–177.*
7. *Zhang, M., Zhao, M., Jian, M., Wang, C., Yu, A., Yin, Z., et al. (2019). Printable Smart Pattern for Multifunctional Energy-Management E-Textile. Matter, 1(1), 168-179.*
8. *Monteiro, S., Candido, V., Braga, F. (2016). Sugarcane bagasse waste in composites for multilayered armor. European Polymer Journal, 78, 173–185.*
9. *Cristaldi, G., Latteri, A., Recca, G. (2010). Composites based on natural fibre fabrics. In, Woven fabric engineering, Dubrovski, P.D., InTech, Rijeka, 317–342.*
10. *Buksnowitz, C., Adusumalli, R., Pahler, A., Sixta, H., Gindl, W. (2012). Acoustical properties of Lyocell, hemp, and flax composites. J. Reinf. Plast. Compos., 29, 3149–3154.*
11. *Liu, Q., Hughes M. (2008). The fracture behaviour and toughness of woven flax fibre reinforced epoxy composites. Composites Part A Applied Science and Manufacturing, 39(10), 1644-1652*
12. *Bensadoun, F., Verpoest, I., Vuure, A.W. Van. (2017). Interlaminar fracture toughness of flax epoxy composites. J Reinf Plast Compos, 36(2),121–136.*
13. *Mouritz, A.P. (2007). Review of z-pinned composite laminates. Compos A, 38, 2383–97.*
14. *Rong, M.Z., Zhang, M.Q., Liu, Y., Zhang, Z.W., Yang, G.C., Zeng, H.M. (2001). Effect of stitching on inplane and interlaminar properties of sisal/epoxy laminates. J Compos Mater, 36, 1505–26.*
15. *Mouritz, A.P., Bannister, M.K., Falzon, P.J., Leong, K.H. (1999). Review of applications for advanced three-dimensional fibre textile composites. Composites Part A, 30,1445–1461.*
16. *Allegri, G., Zhang X. (2007). On the delamination suppression in structural joints by z-fibre pinning. Composites Part A: Applied Science and Manufacturing, 38, 1107–1115.*

17. *Dell'Anno, G., Treiber, J.W.G., Partridge, I.K. (2016). Manufacturing of composite parts reinforced through-thickness by tufting. Robotics and Computer-Integrated Manufacturing, 37, 262-272.*
18. *Sickinger, C., Herrmann, A. (2001). Structural Stitching as a method to design high-performans composites in future, 11th International Techtextil-Symposium for Technical Textiles, Nonwovens and Textile-Reinforced Materials, Germany, 23.-26.04.2001*
19. *Poniecka, A., Barburski, M., Urbaniak, M. Mechanical properties of composites reinforced with technical embroidery made of flax fibers. AUTEX Research Journal DOI 10.2478/aut-2021-0024*
20. *Poniecka, A., Barburski, M., Ranz, D., Cuartero, J., Miralbes, R. (2022). Comparison of mechanical properties of composites reinforced with technical embroidery, UD and woven fabric made of flax fibers. Materials, 15 (7469), 1-18.*
21. *Document available on a web page. Retrieved 3 January 2021. Web site: www.technicalembroidery.co.uk*
22. *EN ISO 527-4:1997; Plastics—Determination of tensile properties—Part 4: Test conditions for isotropic and orthotropic fi-bre-reinforced plastic composites. Available online: https://www.iso.org/standard/4595.html (accessed on 15 March 2021).*
23. *ASTM D 5528-01 Standard Test Method for Mode I Interlaminar Fracture Toughness of Unidirectional Fiber-Reinforced Polymer Matrix Composites1*

DETECTING DAMAGED ZONES ALONG SMART SELF-SENSORY CARBON BASED TRC BY TDR

Mahdi Gaben, Yiska Goldfeld

Faculty of Civil and Environmental Engineering, Technion – Israel Institute of Technology, Haifa, 32000, Israel. corresponding author's e-mail: yiska@technion.ac.il.

Abstract:

The study aims to investigate the ability of smart self-sensory carbon roving to detect damaged zones in TRC structures. State of the art monitoring procedures are based on integrative measurements and accordingly are limited in detecting only the occurrence of damage. This study aims to handle this limitation and offers to adopt the Time Domain Reflectometer (TDR) technique. The TDR concept is widely used in Bayonet Nut Coupling (BNC) cables to identify defects along the cable (opens, shorts, etc.). The current study adopts its principle to carbon rovings. To simulate the BNC cable configuration, the study offers to connect two parallel carbon rovings to the TDR Data Acquisition (DAQ) system. The proposed monitoring technique is investigated by loading two textile reinforced MPC beams under uniaxial tensile loading. Results show the potential of the suggested technique to locate damage zones in TRC structures and highlights its limitation.

Key words:

Time domain reflectometer, Smart carbon rovings, AC measurements, Crack identification technique.

1. Introduction

Intelligent concrete structures with self-sensory capabilities are increasingly relevant in today's-built environment. The technology of carbon-based textile reinforced concrete (TRC) is a potential candidate for the development of such intelligent structures. Textile reinforcement technology is based on a biaxial textile mesh of alkali-resistant glass (AR-glass), carbon or basalt rovings with a high tensile strength and high resistance to corrosion. It allows to construct thin-walled, light and durable concrete elements [2,10,14]. Since the carbon rovings are electrically conductive, they can be used both as the main reinforcement system and as the sensory agent [1,4,5,13,16,17]. The potential of using carbon rovings as an integrated sensory agent has been presented in the literature for various sensory purposes such as: detecting cracking [7], estimating strain [7,13,16,17], monitoring the mechanical loading [1,4,5], identifying infiltration of water through cracked zones [6,12], etc. The commonly used approaches for the electrical measurement are based on direct current (DC) electrical circuits by two-probes monitoring setup [13], four-probes monitoring setup [16], Wheatstone bridge configurations [7,17], or by alternating current (AC) electrical circuits [4,5]. These studies proved the feasibility of the smart sensory concept and focused on the correlation between measured changes in the electrical resistance (ERC), the electrical inductance or the electrical impedance of the carbon roving and the structural response. All the above-mentioned monitoring systems yield integrative measurements quantities that cannot localize damage along the structure. This study aims to detect the damaged zones by adopting the principles of the Time Domain Reflectometer (TDR) technique to smart carbon based TRC structures.
The principle of TDR is traditionally used in Bayonet Nut Coupling (BNC) cables to identify defects along the cable. The electrical configuration of BNC cables consists of a copper wire and an insulation barrier. The latter is placed at a constant distance from the copper wire, and the resistance per unit length is constant and equals to 50 Ohms. This study offers to adopt the idea of the BNC configuration by using embedded continuous carbon rovings to locate damage along TRC elements. Damage in this study defines as cracks. Two parallel carbon rovings are connected to a designated data acquisition (DAQ) system, one roving functions as the signal and the other as the insulation.
The carbon rovings have a unique micro-structure, which is divided into two zones: the inner (core) filaments and external (sleeve) filaments [8,11,15]. The sleeve filaments break due to cracking, which yields changes in the electrical current density distribution along the roving. This phenomenon results in an increase of the impedance. In addition, the impedance is not a constant value along the carbon roving and depends on the length of the roving. These properties may limit a direct implementation of the BNC concept which will be reflected by the monitoring capabilities.
To isolate the influence of the electrical properties of the cement body, the study uses magnesium phosphate cement (MPC) matrix. MPC is a production of acid-based solution, dead burnt magnesia, potassium-based phosphate and ammonium-based phosphate [4]. MPC matrix is characterized by a relatively high impedance value compared to conventional cement-based matrix [4]. As a result, it is a better choice to reduce external environmental emissions.
To demonstrate the proposed sensory concept, the study experimentally investigates two textile reinforced MPC elements under uniaxial tensile loading tests and presents the potentials of the proposed monitoring system.

2. Materials and Method

This study uses a generic production process of textile reinforced cement elements [4-7,12,17]. The mechanical and electrical properties of the textile and the production process of the textile reinforced MPC specimens are discussed in this section.

2.1. Carbon-based textile

Following [4-7,12,17], the current study uses a generic textile mesh. The textile consists of six carbon rovings in the longitudinal direction (0°) and AR-glass rovings in the transverse direction (90°). The

textile has a warp-knitted grid structure with a mesh size of 7-8 mm. The stitch type is pillar. The mechanical and electrical properties of the carbon and the AR-glass rovings are given in Table 1.

Table 1. Material properties of the AR-glass and the carbon rovings [5]

	AR-Glass roving	Carbon roving
Specific mass density [kg/m^3]	2,680	1,810
Modulus of elasticity [GPa]	72	270
Filament Tensile strength [MPa]	1,700	5,000
Filament diameter	19 μm	7 μm
Linear Density [Tex]	2,400	1,600
Electrical resistance [Ω/m]	Infinity	13

2.2. MPC matrix with additive short aramid fibers

The study uses a commercial matrix of mono-potassium phosphate acid produced by ICL Group Ltd. Its commercial name is Phosment. In addition, to improve the ductility of the matrix short aramid fibers (AF) were added to the mixture. The volume fraction of the fibers is determined as 0.5%. The study uses a commercial AF named Technora CF32 produced by Teijin Frontier company Ltd. The short AF are 3mm length12 filaments: 12 μm diameter, the tenacity - 2.3-2.5 N/tex, mass density - 1.39 g/cm3, tensile strength - 3.2-3.5 GPa, modulus of elasticity - 65-85 GPa, elongation break - 3.9-4.5%. The MPC matrix was prepared with a ratio of 1:4 water to dry material.
The tensile and flexural strengths of the matrix (MPC +0.5% short AF) specimens were determined at 14 days according to EN 196-1:2005 [3]. The tensile and compression strengths are 6.611 ± 0.434 MPa and 61.929 ± 6.172 MPa, respectively.

2.3. Carbon-based textile reinforced MPC beams

Two beams are investigated. In each beam, a single textile layer is placed. The geometrical properties of both beams are 500 mm long, 50 mm wide and 8 mm thick. The textile layer is placed in the middle of the cross-section of the beams. The beams are cast in a special mold that enables to slightly pre-tensioned the textile upon casting, see Fig. 1.

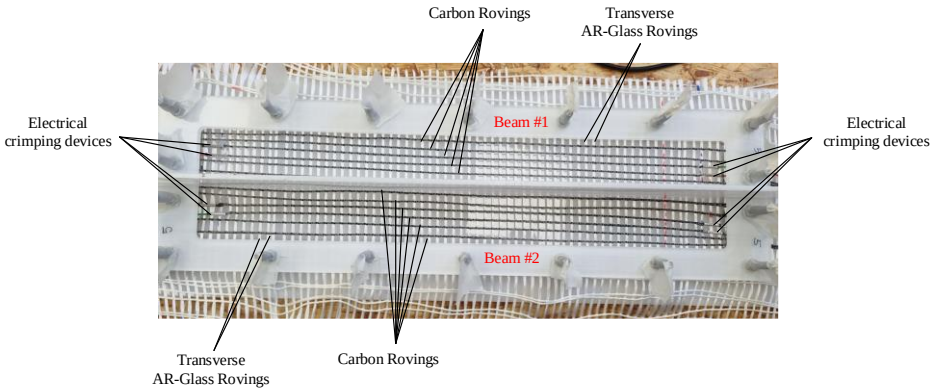

Figure 1. Casting mold for two beams.

2.4. Loading setup

The beams are loaded under a uniaxial tensile loading with a displacement control rate 0.5 mm/min by Instron model 5966. In order to avoid local stress at the ends of the beams, aluminum panels were attached to the ends of the beams, see also [8]. A special uniaxial device was used (Instron screw side action tensile grips model 1710-116) the widths of the supports are 50 mm and they were positioned 20

mm from the beams' edges. Along the loading process, the applies load, the displacement, the impedance spectrum and the crack propagation using the digital image correlation (DIC) technique are measured (LaVision DaVis 10). The loading scheme is shown in Fig. 2.

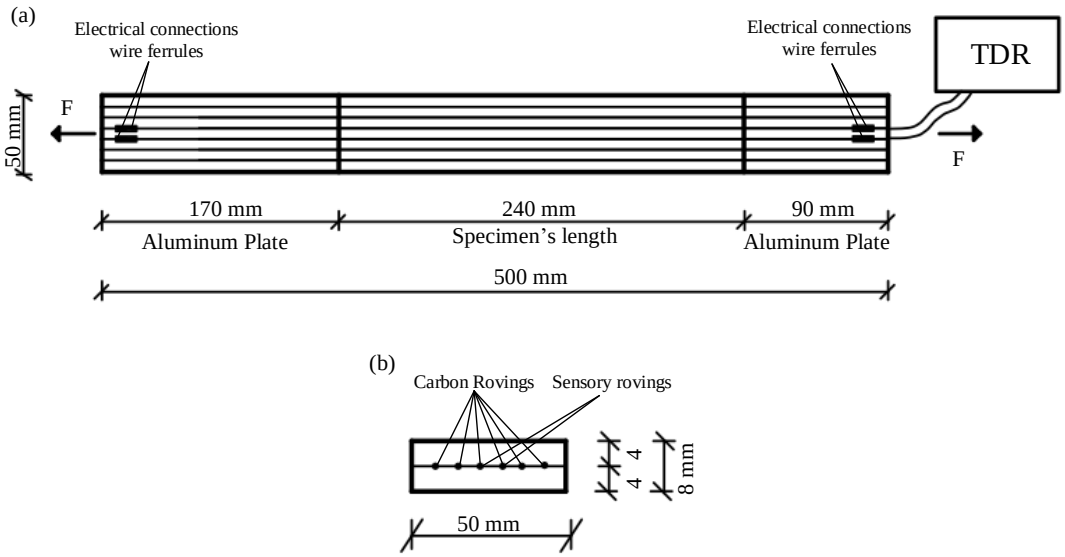

Figure 2. Experimental layout: (a) Uniaxial tensile loading beam; (b) Typical cross-section.

3. Sensing Concept

The study argues that by using TDR analysis, the location of damaged zones along textile reinforced MPC structures can be identified. The idea is based on sending energy pulses by an electrical current into a BNC cable. When the energy pulse encounters a damage, a portion of it is reflected. The reflection time is translated into the position of the damage. Opposed to BNC cables whose resistance per length is constant, the resistance of a carbon roving changes along the roving and depends on the structural health.

The study uses a Fieldfox Handheld Analyzer N9918B with a frequency range of 200kHz-500Mhz with 1600 reading points. Since the resistance of the carbon roving increases with the roving's length, a calibration process determines the location of the damage. The calibration is performed by a magnetic field on a selected known zone along the element. The obtained calibrations are as follow:

$$Beam\ A\text{: } Crack\ location_{[mm]} = 0.2231 \cdot TDR_{index} - 56.66 \quad (1)$$

$$Beam\ B\text{: } Crack\ location_{[mm]} = 0.2583 \cdot TDR_{index} - 45.665 \quad (2)$$

The sensory process is performed by the following main three steps:

First, the measured values are determined by the following processes:

- The impedance spectrums from the TDR were measured every 1 Hz.
- The difference between every two consecutive impedance spectrums was calculated, they referred as impedance spectrum change (ISC).
- For each ISC, the peak to peak (PTP) value was calculated.

Second, the threshold values are estimated by the following process:

- The first 200 ISC were evaluated at an unloaded position and aim to estimate the noise level. The noise level evaluated by the maximum PTP of the readings (for each ISC). In our case the noise level for beam A and beam B are 0.016 Ω and 0.011 Ω, respectively.

- After the loading started, each PTP value higher than 30% of the noise level, is eligible for further investigation and considered as potential damage events.

Third, the identification of damage events is performed by:

- At the potential events the maximum PTP was investigated. Since the formation of cracks yields an integrative increase of the ISC [4,5], it is assumed that the occurrence of damage events should yield a local maximum in the ISC. In such a case, the index of the maximum PTP determines the damaged zone by the calibration presented in Eqs. [1] and [2].

4. Results and discussion

Results of the experimental investigation are given in Figs. 3-6. The impedance response spectrum is measured in a frequency range of 200kHz-500MHz, with 1600 points, in a rate of 1 Hz. Fig, 3a and Fig. 5a present the load-deflection curve, the dashed vertical lines represent the formation of cracks. Cracks are considered as damage and their formation are called event #. Fig, 3b and Fig. 5b present the propagation of the cracks (measured by the DIC technique) versus the vertical deflection of beams A and B, respectively. Fig, 3c and Fig. 5c present the peak-to-peak values of the ISC for beams A and B, respectively. Therefore, the figures present the first and second main steps of the identification procedure. Fig. 4 and Fig. 6 represent a comparison between the identified position of damage by using the TDR analysis (the third step) and the actual position by using the DIC technique for beams A and B, respectively.

From the structural point of view, Fig. 3a and Fig. 5a, it is seen that both beams have similar structural responses. Beam A and beam B have four and three events, respectively. Each event represents a formation of a micro crack. The objective of the monitoring system is to identify these events.

From Fig 3c and Fig. 5c, it is seen that in both beams all the damage events are successfully identified. It is seen that in case of beam A, along with the actual events an additional event was identified, marked in a red circle in the Fig. 3c.

According to the third step for each potential event the PTP profile and its peak was investigated. The position of the damaged zone is calculated by the obtained index and transformed to physical location by the calibration formulas. From Fig. 4a and 6a it is observed that in both beams the first damage zone is successfully identified. Yet, the locations of the next damaged zones were failed to be detected. These results are associated to the degradation of energy pulse along the carbon roving due to two main reasons: first, loss of the energy pulse after an encounter of the previous damage. In our case, a portion of the energy pulse as the first damage occurred; second, since in carbon rovings, the impedance changes along the roving, the ability to distinguish and locate damage zones that are located relatively far from the energy source reduces.

These observations demonstrate the potential of using TDR analysis to locate damaged zones in reinforced MPC structures. Yet, advanced investigation is needed to yield a robust monitoring system.

5. CONCLUSIONS

The paper presented a preliminary demonstration of using TDR technique to locate cracked zones in TRC structures. The goal was to explore the ability of the technique to identify the damaged zones in TRC beams. Two specimens were loaded under uniaxial tensile loading and were monitored along the loading process. It was demonstrated that TDR technique can successfully identify the occurrence of all damage events. The first damaged zones were also successfully identified, while the exact location of the next damaged zones could not be identified. The reasons are associated to the loose of energy signal and the distance from the energy source. Despite of that, this investigation demonstrated the potential of using of TDR analysis for structural health monitoring applications. These preliminary results open the way for the development of advanced investigations that will further bring the concept of self-sensory carbon roving into realization.

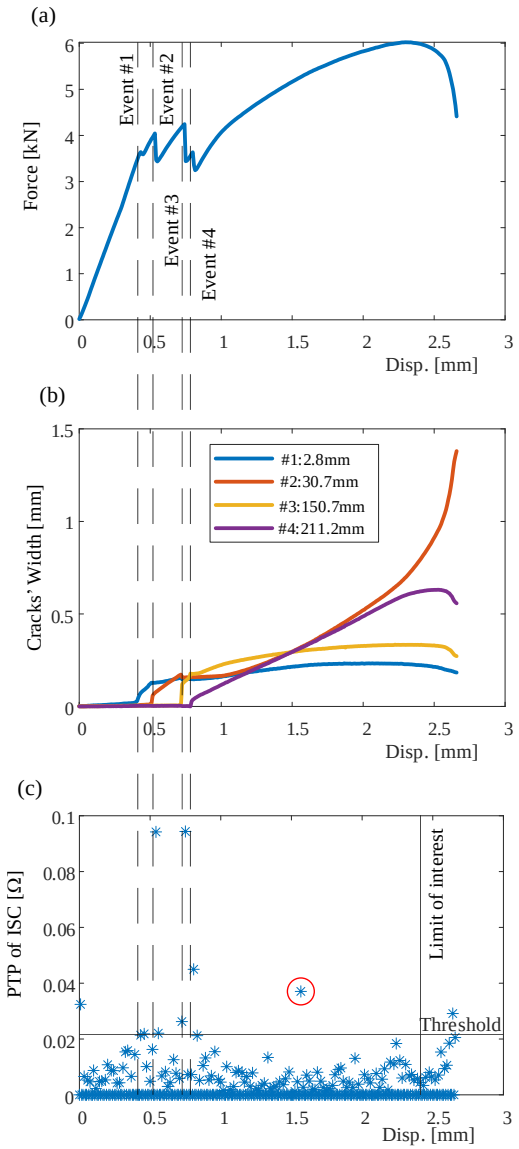

Figure 3. Mechanical and TDR analysis of Beam A: (a) Load- defection curve; (b) PTP of ISC; (c) Cracks' propagation.

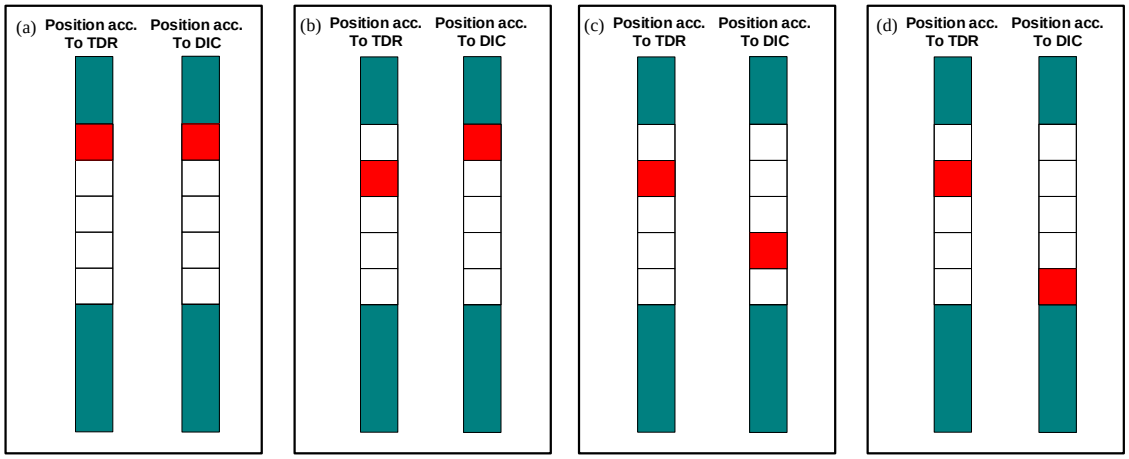

Figure 4. Position of damage comparison between the proposed method and the actual damage by DIC results for Beam A: (a) Event #1; (b) Event #2; (c) Event #3; (d) Event #4.

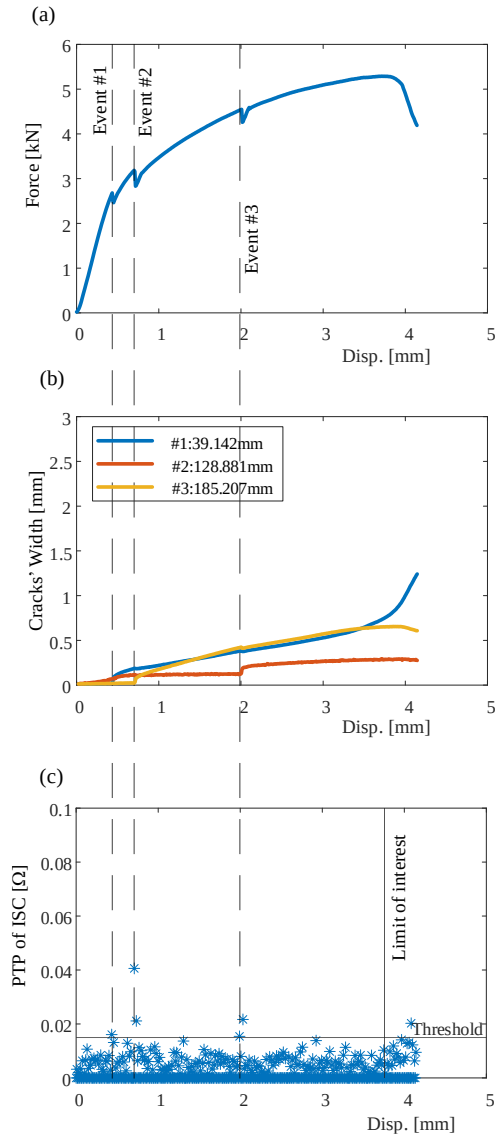

Figure 5. Mechanical and TDR analysis of Beam B: (a) Load- defection curve (b) PTP of ISC; (c) Cracks' propagation.

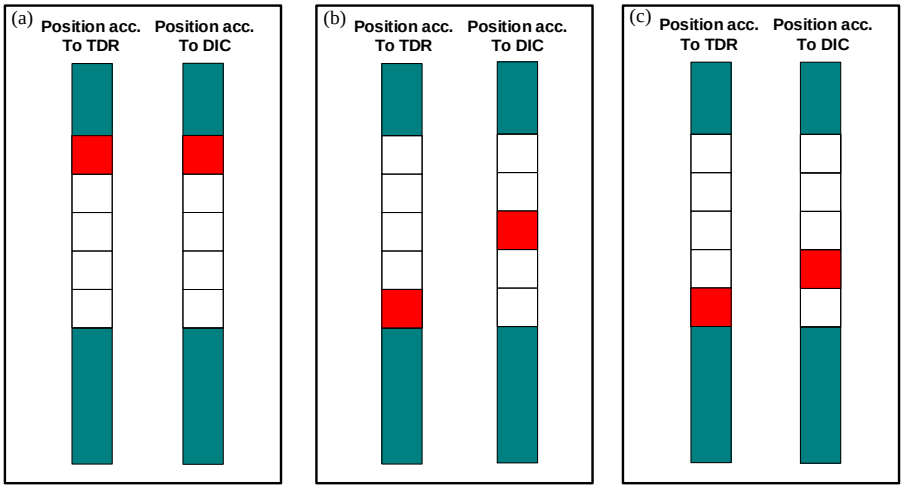

Figure 6. Position of damage comparison between the proposed method and the actual damage by DIC results for Beam B: (a) Event #1; (b) Event #2; (c) Event #3.

ACKNOWLEDGEMENTS

This research was supported by the ISRAEL SCIENCE FOUNDATION (grant No. 1663/21). The authors are thankful for the help of Eng. Barak Ofir and of the technical and administrative staff of the National Building Research Institute at the Technion. The authors acknowledge the support provided by ICL Group Ltd for providing the MPC mixture (Phosment) and by Teijin Frontier company Ltd for providing the short aramid fibers.

References

1. *Christner, C., Horoschenkoff, A., Rapp, H., (2012). Longitudinal and transvers strain sensitivity of embedded carbon fiber sensors, Journal of Composite Materials. 47 (2), 155-167.*
2. *De Andrade Silva, F., Butler, M., Mechtcherine, V., Zhu, D., Mobasher, B., (2011). Strain rate effect on the tensile behavior of textile-reinforced concrete under static and dynamic loading. Materials Science and Engineering: A, 528(3), 1727-1734.*
3. *En, B. S., (2005). 196-1. (2005). Methods of testing cement. Determination of strength. British Standards Institute.*
4. *Gaben, M., Goldfeld, Y., (2022). Enhanced self-sensory measurements for smart carbon-based textile reinforced cement structures. submitted for publication.*
5. *Gaben, M., Goldfeld, Y., (2022). Self-sensory carbon-based textile reinforced concrete beams–Characterization of the structural-electrical response by AC measurements. Sensors and Actuators A: Physical, 334, 113322.*
6. *Goldfeld, Y., Perry, G., (2018). Electrical characterization of smart sensory system using carbon based textile reinforced concrete for leakage detection. Materials and Structures, 51(6), 170.*
7. *Goldfeld, Y., Yosef, L., (2019). Sensing accumulated cracking with smart coated and uncoated carbon based TRC, Measurement. 141, 137-151.*
8. *Häußler-Combe, U., Hartig, J., (2007). Bond and failure mechanisms of textile reinforced concrete (TRC) under uniaxial tensile loading. Cement and Concrete Composites, 29(4), 279-289.*
9. *Hegger, J., Voss, S., (2008). Investigations on the bearing behavior and application potential of textile reinforced concrete. Engineering Structures, 30, 2050-205.*
10. *Peled, A., Bentur, A. (2003). Fabric structure and its reinforcing efficiency in textile reinforced cement composites. Composites Part A: Applied Science and Manufacturing, 34(2), 107-118.*
11. *Perry, G., Dittel, G., Gries, T., Goldfeld, Y., (2021). Monitoring capabilities of various smart self sensory carbon-based textiles to detect water infiltration. Journal of Intelligent Material Systems and Structures, 1045389X211006901.*
12. *Quadflieg, T., Stolyarov, O., Gries, T., (2016). Carbon rovings as strain sensors for structural health monitoring of engineering materials and structures. Journal of strain analysis for engineering design, 51(7), 482-492.*
13. *Shames, A., Horstmann, M., Hegger, J., (2014). Experimental investigations on Textile-Reinforced Concrete (TRC) sandwich sections. Composite Structures, 118, 643-653.*
14. *Soranakom, C., Mobasher, B., (2009). Geometrical and mechanical aspects of fabric bonding and pullout in cement composites. Materials and structures, 42(6), 765-777.*
15. *Wen, S., Wang, S., Chung, D. D. L., (1999). Carbon fiber structural composites as thermistors. Sensors and Actuators A: Physical, 78(2-3), 180-188.*
16. *Yosef, L., Goldfeld, Y., (2020). Smart self-sensory carbon-based textile reinforced concrete structures for structural health monitoring. Structural Health Monitoring, 1475921720951122.*

INTELLIGENT TEXTILE AND FIBER REINFORCED MPC COMPOSITES FOR SHM

Lidor Yosef and Yiska Goldfeld

Technion - Israel institute of technology, Faculty of civil and environmental engineering, Haifa 32000, Israel, corresponding author's e-mail: Yiska@technion.ac.il

Abstract:

This study develops novel intelligent composite structural elements combining three advanced technologies: magnesium phosphate cement (MPC) matrix, smart-self sensory carbon-based textile reinforcement system, and additive short-dispersed fibers. In such system, the carbon rovings simultaneously serve as the main reinforcement system and the sensory agent. The material properties of the MPC matrix include minimization of environmental effects, high flexural strength and enhanced rheological properties which is an advantage in textile reinforcement system. From the sensory point of view, MPC is electrically insulated matrix which enhances the measured electrical signal from the carbon rovings.
Experimental investigation demonstrates the advanced capabilities of the new hybrid structures. The investigation compares between the structural and electrical responses of textile reinforced MPC elements and TRC elements under flexural loading. The structural-electrical correlation enables to further explore new composite configurations and to develop enhanced smart self-sensory systems. The study demonstrates that by merging MPC mixture with textile and fiber reinforcement systems, it is possible to design and construct thin-walled, elements with advanced structural and self-sensing capabilities.

Key words:

Intelligent structures, Advanced structural response, Enhanced sensory capabilities, Textile and fiber reinforcement.

1. Introduction

The technology of textile reinforced cementitious structures (TRC) is based on the synergy between the high compressive strength of the concrete and tensile strength of the textile. The technology enables to construct thin-walled structural elements with advanced structural performance, to reduce the amount of consumed building materials, with the benefit to integrate structural health monitoring (SHM) systems [8-9,12,14,16]. To further enhance the structural and sensory capabilities of the TRC technology, the current study investigates the use of magnesium phosphate cement (MPC) which is a perfect candidate for development of smart TRC structures.

MPC is an eco-friendly material that is characterized by a high early strength [15,18], high corrosion resistance and advanced bonding with existing concretes. These qualities were mainly used for development of rapid retrofitting existing concrete structures and roads [19]. Recent studies investigated the possibility to merge MPC mixture with textile for strengthening of reinforced concrete elements [22]. Furthermore, the improved rheological and electrical properties of the MPC is advantageous for textile reinforced composites from both structural [4] and sensory aspects [20]. The current study investigates the combination of MPC matrix with textile and fiber reinforcement systems for development of light, and optimal structural elements with integrated self-monitoring system.

Generally, textile reinforced cementitious structures are based on Portland cement (PC) matrix. The level of impregnation of the matrix into the roving cross-section affects the load transfer mechanism and govern the overall structural response [10-11,17]. It is affected by the properties of the matrix and the bundle of filaments that characterize rovings, and results in partial roving impregnation. Accordingly, the roving is usually divided into two sub rovings that called sleeve and core [21]. The load transfer mechanism of the sleeve filaments is based on adhesion with the concrete matrix, while the core filaments carry stress by cohesion with the neighboring filaments. The volume fraction of sleeve to core filaments significantly affects the overall structural response. Therefore, the research in this focus on exploring the bond mechanism and the parameters that governed it [3,13]. The resultant macrostructural response of TRC composites can be divided into four main states according to the ACK model. State I, is the healthy state; State II, in which distributed multiple microcracks are formed, is the design state of the element; State III, in which the existing cracks expand and propagate, is related to the damage state; and State IV, in which the rovings are pulled out from the matrix, leads to failure of the element [1].

PC based TRC structures were investigated for SHM purposes such as monitoring the load pattern [2], distinguishing between micro and macro-cracks [5] and detecting accumulated damage [7]. Further research investigated the effect of textile configuration, which change the textile-matrix bond mechanism, on the SHM capabilities [6]. The current study argues that the advanced rheological and electrical properties of MPC matrix enhance the bond mechanism, and accordingly will be reflected by advanced monitoring capabilities. The study investigates three types of composites: textile reinforced PC matrix (TRC), textile reinforced MPC (TR-MPC) and TR-MPC with additive short aramid fibers. The experimental investigation is based on monotonic flexural loading tests and focuses on the effect of the composite configuration on the structural and electrical responses, and the correlation between them.

2. Experimental investigation

2.1 Materials

The study aims to develop new textile reinforced composite elements, with enhanced structural and sensory capabilities. The investigation focuses on three different types of matrices: Portland cement (PC); plain MPC; and MPC with 0.5% of additive short aramid fibers. The PC matrix is classified as a fine-grained matrix. This study uses a commercial mixture (Sika grout

214). The MPC matrix is a commercial potassium-based mixture (K-MPC) called Phosment, produced by ICL LTD. The short aramid fibers (AF) are commercial product of Teijin Fournier LTD, called Technora and their typical length is 3mm. The material properties of the AF are given in Table 1. In case of TR-MPC with additive AF, the fibers were added to the water and then mixed with the dry MPC powder.
The PC and MPC mixtures were prepared with water to dry material ratios of 1:8 and 1:4, respectively. The flexural and compression strengths of the matrices were tested at age of 28 days by using 40/40/160 mm and 50/50/50 mm specimens. The mean compression and flexural strengths and standard deviation of PC, MPC, and MPC with short AF are: (6.33 $\pm$ 0.1,67.99$\pm$0.14), (9.90 $\pm$ 0.42,69.35 $\pm$1.5), (11.29 $\pm$ 0.95,72.75 $\pm$ 2.64).
The textile reinforcement is a generic glass-carbon bi-axial mesh with mesh size of 7-8 mm [4-7] The warp direction is composed of 6 AR-glass rovings and 2 carbon rovings, while in the weft direction only AR-glass rovings are positioned. The material properties of the textile and short fibers are given in Table 1.
The geometrical dimensions of the beam specimens are length 300mm, width 70mm, height 15 mm. Each beam is reinforced with a single textile layer, located 5 mm above the lower face of the beam. The textile layer is slightly pretensioned in the mold before casting, see Fig.1.

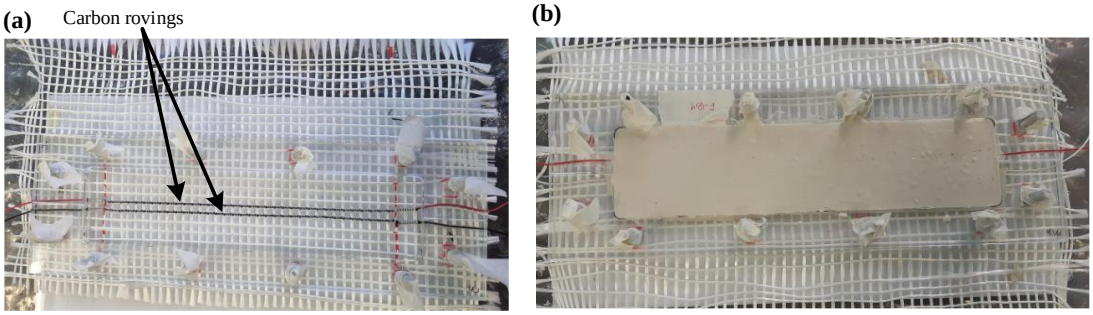

Figure 1. Beam specimen in the mold: (a) Before casting, (b) After casting

Table 1. Material properties of the textile and short fibers [4,5]

	AR-Glass roving	Carbon roving	Aramid fibers (3 mm length)
Specific mass density [g/cm^3]	2.68	1.8	1.39
Modulus of elasticity [GPa]	72	270	65-85
Filament Tensile strength [GPa]	1.7 (elongation 2.4%)	5 (elongation 1.7%)	3.2-3.5 (elongation 3.9-4.5%)
Filament diameter	19 µm	7 µm	12 µm
Linear density [Tex]	2,400	1,600	-
Electrical resistance [Ω/m]	Infinity	13	Infinity

2.2 Methods

The study investigates three different cementitious composites: PC based TRC, textile reinforced MPC (TR-MPC) and TR-MPC with additive short fibers. The specimens were experimentally tested in monotonic flexural loading tests by using a four-points bending scheme [4-7,20]. The beams span length was 210 mm and the distance between the load points was 70 mm. The experiment is performed in a displacement control mode in loading rate of 0.1 mm/min by using an Instron loading machine (Model 5966), see Fig.2(a). The specimens were loaded from the healthy state and up to the ultimate load capacity, the experiments were

terminated at a drop of 15% of the ultimate load. The DIC method was used to monitor the displacement field at the front face of the beam, and to analyze the formation and propagation of cracks. The front face of each beam is photographed along the experiment for the DIC analysis (1 photo every 3 seconds).

The study utilizes the piezoresistive capabilities of the carbon rovings. The sensory concept is adopted from [6] and is based on DC measurements by using a Wheatstone bridge electrical circuit. Each carbon roving functions as electrical resistor that is connected to an individual bridge. The measured voltage changes across the bridge is used to evaluate the integrative electrical resistance change (ERC) of the carbon roving, by using the following equation, see also Fig.2b:

$$R_x = V_{in}\frac{R_c}{V_b + \left(\frac{R_b}{R_a + R_b}\right)V_{in}} - R_c - R_d \quad (1)$$

Where R_x is the rovings integrative resistance, V_{in} is the excitation voltage, R_a, R_b, R_c, R_d are known resistors, and V_b is the measured voltage change across the bridge. The ERC is measured relative to the electrical resistance at the beginning of the experiment, which represents the healthy state. The study also adopts the compensation procedure of environmental parameters such as temperature and moisture by using a non-loaded reference beam [6]. Accordingly, the ERC which is solely related to structural-mechanical change is calculated as follows:

$$\Delta R = R_x - R_0 - \Delta R_{reference} \quad (2)$$

The study explores the structural performance and the structural-electrical correlation for each of the composite beams. The structural electrical correlation is based on two integrative values. The first is the ERC, which is measured over the length of roving, and the second is the strain at the front face of the beam, that is correspondingly calculated over the length of the roving. It means that according to this sensory concept, only an integrative measure of the structural health is obtained, which limit the possibility to identify the exact location of a crack. Yet, it was demonstrated that the integrative measurements yield sufficient information that can be used for SHM purposes [4-7].

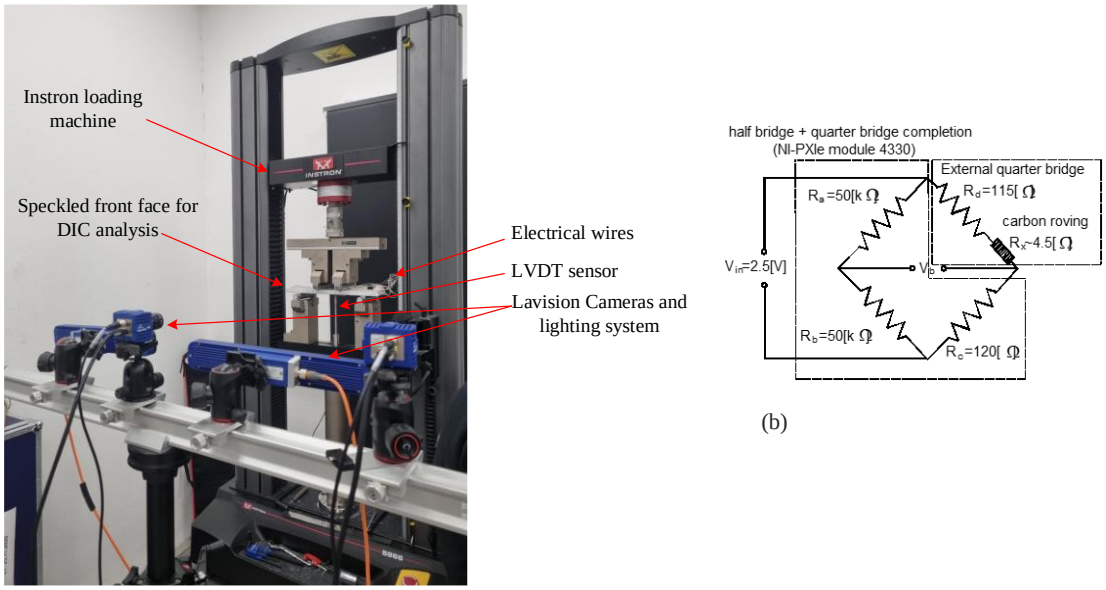

Figure 2. (a) Experimental test setup: Specimen, loading machine and DIC system, (b) DC measurement by Wheatstone's bridge scheme [6]

3. Results and discussion

Fig.3 (a-c) presents the structural and electrical response of the three composite beams. The figure also presents the formation and propagation of cracks along the experiment, see Fig. 3 (d-f). The structural-electrical correlation is presented in Fig.4 by the measured relative ERC versus the integrative strain along the roving. The results highlight several observations:
First, from Fig. 3 it is seen the structural response of the three composites can be divided into the four main structural states that characterized textile reinforced cement beams. Yet, each beam is characterized by a different structural response. The differences between the beams are explained by the matrix properties and especially by the different bond-mechanism between the textile-fiber reinforcement and the matrix. In state I, the differences in the first cracking loads are associated with the higher flexural strength of the MPC matrix (0.92-1.3 KN for TR-MPC and 0.33 KN for the TRC). In state II, the differences are observed by the number and severity of the cracks. While in case of TRC multiple micro-cracks (up to 150 μm) are formed, in the TR-MPC the matrix is relatively brittle which result in formation of only two macro-cracks, see Fig.3(d-e). This behavior is improved by adding short AF to the MPC matrix Fig.3 (c, f). The contribution of the short AF in this state is reflected by higher ductility and by adding new cross links with the matrix that result in multiple microcracks and wider range of State II. In state III, the improved bond mechanism of MPC composites is expressed by enhanced strain hardening behavior and higher ultimate loads that are carried by the improved composite elements (1.21-1.91 KN for TR-MPC and 1.13 KN for the TRC).

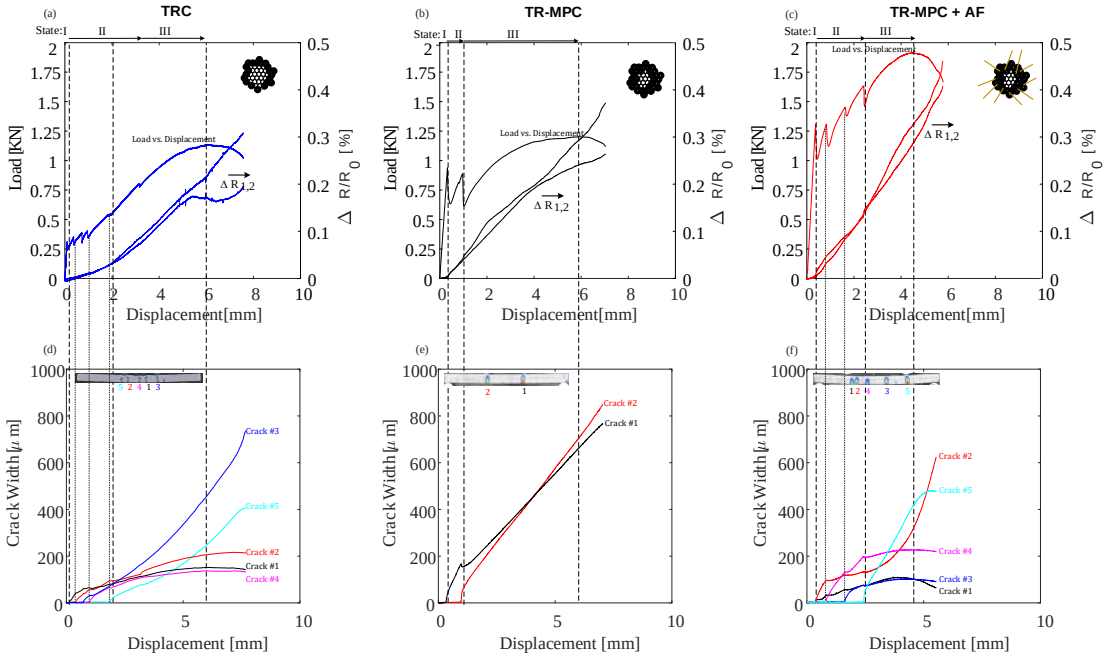

Figure 3. Structural and electrical response of TRC, TR-MPC and TR-MPC +AF: (a-c) load vs. displacement and ERC of the carbon rovings, (d-f) crack formation and propagation analysis.

Second, it is observed that there is a consistent increase in the ERC signal of the three specimens. Yet differences between the trend and intensity of the signals are also observed. In case of MPC based specimens (Fig. 3b-3c) the intensity of the ERC signal is higher along the entire structural-electrical response (0.26-0.31% for TR-MPC and 0.19% for the TRC at the ultimate load). Furthermore, while in TRC specimen (Fig. 3a) the trend of the ERC is dependent on the structural state, in the TR-MPC the trend is relatively linear. These differences are associated with the structural states and the microstructural mechanism of each composite configuration. In case of TRC the mechanism is changing from sleeve controlled in state II, to

core controlled in state III, while in TR-MPC the contribution of the sleeve filaments remains consistent along the entire response, see Fig.3 (b-c).
Third, the different composite configurations yield different structural-electrical correlations. It is associated with the bond mechanism of each composite, and especially the active sub rovings in each state, see Fig.4. In case of TRC, the active sub-roving changes from sleeve to core (State II - State III). As a result, the structural-electrical correlation yields a non-linear correlation function [7]. In case of TR-MPC, the improved rheology is expressed by relatively high-volume fraction of sleeve filaments that are active along the response. It leads to a linear structural-electrical correlation, see Fig. 4. Furthermore, the contribution of the short AF leads to enhanced textile-matrix bond and higher ERC, which is expressed by higher trend of the structural-electrical correlation.
The above results show the advantage of MPC based composites from both the structural and sensory points of view. The improved rheological and electrical properties of the MPC matrix [4,20] result in enhanced structural response and sensing capabilities. The structural-electrical correlation reflects the unique bond mechanism of each composite.

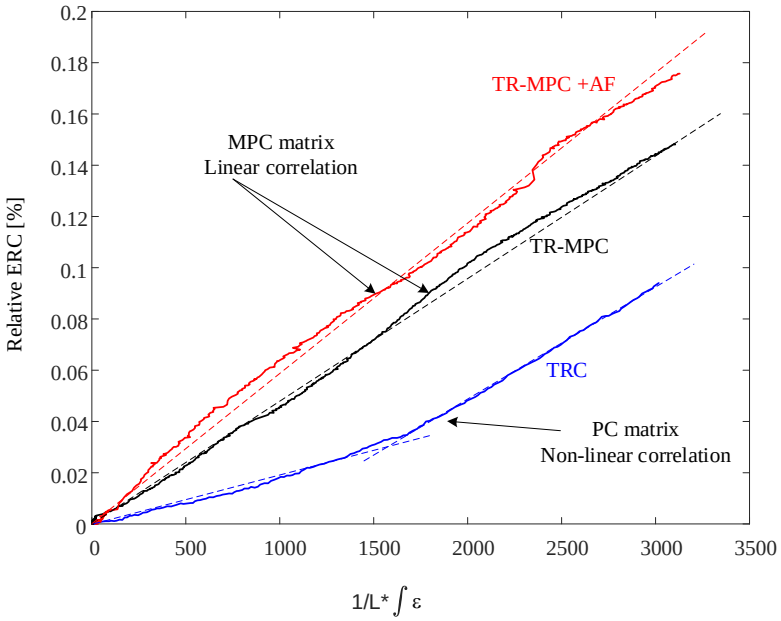

Figure 4. Comparison of the composites structural-electrical correlation: Linear correlation of MPC matrices and nonlinear correlation PC matrix

4. CONCLUSIONS

This study investigated the structural and sensory capabilities of intelligent MPC based composite elements that were made of three types of matrices: PC, MPC and MPC with short additive fibers, reinforced with glass-carbon textile. The structural and electrical behaviors of the composites were investigated in flexural tests from a healthy state and up to the ultimate load. It is seen that the enhanced material properties of the MPC matrix resulted in advanced performance of the thin-walled element compared to the PC based TRC. The MPC based composites exhibited higher cracking loads and ultimate carrying loads. The contribution of the short fibers to the TR-MPC was expressed in enhanced cracking pattern and higher ultimate loads which indicated on the improved textile-matrix bond mechanism. Accordingly, the TR-MPC elements were characterized by enhanced sensory capabilities. It was expressed by higher ERC signal along the entire structural response, linear electrical trend, and higher SNR values. The differences in mechanical and sensory capabilities of the composites are

associated with the matrix properties and the contribution of the dominant sub-roving to the structural-electrical correlation in each composite.

ACKNOWLEDGEMENTS

This research was supported by the Israeli Ministry of Construction and Housing. The authors acknowledge the support provided by ICL Group Ltd for providing the MPC mixture (Phosment) and by Teijin Frontier company Ltd for providing the short aramid fibers. The authors also acknowledge the support provided to this study by the American Technion Society within the framework of the Interdisciplinary Eco-Engineering Research Center: Philip and Harriet Klein Contribution.
The study was conducted at the Technion with the assistance of Eng. Barak Ofir and the technical staff of the National Building Research Institute, their help is gratefully acknowledged.

References

1. *Aveston J., Cooper G., Kelly A., (1971) "The properties of fibre composites", in Conference Proceedings of the National Physical Laboratory, IPC Science and Technology Press Ltd., Guildford, England, pp. 15–26.*
2. *Christner C., Horoschenkoff A., and Rapp H. (2012). Longitudinal and transvers strain sensitivity of embedded carbon fiber sensors, Journal of Composite Materials, 47(2):155-167, 2012.*
3. *Gao S.L., Mäder, E. and Plonka, R. (2004). Coatings for glass fibers in a cementitious matrix, Acta Materialia, Vol. 52, No. 16, pp. 4745-4755.*
4. *Goldfeld, Y., Biton, R. (2022). Experimental study of thin-walled composite elements made of magnesium phosphate cement reinforced by fibers and textile, Submitted for Publication.*
5. *Goldfeld, Y., Quadflieg, T., Ben-Aarosh, S., and Gries, T. (2017a). Micro and macro crack sensing in TRC beam under cyclic loading. Journal of Mechanics of Materials and Structures, 12(5), 579-601.*
6. *Goldfeld Y., Yosef L. (2019). Sensing accumulated cracking with smart coated and uncoated carbon based TRC, Measurement, 141:137-151.*
7. *Goldfeld Y., Yosef L. (2020). Electrical–structural characterization of smart carbon-based textile reinforced concrete beams by integrative gauge factors. Strain. 2020;56:e12344*
8. *Hegger J. and Voss S., "Investigations on the bearing behavior and application potential of textile reinforced concrete." Eng. Struct. 30 (7) (2008) 2050–2056.*
9. *Hegger J., Kulas C., Raupach M. And Büttner T., "Tragverhalten und Dauerhaftigkeit einer schlanken Textilbetonbrücke". Beton- und Stahlbetonbau 106 (2) (2011b) 72–80.*
10. *Lepenies, I., Meyer, C., Schorn, H., & Zastrau, B. (2007). Modeling of load transfer behavior of AR-glass-rovings in textile reinforced concrete. Special Publication, 244, 109-124.*
11. *Mobasher, B., Peled, A., and Pahilajani, J., Pultrusion of fabric reinforced high fly ash blended cement composites, in Sixth Rilem Symposium on Fibre-Reinforced Concrete (FRC), BEFIB 2004, Varenna, Italy, September 20–22, 2004.*
12. *Mobasher B., Dey, V., Cohen, Z., and Peled A. (2014) "Correlation of constitutive response of hybrid textile reinforced concrete from tensile and flexural tests", Cement & Concrete Composites, 53:148-161.*
13. *Perry, G., Dittel, G., Gries, T., and Goldfeld, Y. (2020). Mutual effect of textile binding and coating on the structural performance of TRC beams. Journal of Materials in Civil Engineering, 32(8), 04020232.*
14. *Silva F. D. A., Butler M., Mechtcherine V., Zhu D., and Mobasher B.. "Strain rate effect on the tensile behavior of textile-reinforced concrete under static and dynamic loading". Mater. Sci. Eng. 528 (3) (2011) 1727–1734.*
15. *Sugama T., and Kukacka L.E. (1983). Characteristics of magnesium polyphosphate cements derived from ammonium polyphosphate solutions. Cement and Concrete Research Vol. 13, pp. 499-506.*

16. *Tysmans T., Adriaenssens S., Wastiels J., "Form finding methodology for force modelled anticlastic shells in glass fibre textile reinforced cement composites". Eng Struct 33 (2011) 2603–11.*
17. *Tysmans, T., Adriaenssens, S., Cuypers, H., and Wastiels, J., Structural analysis of small span textile reinforced concrete shells with double curvature, Composites Science and Technology, 69, 1790–1796, 2009.*
18. *Walling S.A., and Provis J. L. (2016). A discussion of the papers "Impact of hydrated magnesium carbonate additives on the carbonation of reactive MgO cements" and "Enhancing the carbonation of MgO cement porous blocks through improved curing conditions", by C Unluer and A Al-Tabbaa". Cem. Concr. Res. 79 (2016) 424−426.*
19. *Yang Q., Zhu B., Wu X., (2000). "Characteristics and durability test of magnesium phosphate cement-based material for rapid repair of concrete". Materials and Structures 33 (4) (2000) 229-234.*
20. *Yosef L., Goldfeld Y., (2022). "Effect of Matrix Electrical and Micro-Structural Properties on the Self-Sensory Capabilities of Carbon-Based Textile Reinforced Composites", submitted for publication.*
21. *Zastrau, B., Lepenies, I., & Richter, M. (2008). On the multi scale modeling of textile reinforced concrete. Technische Mechanik-European Journal of Engineering Mechanics, 28(1), 53-63.*
22. *Zhu C.J., Fang S., Ng P.L., Pundliene I., and Chen J.J, (2020). "Flexural Behavior of Reinforced Concrete Beams Strengthened by Textile Reinforced Magnesium Potassium Phosphate Cement Mortar". Front. Mater. 7:272. doi: 10.3389/fmats.2020.00272.*

THE EFFECT OF POLYMER TYPE AND FIBER ORIENTATION ON THE COMPLIANCE PROPERTIES OF ELECTROSPUN VASCULAR GRAFTS

Suzan Ozdemir[1,*], Janset Oztemur[1], Hande Sezgin[1], Ipek Yalcin-Enis[1]

[1]Istanbul Technical University, Textile Engineering Department, Istanbul, Turkey

[*]ozdemirsu@itu.edu.tr

Abstract:

Vascular diseases are a major source of fatalities globally. However, the lack of accessibility of autologous vessels and the poor efficacy of commercial small-diameter vascular grafts limit surgical alternatives. Researchers therefore aimed to develop vascular prostheses that meet all requirements. Apart from the benefits of tissue-engineered grafts, significant obstacles that still hinder successful grafting include compliance mismatch, dilatation, thrombus development, and the absence of elastin. Among these issues, compliance mismatch between native vessel and artificial vascular scaffold has been mentioned in the literature as a possible cause of intimal hyperplasia, suture site rupture and endothelial and platelet cell damage. As a result, the usage of suitable materials and optimized fabrication techniques are required to achieve better control over the characteristics and functionality of the grafts. In particular, in the case of electrospun vascular grafts, the compliance can be adjusted throughout a broad range of values by adjusting the electrospinning parameters such as material selection, fiber orientation, porosity, and wall thickness. In this study, the electrospun vascular grafts consisting of pure PCL, PLA, and their blends were produced by using two different rotation speeds to achieve the oriented and non-oriented scaffolds. The impact of polymer type and fiber orientation on the compliance properties was evaluated. The results revealed that both material selection and fiber alignment have a significant effect on the compliance levels. PCL100_R grafts had the highest compliance value whereas the PCLPLA50_O scaffold had the lowest.

Key words:

vascular grafts, electrospinning, compliance mismatch, intimal hyperplasia

1. Introduction

Cardiovascular diseases, which account for 32% of all fatalities worldwide, will continue to be the leading global cause of disability and death, according to experts' predictions for the future [1, 2]. There is an urgent and significant need in clinics for tissue engineered small-diameter (<6 mm) blood vessel substitutes due to a lack of availability of autologous vessels and effective commercial products used for bypass surgeries, such as vascular prostheses made of polyethylene terephthalate (PET) or expanded polytetrafluoroethylene (ePTFE), which have low clinical efficacy and a high failure rate after implantation [3, 4].

Tissue engineering faces a great challenge when attempting to replicate the unique design and distinctive mechanical characteristics of the vascular wall in order to fulfill the functional needs of the native tissue [5]. There are several design criteria that affect the properties of vascular grafts, including material selection and constructional parameters including fiber diameters, pore sizes, fiber orientation, wall thickness, and etc. [6]. In tissue engineering applications, the selection of biomaterials has an important role in providing the basic structure for mechanical properties, cell interactions, biocompatibility, biodegradability, anti-toxicity, and cell growth [7]. While natural biodegradable polymers are very successful in biocompatibility and cell activities, synthetic polymers stand out with their properties such as high strength and controllable degradation rate. Each biopolymer has advantages as

well as drawbacks that need to be addressed, and the necessity of combining two or more polymers has been raised as a solution [8]. Polycaprolactone (PCL), which has a highly flexible structure and a long biodegradation period to allow the scaffold enough time for the formation of neo-tissue, is highly demanded for tissue engineering applications [9]. On the other hand, polylactic acid (PLA) is a biomaterial that is usually favored due to its great biocompatibility and outstanding mechanical qualities. However, PCL has lower biocompatibility than PLA, and factors like the brittleness of PLA make the combination of these two materials appealing [10]. Surface production methods and parameters are as important as the selection of biomaterials for the applicability of scaffolds. Electrospinning method is a frequently preferred surface fabrication technique for obtaining three-dimensional structures in different constructions by the modification of various collector systems because it is a simple mechanism to adjust the fiber diameter, pore size and wall thickness of the samples, to obtain fiber orientation, and to facilitate the use of many biopolymers [11]. Thus, all the production parameters should be determined clearly to manufacture the ideal vascular graft that has sufficient characteristics that contribute to the material's performance.

In literature, morphological and biological studies are typically given top priority, whereas mechanical aspects are typically just briefly discussed. To improve the clinical efficacy of vascular grafts exposed to physiological stresses and avoid graft failure due to intimal hyperplasia, thrombosis, aneurysm, blood leakage, and occlusion, sufficient mechanical characteristics that are equivalent to native vessels must be achieved for grafts [12]. The mechanical properties of the scaffold, such as suturability, compliance, tensile strength, burst pressure, and blood permeability, are significantly influenced by the material and architecture of the scaffold [13]. In particular, one of the main reasons for graft failure over extended periods of implantation is compliance mismatch between the native artery and the inelastic artificial graft at the anastomosis sites, which produces low blood flow rates and turbulent blood flow in small-diameter vascular prostheses [14]. The blood flow fluctuations in the vascular scaffold and the stress concentration at the anastomosis regions are caused by the incompatible dimension changes of the vascular prosthesis and the native blood vessel as a reaction to pressure variations inside the lumen, which is known as compliance mismatch [15]. Low patency rates are caused by these mechanical problems, which also contribute to the scaffold material's thrombogenicity, inadequate endothelialization, luminal constriction, and trombosis, which are triggered by intimal hyperplasia [14]. It is notably difficult to create vascular prostheses that are both elastic and strong enough to resist blood pressure because burst strength and compliance are frequently inversely proportional [16]. Numerous studies in the literature demonstrate that the compliance is determined by the material selection and construction characteristics, such as wall thickness, the number of layers, and the orientation of the fibers within the layers [17-19]. Johnson et al. (2015) produced vascular grafts from various polymers and wall thicknesses. The compliance values revealed that both the polymer type and wall thickness were effective on the compliance levels. An increase in wall thickness reduced the compliance values, whereas using flexible materials improved the results [17]. Li et al. (2017) designed composite vascular graft prototypes by integrating a flexible PLA knitted fabric as an inner layer with a soft PCL matrix as an outer layer. The compliance value of all the samples was found to be below 2%/100 mmHg [20]. Also, the measured compliance values of some of the native human blood vessels are given in Table 1.

Table 1. Compliance values of native human blood vessels

Type of Blood Vessel	Compliance	References
Saphenous vein	1.5%/100 mmHg	[21]
Coronary artery	0.0725%/mmHg	[22]
Femoral artery	3.8–6.5%/100mmHg	[23]

In this study, both the radially-oriented and randomly-distributed electrospun fibrous vascular grafts that were made of neat PCL, PLA, and their blend with a weight ratio of 50:50 were fabricated to assess the impact of the polymer selection and the fiber orientation on the compliance properties.

2. Experimental Study

2.1. Materials

The neat or the blended form of PCL (Mn 80,000) and PLA (Mn 230,000; Ingeo 2003 D with 4.3 mol% D-lactide content) were dissolved in a solvent system consisting of chloroform (CH)/acetic acid (AA)/ethanol (ETH) with 8/1/1 wt. at a concentration of 8% w/w. All the polymers and the solvents were supplied from the Sigma Aldrich.

2.2. Methods

Surface fabrication

The prepared neat PCL, neat PLA and PCL/PLA (50:50) solutions were stirred for 4 hours with a magnetic stirrer and immediately electrospun by using electospinning system supplied from Inovenso, Turkey (Nanospinner, Ne100^{+}). The neat and blended polymer solutions were transferred by a 10 ml plastic syringe through a distance from the needle tip which was kept at 20 cm. The mandrel with a rotational speed of 200 rpm and 10000 rpm were used for the fabrication of tubular scaffolds with randomly distributed and radially oriented fibers, respectively. Tubular scaffolds have 6mm inner diameter and the spinning time for all samples was fixed at 40 minutes. The sample codes and details are given in Table 2.

Table 2. Samples codes and details

Sample codes	Blending ratio of PCL/PLA (%)	Rotational speed of the collector (rpm)	Fiber orientation
PCL100_R	100/0	200	Randomly distributed
PCL100_O	100/0	10000	Radial orientation
PCLPLA50_R	50/50	200	Randomly distributed
PCLPLA50_O	50/50	10000	Radial orientation
PLA100_R	0/100	200	Randomly distributed
PLA100_O	0/100	10000	Radial orientation

Compliance

The custom-designed device used to test compliance provided air flow at a physiologically equivalent pressure. After the balloon was inserted through the samples, they were mounted by the sleeves to the nozzles and supplied with air from the system. The pulsatile intraluminal pressure was established at the diastolic and systolic pressures of 80 mmHg and 120 mmHg, respectively. The photos of the samples at these pressures were taken by a camera system, and the diameters at each pressure were measured by the Image J software system. After that, the compliance values were calculated by the formula below;

$$\%compliance = \frac{\frac{R_{p_2} - R_{p_1}}{R_{p_1}}}{p_2 - p_1} \times 10^4 \quad (1)$$

R_{p1} = pressurized radii at diastolic pressure (mm)
R_{p2} = pressurized radii at systolic pressure (mm)
p1 = diastolic pressure (mmHg)
p2 = systolic pressure (mmHg)

3. Results and discussion

The compliance values of each sample group were given with their standard deviations in Table 3. It was clearly observed from the results that the radial fiber orientation reduced the compliance values of the scaffolds. This situation was expected as the oriented fibers are already under stress in that direction and they cannot be stretched as in the randomly oriented fibers [3]. Grasl et al. (2021) also manufactured electrospun vascular grafts made of polyurethane (PU) and PLLA with fiber orientations in different directions and measured the compliance values. It was observed that in PU samples, fiber orientation in any direction caused a reduction in compliance values, whereas PLLA showed similar compliance levels in any direction because of its stiff structure. For example, in PU scaffolds with radially oriented fibers, the compliance was 4.1 ± 0.4 mmHg %/100 mmHg whereas it was 29.7 ± 5.5 mmHg %/100 mmHg in the PU scaffolds with randomly distributed fibers. On the other hand, in PLLA samples the compliance was 1.3 ± 0.4 mmHg %/100 mmHg for the radial orientation whereas it was 1.4 ± 0.4 mmHg %/100 mmHg for the samples with no fiber orientation [24].

On the other hand, scaffolds made of PCL have the highest compliance values in all directions, whereas blended scaffolds showed the lowest compliance among all the samples. As the PCL is a flexible and pliable biopolymer with high strain values, higher compliance results were expected from the PCL100 scaffolds. In addition, PLA is a brittle and stiff material with lower elongation values, PLA100 showed lower compliance than PCL prostheses [25]. In the PCLPLA50 samples, the lowest compliance values were observed because of the mechanical failure caused by the immiscible characteristics of the polymer components. As the blending cannot be reached properly, the phase separation occurs because of the weak adhesion forces between the polymer chains in these scaffolds during the electrospinning process [26].

When the obtained compliance values were compared with the values of the native vessels, it was clear that compliance values of the samples of randomly distributed fibers were higher than those of the saphenous vein and coronary artery, with a compliance of 1.5%/100 mmHg and 0.0725%/mmHg, respectively [21, 22]. Additionally, oriented samples also had higher compliance values than the coronary artery. Despite the fiber orientation lowers the compliance, it also known that it contributes to mechanical characteristics of the scaffolds such as tensile strength and burst pressure [27]. Thus, both of the structures can be utilized for different approaches in multilayer vascular graft strategies.

Table 3. Compliance values of the scaffolds at a pressure range of 80 -120 mmHg

Sample codes	Compliance ± SD (%/100 mmHg)
PCL100_R	2,494 ± 0,791
PCL100_O	1,155 ± 0,553
PCLPLA50_R	1,542 ± 0,783
PCLPLA50_O	0,864 ± 0,350
PLA100_R	1,603 ± 1,326
PLA100_O	1,078 ± 0,353

4. CONCLUSIONS

In this study, PCL, PLA, and PCL/PLA blended samples were fabricated by using two rotational speeds to achieve scaffolds with randomly distributed and radially oriented fibers. The effect of the polymer type and the fiber orientation of the samples was confirmed by the compliance test results. It was seen that PCL100_R had the highest compliance value among all the samples, as it has much more elastomeric polymer and fibers without high tension. On the other hand, the PCLPLA50_O sample had the lowest compliance values because of the incompatibility of the polymer blending and stretched fibers by orientation. Although the samples with randomly oriented fibers had adequate compliance levels,

combining the advantages of both structures by designing multilayered grafts should be considered to optimize the other mechanical and biological characteristics of these scaffolds.

ACKNOWLEDGEMENTS

This study is funded by TUBITAK Project (Grant no:121M089) and ITU Scientific Research Project (Grant no: 43368)

References

1. *Fayon, A., Menu, P., & el Omar, R. (2021). Cellularized small-caliber tissue-engineered vascular grafts: looking for the ultimate gold standard. In npj Regenerative Medicine (Vol. 6, Issue 1). Nature Research. https://doi.org/10.1038/s41536-021-00155-x*
2. *Tran, N., Le, A., Ho, M., Dang, N., Thi Thanh, H. H., Truong, L., Huynh, D. P., & Hiep, N. T. (2020). Polyurethane/polycaprolactone membrane grafted with conjugated linoleic acid for artificial vascular graft application. Science and Technology of Advanced Materials, 21(1), 56–66. https://doi.org/10.1080/14686996.2020.1718549*
3. *Nezarati, R. M., Eifert, M. B., Dempsey, D. K., & Cosgriff-Hernandez, E. (2015). Electrospun vascular grafts with improved compliance matching to native vessels. Journal of Biomedical Materials Research - Part B Applied Biomaterials, 103(2), 313–323. https://doi.org/10.1002/jbm.b.33201*
4. *Ye, L., Takagi, T., Tu, C., Hagiwara, A., Geng, X., & Feng, Z. (2021). The performance of heparin modified poly(ε-caprolactone) small diameter tissue engineering vascular graft in canine—A long-term pilot experiment in vivo. Journal of Biomedical Materials Research - Part A, 109(12), 2493–2505. https://doi.org/10.1002/jbm.a.37243*
5. *Nerem, R. M., & Seliktar, D. (2001). Vascular tissue engineering. In Annual Review of Biomedical Engineering (Vol. 3, pp. 225–243). https://doi.org/10.1146/annurev.bioeng.3.1.225*
6. *Yalcin Enis, I., & Gok Sadikoglu, T. (2018). Design parameters for electrospun biodegradable vascular grafts. In Journal of Industrial Textiles (Vol. 47, Issue 8, pp. 2205–2227). SAGE Publications Ltd. https://doi.org/10.1177/1528083716654470*
7. *Yu, E., Mi, H. Y., Zhang, J., Thomson, J. A., & Turng, L. S. (2018). Development of biomimetic thermoplastic polyurethane/fibroin small-diameter vascular grafts via a novel electrospinning approach. Journal of Biomedical Materials Research - Part A, 106(4), 985–996. https://doi.org/10.1002/jbm.a.36297*
8. *Shalumon, K. T., Deepthi, S., Anupama, M. S., Nair, S. v., Jayakumar, R., & Chennazhi, K. P. (2015). Fabrication of poly (l-lactic acid)/gelatin composite tubular scaffolds for vascular tissue engineering. International Journal of Biological Macromolecules, 72, 1048–1055. https://doi.org/10.1016/j.ijbiomac.2014.09.058*
9. *Mohamed, R. M., & Yusoh, K. (2015). A Review on the Recent Research of Polycaprolactone (PCL). Advanced Materials Research, 1134, 249–255. https://doi.org/10.4028/www.scientific.net/amr.1134.249*
10. *Patrício, T., Domingos, M., Gloria, A., & Bártolo, P. (2013). Characterisation of PCL and PCL/PLA scaffolds for tissue engineering. Procedia CIRP, 5, 110–114. https://doi.org/10.1016/j.procir.2013.01.022*
11. *Li, S., Sengupta, D., & Chien, S. (2014). Vascular tissue engineering: From in vitro to in situ. In Wiley Interdisciplinary Reviews: Systems Biology and Medicine (Vol. 6, Issue 1, pp. 61–76). https://doi.org/10.1002/wsbm.1246*
12. *Johnson, R., Ding, Y., Nagiah, N., Monnet, E., & Tan, W. (2019). Coaxially-structured fibres with tailored material properties for vascular graft implant. Materials Science and Engineering C, 97, 1–11. https://doi.org/10.1016/j.msec.2018.11.036*
13. *Hasan, A., Memic, A., Annabi, N., Hossain, M., Paul, A., Dokmeci, M. R., Dehghani, F., & Khademhosseini, A. (2014). Electrospun scaffolds for tissue engineering of vascular grafts. In Acta*

Biomaterialia (Vol. 10, Issue 1, pp. 11–25). Elsevier Ltd. https://doi.org/10.1016/j.actbio.2013.08.022

14. *Hiob, M. A., She, S., Muiznieks, L. D., & Weiss, A. S. (2017). Biomaterials and Modifications in the Development of Small-Diameter Vascular Grafts. ACS Biomaterials Science and Engineering, 3(5), 712–723. https://doi.org/10.1021/acsbiomaterials.6b00220*
15. *Zhang, Y., Li, X. S., Guex, A. G., Liu, S. S., Müller, E., Malini, R. I., Zhao, H. J., Rottmar, M., Maniura-Weber, K., Rossi, R. M., & Spano, F. (2017). A compliant and biomimetic three-layered vascular graft for small blood vessels. Biofabrication, 9(2). https://doi.org/10.1088/1758-5090/aa6bae*
16. *Fernández-Colino, A., Wolf, F., Rütten, S., Schmitz-Rode, T., Rodríguez-Cabello, J. C., Jockenhoevel, S., & Mela, P. (2019). Small Caliber Compliant Vascular Grafts Based on Elastin-Like Recombinamers for in situ Tissue Engineering. Frontiers in Bioengineering and Biotechnology, 7. https://doi.org/10.3389/fbioe.2019.00340*
17. *Devan Ohst, J. J. (2015). Development of Novel, Bioresorbable, Small-Diameter Electrospun Vascular Grafts. Journal of Tissue Science & Engineering, 06(02). https://doi.org/10.4172/2157-7552.1000151*
18. *Kim, S. H., Mun, C. H., Jung, Y., Kim, S. H., Kim, D. I., & Kim, S. H. (2013). Mechanical properties of compliant double layered poly(L-lactide-co-ε- caprolactone) vascular graft. Macromolecular Research, 21(8), 886–891. https://doi.org/10.1007/s13233-013-1095-5*
19. *Matsuda, T., Ihara, M., Inoguchi, H., Kwon, I. K., Takamizawa, K., & Kidoaki, S. (2005). Mechano-active scaffold design of small-diameter artificial graft made of electrospun segmented polyurethane fabrics. Journal of Biomedical Materials Research - Part A, 73(1), 125–131. https://doi.org/10.1002/jbm.a.30260*
20. *Li, C., Wang, F., Douglas, G., Zhang, Z., Guidoin, R., & Wang, L. (2017). Comprehensive mechanical characterization of PLA fabric combined with PCL to form a composite structure vascular graft. Journal of the Mechanical Behavior of Biomedical Materials, 69, 39–49. https://doi.org/10.1016/j.jmbbm.2016.11.005*
21. *McClure, M. J., Simpson, D. G., & Bowlin, G. L. (2012). Tri-layered vascular grafts composed of polycaprolactone, elastin, collagen, and silk: Optimization of graft properties. Journal of the Mechanical Behavior of Biomedical Materials, 10, 48–61. https://doi.org/10.1016/j.jmbbm.2012.02.026*
22. *Bouchet, M., Gauthier, M., Maire, M., Ajji, A., & Lerouge, S. (2019). Towards compliant small-diameter vascular grafts: Predictive analytical model and experiments. Materials Science and Engineering C, 100, 715–723. https://doi.org/10.1016/j.msec.2019.03.023*
23. *Xing, M. Y., Yu, C. L., Wu, Y. F., Wang, L., & Guan, G. P. (2020). Preparation and characterization of a polyvinyl alcohol/polyacrylamide hydrogel vascular graft reinforced with a braided fiber stent. Textile Research Journal, 90(13–14), 1537–1548. https://doi.org/10.1177/0040517519896753*
24. *Grasl, C., Stoiber, M., Röhrich, M., Moscato, F., Bergmeister, H., & Schima, H. (2021). Electrospinning of small diameter vascular grafts with preferential fiber directions and comparison of their mechanical behavior with native rat aortas. Materials Science and Engineering C, 124. https://doi.org/10.1016/j.msec.2021.112085*
25. *Zahedi, P., Karami, Z., Rezaeian, I., Jafari, S. H., Mahdaviani, P., Abdolghaffari, A. H., & Abdollahi, M. (2012). Preparation and performance evaluation of tetracycline hydrochloride loaded wound dressing mats based on electrospun nanofibrous poly(lactic acid)/poly(e-caprolactone) blends. Journal of Applied Polymer Science, 124(5), 4174–4183. https://doi.org/10.1002/app.35372*
26. *Carvalho, J. R. G., Conde, G., Antonioli, M. L., Dias, P. P., Vasconcelos, R. O., Taboga, S. R., Canola, P. A., Chinelatto, M. A., Pereira, G. T., & Ferraz, G. C. (2020). Biocompatibility and biodegradation of poly(lactic acid) (PLA) and an immiscible PLA/poly(ε-caprolactone) (PCL) blend compatibilized by poly(ε-caprolactone-b-tetrahydrofuran) implanted in horses. Polymer Journal, 52(6), 629–643. https://doi.org/10.1038/s41428-020-0308-y*
27. *Ozdemir, S., Yalcin-Enis, I., Yalcinkaya, B., & Yalcinkaya, F. (2022). An Investigation of the Constructional Design Components Affecting the Mechanical Response and Cellular Activity of Electrospun Vascular Grafts. Membranes, 12(10), 929. https://doi.org/10.3390/membranes12100929*

A PRELIMINARY STUDY EXAMINING THE BURST STRENGTH OF VASCULAR TUBULAR SCAFFOLDS

Janset Oztemur*, Suzan Özdemir, Hande Sezgin & Ipek Yalcin-Enis

Textile Engineering Department, Istanbul Technical University, Istanbul

*oztemurj@itu.edu.tr

Abstract:

In this study, neat PCL, neat PLA and PLA/PCL (50/50) based tubular surfaces are produced by electrospinning to simulate the native blood vessel structure and to investigate the effects of both graft material and fiber orientation on burst strength. The burst pressure values of these vascular graft structures that designed with both randomly oriented fibers and oriented fibers, measured by a custom- burst pressure tester, and the results are compared. The results show that fiber orientation have a great influence on burst pressure, regardless of the type of biomaterial. It is determined that grafts with oriented fibers have at least twice the burst strength than those with random fibers. The findings indicate that changing the graft material has also an effect on burst strength. When the results are analyzed by polymer type, although the PLA100_O sample has the highest burst strength among all oriented fiber sample groups, it is better to determine the vascular graft candidate by taking into account radial elasticity.

Key words:

Vascular graft, fiber orientation, burst pressure, mechanical properties, electrospinning

1. Introduction

According to data from the World Health Organization, among various chronic and non-chronic diseases, cardiovascular diseases have a mortality rate of 31%, making them the most common cause of death [1]. Although blood vessel replacement is the most popular and recommended treatment for cardiovascular diseases, its usage is constrained due to a shortage of accessible vessel resources, donor site morbidity, vasoplasma problems, dimensional incompatibility, and poor quality [2]. Vascular grafts now assist the development of the native artery by enabling surviving cells to adhere, develop, and proliferate. While materials like polyethylene terephthalate (PET), polytetrafluoroethylene (PTFE), and polyurethane (PU) have been effectively employed in large-diameter grafts in the past, an adequate success rate for small-caliber grafts has not been attained [3]. The use of these materials in small-diameter vascular grafts results in large-scale thrombosis (tendency to produce clots), restenosis (stenosis of the vessel and consequent blood flow limitation), and various infections. They also have properties like insufficient structural porosity, insufficient cell adhesion and proliferation, and low level radial elasticity [4]. For this reason, researchers are looking for novel vascular graft materials that can imitate the injured artery in all of its characteristics.

Due to its exceptional mechanical qualities, including high elongation, slow biodegradation time, biocompatibility, and cell survival, polycaprolactone (PCL) is a particularly desirable material for vascular graft applications [5]. Moreover, another aliphatic polyester, polylactic acid (PLA), is also in demand because of its high strength, biocompatibility, and biodegradability [6].

On the other hand, vascular grafts are successful to the extent that they can mimic native vessels and approximate the artificial tissue to native tissues in all their properties. The designed vascular grafts should match the native vascular structure, which is a very complex structure, in terms of physical, histological, topographic and biological properties as well as mechanical properties [7]. The vascular structure, which is subjected to many loads such as blood pressure and stress cycling, must have burst strength to prevent aneurysmal expansion [8]. The burst pressure values of the saphenous artery and the internal mammary artery can be seen in Table 1 (Table 1).

Table 1. Burst strength values of native human blood vessels

Type of Blood Vessel	Burst Pressure (mmHg)	Reference
Saphenous vein	1599±877	[9,10]
Internal mammary artery	3196±1264	[9]

Studies on vascular graft designs that include burst strength are regularly reported in the literature. The burst strength values in the study by Gao et al. (2019), in which they developed PCL and poly(lactide-co-glycolide) (PLGA) blend-based vascular grafts, were found to be extremely similar to the human blood vessel strength properties, and the burst resistance was over 1500 mmHg [11]. Yalcin-Enis et al. (2017) designed surfaces with randomly oriented fibers and oriented fibers using PCL and poly(L-lactide) caprolactone (PLC) with various molecular weights, and then they examined the mechanical strength of those surfaces. The study's findings showed that the molecular weight and surface orientation both affected the burst strength of the graft formations [12].
The graft structures developed within the scope of the study aim to examine the effects of the raw materials and the fiber orientation on burst strength, as well as an imitation of the native vessel structure with synthetic materials. In this context, tubular scaffolds are produced from both neat PLA and PCL and blend forms of these materials in 50/50 ratios, and the effects of material and fiber orientation on the burst strength of scaffolds are examined.

2. Experimental

2.1. Materials

PCL (Mn 80,000), PLA (Mn 230,000; Ingeo 2003 D with 4.3 mol% D-lactide content), and the components of solvent systems (chloroform (CHL), ethanol (ETH), and acetic acid (AA)) are supplied from Sigma Aldrich.

2.2. Methods

Neat PCL, neat PLA, and PLA/PCL (50/50) are dissolved in CHL/ETH/AA (8/1/1 wt.) at 8% polymer concentrations. Each polymer solution system is stirred for 2 hours at room temperature. Tubular vascular graft structures with 6 mm diameter are fabricated using electrospinning set-up with rotating feeding unit that supplied from Inovenso, Turkey (Nanospinner, Ne100+).

Table 2. Sample codes and descriptions

Sample Code	PCL ratio (%)	PLA ratio (%)	Production Rotational Speed (rpm)	Fiber Orientation
PCL100_O	100	0	10000	Oriented
PCL100_R	100	0	200	Random
PCLPLA50_O	50	50	10000	Oriented
PCLPLA50_R	50	50	200	Random
PLA100_O	0	100	10000	Oriented
PLA100_R	0	100	200	Random

Moreover, graft surfaces are produced at two different rotational speeds; 200 rpm for randomly oriented fibers and 10000 rpm for oriented fibers. Sample codes and descriptions are given in Table 2. For textile fabrics, the burst strength analysis is often applied in a planar form. Due to their constrained size, tubular samples cannot be tested using this implementation. For that reason, the burst pressure properties of the tubular graft structures are measured by custom design burst tester (Inovenso, Turkey, Figure 1) developed within the scope of the study. The following succinctly describes the measuring methodology for the burst pressure in the aforementioned device; the sample is secured to the ends, and pressure from the air inlets is applied to it.The pressure value is then read from the screen and recorded when the sample bursts.

3. Results and Discussion

Burst strength test results are given in the Table 3. As can be clearly seen from the table, the burst resistance of vascular graft samples with fiber orientation is considerably higher than those of samples with randomly distributed fibers. Examining the burst pressure readings of each sample group reveals that the fiber orientation increases the burst pressure value of each sample by two to three times. This situation is also encountered in vascular graft studies in the literature. Tubular grafts were created by McClure et al. (2009) using a variety of biomaterials, including neat PCL, PCL:silk, neat polydioxanone (PDO), and PDO:silk-based, at two distinct rotational speeds, 500 and 8000 rpm. According to the study, grafts produced at high rotational speeds (8000 rpm), independent of the kind of material used, had greater burst pressure value (3095, 2009, 3336, and 1256 mmHg for PCL, PCL:silk, PDO, and PDO:silk, respectively) with better-aligned fibers than grafts with randomly aligned fibers (2202, 1237, 1152 and 834 mmHg for PCL, PCL:silk, PDO, and PDO:silk, respectively) [13]. Grasl et al. (2021), on the other hand, produced thermoplastic polyurethane (PUR) and polylactid acid (PLLA) based vascular graft structures with both circumferential and axial fiber orientation as well as random fibers. In both PUR and PLLA graft samples, it was observed that the burst resistance was better on the surfaces with oriented fibers (894 mmHg for PUR, and 7641 mmHg for PLLA as circumferentially oriented, and 606 mmHg for PUR and 1587 mmHg for PLLA as axially oriented) compared to the surfaces with random fibers (200 mmHg for PUR, and 570 mmHg for PLLA) [14].

The ideal vascular graft should be similar to native arteries to minimize issues related to mismatch, have enough mechanical strength to resist arterial pressures, and pulse-rate blood flow to prevent aneurysms [15]. Moreover, human saphenous vein burst strength is frequently used as a benchmark for the burst strength of other manufactured grafts since it is considered the "gold standard" of vascular grafts [13]. The PCL100_O, PCLPLA50_O, and PLA100_O samples are found to be highly successful in terms of burst resistance and their burst pressure values are found greater than the burst resistance of the human saphenous vein which is 1599 mmHg [9,10].

Table 3. Burst pressure results of vascular graft samples with standard deviations (SD).

Sample	Burst Pressure ± SD (mmHg)
PCL100_O	1449,0±10,6
PCL100_R	730,3±94,45
PCLPLA50_O	2001,0±44,6
PCLPLA50_R	702,5±39,7
PLA100_O	2362,5±109,6
PLA100_R	936,5±10,6

On the other hand, the data also demonstrate how the type of biomaterial affects burst resistance. The PLA100_O and the PLA100_R are found to have the highest burst strengths among the all sample groups with orientated fibers and random fibers, respectively. This is a result of PLA's improved mechanical properties [16]. Although PLA has a great mechanical strength, its stiff structure prevents it from possessing the flexibility that vascular grafts should have [6]. PCL, on the other hand, has a relatively lower burst resistance than PLA. The beneficial effect of the PCL/PLA combination becomes

apparent at this point. As can be seen in Table 3, PCLPLA50_O has a sufficient burst resistance at about 2001 mmHg. In addition, it was noticed during testing that this sample (PCLPLA50_O) has a much more flexible structure than PLA100_O.

4. CONCLUSIONS

The purpose of the study is to produce PCL, PLA, and PCL/PLA-based vascular graft constructions in two different rotational speeds (at 200 and 10000 rpm) to test the burst strength of tubular structures with both orientated fibers and randomly distributed fibers. In order to develop a structure that closely mimics the behavior of the native vessel, it is first determined how fiber orientation and material selection influence burst pressure. When the results are examined, it is seen that oriented fibers are effective in burst resistance and PLA100_O has the highest value with 2362 mmHg. However, in native artery replacement, the elastic structure of the material is of great importance as well as the burst resistance of the material. Since the rigid structure of PLA does not match the characteristic elastic structure of the native artery, PCLPLA50_O sample is thought to be a more suitable substitute among the samples produced considering both properties. Nevertheless, examining the radial elasticity of the material to be used in vascular grafts is important in terms of material selection.

ACKNOWLEDGEMENTS

This study is supported by the TUBITAK (The Scientific and Technological Research Council of Turkey) under grant no: 121M309 and ITU Scientific Research Projects under grant no: 43368.

References

1. Ghiasi, M. M., Zendehboudi, S., & Mohsenipour, A. A. (2020). Decision tree-based diagnosis of coronary artery disease: CART model. Computer Methods and Programs in Biomedicine, 192, 105400. https://doi.org/10.1016/j.cmpb.2020.105400
2. Hao, D., Fan, Y., Xiao, W., Liu, R., Pivetti, C., Walimbe, T., … Wang, A. (2020). Rapid endothelialization of small diameter vascular grafts by a bioactive integrin-binding ligand specifically targeting endothelial progenitor cells and endothelial cells. Acta Biomaterialia, 108, 178–193. https://doi.org/10.1016/j.actbio.2020.03.005
3. Zhang, F., Bambharoliya, T., Xie, Y., Liu, L., Celik, H., Wang, L., … King, M. W. (2021). A hybrid vascular graft harnessing the superior mechanical properties of synthetic fibers and the biological performance of collagen filaments. Materials Science and Engineering C, 118(May 2020), 111418. https://doi.org/10.1016/j.msec.2020.111418
4. Spadaccio, C., Nappi, F., De Marco, F., Sedati, P., Sutherland, F. W. H., Chello, M., … Rainer, A. (2016). Preliminary in vivo evaluation of a hybrid armored vascular graft combining electrospinning and additive manufacturing techniques. Drug Target Insights, 10, 1–7. https://doi.org/10.4137/DTI.s35202
5. Yalcin, I., Horakova, J., Mikes, P., Sadikoglu, T. G., Domin, R., & Lukas, D. (2014). Design of Polycaprolactone Vascular Grafts. Journal of Industrial Textiles, 45(5). https://doi.org/10.1177/1528083714540701
6. Oztemur, J., & Yalcin-Enis, I. (2021). Development of biodegradable webs of PLA/PCL blends prepared via electrospinning: Morphological, chemical, and thermal characterization. Journal of Biomedical Materials Research - Part B Applied Biomaterials, 109(11), 1844–1856. https://doi.org/10.1002/jbm.b.34846
7. Oztemur, J., & Yalcin Enis, I. (2020). The Role of Biopolymer Selection in the Design of Electrospun Small Caliber Vascular Grafts to Replace the Native Arterial Structure. In A. Hayaloğlu (Ed.), Theory and Research in Engineering (First, pp. 167–192). Gece Kitaplığı.
8. Hiob, M. A., She, S., Muiznieks, L. D., & Weiss, A. S. (2017). Biomaterials and Modifications in the Development of Small-Diameter Vascular Grafts. ACS Biomaterials Science and Engineering, 3(5), 712–723. https://doi.org/10.1021/acsbiomaterials.6b00220

9. Konig, G., McAllister, T. N., Dusserre, N., Garrido, S. A., Iyican, C., Marini, A., … L'Heureux, N. (2009). Mechanical properties of completely autologous human tissue engineered blood vessels compared to human saphenous vein and mammary artery. Biomaterials, 30(8), 1542–1550. https://doi.org/10.1016/j.biomaterials.2008.11.011
10. Zamani, M., Khafaji, M., Naji, M., Vossoughi, M., Alemzadeh, I., & Haghighipour, N. (2017). A Biomimetic Heparinized Composite Silk-Based Vascular Scaffold with sustained Antithrombogenicity. Scientific Reports, 7(1), 1–14. https://doi.org/10.1038/s41598-017-04510-1
11. Gao, J., Chen, S., Tang, D., Jiang, L., Shi, J., & Wang, S. (2019). Mechanical Properties and Degradability of Electrospun PCL/PLGA Blended Scaffolds as Vascular Grafts. Transactions of Tianjin University, 25(2), 152–160. https://doi.org/10.1007/s12209-018-0152-8
12. Yalcin Enis, I., Horakova, J., Gok Sadikoglu, T., Novak, O., & Lukas, D. (2017). Mechanical investigation of bilayer vascular grafts electrospun from aliphatic polyesters. Polymers for Advanced Technologies, 28(2), 201–213. https://doi.org/10.1002/pat.3875
13. McClure, M. J., Sell, S. A., Ayres, C. E., Simpson, D. G., & Bowlin, G. L. (2009). Electrospinning-aligned and random polydioxanone-polycaprolactone-silk fibroin-blended scaffolds: Geometry for a vascular matrix. *Biomedical Materials*, *4*(5). https://doi.org/10.1088/1748-6041/4/5/055010
14. Grasl, C., Stoiber, M., Röhrich, M., Moscato, F., Bergmeister, H., & Schima, H. (2021). Electrospinning of small diameter vascular grafts with preferential fiber directions and comparison of their mechanical behavior with native rat aortas. *Materials Science and Engineering C*, *124*(October 2020). https://doi.org/10.1016/j.msec.2021.112085
15. De Valence, S., Tille, J. C., Giliberto, J. P., Mrowczynski, W., Gurny, R., Walpoth, B. H., & Möller, M. (2012). Advantages of bilayered vascular grafts for surgical applicability and tissue regeneration. *Acta Biomaterialia*, *8*(11), 3914–3920. https://doi.org/10.1016/j.actbio.2012.06.035
16. Pawar, R. P., Tekale, S. U., Shisodia, S. U., Totre, J. T., & Domb, A. J. (2014). *Biomedical Applications of Poly (Lactic Acid)*. 40–51.

FABRICATION AND CHARACTERIZATION OF ELECTROSPUN ANTHOCYANIN-LOADED POLYLACTIDE NANOFIBERS

Handan Palak[1] , Burçak Karagüzel Kayaoglu[1]

[1] Department of Textile Engineering, Faculty of Textile Technologies and Design, Istanbul Technical University, Gumussuyu Campus, Inonu Cad., No. 65, Istanbul, Turkey.
palakh@itu.edu.tr

Abstract:

In this study, morphological, chemical and thermal characteristics of biobased and biodegradable anthocyanin-loaded polylactide (PLA) nanofibrous membranes were investigated. To prepare electrospinning solutions, PLA was dissolved at a concentration of 10% (wv^{-1}) in a solvent system of chloroform/dimethylformamide (75/25% vv^{-1}), and anthocyanin at different concentrations (1, 2, and 3% wv^{-1}) was added into the polymer solutions. The prepared solutions were electrospun by using a single syringe electrospinning setup. The morphological, chemical and thermal structure of the neat and anthocyanin-loaded PLA nanofibrous membranes were characterized via Scanning Electron Microscopy (SEM), Fourier Transform Infrared Spectroscopy (FT-IR), and Differential Scanning Calorimetry (DSC), respectively. The FT-IR spectra proved the incorporation of anthocyanin into nanofibrous membranes successfully. It was observed that when anthocyanin was added into the polymer solution; bead-free nanofibers were produced, and when the concentration of anthocyanin was increased, mean fiber diameter increased as well. In addition, anthocyanin loading did not affect the crystallization behavior of PLA; however, the glass transition temperature (T_g) of the nanofibrous membranes including no anthocyanin in the structure was higher than those of the other membranes including anthocyanin.

Key words:

Polylactide (PLA), anthocyanin, nanofibers, electrospinning, bio-based

1. Introduction

Electrospinning is a practical technique to fabricate ultrafine polymer fibers in different diameters ranging from nanometers to micrometers by applying an electric field on the polymer solution. Electrospun nanofibrous membranes (ENMs) show unique characteristics, i.e., high specific surface area, high porosity, small pore size and high absorbance capacity [1]. ENMs can also be produced by incorporating various compounds such as pigments, nanoparticles, antimicrobials and drugs into the structure to improve their properties for use in different application areas.

The need of using sustainable and biobased polymers increases globally due to environmental concerns. PLA is a biobased, biodegradable and biocompatible aliphatic polyester, which is derived from renewable resources, i.e., corn starch and sugar cane. Due to its good mechanical and thermal properties, PLA is used in various engineering applications instead of petroleum-based polymers i.e., polyethylene terephthalate (PET) and polystyrene (PS) [12]. PLA was also used in the development of electrospun nanofibrous mats for biosensors [2], active food packaging [3, 4, 6,10] and pH indicator [7, 9] applications.

Anthocyanin from natural sources, i.e., black carrots, red cabbage, grape, blueberry, etc., is a water-soluble, non-toxic and commercially available natural pigment. It is stable against photodegradation and color resistant at higher temperatures. In addition, anthocyanin has strong bioactivities, including

antioxidant, anti-inflammatory, antibacterial activities [14]. It is mostly used for developing halochromic/pH-sensitive materials since it is able to change its color with the change of pH [8, 14].

In this study, it is aimed to develop biobased-biodegradable anthocyanin-loaded PLA nanofibrous membranes, and reveal the effect of anthocyanin loading on the morphological, chemical and thermal characteristics of the membranes. The proposed anthocyanin-loaded nanofibrous membranes have a potential to be further developed as pH-sensitive ENMs for protective clothing, filtration, wound dressings, and food packaging applications.

2. Experimental

2.1. Materials

Commercial grade of PLA (4060D) was supplied from NatureWorks LLC (USA) (Table 1). Chloroform (CHL, molecular weight: 119.38 g/mol, 99% purity, Sigma-Aldrich) and N,N-dimethylformamide (DMF, molecular weight: 73.09 g/mol, 99% purity, Sigma-Aldrich) were used as solvents (Table 2). Black carrot anthocyanin in powder form was supplied from GemmaNatural (Turkey).

Table 1. Properties of the PLA grade [12]

Grade	D-content (mol%)	Melt flow rate g/10min (210°C)	Molecular weight (kg/mol)	Polydispersity index
4060D (Amorphous)	12	7-10	190	1.9

Table 2. Properties of the solvents

Solvent	Boiling Point (°C)	Dielectric constant (ε)	Hansen solubility parameter, δ ($MPa^{1/2}$)
DMF	153	36.70	24.2
CHL	61	4.80	18.7

2.2. Methods

The polymer solutions were prepared by dissolving PLA at a concentration of 10% (wv^{-1}) in a binary solvent system (CHL/DMF: 75/25% vv^{-1}) for 4h at 50°C [4]. Anthocyanin at different concentrations (1, 2, and 3% wv^{-1}) was magnetically stirred in DMF for 2h. Then, it was added into the polymer solutions, and final polymer solutions including anthocyanin were ultrasonicated for 1h, then magnetically stirred for 16h at room temperature.

The prepared polymer solutions were used in an electrospinning device of Nanospinner24 (Inovenso) for producing nanofibrous mats. The applied voltage was in a range of 10-12 kV and tip-to-collector distance and feed rate were fixed at 12-13 cm and 2.5 ml/h, respectively. The nanofibrous mats were electrospun and deposited on a cylindrical rotary collector rotating at 60 rpm. Electrospun nanofibrous mats were produced at room temperature with a relative humidity (RH) of ~40-50%.

The morphology of nanofibrous membranes was examined with a Tescan Vega3 scanning electron microscope (SEM). Before imaging, samples were placed into a Quorum Sputter Coater to be coated with a thin layer of Au/Pd for 2 min. To measure the diameter of the nanofibers, SEM images were analyzed with ImageJ software. 100 measurements were taken on each sample, and average nanofiber diameters were calculated. In order to identify the bonds and functional groups of nanofibrous mats, Perkin Elmer Spectrum 65 FTIR-ATR spectrometer was used. In order to analyze the thermal and crystallization behavior of nanofibrous membranes, a differential scanning calorimetry (DSC), Perkin Elmer DSC400, was used. The samples were heated from 25°C to 200°C at a heating rate of 10°C/min and then cooled to 25°C at a rate of 10°C/min.

3. Results and discussion

3.1. Morphological analysis

SEM images of electrospun nanofibers are shown in Fig. 1(a–d). Bead formation was observed on the PLA nanofibers (Fig. 1a) since an inherent amorphous structure led to lower levels of polymer chain entanglement [13]. On the other hand, the viscosity increased after 1% wv^{-1} anthocyanin was added into the polymer solution; thus, bead-free uniform nanofibers were produced (Fig. 1b), and the mean fiber diameter increased from 327 ± 101 nm to 481 ± 90 nm. Similarly, once the concentration of anthocyanin was increased to 2% (Fig. 1c), and 3% (wv^{-1}) (Fig. 1d), uniform fibers having a larger mean diameter, i.e., 590± 130 nm and 629± 86 nm respectively, were produced.

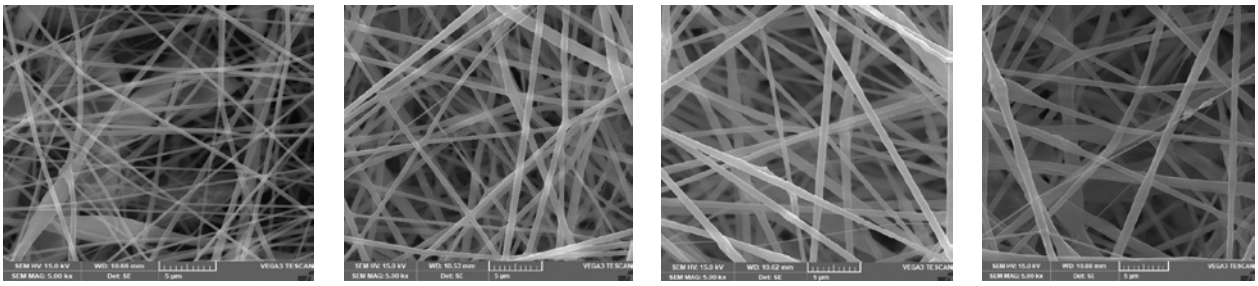

(a) **(b)** **(c)** **(d)**

Figure 1. SEM images and the fiber diameter distribution of nanofibers produced with 10% PLA including 0% (a), 1% (b), 2% (c) and 3% (d) (wv^{-1}) anthocyanin

3.2. FT-IR spectrum analysis

Figure 2a shows the FT-IR spectra of PLA and anthocyanin, whereas Figure 2b shows the FT-IR spectra of nanofibrous PLA membranes without any additive, and with anthocyanin. The spectra of nanofibrous membranes were similar to the spectrum of PLA since it is the dominant component of the nanofibrous membranes. Since the anthocyanin concentration was the highest, the specific band of anthocyanin at 3279 cm^{-1} was mainly remarkable in the FT-IR spectrum of PLA+3% anthocyanin membrane. Relatively strong bands were observed in the region of 1400 cm^{-1} to 1080 cm^{-1} for the nanofibrous membranes containing anthocyanin, proving the formation of C-O asymmetric stretching, C-O-C and CH_2 vibrations groups in the structure [5].

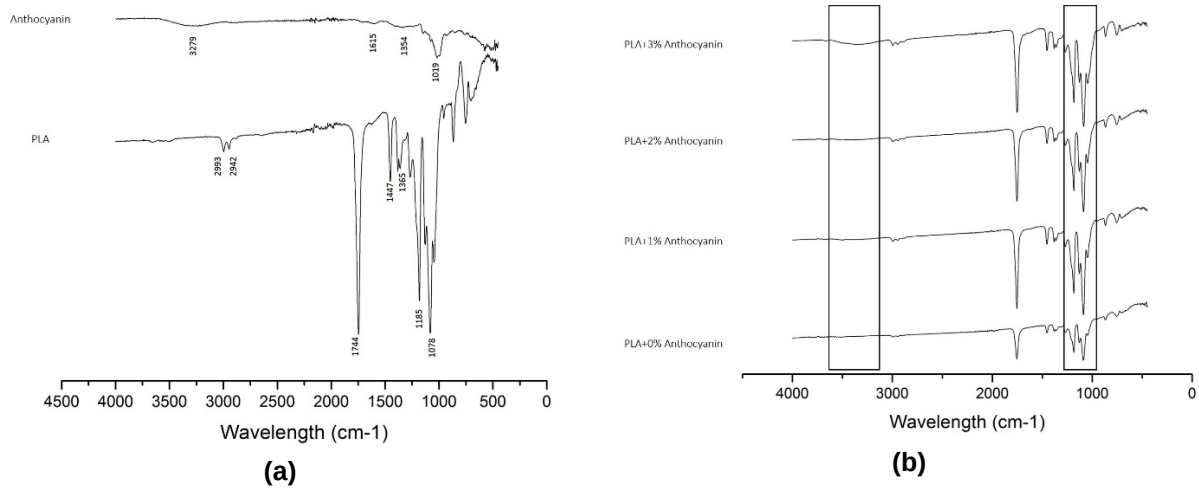

(a) **(b)**

Figure 2. (a) FT-IR spectra of PLA and anthocyanin, (b) FT-IR spectra of nanofibrous PLA mats with and without anthocyanin loading

3.3. DSC analysis

Figure 3 shows the DSC heating and cooling thermograms of the nanofibrous membranes. The nanofibrous membranes did not show any crystallinity even under such stretching force during fiber formation [13]. Moreover, the addition of anthocyanin did not affect the crystallization behaviour of PLA. The glass transition temperature (T_g) of nanofibrous membrane containing no anthocyanin in the structure was higher than those of the membranes containing anthocyanin. This may be attributed to the fact that natural pigment enters between polymer chains and acts as plasticizers by increasing polymer chain mobility [2].

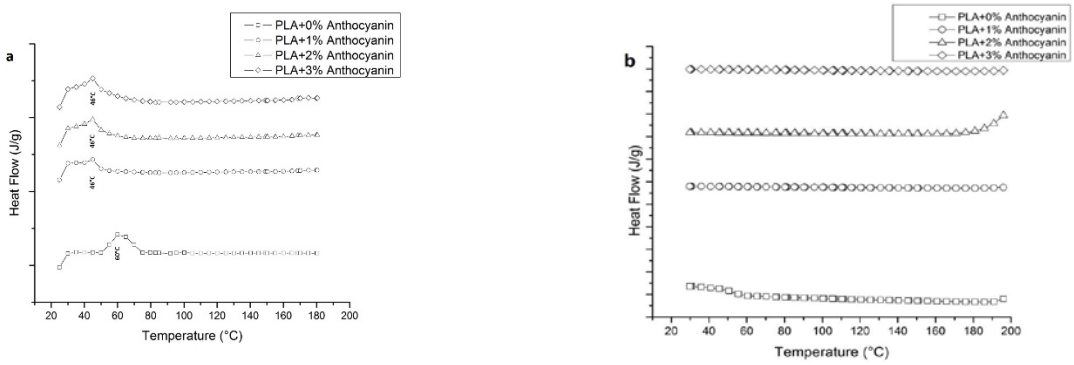

Figure 3. Differential scanning calorimetry heating (a) and cooling (b) thermograms of nanofibrous mats.

4. CONCLUSIONS

In this study, anthocyanin-loaded PLA based nanofibrous membranes were successfully produced by electrospinning method. SEM analysis indicated that PLA fibers were obtained at nanoscale. When the concentration of anthocyanin was increased, uniform fibers having a larger mean diameter were produced. FTIR analysis indicated that the spectra are mainly dominated by the characteristic peaks of PLA. The main peak of anthocyanin was also observed in the spectra, which means that it was successfully loaded into the nanofibrous membranes. The addition of anthocyanin did not affect the crystallization behaviour of PLA, and nanofibrous membranes did not show any crystallinity. The T_g of nanofibrous membrane which has no anthocyanin in the structure was higher than those of the other membranes containing anthocyanin due to plasticizing effect of the anthocyanin pigment. It was concluded that anthocyanin loading did not have a negative effect on the characteristic properties of PLA based nanofibrous membranes. For further studies, the proposed anthocyanin-loaded nanofibrous membranes can be developed as pH-sensitive ENMs for the applications areas of tissue engineering, protective clothing, filtration, and food packaging.

ACKNOWLEDGEMENTS

Authors acknowledge Istanbul Technical University Scientific Research Projects Fund under Grant No. BAP 43661 for the financial support.

References

1. *Agarwal, A., Raheja, A., Natarajan, T. S., & Chandra, T. S. (2012). Development of universal pH sensing electrospun nanofibers. Sensors and Actuators, B: Chemical, 161(1), 1097–1101.*
2. *Aliheidari, N., Aliahmad, N., Agarwal, M., et al. (2019). Electrospun nanofibers for label-free sensor applications. Sensors; 19(16): 3587.*
3. *Altan, A., Aytac, Z., & Uyar, T. (2018). "Carvacrol loaded electrospun fibrous films from zein and poly(lactic acid) for active food packaging", Food Hydrocolloids, 81, 48–59.*
4. *Aydogdu, A., Yildiz, E., Ayhan, Z., Aydogdu, Y., Sumnu, G., & Sahin, S. (2019). "Nanostructured poly(lactic acid)/soy protein/HPMC films by electrospinning for potential applications in food industry", European Polymer Journal, 112, 477–486.*
5. *Jaleel, K.A., Zubair, J.A., and Masa, J. M. A.-B. (2017). Effects of natural pigments on the poly(methyl methacrylate) biopolymer. J Cancer Sci Ther, 9(1).*
6. *Kayaci, F., Umu, C., Tekinay, T. & Uyar, T. (2013). "Antibacterial electrospun poly(lactic acid) (pla) nanofibrous webs incorporating triclosan/cyclodextrin inclusion complexes", J. Agric. Food Chem. 61, 3901−3908.*
7. *Kuntzler, S.G, Costa, J.A.V, Brizio, A.P.D.R.,& de Morais, M.G. (2020). Development of a colorimetric pH indicator using nano fibers containing Spirulina sp. LEB 18, Food Chemistry, 328, 126768.*
8. *Maftoonazad, N., & Ramaswamy, H. (2019). Design and testing of an electrospun nanofiber mat as a pH biosensor and monitor the pH associated quality in fresh date fruit (Rutab). Polymer Testing, 75, 76–84.*
9. *Moreira, J. B., Terra, A. L. M., Costa, J. A. V., & Morais, M. G. de. (2018). "Development of pH indicator from PLA/PEO ultrafine fibers containing pigment of microalgae origin", International Journal of Biological Macromolecules, 118, 1855–1862.*
10. *Munteanu, B.S, Aytac, Z., Pricope, G.M., Uyar, T. & Vasile, C. (2014). "Polylactic acid (PLA)/Silver-NP/VitaminE bionanocomposite electrospun nanofibers with antibacterial and antioxidant activity", J Nanopart Res, 16:2643.*
11. *Natureworks Ingeo (2022, October)* https://www.natureworksllc.com/Products
12. *Nofar, M., Maani, A., Sojoudi, H., Heuzey, M. C., & Carreau, P. J. (2015). Interfacial and rheological properties of PLA/PBAT and PLA/PBSA blends and their morphological stability under shear flow. Journal of Rheology, 59(2), 317–333.*
13. *Palak, H., Güler, E., Nofar, M., & Karagüzel Kayaoğlu, B. (2022). Effects of D-lactide content and molecular weight on the morphological, thermal, and mechanical properties of electrospun nanofiber polylactide mats. Journal of Industrial Textiles, 51(2S), 3030S–3056S.*
14. *Prietto, L., Pinto, V.Z., El Halal, S.L.M., Morais, M.G., et al. (2007). Ultrafine fibers of zein and anthocyanins as natural pH indicator. Journal of the Science of Food and Agriculture, 98, 2735-2741.*
15. *Sun, X. Zhoua,T. Weia, C., Lan, W., Zhao, Y. et al. (2018) Antibacterial effect and mechanism of anthocyanin rich Chinese wild blueberry extract on various foodborne pathogens, Food Control, 94 155-161.*

IMPROVING LOCAL THERMAL COMFORT IN BUILDINGS: A STUDY OF PROPERTIES OF HEATING TEXTILE COMPOSITES IN CONSTRUCTION INDUSTRY

Anna Kania, Marcin Barburski

Lodz University of Technology, Faculty of Material Technologies and Textile Design, Institute of Architecture of Textiles, ul. Żeromskiego 116, 90-543 Łódź Poland

Abstract:

The focus of this study is to analyze heating and insulating properties of textiles utilized in the construction industry. Research regarding textile heating composites typically centers around their use in the fashion industry and personal thermal comfort. Therefore, the study focuses on the application of textile heating composites as a method for improving the local thermal comfort of the user. The aim of this project was to analyze and describe the heating and insulating properties of electroconductive yarns and insulating textiles used in the construction industry. This goal was achieved by building physical samples that underwent heating tests. The next step was to compare the examined properties and select the best combination of yarn and fabric, which was then tested in the target environment. It was concluded that the best heating results are achieved with steel thread embroidered on fiberglass mesh and combined with extruded polystyrene that can be used to improve the local thermal comfort of the user.

Key words:

electroconductive yarns, heating, embroidery, personal thermal comfort, composite, building

1. Introduction

The search for new materials with better and better properties has led to the creation of a new group of materials known as composite materials. When designing innovative composite materials, they consider the operating conditions and the loads under which they will work. The rapidly growing industry related to the production of composite combines issues in the field of textiles, metallurgy, mechanics and chemistry of polymers, and plastics processing. [4]

A special field of composites is the combination of textiles and electronics, known as textronics. Programmable products can be produced through technical embroidery, weaving, or wreathing, and thanks to the use of flat textile products, they are flexible and portable. Popular applications of textronics are actively heating clothes or garments that measure basic life parameters. [1], [8], [10]

Heating textile composites have been described and tested mainly in the application of the fashion industry and personal thermal comfort products. [2], [9] For building heating usually used are classic heating systems with radiators connected directly to the power plant or to local water heating systems. [5], [7] Floor heating is used less frequently, usually in combination with one of the aforementioned heating methods, as an additional element increasing the local thermal comfort of the user. [11]

Thermal comfort is a mental state in which a person subjectively feels a sense of warmth. It depends on two kinds of factors:

- Thermal conditions, including air temperature, humidity, air movement, and radiant temperature, e.g., cool air near a window.
- Workers' individual personal factors, such as level of physical activity and clothing. Physical factors such as weight, gender, and age are also important variables. [6]

2. Experimental

2.1. Materials and fabrication procedures

A steel thread with a nominal electrical resistance of 27Ω per meter, a silvered thread with a nominal electrical resistance of 80Ω per meter, and a carbon rowing of unknown nominal electrical resistance were used to create a technical embroidery on a fiberglass mesh of 330g/m^2 density and 30mm thick extruded polystyrene was used as insulation material, covered with 5mm thick expanded polystyrene with an aluminum layer on top (Figure 1C). The polystyrene was combined with a designated glue, and the fiberglass mesh with the embroidery was then placed on top of it (Figure 1B) using heat-resistant and nonconducting glue. All fitting packet was cowered by Jacquard woven fabric. (Figure 1A)

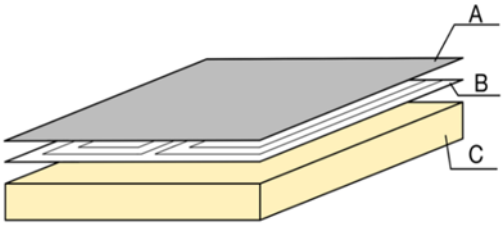

Figure 1. Schematics of samples. A – Jacquard woven fabric, B – heating embroidery on fiberglass mesh, C – extruded polystyrene

The first samples were made with a single thread as shown in Figure 2, in a shape of a square with 50 cm long sides and 1 cm distance between single lines for steel and silvered threads.

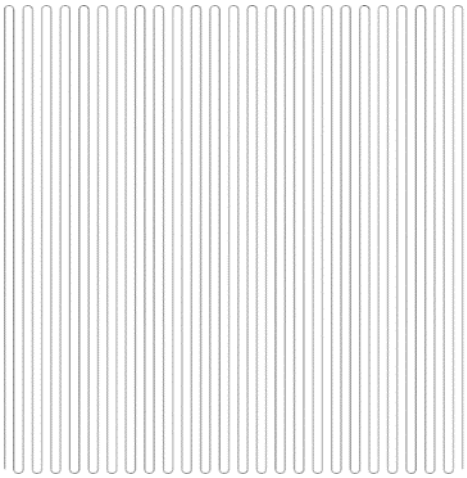

Figure 2. Pattern used to make first samples

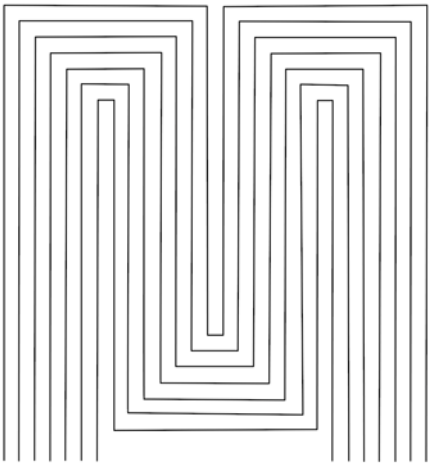

Figure 3. Pattern used to make second samples

The pattern was adjusted accordingly for the carbon rowing with 2 cm distance between the lines. Next samples were made with multiple threads, as shown in Figure 3, also in a shape of a square and 1 cm distance between single lines for steel and silvered threads, but with 30 cm long sides. The pattern was adjusted accordingly for the carbon roving with 1,5 cm distance between the lines. In samples made with the pattern from Figure 2, the ends were connected directly to the energy source, while in samples made with the pattern from Figure 3, the ends were connected to form a parallel circuit, and then connected to the power source. Samples were then covered with a layer of jacquard woven fabrics made by Marta Rzeźniczak (Institute of Architecture of Textile, Lodz University of Technology).

2.2. Experimental procedures

First samples were tested to measure the electric resistance and the minimum voltage needed for a heating effect. Then after adjusting the pattern, samples were made in different configurations: 1) steel

thread embroidered on fiberglass mesh, 2) embroidery on fiberglass mesh attached to polystyrene, 3) embroidery on fiberglass mesh attached to polystyrene and covered with the jacquard. Corresponding samples were made using carbon fiber. The samples were then connected individually to a DC power source with an effective voltage of 22V and were investigated under thermal camera ThermaCAM E65 for maximal temperature, the time needed to reach maximal temperature, and the time needed for cooling down to a temperature of 24°C. The temperature of the environment was 21,2°C. Then the steel thread sample covered with jacquard was tested for current-voltage characteristics and temperature as a function of voltage using the same DC source as before. The active power of the system was calculated using the current-voltage characteristic. The sample was also tested for heat conduction coefficient to see whether the embroidery and jacquard influenced the declared coefficient of extruded polystyrene (XPS).

3. Results and discussion

3.1. Minimal voltage

The samples were tested for approximate electric resistance to estimate the minimum voltage needed for the heating effect. The results were as follows: steel thread – 550Ω, carbon fiber - 640Ω, slivered thread - 3300Ω. Because of the significantly bigger resistance of the silvered thread, it was eliminated from further research as ineffective. The minimum voltage needed for the heating effect oscillated between 240V-300V. To reduce voltage to safe quantities, the pattern was adjusted to accommodate shorter lengths of threads and parallel circuits.

3.2. Thermal camera observation

Samples made with the adjusted pattern were observed under a thermal camera, as shown in Figure 4 and Table 1. The best results were achieved with steel thread covered with jacquard woven fabric. Despite longer heating time than just extruded polystyrene with steel thread embroidery on fiberglass mesh, it achieves a similar temperature and is more user-friendly – the electroconductive threads are covered, so there is no danger of accidental burn or short circuit. The carbon rowing heated up to lower temperatures needed more time to reach maximum temperature and cooled down faster. Overall, steel thread performed better, with shorter times of heating up and longer times of cooldown. The jacquard cover didn't have a big impact on the maximum temperature, slightly changing the heating curve in comparison to just the embroidery and polystyrene combination (Figure 4).

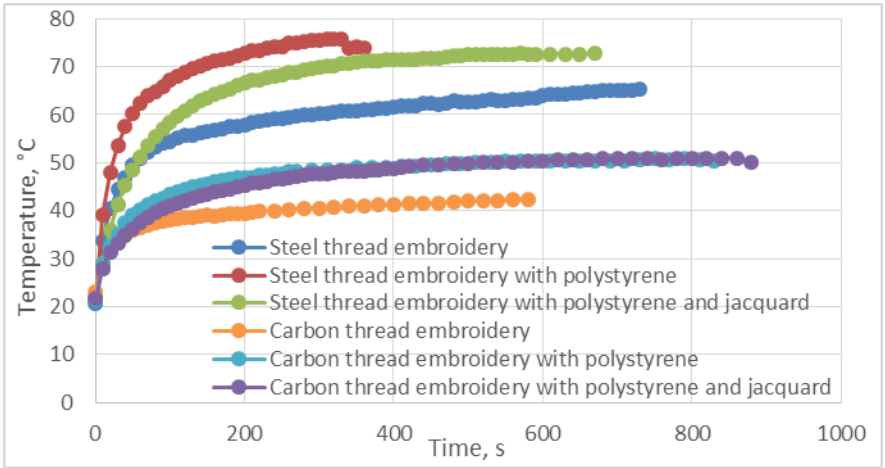

Figure 4. Comparison of temperatures and heating times of different samples

Table 1. Results of observation under a thermal camera

Lp	Sample	Maximal reached temperature, °C	Heating time, s	Cooling time, s
1	Steel thread embroidery	65,3	740	240
2	Steel thread embroidery with polystyrene	75,7	360	679
3	Steel thread embroidery with polystyrene and jacquard	72,9	670	943
4	Carbon thread embroidery	42,4	580	191
5	Carbon thread embroidery with polystyrene	50,9	830	567
6	Carbon thread embroidery with polystyrene and jacquard	51	880	732

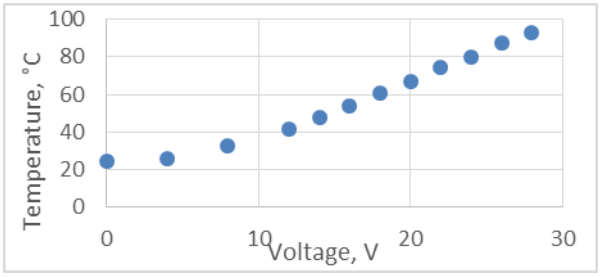

Figure 5. Temperature as a function of voltage for steel thread embroidery on fiberglass mesh with XPS and jacquard woven fabric

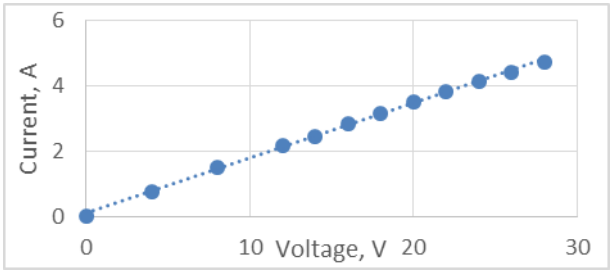

Figure 6. Current-voltage characteristic for steel thread embroidery on fiberglass mesh with XPS and jacquard woven fabric cover

3.3. Steel thread sample with jacquard woven fabric covering

After comparing results from previous tests, it was concluded that further research will be conducted on a sample made with steel thread with the jacquard covering. As shown in Figure 5, the maximal measured temperature within safe for humans voltages was 93°C. Apart from the initial heating voltage between 0V and 10V, the dependence between voltage and temperature is linear (Figure 6). It may prove to be useful in further research and developing control systems. The current-voltage characteristic on Figure 5. demonstrates that there are no statistically important differences in resistance due to heating. It was used to calculate the active power of the sample, as shown in Table 2. Comparing it with the power needed to heat a square meter of a room [3] it may be concluded that there should not be a significant difference between the energy efficiency of radiators and the presented composite.

Table 2. Active power as function of time

Temperature °C	25,8	32,8	41,5	47,5	53,8	60,6	67	74,2	79,5	87,5	93
Active power W	3,04	11,89	25,97	34,4	45,12	57,02	70,04	83,6	98,88	114,92	132,16

4. CONCLUSIONS

The presented study showcased the heating potential and characteristics of different electro-conductive threads. The samples were made using steel thread, silvered thread, and carbon roving, which were embroidered on fiberglass mesh. Then they were glued on extruded polystyrene and covered with jacquard woven fabric. Their electric resistance, heating potential and time, cooling time, and temperature as a function of voltage were measured. Current-voltage characteristic was made and used to calculate the active power of the sample. The main results are summarized below:

1. After comparing electric resistance and maximal temperatures reached by different threads, the steel thread was chosen as the overall best material for heating purposes.
2. There is no statistically significant difference between the performances of the sample on extruded polystyrene with the jacquard woven fabric cover and the one without the cover.
3. The studied composite has comparable active power to those of typical radiators, therefore being an equally energy-efficient source of heating.

Considering all the above, it can be concluded, that textile composites are a good mode of improving local thermal comfort.

ACKNOWLEDGEMENTS

The authors would like to thank Witold Grymin from the Department of Building Materials Physics and Sustainable Design, Lodz University of Technology for supporting them during this work and helping in laboratory work with a full of patience and kindness. The article was written when the first author was a student of E2TOP project at Lodz University of Technology.

References

1. *Bonaldi, R.R. (2018). High Performance Apparel. Woodhead Publishing (Cambridge)*
2. *Couto, S., Campos, J.B.L.M., Neves, S.F., Mayor, T.S., (2015). Advances in the optimization of apparel heating products: A numerical approach to study heat transport through a blanket with an embedded smart heating system, Applied Thermal Engineering, 87*
3. *Kacznow, S. (2022). Dobór mocy grzejników. Retrieved October 20, 2022. www.egrzejniki.pl*
4. *Long, A. C. (2007). Composites Forming Technologies. Woodhead Publishing (Cambridge)*
5. *Łukasiewicz, E., Shamoushaki, M. (2017). Heating potential of undeveloped geothermal water intakes in Poland in the context of sustainable development and air protection, Water Resources and Industry, 27*
6. *Pawłowski, K. (2017). Projektowanie ścian w budownictwie energooszczędnym. Grupa Medium (Warszawa)*
7. *Szulgowska-Zgrzywa, M., Piechurski, K., Stefanowicz, E., Baborska-Narożny, M. (2022). Multi-criteria assessment of the scenarios of changing the heating system in apartments in historical buildings in Wroclaw (Poland) – Case study, Energy and Buildings, 254*
8. *Tunakova, V., Gregr, J. (2010). Electrical conductivity measurements of fibers and yarns. Retrieved October 20, 2022. www.researchgate.net*
9. *Wang, F., Kang, Z., Zhou, J. (2019). Model validation and parametric study on a personal heating clothing system (PHCS) to help occupants attain thermal comfort in unheated buildings, Building and Environment, 162*
10. *Xue, P., Tao, X., Leung, M., Zhang, H. (2005). Wearable Electronics and Photonics. Woodhead Publishing (Cambridge)*
11. *Zembrowski, J. (2017). Sekrety tworzenia murowanych domów bez błędów. Biuro Doradztwa Budowlanego (Białystok)*

DESIGN AND INVESTIGATION THE OPERATION OF TEXTILE BASED ELECTRODES FOR ELECTROTHERAPY

Roya Aghadavood*, Radek Martinek*, Zahra Shahbaz, Tahereh Kheiri**, Mohsen Shanbeh****

*Department of Cybernetics and Biomedical Engineering, VSB - Technical University of Ostrava, 17.listopadu 2172/15, 708 00 Ostrava-Poruba, Czech Republic, +420774812276, roya.aghadavod.marnani.st@vsb.cz. radek.martinek@vsb.cz.

**Department of Textile Engineering, Isfahan University of Technology, Isfahan 84156-83111, Iran, +98-(0)31-33912425, +98-(0)31-33912444,z.shahbaz@tx.iut.ac.ir, t.kheiri@tx.iut.ac.ir, mshahnbeh@iut.ac.ir

Abstract:

Electrostimulation is a way of treatment various nerve and muscle injuries as well as acute and chronic pain conditions. The electrotherapy which is increasingly used in physiotherapy, muscle is exposed to an electrical pulse in order to activate excitable tissue using external electrodes with the aim of building muscle strength, enhancement healing, improvement in patient's mobility or reducing painTextile based electrodes are significantly noticed in the aspects of being flexible and re-usable and no needs of hydrogels, thereby avoiding skin irritation and allergic reactions and enhancing user comfort. This article presents a kind of textile based electrodes made of conductive yarns containing stainless steel/plyester blend fiber. The embroidery technique was used to prepare the textile based electrodes.Samples were examined on 10 people with pain in their bodies in a hospital without being moisturised. The purpose of this study is to asses the performance of 3 different textile based electrodes, considering the conductivity of the yarns which have been used to produce textile based electrodes, the usfulness of them for electrotherapy and comparing them with rubber electrodes commonly are used in clinics regularly.

Key words:

Electrostimulation, Electrotherapy, Rubber electrode, Textile electrodes, Conductive yarn, Embroidery.

1. Introduction

"Smart textiles" are novel topics in research area which is related to new generation of fiber assemblies and apparel systems that are able to react with, sense and be adapted to surrounding conditions or stimuli in a manual or programmed manner. Fiber and also textile based electronics have extreme flexibility as well as wearing comfort. In addition, their fabrication is low-cost and have environmentally friendly process by means of conventional facilities, often with no need of special conditions. The most relevant definition of smart textiles is textiles that interact external situations [7]**.** To date, conductive textiles or in another words electro-conductive textiles have wide variety of applications in smart textiles are currently under investigation by many researchers. There are three ways to make a fabric conductive, using conductive fiber materials, conductive fiber coatings, or conductive coating or finishing methods on the whole textile fabrics [2]**.**

Electrotherapy involves a wide range of techniques and devices and used as longterm treatment for post-acute rehabilitation patients delivered over a period of eight to sixteen weeks. In this type of therapy human body is exposed to a low-level current in order to become activated or stimulated. In contrast of internal electrodes used with in the body surface electrodes are applied on the skin. Among surface electrodes, the disposable rubber electrodes, need using an additional hydrogel or electrode cream as

an electrolyte interface between the skin and the electrode in order to improve skin contact and ensure a continuous current flow. As well as investigating the contact between the electrode and human skin, natural changes in the skin such as changes of humidity, temperature, structure should be paied atteintion. The surface resistance of the electrode must ne in a small value and also it is one of the most significant parameters of a proper electro stimulation process. In order to have a lower surface resistance yarns characterised by high conductivity for instance silver polyamide yarns or cotton yarns wrapped round by stainless steel can be used [10].

Previous works investigated suitable stimulation parameters using TENS electrodes, designed garments able to deliver functional electrical estimulation[9]. In spite of the majority medical use of rubber electrodes, they have been found to cause skin irritation, shocking and skin burns in some patients. While wearable conductive textile electrodes provide alternative, skin comfort and high elasticity for users. Baheti et al. dealt with the deposition of silver particle onto knitted fabrics for possible application in electrotherapy. A knitted fabric with deposited silver particles was used in electrotherapy and its operation on some properties as well as electrical conductivity, physiological comfort, antibacterial, and durability were investigated. When there is a variety of human body movements small electrical resistance changes were observed during the extension to 80% and as the results, it can be noticed that the electrical resistance will increase significantly after the 90% extension. Besides, as other findings of this paper, it can be noted that no significant changes in fabric properties such as air permeability, water vapor permeability, fabric porosity, and conductivity were observed [1].Three types of knitwear with a similar surface weight with different raw material composition were fabricated by Skrzetuska et al. Embroidery machine and film printing were used in stimulating electrode fabrication. Friction, washing and mechanical tests were investigated. As a result, they found that the best textile material for film printing process in electrode fabrication is viscose knitwear[8]. Garments with the ability to deliver functional electrical stimulation were designed by Moineau et al. Electrodes knitted by means of conductive yarn were moistened before use[6]. Another study on dry and wet textile electrodes in electrotherapy demonstrated that using dry electrodes can cause pain when the current is in a low range; on the other hand, the wet textile based electrodes which were tested alongside the dry and common hydrogel electrodes showed no sign of pain during the process which is due to pain-sensing fiber that can be activated more feasible with the dry electrodes than the wet and hydrogel ones [11]. Considering the differences between wet and dry electrodes, there is another study which confirms the preference of wet textile electrodes over the dry ones. Euler et al has compared six various of knitted electrodes in wet and dry state. The study shows that wet electrodes have less contact impedance than dry knitted electrodes. From the results it can be noted that dry textile electrodes have their best performance with an uneven surface. At the same time the wet textle based electrodes are more acceptable with a smooth surface. Nevertheless it is noticed that the dry textile based electrodes performance can be improved by putting pressure on the system[3]. Liu et al in a novel study has investigated a textile based electrode for electrotherapy which had an acceptable result in reducing pain on subjects[5]. Hunold et al has investigated a novel textile based electrode which is integrated with flexible caps; also a comparison between these novel electrodes and conventional rubber electrodes were studied. The results showed that the flexible cap used with textile based electrodes made them more comfortable as wearable electrodes[4].

2. Experimental

2.1. Materials

In this study textile based electrodes are made of Stainless steel/polyester staple fiber blend yarn (produced by Xiamen JL-fiber Science and Technology Co. Ltd., Xiamen, China). The fineness of stainless-steel fiber was 12 microns. Properties of the conductive yarns are presented in Table 1. Electrodes were made on a stretchable woven fabric in 6*6 square centimeter dimension. The weave design of this fabric was plain. Mass per unit area of the used fabric was 0.0113 g / cm^2. A couple of electrodes were prepared from each yarn, one of them as phase and the other one as zero, therefor we

had six samples that their features are noted in Table 2. Surface electrical resistance of each electrod were measured by using a foure prob. The warp yarn of based woven fabric was multifialment Polyester/Spandex(75den/20den) intemingled yarn. Weft yarn was Polyester/viscose(65/35%) ring spun yarn with linear density of 20 tex. The connector attached to the surface of each electrode by using conductive silver glue. Rubber electrodes has been used as reference one in order to evaluate the performance of the textile based electrodes. Prepared textile based electrodes are shown in Fig 1. A two-channel Berjis ST-90 physiotherapy system was used as an electricity resource to provide electrical current. That provided electrical current transferred to the surface of the textile based electrode through a wire which used as a connector. The rubber electrode is shown in fig 2.

Table 1. Properties of the yarn

Properties / Yarn Code	Blend Ratio (Stainless steel/PET)	Strength (cN/Tex)	Linear Resistance (Ω/cm)	Diameter (μm)	Extension (%)
A	80%/20%	32.22	5.31	447.14	6.78
B	40%/60%	120.05	23.07	249.46	3.24
C	28%/72%	125.84	29.82	248.25	3.08

Table 2. Properties of the samples

Electrode Code	Yarn Code	Surface electrical resistance ($\Omega/square$)	Weight (g)	Thickness (mm)
1	A	2.25	1.83	1.28
2	B	16.6	1.09	0.95
3	C	26	1.72	1.15

a) b) c)

Figure 1. Textile based electrodes: (a): The electrode from yarn C and its connector, (b): The electrode from yarn B and its connector, (c): The electrode from yarn A and its connector

Figure 2. Rubber electrode

2.2. Methods

In this study conductive yarns containing 28, 40 and 80 percent of stainless steel fibers and 72, 60 and 20 percent of polyester fibers, respectively were used to develop textile based electrodes with the dimension of 6*6 square centimeter. Conductive yarns were embroidered on mentioned fabric by means of Jack JK-9100B sewing machine. Moreover, connectors have been used in order to connect the textile electrodes to the two-channel Berjis ST-90 physiotherapy system. Textile based electrodes were placed on different parts of patient's body such as patient's arm, leg, calf, knee and back. As an example, electrodes position on the patient's arm is illustrated in Fig 3(a) and also Fig 3(b) shows textile based electrodes which was worn around the forearm of one of the authors. These textile based electrodes were located in wet spong pads. Spongy pads are shown in Fig 4.

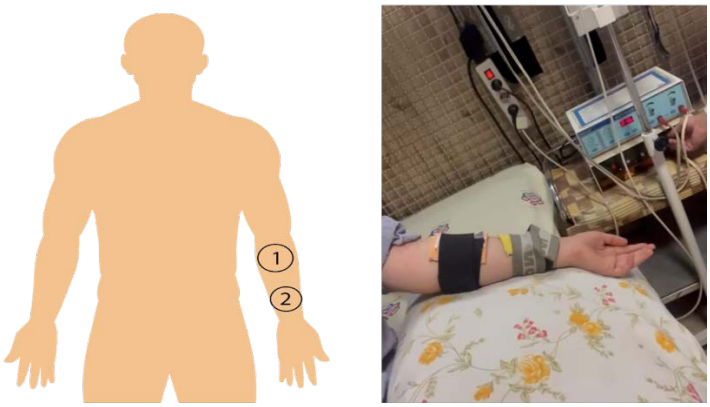

Figure 3. a) Electrodes positions on the patient's arm, b) Clinical test of textile based electrodes on forearm position

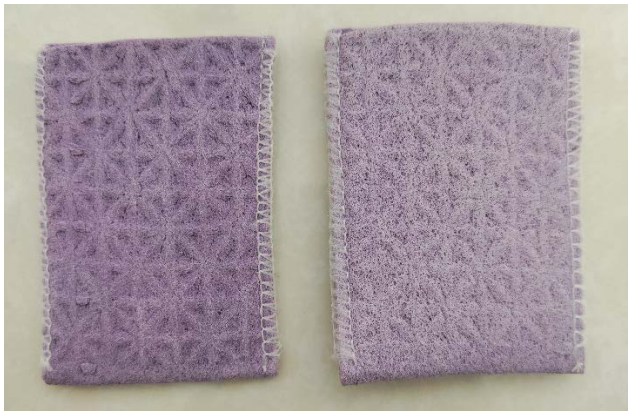

Figure 4. Spong pads

3. Results and discussion

In our experiments we compared the performance of textile based electrodes with conventional rubber ones. Results showed that textile based electrodes had a comparable performance with rubber electrodes during the electrotherapy. We confirmed that the textile based electrodes had a desirable current during the electrotherapy for all the patients on all parts of their bodies. According to the results, textile based electrodes illustrated similar electrical current with rubber electrodes as the patients were

therapied and no clear differences has been observed in the performance of rubber and textile based electrodes. The electrical conductivity of electrodes could be one of the main factors which has been considered in this study. The result revealed that the electrical current using dry textile electrodes did not increased as the conductivity increased and transferred current did not change. All the textile based electrodes with different conductivity performed equally.

4. CONCLUSIONS

In this study textile based electrodes, which prepared by swing conductive stainless steel yarns on a stretchable woven fabric by using Jack JK-9100B sewing machine, have been presented as an alternative for conventional rubber electrodes. Both electrodes were placed in a pad and no skin irritation was observed while using pad. The results showed that textile electrodes performed well throughout the therapy. Furthermore, according to the result, increasing the conductivity won't lead to improve textile electrodes efficiency in transferring the electrical current. Compared to the rubber electrodes prepared electrodes exhibited similar and comparable performance. It seems that the use of textile based electrodes for using in electrotherapy instead of conventional electrodes has many potential and in future we aim at work on the life time and durability of these electrodes and also effect of dimension and structure of them on their performance.

ACKNOWLEDGEMENTS

The authors would like to thank Dr. Saneie for his encouragement, support and cooperation in collecting data used in this study.

References

1. *Ali, A., Baheti, V., Militky, J., & Khan, Z. (2018). Utility of silver-coated fabrics as electrodes in electrotherapy applications. Journal of Applied Polymer Science, 135(23), 46357.*
2. *Ehrmann, A., & Blachowicz, T. (2017). Conductive yarns, fabrics, and coatings. In Examination of Textiles with Mathematical and Physical Methods (pp. 13-29). Springer, Cham.*
3. *Euler, L., Guo, L., & Persson, N. K. (2021). Textile electrodes: Influence of knitting construction and pressure on the contact impedance. Sensors, 21(5), 1578.*
4. *Hunold, A., Ortega, D., Schellhorn, K., & Haueisen, J. (2020). Novel flexible cap for application of transcranial electrical stimulation: a usability study. Biomedical engineering online, 19(1), 1-11.*
5. *Liu, M., Ward, T., Young, D., Matos, H., Wei, Y., Adams, J., & Yang, K. (2020). Electronic textiles based wearable electrotherapy for pain relief. Sensors and Actuators A: Physical, 303, 111701.*
6. *Moineau, B., Marquez-Chin, C., Alizadeh-Meghrazi, M., & Popovic, M. R. (2019). Garments for functional electrical stimulation: design and proofs of concept. Journal of Rehabilitation and Assistive Technologies Engineering, 6, 2055668319854340.*
7. *Persson, N. K., Martinez, J. G., Zhong, Y., Maziz, A., & Jager, E. W. (2018). Actuating textiles: next generation of smart textiles. Advanced Materials Technologies, 3(10), 1700397.*
8. *Skrzetuska, E., Michalak, D., & Krucińska, I. (2021). Design and analysis of electrodes for electrostimulation (TENS) using the technique of film printing and embroidery in textiles. Sensors, 21(14), 4789.*
9. *Tao, X. (Ed.). (2015). Handbook of smart textiles (pp. 293-316). Singapore, Springer.*
10. *Tokarska, M. (2011). Research of Textile Electrodes for Electrotheraphy. Fibres & Textiles in Eastern Europe, 19(5), 88.*
11. *Zhou, H., Lu, Y., Chen, W., Wu, Z., Zou, H., Krundel, L., & Li, G. (2015). Stimulating the comfort of textile electrodes in wearable neuromuscular electrical stimulation. Sensors, 15(7), 17241-17257.*

SOLUTION BLOWN OF PLA NANOFIBER CONTAINING OZONATED MORMODICA OIL AND ITS MICROCAPSULES TO OBTAIN ANTIBACTERIAL MEDICAL TEXTILES SURFACES

Koray Pektaş[1], Onur Balcı[1], Mehmet Orhan[2]

[1]Kahramanmaraş Sütçü İmam University, Faculty of Engineering and Architecture, Textile Engineering Department, Avşar Campus, 46100, Onikişubat/ Kahramanmaraş /Türkiye, koraypektas@ksu.edu.tr, +90 344 300 1644, +90 506 948 1683

[1]Kahramanmaraş Sütçü İmam University, Faculty of Engineering and Architecture, Textile Engineering Department, Avşar Campus, 46100, Onikişubat/ Kahramanmaraş /Türkiye, obalci@ksu.edu.tr, +90 344 300 1648

[2]Uludağ University, Faculty of Engineering and Architecture, Textile Engineering Department, Görükle Campus, 16059, Nilüfer/ Bursa/Türkiye, morhan@uludag.edu.tr, +90 224 294 1903

corresponding author e-mail: koraypektas@ksu.edu.tr

Abstract:

In the scope of the study, it was aimed to obtain antibacterial nanofiber surfaces containing Momordica oil, its ozonated oil form and its microcapsules forms. First of all, Mormodica oil was exposed to ozone gas for 135 min. After that, crude and ozonated mormodica oil were microencapsulated by using simple coacervation. Subsequently, %10 PLA polymer solution were prepared and used for obtaining PLA nanofiber surface by using solution blowing spinning. Besides, PLA polymer solution were mixed with crude mormodica oil, ozonated mormodica oil and their microcapsules forms and then these solutions were spun by using solution blowing spinning. Obtained ozonated oil, microcapsules and nanofiber surfaces were characterized via measurement of total unsaturated fatty acid amount in the oils, scanning electron microscope, FT-IR analysis and antibacterial activity test. The data showed that mormodica oil were ozonated. Microencapsulation process was done successfully and obtained nanofiber containing mormodica oil and its microcapsules. Moreover antibacterial activity showed that mormodica oil and ozonated mormodica oil showed antibacterial activity against to S.aureus and E.coli bacteria according to the disc diffusion method. The nanofiber surfaces containing ozonated oil and its microcapsules showed antibacterial activity against to S.aureus and E.coli bacteria according to the ASTM E 2149-01 method. As a result, it was obtained biodegradable nanofiber containing microcapsules and showing antibacterial activity.

Key words:

Solution blowing spinning, PLA, ozonated oil, microencapsulation, antibacterial activity

1. Introduction

Recently, the ozone (O_3) is applied to treat many illnesses such as cellulite, burnt, ulcer, chronic wounds, immune system illnesses etc. On examining these treatments, it is seen that the ozone is used both directly and ozonated vegetable oils in treatment of illnesses. However, comparing to ozone gas and the ozonated water, the ozonated oils have an advantage that the ozone is bonded to oil via unsaturated

fatty acids. Thus, the ozone could be stored as ozonide and its effect goes a long [1-3]. The ozonides, which show anti-bacterial and anti-fungal activity, carry O_2 into lesion without sparking off skin irritation [4].

On the other hand, the microencapsulation is a preferable method to transfer ozonated oil onto textile surfaces. The microencapsulation is a caging method that liquid or solid particles, which are located small droplets, are hindered in a thin film. The microencapsulation is formed by many methods such as in-situ polymerization, interfacial polymerization, coacervation, spray drying etc. [1,5]. But the coacervation methods are common to encapsulate oils among them [6].

Solution blown technique is a spinning method that inspired from both meltblown and electro spinning method, generate micro and nanofiber surfaces [7]. On examining literature on solution blowing spinning, there are much more studies on nanofiber spinning while there are a few studies on medical textile surfaces [8-11].

In this study, it was aimed to obtain biodegradable antibacterial nanofiber surfaces containing Momordica oil, its ozonated oil form and its microcapsules forms. To get these functionality, mormodica oil, ozonated mormodica oil and their microcapsules were mixed PLA polymer solution and spun together. After that, a set of tests and analyses were employed both mormodica oil and obtained nanofiber surface.

2. Experimental

2.1. Materials

In the scope of this study, mormodica oil and its ozonated form were used as an active material. Arabic gum was used as shell material for microencapsulation process. PLA polymer was used for obtaining biodegradable nanofiber surfaces. Chloroform was used for dissolving the PLA polymer. 30 g/m^2 Polypropylene non-woven surfaces was used as a ground surface to collect PLA nanofiber.

2.2. Methods

Crude mormodica oil were exposed to ozone gas for 135 min in a glass reaction column and then ozonated mormodica oil obtained (Figure 1).

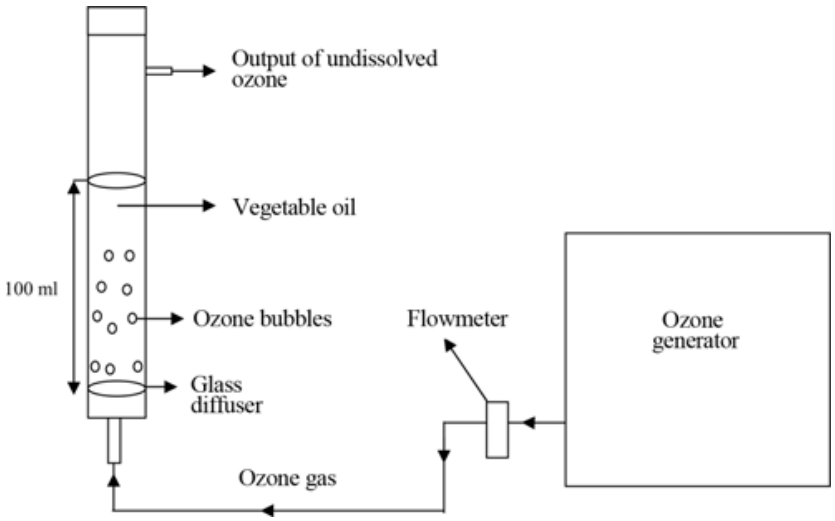

Figure 1. Schematic drawing of the ozonation process

As for the microencapsulation of the crude and ozonated mormodica oil, simple coacervation method was used and flow chart of the microencapsulation process was given in Figure 2.

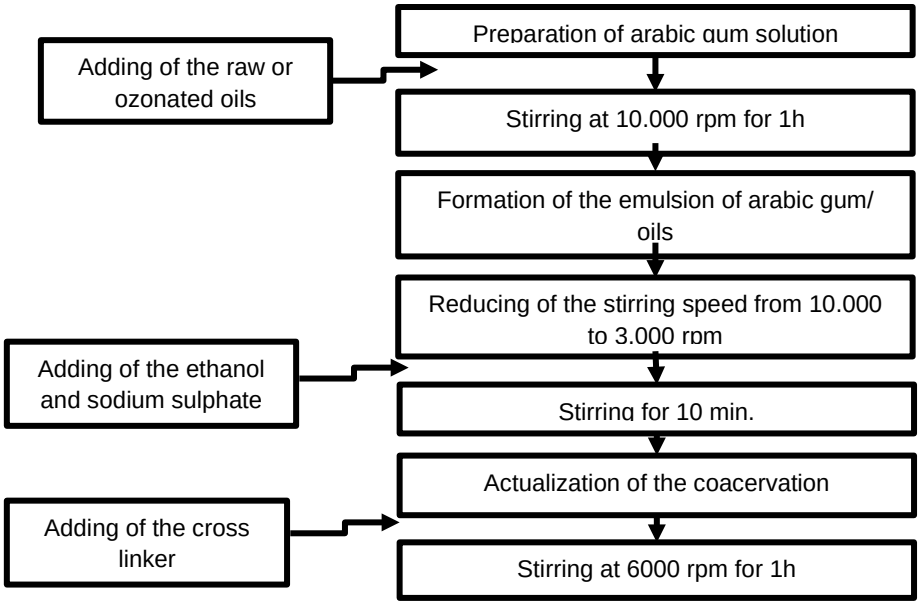

Figure 2. Flow chart of the microencapsulation process

Solution blowing spinning was used for obtaining PLA nanofiber. With this purpose, 10g PLA polymer was dissolved in the chloroform (100ml) for 2 hours at 60℃. Then the polymer solution was cooled to room temperature. After that solution blowing spinning parameters were adjusted and PLA nanofiber were obtained. To obtain PLA nanofiber containing oil and microcapsules, 1 ml oil or microcapsule solution poured into the 20 ml PLA polymer solution. Then fiber spinning containing oil or microcapsules were employed. Fiber spinning parameter of the solution blowing spinning were given below.

- Solution feeding rate: 10ml/h.
- Air pressure: 2 bar
- Working distance: 37 cm
- Working time: 30 min.
- Distance between inner and outer nozzle: 2 mm

As for the characterization of the oils, total unsaturated fatty acid amount was determined by using GC and FT-IR analyses was done to observe change of the spectrum after ozonation process. Besides, disc diffusion method was used for investigating antibacterial activity of the oils. SEM images were taken for observe nanofiber morphology. Antibacterial activity of the nanofiber surfaces was analyzed according to the ASTM E 2149-01.

3. Results and discussion

Total unsaturated fatty acid amounts of the oil were given in Table1.

Table 1. Total unsaturated fatty acid amount of the oils

Unsaturated fatty acid (%)	Mormodica oil	Ozonated mormodica oil
Oleic acid	42,457	11,413
Linoleic acid	38,949	3.309
Total unsaturated fatty acid amount	81,406	14,722

Total unsaturated fatty acid amount of the oils showed that unsaturated fatty acid amount decreased after ozonation process. Because the bound of the =C-H in the crude oil were broken and replace C-O bound. during the ozonation process. To support this hypothesis, FT-IR spectrum of the oil were investigated. FT-IR spectrum of the oil (Figure 3) showed that C-O bound was seen at 1100cm^{-1} after ozonation process and it was proof of the ozonation of the mormodica oil was done successful.

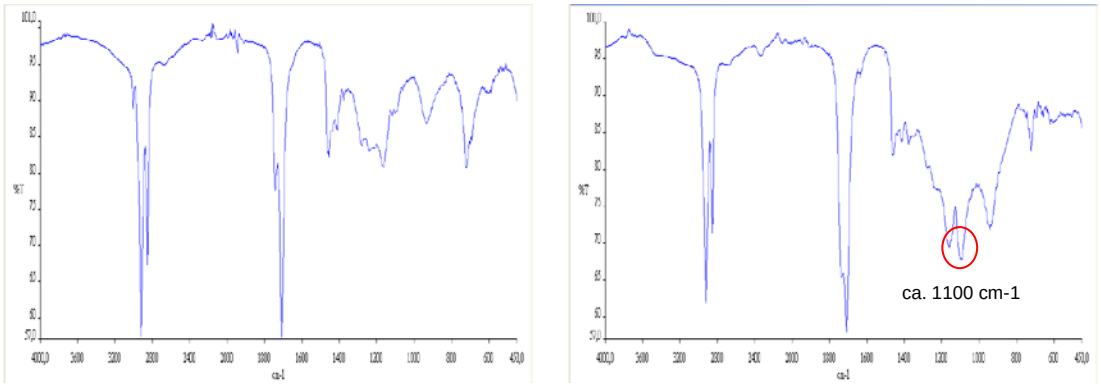

a. b.

Figure 3. FT-IR spectrum of the oil a.mormodica oil b. ozonated mormordica oil

On examining of the antibacterial activity of the crude and ozonated mormodica oil (Table 2), it was seen that both of them had antibacterial activity against to both gram negative (*E.coli*) and gram positive (*S.aureus*) bacteria with different inhibition zone. Besides, it was seen that antibacterial activity of the ozonated mormodica oil was higher than the crude one.

Table 2. Antibacterial activity of the crude and ozonated mormodica oil

Oil Sample	Inhibition zone diameter (mm)	
	S.aureus	E.coli
Crude mormodica oil	100	100
Ozanated mormodica oil	160	130

After characterization of the mormodica oil and ozonated one, PLA nanofiber surface were observed via SEM images. Upon observing of the PLA nanofiber morphology, it was seen that ground non-woven surfaces had micrometer fiber diameter while crude PLA fiber, containing oil and microcapsules ones had nanometer fiber diameter but some beads formations were observed. It was thought that nanofiber spinning parameter could change to hinder bead formations. Moreover, it was seen that microcapsules in the PLA nanofiber were seen as spherical shape.

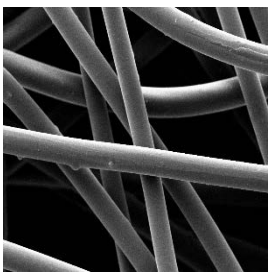

30 g/m^2 Polypropylene

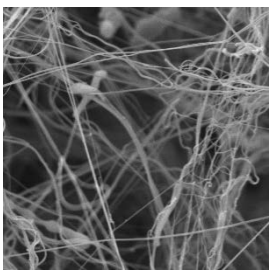

Crude PLA nanofiber

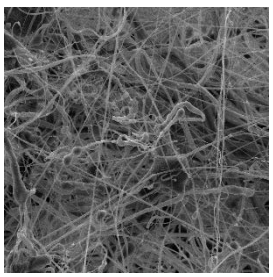

PLA nanofiber containing mormodica oil

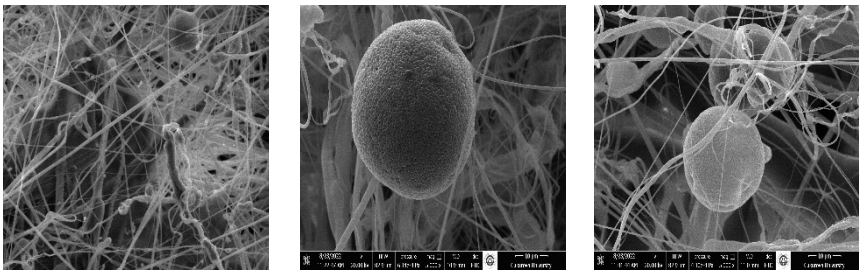

PLA nanofiber containing ozonated mormodica oil | PLA nanofiber containing mormodica oil microcapsules | PLA nanofiber containing ozonated mormodica oil microcapsules

Figure 4. SEM images of the nanofiber

Antibacterial activity of the polypropylene non-woven and nanofiber surface against to gram negative (*E.coli*) and gram positive (*S.aureus*) bacteria showed that all surface had the antibacterial activity. However, of all the sample, PLA nanofiber containing crude mormodica oil and ozonated one had higher antibacterial activity against to *S.aureus.* On the other hand all sample did not show antibacterial activity against to *E.coli (Table 3). This situation could be explained by lack of the amount of oil in the nanofiber. Because it was seen that antibacterial activity of the oil increased in tandem with the escalading of the oil amount according to the disc diffusion method. Thus, the more oil is contained in the nanofiber, the more antibacterial activity is observed.*

Table 3. Antibacterial activity of the non-woven and nanofiber surfaces

Sample	Bacteria reduction/proliferation (%)	
	S.aureus	***E.coli***
Polypropylene ground non-woven surface	-88,25	-11,48
PLA nanofiber	-83,51	-12,41
PLA nanofiber containing mormodica oil	-99,37	-11,11
PLA nanofiber containing ozonated mormodica oil	-100,00	-40,74
PLA nanofiber containing mormodica oil micro capsules	-81,40	-11,67
PLA nanofiber containing ozonated mormodica oil micro capsules	-98,72	-10,19

4. CONCLUSIONS

In the scope of this study, ozonated oil showing antibacterial activity were obtained. After that, crude and ozonated mormodica oil were microencapsulated via simple coacervation successfully. PLA nanofibers were spun by solution blowing spinning. Moreover, PLA nanofiber containing oil and microcapsules were spun successfully but some beads formation in the surfaces was observed. Nevertheless, All surface show antibacterial activity against to *S.aureus* while they did not show antibacterial activity against to *E.coli.* For further studies, it is thought that fiber formation parameters of the solution blowing spinning for PLA polymer will investigate deeply and will try to obtain antibacterial activity of the surfaces against to gram negative bacteria (*E.coli*).

ACKNOWLEDGEMENTS

This study (5220045) is funded by The Scientific and Technological Research Council of Turkey, Republic of Turkey (TUBITAK). We would like to thank warmly TUBITAK for supporting this study

References

1. Beşen, B. S., Güneşoğlu, C., Balci, O., & Sütçü, K. (2016). Antibacterial Finishing of 100% Cotton Fabric with with β-Cyclodextrin-Ozonated Olive Oil Inclusion Complex. AATCC Journal of Research, 3(6), 12–18. https://doi.org/10.14504/ajr.3.6.3
2. Beşen, B. S., Güneşoğlu, C., Balci, O., Sütçü, K., Balcı, O., Güneşoğlu, C., İrem Tatlı, I. (2016). Obtaining medical textiles including microcapsules of the ozonated vegetable oils. AATCC Journal of Research, 3(6), 12–18. https://doi.org/10.1007/s12221-017-1212-8
3. Sancar BEŞEN, B., Balci, O., Orhan, M., Güneşoğlu, C., İrem TATLI, İ., Sütçü İmam Üniversitesi, K., … Botanik Anabilim Dalı, F. (2015). Ozonlanmış Yağlar ile İşlem Uygulanmış Dokusuz Yüzeylerin Antibakteriyel Etkinliklerinin İncelenmesi An Investigation on Antibacterial Activities of Nonwovens Treated with Ozonated Oils. Journal of Textiles and Engineer, 22(100), 25. https://doi.org/10.7216/1300759920152210003
4. Öcal, E., (2013), Ozon Yağının Kapsül Formasyonu Üzerindeki Etkisi. Uzmanlık Tezi. Hacettepe Üniversitesi Tıp Fakültesi. Ankara. s.14
5. Karthikeyan, M., Ramachandran, T., Shanmugasundaram, O.L., (2014), "Synthesis, Characterization, and Development of Thermally Enhanced Cotton Fabric Using Nanoencapsulated Phase Change Materials Containing Paraffin Wax", The Journal of The Textile Institute, DOI: 10.1080/00405000.2014.886368
6. Özyıldız, F., Karagönüllü, S., Basal, G., Uzel, A., Bayraktar, O., (2012), "Micro-encapsulation of Ozonated Red Pepper Seed Oil with Antimicrobial Activity and Application to Nonwoven Fabric", The Society for Applied Microbiology, Letters in Applied Microbiology, vol.56, pp.168-179.
7. Medeiros, E. S., Glenn, G. M., Klamczynski, A. P., Orts, W. J., & Mattoso, L. H. C. (2009). Solution blow spinning: A new method to produce micro- and nanofibers from polymer solutions. Journal of Applied Polymer Science, 113(4), 2322–2330. https://doi.org/10.1002/app.30275
8. Calisir, M. D., & Kilic, A. (2020). A comparative study on SiO2 nanofiber production via two novel non-electrospinning methods: Centrifugal spinning vs solution blowing. Materials Letters, 258, 126751. https://doi.org/10.1016/j.matlet.2019.126751
9. Polat, Y., Calisir, M., Gungor, M., Sagirli, M. N., Atakan, R., Akgul, Y., … Kiliç, A. (2019). Solution blown nanofibrous air filters modified with glass microparticles. Journal of Industrial Textiles, 1–14. https://doi.org/10.1177/1528083719888674
10. Shi, L., Zhuang, X., Tao, X., Cheng, B., & Kang, W. (2013). Solution blowing nylon 6 nanofiber mats for air filtration. Fibers and Polymers, 14(9), 1485–1490. https://doi.org/10.1007/s12221-013-1485-5
11. Sinha-Ray, S., Sinha-Ray, S., Yarin, A. L., & Pourdeyhimi, B. (2015). Application of solution-blown 20-50nm nanofibers in filtration of nanoparticles: The efficient van der Waals collectors. Journal of Membrane Science, 485, 132–150. https://doi.org/10.1016/j.memsci.2015.02.026
12. Liu, Y., Zhang, G., Zhuang, X., Li, S., Shi, L., Kang, W., … Xu, X. (2019). Solution blown nylon 6 nanofibrous membrane as scaffold for nanofiltration. Polymers, 11(2), 1–15. https://doi.org/10.3390/POLYM11020364

CHITOSAN ADDED COMPOSITE VISCOSE YARN AND ITS POTENTIAL APPLICATION FOR DENIM FABRIC DEVELOPMENT

Ahmet Korkmaz[1], Osman Babaarslan [2]

[1]R&D Department, Çalik Denim Textile AŞ., Yeşilyurt, Malatya, Turkey
[2]Cukurova University, Department of Textile Engineering, Adana, Turkey
ahmet.korkmaz@calikdenim.com.tr
teksob@cu.edu.tr

Abstract:

The rapid increase in consumption has led to the decrease and even extinction of natural resources on earth. The textile industry also has an important place in terms of consumption. The transition to more sustainable biodegradable products instead of established fossil-based materials has increased rapidly due to textile manufacturers and related industries, legal regulations, social responsibility commitments and increasing ecological awareness of customers. Developing new environmentally friendly, biodegradable material groups with new technologies or by modifying existing technologies has been the main goal of many researchers. In this context, we aimed to develop denim fabric that is effective against strong hospital bacteria by using the yarn containing biopolymer chitosan as a weft in denim production.
Chitosan finds wide application in the textile industry due to its biodegradability, antibacterial activity and many more functionalities. Chitosan is used in biomedical textile applications in the textile industry, either as a wound healing, hemostatic (blood stopper), antibacterial, antifungal, either alone or modified to various derivatives or combined with other materials. In this context, instead of using chitosan as a coating material in our studies, chitosan-containing yarn was used in the production of denim fabric in order to distribute the chitosan more homogeneously and to increase the washing resistance. As a result, it was determined that the denim fabric developed by using chitosan-based yarn in weft in denim production reduces hospital bacteria (MRSA-Methicillin resistant staphylococcus aureus) by > 99%.

Key words:

Chitosan, antibacterial, denim fabric, biodegradability, MRSA, medical textiles

1. Introduction

Seafood producing companies around the world throw large quantities of crab and shrimp shells into the environment without reuse. In recent years, intensive studies of researchers about the reuse of wastes has also included shrimp and crab shells, and these wastes are evaluated by chemical or biological methods and new products are obtained. Chitin and its most important derivative, chitosan, are among the products obtained in this way. The wastes of the shrimps, whose meat is separated in the processing plants, constitute approximately 40-56% of the total product. Shell wastes also contain very valuable bioactive components such as antioxidants, peptones, amino acids, peptides, proteins, minerals, enzymes, lipids and other beneficial nutrients. The raw material requirement for the production of chitin is met from shrimp (56,000 tons), various shellfish (39,000 tons), mushrooms (32000 tons), oysters (23000 tons). In Figure1, the production process of the chitin is shown.

Figure 1. Production process of chitin (5)

Chitosan is a biopolymer obtained by deacetylation of chitin (β-(1-4)-poly-N-acetyl-D-glucosamine), which is the most common in nature after cellulose. In Figure 2, the production process of the chitin with the chemical method is shown.

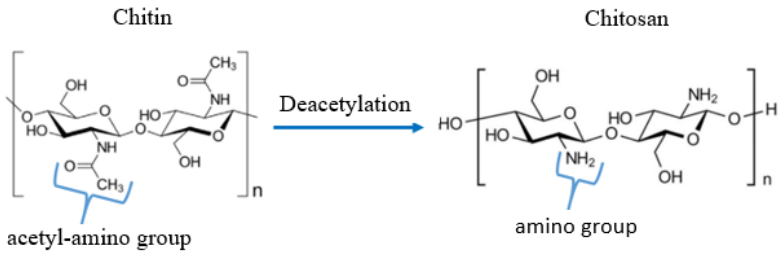

Figure 2. Chitosan from chitin via deacetylation (5).

Chitosan, a natural biopolymer with biocompatible, non-toxic and antibacterial properties, can be used in different forms such as solution, powder, fiber and film (12). The reason for the analgesic effect of chitosan is due to its polycationic structure. The biodegradability of chitosan is due to the fact that chitosan is not only a polymer carrying amino groups, but also a polysaccharide, which as a result contains brittle glycosidic bonds. (7).

The presence of amino groups in the chitosan structure (Figure 3) distinguishes it from chitosan, and this difference gives the polymer many special properties. The amino groups in the chitosan structure can be protonated by providing solubility in diluted acidic aqueous solutions. In contrast, the practical applications of chitin, if any, are extremely limited due to its poor solubility (2).

In addition, due to these amino groups, chitosan efficiently complexes various species such as metal ions and is therefore often used in wastewater treatment, purification by recovery of heavy metals (Rinaudo 2006).The hemostatic property of chitosan can also be associated with the presence of positive charges present in chitosan. This is because the membranes of red blood cells are negatively charged and therefore can interact with the positively charged chitosan. The fact that chitin has less hemostatic properties than chitosan tends to confirm this explanation (2).

Chitosan can be converted into many forms such as hydrogel, sponge, membrane, film, depending on the area of use. As it is known, sponges are open-pore foams and can absorb large amounts of liquid due to their microporosity. Chitosan-based sponges are mostly used as wound-healing materials, as they can absorb wound exudates while aiding tissue regeneration. Chitosan sponges also find application in bone tissue engineering as filling material (9, 8).

Stegmaier et al. investigated the use of chitosan as a sizing agent with appropriate modification in the textile industry. As a result of these studies, economic and ecological advantages in sizing have been demonstrated by increasing the weaving efficiency based on the reduction of yarn breaks with chitosan-based sizing (11).

The use of chitosan as an absorbent in the removal of dyes to treat textile wastes has been investigated. In this context, chitosan was found to be very effective in removing dianix orange S-G, a disperse dye, from wastewater. Dye removal was carried out using the ability of chitosan to dissolve in acidic medium and reform in basic medium (14).

Chitosan has been used as an aid to increase the uptake of anionic dyes in textile dyeing. Chitosan is used instead of salt in reactive dye dyeing of cotton fabric. Cellulosic fiber takes a negative charge in the aqueous medium and repels the negatively charged dye anion during dyeing. Such repulsion between fiber and dye is avoided by using salt in the dyebath for reactive dyes.

By treating cotton fabric with chitosan, Ashenafi et al. revealed that surface modification of cotton provides better dyeing properties and the best possibility for salt-free dyeing of cotton may be the use of chitosan (1).

Erdoğan et al. aimed to develop a new generation of environmentally friendly antibacterial finishes by using chitosan as a binder for nano-silver coatings. In the study, chitosan formed a colorless film and formed a matrix that allowed nano-Ag particles to accumulate homogeneously on the fabric surface, and as a result, a very strong anti-nacterial effect was observed (4).

Chitosan can be crosslinked with cellulose using polycarboxylic acids, thus providing better bonding between chitosan and cotton fabric. A good wrinkle recovery was obtained in cotton as a result of the cross-linking of chitosan and cellulose by polycarboxylic acids (13).

Ivanova et al. developed super hydrophobic and anti-bacterial textiles using chitosan-based nanoparticles for biomedical applications (6). In their studies, Raeisi obtained superhydrophobic cotton fabrics by using chitosan and titanium dioxide (TiO_2) nanocomposites (10).

MRSA (also known as supervirus) stands for methicillin-resistant Staphylococcus. MRSA is a "staph" germ (bacteria) that does not get better with the type of antibiotics that usually cure staph infections. These kind of staph germs are spread by skin-to-skin contact. Healthcare personnels or visitors to a hospital may carry staph germs on their body which can spread to a patient. After entering to the body through open wounds, burns or cuts can this staph germ spread to bones, joints, the blood, or any organ, such as the lungs, heart, or brain and can cause serious health problems. If we list the groups at risk in addition to healthcare personnel: athletes who share items such as towels or razors, draggie, people who had surgery in the past year, children in day care, members of the military.

Denim is a textile product that can be worn by people of all ages and kinds. From this point of view we aimed to developped a denim fabric, which controbute to reduction of super virus MRSA spreading among both healthcare personnel, hospital visitors and above mentioned people at risk. In line with this purpose we used chitosan containing weft yarn in denim.

2. Experimental

2.1. Materials

The application of chitosan to cotton fabrics has mostly been in the form of microcapsules of powdered chitosan or in the form of coating by dissolving in acid. In order to make chitosan more homogeneous and permanent in denim fabric, chitosan-based yarn was supplied in this study. For the denim production was used Ne 30/1 chitosan-based yarn as weft.

The physical properties of chitosan containing yarn as weft in denim production are shown in table 1. When yarns are compared especially in terms of hardness and elongation, it is seen that chitosan-based yarn is better.

Table 1. The physical properties of in denim production used yarn.

Yarn	Ne	%U	Hairness	Elongation	Stiffness
Chitosan viscose yarn	30/1	10,1	4,73	9,21	17,96
Combed cotton yarn	30/1	10,5	5	5,5	15,5-16

2.2. Methods

The developed denim with chitosan rayon yarn and cotton yarn in weft is weaved according to procedure in table 2. The processes applied to the weaved denim fabrics are summarized in Figure 3.

Table 2. Weaving procedure

	Warp Yarn	Warp Yarn Number Ne	Weft Yarn	Weft Yarn Number Ne	Weft density	Weaving Type	Warp Wire Count	Comb Width	Comb No/Number of wire through
Sample 2	%100 CO	20/1	%100 CO	30/1	27,5	3/1 Z	5880	210	140/2
Sample 1	%100 CO	20/1	Chitosan based	30/1	27,5	3/1 Z	5096	182	70/4

Figure 3. Applied processes to the weaved denim fabric

3. Results and discussion

FT-IR Analysis of chitosan containing yarn;
The FT-IR spectra for commercial chitosan powder in comparison with chitosan rayon yarn, which is used as weft in denim is illustrated in Fig. 4. The main characteristic peaks of commercial chitosan powder are at 3357 (–OH & -NH stretch), 2974 (C–H stretch), 1647 and (N–H bend), 1374 (bridge O stretch), and 1024 cm^{-1}(C–O stretch). Whereas the main corresponding peaks of chitosan rayon yarn were at 3350, 2880, 1652, 1378 and 1024 cm^{-1} respectively.

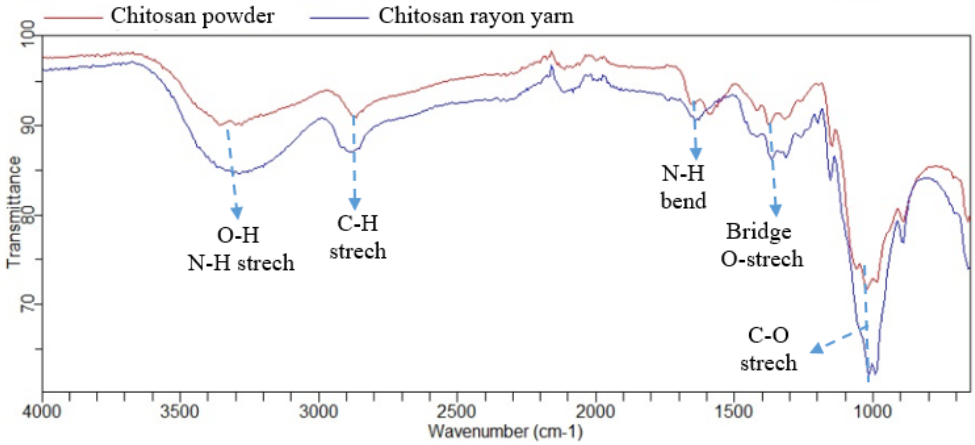

Figure 4. FT-IR spectra of commercial chitosan powder and chitosan viscose yarn

SEM/analysis**;**
To compare the structure of the chitosan containing rayon yarn with cotton yarn cross-section of fibers were studied using SEM. When the cross-section images of chitosan containing yarn are compared with commercial viscose rayon fiber product, the similarity can be seen in figure 6. The both fibre have close to circular cross-section.

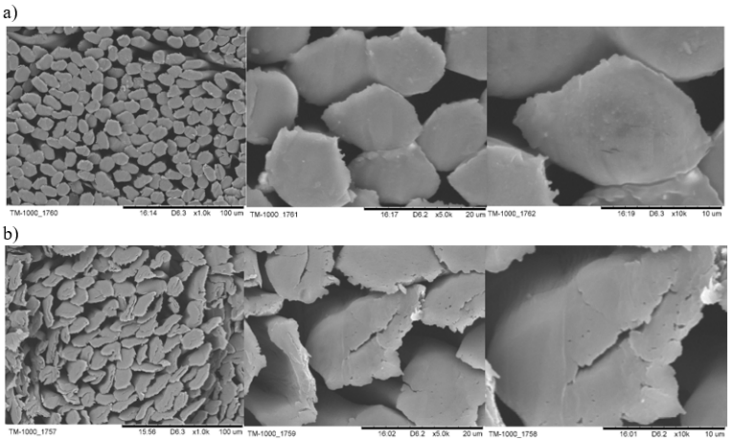

Figure 5. SEM Pictures of a) Cross section of chitosan containing rayon yarn Ne 30/1 (1000/5000/10000) b) Cross section of cotton yarn Ne 30/1, (1000/5000/10000)

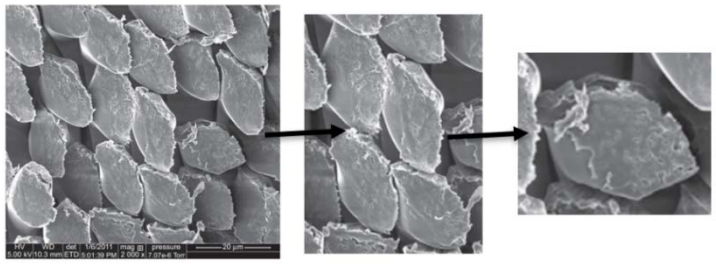

Figure 6. Lyocell rayon fiber cross-sectional view SEM (3)

Physical Properties of Weaved Denim;
The weaved two denim fabrics with the same warp and different weft were compared relates to their physical properties. Dry-wash crocking results of both fabrics seems to be practically same. According to tear result of chitosan containing yarn compared with Ne 30/1 cotton yarn in weft is more durable than cotton yarn (table 3).

Table 3: Physical Properties of weaved denim

Weft Yarn	WEIGTH		WEIGTH		CROCKING		STIFFNESS	pH	TENSİLE (kgf)		TEAR (grf)	
	DRY gr/m²	WASH gr/m²	DRY oz/yd²	WASH oz/Yd²	DRY	WET			WARP	WEFT	WARP	WEFT
Ne 30/1 Chitosan containing	176	177	5,2	5,2	2-3	1-2	0,28	4,54	43	24	3588	2936
Ne 30/1 Cotton	189	173	5,6	5,1	3	1-2	0,25	4,87	40	26	3719	2675

Determination of antibacterial activity: The antibacterial activity of developped denim with chitosan containing yarn in weft was determined acoording to AATCC 100:2019 standards with the test organism staphylococcus aureus MRSA (ATCC 33591) in Intertek Testing Services Taiwan Ltd. As can be seen from the result in Table 3, the super bacteria MRSA is reduced by more than 99.92 % on the developed denim fabric.

Table 4. Antibacterial activity test result of developed denim fabric

Name Of Test Bacteria (Strain Number)	*Methicillin resistant staphylococcus aureus* (ATCC 33591)
The number of bacteria recovered from the inoculated viability control fabric swatches immediately after inoculation ("0" contact time) (D)	1.5 $X10^5$ CFU/Sample
The number of bacteria recovered from the inoculated viability control fabric swatches incubated over 24 hours contact period (B)	1.8 $X10^7$ CFU/Sample
The number of bacteria recovered from the inoculated tested sample swatches immediately after inoculation ("0" contact time) (C)	1.3 $X10^5$ CFU/Sample
The number of bacteria recovered from the inoculated tested sample swatches incubated over 24 hours contact period (A)	<100 CFU/Sample
Growth value (F)	2.08
Percent reduction of Bacteria (R)	>99.92%

After 24 hours of incubation the reduction in methicillin staphylococcus aureus MRSA (ATCC 33591) is depicted in Figure 7.

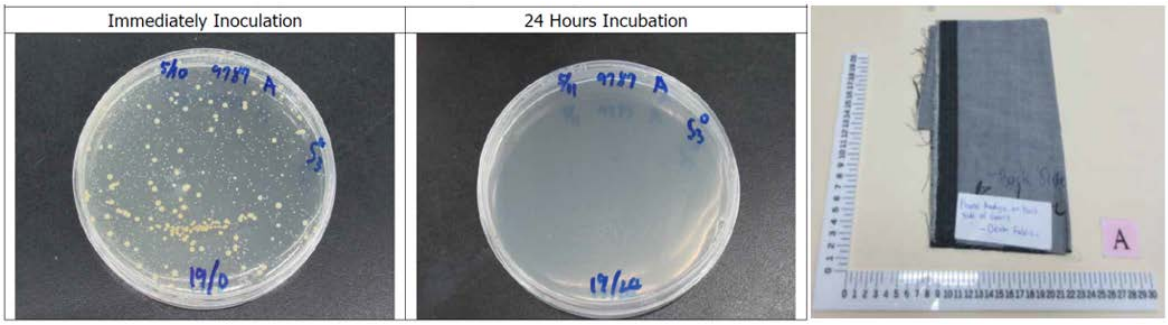

Figure 7. Reduction of MRSA after 24 hours incubation

The positively charged ions provided by Chitosan concentrate on the surface of the fabric and provide antibacterial protection to the fabric. When bacteria containing negative ions come into contact with the chitosan surface on the fabric; The positively charged ions bind to the bacteria and cause their enzymes to break down. The enzymes are then unable to produce energy, which inhibits the bacteria from multiplying and the bacteria eventually die.

4. CONCLUSIONS

Chitosan is a biopolymer with biocompatible, non-toxic and antibacterial properties which is the most common in nature after cellulose. In this work, it is aimed to create a denim fabric containing chitosan rayon yarn. For this purpose, we provided with wet spinning method produced chitosan containing yarn in order to use as weft yarn in denim. The antibacterial activity of developped denim with chitosan containing yarn in weft was determined acoording to AATCC 100:2019 standards with the test organism staphylococcus aureus MRSA (ATCC 33591) in Intertek Testing Services Taiwan Ltd. The super bacteria MRSA is reduced by more than 99.92 % on the developed denim fabric. As far as we know, it exists any study in the literature related to the use of chitosan as weft yarn in denim related to activity gains methicillin staphylococcus aureus MRSA (ATCC 33591).

Denim is a textile product that can be worn by people of all ages and kinds. From this point of view we succeed to developped a denim fabric, which controbute to reduction of super virus MRSA spreading among both healthcare personnel, hospital visitors and soldiers, athletes at risk. If this product is used by healthcare personnel or hospital visitors can protect their health and reduce the casualties of patients caused by MRSA nosocomial infections, and reduce huge medical expenses.

ACKNOWLEDGEMENTS

ÇALIK DENİM TEKSTİL A.Ş., which provides all kinds of technical and administrative support during the management and execution phases of this study. We would like to thank the management.

References

1. *Bethlehem, A., Studies on dyeing properties of chitosan modified cellulosic fiber, Journal of Textile Engineering & Fashion Technology. 2020;6(1):37–42.*
2. *Croisier, F., 2013, Chitosan-based biomaterials for tissue engineering European Polymer Journal 49 (2013) 780–792*
3. *Chen, J., 2015. Synthetic textile fibers: regenerated cellulose fibers. In: Sinclair, R. (Ed.), Textiles and Fashion. Woodhead Publishing in Association with the Textile Institute. http://dx.doi.org/10.1016/B978-1-84569-931-4.00004-0*
4. *Erdoğan, S., Textilefinishing with chitosan and silver nanoparticles against Escherichia coli ATCC 8739, Trakya University Journal of Natural Sciences, 21(1): 21-32, 2020 ISSN 2147-0294, e-ISSN 2528-9691 DOI: 10.23902/trkjnat.641367*
5. *Kuzgun N., Chitosan Production, Chitosan Properties and Usage Areas., Türk Bilimsel Derlemeler Dergisi 6 (2): 16-21, 2013*
6. *Ivanova, N.A., Superhydrophobic chitosan-based coatings for textile processing, Applied Surface Science 263 (2012) 783–787*
7. *Ibrahim, H. M., 2015, Concepts, Compounds and the Alternatives of Antibacterials, Chitosan as a Biomaterial — Structure, Properties, and Electrospun Nanofibers. 10.5772/59522(Chapter 4), doi:10.5772/61300*
8. *Lee Y-M, Park Y-J, Lee S-J, Ku Y, Han S-B, Choi S-M, et al. Tissue engineered bone formation using chitosan/tricalcium phosphate sponges. J Periodontol 2000;71:410–7.*
9. *Costa-Pinto AR, Reis RL, Neves NM. Scaffolds based bone tissue engineering: the role of chitosan. Tissue Eng Part B, 2011;17:331–47.*
10. *Raeisi, M., Superhydrophobic cotton fabrics coated by chitosan and titanium dioxide nanoparticles with enhanced antibacterial and UV-protecting properties International Journal of Biological Macromolecules 171 (2021) 158–165*
11. *Stegmaier, T., Chitosan – A Sizing Agent in Fabric Production – Development and Ecological Evaluation, Clean 2008, 36 (3), 279 – 286*
12. *Şahan, G., 2014, Kitosan biyopolimerinin formları ve tekstil uygulamaları, XIII. Uluslararası İzmir Tekstil ve Hazır Giyim Sempozyumu,170*
13. *Sunder, Edwin A., 2014, Croslinking of Chitosan with Cotton using Polycarboxylic Acids, International Journal of Engineering Research & Technology (IJERT), ISSN: 2278-0181, Vol 3 Issue 4,*
14. *Vithanage, A.H., 2015, Textile Dye Removal in Wastewater Using Chitosan, Annual Sessions of IESL, pp. [1 - 10], doi:10.4028/www. scientific.net /AMR.610-613.3394*

DESIGN OF ELECTRONICALLY CONTROLLED JACQUARD MACHINE FOR MULTI-SHED WEAVING MACHINES

Raşit ARSOY[1], Selçuk ASLAN[2]

[1]Faculty of fine arts, Department of Textile and Fashion Design, Kafkas University, rasitarsoy@gmail.com, 507-777-62-50, Kars 36000, Turkey.

[2]Fine Arts Vocational School, Department of Design, Kafkas University, Kars 36000, Turkey.

Abstract:

The Jacquard shed opening system, which makes it possible to open the shed by controlling the warp threads in groups and obtain different designs and shapes, differs from other shed opening systems in that each group of warp threads and each of them can be controlled as needed. The various warp movements, which are limited by the number of frames in other shedding systems, are limited by the number of sinkers in the Jacquard system. Since all known Jacquard shedding systems are designed for operation with single shed weaving machines, they cannot be used for shedding on multiple weaving machines. In this study, a new electronically controlled jacquard machine for multiple shed weaving machines was developed, which eliminates this problem and enables the opening of the weaving compartments by controlling the warp threads individually in multiple shed weaving machines, thus allowing the weaving of all known jacquard fabric patterns.

The technological and kinematic schemes of the jacquard machine were prepared taking into account the type of fabric to be produced, the operating principles of the weft insertion and shedding mechanisms to be used in the machine to be developed, and the expectations for improving the technical and economic indicators of the machine.

The electronically controlled pattern reading system, which consists of modules in the machine, converts the electronic data into mechanical data to ensure shedding. In the cam shedding mechanism, which transmits motion to the knives in the form of a stepped shaft in the multiple weaving machine, the warp threads are placed on the knives so that they can move vertically. They are controlled by specially structured sinkers which, in contact with the blades, move from the lower to the upper state with the help of the blades and from the upper to the lower state with the help of springs. When the warp threads are to remain in the upper position according to the pattern, the sinkers are interlocked by electromagnets to form an undulating nozzle corresponding to the fabric pattern.

By arranging the interlocking projections along the sinker, it is possible to match the density of the sinker to the density of the warp threads.

Since the machine allows weaving of all known jacquard fabrics, the problem of not being able to produce weaves other than the rag foot weave, which is considered one of the major drawbacks of multiple shed weaving machines, has been solved.

Key words:

Jacquard, Shed, Weaving, Plate, Thread

1. Introduction

The Jacquard shed opening system, which makes it possible to open the shed by controlling the warp threads in groups and obtain different designs and shapes, differs from other shed opening systems in that each group of warp threads and each of them can be controlled as needed [1, 2, 3, 11]. The various warp movements, which are limited by the number of frames in other shedding systems, are limited by the number of sinkers in the Jacquard system.

According to motion control systems, Jacquard machines can be mechanically and electronically controlled. Today, electronic control systems are used in all Jacquard machines.
To enable the production of more complex patterns, research is being carried out into the design of Jacquard machines that allow individual control of the warp threads.
In the invention of Jonathan F. McIntyre, information is given on the construction of an electronically controlled device that can control the warp threads individually [7].
Walter Keim and Kurt Jhile did the work on an electromagnetic basis. A common electromagnet between the hooks is used to control the shed in a certain position according to the scheme. The electromagnet is attached to the case so that it can be tilted or pivoted about an axis. In the pattern reading position, each hook moves mechanically to approach the pole of the electromagnet, especially to lean against it [9].
Chi Zhang introduced the basic design technologies of jacquard knitting integrated control system, the structure of integrated control system. The results of this project provided some theoretical and practical implications for the development of electronic jacquard control system [4].
M. Kaplan's project involved the manufacture, development and improvement of a prototype pattern loom using a Jacquard shedding machine. It was found that a more complex pattern could be produced by individual manipulation of the warp threads using the Jacquard mechanism [6].
Since all known Jacquard shedding systems are designed to operate on single shed weaving machines, they cannot be used for shedding on multiple shed weaving machines.
In this paper, information is given on the design structure of a new Jacquard machine for multiple shed weaving machines, developed by me, which eliminates this problem and enables shedding by controlling the warp threads one by one on multiple shed weaving machines, allowing all known Jacquard fabric patterns to be woven.

2. Materials and methods

The development of a new Jacquard machine requires in-depth knowledge of fabric theory and extensive knowledge of existing designs of known Jacquard machines and mechanisms. Due to the necessity of performing these operations and the complexity of the Jacquard machine design, care was taken to ensure that the design steps listed below were fully implemented in the design [11, 21]:
1. For the design of the Jacquard machine, the technological task was developed. At the same time, the characteristics of the technological process were carefully studied and the mechanical properties of the new machine were critically evaluated;
The design structures of existing Jacquard machines were studied, patents and technical literature were studied to determine the functionality of the machine to be designed, the main directions of its production perspective and the development prospects;
2. The technological and kinematic schemes of the jacquard machine were prepared taking into account the type of fabric to be produced, the operating principles of the weft insertion and shedding mechanisms to be used in the machine to be developed, and the expectations for improving the technical and economic indicators of the machine;
Figure 1 shows the technology diagram of the wave shed fabric forming system [21]. The shuttle 9 carrying the weft 10 moves at constant speed in the direction shown in the figure in a nozzle A which opens in front of it and closes behind it in a wave-like manner. The number of sheds depends on the dimensions of the shuttle and the width of the fabric. The fabric forming process is realized by

compressing the weft threads introduced into the shed to the fabric line with the help of the special weaving blade number 11 in wave motion.

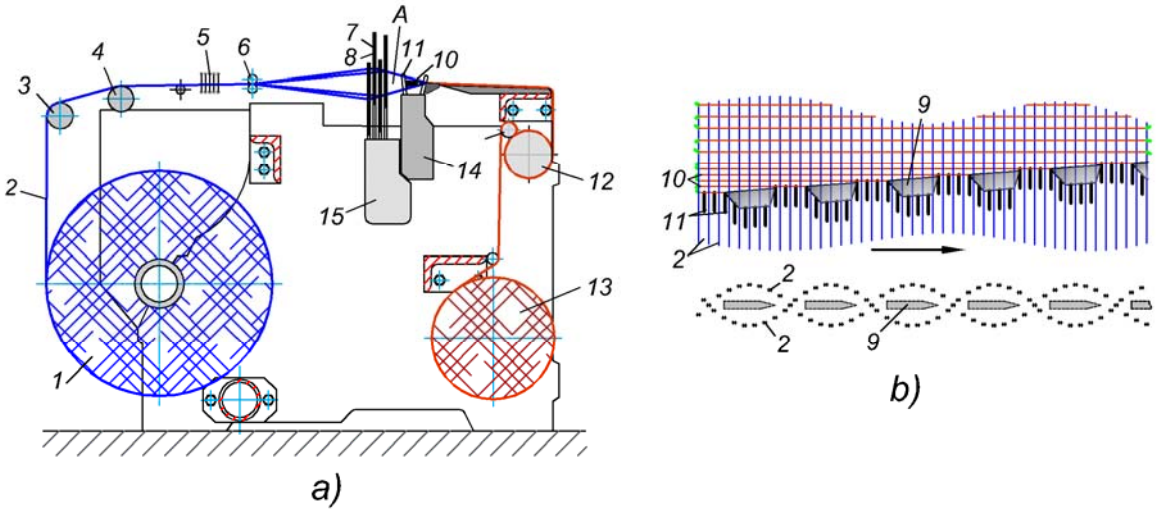

Figure 1. Technological scheme of the multiphase weaving machine with wave shed: a) technological scheme; b) threading the weft threads through the shed

It is not so easy to transfer the movement to the shuttles in the closed shed. Many methods have been proposed for this purpose. One of the methods is to use the weight of the shuttle as the force that stabilizes the shuttle in the shed. When the teeth of the weaving blade number 11 move from left to right, the shuttles move in the horizontal direction at a certain speed under the influence of the friction force.

The main technical scheme of the machine is similar to the known technical schemes. The warp yarns No. 2 opening from the warp beam No. 1 pass through the warp bridge No.3, the warp control system No. 6 and the shafts No. 4, 6, through the eyelets of the reeds No. 8 attached to the frames No. 7 of the shedding mechanism and through the comb teeth No. 11 and reach the fabric forming zone. After the finished fabric has passed the fabric tension shaft No. 12, it is wound onto the fabric beam No. 13.

The motion on the frames is transmitted by the shed forming mechanism No. 15 and the motion on the card teeth No. 11 is transmitted by the weaving blade mechanism No. 14.

When forming a shed, several frames are used to form the shed in the shape of a wave and to allow wave-like movement of the shed along the width of the warp threads.

The main advantages of this technology are that the fabric formation is similar to the classical methods, the machine works at low speeds and has a high efficiency.

The main disadvantage of this technology is that it can be used only for the production of one type of fabrics, namely rag fabrics [1, 21, 24].

Presentation of the newly developed machine.

In this study, a new electronically controlled Jacquard machine for multiple shed weaving machines was designed by analyzing the design structures of existing Jacquard machines, patents on the design of shedding systems of multiple shed weaving machines, technical literature and publications on this subject in technical journals [10-22, 24].

In order to make the working principle of the designed Jacquard machine easy to understand, the machine is presented with seven technical drawings:

Fig. 2 - General view of the Jacquard machine mounted on the weaving machine and B-B cross-section of the machine in the front view plane;

Fig. 3 - A-A cross-section of the Jacquard machine in the left view plane;

Fig. 4 - Schematic describing the operation of the electronically controlled interlock mechanism;

Fig. 5 - Cross-section C-C illustrating the assembly and guiding of the sinkers;

Fig. 6- Scheme explaining the formation of the wavy nozzle on the machine;

Fig. 7 - Three-dimensional view of the Jacquard machine explaining its structure and operation;

Fig. 8 - Three-dimensional view of the sinker.

The movement to the Jacquard machine is transmitted from the main shaft of the weaving machine through a 17-18 bevel gear. The machine consists of a computerized electronically controlled pattern reading system, a cam mechanism numbered 4-5 that transmits a wave-like motion to the knives, and a system that transmits motion from the knives to the warp threads according to the pattern.

In the shedding mechanism with cams No. 4-5 transmitting a stepped wave-like motion to the drop wires No. 6, the warp threads No. 1 are placed on the drop wires in such a way that they can move vertically from the lower to the upper layer of the drop wires with the help of the springs 16, in the opposite direction, from the upper layer to the lower layer, they are guided by the specially structured sinkers 8 in contact with the drop wires 6.

The design structure of the sinkers, which transmit the movement to the warp threads depending on the pattern, is shown in Figure 8. The plate, made of thin steel bar, has a locking projection E at the lower end and a slot D at the other end, through which the knives can move freely when the sinkers are locked.

The electronically controlled pattern reading system consists of No. 9 modules. The task of the modules in the machine is to convert the electronic data into mechanical data (the pattern in the computer into a mechanical movement) to ensure the formation of the nozzle. This operation is performed by the electromagnet No. 11 with the latches No. 10. When the warp threads are to remain in the upper position according to the pattern, a magnetic field is generated with the help of the given electric current, and the latches are mobilized. The end of the latch 10, which is pulled and rotated during magnetization, enters the slot E opened on the board and ensures that it is locked and the warp threads remain in the upper position. When the warp threads are to be lowered, the power supply to the module is interrupted. In this case, the end of the pawl rotating in the negative direction comes out of the slot with the help of the spring 12 and the sinker is released and moves together with the knife to the lower position. Lowering of the sinker together with the knife is ensured by the spring 16 connected to the sinker by the thread No. 15.

The number of electronic control modules corresponds to the number of sinkers used in the machine. Since the width of the modules is greater than the thickness of the blanks, the modules are arranged in several rows. The number of rows is specified in the pattern.

Figure 6 shows that a stepped, corrugated nozzle is formed in the machine. The number of stages of the nozzle depends on the number of blades that form the nozzle. It is recommended that this number is above 8.

In cross-section A-A in the left view plane of the machine, the number of blades is indicated as six, and in Figure 7, which explains the three-dimensional view of the machine, the number of blades is indicated as four to make the figure understandable.

To ensure a high density of platinum, two blades are attached to each arm. Thus, if the sinker thickness is 0.25 mm and the distance between the sinkers is 0.5 mm, the warp density is assumed to be 40 per 1 cm.

The eccentrics No. 4 mounted on the spindle No. 23, driven by the main spindle of the loom in a ratio of 1:1, perform a rotational movement and transmit a displacement in the vertical direction corresponding to the height of the shed to the blades 6 arranged at the ends of the arms 5 (Fig. 2).

In order to obtain a mountain-shaped nozzle, the eccentrics No. 4 are arranged on the shaft at equal angles according to the number of blades forming the stepped nozzle. If we express the number of blades with n, the insertion angle of the eccentrics results from the equation $\phi = 360o/n$.

The infinite wave-like movement of the blades is transmitted to the warp threads via the sinkers (8) and the threads 15, which connect the warp threads to the sinkers.

The positions of the shuttles No. 20 and the warp threads in the shaft nozzle are shown in Figures 6 and 7.

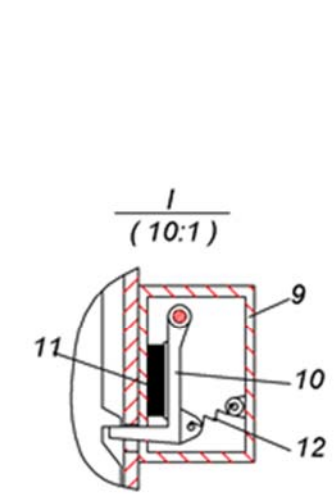

Fig. 4

Fig. 2

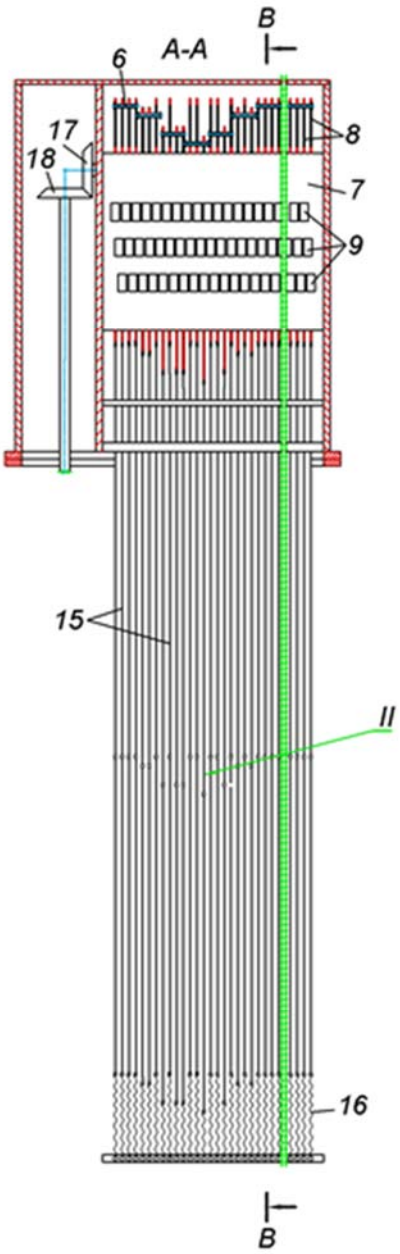

Fig. 3

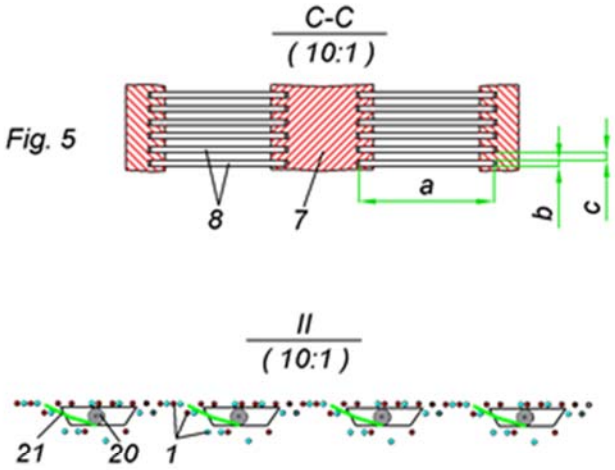

Fig. 5

Fig. 6

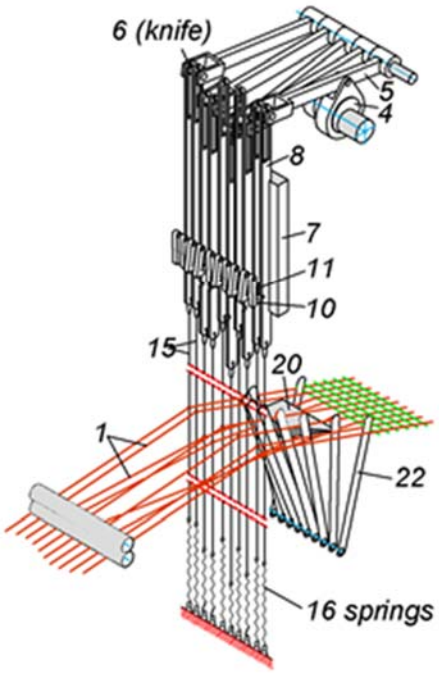

Fig. 7

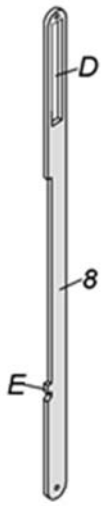

Fig. 8

3. Results

1. In the cam shedding mechanism (4,5), which transmits motion to the knives (6) in the form of a stepped shaft in the multiple weaving machine, the warp threads (1) are placed on the knives so that they can move vertically. They are controlled by specially structured sinkers (8) which, in contact with the blades, move from the lower to the upper state with the help of the blades (6) and from the upper to the lower state with the help of springs (16). When the warp threads are to remain in the upper position according to the pattern, the sinkers are interlocked by electromagnets (10, 11) to form an undulating nozzle corresponding to the fabric pattern.

2. By arranging the interlocking projections (E) along the sinker, it is possible to match the density of the sinker to the density of the warp threads.

3. Since the machine allows weaving of all known jacquard fabrics, the problem of not being able to produce weaves other than the rag foot weave, which is considered one of the major drawbacks of multiple shed weaving machines, has been solved.

References

1. *Adanur, S. (2001). Handbook of Weaving (1st ed.). CRC Press.*
2. *Başer G. (2004.)Dokuma Tekniği ve Sanatı. Punto Yayınları, Cilt 1, İzmir.*
3. *Eren R. (2009). Dokuma Temel Bilgileri. U.Ü. Mühendislik-Mimarlık Fakültesi Tekstil Mühendisliği Bölümü ders notları.*
4. *Chi Zhang, Jiangang Zhang, Xiaoguang Wu, Chengjun Zhang. (2010). Key Technology in Embedded Control System of Jacquard Knitting. International Conference on Mechatronics and Automation August, 4-7, Xi'an, China.*
5. *Nithya G., Sritha P., Gopika N.P. (2022). Design of PIC Microcontroller based Automatic Control System for Electronic Jacquard Mechanism. International Journal of Electrical Engineering and Technology. ISSN 2249-3085, Volume 12, Number 1, pp. 55-61.*
6. *Kaplan M., Ala D.M., Çelik N. (2019). Desıgn of an Electronıc Jacquard Samplıng Loom. İcontex, 2nd international congress of innovative textile, ss 66-69.*
7. *Keim W., Jhile K. (1990). Hook Control Devıce for an Open Shed Jacquard Machıne. Patent Number: 4,936,357. Date of Patent: Jun. 26.*
8. *Jonathan F. M., Malcolm G. B., Ian T. (1995). Electrically Controlled Jacquard Selection Apparatus. Patent Number: 5,464,046. Date of Patent: Nov. 7*
9. *Panneerselvam R. G., Yuvaraj D., Bhanu V. (2020). Use of indigenous electronic jacquard in handloom for weaving fashionable silk sarees. Dogo Rangsang Research Journal, UGC Care Group I Journal, ISSN : 2347-7180, Vol-10, Issue-07, No. 16 July.*
10. *Браун Д. (2004). Patent RU2359076C2. (FR), Зевообразующее устройство, ткацкий станок, Оборудованный таким устройством, и способ образования зева с использованием такого устройства*
11. *Буданов К.Д., Мартиросов А.А., Попов Э.А., Туваева А.А. (1975). Расчет и проектирование текстильного оборудования. Учебное пособие. — М.: Машиностроение, 390 с.*
12. *Галкин А.А. Ковалев Г.И. Губин В.В. Сидоров В.Ю. Галкин А.А. Малафеев Р.М. (2000). Зевообразующее устройство ткацкого станка с волнообразно подвижным зевом. Patent RU2177057C1.*
13. *Губин В.В. Ковалев Г.И. Галкин А.А. Сидоров В.Ю.Малафеев Р.М. (2000). Устройство управления жаккардовым зевообразующим механизмом ткацкого станка с волнообразно подвижным зевом. Patent RU2178471C1.*
14. *Ковалев Г.И. Макаров В.А. Комаров Ю.И. (1976). Зевообразующее устройство ткацкого станка с волнообразно подвижным зевом. Patent SU669772A1.*

15. *Ковалев Г.И. Галкин А.А. Сидоров В.Ю.Губин В.В. Галкин А.А. Малафеев Р.М. (2000). Зеленская В.В. Зевообразующее устройство ткацкого станка с волнообразно подвижным зевом. Patent RU2173358C1.*
16. *Ковалев Г. И., Лощилин Е. Д. (1989). Зевообразующее устройство ткацкого станка с волнообразно подвижным зевом. Patent SU1677105A1.*
17. *Люциано К. (1982). Зевообразовательный механизм для ткацкого станка с волнообразно подвижным зевом. Patent SU1313357A3.*
18. *Люциано К. (1982). Зевообразующее устройство для ткацкого станка с волнообразным подвижным зевом. Patent SU1313357A3.*
19. *Люциано К. (1982). Зевообразующее устройство ткацкого станка с волнообразно подвижным зевом. Patent SU1313357.*
20. *Мартынкин Ф. Ф., Виноградов И. Г., Колосова Т. И. (1980). Зевообразовательный механизм для ткацкого станка с волнообразно подвижным зевом. Patent SU973679A1.*
21. *Талавашек О., Сватый В. (1985). Бесчелночные ткацкие станки. Пер. с чеш. - М.: Легпромбытиздат, 335 с.*
22. *Хайнрих М., Вернер Х. (1972). Зевообразовательный механизм для ткацкого станка с волнообразно подвижным зевом. Patent SU557129A1.*
23. *https://www.derstekstil.name.tr/dokuma-makinelerinin-ana-elemanlari.html*
24. *https://www.derstekstil.name.tr/jakarli-agizlik-acma-sistemleri.html*

THERMAL AGING EFFECT ON THE PHYSIO-MECHANICAL PROPERTIES OF TEXTILES USED FOR THE REINFORCEMENT OF CONVEYOR BELTS

Tsegaye Sh. Lemmi & Marcin Barburski

Lodz University of Technology, Faculty of Material Technologies and Textile Design, Institute of Architecture of Textiles, Stefana Żeromskiego 116, 90-924, Lodz, Poland. Corresponding author email: marcin.barbusrki@p.lodz.pl

Abstract:

The use of textiles produced from high tenacity(HT) polyester yarns as a reinforcement material in the mechanical rubber goods industries, mainly in the conveyor belt, is extensively increasing due to their high tensile strength, flexibility, thermal stability, modulus of elasticity, and light weightiness. To achieve the desired property of a conveyor belt, the reinforcement components undergo various processing stages; among those stages vulcanizing the reinforcement materials under high temperatures is the crucial process that determines the physical and mechanical properties of the conveyor belt. The main aim of this work was to analyze the effect of vulcanization parameters on the physio-mechanical properties of high tenacity polyester yarns and fabrics that are utilized to reinforce a conveyor belt. An extensive experimental study was conducted on a pre-activated HT polyester yarn of different linear densities and woven fabrics produced for the purpose of conveyor belt reinforcement by subjecting the yarns and fabrics to various aging temperatures for a certain period of aging time. Following the experiments, a comprehensive study and analysis were conducted on the tensile property of the yarns and fabrics. The finding revealed that thermal aging has an immense impact on determining the tensile strength and elongation of the yarn and woven fabric, which also has a direct influence on the properties of the conveyor belt. The analysis of experimental test results of polyester yarns and woven fabrics revealed that vulcanizing textile-reinforced conveyor belt at high temperatures (220 °C) could deteriorate the tensile strength and increase the elongation at break of the yarn, fabric, or belt.

Keywords:

Polyester, yarn, woven fabric, conveyor belt, vulcanization, tensile strength.

1. Introduction

Nowadays, the demand for bulk materials transportation in mining, agriculture, construction, transport, power, and other industries with higher efficiency and reasonable transportation cost advances the revolution of conveyor belt technology. Thus, the requirement for lightweight conveyor belts in these sectors is immensely increasing, and textile-rubber reinforcement technology is coming to hand in modern heavy-duty transporting technology. In modern mechanical rubber reinforcement technology, primarily for conveyor belt reinforcement, textiles woven from a high tenacity polyester yarn in a warp direction and polyamide 66 in a weft direction are widely utilized. This is due to the fact that high-tenacity polyester yarn offers significant performance advantages over natural, regenerated, and other synthetic fibers. High warp modulus, which reduces fabric stretch and expansion under a load, superior tear resistance, and high tensile strength are some of these characteristics. Additionally, high-tenacity polyester is less sensitive to moisture and rot conditions; consequently, conveyor belt durability in these environmental circumstances is good [1].

The high demand of industries for lightweight conveyor belts draws the attention of many scholars to research how various processing parameters can influence the composition of the conveyor belt

properties. Barburski et al. [2] investigated the impact of heat treatment on the woven fabrics used as a carcass of the conveyor belt at different production stages of the conveyor belt. The study revealed that fabric weave structure and duration of thermal treatment have an influence on the physical properties of the woven fabric. Amr et al. [3] also studied the effect of the number of plies of the reinforcing material, the speed, and the loading direction on the tensile property of textile-reinforced conveyor belts using the Taguchi method. Rudawska et al. [4] also analyzed the impact of temperature and humidity on the tensile property of textile-reinforced conveyor belts. Lemmi et al. [1] [5] in detail investigated the effects of thermal aging and vulcanization parameters on the tensile strength, elongation, and surface structure of the polyester yarn, EP woven fabric, and multi-ply conveyor belts. Also, different researchers provided fundamental information concerning the conveyor belt design and woven fabric structure used for the intent of conveyor belt reinforcement [6][7]. In previous works various scholars researched in the area of factors that affect the properties of conveyor belt [8-13]. However, the effect of vulcanization process on the mechanical properties of textiles used for the reinforcement of conveyor has been left behind. The main goal of this work was to analyze the effect of vulcanization parameters on the physio-mechanical properties of high tenacity polyester yarns and fabrics that are utilized to reinforce a conveyor belt.

2. Materials and methods

2.1 Materials

In order to analyze the thermal aging effect on the properties of textiles used for the reinforcement of mechanical rubber goods, especially conveyor belts, a comprehensive study was conducted on high tenacity polyester(poly(ethylene terephthalate)) yarn and technical fabrics woven from HT polyester yarn in a warp direction and polyamide 66 yarn in the weft direction. The yarn and fabric samples were supplied by Kordárna, A.s company, the Czech Republic. The detailed property of the yarns and fabrics used to conduct this work is provided in Tables 1 and 2, respectively.

Table 1. Properties of High Tenacity Polyester Yarn sample [Lemmi et al., 2021].

Yarn type	***Property***				
	Linear density (tex)	Breaking force (N)	Breaking tenacity (cN/tex)	Elongation at break (%)	Hot air shrinkage (%)
High Tenacity Polyester	110	89.90	81.00	13.50	5.50

Table 2. Properties of Technical dipped woven fabric sample [Lemmi et al., 2021].

Fabric Type	**Fabric Properties**						
	Warp Yarn	Weft Yarn	Warp Count Ends/cm	Weft Count Picks/cm	Mass per unit Area (g/m2)	Crimp of Warp (%)	Weave Type
EP 200 - Dipped*	Polyester	PA 66	9.10 ± 0.25	4.50 ± 0.15	631 ± 10	2.50	Plain weave

* **E**-HT polyester yarn, **P**- Polyamide 66, **200** – nominal strength of the fabric sample in $kNm^{-1,}$ **Dipped**- the sample was dipped in resorcinol–formaldehyde–latex (RFL) solution to enhance the adhesiveness of the textile to rubber material.

2.2 Methods

Determining the impact of vulcanization process parameters on the tensile property of the conveyor belt carcass is difficult because of the complex structural composition of the conveyor belt. In this work, the following methods were employed to ascertain the effect of thermal aging on the properties of textile fabrics and yarns. High-tenacity polyester yarn and EP woven fabric samples were aged under the thermal aging temperature of 140, 160, and 220 °C for a duration of 35 minutes in an industrial oven. Following that, a multi-ply conveyor belt reinforced with a woven fabric of the same parameter was produced. The vulcanization temperature and duration used to vulcanize the conveyor belt was similar to the thermal aging used to age the fabric samples. Besides this, the samples used to reinforce the belt have the same property as the fabric samples on which the thermal aging investigation was conducted. Finally, the fabric samples were removed from the belt (Figure 1) to analyze the effect of the vulcanization process on the properties of the fabric used to reinforce the belt. The tensile property of the yarn and fabric samples pre-and post-thermal aging were tested in accordance with ISO 2062:2009 [14] and ISO 13934-1:2013 [15]. A Zwick/Roell tensile testing machine with a constant rate of extension, 2.5kN load cell, 250 mm/min crosshead speed, and a gauge length of 250mm was used to test the tensile property of the yarn samples. Also, for the tensile property testing of woven fabrics, the Zwick/Roell tensile testing machine of 150 kN load cell, testing the speed of 100 mm/min with a mechanical extensometer and the specimen width of 50 mm and 250 mm length between clamps were used. All experimental tests were conducted in standard laboratory conditions.

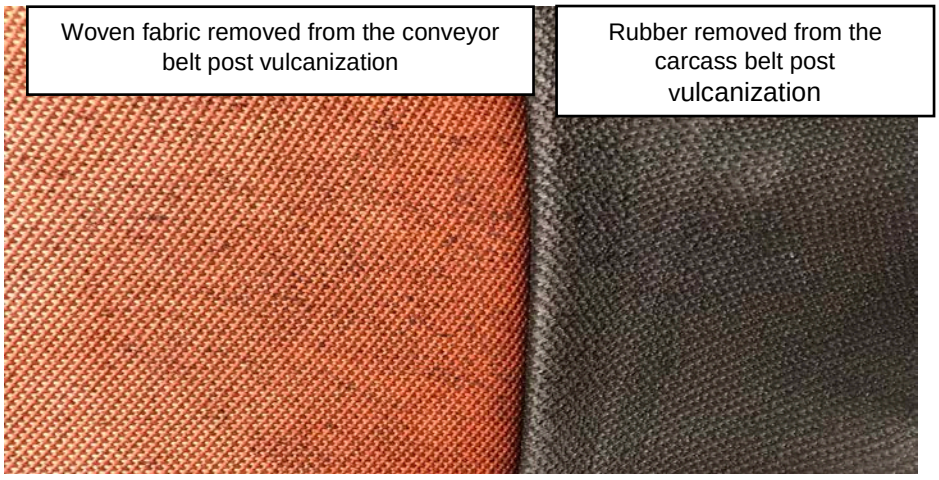

Figure 1. Woven fabric removed from conveyor belt reinforcement [Lemmi et al., 2021].

3. Results and Discussion

3.1 The effect of thermal aging parameters on the tenacity and percentage elongation of high tenacity polyester yarn

By altering the aging temperatures, the impact of thermal aging factors on the tenacity of polyester yarn was studied. As shown in Figure 2, there were no considerable changes in the tenacity of the yarn samples aged at 160 °C and 200 °C compared to the tenacity of the unaged yarn.
However, compared to the tenacity of the unaged yarn samples, the tenacity of yarn samples aged at 220 °C was drastically decreased. This indicates that the aging of polyester yarns way above its glass transition temperature (≈180 ℃) and around the melting point (≈260 ℃) can degrade the tenacity of the yarn.

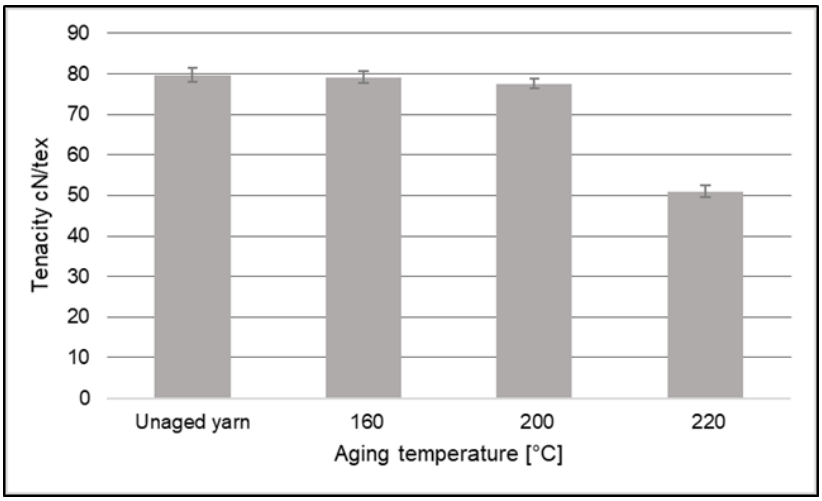

Figure 2. Impact of thermal aging on the tenacity of HT polyester yarn.

However, as shown in Figure 3, the aging of polyester yarns above the fiber's glass transition increases the yarn's percentage elongation. Unlike the tenacity, the percentage elongation of the yarn is incremented as the aging temperature approaches to the melting point of the yarn.

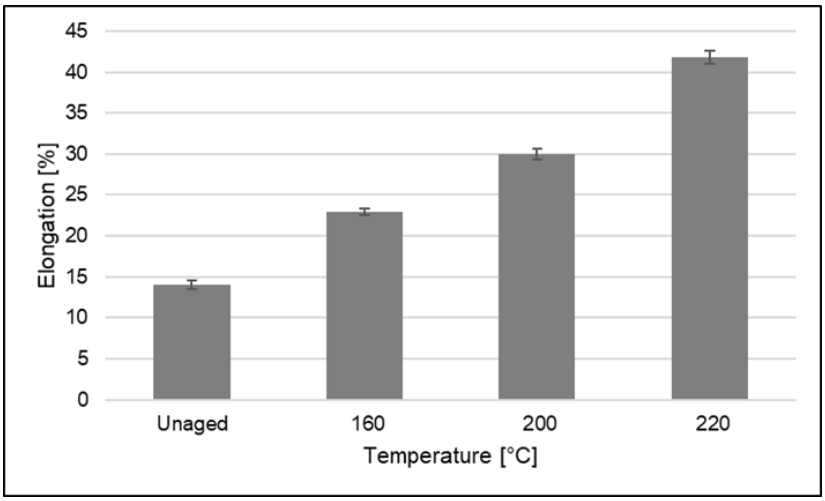

Figure 3. Effect of thermal aging on the percentage elongation of yarn.

3.2 Influence of thermal aging parameters on the tensile strength of woven fabrics

In Figure 4, the impact of thermal aging on the woven fabrics aged in an industrial oven and the fabric removed from a conveyor belt post-vulcanization process were compared. Regardless of the thermal aging medium, the tensile strength of the fabric samples was degraded compared to the unaged fabric samples.

Nevertheless, severe deterioration of the fabric's tensile strength was observed for the samples aged at 220 °C in the case of both mediums of aging. Moreover, the samples removed from the vulcanized conveyor belt were almost destroyed at 220 °C; this discrepancy resulted from the fact that the fabrics aged in the oven were aged under no pressure, whereas the fabric used as the carcass of the conveyor belt was vulcanized under high pressure, which affects the tensile strength of the fabric. Therefore, vulcanizing of EP textile reinforced conveyor at or above 220 °C cannot be recommended regardless of the vulcanization duration.

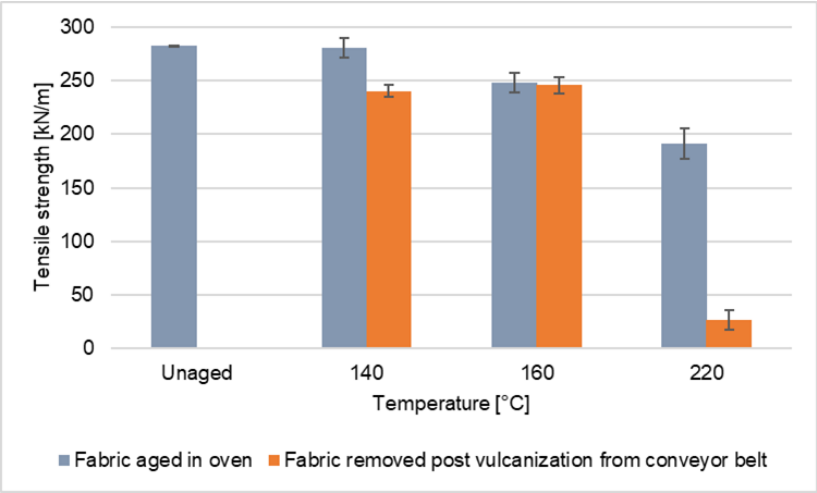

Figure 4. Effect of thermal aging on the tensile strength of the woven fabric.

3.3 Impact of thermal aging on the elongation of woven fabric

In determining the performance of the conveyor belt in varying stress levels, the percentage elongation of the conveyor belt has a significant impact. Hence, this property must be scrutinized during material choice for the reinforcement of the belt. As shown in Figure 5, the percentage elongation of the fabrics aged below Tg temperature of polyester (≈180 ℃) was around 5% higher compared to the unaged fabric. However, the fabric samples aged in an industrial oven at 220 °C were highly elongated, which is not recommended for the conveyor belt design. In order to reduce power fluctuation on the drive sharing of rollers, increase the service life of the belt and prevent the driving motor from burning out, always a conveyor belt with low percentage elongation is recommended. In addition, the elongation of the sample removed from the conveyor belt was fully deteriorated at 220 °C due to the fact that the sample was broken under a minor applied force.

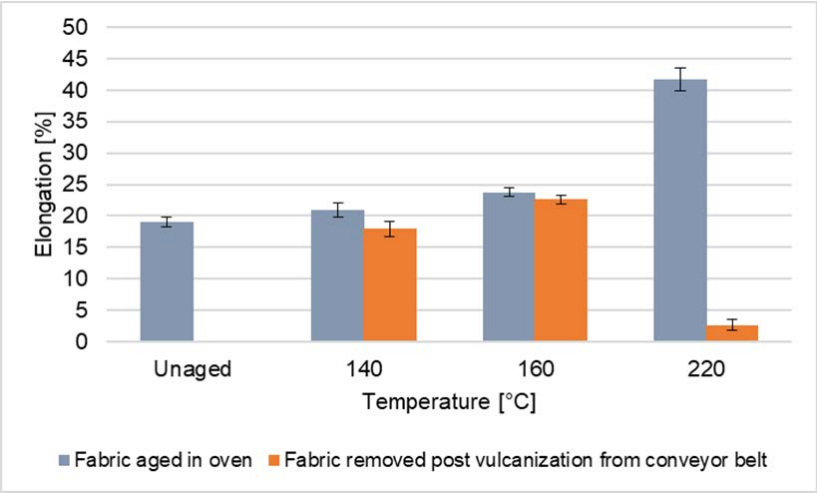

Figure 5. Effect of thermal aging on elongation of woven fabric.

4. CONCLUSIONS

The influence of aging temperature on the tensile properties of high tenacity polyester yarn and EP fabric was investigated by subjecting the yarn and fabric samples to different aging conditions used in the normal vulcanization process of conveyor belts. From the experimental results obtained, the tensile strength and percentage elongation of the polyester yarn and EP fabric is highly dependent on the aging temperature. Irrespective of the aging stage and medium of aging, the tensile strength of the samples subjected to thermal aging at 220 ℃ was decreased. However, the percentage elongation of yarn and Ep fabric samples aged in an industrial oven was shown higher percentage elongation, but the elongation of the sample removed from the conveyor belt vulcanized at 220 ℃ was lower than expected. Therefore, vulcanizing a conveyor belt reinforced by EP woven fabric at or above 220 ℃ is not recommended as it deteriorates the tensile property of the conveyor belt's constituent materials. Therefore, from the experimental analysis conducted, the optimum temperature to vulcanize EP reinforced conveyor belt is 160 ℃ for the duration of 35 minutes, depending on the number of plies of the conveyor belt.

ACKNOWLEDGMENTS

The authors are grateful for the support provided by Sempertrans Bełchatów Sp. z o.o R&D department for providing the laboratory equipment needed to accomplish the goal of this work. This paper was completed while the first author was a Doctoral Candidate in the Interdisciplinary Doctoral School at the Lodz University of Technology, Poland.

References

1. *Lemmi, T.S.; Barburski, M.; Kabziński, A.; Frukacz, K. (**2021**). Effect of thermal aging on the mechanical properties of high tenacity polyester yarn. Materials, 14(1666), pp.1-11, DOI:10.3390/ma14071666.*
2. *Barburski, M.; Góralczyk, M.; Snycerski, M. (**2015**). Analysis of changes in the internal structure of PA6.6/PET fabrics of different weave patterns under heat treatment. Fibres Text. East. Eur, 23, 46–51, doi:10.5604/12303666.1152722.*
3. *Ali, A.A.; Abdellah, M.Y.; Hassan, M.K.; Mohamed, S.T.(**2018**). Optimization of tensile strength of reinforced rubber using Taguchi method. Int. J. Sci. Eng. Res., 9, 180–186.*
4. *Rudawska, A.; Madleňák, R.; Madleňáková, L.; Droździel, P. (**2020**). Investigation of the effect of operational factors on conveyor belt mechanical properties. Appl. Sci., 10, 4201, doi:10.3390/APP10124201.*
5. *Lemmi, T.S.; Barburski, M.; Kabziński, A.; Frukacz, K. (**2021**). Effect of thermal aging on the mechanical properties of high tenacity polyester yarn. Materials, 14, 1666, doi:10.3390/ ma14071666.*
6. *Kabzinski, A. (**2010**). Rubber textile composites. Application of fabrics in conveyor belts. Tech. Wyr. Wlókiennicze, 18, 59–63.*
7. *Naga, K.; Ananth, S.; Rakesh, V.; Visweswarao, P. K.(**2013**). Design and selecting the proper conveyor-belt. Int. J. Adv. Eng. Technol. E, IV, 43–49.*
8. *Bajda, M.; Hardygóra, M.(2021). Analysis of reasons for reduced strength of multiply conveyor belt splices. Energies, 14, 1-21, 1512, doi: 10.3390/en14051512.*
9. *Ambriško, Ľ.; Marasová, D.; Grendel, P.(**2016**). Determination the effect of factors affecting the tensile strength of fabric conveyor belts. Maint. Reliab., 18, 1, 110–116, doi: http://dx.doi.org/10.17531/ein.2016.1.14.*
10. *Alvarez, A. A.; Alexander, A.; Soto, R.; Luís, J.; Rivera, V.; Concepción, A. D.(**2021**). Adhesion quality assessment of textile conveyor belts through experimental methods and mathematical modeling. Qual. Manag., 22, 181, 64–67.*

11. *Chou, C. S.; Liu, C. L.; Chuang, W. C. (**2013**). Optimum conditions for vulcanizing a fabric conveyor belt with better adhesive strength and less abrasion. Mater. Des., 44, 172–178, doi: 10.1016/j.matdes.2012.07.029.*
12. *Yao, Y.; Zhang B.(**2020**). Influence of the elastic modulus of a conveyor belt on the power allocation of multi-drive conveyors. PLoS One, 15, 7, 1–16, doi: 10.1371/journal.pone.0235768.*
13. *Rudawska, A.; Madleňák, R.; Madleňáková, L.; Droździel, P.(**2020**) Investigation of the effect of operational factors on conveyor belt mechanical properties. Appl. Sci., 10, 12, 1–17, doi: 10.3390/APP10124201.*
14. *ISO. Textiles—yarns from packages—determination of single-end breaking force and elongation at break using constant rate of extension (CRE) tester; ISO 2062:**2009**; ISO: Geneva, Switzerland, 2009.*
15. *ISO. Textiles—Tensile Properties of Fabrics—Part 1: Determination of Maximum Force and Elongation at Maximum Force Using the Strip Method; ISO 13934-1:**2013**; ISO: Geneva, Switzerland, 2013.*

INVESTIGATING THE APPLICATION OF TERRA DYE ON COTTON KNITTED FABRICS

Anagha Vaidya Soocheta; Sanskrita Singh Bhundoo

Department of Applied Sustainability and Enterprise Development, University of Mauritius, Reduit, Mauritius

a.soocheta@uom.ac.mu, mobile +23057593959
sanskrita.bhundoo@umail.uom.ac.mu

Abstract:

Today, sustainable textile dyeing technologies are being researched with a purpose of developing eco-friendly dyes that are cost effective and resource efficient. Natural Earth Pigments also known as native earth pigments, earth colours, earth ochres, iron oxide pigments etc. come from naturally occurring minerals, typically iron oxide or manganese oxide. Terra dye is a sustainable and environment friendly dye which has been derived from pigmented earth and without the use of harsh toxic chemicals. It is 100% natural, obtained from the extraction of minerals. The study investigates the application of 'Terra dye' on cotton knitted fabrics. 100% Cotton Jersey and 100% Cotton Fleece fabrics were used. The terra dyed fabrics were tested for their properties of colour uptake, bleeding, rubbing fastness, resistance to light and washing fastness. The effect of different fixing agents was investigated. The results of the lab trials and testing, conclude that Terra dye has good prospects of being used in dyeing.

Key words:

Application; Natural Earth Pigments; Terra Dye; 100% Cotton fabrics

1. Introduction

New sustainable textile dyeing technologies are being researched and developed with the aim of developing sustainable dyes that are more cost effective, resource efficient causing no harm to the planet. (TS Jeans Care, 2022). Terra is the Latin name for the earth. It is the name of the Goddess that protects the planet. The name has a direct connection to the innovative eco-friendly earth dyes. Terra dye is a sustainable and environment friendly dye which has been derived from pigmented earths and with no use of harsh toxic chemicals. It is 100% natural as it is obtained from the extraction of minerals. Through the process of grinding, geological material can become a pigment powder. Mineral deposits present give colouration to the earth pigments. Earth pigments are insoluble in water and are physically and chemically unaffected by the mediums they mix with. Furthermore, it caters for 50% water savings and 50% less use of energy as compared to a conventional pigment dye. Terra dye has some inherent disadvantages. This pigment dye may not be harmful to the environment but processes such as mining and quarrying required during extraction of earth pigments may be highly polluting. Dyes collected from natural earth pigments may lead to a variance in the colour of the dye due to factors contributing to the source itself such as climate, location of earth pigment and volcanic eruptions.

Mauritius, is a volcanic island. It has at Chamarel a rare and impressive geological phenomenon of the seven coloured. As seen in figure 1 the colours of the earth are blend together, like ochre and mauve, brown and pink, and shade in-between.The colours are seen to move from brown to ochre, from mauve to pink and into dozens of variations. The island with such diversified earth colour palatte provide scope for exploring terra dyes. The study investigates the application of 'Terra dye' on 100% Cotton Jersey and 100% Cotton Fleece knitted fabrics.

2. Experimental Method

2.1. Materials

100% Greige cotton jersey and cotton fleece knitted fabrics were used (Figure 2.1 (a) (b)). Five Terra dyes as seen n figure 2.2 (a) (b) (c) (d) (e), trade names “Giallo Artiglieria” (Yellow), “Verde Similcromo” (Green), “Rosso Laccato Scuro” (Pink), “Rosso Ercolano” (Red Earth) and “Mineral Black” were utilised. The Terra dyes and fabrics were provided by Consolidated Fabrics Ltd.

a)

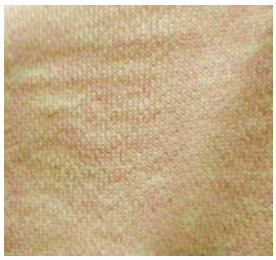

b)

Figure 2.1 (a) (b). Greige Cotton Jersey and Fleece knitted fabric

a) Giallo Artiglieria (Yellow)

b) Verde Similcromo (Green)

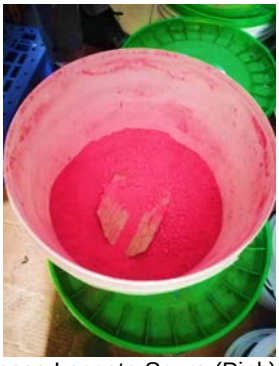

c) Rosso Laccato Scuro (Pink)

(d) Rosso Ercolano (Red Earth)

(e) Mineral Black

Figure 2.2 a) b) c) d) e). Terra Dyes

2.2. Pre-treatment of Fabric

Semi Bleach: The fabrics were semi bleached in a Fong’s industrial dyeing machine as shown in Figure 2.3. Machine was preheated at 50ºC for 10 minutes and 158 Litres of water was filled. 160g of Ronwet, a wetting agent, was added. 25 kgs of the fabric was loaded. 160 g of Imerol NFL, a detergent, 64 g of Prestogen FCB, a stabiliser and 32 g of Ronlube, an anti-crease, was added into the machine. After 5 mins, 633g of liquid Caustic Soda was poured into the bath. 640g of Hydrogen Peroxide was added and the temperature was increased at 3ºC per minute until it reached 110ºC. for 20 minutes. Nevocid, an acid, was injected into machine trough pipe system. The pH was maintained between 6-7. 64g of Bactosol, a peroxide added to neutralize the liquor. The fabric was rinsed with water and dried

Scouring: A batch 4 kg fabric was scoured in Rotary machine as shown in Figure 2.4 (a) & (b) with 0.50g/L Asutol and 60g Ronwet, wetting agent to remove impurities present before proceeding with dyeing. The Cotton Jersey and Cotton Fleece fabrics scoured as per the scouring profile seen in Figure 2.5.

Figure 2.3. Pretreatment

Figure 2.4 (a) & (b). Scouring process in Rotary

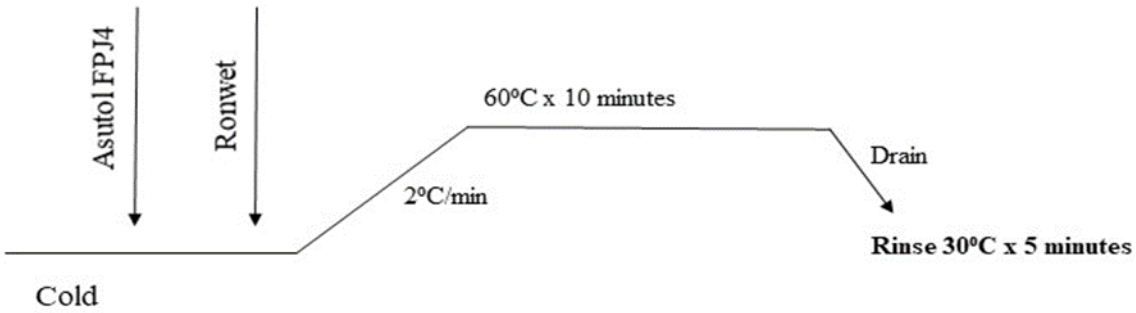

Figure 2.5. Scouring Profile (Adapted - Tropic Knits Washplant Dyehouse Recipe Card, 2022)

2.3. Dyeing of Cotton Fabrics with Terra Dyes

120 L of cold water was filled into the Rotary machine. 120 grams of Terra dye pigment was mixed with 1 litre of cold water until the pigment was completely diffused into the water. The dye was then poured slowly into the machine through a strainer to filter remaining undissolved dye pigments. The machine was run for 15 minutes and temperature raised to 60ºC. The steam valve was opened to allow steam to be gradually released at 1ºC per minute from the steam pipe into the machine to control even dyeing. After 15 minutes, hydro extraction was carried out in which the dyed water was drained out of the machine.

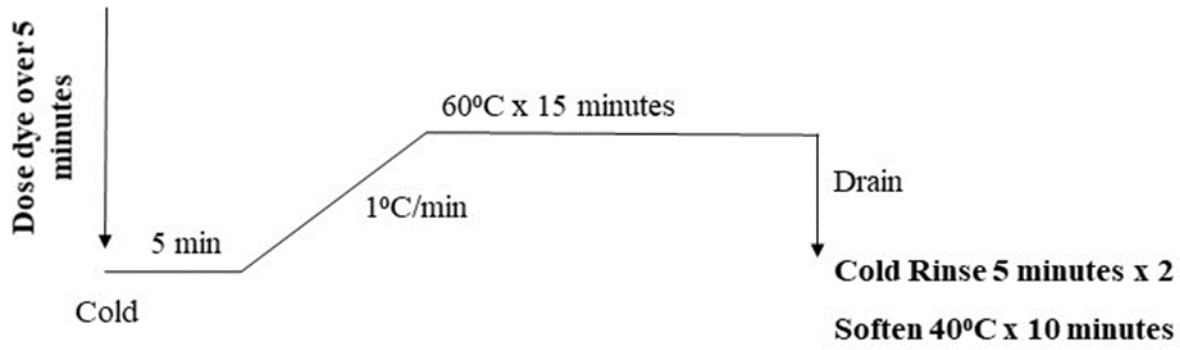

Figure 2.6. Dyeing Profile Terra dye (Adapted -Tropic Knits Washplant-Dyehouse Recipe card, 2022)

The fabrics were rinsed twice with cold water for 5 minutes. 120g of Acasoft, a softener was then added at 40ºC and machine was run for further10 minutes. The fabrics were dried. Figure 2.6. shows the dyeing profile used for Terra dyeing.

2.4. Dyeing of Cotton Fabrics with Terra Dyes using Cationisation method

1 kg of Cotton Jersey and Cotton Fleece were dyed with Terra dye trade name “Sand” which is of a yellow Ochre colour. Cationisation method involves the use of binder, to fix the dye pigment onto the fabric and achieve good colourfastness.

Scouring: The fabrics were scoured with 0.50 g/L Asutol prior to dyeing using the scouring profile as seen in Figure 2.7. After hydro extraction, the machine was filled with 30 litres of water to proceed with cationisation.

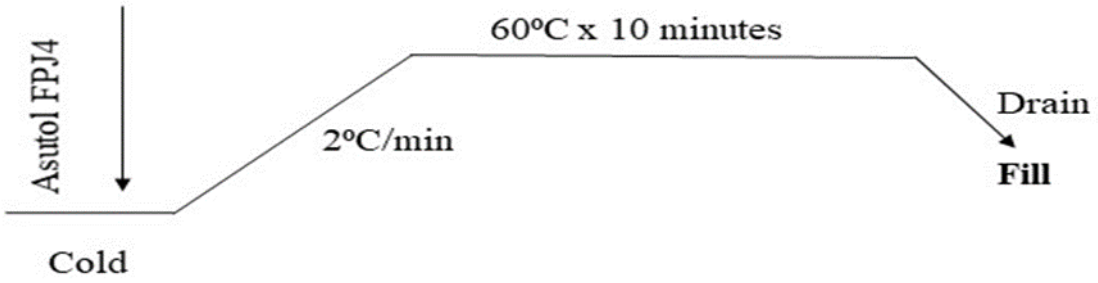

Figure 2.7. Scouring Profile (Adapted -Tropic Knits Washplant - Dyehouse Recipe Card, 2022)

Cationisation: 30 grams of Dye prep (Binder) was well diluted, filtered and poured into the Rotary machine and the machine was run for 3 minutes. The machine was heated to 50ºC at 2ºC per minute. Machine was run for 15 minutes at 50ºC. After 15 minutes, 30 grams of Soda Ash was added and machine was run for another 15 minutes. The pH was maintained in the range of 8-10. Hydro extraction was carried out before cold rinsing for 5 minutes twice. Catonisation profile is seen in Figure 2.8

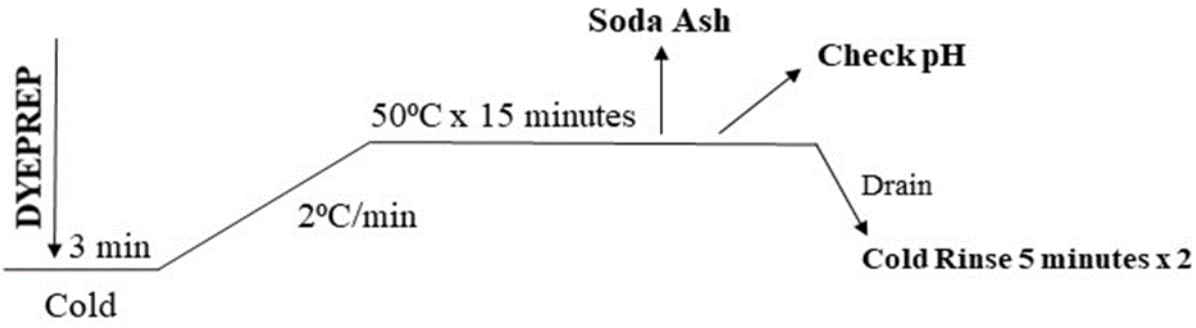

Figure 2.8. Cationisation Profile (Adapted- Tropic Knits Washplant - Dyehouse Recipe Card, 2022)

Pigmentation: Machine was filled with cold water. 6 grams of Acetic acid added and run for 5 minutes. The pH was maintained at 4.5 before dosing 100 grams of dye pigment into the machine. Machine was heated 1ºC per minute to a temperature of 50ºC for 20 minutes. 60 grams of Fixacryl CFD, a dye fixer, was added and machine was run for 10 minutes. Water was drained and fabric was cold rinsed for 5 minutes. Figure 2.9 shows the pigmentation profile.

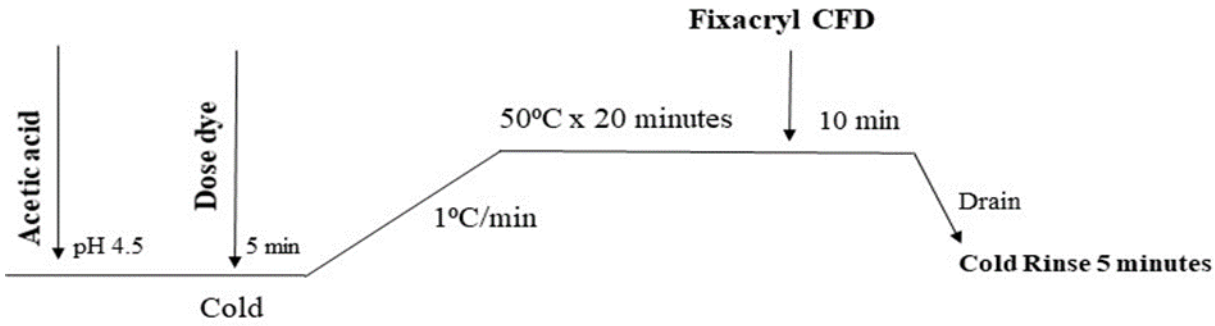

Figure 2.9. Pigmentation profile (Adapted -Tropic Knits Washplant - Dyehouse Recipe Card, 2022)

Softening: Fresh cold water was filled in machine. pH of water was adjusted to 5.5-6 by adding acid and machine was run for 3 mins (Figure 2.10). 40 grams of Acaflakes RT New, softener, was added to the bath. The machine was heated at 2ºC per minute to a temperature of 40ºC and run for 10 minutes. Hydro extraction was carried out and the fabrics were tumble dried at 105ºC for 60 minutes.

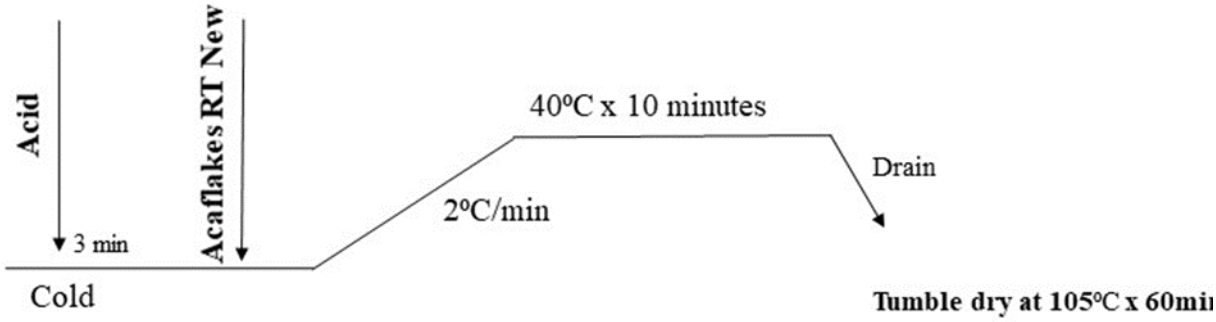

Figure 2.10. Softening profile (Adapted from Tropic Knits Washplant - Dyehouse Recipe Card, 2022)

2.5. Finishing

Dyed fabric samples were padded with different fixatives in separate batches - 200g Sodium Sulphate (Salt), 5 ml Acetic acid, 200g Sodium Carbonate (Soda Ash), 200g Sodium Bicarbonate (Baking Soda) and 40g Hifix, a cationic fixing agent. A rapid pad mangle machine was utilised for padding process.

Padding: 1 litre of water was boiled at a temperature of 100ºC. 200 grams of Sodium Sulphate was added, stirred continuously to dissolve and allowed to cool. This solution was used for padding and samples were oven dried. Same process was used for each fixative.

2.6. Evaluation

Grams per Square Metre (GSM): The GSM of both Cotton Jersey and Fleece were measured when at "greige" state, after semi-bleaching, dyeing and finishing process. The fabrics were ring cut matched with circular standard template and weighted on an electronic balance.

Pantone CAPSURE: Pantone Capsure apparatus Figure 2.11 was utilised to match dye colour of fabric with pantone colour libraries to obtain colour name and code.

Rubbing Fastness: Dyed Cotton Jersey and Fleece specimens were cut in dimension 25cm x 5 cm for both dry and wet rubbing test. The test was carried out in a crock meter whereby the rubbing fringe was covered with a dry crocking cloth and held in position with a spring clip. Fabric specimen was placed on rubbing area and was held by the clamping device's pins passing through the fabric and into holes on the base. Along the warp direction, the fringe was moved forth and back 10 times in 10 seconds at the rate of one turn per second. Same procedure is carried out for wet rubbing test. In the latter case, the

crocking cloth is wetted, squeezed and dried at room temperature after rubbing which was later matched with greyscale for assessing staining. (Figure 2.12)

Figure 2.11. Pantone

Figure 2.12. Samples Rub fastness

Wash Fastness: Microfiber was sewn on top of all dyed samples. Soap solution was prepared with 5g of ECE detergent and 2g of Sodium Carbonate per litre of water. Solution of liquor ratio 50:1 was poured in each container for each sample and was put in machine at 60ºC for 30 minutes and was flat dried (Figure 2.13). Samples were assessed with greyscale for staining.

Light Fastness: Pieces of Blue Wool was stick onto a piece of cardboard of dimension 12.8 cm x 4.9 cm and was used to act as control. On 5 other pieces of cardboard, the dyed samples were cut and glued. The machine was set for 103 hours. Samples were cross-checked each 6 hours for any colour change. Changes in colour were matched with greyscale standard in a light cabinet. The blue wool had to fade to a contrast equal to a grade of 2/3 according greyscale. (Figure 2.14(a) (b)).

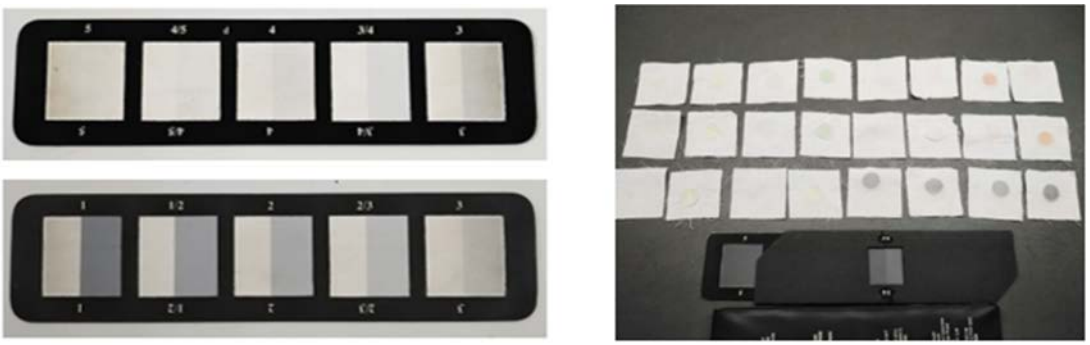

Figure 2.13. Assessing crocking cloth with greyscale for staining

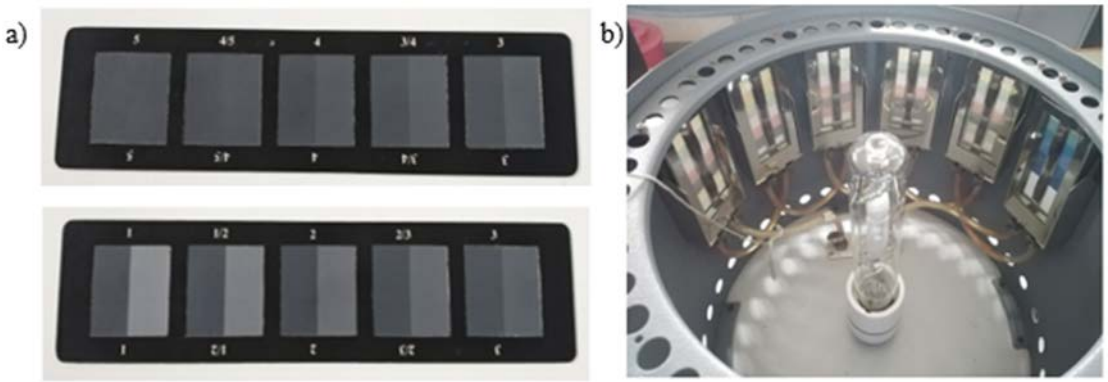

Figure 2.14 (a) Greyscale for assessing colour change (b) Samples in light fastness machine

3. Results and discussion

3.1. Pre-treatment of Fabric

Semi-bleaching: With visual inspection, a major change in fabric colour can be observed. The natural yellowish brown colour the fabric was removed to a uniform degree of whiteness. (Figure 3.1 (a) & (b))

a) b)

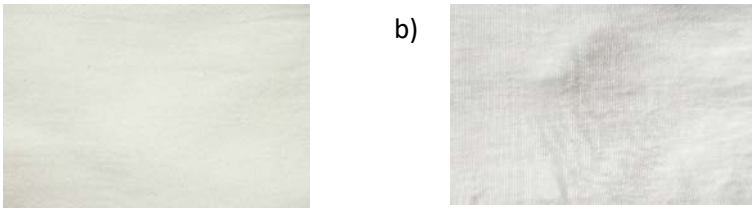

Figure 3.1 (a) (b). Semi-bleached Cotton Jersey and Fleece fabric

Fabric Mass weight loss: Table 3.1 shows the weight loss occurred due to the amount of fibres being treated with the addition of Hydrogen peroxide (H_2O_2) during semi-bleach process. It can be observed that weight loss for Fleece is less than Jersey fabric.

Table 3.1 Mass of Fabric

Fabric Type	Before Semi-bleaching	After Semi-bleaching
100% Cotton Jersey	25 kg	21.5 kg
100% Cotton Fleece	25 kg	22 kg

3.2. Spectrophotometric Whiteness Test

As seen in figure 3.2 (a) (b), a Standard Whiteness of 72.42 was obtained for semi-bleached Cotton fleece and 70.63 for jersey fabric.

(a) (b)

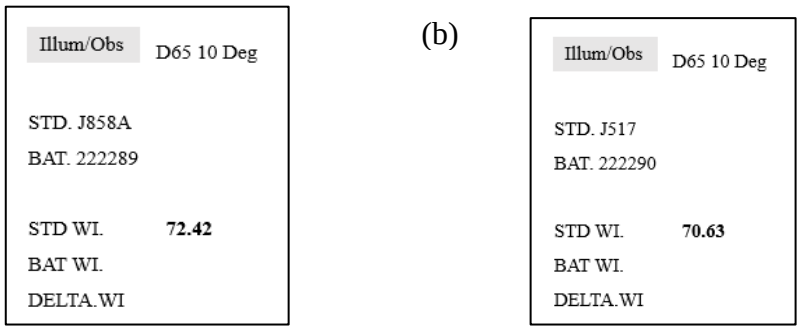

Figure 3.2 (a) (b) Whiteness test Datacolour Spectrophotometer

Illum/Obs D65 10 Deg refers to a light source name which is a simulation of natural day light.
STD refers to standard of fabric.
BAT refers to the batch number of fabric lot.
STD WI refers to the Standard Whiteness

3.3 Dyeing with Terra dyes

Table 3.2 shows the colour codes and names obtained for the jersey and fleece cotton fabrics dyed with terra dyes. Pantone CAPSURE apparatus was used to obtain the colour codes and names.

Table 3.2. Pantone Color and Code

Terra Dye	Jersey Cotton	Fleece Cotton
Giallo Artiglieria (Yellow)	PANTONE 12-0817 TCX Apricot Gelato	PANTONE 12-0822 TCX Golden Fleece
Verde Similcromo (Green)	PANTONE 13-6208 TCX Bok Choy	PANTONE 15-6315 TCX Smoke Green
Rosso Laccato Scuro (Pink)	PANTONE 13-1904 TCX Chalk Pink	PANTONE 14-1905 TCX Lotus
Rosso Ercolano (Red Earth)	PANTONE 16-1522 TCX Rose Dawn	PANTONE 16-1516 TCX Cameo Brown
Mineral Black	PANTONE 18-4005 TCX Steel Gray	PANTONE 18-5203 TCX Pewter
Sand (With Binder)	PANTONE 13-1025 TCX Impala	PANTONE 14-0936 TCX Sahara Sun

3.4. Padding and Finishing

Padding process with Sodium Sulphate: Rosso Ercolano and Mineral black was seen to bleed colour in the bath. For lighter dye shades, no major change was observed in the solution during padding process. White patches of salt were observed on fabric surface after being oven dried and fabric feel became rough.
Padding process with Sodium Carbonate: Slight bleeding was observed for light coloured samples whereas dark shade bleed much more. Fabric were smooth after drying with showed no tendency of curling.
Padding process with Sodium Bicarbonate, Acetic acid & Cationic Fixing agent: Darker dye shades continued to bleed. Fabric remained soft with good drape with even dyeing. Similar results were achieved for acetic acid and cationic fixing agent.

3.5. Grams per Square Metre (GSM)

It can be observed that both fabrics gained weight after semi-bleaching process. This may be due to the fact that curling tendency of knitted fabrics and shrinkage occurred increased the weight. Furthermore, an additional increase in GSM was observed after dyeing due to the reason that the dye pigment weight has add up to the fabric weight. Fleece fabric is gaining more mass due to its compact and thick structure. GSM has increased much more after the addition of fixatives, and fabrics have become much heavier.

3.6. Dry and Wet Rubbing Fastness of Terra dyes

In the greyscale, the fastness ratings range from 1 (Poor) to 5 (Excellent). Very good results (3.5-4.5) were obtained for all dry rub tests indicating that less staining occurred with amount of unfixed dyes present in fabric. However, for wet rubbing, an average wet rubbing fastness (3) was obtained for non-treated fabrics as unfixed dyes dissolved in water and stained the crocking cloth. Small fuzzy balls(pills) of fibres can be seen on crocking cloth. On the other hand, lighter shade samples treated with Sodium Sulphate, Sodium Carbonate, Sodium Bicarbonate, Acetic acid and Cationic fixing agent obtained excellent results (4-4.5). Only the darker shades wet rubbing fastness could not have been improved with addition of fixatives. (Figure 3.3 (a) (b)).

a)

Terra dye colour	100% Cotton Jersey	100% Cotton Fleece
Giallo Artiglieria (Yellow)	4	4
Verde Similcromo (Green)	4	4
Rosso Laccato Scuro (Pink)	4.5	4.5
Rosso Ercolano (Red Earth)	4	4
Mineral Black	3.5	3.5
Sand (Binder)	4.5	4.5

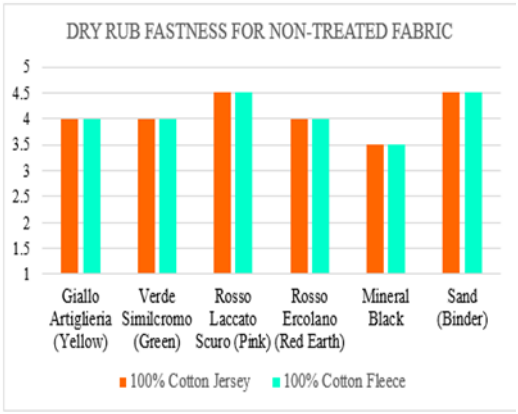

b)

Terra dye colour	100% Cotton Jersey	100% Cotton Fleece
Giallo Artiglieria (Yellow)	3	3
Verde Similcromo (Green)	3	3
Rosso Laccato Scuro (Pink)	3	3
Rosso Ercolano (Red Earth)	3	3
Mineral Black	3	3
Sand (Binder)	3	3

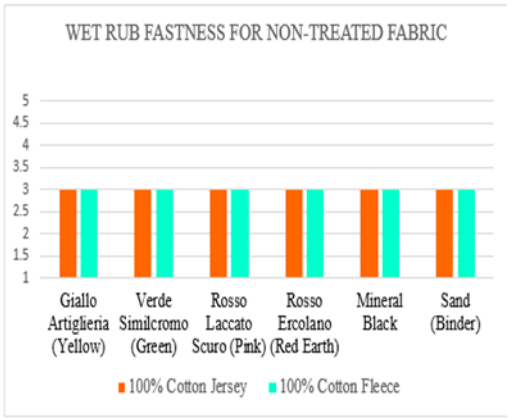

Figure 3.3 (a) (b). Dry and Wet Rub fastness for treated fabrics

3.7. Results for Wash Fastness test

Staining on microfiber were assessed with greyscale in order to determine whether the dye used stains other fibres and whether garment with this dye can be washed together in washing machine at home. (Table 3.3). Non-treated terra dye samples slightly stained almost all fibres. Lighter shades did not stain the multifibre when compared to darker shades. For the Sodium Sulphate samples, the white salt patches present on fabric was washed away. For Sodium Carbonate, Sodium Bicarbonate and Acetic acid, quite good results were obtained as dye shade strength was the same after washing and did not bleed much. Lighter dye shades did not affect the multifibre at all. Excellent results were achieved for cationic fixing agent samples as no major staining was observed.

Table 3.3 Fastness to washing test results

Sample Type	Dye Colour	Staining on Multifibre					
		Acetate	**Cotton**	**Nylon**	**Polyester**	**Acrylic**	**Wool**
Non-treated	Yellow Jersey	5 (No change)					
	Yellow Fleece	4/5	4/5	3(Pink)	4/5	4/5	4/5
	Green Jersey	5 (No change)					
	Green Fleece	5 (No change)					
	Pink Jersey	4/5	5	4/5	4/5	5 (No change)	
	Pink Fleece	4/5	4/5	4	4/5	4/5	4/5
	Red Jersey	5 (No change)		4/5	4/5	4/5	4/5
	Red Fleece	4	4/5	4	4/5	4/5	4
	Black Jersey	4/5	4/5	4/5	4/5	5 (No change)	
	Black Fleece	4/5	4/5	4/5	4/5	4/5	5
	Sand Jersey	5 (No change)					
	Sand Fleece	5 (No change)					
Sodium Sulphate	Yellow Jersey	5 (No change)					
	Yellow Fleece	5 (No change)					
	Green Jersey	5 (No change)					
	Green Fleece	5 (No change)					
	Pink Jersey	5 (No change)		4/5	4/5	5 (No change)	
	Pink Fleece	5 (No change)		4/5	4/5	5 (No change)	
	Red Jersey	4/5	5	5	4/5	4/5	5
	Red Fleece	4/5	4/5	4/5	4/5	4/5	5
	Black Jersey	5	5	4/5	5	5	5
	Black Fleece	4/5	4/5	4/5	4/5	4/5	4/5
Sodium Carbonate	Yellow Jersey	5 (No change)					
	Yellow Fleece	5 (No change)					
	Green Jersey	5 (No change)					
	Green Fleece	5 (No change)					
	Pink Jersey	4/5	5	4/5	5 (No change)		
	Pink Fleece	4/5	5	4/5	5 (No change)		
	Red Jersey	4/5	5	4/5	5 (No change)		
	Red Fleece	4/5	4/5	4/5	4/5	4/5	5
	Black Jersey	5 (No change)					
	Black Fleece	4/5	4/5	4/5	4/5	4/5	5
Sodium Bicarbonate	Yellow Jersey	5 (No change)					
	Yellow Fleece	5 (No change)					
	Green Jersey	5 (No change)					
	Green Fleece	5 (No change)					
	Pink Jersey	4/5	5	4/5	5	4/5	5
	Pink Fleece	4/5					5
	Red Jersey	4/5			5 (No change)		
	Red Fleece	4/5					

	Black Jersey	5 (No change)				
	Black Fleece	4/5				5 (No change)
Acetic Acid	Yellow Jersey	5 (No change)				
	Yellow Fleece	5 (No change)				
	Green Jersey	5 (No change)				
	Green Fleece	5 (No change)				
	Pink Jersey	4/5	5	4/5		5 (No change)
	Pink Fleece	4/5				5 (No change)
	Red Jersey	4/5			5 (No change)	
	Red Fleece	4	4/5			5
	Black Jersey	4/5				
	Black Fleece	4/5				
Cationic Fixing agent	Yellow Jersey	5 (No change)				
	Yellow Fleece	5 (No change)				
	Green Jersey	5 (No change)				
	Green Fleece	5 (No change)				
	Pink Jersey	5 (No change)				
	Pink Fleece	5 (No change)				
	Red Jersey	4/5	5 (No change)		4/5	5
	Red Fleece	4	4/5	4	4	4/5
	Black Jersey	4/5				
	Black Fleece	4/5				

3.8. Light Fastness test

After being exposed to UV light for 103 hours, the samples (Figure 3.4.) were assessed with colour change greyscale. The obtained results are seen in Table 3.4. Slight colour changes could be observed in lighter samples whereas a major colour difference was observed in darker samples. The darker the colour, the more the fading away of the shade is noticeable. Sodium Carbonate and Bicarbonate samples fairly resisted to light. Presence of salt in sample has made the colour to fade more rapidly compared to the other samples. Samples with Acetic acid and Cationic fixing agent resulted in good resistance to light.

Figure 3.4 Samples after light fastness

Table 3.4 Light fastness test results

Number of hours	Non-treated	Sodium Sulphate	Sodium Carbonate	Sodium Bicarbonate	Acetic acid	Cationic Fixing agent
Light dye shades						
6 hours	5	4/5	4/5	5	4/5	5
18 hours	5	4	4/5	5	4/5	5
42 hours	4/5	4	4	4/5	4/5	4/5
103 hours	4/5	3/4	4	4	4	4/5
Dark dye shades						
6 hours	4/5	4/5	4/5	5	4/5	5
18 hours	4	3/4	4	5	4/5	5
42 hours	3/4	3	3/4	4/5	4/5	4/5
103 hours	3	2/3	3	4	4	4/5

4. CONCLUSIONS

This study has provided an in-depth understanding of Terra dye. The study investigates the application of 'Terra dye' on 100% Cotton Jersey and 100% Cotton Fleece knitted fabrics. The fabrics were semi bleached in an industrial dyeing machine with Asutol and Ronwet to remove impurities present before dyeing. Data colour spectrophotometer was used to test the degree of whiteness. The scoured fabrics were dyed in a rotary dyeing machine. Five colours of Terra dye namely Giallo Artiglieria (Yellow), Verde Similcromo (Green), Rosso Laccato Scuro (Pink), Rosso Ercolano (Red Earth) and Mineral Black (Black) were used. The fabrics were rinsed thoroughly and treated with Acasoft, softener. The dyed fabrics were treated with fixing agents namely Sodium Sulphate (Salt), Acetic acid, Sodium Carbonate (Soda Ash), Sodium Bicarbonate (Baking Soda) and Hifix, a cationic fixing agent using the rapid padding mangle. Dyeing using the Cationisation method was carried out with 'Sand Terra dye'. Cationisation method involved the use of binder to fix the dye pigment onto fabric surface to achieve good colourfastness. Pantone Capsure apparatus was utilised to match the fabric dye colour with pantone colour libraries and obtain the pantone colour name and code. Very good results were obtained for all dry rub tests and an average wet rubbing fastness was observed that stained the crocking cloth. The dye could not achieve darker colour strength or fix the dye pigments permanently on the fabric surface. It was seen that the bleeding of dye from the fabric could be reduced by use of cationisation method and cationic fixing agent. Samples with Acetic acid and Cationic fixing agent resulted in good resistance to light. The results of the lab trials and testing, conclude that Terra dye has good prospects of being used in dyeing. These Eco-friendly pigments obtained from natural sources show potential to make it into the mainstream fashion.

ACKNOWLEDGEMENTS

Acknowledgements are due to Mr Shiva Chinappen CDL Knits Ltd for arranging and providing with the required materials, equipment and facilities; Mr M.Seeburn for providing dyeing facilities at the Wash plant of Tropic Knits Ltd.; Mr V.Jeepah for assisting with the dyeing processes.

References

1. *Corbman, b., 1985. Textiles. 6th ed. New york: Macgraw-hill, pp.107-255*
2. *Dr Mukhopadhyay, S., 2022. The polymer system of cotton.*
3. *Esteve-Turrillas, F. and de la Guardia, M., 2017. Environmental impact of Recover cotton in textile industry. Resources, Conservation and Recycling, 116, pp.107-115.*
4. *Fao.org. 2016. FAOSTAT. [online] Available at: <https://www.fao.org/faostat/en/> [Accessed 18 January 2022].*
5. *Fibre2fashion.com. 2022. Bleaching of Cotton Textile Material - Bleaching Of Cotton Fibre. [online] Available at: <https://www.fibre2fashion.com/industry-article/7071/problems-in-bleaching-for-cotton-textile-material> [Accessed 20 April 2022].*
6. *KEMI, Swedish Chemicals Agency, 2016. Hazardous chemical substances in textiles. Arkitektkopia, Stockholm 2016.*
7. *Kerr, J., 2022. Soil Morphological Characteristics — MARLIN - Septic Tank Cleaning, Inspection, Installation, and Repair. [online] MARLIN - Septic Tank Cleaning, Inspection, Installation, and Repair. Available at: <https://www.marlinw.com/understanding-onsite-wastewater/2019/7/19/soil-morphological-characteristics> [Accessed 8 January 2022].*
8. *Mondal, M., 2021. Fundamentals of natural fibres and textiles. Duxford: Woodhead Publishing.*
9. *Orvis, 2022. Terra Dye Organic Cotton Scoopneck Short-Sleeved Tee. [online] Orvis.com. Available at: <https://www.orvis.com/terra-dye-organic-cotton-scoopneck-short-sleeved-tee/29CN.html> [Accessed 16 January 2022].*
10. *Pantone.com. 2022. PANTONE® USA | PANTONE® - Find a Pantone Color | Quick Online Color Tool. [online] Available at: <https://www.pantone.com/connect/14-0936-TCX> [Accessed 15 June 2022].*

11. *Shawn, A., 2021. chemical Composition of Cotton Fiber. [online] Textile Learner. Available at: <https://textilelearner.net/chemical-composition-of-cotton-fiber/> [Accessed 16 January 2022].*
12. *Soil Survey Manual, 1951 [ebook] U.S Department of Agriculture Miscellaneous Publication, pp.238-240. Available at: <https://books.google.mu/books?id=8JJzAAAAIAAJ&printsec=frontcover#v=onepage&q&f=false> [Accessed 15 January 2022].*
13. *The Earth Pigments Company, LLC. 2022. A Brief Look on Pigments Through the Ages. [online] Available at: <https://www.earthpigments.com/blog/a-brief-look-on-pigments-through-the-ages/> [Accessed 10 January 2022].*
14. *Tsjeanscare.wixsite.com. 2022. [online] Available at: <https://tsjeanscare.wixsite.com/tsjeanscare/researchanddevelopment> [Accessed 14 March 2022].*
15. *Willis, S. 2021. How Sustainable Dyeing is Changing the Textile Industry. [online] Available at: <https://www.plugandplaytechcenter.com/resources/how-sustainable-dyeing-changing-textile-industry/> [Accessed 11 February 2022].*
16. *Zaitex, 2022. ZETATERRA eco-friendly dyes from natural resources. [online] zaitexfashion.com. Available at: <https://zaitexfashion.com/zetaterra> [Accessed 29 July 2022].*

NOVEL ELASTIC WARP KNITTED FABRIC WITH PERFORATION

Liudmyla Melnyk, Olena Kyzymchuk

Kyiv National University of Technologies and Design, Ukraine, Nemyrovycha-Danchenko str. 2, Kyiv, 01011, Ukraine, melnik.lm@knutd.edu.ua, kyzymchuk_knutd@ukr.net

Abstract:

The aim of this project is to create novel elastic knitted materials with improved comfort for medical products. In this context, warp knitted structures were produced using different weft threads laying in. The elastic warp knitted fabric produced with transverse weft threads for the whole width was used as a reference sample. It is widely used in medical products. Laying in weft threads with a partial set according to a certain repeat allows us to get structures in which there is no connection in adjacent wales in certain places. This leads to the formation of through holes in the structure. As a result of increased permeability, comfort properties are improving. The structure, functional and comfort properties of developed and reference elastic warp knitted fabrics were investigated. It was found that novel elastic fabrics have higher values of comfort indicators and provide the necessary functional properties.

Key words:

elastic fabric, warp knitting, permeability, perforation.

1. Introduction

The demand for such medical products as bandages and corsets is growing every year [1]. For the treatment of diseases of the thoracic, lumbar and sacral regions, simple medicines are not enough, but also supportive devices are needed. The manufacturing of textile products for preventive and rehabilitation purposes is relevant in the socio-economic aspect as well. They allow you to normalize body motion and human well-being; to ensure the limits of a normal state in the life cycle, to preserve health, and to prevent future disease development. The history of the creation and development of medical and preventive products goes back decades, during which the product designs have undergone significant changes. They gained the greatest development with the appearance of elastic textile bands and fabrics [2].

Different textile technology (braiding, weaving, knitting, and non-weaving) are used for the manufacture of medical products. Knitting is the most promising method because of favorable technical and economic indicators as well as product quality [3]. Knitted fabrics with their huge variety of interlooping, differences in the raw material composition, stitch density, thickness, and so on have got a wide range of physical-mechanical and comfort properties. In addition, they also ensure a good fit for the different shapes of the body surface.

High stretchability and elasticity are the main functional properties of knitted fabric for rehabilitation products. It is provided by the use of elastomers such as polyurethane or latex threads and is determined by their location. In weft knitting, elastomeric threads are used as a transverse weft (coursewise stretching fabric) [4] or for loops formation (bi-stretching fabric) [5], while in warp knitting, elastomeric threads are usually vertically laid (walewise stretching fabric) [6]. It should be noted that the warp-knitted band manufactured on the Crochet knitting machine is the preferred material for corsets and bandages

[7]. The pillar stitch with the closed loop is ground interlooping. The elastomer threads are laid longitudinally in every wale and positioned between the loop`s overlap and underlap. They are fed into knitting zone with up to 270% pre-elongation. The weft filling yarns are used for connecting the separate chains into the fabric and are laid for the whole width on both sides of elastomeric threads to cover them better. Such fabric has very compact structure (Figure 1) with high stitch density vertically as a result of elastomer relaxation after knitting.

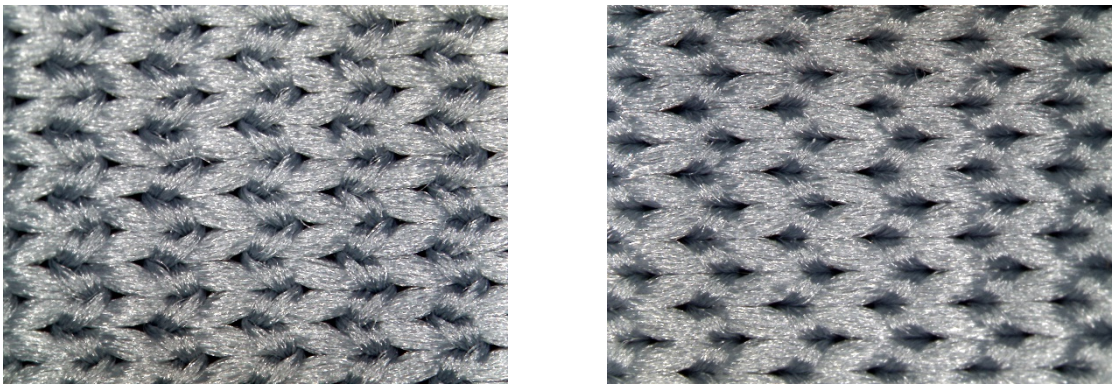

a b

Figure 1. Photos of elastic warp knitted fabric: a – face side; b – back side

The comfort is the second important aspect of developing elastic materials for medical and preventive products [8]. is a complex parameter because it involves both objective (permeability, hygroscopicity, thermal conductivity) and subjective (individual human approach) scores [9]. It is paid considerable attention now. These requirements are usually provided by the raw material composition [10].

The goal of this research is to develop novel elastic warp knitted material with through holes in terms of improving the permeability and future providing a higher comfort level of medical products.

2. Experimental part

2.1. Materials

Four fabric variants differ by transvers weft (Table 1) were produced on 15-gauge T.C.H crochet knitting machine. Technological parameters as yarn feeding tension, fabric takedown load, and the number of used needles were kept constant for all samples.

Table 1. Elastic warp knitted fabric

Cod	Linear density of weft thread	Variant of weft
AW	33.4 tex * 2	whole width
AP	33.4 tex * 2	patterned
BW	33.4 tex * 4	whole width
BP	33.4 tex * 4	patterned

The 16.7 tex polyester threads are used as ground (1st guide bar) for pillar stitches (Fig. 2.a) and 0.8 mm diameter polyurethan threads (3rd guide bar) are used as longitudinal elastomer component (Fig. 2.b). Both guide bars are fully threaded.

The 33.4 tex (96 filaments) polyester threads of 2-ply (A variant) and 4-ply (B variant) were used as weft in transverse direction. In order to create novel structure and to study the effect of interlooping on fabric properties two variants of weft yarn laying-in repeat were used:

- the whole width weft (W variant) introduced by special feeders on both sides of elastomer threads in opposite directions (reference samples);
- the patterned weft (P variant) introduced by incomplete (1 in, 5 out) guide bars (Figure 3) on both sides of elastomer threads in same directions (novel structure).

Figure 2. Lapping diagram: a – 1st guide bar (pillar stitch); b – 3rd guide bar (elastomer thread)

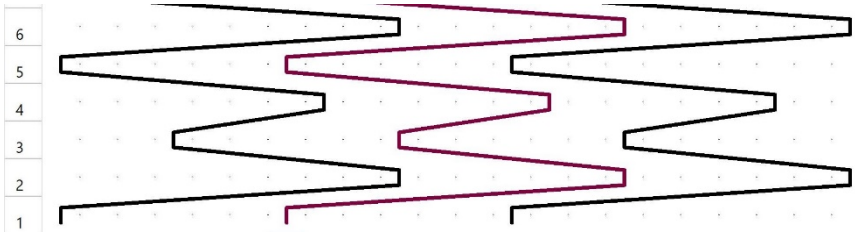

Figure 3. Lapping diagram for: 2nd and 4th guide bars (patterned weft)

The lapping diagrams on figures 2 and 3 were created by using Warp Knitting Pattern Editor of TexMind [11].

2.2. Methods

The structural properties of the fabrics were tested using the following standards: BS EN 14971:2006 [12] for stitch density, ISO 5084: 1996 [13] for thickness, and ASTM D3776 [14] for mass per unit area. The mean value for 10 parallel measurements were used for result analyses.

Photos of fabrics were taken on a digital microscope Microsafe ShinyVision MM-2288-5X-BN. Loop size and hole areas were measured by ImageJ software (Figure 4). The mean value for 10 parallel measurements were used for result analyses.

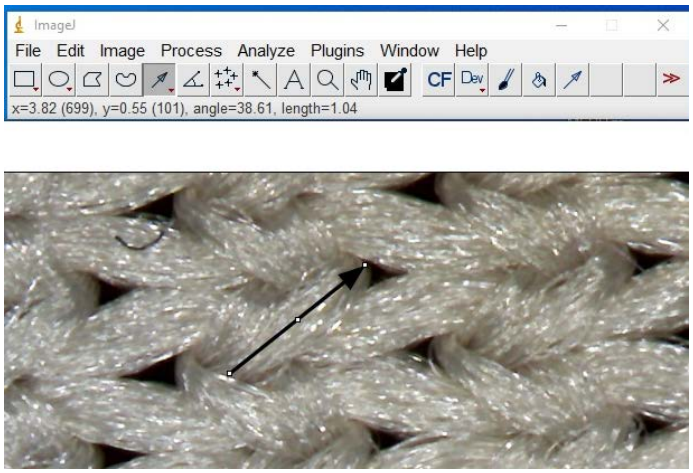

Figure 4. Measurement with ImageJ software

The study of stretchability and elasticity of elastic warp-knitted fabric was performed according to BS EN ISO 20932-1:2020 [15] on Zwick Roell Z010. Required cycling limits are the following: gauge length settings 100 mm; the number of cycles 5; cycling load 35 N, recovery period 30 min. 3 specimens (300 mm x 50 mm) were tested for each fabric's variant. The following indicators are calculated from obtained data: elongation, permanent deformation, recovered elongation and elastic recovery.

Comfort properties of the fabrics were tested using the following standard methods:

- Air permeability is according ISO 9237:1995 [15] on Textest FX 3300 (pressure of 100 Pa and sample area of 20 cm2). Each fabric sample was tested 10 times.
- Thermal conductivity is according ISO 8301: 1991 [16] on Alambeta (Sensora instruments). Each fabric sample was tested 3 times.
- Water vapour resistance is according TS EN ISO 11092:2014 [17] on Permetest. Each fabric sample was tested 5 times.

3. Results and discussion

3.1. Fabric structure

The fabrics with the patterned weft yarns (variants AP and BP) have got through holes in 3rd and 4th courses of repeat at places where no connection between the two adjacent weft yarns (Figure 3). The photos of fabric after knitting and relaxation during 48 hours in standard environmental conditions (20 °C and 101 kPa) are presented in Figure 5. The measurement results of stitch size and hole areas are presented in Table 2.

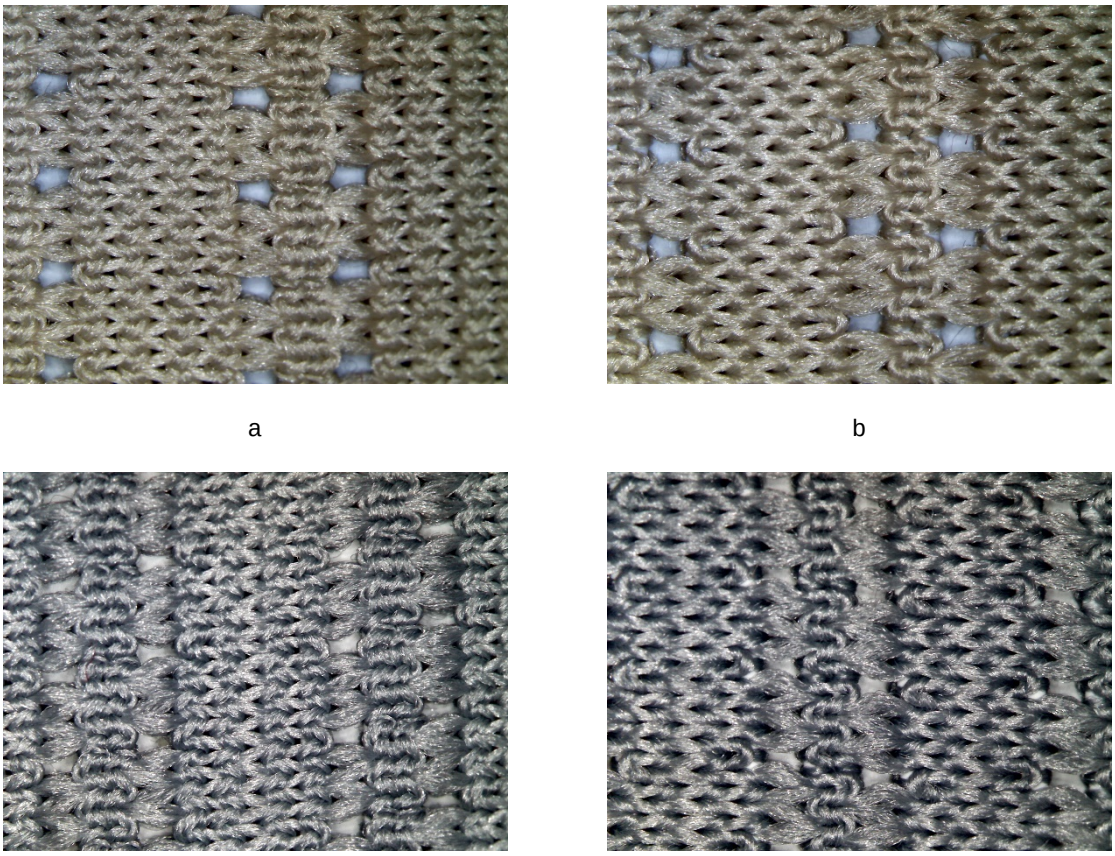

Figure 5. Photos of novel elastic warp knitted fabric:
a – AP face side; b – AP back side; c – BP face side; d – BP back side

As a result of the analysis of the stitch size (loop`s width and height), it was established that the novel fabrics with perforation correspond to the reference elastic warp-knitted fabrics. There is a difference in loop positioning only. For fabric with a 2-ply weft yarn, the loop skeleton is more inclined to the horizontal line. It is the result of both the total linear density of weft yarn and better conditions for elastomer relaxation.

Table 2. Stitch size and hole area of elastic warp knitted fabric

Cod	Loop`s width, W [mm]	Loop`s height, W [mm]	Angle to horizontal [°]	Hole`s area, S [mm^2]
Reference samples				
AW	1.05	0.76	38.8	-
BW	0.96	0.76	42.9	-
Developed structure				
AP	1.04	0.73	38.7	0.74 ± 0.01
BP	1.01	0.79	40.3	0.45 ± 0.01

It should be noted that the size of the through holes is larger for AP fabric despite the smaller loop`s height. It is because the ticker weft yarn in BP fabric fills the part of a hole.

3.2. Structural parameters

The structural parameters of elastic warp knitted fabrics are presented in Table 3.

The total linear density of weft threads affects the stitch length. The loop`s length for fabrics with 4-ply weft yarn is 5.5 % longer than for fabrics with 2-ply weft yarn. The length of elastomer per stitch for BP fabric is longer than for AP fabric as well. Research results show that weft yarn repeat affects its length only. The weft length per stitch for developed fabrics is 10% less than that for reference ones.

It is obvious that all knitted fabrics have the same stitch density horizontally (62 wales per 100 mm) because the distance between the wales is determined by the needle pitch. There is difference in stitch density vertically. For the reference samples the density of BW fabric is 35 stitches (17 %) less than AW fabric. The difference for developed structure is not so big. It is only 7 stitches (4 %).

Table 3. Parameters of elastic warp knitted fabric

Cod	Stitch length [mm]			Stitch density per 100 mm		Thickness [mm]	Mass per unit area [g/sq.m]
	loop	elastomer	weft	wales	courses		
Reference samples							
AW	5,50 ± 0,01	0.50	1.67 ± 0.01	62	204 ± 3	1.48 ± 0.01	809.4 ± 4.2
BW	5,82 ± 0,01	0.53	1.70 ± 0.01	62	168 ± 2	1.68 ± 0.02	947.7 ± 4.6
Developed structure							
AP	5,56 ± 0,02	0.51	1.50 ± 0.02	62	193 ± 3	1.69 ± 0.02	794.2 ± 4.0
BP	5,79 ± 0,02	0.51	1.51 ± 0.02	62	186 ± 3	1.78 ± 0.02	886.0 ± 4.6

As for thickness, the fabrics with 4-ply weft yarn are thicker than the corresponding fabrics with 2-ply weft yarn (Figure 6). It was found that developed fabrics are thicker than reference ones. It is the result of the overlapping of two weft threads in the contact areas. Developed elastic warp-knitted fabrics have reduced mass (Figure 7) that leads to a decrease in materials consumption and weight of the final product.

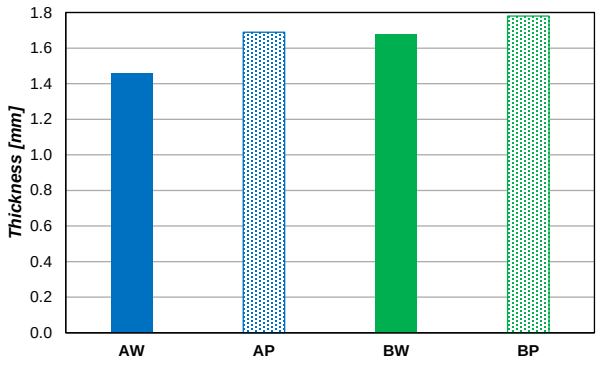

Figure 6. The thickness of elastic warp knitted fabric

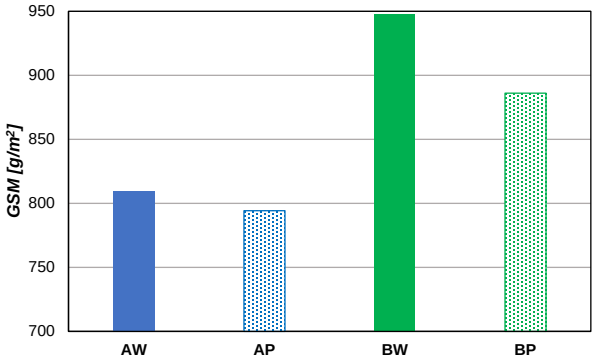

Figure 7. The mass of elastic warp knitted fabric

3.3. Elasticity

The research results for elasticity of elastic warp knitted fabric are presented in Table 4. They show that both reference and novel elastic warp knitted fabric with perforation provides a high level of stretchability and elasticity. The fabrics` elongation is more than 140 [%] and only for the AP variant is 127 [%] but it is quite high. A permanent deformation does not exceed 3 [%]. All studied elastic warp knitted fabrics provide high level of elasticity: elastic recovery is more than 98%.

Table 4. Elasticity of elastic warp knitted fabrics

Cod	Elongation, S [%]	Permanent deformation, C [%]	Recovered elongation, D [%]	Elastic recovery, R [%]
Reference samples				
AW	147 ± 2	2.3 ± 0.3	144	98.4
BW	142 ± 3	0.3 ± 0.0	142	99.8
Developed structure				
AP	127 ± 1	1.7 ± 0.3	125	98.7
BP	142 ± 3	3.0 ± 0.5	139	97.9

3.4. Air permeability

The results of the fabrics` air permeability testing are presented in Figure 8. Predictably, novel fabrics have much greater value because of through holes. The value is greater for fabrics with 2-ply weft yarn both reference and developed structures.

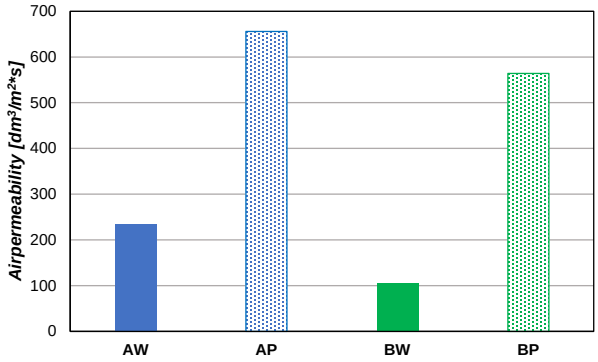

Figure 8. The air permeability of elastic warp knitted fabric

3.5. Water vapor permeability

Research results obtained at the Permeatest instrument are presented in Table 5.

The reference elastic warp knitted fabrics AW and BW have 30-31% relative water vapour permeability (RWVP) that is not affected by the total linear density of transverse weft threads. The novel elastic warp knitted fabrics has improved water vapour permeability that depends on the total linear density of transverse weft threads. AW sample has 8% higher RWVP compared to BP sample.

Table 5. Water vapor properties of elastic warp knitted fabrics

Cod	Relative Water Vapour Permeability, RWVP [%]	Water Vapour Resistance, Ret [Pa·m^2·W^{-1}]
Reference samples		
AW	30 ± 1.1	10.7 ± 0.43
BW	31 ± 1.1	12.9 ± 0.54
Developed structure		
AP	41 ± 1.2	8.1 ± 0.25
BP	33 ± 0.8	9.6 ± 0.48

The Water Vapour Resistance coefficient (Ret) of novel elastic warp knitted fabrics is lover compared to reference samples. It allows developed fabric to be used in medical products for moderate efforts. They are more pleasant to wear during physical activity.

3.6. Thermal properties

Research results obtained at the Alambeta instrument are presented in Table 6.

The decrease in the thermal conductivity coefficient and the increase in the thermal resistance coefficient indicate the lower thermal insulation properties for novel elastic warp-knitted fabrics (AP and BP). As described before, the novel fabric is developed for medical products used daily and worn on underwear or even on the body directly. In this case, the lower thermal insulation properties lead to improving the comfort of products.

Table 6. Thermal properties of elastic warp knitted fabrics

Cod	Thermal conductivity coefficient $\lambda\ 10^3$ [$W \cdot m^{-1} \cdot K^{-1}$]	Thermal diffusivity coefficient, $a\ 10^{-6}$ [$m^2 \cdot c^{-1}$]	Thermal absorptivity coefficient, b [$W \cdot s^{1/2} \cdot m^{-2} \cdot K^{-1}$]	Thermal resistivity coefficient, $R\ 10^{-3}$ [$K \cdot m^2 \cdot W^{-1}$]
Reference samples				
AW	76.3 ± 0.9	0.105 ± 0.009	236 ± 7	19.2 ± 0.3
BW	78.7 ± 0.6	0.056 ± 0.003	333 ± 7	20.6 ± 0.2
Developed structure				
AP	66.1 ± 0.7	0.071 ± 0.003	248 ± 3	25.6 ± 0.2
BP	63.7 ± 0.6	0.095 ± 0.001	206 ± 2	28.0 ± 0.3

4. CONCLUSIONS

Taking into account the fact that elastic warp-knitted fabrics are widely used for the production of medical support products, new structures with perforations were developed. In contrast to the widespread fabrics with the whole-width weft, weft threads are laid according to a certain repeat and used incomplete threading of the guide bar. Through holes are formed in courses where there are no contacts between two adjacent weft threads. The conducted research showed that the main functional properties of the novel fabrics (stretchability and elasticity) correspond to the properties of the reference fabrics. Due to the presence of perforations, the comfort of the products is improved: air and water vapour permeability indicators have significantly increased and thermal protection indicators have decreased.

ACKNOWLEDGEMENTS

This research was done at Ege University within the 2221 project "Research and Development of Comfortable Elastic Textile Materials as a Medical Support Product" with support from The Scientific and Technological Research Council of Turkey. The authors would like to thank Philipp Schwartz Initiative for Ukrainian scientist as well for supporting the future development of project at Technical University Dresden.

References

1. *IMARC Group, Medical Textiles Market: Global Industry Trends, Share, Size, Growth, Opportunity and Forecast 2022-2027 (https://www.imarcgroup.com/medical-textiles-market)*
2. *Melnyk L.M., Kyzymchuk O.P. (2012) The utilization of elastic knitted materials in the medical-preventive goods. Bulletin of Kyiv National University of Technologies and Design, 4, 139-145. – in Ukranian*
3. *Sadhan Chandra R. (2012). 27 - Scope of knitting in the manufacture of medical textiles. In: Sadhan Chandra R, editor. Fundamentals and Advances in Knitting Technology: Woodhead Publishing India, 326-9.*

4. *Kyzymchuk, O. & Melnyk, L. (2016). Influence of miss knit repeat on parameters and properties of elasticized knitted fabric, IOP Conf. Series: Materials Science and Engineering, 141, 012006. DOI: 10.1088/1757-899X/141/1/012006.*
5. *Pavko-Cuden A. (2010) Parameters of Compact Single Weft Knitted Structure (Part 2): Loop Modules and Munden Constants – Compact and Supercompact Structure. Tekstilec, 53 (10–12), 259–272*
6. *Kyzymchuk, O., Melnyk, L., Arabuli, S. (2020). Study of Elastic Warp Knitted Bands: Production and Properties. Tekstilec, 63(2), 113-23. DOI: 10.14502/Tekstilec2020.63.113-123*
7. *Kyzymchuk, O., Melnyk, L. (2018) Stretch properties of elastic knitted fabric with pillar stitch. Journal of Engineered Fibers and Fabrics, 13 (4): 1-10. DOI : 10.1177/1558925018820722*
8. *Ng Sau-Fun, Hui Chi-Leung & Wong Lai-Fan (2011) Development of medical garments and apparel for the elderly and the disabled, Textile Progress, 43:4, 235-285, DOI: 10.1080/00405167.2011.573240*
9. *Mallikarjunan K., Senior L. (2011) Comfort and Thermo Physiological Characteristics of Multilayered Fabrics for Medical Textiles, Journal of Textile and Apparel, Technology and Management, 7 (1), 1–15.*
10. *Oglakcioglu N. (2016) Design of functional knitted fabrics for medical corsets with high clothing comfort characteristics. Journal of Industrial Textiles. 45(5), 1009-1025. doi:10.1177/1528083714551438*
11. *Warp Knitting Pattern Editor. TexMind. Web site: http://texmind.com/wp/products/warp-knitting-software/*
12. *BS EN 14971:2006 Textiles. Knitted fabrics. Determination of number of stitches per unit of length and unit area*
13. *ISO 5084: 1996 Textiles - Determination of thickness of textiles and textile products*
14. *ASTM D3776. Standard Test Methods for Mass Per Unit Area (Weight) of Fabric.*
15. *BS EN ISO 20932-1:2020+A1:2021 Textiles. Determination of the elasticity of fabrics. Strip tests.*
16. *ISO 9237:1995, Textiles -- Determination of the permeability of fabrics to air*
17. *ISO 8301:1991 Thermal insulation; determination of steady-state thermal resistance and related properties; heat flow meter apparatus.*
18. *TS EN ISO 11092:2014 Textiles. Physiological effects. Measurement of thermal and water-vapour resistance under steady-state conditions*

INVESTIGATION OF STRUCTURAL AND PERFORMANCE PROPERTIES OF HEMP-CONTAINING KNITTED FABRICS WITH DIFFERENT COMPOSITIONS

Korhan Sen[1*], Aysegul Kaya[1], Goksu Kanık[1]

1TYH Uluslararası Tekstil Pazarlama A.Ş., Istanbul R&D Center, Oruc Reis Street No:7, P.O. Box 34197, Istanbul, Turkey.

***Corresponding author**

[1*]TYH Tekstil Istanbul R&D Center Istanbul, Turkey, korhansen@tyh.com.tr, (+905378839203)
[1]TYH Tekstil Istanbul R&D Center Istanbul, Turkey, aysegulkaya@tyh.com.tr, (+905433738577)
[1]TYH Tekstil Istanbul R&D Center Istanbul, Turkey, goksukanik@tyh.com.tr, (+905546247098)

Abstract:

The growing relevance of sustainable materials has increased the importance of hemp-containing products obtained from natural fibers. When the raw materials used in the garment industry are examined, it is observed that the market share of hemp-containing fibers is low in percentage. Researching the production techniques and methods of fabrics to be obtained from hemp fiber and adapting them to the use of clothing will contribute significantly to the development of the hemp product range. It is aimed that these fabrics to be developed will pass tests in accordance with end-consumer standards. In this study, structural and performance properties of hemp fiber were examined and alternatives were produced instead of conventional methods for a sustainable world. In line with the sustainability strategy, there are advantages of hemp fibers in terms of water consumption, environmental impact compared to cotton fiber. Within the scope, studies were carried out to develop single jersey knitted fabrics by hemp- containing at different compositions such as 70 % cotton/ 30 %hemp, 80 % cotton/ 20 %hemp and 90 % cotton/ 10 %hemp, %100 cotton fabric having the similar structural properties was taken as a control sample. As a result, prototype tests were performed considering the structural and performance properties of the developed fabrics.

Key words:

Textile Ecology, Sustainability, Hemp Fiber, Cotton Fiber, Knitting, Water Consumption

1. Introduction

The textile and apparel industry, which is one of the most important requirements of people, should continue its activities by considering human and environmental health and, accordingly, sustainable development. The concept of “textile ecology” is important to ensure sustainability in the textile industry. In this context, hemp, a biodegradable fiber, has come to the fore again [1].

Due to its many environmentally friendly features, the use of hemp fiber in sustainable textile design and production also allows it to be evaluated within the scope of slow and ecological fashion. There are many studies conducted on reusing hemp fibers by recycling them with chemical methods, and this shows its sustainability. Hemp is a more environmentally friendly, economical and sustainable type of raw material compared to similar raw materials [2].

Hemp is an industrial plant which has an annual, herbaceous and multi-use potential in the cannabis. Cannabis is a woody annual plant from the Cannabaceae family. Today, there are two subspecies of hemp. These are; Cannabis sativa and Cannabis indica. The type that is important for industrial applications and used in fiber production is Cannabis sativa. [3].

Since it does not demand much water, it contributes to the protection of water resources. It produces a high amount of oxygen and does not require pesticides and fertilization as it does not have any agricultural pests. Hemp acts as a carbon sink due to CO_2 absorption, and it has been revealed that hemp plants help maintain strong soil structure, protecting them against landslides due to their roots located at a depth of about 1 meter underneath. According to the related literature, compared to cotton cultivation, it was determined that the water footprint of industrial hemp (2719 l/kg) is less than 1/3 of the water footprint of cotton (10000 l/kg) [4].

On the other hand, it has been observed that 60% of hemp is returned to the soil as a nutrient when dried in the field. In this context, literature research has shown that the environmental impact of hemp raw materials is low and can be an important resource in ensuring sustainability in the textile industry. Looking at the physical structure of hemp fiber, hemp fiber has a hollow structure. It has a large lumen and this lumen constitutes approximately 1/2 - 1/3 of the total cross-sectional area. It is larger than ramie, flax, and cotton. Since there are many hydrophilic molecules that can easily combine water molecules, hemp fiber has good moisture absorption with a commercial moisture value of 10.8%. It also has a much higher moisture holding capacity than cotton fiber with a commercial moisture value of 8.5%. Hemp fiber with a polygonal cross-section has a hollow structure with a lot of air inside, which can increase insulation. At the same time, it effectively prevents the formation of anaerobic bacteria. Hemp fiber can block up to 90% of ultraviolet sunlight without any treatment, and this is because of its high lignin content, which can absorb ultraviolet light [5-7].

Within the scope, the development studies with a composition of 70 % cotton/ 30 %hemp, 80 % cotton/ 20 %hemp and 90 % cotton/ 10 %hemp single jersey knitted fabrics in navy blue color with Ne number 20/1 were carried out. These fabrics were compared to %100 cotton fabric with similar properties. The mass per unit area value of the cotton fabric is 175 g/m^2 and the width is 185 cm. Procurement studies were carried out to determine the fabric formulation and content. Since hemp fiber is limited, the duration of the studies has been extended. Fabric development studies were carried out with another supplier.

Defects in raw material production due to the pandemic and the fact that hemp yarn quality is not suitable for knitting made prototype development studies difficult. Since hemp is seen as the cotton fiber of the future, TYH Tekstil attaches importance to the use of hemp- containing yarns. Therefore, despite the failures, the studies continued. As a result, structural and performance tests such as pilling, fastness, fiber analysis (quantitative/microscopic count- qualitative method) and bursting strength were made on the developed fabrics and comparisons were made between both fabrics.

2. Experimental

2.1. Materials

Single jersey knitted fabrics with Ne 20/1 yarn counts in different weights and compositions from natural fibers were used in this study. The structural parameters of the fabric samples used in this study are listed in Table 1.

Table 1. Properties of TYH fabrics

Properties of Fabrics	Fabric-1	Fabric-2	Fabric-3	Fabric-4
Raw Material	100% cotton	90 % Cotton 10 %Hemp	80 % Cotton 20 %Hemp	70 % Cotton 30 %Hemp
Type Knitting	Single jersey			
Unit Weight (gr/m²)	175	170	170	160
Yarn Count (Ne)	20/1			
Color	Navy Blue- 654-860.qtx			

2.2. Methods

To ensure compatibility between fabrics, first of all, the structural properties of the developed fabrics were evaluated. Washing fastness, rubbing fastness (dry and wet), water fastness, perspiration fastness, pH tests, pilling test with ICI Pilling Box and Pilling Martin Dale were performed. In addition, fiber analysis (quantitative/microscopic count- qualitative method), bursting strength test was determined. Test sample fabrics were adjusted according to standard conditions before test and analyzes (21 ± 1 °C, 65 ± 2% relative humidity).

In this study, these tests applied to the fabrics have been conducted in accordance with certain standards. Tests and related standards are given in Table 2.

Table 2. Tests and Standards

Test	Standard
Washing Fastness (Gyrowash)	ISO 105 C06 AIS
Rubbing Fastness (Dry-Wet)	EN ISO 105 – X12
Water Fastness	EN ISO 105 – E01
Perspiration Fastness	EN ISO 105 – E05
pH	ISO 3071 – 1980
ICI Pilling Box	ISO 12945 – 1
Pilling Martin Dale	EN ISO 12947
Fiber Analysis (quantitative/microscopic count)	AATCC 20 A
Fiber Analysis (qualitative method)	TS 4739:1986 (Metot:1)
Bursting Strength	ISO 13938-2:2019

Hemp-containing yarns could not be knitted due to the strength problem. Both yarns created bursting images during knitting. Yarn repair works were started by checking the strength, pilling and fastness values of the fabrics and improving the production conditions of the yarns. It has been observed that the working performance is low during knitting due to waiting after fixation with yarns. The fixation is a process performed to provide yarn relaxation and proper working form.

The drier the environment in the waiting conditions of the yarn, the shorter the deterioration of this form. If the standard weather conditions (closed warehouses out of the sun) are provided, it is not affected by the waiting period. When the incoming yarns were examined, it was observed that they were subject to the post-shipment transfer process and the yarn was very dry. This situation directly affects the breaking and working performance. Double fixation was applied for improvement studies. It has been tried to improve the working performances by re-transferring-fixing the yarns.

3. Results and discussion

Fastness is a color strength of textile product to withstand the factors encountered during both its production and use. It is a major quality feature in dyed textile products. Knowing the fastness of the textile material is important for the preparation of care labels [8]. Thus, washing fastness, rubbing fastness (dry and wet), water fastness, perspiration fastness and pH tests were applied. Table 3 shows the results of these testing. These tests were carried out in the company's laboratory. As can be seen from Table 3, it was determined that the developed knitted fabrics presented good fastness results. Test results were evaluated according to the company's acceptance value and customer criteria.

Table 3. Structural Tests of the fabrics and results

Physical Test	Fabric-1	Fabric-2	Fabric-3	Fabric-4
Washing Fastness	4/5	4/5	4/5	4
Dry Rubbing Fastness	4/5	4	4/5	4/5
Wet Rubbing Fastness	3/4	4	4	4
Water Fastness	4/5	4	4	3/4
Perspiration Fastness	4/5	4	4/5	4
pH	6.8	6.9	6.9	6.8
ICI Pilling Box	4	4	4	3/4
Pilling Martin Dale	4	3/4	4	3

In addition, the pilling problem, one of the important problems in textile, disturbing both the producer and the consumer and also affecting the fabric quality. Test devices and methods used together with the factors affecting pilling are also very important in terms of evaluating the pilling performance of fabrics [9]. In this context, as a fabric pilling analysis, Martin Dale test according to EN ISO 12947 standard and ICI Pilling Box test according to ISO 12945-1 standard were performed on the developed knitted fabrics as seen in Table 3. Martin Dale test results were determined as 3/4 and 4, ICI Pilling Box test as 4. These results have been accepted as valid according to standards.

In the literature, effect of the parameters, affecting the evenness also mechanical and structural properties of blended yarns with different hemp compositions, and the regression equation between blending ratio and yarn mechanical property was investigated. Based on this equation, blended yarns were produced in different compositions by using polyester, hemp and cotton fibers in the experiment. When the results were examined, it was observed that the unevenness of the hemp blended yarn increased as the hemp fiber ratio in the yarn increased. Since hemp fiber has longer fiber length, higher initial modulus, irregular fiber cross-section and greater surface friction than polyester and cotton, in addition to its stiffness, its distribution in the yarn is greatly affected by the content. Due to its mechanical properties, hemp fiber is affected by its distribution in the yarn. It has been found that, due to their smooth surface and low holding force, they are easy to slide from each other, although they have high strength when stretched. It has also been observed that when hemp fiber is blended with polyester and cotton in specific rate, the adhesive strength increases again under the effect of twisting [7, 10].
Bursting strength test were performed in the relevant parts of the product as a performance test. In this context, the performance tests of the fabrics are presented in Table 4.

Table 4. Performance tests of the fabrics and results

Performance Test	Fabric-1	Fabric-2	Fabric-3	Fabric-4
Bursting Strength, (kPa)	603.3	489.2	525.95	460.05
Distance To Burst, (mm)	16.1	10.6	10.8	10.5

Examining the test results, the rigid structure of the hemp fiber improves the strength of the fabric up to a certain point, and when that point is exceeded, hemp fibers begin to fall out. Thus, it reduces strength and more fiber fall out occurred in the Fabric-4 (70 % Cotton/ 30 %Hemp) compared to others. In the test results, it was observed that the Fabric-3 (80 % Cotton/ 20 %Hemp) gave ideal results close to cotton. In terms of structural properties, the Fabric-3 (80 % Cotton/ 20 %Hemp) gave better results than other hemp blended fabrics. This fabric can be an alternative fabric to cotton fibers. The optical microscope images of hemp and cotton fibers are shown in Figure 1.

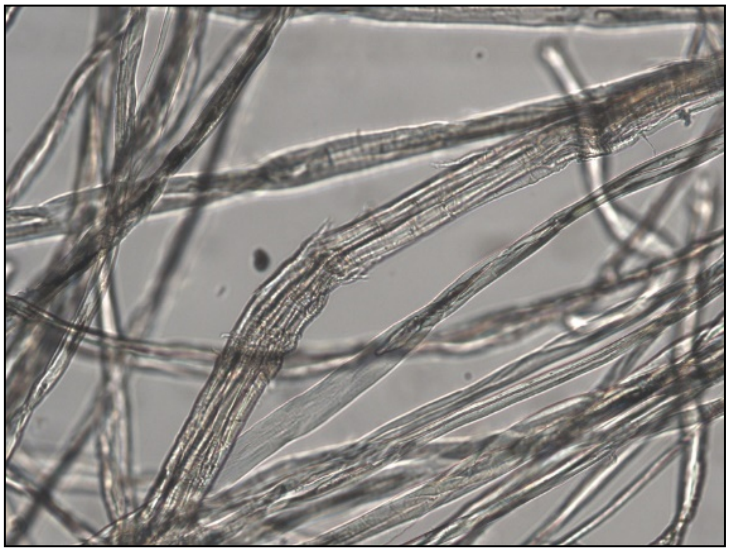

Figure 1. Structure of cotton/hemp fibers

The fibers in the middle in the image are hemp fibers, as seen in the Figure 1. Under a microscope a cotton fiber looks like a twisted ribbon or a collapsed and twisted ribbon or a collapsed and twisted tube. These twists are called convolutions [11]. Hemp has more twisted ribbon than cotton fiber.

During the growth phase of the plant, there is no change in the number of fibers, but the length of the fiber's increases. In the hemp plant, the fiber thickness increases from the stem down. The fiber lengths are determined by the distance between the ribbon. The glossy hemp fibers are yellow-brown, and the cross-section of the fiber is polygonal [7, 12].

4. CONCLUSIONS

The fact that the products obtained from synthetic fibers are petroleum-based increase the CO_2 emission and carbon footprint. Natural fibers are mostly preferred in clothing products used in our daily lives. On the other hand, hemp fibers have become an alternative to cotton since the cultivation process of cotton fibers, which is the most preferred natural fiber, includes abundant irrigation and pesticide and chemical fertilizer applications that cause many health problems. For this purpose, TYH Tekstil has given importance to research and development studies in this field, considering hemp fibers as the cotton of the future.

Many problems have been encountered in hemp fiber, from the fiber stage to the fabric stage. Despite all the problems, fabrics have been developed. Studies were carried out to develop single jersey knitted fabrics from blending raw materials containing hemp at different composition such as 70 % cotton/ 30 %hemp, 80 % cotton/ 20 %hemp and 90 % cotton/ 10 %hemp, %100 cotton fabric having the similar structural properties was taken as a control sample. The structural and performance properties of the fabrics developed in the test results are evaluated. Results show that compared to other hemp-containing knitted fabrics, 80% cotton/ 20% hemp blended knitted fabric was considered more suitable for use in knitting. Consequently, this study reveals that composition is not the decisive factor, although it is commonly assumed that the strength reduces as the hemp ratio increase. The rigid structure of the

hemp fiber improves the strength of the fabric up to a certain point, and when that point is exceeded, hemp fibers begin to fall out. Thus, it reduces strength and more fiber fall out occurred in the Fabric-4 (70 % Cotton/ 30 %Hemp) compared to others.

Hemp fiber is very popular nowadays due to the rising of environmental concerns. This popularity depends on its ecological properties and superior daily usage performance. This paper gives information about hemp fiber properties and its advantages. The aim of this paper is to highlight the importance of hemp-containing textiles for today's world textile market. As a suggestion, in the light of this study, experiments can be made on different fabric compositions to find the rate at which fiber fall out starts. Factors affecting the fall out can be determined and studies can be carried out to solve this problem. As a result, its use can be spread by increasing the hemp mixture to the highest possible rate. It's observed that defects are related to strength properties according to performance test in this study. TYH Tekstil Istanbul R&D Center is open to cooperate for innovative studies and suggestions.

ACKNOWLEDGEMENTS

This study is conducting in an apparel company's R&D Center as an R&D project. This work would not have been possible without his endless support of dear Mr. Mehmet Kaya, the director of TYH Tekstil A.Ş. We are especially indebted to him and TYH Tekstil. We would also like to show my gratitude to all of those with whom We have had the pleasure to work during this study and other related projects.

References

1. *Kumar, R. (2017). Prospects Of Sustainable Fashion Design Innovation. International Journal of Textile and Fashion Technology, Volume 7, Issue 6, 5-14.*
2. *Gedik, G., Avinc, O., (2020). Hemp Fiber as a Sustainable Raw Material Source for Textile Industry: Can We Use Its Potential for More Eco-Friendly Production? Sustainability in the Textile and Apparel Industries, 87–109.*
3. *Kurtuldu, E., Ismal, Ö.E. (2019). The Fiber Appreciated Again in Sustainable Textile Production and Design: Hemp (in Turkish). Faculty of Fine Arts Art Journal, Volume 12, Issue 24, 694- 718.*
4. *Averink, J. (2015). Global water footprint of industrial hemp textile (Master's thesis, University of Twente).*
5. *Ahmed, F., Islam, Z., Mahmud, S., Sarker, E., Islam, R. (2022). Hemp as a potential raw material toward a sustainable world: A review. Heliyon. Volume 8, Issue 1. 1-15.*
6. *Zimniewska, M. Hemp Fibre Properties and Processing Target Textile: A Review. Materials 2022, 15, 1901.*
7. *Kaya, S., Oner, E. (2020). Production, Characteristics and Applications of Hemp Fibres in Textile Industry (in Turkish). The Journal of Graduate School of Natural and Applied Sciences of Mehmet Akif Ersoy University Volume 11, Issue 1 108-123.*
8. *Tolek, S., Kadem, F.D. (2016). An investigation on color analysis and Fastness properties of the denim fabric Dyed with a different method (in Turkish). Tekstil ve Konfeksiyon, Volume 26, Issue 2, 199-204.*
9. *Okur, A. (1998). Pillling of fabrics: formation, affecting factors and testing methods (in Turkish). Tekstil ve Mühendis, Volume 45-46, 10-18.*
10. *Zhang, H., Zhang, J., Gao, Y. (2014). Study on the relationship between blending ratio and performance of hemp/polyester yarn. Journal of Natural Fibers, Volume 11, Issue 2, 136-143.*
11. *Mondal, I.H. (2021). Fundamentals of Natural Fibres and Textiles. A volume in The Textile Institute Book Series, Cover for Fundamentals of Natural Fibres and Textiles.*
12. *Gedik, G., Avinç, O. O., Yavas, A. (2010). Hemp Fiber Properties and Its Advantages in Textile Industry (in Turkish). Electronic Journal of Textile Technologies, Volume 4, Issue 3, 39-48.*

POLYACRYLONITRILE NONWOVENS FOR THE PRODUCTION OF CARBON MATERIALS SUPPORTING THE REGENERATION OF BONE AND CARTILAGE TISSUES

Maciej Boguń[1], Katarzyna Śledzińska[1], Małgorzata Giełdowska[1], Paulina Król[1], Irena Kamińska[1], Sylwia Magdziarz[1,2]

[1]Łukasiewicz Research Network, Lodz Institute of Technology, 19/27 Marii Skłodowskiej-Curie, Lodz, Poland, mail: info@lit.lukasiewicz.gov.pl, tel. +48 42 307 09 01

[2]Institute of Organic Chemistry, Faculty of Chemistry, Lodz University of Technology, 116 Zeromskiego, 90-924 Lodz, Poland

corresponding author e-mail: maciej.bogun@lit.lukasiewicz.gov.pl

Abstract:

The influence of the change in surface weight on the physical properties of oxidized polyacrylonitrile precursor nonwovens intended for the production of carbon materials used in tissue engineering was studied. Thermal insulation properties of the nonwovens and their behavior during incubation in phosphate buffered saline (PBS) were investigated. Initial carbonization tests showed that from the point of view of carbonization and further application of carbon materials, the most effective was the use of a surface weight of about 120 g/m^2. At the same time, for the research conducted on the incubation of nonwovens in PBS, no significant change in the pH of the solution was found.

Key words:

polyacrylonitrile fibers, nonwovens, PBS incubation, thermal insulation properties

1. Introduction

One of directions in the development of contemporary medicine is the search for new materials that will support the process of tissue regeneration. Among these types of materials, carbon fibers, carbon nanostructures and composites with their participation are of particular importance. They have been used in many solutions in modern medicine [1-5]. In this case, it is important to properly select both the carbon fiber precursor and the carbonization process itself so that the produced carbon structure and its properties are appropriate for the intended purpose [6,7]. When thermal insulation properties of precursor nonwovens are known, it possible to select the most favorable conditions for the carbonization process in order to obtain a carbon nonwoven fabric with the same chemical structure in the entire bulk. This is extremely important from the point of view of medical application of carbon nonwovens, which will constitute the scaffolding of hybrid carbon-polymer biomaterials. At the same time, knowledge of the impact of the carbonization process on the liquid absorption capacity, changes in pH and conductivity of the incubated medium allows us to shape the behavior of the biomaterial in vitro and in vivo.
The aim of this study was to examine thermal insulation properties of the produced precursor nonwovens with two surface weights and to investigate the incubation of the nonwovens in a phosphate-buffered saline (PBS) solution.

2. Experimental

2.1. Materials

Oxidized polyacrylonitrile fibers from Toray (Hungary) were used for the production of nonwovens. Figure 1 shows a cross-section and longitudinal view of the fibers used. Medical grade phosphate-buffered saline solution (PBS) was used for incubation tests.

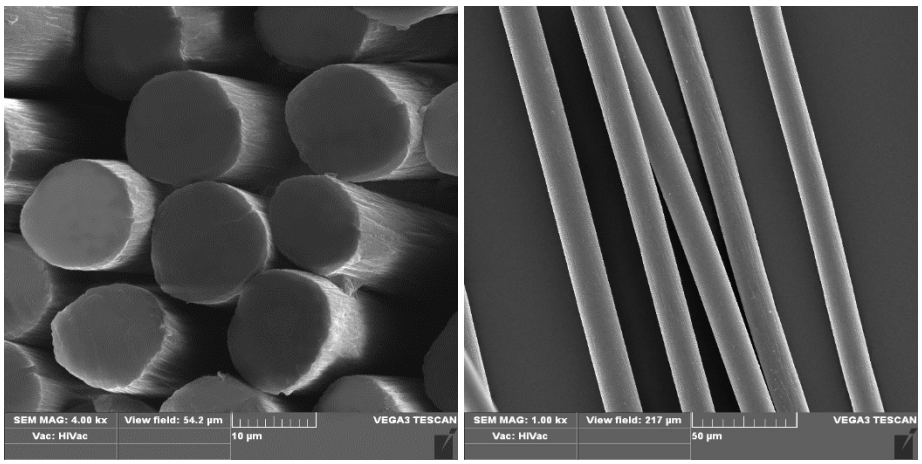

Figure 1. SEM pictures of the precursor fibers used

2.2. Methods

The nonwovens were produced using a mechanical fleece forming system with a laboratory carding machine. Then, the obtained fleece was subjected to the needling process on a HEUER type ROM 30LP/120/11/900 needle punching machine.
Measurements of the surface topography (SEM analysis) of the materials were carried out on a VEGA3 TESCAN (Tescan Osay Holding, Brno, Czech Republic)
To test the thermal insulation properties, the Alambeta device (Sensora, Czech Republic) was used, by means of which thermal conductivity, thermal diffusivity, thermal absorption, thermal resistance, quotient of the maximum and stationary heat flow density were measured.
The incubation of the nonwovens in PBS was examined at specific intervals. The pH and conductivity of the incubated medium was determined with an immersion probe.

3. Results and discussion

The study of thermal insulation properties shows that an increase of the surface weight from 120 g/m^2 to 600 g/m^2 causes an increase in thermal insulation parameters. This is typical because of a similar structure of the material used and differences in its thickness. There are significant differences in all tested thermal insulation parameters. The exception is heat flow density, which is at a similar level for both surface weights (Table 1). When analyzing results of the test and carrying out the process of carbonization of nonwovens, it should be stated that the increase of the surface weight results in quality deterioration of the produced carbon materials. It should be noted, however, that in the case of medical use of this type of biomaterial, the carbonization process is carried out to a temperature 1200°C. At the same time, as part of the work, research was carried out on the incubation of the produced nonwovens in the PBS medium at various intervals. Figures 2 and 3 show the results of changes in pH and conductivity of the incubated medium after keeping the nonwovens in it for various periods.

Table 1. Thermal insulation parameters for precursor nonwovens

Sample	λ $Wm^{-1}K^{-1}$	a m^2s^{-1}	b $Wm^{-2}s^{1/2}K^{-1}$	r Km^2W^{-1}	h mm	p -	q_{max} Wm^{-2}
OPAN 120	0,0368 ±0,0006	6,61E-07 ±1,04E-07	45,6 ±3,1	0,0712 ±0,0006	2,62 ±0,04	3,70 ±0,32	0,531 ±0,046
OPAN 600	0,0475 ±0,0019	4,37E-07 ±1,19E-07	73,1 ±8,3	0,1302 ±0,0066	6,17 ±0,16	5,86 ±0,78	0,528 ±0,065

where: λ – thermal conductivity; a – thermal diffusivity; b – thermal absorption; r – thermal resistance; h – thickness; p – the quotient of the maximum and stationary heat flow; q_{max} – maximum heat flow

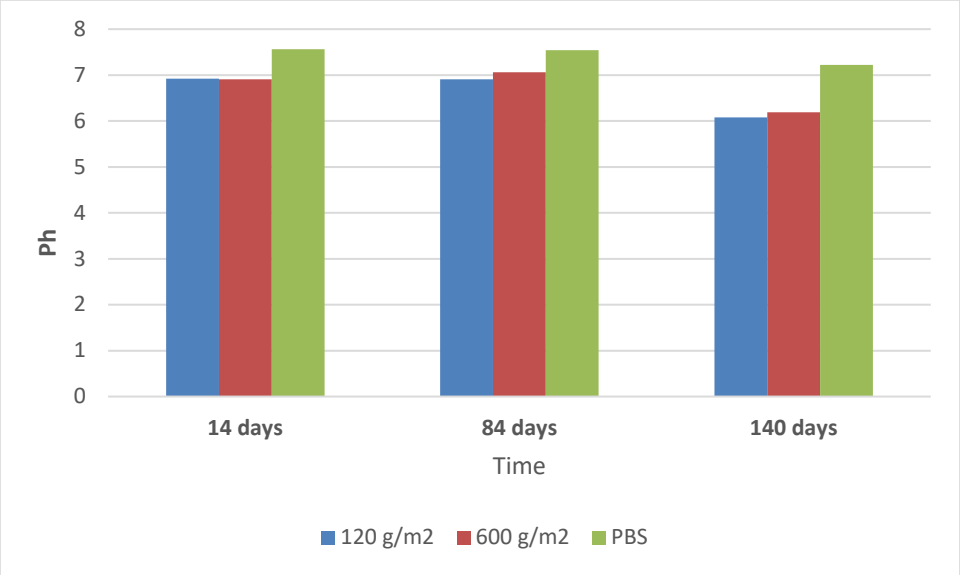

Figure 2. Changes in the pH of the incubation medium over time

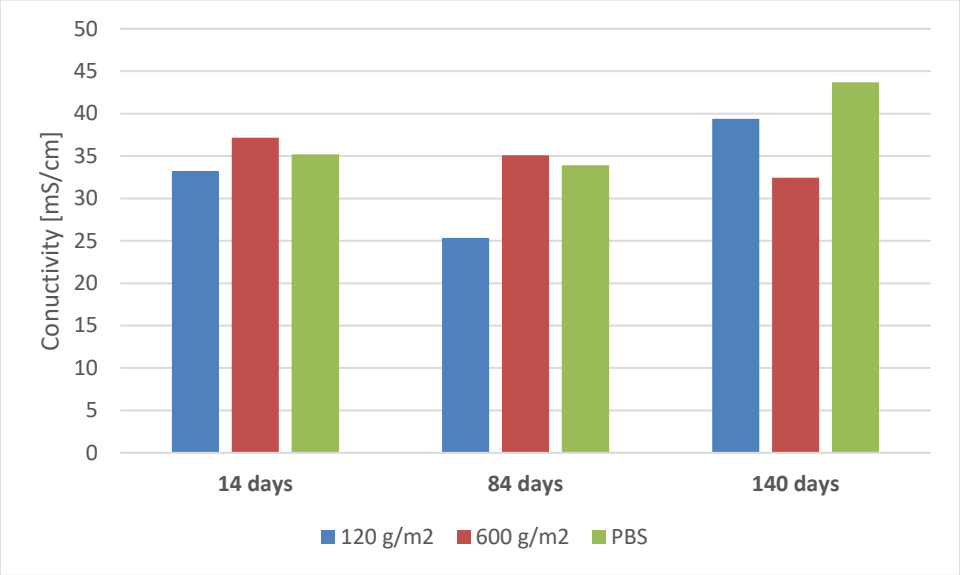

Figure 3. Changes in the conductivity of the incubation medium over time

The conducted research shows that the surface weight is of no great importance for the pH of the medium. In both cases, the change of pH ranges from 6 to 7. On the other hand, in the case of

conductivity, the influence of the surface weight of the nonwoven on changes of this parameter is visible. The incubation medium in which the nonwovens with a lower surface weight were kept shows an increase in conductivity over time, unlike the medium in which the nonwovens with a surface weight of 600 g/m^2 were incubated.

4. CONCLUSIONS

It follows from the research on thermal insulation properties that the surface weight of nonwovens can have a significant influence on the carbonization effectiveness. This may result in differences in the properties of the carbon material in the entire bulk. In the case of medical use of carbon structures, it is important that the carbon structure produced during the carbonization process is homogeneous. In this case, the lack of homogeneity in the chemical structure may result in the formation of inflammations in vivo. Research on the incubation of nonwovens with different surface weights in the assumed time intervals showed differences in the parameters tested. Therefore, it is important to reconcile many opposing interdependencies in the design of biomaterials, so that the material constructed in this case, being a type of GBR membrane (guide bone regeneration), contributes to the effective process of tissue regeneration.

ACKNOWLEDGEMENTS

This research was funded by the National Science Centre, Poland, grant number UMO-2018/31/B/ST8/02418

References

1. *Frączyk, J., Magdziarz, S., Stodolak-Zych, E., Dzierzkowska E., Puchowicz, D., Kamińska, I., Giełdowska, M., Boguń, M. (2021), Chemical Modification as a Method of Improving Biocompatibility of Carbon Nonwovens. Materials 14(12), 3198*
2. *Rajzer I., Rom, M., Błażewicz, M. (2010), Production of carbon fibres modified with ceramic powders for medical applictaions. Fibers and Polymers 11, 615-624*
3. *Trabelsi, M., Mamun A., Klöcker, M., Sabantina, L., Großerchode, Ch., Blachowicz, T., Ehrmann, A. (2019), Increased mechanical properties of carbon nanofiber mats for possible medical applications. Fibers 7(11), 98*
4. *Yadav, D., Amini, F., Ehrmann, A. (2020), Recent advances in carbon nanofibers and their applications – a review.(European Polymer Journal 138, 109963*
5. *Chua, C.Y.X., Liu, H.-Ch., Di Trani, N., Susnjar, A., Ho, J., Scorrano, G., Rhudy, J., Sizovs, A., Lolli, G., Hernandez, N., Nucci, M.C, Cicalo, R., Ferrari, M., Grattoni, A. (2021), Carbon fiber reinforced polymers for implantable medical devices. Biomaterials 271, 120719*
6. *Fraczek-Szczypta, A., Rabiej, S., Szparaga, G., Pabjanczyk-Wlazlo, E., Krol, P., Brzezinska, M., Blazewicz, S., Bogun, M. (2015), The structure and properties of the carbon non-wovens modified with bioactive nanoceramics for medical applications. Materials Science & Engineering C: Materials for Biological Applications 51, 336-345*
7. *Morawska-Chochół, A., Domalik-Pyzik, P., Menaszek, E., Sterna, J., Bielecki, W., Bonecka, J., Boguń, M., Chłopek, J. (2018), Biodegradable intramedullary nails reinforced with carbon and alginate fibers: in vitro and in vivo biocompatibility. Journal Applied Biomaterials&Functional Materials 16(1), 36-41*

A STUDY – GENESIS OF FIBRE FRAGMENTS

Jana Novotná

Technical University of Liberec, Dep. of Material Engineering, Liberec, Czech. Rep.,
e-mail: jana.novotna3@tul.cz

Abstract:

One of our society's long-standing environmental problems is the presence of textile fiber fragments in the air and all types of water worldwide. In addition to chronic effects on the human body, fibre fragments can also harm living organisms. In recent years, there has been an increasing number of scientific publications on this topic. This study looks at the current state of the art on fibre fragments and highlights the causes of fibre fragments.

Key words:

textile fibre fragments, textile fibres, microplastics, microfibers

1. Introduction

The global production of fibres (synthetic and natural) has been steadily increasing, as shown in Figure 1 [1]. In the new millennium, synthetic fibres have surpassed natural fibres in production. Synthetic fibres now dominate the textile market and are expected to continue. Recycled fibres will also increase as EU legislation will come into force in 2025, placing textiles in the circular economy system [2].

The textile, leather and clothing industries leave a significant ecological footprint and are resource and waste intensive. The EU population produced an average of 5 kg/year of textile waste per capita in 2020 [3]. At the same time, the annual global emission of synthetic fibre fragments from textiles is estimated to be approximately 500,000 mt/year [1]. At the same time, China is the world's largest producer of synthetic fibres, which produces 66% of all synthetic fibres [4].

Due to the worldwide variety of textile products and a large number of producers, as well as the import and export of textile goods, the spectrum of fibre fragments in the environment is extensive, and the origin of these fragments cannot be guaranteed with certainty, e.g. geographically.

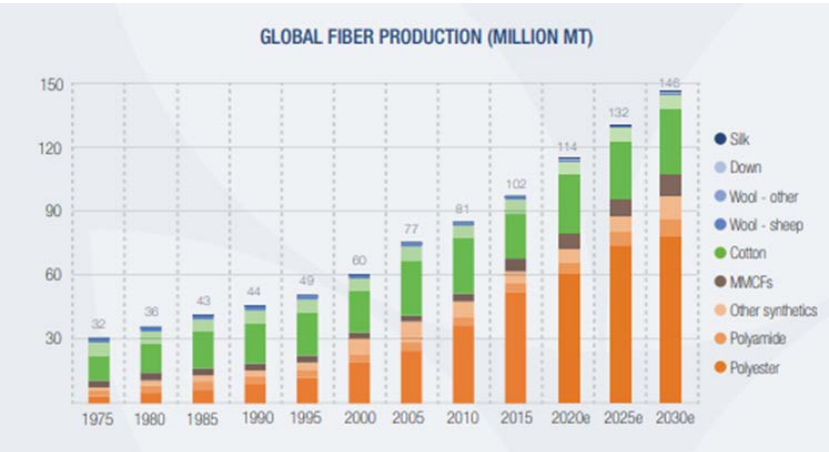

Figure 1. Global Fibre production [1]

2. Terminology

The protruding fibres are released from the textile structures, especially during maintenance (washing and drying). The use of flat textiles causes mechanical stresses, which can manifest as visible changes in the surface, an example being the breaking of the yarn due to weak interactions between the fibres. In both cases, these are irreversible destructive changes, and fibre loosening occurs.

However, the processes of washing, drying and use of textiles can also cause loosening of the fibres, i.e. fragmentation of the fibre ends, and thus the formation of microfibres, an example of which is shown in Figure 2 (a). Fibre degradation and breakage of the fibre structure can also occur, as seen in Figure 2 (b). In these cases, irreversible destructive changes are also involved, and microfibrils are released.

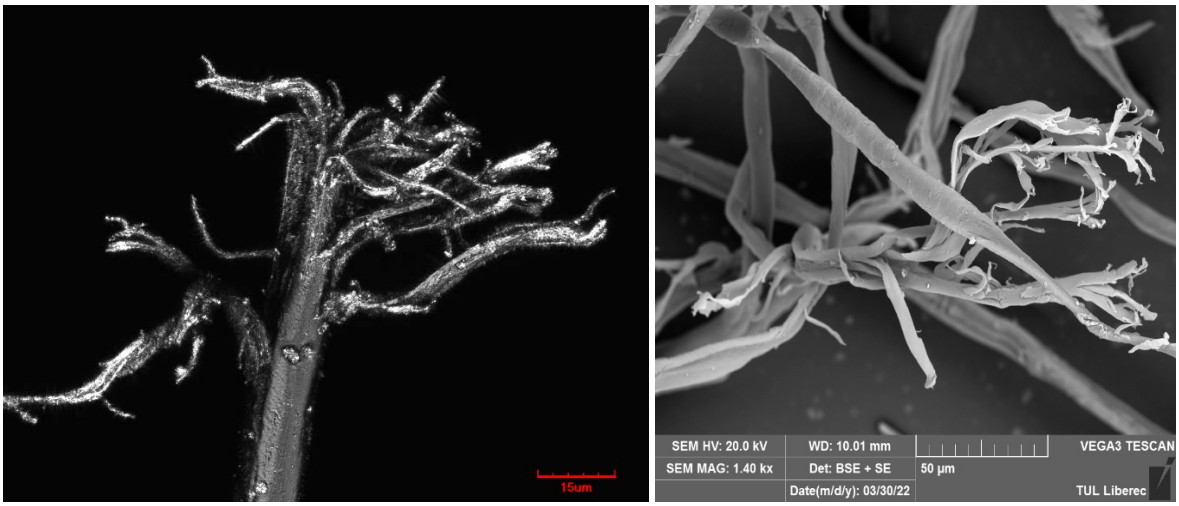

(a) (b)

Figure 2. Confocal microscope and SEM image of cotton fibers: (a) fibrillation of the fiber end, (b) fiber breakage due to mechanical stress

In general, microplastics are plastic particles smaller than 5mm, the primary ones are produced by washing clothes or by tyre abrasion, and the secondary ones are mainly produced by decomposing larger plastic objects such as plastic bags and bottles [5]. However, for example, in the article Accumulation of microplastic on shorelines worldwide: sources and sinks [6], dimensions up to 1mm are defined. Generally, these are particles of synthetic origin of arbitrary shapes.

While in the textile industry, textile fibers with a size of 10-30 µm are referred to as microfibers [7][8]. At the same time, the term microfibers are used by textile experts to refer to materials released from textile structures during maintenance, especially during washing and drying and during use. Thus, these are elongated formations of a mainly needle-like type.

Finally, the term fibre fragments and fibre fragmentation is recommended by the Microfibre Consortium (TMC) [9] and the American Association of Textile Chemists and Colorists (AATCC) [10] as a more appropriate term to use instead of the terms microfibres and microplastics.

3. Causes of fibrous fragments

Several factors influence the emission of fibres from textiles, such as the type of textile fibres (Physico-chemical properties of the material), the type of yarn (twist, uniformity, hairiness, length of fibres) and the construction of the textile (including the type of preparation technology) from which the fibres come (fabrics, knits, non-wovens), and another factor is the finishing of the textile materials.

Another significant factor influencing the release of fibres is the rate of fragment shedding, which is affected by the type and method of maintenance of the textile (washing, drying), and also has a non-negligible influence on the way the textile is used (mechanical stress), and last but not least, the effect of UV radiation (degradation of the textile). Further systematic research is needed to assess and distinguish the extent to which individual factors influence the process of microfibre emission.

The release of fibre fragments into the environment also releases chemicals carried by the fibres (dyes, refining) along with the fibre fragments. Most research to date has focused on the presence of fibre fragments in the aquatic environment [11][12][13]. The presence of fibre fragments is not limited to this environment; fibres are also transported by air. Especially in textile plants, the concentration of these microfibres is high, and their release can negatively affect workers. Microfibres can be eliminated through the digestive tract. Still, some of them accumulate in the body, not only in humans but also in animals, which are often part of the food chain. Due to fibre fragments' chemical and physical properties, microplastics penetrate cells and tissues and accumulate in the human body (lungs, gastrointestinal tract, blood and lymphatic vessels) [14].

One of the consequences of fibre release is the fuzzing of textiles. Pilling form on the surface of textiles when fibres are pulled from the fabric's surface and become entangled during use. The level of pilling is determined by the rate of several processes occurring in parallel. These processes include the entanglement of fibres, which leads to the formation of pilling; the drawing of additional fibres to the surface; and the abrasion of fibres and pilling [15]. The rate of these processes depends on the properties of the fibres, yarns and surface textiles.

3.1. Effect of yarn composition and type of construction of the flat fabric

The proportion of fibre components in the yarn construction plays an essential role in releasing fibre fragments during washing and forming wrinkles. Yarns made from 100% synthetic materials release more fibre fragments than those made from natural fibres. The friction between fibres during yarn formation is low because synthetic fibres do not have a natural convolution structure or crimp [16]. In yarns made from 100 % cellulosic fibres, the fibres swell during washing due to the action of water and detergent. Due to the mechanical action of the washing cycle, these fibres can be more easily unravelled, as shown in Figure 3.

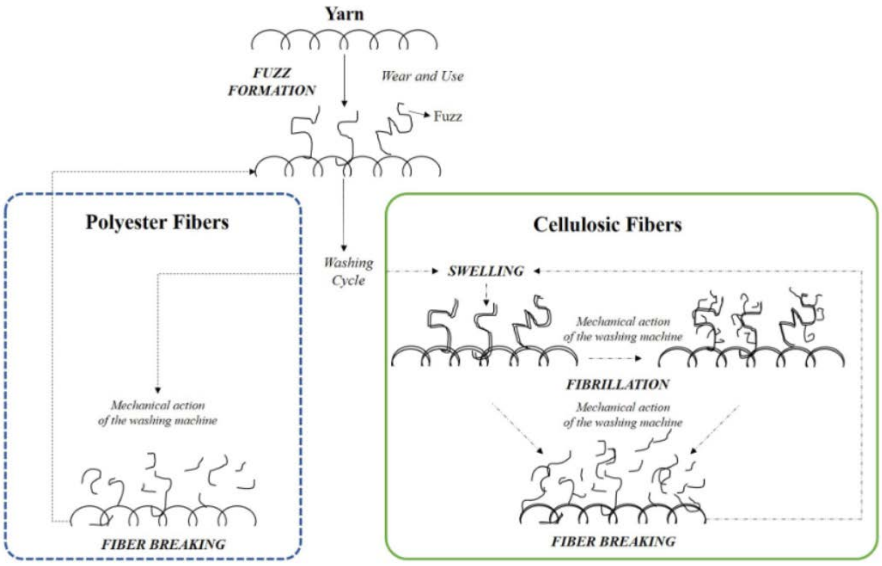

Figure 3. Proposed mechanism for the microfibers release during laundering from fabrics and yarns made of polyester fibers (blue dashed line, left) and cellulosic fibers (green solid line, right)[16]

For example, the impact of yarn construction is addressed in the study Microfiber Release to Water, Via Laundering, and Air, via Everyday Use: A Comparison between Polyester Clothing with Differing Textile Parameters [17]. It has been found that continuous filament yarns have less release of fibre fragments than short-staple yarns.

The structure of flat textiles influences the generation of fiber fragments; for example, knitted fabrics with an open loop structure or pile structure release significantly more fiber fragments than plain woven fabrics [18].

3.2. Effect of treatment and maintenance of textiles

In general, higher washing temperatures lead to fibre degradation. At the same time, liquid detergents based on non-ionic detergents are preferable to products containing anionic detergents with inorganic salts and abrasives [19]. Long wash cycles with high speeds increase the likelihood of fiber debris release. Drying in a tumble dryer noticeably increases the release of fibre fragments.

4. Organisation and initiatives

In 2022, the European Topic Centre on Waste and Materials in the Green Economy (ETC/WMGE) [20] published a document outlining initiatives to mitigate or avoid the emission of fibre fragments from textiles. In Europe, this issue is mainly addressed by The Microfiber Consortium (TMC) [9], Euratex [21] and the European Environment Agency [22]. The logos of the organisations are shown in Figure 4. Globally, the Cross Industry Agreement (CIA) is concerned with preventing the release of microfibres during production and washing and standardising the measurement of the release of fibre fragments.

Figure 4. European organisations working on the issue of fibre fragments in the environment [9] [21][22]

In the UK in particular, there are a growing number of initiatives addressing the issue of the impact of textile fibres on the human body, for example, HUBBUB, a company trying to raise awareness among ordinary consumers about the effect of washing on the formation of microfibres, primarily through social media [23]. WRAP: an association of fashion retailers, charity retailers and textile recycling companies aiming to reduce the environmental impact of clothing consumption [24].

Recommendations to reduce the spread of fibre fragments through the environment for ordinary consumers include: limiting the purchase of textiles, washing less frequently, washing clothes in hot water to a maximum of 30˚C, and using micro-filters in washing machines [11-13]. A roadmap to achieve zero environmental fibre fragments by 2030 is specified in Figure 5.

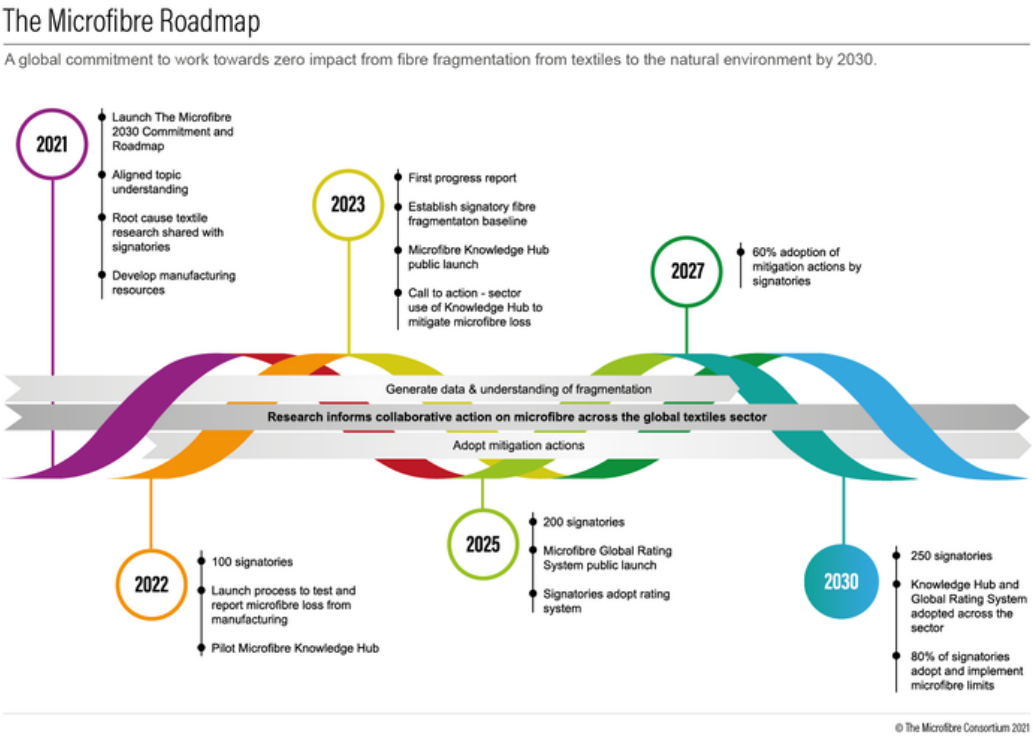

Figure 5. A plan to achieve zero impact of fibre fragmentation on the natural environment [9]

5. Conclusion and recommendations

The topic of fibre fragmentation generation concerns manufacturers and general consumers of textile structures, as well as specialists in the field of water purification or physicians dealing with environmental impacts on the human body, and even ecologists focused on sustainable development and ecological conservation. Collaboration between experts across disciplines is required to accurately determine the hazardousness of textile fibre fragments. From a textile point of view, in particular, it is necessary to define the relationship and interdependencies between the type of textile fibre, the type of textile structure and the tendency of the material to behave during use, treatment and UV degradation.

A concrete solution developed by The Microfiber Consortium [9] includes a roadmap to achieve zero impact of fibre fragmentation on the natural environment and is presented in Figure 5. In particular, this plan consists of disseminating information on fibre fragmentation issues to as many consumers, research organisations and manufacturing plants as possible.

In the future, one of the ancillary solutions could be the classification of textile materials containing synthetic fibres according to their safety, i.e. stability in terms of generating a minimum amount of fibre fragments.

A solution that eliminates or at least limits the occurrence of loose fibre fragments is of global importance concerning the environment. Therefore, more research work is needed to address this issue.

ACKNOWLEDGEMENTS

Author is grateful for the useful help to Ing. J. Grabmüllerová and Ing. J. Nováková.

References

1. *Preferred Fiber and Materials Market Report [online]. 2020. Available from: https://textileexchange.org/2020-preferred-fiber-and-materials-market-report-pfmr-released-2/*
2. *EU, 2018, Directive (EU) 2018/850 of the European Parliament and of the Council of 30 May 2018 amending Directive 1999/31/EC on the landfill of waste (text with EEA relevance), OJ L 150, 14.6.2018 [online]. 2018. Available from: https://eur-lex.europa.eu/legal-content/EN/ALL/?uri=CELEX:32018L0850*
3. *Data on the EU Textile Ecosystem and its Competitiveness [online]. 2021. Available from: https://data.europa.eu/doi/10.2873/23948*
4. *BEVERLEY, H., L. KIRSI a K.I. GRIMSTAD. Microplastic pollution from textiles: a literature review, consumption research norway -Oslo and akershus university college of applied Sciences [online]. 2018. Dostupné z: https://oda.oslomet.no/oda-xmlui/handle/20.500.12199/5360*
5. *EU. Microplastics:sources, effects and solutions. 2018 [online]. Available from: https://www.europarl.europa.eu/news/en/headlines/society/20181116STO19217/microplastics-sources-effects-and-solutions*
6. *MA, Browne, Crump P, Niven SJ, Teuten E, Tonkin A, Galloway T a Thompson R. Accumulation of microplastic on shorelines woldwide: sources and sinks. Environ Sci Technol. [online]. 2011, 45(21), 9175–9179. Available from: doi:10.1021/es201811s*
7. *HOSSEINI RAVANDI, S.A. a M. VALIZADEH. Properties of fibers and fabrics that contribute to human comfort. Improving Comfort in Clothing [online]. 2011, 61–78. Available from: doi:10.1533/9780857090645.1.61*
8. *MILITKÝ, Jiří (TUL). Textilní vlákna. Liberec: TUL, 2002.*
9. *THE MICROFIBRE CONSORTIUM [online]. 2020. Available from: https://www.microfibreconsortium.com/*
10. *WOOD, K.M. a C. BOX. California microfiber update: textile perspective [online]. 2020. Available from: https://marinedebris.noaa.gov/reports/california-microfiber-update-textile-perspective-proceedings*
11. *GEYER, Roland, Jenna R. JAMBECK a Kara Lavender LAW. Production, use, and fate of all plastics ever made. SCIENCE ADVANCES [online]. 2017, 3(7), 6. Available from: doi:10.1126/sciadv.1700782*
12. *NEVES, Diogo, Paula SOBRAL, Joana Lia FERREIRA a Tânia PEREIRA. Ingestion of microplastics by commercial fish off the Portuguese coast. Marine Pollution Bulletin [online]. 2015, 101(1), 119–126. ISSN 0025-326X. Available from: doi:10.1016/J.MARPOLBUL.2015.11.008*
13. *FERREIRA, Marta, Jameel THOMPSON, Andrew PARIS, David ROHINDRA a Ciro RICO. Presence of microplastics in water, sediments and fish species in an urban coastal environment of Fiji, a Pacific small island developing state. Marine Pollution Bulletin [online]. 2020, 153, 110991. ISSN 0025-326X. Available from: doi:10.1016/J.MARPOLBUL.2020.110991*
14. *PRATA, Joana Correia, João P. DA COSTA, Isabel LOPES, Armando C. DUARTE a Teresa ROCHA-SANTOS. Environmental exposure to microplastics: An overview on possible human health effects. Science of The Total Environment [online]. 2020, 702, 134455. ISSN 0048-9697. Available from: doi:10.1016/J.SCITOTENV.2019.134455*
15. *ČSN EN ISO 12945-2 (800837) Textilie - Stanovení sklonu plošných textilií ke žmolkování, rozvláknění nebo viditelným změnám povrchu - Část 2: Modifikovaná metoda Martindale. 2021*
16. *ZAMBRANO, Marielis C., Joel J. PAWLAK, Jesse DAYSTAR, Mary ANKENY, Jay J. CHENG a Richard A. VENDITTI. Microfibers generated from the laundering of cotton, rayon and polyester based fabrics and their aquatic biodegradation. Marine Pollution Bulletin [online]. 2019, 142, 394–407. ISSN 18793363. Available from: doi:10.1016/j.marpolbul.2019.02.062*
17. *FALCO, Francesca De Falco, Mariacristina COCCA, Maurizio AVELLA a Richard C. THOMPSON. Microfiber Release to Water, Via Laundering, and to Air, via Everyday Use: A Comparison between Polyester Clothing with Differing Textile Parameters. Environmental Science & Technology [online]. 2020, 54(6), 3288–3296. Available*

from: doi:10.1021/acs.est.9b06892

18. *CARNEY ALMROTH, Bethanie M, Linn ÅSTRÖM, Sofia ROSLUND, Hanna PETERSSON, Mats JOHANSSON a Nils-Krister PERSSON. Quantifying shedding of synthetic fibers from textiles; a source of microplastics released into the environment [online]. nedatováno. Available from: doi:10.1007/s11356-017-0528-7*
19. *PERIYASAMY, Aravin Prince a Ali TEHRANI-BAGHA. A review on microplastic emission from textile materials and its reduction techniques. Polymer Degradation and Stability [online]. 2022, 199, 109901. ISSN 0141-3910. Available from: doi:10.1016/J.POLYMDEGRADSTAB.2022.109901*
20. *EVELIEN DILS. ETC/CE Report 1/2022: Microplastic pollution from textile consumption in Europe [online]. 2022. Available from: https://www.eea.europa.eu/publications/microplastics-from-textiles-towards-a*
21. *Euratex [online]. 2022. Available from: https://euratex.eu/*
22. *European Enviromental Agency [online]. 2022. Available from: https://www.eea.europa.eu/*
23. *HUBBUB. What is in My Wash? [online]. 2018. Available from: https://www.hubbub.org.uk/whats-in-my-wash-plastic-microfibres-campaign*
24. *Sustainable Clothing Action Plan 2020 Commitment [online]. 2020. Available from: doi:https://wrap.org.uk/taking-action/textiles/initiatives/scap-2020*

DEVELOPMENT OF MAGNETISABLE FIBRES FOR REORIENTING FIBRES IN CARDED WEBS BY USE OF A MAGNETIC FIELD

Lena Kölsch[1]; Holger Fischer[1]; Christopher Albe[2]; Katharina Heilos[2]; Oliver Schnock[1]; Dennis Kirchhöfer[1]

[1]Faserinstitut Bremen e.V. FIBRE, Bremen (DE), koelsch@faserinstitut.de
[2]Sächsisches Textilforschungsinstitut e.V. STFI, Chemnitz (DE), Christopher.Albe@stfi.de

Abstract:

In the field of processing high-performance fibres into nonwovens, fibre orientation is a critical factor for the properties of the nonwovens. In the project Falona (INNO-KOM, project no. 49VF210027 & 49VF210033), two research institutes are developing and investigating a method for reorienting fibres in carded webs using a magnetic field. To achieve magnetisability of the fibres, the partners are investigating two different research approaches. In the first research approach (at STFI), the fibres are coated with a magnetic fluid, while in the second approach (at FIBRE), hollow fibres filled with a magnetisable fluid are considered. These two approaches are intended to allow fibre alignment in the carded web in a way that is gentle on the fibers, combined with the possibility of creating a magnetic composite. The focus of the article is on the manufacturing process of magnetisable fibres and the first results.

Key words:

Liquid-core fibre; magnetisable fibres; fibre orientation; magnetic field; carded web

1. Introduction

The growth predictions for carbon fibre-reinforced plastics (CFRP) are excellent, due to their outstanding properties. As a consequence the amount of CFRP waste is growing simultaneously with the increasing consumption. This comprises scraps from production as well as end-of-life waste. Due to the high economical value of CFRP there is enlarged interest in effective recycling of these materials. These materials can be recycled by milling or shredding the CFRP and subsequent pyrolysis to recover recycled carbon fibres (rCF). Result of preliminary work was processing of long, but not endless recycled carbon fibres by means of the carding principle, using either 100 % carbon fibres or blends with natural fibres and / or synthetic fibres in pilot plant scale [1]. Subsequently, within the frame of the research project RecyCarb [2,3] the research was continued on process scale-up and setting up a qualified value-added chain for recycled carbon fibres (rCF) by closing the technological gap between rCF und functional high-value re-use.

The fibre orientation in these nonwovens is substantially lower than in wovens or unidirectionally arranged rovings. Actually the fibre orientation in carded webs is a MD/CD ratio of approx. 6:1 [2]. Modifications of this mechanical process can lead to higher MD/CD ratios of 7:1 to 8:1, but are accompanied by strong fibre damage [4]. Due to the comparable low fibre orientation there are actually only applications with lower demand on mechanical properties on the market for rCFRP.

For this reason new processes for optimisation of the fibre orientation are necessary. Aim of the project Falona is to develop two different approaches using magnetic fields to enhance the fibre

orientation in carded webs. The first approach is driven by the partner STFI using high-performance fibers (carbon and glass fibres) treated with a fibre auxiliary modified with particles by spraying after web formation. The second approach is driven by the partner FIBRE and aims to use thermoplastic hollow fibres, filled with a magnetisable liquid. The filled hollow fibres are subsequently processed in the carding process either in combination with high-performance fibres or as a 100% variant. The processes to be developed shall enable fibre-friendly alignment of the fibres in the web by using a magnetic field using Helmholtz coils.

The focus of the article is on the manufacturing process of magnetisable fibres and the first results.

2. Experimental

Hollow fibres were produced on a melt-spinning line (cf. Figure 1, Fourné Maschinenbau GmbH, Alfter-Impekoven, DE) with throughput 0.5 – 7 kg/h, process temperature up to 400°C, spinning speed up to 900 m/min, one heatable godet-mono & three heatable godet-duos enabling max. stretching 1:9 and yarn-count 100 – 3500 dtex. The line is suitable for standard and high-performance thermoplastics and biopolymers. A Bi-Co spinneret for hollow fibers with 18 holes was used. In a first step, oil-filled hollow fibres were produced from PE (polyethylene LE9168 borealis and refined soy oil from chemiekontor). The fibres were produced by using the melt spinning process, in which the polymer is melted in an extruder and transported to the spinneret. Oil and polymer are then combined in the spinneret. The oil is pre-heated by a heating hose in order to guarantee that the oil does not cool down the hot spinneret too much. The pressure and temperature are controlled by sensors. After passing the spinneret the oil-filled hollow fibres form, which are then passed over godets and stretched to increase strength. In the second step, magnetic iron dioxide particles (BAYOXIDE E 8706, Lanxess) were mixed into the oil and this was used as core liquid for the production of the magnetisable oil-filled hollow fibres.

Figure 1. Melt-Spinning System used in this work.

3. First Results

Oil-filled fibres with homogeneous cross-section could be successfully produced (cf. Figure 2, left). The outer diameter of the fibres is approximately 120 µm and the inner diameter is 60 µm.

Also, fibres filled with the particle/oil mixture could be produced, which respond to a magnetic field. The particle content of the fibres was 10 percent by weight. The outer diameter of the fibres here is approximately 600 µm and the inner diameter is 20 µm (cf. Figure 2, right). Actually, particle contents up to 30% have been reached.

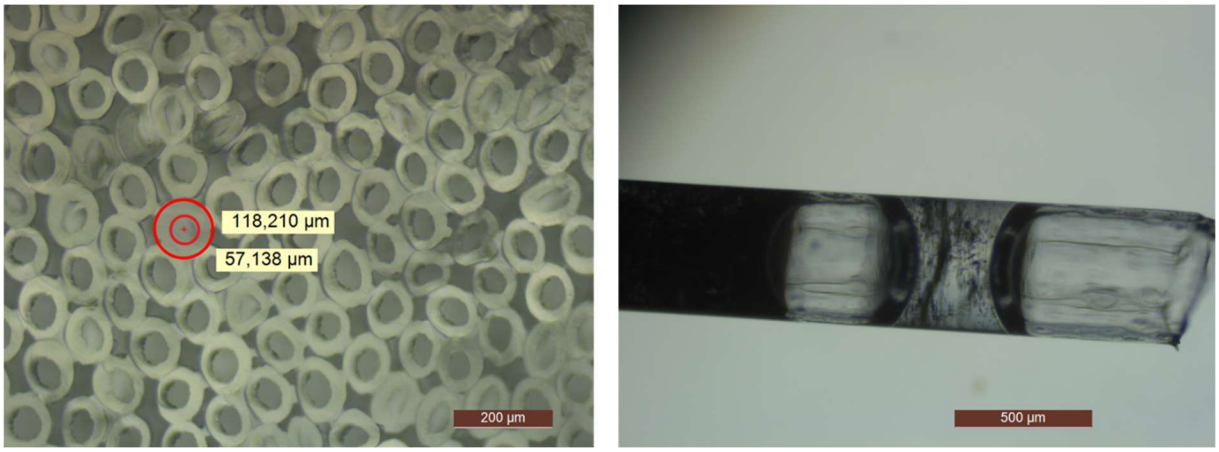

Figure 2. Cross-section of oil-filled hollow fibres (left) and a fibre filled with the particle/oil mixture (right).

An experimental setup for the generation of a homogeneous magnetic field with parallel magnetic field lines was developed, on the basis of which the fibers, which were produced with the process shown in Figure 3b), are to be oriented in the further project progress (cf. Figure 3a)).

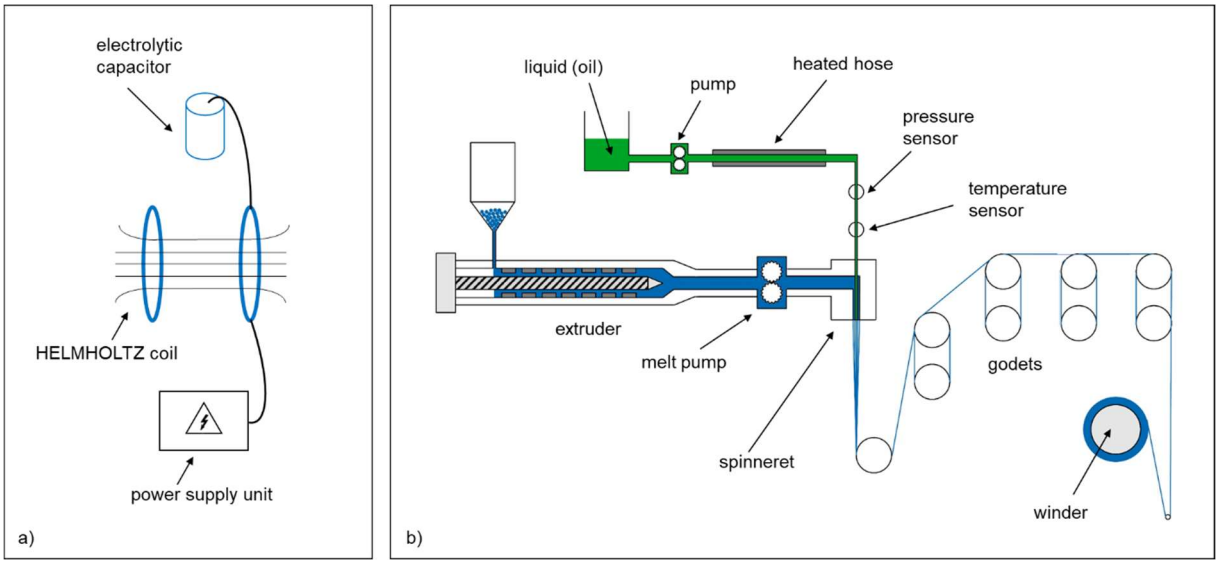

Figure 3. Experimental setup for the generation of a homogeneous magnetic field a) and the principle of the melt-spinning process b).

4. Conclusions and Outlook

Hollow fibres filled with oil containing various shares of magnetisable particles have been produced successfully. In parallel, the process parameters for fibre production have been optimised. Subsequently the fibres have been processed to staple fibres, including thermal closing of the fibre ends. This prevents loss of liquid. Actually, orientation of single fibres in a magnetic field has been tested successfully.

Next steps of the project work will be carding of the staple fibres into webs and subsequent orientation improvement in the magnetic field. The degree of orientation will be accessed by using an image analysis system. Finally it is planned to produce composites from the magnetisable fibre webs using the vacuum infusion process to obtain information about the achievable mechanical properties.

ACKNOWLEDGEMENTS

The authors are much indebted to the federal ministry of economic affairs and climate action for funding this research within the programme INNO-KOM (No. 49VF210027 & 49VF210033).

Supported by:

Federal Ministry for Economic Affairs and Climate Action

on the basis of a decision by the German Bundestag

References

1. *Hofmann M., Gulich B. (2015). Nonwovens for composites — recycling carbon waste in the form of long fibres. JEC Composites Magazine, No. 98, 50 – 51. ISSN 1639-965X.*
2. *Fischer H., Heilos K., Hofmann M., et al. (2019). RecyCarb — Ganzheitliche verfahrenstechnische Betrachtung und prozessbegleitendes Monitoring von Qualitätsparametern bei der Aufbereitung von Carbonfaserabfällen und deren hochwertigen Wiedereinsatz in textilen Flächengebilden als Basismaterial für Faserverbundwerkstoffe der Zukunft. In series: Forschungsberichte aus dem Faserinstitut Bremen no. 60. Books on Demand GmbH, Norderstedt, DE. ISSN 1618-7016. ISBN 978-3-7494-3150-2.*
3. *Heilos, K.; Fischer, H.; Hofmann, M., Miene, A. (2020). Nonwovens made of Recycled Carbon Fibres (rCF) used for Production of Sophisticated Carbon Fibre-Reinforced Plastics. Fibres and Textiles / Vlákna a Textil 27(3), 65 – 75. ISSN 1335-0617.*
4. *Stegschuster, G., Schlichter, S. (2017). Web Based Composites — Prozessketten und Produkte. Presentation, 32. Hofer Vliesstofftage, 9. November 2017, Freiheitshalle Hof., Hochschule Hof, Hof, DE.*

TENSILE STRENGTH PROPERTIES COMPARISON OF PARTIALLY ORIENTED MULTIFILAMENT YARNS (POY) FROM RECYCLED AND VIRGIN POLYESTER

Mehmet Erdem İnce[1], Emel Çelik

Gaziantep University, Textile Engineering Department, 27310, Şehitkamil, Gaziantep, Türkiye.
[1]einceg@gantep.edu.tr; meince@ncsu.edu, Tel: +90 342 317 27 30 Fax: +90 342 317 27 06

Abstract:

This study is about using recycled polyester in filament yarn production. In this context, the response of partially oriented filament yarns produced from recycled and virgin polyester to the tensile force was compared. The test speed was also considered as additional input factors. The load-elongation curve was divided into three as the first linear region, the middle horizontal plateau region and the last linear region. For the initial part of the study, the maximum force (ultimate tensile strength) and the extension at the maximum force were considered. How the polymer type of the yarn and the test speed affected the peak point properties was revealed with detailed data analysis and explanatory/visual graphics using the JUMP® statistical software package. While virgin and recycled yarn exhibited the same amount of maximum force performance, the recycled yarn extended more than the virgin yarn at statistically significant level. Higher test speed resulted in higher maximum force performance, while it did affect the extensibility of the yarn at statistically significant level.

Key words:

polyester, recycled polyester, partially oriented yarn, polyester filament yarn, yarn tensile strength

1. Introduction

The usage area of plastic materials is increasing rapidly because they are lighter and easier to process than traditional materials such as metal and ceramic. On the other hand, the rapid increase in the world population and the emergence of new application areas of plastics increase their consumption steadily [1]. Polyester polymer is among the most consumed plastic materials. In this context, reuse of end-of-life polyester polymer through recycling is important in terms of both reducing the plastic waste load and sustainability [3]. This study is within the scope of reuse of recycled polyester polymer by directing it into the textile yarn production chain [2]. In this context, the tensile force response of the partially oriented multi-filament yarn (POY) from recycled polyester was examined and compared with that of the POY from virgin polyester. Thus, it was clearly revealed to what extent the recycling process changes the tensile strength properties of the polyester polymer.

In order to increase the parallelism between the polymer chains and increase the yarn strength, the partially oriented polyester yarn is subjected to tensile loads at different deformation rates in the subsequent drafting processes. Therefore, revealing the responses of POYs from virgin and recycled polymers to tensile deformation under different deformation rates is important in terms of determining the strength properties of the fully drawn yarn (FDY). In this study, the tensile properties of partially oriented polyester yarns produced under the same conditions from virgin and recycled polymers was compared. Whether virgin and recycled polyester yarns differ in terms of tensile strength performance, how they respond to different deformation rates was demonstrated with detailed statistical data analysis and self-explanatory visual graphics.

2. Experimental

2.1. Materials

Within the scope of this study, it was planned to use multifilament partially oriented polyester yarns (Figure 1) produced under the same conditions form recycled and virgin polymer with a yarn count of 510 deniers. Yarns were subjected to tensile test in the Titan® test device (Figure 2) available in Gaziantep University, Textile Engineering Department. The experimental study plan is given in Table 1. The clamping distance (i.e. the gauge length) was fixed as 250 mm.

Figure 1. Virgin (two bobbins on the left) and recycled (two bobbins on the right) partially oriented polyester multifilament yarns

Figure 2. Titan® brand yarn and fabric strength tester

Table 1. Experimental study plan

Polymer type	Test speed [mm/min]
Virgin PES	50
Recycled PES	750
	1500

2.2. ***Methods***

The typical load-deformation curve was be divided into three main regions (Figure 3) and analyzed. For this part of the study, only the peak (final maximum force or the tensile strength) point was taken into account. How these maximum point properties were affected by polymer type and test speed was revealed in here.

For the future part of the study, additional analysis will be done for the following outputs

1) modulus of elasticity for the first linear elastic region,

2) the deformation energy for the first linear elastic region

3) the transition force and the transition elongation to the middle horizontal plateau region

4) the deformation energy for the middle horizontal plateau region

5) the transition force and the transition elongation to the last linear region

6) the modulus of elasticity for the last linear elastic region

7) the deformation energy for the last linear elastic region

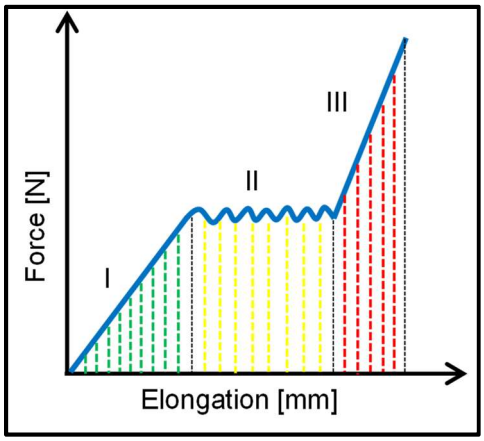

Figure 3. Typical load-elongation curve and its zones for the partially oriented multifilament polyester yarn
I: First linear elastic region, **II**: Middle horizontal plateau region (chain alignment), **III**: Last linear region

3. Results and discussion

Figure 4 and 5 shows the force versus extension curves of the virgin and recycle PES yarn, respectively, at various test speeds.

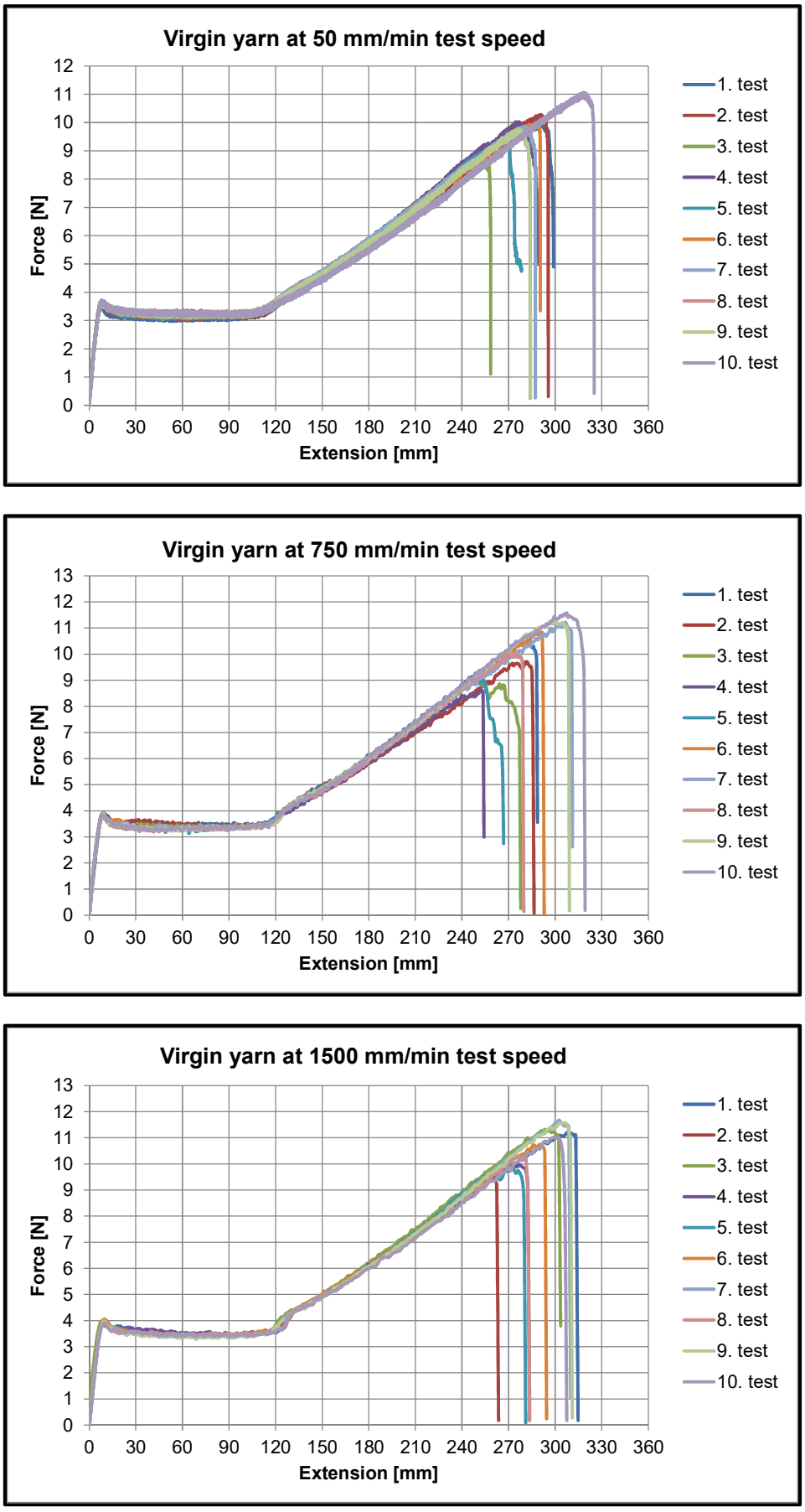

Figure 4. Force-extension curves of the virgin PES yarn at various speeds

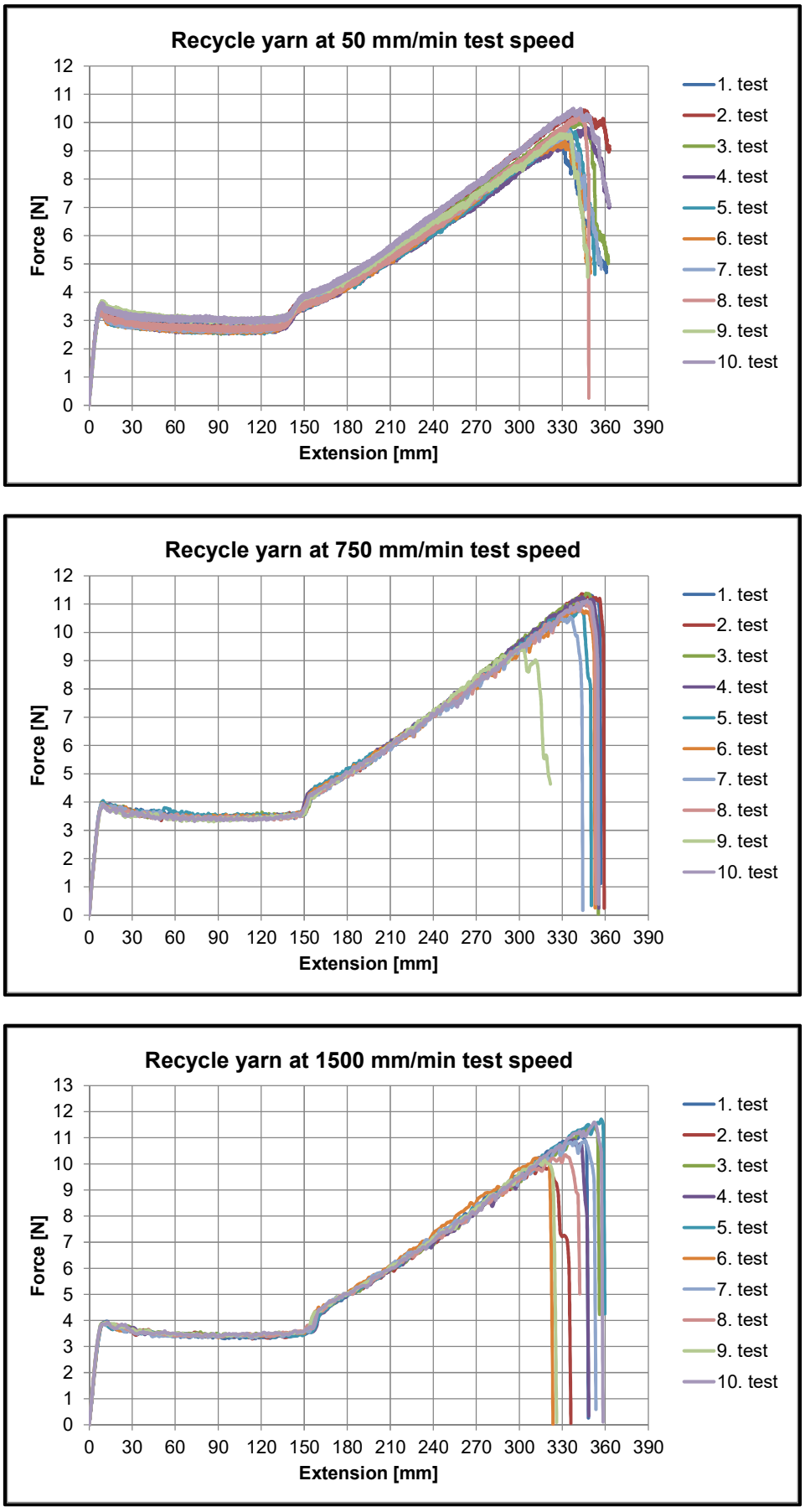

Figure 5. Force-extension curves of the recycle PES yarn at various speeds

Figure 6 and Table 2 show the effect of polymer type on the maximum tensile force. The recycled PES yarn exhibited higher maximum force than the virgin PES yarn; however, this difference did not reach at statistically significant level. Besides, variance analysis showed that both yarns displayed the same amount of maximum force variability (variance).

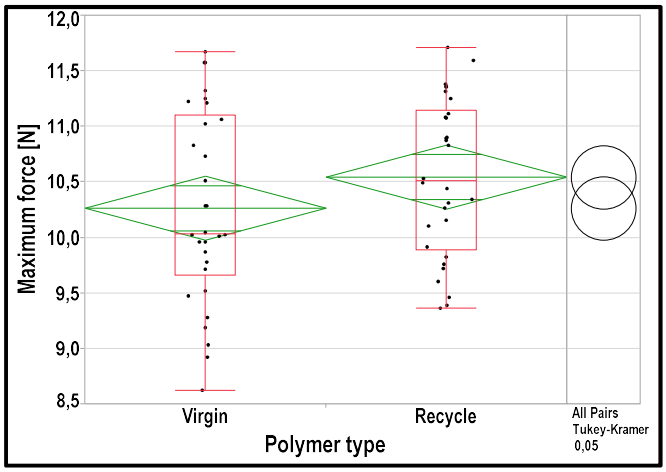

Figure 6. The effect of polymer type on maximum force

Note: The horizontal green line dividing the green diamond corresponds to the mean, while the distance between the lower and upper corners of the green diamond shows the confidence interval based on the 95% confidence level. One comparison circle for the mean calculated at each sublevel level is given in the right-hand column. The circles representing means that differ significantly from each other (α = 0.05) either do not intersect or intersect slightly.

Table 2. The effect of polymer type on maximum force

Property	Polymer type		n	mean	sd	LL	UL	p-value
Maximum force [N]	Recycle	A	30	10.54	0.71	10.26	10.83	0.1728
	Virgin	A	30	10.27	0.86	9.98	10.55	

Note: Levels that are not combined with the same alphabetic capital letter differ significantly from each other (α = 0.05). **n**: number of measurements, **sd**: standard deviation, **LL**: lower limit, **UL**: upper limit. The limits were established according to the 95% confidence level. A p-value less than 0.05 is an indication that the difference between at least two levels is statistically significant and is colored red.

Figure 7 and Table 3 shows the effect of polymer type on the extension at maximum force. Polymer type exhibited statistically significant effect on the extension, and the recycled PES yarn displayed significantly higher extension than the virgin PES yarn. Higher extensibility of the recycled PES yarn can be attributed to its higher impurity as compared with the virgin PES yarn. The recycled yarn also exhibited statistically significantly lower extension variability than the virgin yarn.

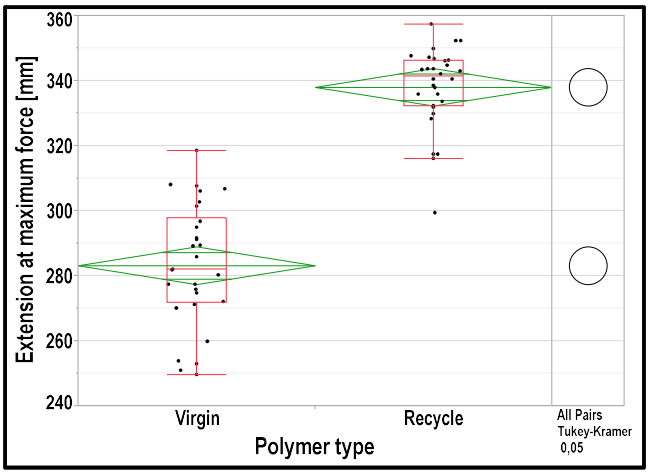

Figure 7. The effect of polymer type on the extension at maximum force

Table 3. The effect of polymer type on the extension at maximum force

Property	Polymer type			n	mean	sd	LL	UL	p-value
Extension at maximum force [mm]	Recycle	A		30	337.97	12.56	332.17	343.76	<0,0001
	Virgin		B	30	283.08	18.58	277.29	288.88	

Increase in test speed improved the maximum force performances of the yarns at statistically significant level (Figure 8 and Table 4). This result can be attributed to the reaction that occurs as a result of forcing the yarn to break before the polymer chains become fully parallelized.

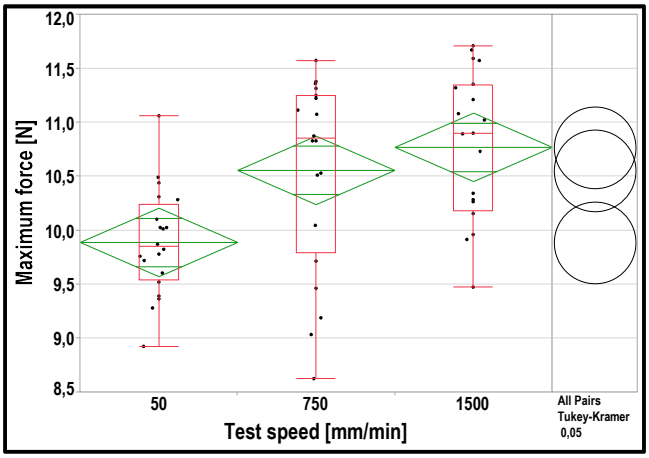

Figure 8. The effect of test speed on the maximum force

Table 4. The effect of test speed on the maximum force

Property	Test speed [mm/min]			n	mean	sd	LL	UL	p-value
Maximum force [N]	1500	A		20	10,77	0,68	10,45	11,09	0,0006
	750	A		20	10,56	0,90	10,24	10,88	
	50		B	20	9,89	0,12	9,57	10,20	

Figure 9 and Table 5 show the effect of test speed on the extension. The test speed slightly increased the extensibility of the yarn; however this increase did not reach at the statistically significant level.

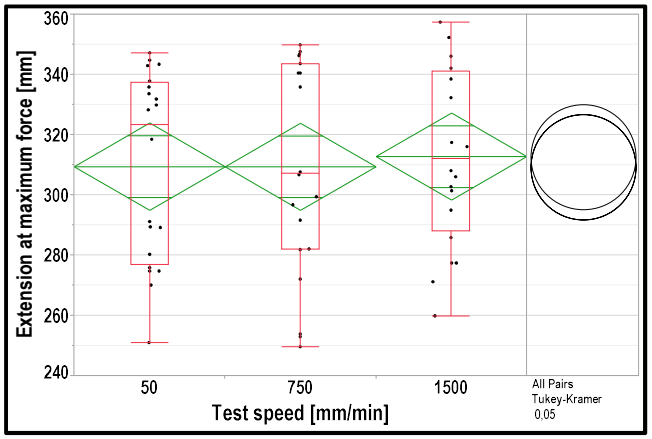

Figure 9. The effect of test speed on the extension at maximum force

Table 5. The effect of test speed on the extension at maximum force

Property	Test speed [mm/min]		n	mean	sd	LL	UL	p-value
Extension at maximum force [mm]	1500	A	20	312.77	29.50	298.29	327.25	0.9304
	50	A	20	309.44	31.55	294.95	323.92	
	750	A	20	309.37	35.67	294.89	323.85	

4. CONCLUSIONS

In this study, the yarns from virgin and recycled PES polymer were subjected to tensile strength test at various test speeds. Thus the effect of two factors, the polymer type and the test speed on the peak tensile force properties of the virgin and recycled yarn was examined. While virgin and recycled PES yarns exhibited the same maximum force, the recycled yarn extended significantly higher than the virgin yarn, which was attributed to the impurity of the virgin yarn. On the other hand, the test speed significantly increased the maximum force, while it did not change the extension at maximum force at statistically significant level.

References

1. *Callister, W. D. (2007). Material Science and Engineering An Introduction. (7th ed.). John Wiley & Sons, Inc.*
2. *Esi, B., Baykal, P. D. (2020). Investigation of tensile strength and elongation properties of chenille upholstery fabrics including recycling polyester yarns. Journal of Engineered Fibers and Fabrics, 15, 1-10.*
3. *Nistic`o, R. (2020). Polyethylene terephthalate (PET) in the packaging industry. Polymer Testing, 90, 1-18.*

ANALYSIS OF MASS IRREGULARITY OF WORSTED RING AND COMPACT STAPLE SPUN YARNS

Petra Jirásková, Eva Moučková

Technical University of Liberec, Faculty of Textile Engineering, Department of Technologies and Structures, Studentská 2, 461 17 Liberec 1, The Czech Republic
Telephone: +420 48 535 3328; Fax: +420 48 535 3542, petra.jiraskova@tul.cz

Abstract:

The paper deals with the analysis of staple spun yarns mass irregularity. This analysis is focused on the transformation of the roving mass irregularity into the yarn mass irregularity by a drafting arrangement of a ring frame and a compact spinning machine. The transformation of mass irregularity is expressed by means of an experimentally determined modulus of the relative transfer function, which are compared with the modulus of the theoretical relative transfer function. The experiment is realized on a set of worsted staple spun yarns of various counts produced on the ring and on the compact spinning machine.

Key words:

Compact spinning, ring spinning, draft, condensing zone, mass irregularity, modulus of relative transfer function

1. Introduction

The mass irregularity of linear textiles is caused by various factors [1]. The total mass irregularity of staple spun yarns is given by:

1) the mass irregularity caused by the fibres themselves and the principle of yarn formation;
2) the mass irregularity caused by yarn production processes and the machines themselves.

The processes in the staple spun yarn production that have a major effect on the mass irregularity are attenuation and doubling [2]. It is known from the theory of mass irregularity that the attenuation process, which is expressed by a draft, has a negative effect on the mass irregularity – the mass irregularity is deteriorated by a draft [3 - 7]. On the contrary, the doubling has a positive effect on the mass irregularity, it balances it. The doubling is one of methods for mass irregularity equalizing and it is realized in the operation “doubling and drafting”.

At the ring spinning machines and the compact spinning machines, the attenuation of fibrous assembly without simultaneous doubling is realized in a drafting arrangement. The level of attenuation is given by so called total draft ratio [2]. In the case of compact spinning machine, the condensing zone is added to the drafting arrangement. The compression of drawn fibrous ribbon results in an overall narrowing of the fibre ribbon, and in a greater mutual adhesion of the fibres. Thus, the twisting triangle is partially eliminated and consequently different tension of the fibres in the twisted ribbon is reduced compared to ring spinning frame. Due to condensation, the fibres are more tightly bound in the body of the ribbon and when twisted, the ends of fibres are more tightly boned in the body of the yarn. The hairiness of resulting yarn is therefore lower and at the same time the yarn has a higher tenacity and breaking elongation when using the same twist level compared to the conventional ring spun yarns. Compact spinning machine manufacturers state that compression in the additional condensing zone results in reduction of yarn mass irregularity and number of faults in the resulting yarn. This is confirmed by the results of studies, for example [12 – 16], in which properties of compact and conventional ring spun yarns have been compared.

The aim of this work is to analyze the effect of the drafting arrangement of conventional ring spinning machine and drafting arrangement with additional condensing zone of the compact spinning machine on structure of worsted spun yarns mass irregularity, strictly speaking on the extent of change of corresponding harmonic components of mass irregularity. For this, we express the transformation of the roving mass irregularity into the yarn mass irregularity due to the drafting arrangement with the condensing zone using the so called experimentally determined modulus of relative transfer function [7 - 9]. We compare the results with the experimentally determined modulus of relative transfer function of drafting device of the conventional ring spinning machine and with the theoretical modulus of relative transfer function of defined ideal drafting process.

2. Experimental

2.1. Materials

For the experiment, the set of worsted ring and worsted compact staple spun yarns of the same parameters and fibre raw material was prepared. The yarns of the same count and the same twist were successively spun on the ring spinning machine and the compact spinning machine from the same roving bobbins. The spinning system of worsted ring and compact yarns was the same, the only difference was in the used spinning frame. The technology of yarn production included preparation for combing (preparatory gilling), tops re-combing, doubling and drawing after combing (finisher gilling), roving formation and spinning. The roving was manufactured using the finisher. The three-rollers double-aprons drafting mechanism was used on the ring spinning machine. In the case of the compact spinning machine, the condensing zone with the lattice apron (Suessen type) was added to the this drafting device. An overview of the experimental yarns and rovings are mentioned in Table 1. Basic parameters of used fibres are presented in Table 2.

Table 1. Basic parameters of staple spun yarns and rovings used for the experiment

Fibre raw material	Spinning technology	Nominal roving count [tex]	Nominal yarn count [tex]	Nominal yarn twist [m^{-1}]	Total draft on ring/compact spinning machine
100% WO	worsted compact	360	16.7	650	21.6
	worsted ring				
100% WO	worsted compact	280	11.1	850	25.2
	worsted ring				
100% WO	worsted compact	440	20.8	750	21.12
	worsted ring				
80% WO / 20% PA	worsted compact	200	10	900	20
	worsted ring				

Mass irregularity of yarns and rovings were measured using Uster Tester IV–SX device. In order to verify the assumptions about the influence of the condensing zone of the compact spinning machine on the other properties of the final yarns, ring and compact spun yarns were subjected to measurements of yarn faults (imperfections) and hairiness on the Uster Tester IV–SX too. The measurement was carried out under the following conditions: yarns: speed of measurement 400 $m.min^{-1}$, time of measurement: 2.5 min; roving: speed of measurement 10 $m.min^{-1}$, time of measurement: 5 min.

Table 2. Main parameters of fibers used for yarn production

Yarn Count [tex]	16.7	11.1	20.8	10
Mean fiber length [mm]	73.7	72	79.5	89

2.2. Methods

The effect of spinning processes on a change in mass irregularity of linear fibrous product, eventually in its structure can be described by so-called modules of relative transfer function of the appropriate process (in this case it is the effect of attenuation in a drafting arrangement of ring spinning machine). The drafting arrangement can be considered as a dynamic system [7] with the continuous input and output of linear fibrous product. For this system, the transfer function, or rather modulus of relative transfer function can be expressed. According to the theory of random functions, the modulus of relative transfer function is expressed by the ratio of the amplitudes of the output and input signals related to respective mean value of fineness of input and output linear fibers product [17]. The input or output signal is a function that expresses the course of the mass of short length sections of corresponding fibrous products depending on the length of these products.

2.2.1 Experimental modulus of relative transfer function

In this work, the transformation of mass irregularity by the drafting device is expressed by the so called experimentally determined modulus of relative transfer function. For the determination of this modulus, we assume that the structure of roving mass irregularity on the wavelength λ_{roving} shows itself in the yarn at the wavelength enlarged due to the total draft (P) both on the compact and conventional ring spinning machine ($\lambda_{roving} \cdot P$). The mass irregularity of the roving at the short wavelengths will be deepened due to the draft. The experimental modules of relative transfer function were determined according to equation (1):

$$\left|F^{*}_{\exp}(\lambda)\right| = \frac{CV_{yarn}\ (\lambda_{roving} \cdot P)}{CV_{roving}\ \left(\lambda_{roving}\right)} \qquad (1),$$

where: $\left|F^{*}_{\exp}(\lambda)\right|$ is the experimentally determined modulus of relative transfer function of drafting mechanism; $CV_{yarn}(\lambda_{roving..}P)$ is the variation coefficient of harmonic component of yarn mass irregularity with wavelength corresponding to wavelength of roving λ_{roving} [m] enlarged by draft P [%]; $CV_{roving}(\lambda_{roving})$ is the variation coefficient of harmonic component of roving mass irregularity with wavelength λ_{roving} [%]; P is the total draft ratio of drafting mechanism of ring spinning frame.

To express the structure of mass irregularity of the linear fibrous product, here represented by mass fluctuations at short wavelengths, we used mass spectrograms of rovings and yarns. The spectrogram shows a distribution of amplitudes of harmonic component, or variation coefficients of harmonic component of mass fluctuation, of roving (input signal) and yarns (output signal) depending on wavelength.

2.2.2 Transformation of mass irregularity by drafting device

The theoretical model of the transformation of mass irregularity through the drafting arrangement is based on the assumption of an ideal draft. The ideal draft occurs when the movement of all fibers is controlled by the feeding (back) and delivery (front) rollers. Other conditions must be met to achieve the ideal draft: the length of all fibers is the same and the distances of the leading ends of the fibers with respect to each other are constant; the fibers are fed and clamped by the feeding rollers and their speed is thus the same as that of the feeding rollers, and at the moment when the leading ends of the fibers are clamped by the delivery pair of roller, their speed will change to the speed of the delivery rollers. In practice, real staple fibers are spun, their length varies. The design of drafting device must be such that the movement of the fibers is most controlled and approaching to the conditions of ideal draft. Therefore, three-roller double-apron drafting devices are used on the ring and compact spinning machines where the aprons control the movement of fibers.

Characteristics of dynamic model of drafting system were derived from the transfer function for the case of the drafting system with a general speed field [17]. For mentioned conditions of the ideal draft, the transfer function of drafting system [11], and then modulus of relative transfer function [9] were derived. Equation (2) expresses the modulus of relative transfer function:

$$\left|F_p^*(\lambda)\right| = \left| P \frac{\sin\frac{\pi\, l}{\lambda}}{\sin\frac{\pi\, l\, P}{\lambda}} \right| \tag{2}$$

where: $\left|F_p^*(\lambda)\right|$ is theoretical modulus of relative transfer function of drafting mechanisms as a function of wavelength λ; λ is the wavelength of harmonic component of mass irregularity of result fibrous product [m], l is the mean fiber length [m]; P is the total draft ratio.

From the yarn mass spectrogram, the average fiber length in the yarn can be determined as a projection of the fiber length into the yarn axis [18]. According to [18], average fiber length $\bar{l}\,[m]$ can be calculated from wavelength λ_{max} [m] corresponding to maximum amplitude of harmonic component of yarn mass irregularity by equation (3):

$$\bar{l} = \frac{\lambda_{\max}}{2.82} \tag{3}$$

3. Results and discussion

The results of yarn faults and yarn hairiness, presented in Table 3, show that tested worsted compact spun yarns have lower hairiness and lower number of yarn faults compared to ring spun yarns. These results confirmed the assumptions about the positive effect of the compact spinning machine's condensing zone on the properties of the final yarn.

Table 3. Selected results of yarn faults and yarn hairiness measurements

Fibres material/ Yarn count [tex]	Spinning technology	Thin -50% [1/km] 95% conf. int.	Thick +50%[1/km] 95% conf. int.	Neps +200% [1/km] 95% conf. int.	Hairiness H [1] 95% conf. int.
100% WO 16.7 tex	compact	130.08 (126.32÷133.85)	12.92 (12.11÷ 13.73)	17.33 (16.49 ÷ 18.18)	4.17 (4.13 ÷ 4.21)
	ring	141.35 (139.65÷143.05)	16.59 (15.90 ÷17.28)	17.12 (16.54 ÷ 17.70)	5.07 (5.06 ÷ 5.08)
100% WO 11.1 tex	compact	456.24 (451.05÷461.43)	38.18 (37.31 ÷39.04)	28.94 (28.15÷ 29.73)	3.67 (3.63 ÷ 3.71)
	ring	472.39 (467.59÷477.19)	70.28 (68.73 ÷71.82)	59.33 (56.51 ÷ 62.16)	4.73 (4.72 ÷ 4.74)
100% WO 20.3 tex	compact	36.61 (35.25 ÷37.97)	7.67 (7.29 ÷8.04)	12.56 (12.11 ÷ 13.00)	3.77 (3.75 ÷ 3.79)
	ring	37.67 (36.29 ÷39.05)	6.36 (6.23 ÷6.48)	11.20 (10.59 ÷ 11.80)	4.42 (4.39 ÷ 4.44)
80% WO/20% PA 10 tex	compact	268.28 (264.51÷272.05)	21.94 (21.35 ÷22.54)	31.56 (30.81 ÷ 32.30)	3.38 (3.35 ÷ 3.41)
	ring	532.06 (515.06÷548.47)	77.44 (73.46 ÷81.42)	52.50 (50.93 ÷ 54.07)	3.76 (3.74 ÷ 3.78)

The results of rovings mass irregularity measurements are mentioned in Table 4, selected results of yarn mass irregularity measurements are presented in Table 5. Compared to worsted ring spun yarns,

CVm values of tested compact spun yarns mass irregularity are lower, but the differences in appropriate mean values are statistically and technologically insignificant. Also, tested compact spun yarns have lower values of mass irregularity *CV(1m)*, *CV(10m)* and *CV(50m)* compared tested ring spun yarns (see Table 5). However, the differences between mean values of ring spun yarns mass irregularities and compact spun yarns mass irregularities are statistically insignificant.

Table 4. Selected parameters of rovings mass irregularity measurements

Fibres material	Nominal roving count [tex]	CVm [%]	Confidence interval [%]
100% WO	360	5.73	(5.30 ; 6.15)
100% WO	280	6.97	(6.56 ; 7.29)
100% WO	440	6.45	(4.85 ; 8.05)
80% WO / 20% PA	200	5.95	(5.93 ; 6.07)

Table 5. Selected parameters of yarn mass irregularity measurements

Fibres material/ Yarn count [tex]	Method of spinning	CVm [%] 95% conf. int.	CV(1m) [%] 95% conf. int.	CV(10m) [%] 95% conf. int.	CV(50m) [%] 95% conf. int.
100% WO 16.7 tex	compact	17.47 (17.10 ÷17.53)	6.83 (6.69 ÷ 6.98)	3.20 (2.88 ÷ 3.52)	1.77 (1.60 ÷ 1.92)
	ring	17.49 (17.27 ÷17.70)	6.82 (6.63 ÷ 7.00)	3.29 (3.13 ÷ 3.44)	1.94 (1.91 ÷ 2.36)
100% WO 11.1 tex	compact	20.54 (20.26 ÷20.81)	8.56 (8.22 ÷ 8.90)	4.77 (4.58 ÷ 4.95)	2.54 (2.32 ÷ 2.76)
	ring	20.65 (20.41 ÷20.88)	8.00 (7.68 ÷ 8.32)	4.89 (4.53 ÷ 5.25)	3.11 (1.27 ÷ 1.62)
100% WO 20.8 tex	compact	15.37 (15.22 ÷15.51)	6.24 (6.11 ÷6.37)	4.69 (4.52 ÷ 2.9)	2.04 (1.77 ÷ 2.31)
	ring	15.49 (15.33 ÷15.64)	6.36 (6.23 ÷6.48)	3.45 (3.31 ÷ 3.58)	2.33 (2.10 ÷ 2.56)
80% WO/20% PA 10 tex	compact	18.92 (18.76 ÷19.07)	7.38 (7.17 ÷7.59)	3.85 (3.61 ÷ 4.09)	2.23 (1.91 ÷ 2.55)
	ring	20.86 (20.07 ÷21.65)	7.58 (7.34 ÷7.81)	3.88 (3.62 ÷ 4.14)	2.17 (1.82 ÷ 2.51)

For the analysis of yarn mass irregularity structure, or the effect of the additional condensing zone of the drafting system of the compact spinning machine and effect of drafting system of ring spinning machine on the yarn mass irregularity, the experimental modules of the relative transfer functions $\left|F^{*}_{\exp}(\lambda)\right|$ were calculated according to equation (1). The coefficients of variation of the harmonic components were read from measured mass spectrogram data. From this data, the average mass spectrograms of individual yarns and roving and consequently average modules of relative transfer function were calculated. The average spectrogram of compact staple spun yarn 80 WO/20PA of yarn count 10 tex is shown in Figure 1.

The courses of average experimentally determined modulus of relative transfer function of the drafting device of ring spinning machine and the drafting device with additional compacting zone of compact spinning machine were compared with each other. Further, these courses were compared with courses of theoretical modulus of relative transfer function $\left|F^{*}_{p}(\lambda)\right|$, calculated using equation (2), or strictly speaking with their envelope curves. The courses of experimental modulus of relative transfer

functions $\left|F^*_{\exp}(\lambda)\right|$ of tested compact and ring spun yarns, envelope curve of theoretical modulus of relative transfer functions are mentioned in Figures 3 – 6. The black line indicates the value of the modulus $\left|F^*_{\exp}(\lambda)\right|$ = 1.

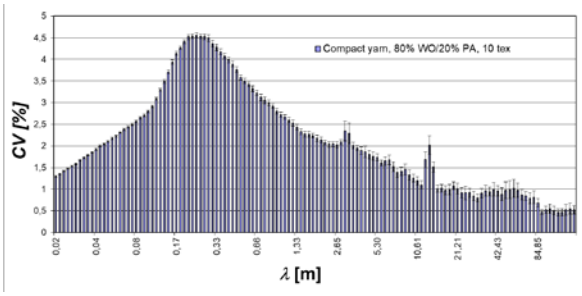

Figure 1. Average mass spectrogram, compact spun yarn, 80% WO/20% PA, yarn count 10 tex

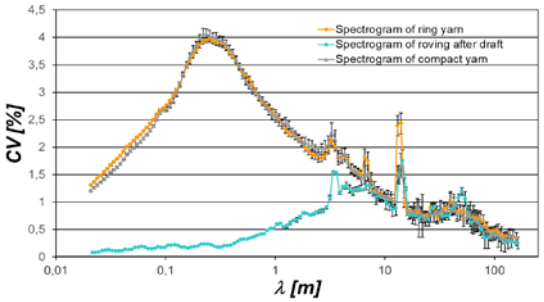

Figure 2. Mass spectrogram of compact and ring spun yarns of count 16.7 tex and mass spectrogram of roving in dependence on wavelength

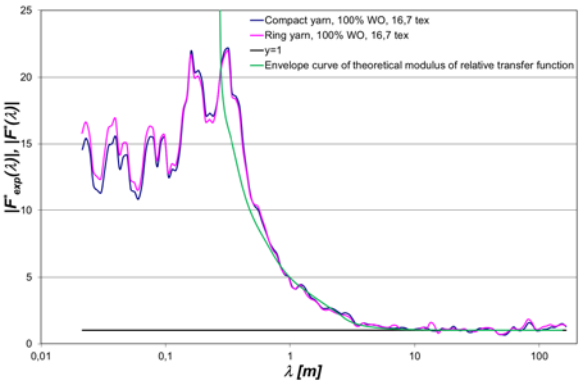

Figure 3. Experimental modulus of relative transfer function of drafting mechanism – compact / ring spinning machine and envelope curve of theoretical modulus of relative transfer function; yarn count 16.7 tex

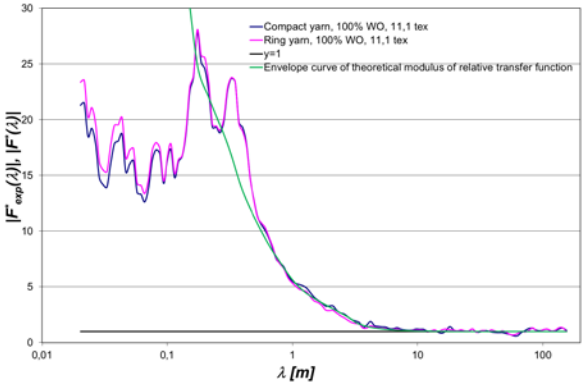

Figure 4. Experimental modulus of relative transfer function of drafting mechanism – compact / ring spinning machine and envelope curve of theoretical modulus of relative transfer function; yarn count 11.1 tex

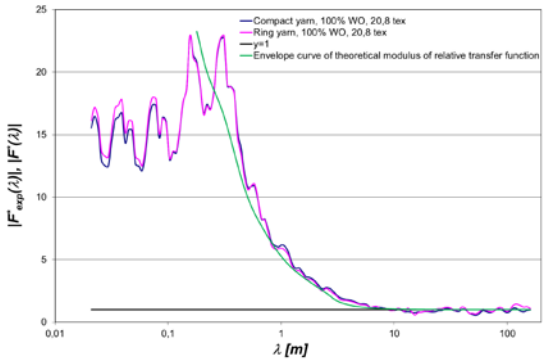

Figure 5. Experimental modulus of relative transfer function of drafting mechanism – compact / ring spinning frame and envelope curve of theoretical modulus of relative transfer function; yarn count 20.8 tex

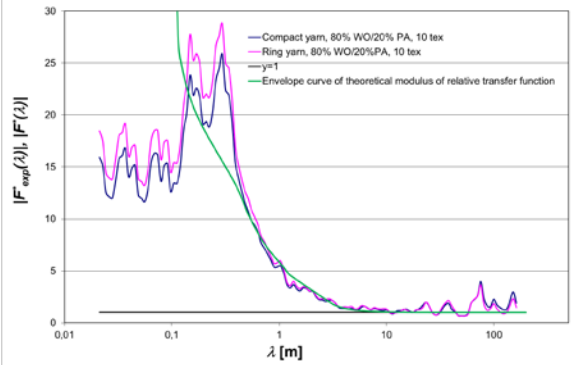

Figure 6. Experimental modulus of relative transfer function of drafting mechanism – compact / ring spinning machine and envelope curve of theoretical modulus of relative transfer function; yarn count 10 tex

From the course of experimental modules of relative transfer function it is evident that modules values are $\left|F^*_{\exp}(\lambda)\right| \rangle 1$. According to the assumptions, the drafting devices of the ring as well as compact spinning machine deepen the mass irregularity, especially at short wavelengths (up to $\lambda \approx$ 1m), where

the modules values increase sharply towards to shorter wavelengths. The increase (deepening) in mass irregularity due to the draft at the ring as well as compact spinning machine is not compensated by any systems or mechanisms that would reduce the mass irregularity. The values of the experimental and theoretical modules of the relative transfer function at wavelengths λ > 1 m fluctuate around the value 1. The fluctuations are caused by the mass irregularity of rovings, but, in most cases, no statistically significant differences were observed between the mean values of the variation coefficients of harmonic components of the roving and yarn mass irregularity at the respective wavelengths (see Figure 2).

The values of the experimental modules of the relative transfer function of drafting device with additional condensing zone of the compact spinning machine are lower than those of drafting device of the ring spinning machine. It means that the drafting device with condensing zone of the compact spinning machine deepens the mass irregularity less than the drafting device of the ring spinning frame. To explain this result, we read the wavelengths corresponding to the maximum amplitude of the harmonic components of the mass irregularity from the average mass spectrograms of compact and ring spun yarns and calculated the mean fibre lengths according to equation (3). The results are presented in Table 6 and it is clear from them that the compact spun yarns appears to be made of longer fibres. This is probably due to the effect of the compaction zone; due to the condensation of the fibre ribbon and the small tension in the compaction zone, the fibres in the twisted ribbon are held in a more straighten state and therefore appear longer. However, we have to note that the differences in the mean values of the experimentally determined modules of the relative transfer functions of the drafting systems of both the compact and ring spinning machines are small and statistically insignificant.

Table 6. Mean fiber length determined from the mass spectrogram of yarn

Mean fiber length [mm]	16.7 tex	11.1 tex	20.8 tex	10 tex
Compact spun yarns	89.08	89.08	93.70	83.12
Ring spun yarns	83.11	77.55	89.07	83.12

Comparing the course of the experimental modulus of relative transfer function with the envelope curve of the theoretical modulus of relative transfer function (see Fig. 3-6), it is clear that courses are very similar. The theoretical modules of relative transfer function are based on the assumption of ideal draft, i.e., a step change in the fibre speed in the drafting field; therefore, theoretical modulus take relatively high values at short wavelengths compared to experimental modules. When drafting a bundle of real fibres, the conditions for ideal draft are not met and due to the effect of floating fibres, fibres speed gradually changes.

4. CONCLUSIONS

The work was focused on the analysis of the effect of the drafting devices of both ring and compact spinning machines on the transformation of the mass irregularity of roving into the yarn with a focus on monitoring the effect of the additional condensing zone of the compact spinning machine on the mass irregularity of the resulting yarn. Experimentally determined and theoretical modules of relative transfer function were used for the analysis. From the presented results it is evident that the drafting systems of the both compact and ring spinning machines deepen the mass irregularity, especially at short wavelengths (λ < 1m), where the modules take values higher than 1 due to drafting of the real fibre bundle. Lower values of mass irregularity and imperfections of compact spun yarns compared to those of ring spun yarns were verified but with the statistically insignificant differences in mean values of mass irregularity of compact and ring spun yarns. The reason for lower values of compact spun yarns mass irregularity could be the effect of additional compacting zone, which causes the fibre ribbon to

become more compact and, due to the small tension draft, it supports a slightly higher fibre straightening in the fibre ribbon compared to ring spun yarn. The higher level of fibre straightening in the compact yarns was demonstrated by the higher average fibre length determined from the yarn mass spectrogram. The behaviour of the real fibres in spinning processes is difficult to predict, but a more compact fibre ribbon is a good prerequisite for a lower mass irregularity of the final yarn, assuming that the technological and technical spinning parameters are optimally set at the individual technological stages.

References

1. *Foster, G. A. R. (1951). Fiber motion in roller drafting. Journal of the Textile Institute Transaction. 42(9). T335-T374.*
2. *Grishin, P. A. (1954). Theory of drafting and its practical applications. Journal of the Textile Institute Transaction. 45 (3). T167-T266*.
3. *Lin,Q., Oxenham, W., Yu, C. (2012). Effect of accelerated point distribution on sliver irregularity. Part I: characterization of accelerated point distribution. Journal of the Textile Institute, 103 (5). 549-557.*
4. *Lin,Q., Oxenham, W., Yu, C. A study of the drafting force in roller drafting and its influence on sliver irregularity, Journal of the Textile Institute. 102(11). 994-1001.*
5. *Graham, J. S., Bragg, C. K. (1972). Drafting force measurement as an aid to cotton spinning. Textile research Journal. 42(3). 175-181.*
6. *Balasubramanian, N (1969). A study of the irregularities added in apron drafting. The Textile Research Journal. 39(2). 155-165.*
7. *Cihlářová, E. (2005). Transformation of roving mass irregularity into yarn mass irregularity. Proceedings of 5th World Textile Conference Autex. University of Maribor, Department of Textile (Maribor). ISBN 86-435-0709-1. 494-499.*
8. *Balda, M., Bošek, M., Dráp, Z. (1968). Základy automatizace. SNTL Praha. (Prague).*
9. *Ursíny, P. (2009). Předení II. Technická univerzita v Liberci (Liberec).*
10. *Moučková, E., Ursíny, P., Jirásková, P., Kim, Y.: Influence of drafting on mass irregularity of cotton ring yarns. 20th International Conference Structure and Structural Mechanics of Textiles: 2014, Liberec, Czech Republic.* Liberec: TU Liberec, s. 151-154, ISBN 978-80-7494-139-9.
11. *Sevosťanov, A.G., Chavkin, V. P., Divinskij, L. A. (1967). Kinematičeskaja teorija vytjagivanija voloknistogo produkta. Izvestija vyšších učebnych zavedenij, Technologia Textilnoj promyšlennosti, 1967 (5). 68-75.*
12. *Khurshid, M.F., Nadeem, K., Asad, M., Chaudhry, M.A., Amanullah, M.: Comparative Analysis of Cotton Yarn Properties Spun on Pneumatic Compact Spinning Systems, Fibres & Textiles in Eastern Europe, 2013, 21, 5(101), 30-34*
13. *Guldemet Basal, G., Oxenham, W.: Comparison of Properties and Structures of Compact and Conventional Spun Yarns, Textile Research Journal, 2006, Vol. 76(7), 567 – 575*
14. *Nikolič, M., Stjepanovič Z., Lesjak,F., Štritof, A.: Compact Spinning for Improved Quality of Ring-Spun Yarn, Fibres & Textiles in Eastern Europe, October/December 2003, Vol. 11, No. 4 (43)*
15. *Rashid, M. R., Ahmed, E., Azad, A.K., Ullah, A.N.M.A :Comparative Study On Cotton Yarn Quality Made From Compact And Conventional Ring Frame, Journal of Innovation & Development Strategy, Volume:5, Issue: 3, December 2011*
16. *Çelik, P., Kadoğlu, H.: A Research on the Compact Spinning for Long Staple Yarns, Fibres & Textiles in Eastern Europe, October/December 2004, Vol. 12, No. 4 (48)*
17. *Yan, G.S., Yu, C.W. (2009). The influence of fiber length distribution on the accelerated points in drafting: A new perspective on drafting proces. Fibres and Polymers, 10(2), 217-220.*
18. *Uster Technologies AG: Uster Tester IV Application Handbook, V1.0/400 106-04010, Uster, (2001).*

THE INFLUENCE OF VARIOUS PORTION OF COTTON WASTE AND WAY OF CLEANING ON QUALITY OF OPEN-END ROTOR YARNS

Gabriela Krupincová

Technical University of Liberec, Faculty of Textile Engineering, Department of technologies and structures, Liberec, Czech Republic, gabriela.krupincova@tul.cz

Abstract:

Nowadays, recycling and reuse of natural resources has become an important topic. The adaptation of technological lines is crucial for the production of yarn from recovered or reclaimed waste fibers with lower length and possible higher contamination. The way of cleaning is a key factor of waste fibre processing into yarn repeatedly. This study is oriented to the investigation of open-end rotor yarn quality in gray and dyed form, which were spun from various portions of cotton waste from 0% to 100% on R37 Rieter spinning machine with exchangeable cleaning channels. The standard cleaning channel C is complemented by two others. The cleaning channel A is suitable for processing of cotton waste, when the amount of impurities in the raw fibrous material is low and the high quality of final yarn is requested. The maximisation of fiber yields predominating on removing impurities and reducing the generation of waste during spinning is the philosophy of innovative way of cleaning W. The standard quality indicators of fibers and yarns were measured. The generalised analysis of variance were used to prove whether the quality of yarn is significantly influenced by selected predictors (quality of fibers, state of yarn, way of cleaning and level of twist). The experiment verified that the open-end rotor spun yarn 29.5tex can be produced from the mixture of cotton waste with or without addition of virgin cotton fibers via selection of spinning strategy (way of cleaning) and suitable level of twist. The use of cleaning method W deteriorates some partial yarn quality indicators, but the shift of yarn quality is mostly within the USP™ level for given quality groups of USTER®STATISTICS. Most yarns are at the 6%-25% qualitative level except the yarns produced from 100% waste which is comparable with 51% -75% qualitative level sufficient for selected end use.

Key words:

open-end rotor yarn; yarn quality; cotton waste; cleaning innovations

1. Introduction

The decrease of natural resources forced the industry to find new opportunities for recycling or reuse of products, which ended their life cycle. The textile waste is usually termed in respect to the place of origin. In general, there are three main categories for textile cotton waste description [11, 12, 18 and 19]. Pre-consumer industrial cotton waste, which relates to the processing from fiber to yarn structure (e.g. blowroom waste, carding stripes, pneumafil waste, combing noils, broken webs or slivers, yarns remains) and post-consumer industrial cotton waste, which is generated during yarns processing to final products (e.g. yarns remains from weaving or knitting, fabric scraps from sewing). When the textile products finish their life cycle then the waste is named as post-consumer cotton waste. The recovering of fibers from pre-consumer waste, especially from spinning companies, is technically mastered and used for a long time to produce the yarns with optimal quality for given end use with economic benefits [11, 12, 18 and 19]. The post-production textile waste obtained from fabric weaving, finishing and processing into final products or from used clothes challenges the industry these days [6-9, 18 and 19]. The cost effective recovering of fibers from waste is limited by the technology, which is adopted and still improved. The cleaning is a key factor of processing of raw fiber materials into yarns.

The cotton fibers recovered from waste can be generally processed by two types of strategies, which differs in the philosophy of cleaning. The first one is oriented to processing of pre-consumer industrial

cotton waste were the carrier components is raw fibrous material with optimal fiber length (e.g. for 100% Cotton yarn - the mixture of virgin cotton fibers and noils or fibers recovered from spinning process at minimal amount of 0% - 15%). In this specific case, the main aim of each technological step is to get the highest quality of semi-products and finally the yarns with optimal quality for selected end application. In this case, from the point of view of philosophy of cleaning the removal of dust and trash predominates on recovering good fibers from waste [11, 12, 18 and 19]. On the other side of the spectrum stands the philosophy, where the minimization of good fibers separation predominates on removing impurities. This concept allows the processing of cotton fibers recycled from industrial post-consumer waste or post-consumer waste from clothing and hard workable cotton waste from spinning process. The quality of these types of fibers is influenced by the current options of technologies used for mechanical recovering or reclaiming of cotton fibers again to the spinning process. The lower length of fibers and its higher variability as well as the possible higher contamination of cotton fibers by trash and dust obtained from reopening of woven or knitted scraps or yarn remains requires use of carrier components at minimal amounts of 0% - 15%. The application of the second strategy leads to potential deterioration of yarn quality from the point of view of qualitative characteristics (e. g. yarn unevenness, hairiness, number of faults, strength and elongation) and also the rustic appearance caused by incorporation of plant particles into yarn structure.

At present time for some specific textile products, the customers accept the ecological criterion as one of priority for the selection of goods. For this reason, the fiber-to-yarn process can be adapted and the demands on quality of yarn is primarily given by workability into the final product because the user requirements including durability is changed due to change of customers sensitivity to e.g. structure uniformity, egality of staining and so on. Denim fabrics with a worn look or cotton goods (linen, home textile) with a natural look might be good examples. The way of cleaning during spinning is essential and the main aim of this article is to prove, whether the innovative way of cleaning together with the amount of waste can influence the quality of open-end rotor spun yarns for application in weaving. The quality of gray and dyed yarn is analysed because in these forms are usually used for processing into home textile or denim fabrics. The experiment suitably complements the results presented in [6-9, 18 and 19], where the authors study the influence of amount of waste on open-end rotor spun yarns together with other influencing factors like the type of waste and the way of its preclearing, levels of yarn construction parameters and way of spinning settings.

2. Experimental – Materials and methods

The experiment was carried out in five levels of blending portions of cotton waste from 100% to 0%. The blowroom waste (mixture of waste from fibre pre-treatment, cleaning and mixing, flat stripes, hard card waste, remains of sliver from doubling and drawing and noils) was blended with virgin cotton fibers. The virgin cotton and cotton waste were pre-treated and blended on mixer at the blowroom and than fed into carding machine. The carding, doubling and drawing followed the standard way. The spinning of open-end rotor yarns were realised on the Rieter R37 spinning machine, which allows the use of three types of trash channels (A, C, W). The exchangeable trash channel A is primarily recommended for processing of wastes, where the priority is to have high quality yarn at the end of the spinning process. In other words, the potential exclusion of good fibres together with impurities or fiber neps is possible more often, the amount of generated waste is higher and grows with contamination of input raw fibre material. Similarly the exchangeable trash channel C allows removing the impurities or fiber neps at optimum level mostly for virgin raw materials or wastes with low level of contamination for a wide range of yarn counts. The cleaning by applying these two kinds of exchangeable trash channels follows the philosophy of the first strategy of spinning mentioned above. Contrary to the exchangeable trash channel W minimises the waste generation and allows maximisation of fiber yields into yarn. On the other hand, when the exchangeable trash channel W is used, the impurities (trash and dust particles) or fiber neps can be possibly incorporated into yarn structure more often, can deteriorate yarn quality and can cause the rustic appearance.

To be able to select suitable yarn construction parameters and optimal settings for spinning, the quality of fibers via standard length parameters and possible contamination with dust, trash or fiber neps were examined from samples selected from slivers by using Trash Tester and USER AFIS® PRO, see table 1. It is visible that the fibre length parameters together with its variability, short fiber content and amount of impurities or neps decreases as the amount of cotton waste decreases. In respect to these results the optimal settings and parts for yarn production on Rieter R37 spinning machine were selected [14-15]. Yarns were produced with 29.5 tex count and the level of twist were optimised in accordance with fibre length parameters for each blends of carrier component (virgin cotton). The rotor type S533 together with a draw off nozzle SR7KS type and 6 kPa spinning under pressure were used for preparation of 30 yarn samples in gray and dyed form. The dyeing of yarn samples was realised by the standard all-in-one technology by using Thies apparatus, and hues typically used for home textile were applied. The yarns were rewound to perforated tubes with soft coils and minimally cleaned before dyeing realization because it is a part of the typical dyeing process. The vat dyes (Indantre) were applied because of their excellent colour fastness in washing and lightfastness. The specific dyeing recipe and procedure recommended by the producer of pigments were used for all selected hues (light grey – for cleaning A, light green – for cleaning C, dark green – for cleaning W). The earlier experience shows that the unanchored fibers or fiber fragments from the yarn surface are released into the dyeing bath to the extent that the yarns made of waste fibers are processed. Therefore the quality of yarns in gray and dyed form is analysed and the significance of change in their quality is evaluated.

Table 1. Selected qualitative parameters of fiber blends

	Material type	**CO waste 100%**	**CO waste /CO 75%/25%**	**CO waste/CO 50%/50%**	**CO waste /CO 25%/75%**	**CO 100%**
Trash Tester	*Good fibers* [%]	98.15	98.67	99.05	99.43	99.71
	Coarse impurities [%]	1.61	1.1	0.74	0.43	0.17
	Dust [%]	0.07	0.06	0.05	0.03	0.05
	Short fibers [%]	0.17	0.17	0.16	0.11	0.07
Uster Afis	$L_{(w)}$ [mm]	21	21.7	22.7	23.1	23.6
	CV $L_{(w)}$ [%]	40	38.4	36.5	35.5	34
	$UQL_{(w)}$ [mm]	26.9	27.6	28.5	29.0	29.3
	$SFC_{(w)}$ % < 12,7	17.2	15.0	12.2	11.3	9.8
	$L_{(n)}$ [mm]	16.1	17	18.1	18.7	19.6
	CV $L_{(n)}$ [%]	54.9	53.1	50.2	48.3	45.2
	$SFC_{(n)}$ % < 12,7	38.2	34.7	30.0	28.1	24.1
	$L_{5,0\ \%}$ [mm]	31.4	32.2	32.8	33.2	33.5
	Neps [Cnt / g]	412	289	196	138	74
	Dust [Cnt / g]	1004	711	486	350	146
	Trash [Cnt / g]	122	92	50	32	9

Table 2. Rieter R37 machine settings

Material type	**CO waste 100%**	**CO waste /CO 75%/25%**	**CO waste/CO 50%/50%**	**CO waste /CO 25%/75%**	**CO 100%**
Sliver count [tex]	6000	6000	6000	6000	6000
Yarn count [tex]	29.5	29.5	29.5	29.5	29.5
Draft	203	203	203	203	203
Twist [m^{-1}]	985	932	901	827	796
Phrix twist coeff. [$ktex^{2/3}m^{-1}$]	94	89	86	79	76
Rotor RPM [min^{-1}]	100000	100000	100000	105000	110000
Opening roll RPM [min^{-1}]	10000	10000	10000	9500	9000
Delivery speed [m min^{-1}]	102	107	111	127	138
Trash channel	A, C, W	A, C, W	A, C, W	A, C, W	A, C, W

The typical set of yarn qualitative structure and mechanical indicators were evaluated together with the yarn abrasion resistance and lint generation to analyse whether the factors (portion of waste – quality of fibers, way of cleaning, form of yarn, level of twist) can influence the quality of yarn. All fiber materials,

slivers, and yarn samples were standard atmosphere conditioned (temperature of 20°C ± 2°C and humidity of 65% ± 2%) in accordance with EN ISO 139 [3]. Yarn samples were selected with respect to EN ISO 12751 [2]. Compliance of nominal and experimental yarn counts was realised in accordance with EN ISO 2060 [4] (testing length of 100 m, 5x). The yarn unevenness CV_m, number of faults (*Thin − 40%*, *Thin − 50%*, *Thick + 35%*, *Thick + 50%*, *Neps + 200%*, and *Neps + 280%*), and hairiness index *H* were evaluated using USTER® TESTER 4SX (a testing speed of 400 m min^{-1} and a testing length of 1 km for each bobbin, 5x) in accordance with ČSN 80 0706 [1]. The amount of trash and dust counts in yarns were verified using USTER ® TESTER 5. The sum criteria of yarn hairiness S_{12} and S_3 were analysed using ZWEIGLE G 567 (testing speed of 50 m min^{-1}, testing length of 100 m, 5x). The yarn tenacity *F* and yarn breaking elongation ε were measured by INSTRON TESTER in accordance with EN ISO 2062 [5] (pretension of 0.5 cNtex^{-1}, testing speed of 500 m min^{-1}, testing length of 500 mm, 50x). Yarn abrasion resistance *o* as a number of strokes to yarn destruction was evaluated by Zweigle 552 (emery paper P 800, the type of abrasive grains alpha Al_2O_3 and pretension of 20 g, 60x) in accordance with IN 32-102-01/01 [10]. Lint generation was measured using Lawson Hemphill constant tension transport (CTT) as the amount of separated abraded lint from a 1-km-long-yarn section when the wrapped yarns were evaluated (testing speed of 100 m min^{-1}, input pretension of yarn 0.5 g tex^{-1}, recommended yarn-to-yarn wrapping angle changed to 540° due to yarn breakages, and tested yarn length of 1000 m) [13] and the result is expressed as the mass of lint in milligrams per kilometre.

3. Results and discussion

To be able to assess extent to which selected numerical response variable of yarn characteristics is influenced by qualitative factors (as way of cleaning and state of yarn) and/or quantitative numeric variables (as waste portion – resulting in various fibre quality defined by fibre length $L_{(w)}$, fiber length variability $CV_{L(w)}$, short fiber content $SFC_{(w)}$ and yarn twist *Z*) the generalised analysis of variance GANOVA was used (1). Observations Z_i at n_j different levels of predictor factor X_j and various values of the predictor variable Y_k can be described by linear regression model with unknown parameters, where α_0 is the absolute term (overall mean value), α_j is an (n_j x 1) vector of latent parameters for *j*-th factor and β_k is the regression coefficient for *k*-th variable. Random error ε_{ij} is assumed to have normal distribution with zero mean, $\varepsilon \sim N(0, \sigma^2)$ [16]. The influence of six selected predictors (type of fiber blend—five levels; way of cleaning —three levels; yarn twist—five levels; yarn state—two levels) on yarn quality (in terms of CV_m, *H*, S_{12}, S_3, *F*, ε, *o*, and *Lint generation*) was verified by GANOVA at a significance level of α = 5%. Table 3 summarises results of the sum of squares, *F* statistic, and *p*-value for all individual predictors, the significant results are marked bold.

$$Z = \alpha_0 + \sum_j \alpha_j X_j + \sum_k \beta_k Y_k + \varepsilon \quad (1)$$

Table 3. The GANOVA results for individual predictors

Predictor	Sum of squares	*F*-statistic	*p*-value	Predictor	Sum of squares	*F*-statistic	*p*-value
CV_m [%]				**F [cNtex^{-1}]**			
$L_{(w)}$ [mm]	**3.081**	**3.960**	**0.01219758**	**$L_{(w)}$ [mm]**	**29.574**	**14.229**	**0.0000028**
$CV_{L(w)}$ [%]	**3.081**	**3.960**	**0.01219758**	**$CV_{L(w)}$ [%]**	**29.574**	**14.229**	**0.0000028**
$SFC_{(w)}$ [%]	**3.081**	**3.960**	**0.01219758**	**$SFC_{(w)}$ [%]**	**29.574**	**14.229**	**0.0000028**
yarn state	**3.703**	**24.455**	**0.00003884**	**yarn state**	**9.850**	**8.431**	**0.0074288**
cleaning	0.301	0.531	0.59425145	cleaning	2.018	0.672	0.5193042
Z [m^{-1}]	**2.764**	**3.336**	**0.02479796**	**Z [m^{-1}]**	**27.775**	**11.738**	**0.0000140**
H [−]				**ε [%]**			
$L_{(w)}$ [mm]	**4.007**	**25.566**	**0.00000001**	**$L_{(w)}$ [mm]**	**2.667**	**5.502**	**0.0023995**
$CV_{L(w)}$ [%]	**4.007**	**25.566**	**0.00000001**	**$CV_{L(w)}$ [%]**	**2.667**	**5.502**	**0.0023995**
$SFC_{(w)}$ [%]	**4.007**	**25.566**	**0.00000001**	**$SFC_{(w)}$ [%]**	**2.667**	**5.502**	**0.0023995**
yarn state	0.084	0.481	0.49399816	**yarn state**	**1.001**	**5.968**	**0.0216717**
cleaning	0.112	0.311	0.73563053	cleaning	0.501	1.301	0.2893773

Z [m^{-1}]	**4.001**	**25.354**	**0.00000001**	**Z [m^{-1}]**	**1.931**	**3.205**	**0.0288936**
S_{12} [100 m^{-1}]				**o [-]**			
$L_{(w)}$ [mm]	**6275376**	**4.960**	**0.00416722**	$L_{(w)}$ [mm]	5186	0.535	0.7113009
$CV_{L(w)}$ [%]	**6275376**	**4.960**	**0.00416722**	$CV_{L(w)}$ [%]	5186	0.535	0.7113009
$SFC_{(w)}$ [%]	**6275376**	**4.960**	**0.00416722**	$SFC_{(w)}$ [%]	5186	0.535	0.7113009
yarn state	1852071	4.205	0.05049964	**yarn state**	**55987**	**159.959**	**0.000000000001**
cleaning	60960	0.058	0.94351392	cleaning	323	0.067	0.9356303
Z [m^{-1}]	**5646814**	**4.134**	**0.01006140**	Z [m^{-1}]	5264	0.544	0.7051850
S_3 [100 m^{-1}]				***Lint generation* [mgkm^{-1}]**			
$L_{(w)}$ [mm]	116795	0.927	0.46331870	**$L_{(w)}$ [mm]**	**6975**	**32**	**0.0000000010**
$CV_{L(w)}$ [%]	116795	0.927	0.46331870	**$CV_{L(w)}$ [%]**	**6975**	**32**	**0.0000000010**
$SFC_{(w)}$ [%]	116795	0.927	0.46331870	**$SFC_{(w)}$ [%]**	**6975**	**32**	**0.0000000010**
yarn state	**341120**	**16.969**	**0.00034228**	yarn state	0.51483	0.0017	0.9671324172
cleaning	1143	0.017	0.98306741	cleaning	728	1,293	0.2915692188
Z [m^{-1}]	135659	1.104	0.37591637	**Z [m^{-1}]**	**6303**	**19.441**	**0.0000001649**

GANOVA confirmed that the fiber length in terms of $L_{(w)}$, $CV_{L(w)}$ and $SFC_{(w)}$ as well as the level of twist Z significantly influence CV_m, H, S_{12}, F, ε and *Lint generation*. The fiber length influences the quality of sliver mainly in terms of its cohesiveness. Too short fiber length, its higher variability and higher short fibers content can negatively influence the quality of sliver after the operation of doubling and drawing due to floating fibers and finally influence the quality of yarn. The fact whether the yarn is in gray or dyed form is significant only for the CV_m, S_3, F, ε, o . The reason is probably hidden in a fact, that the yarn for the dying process had to be rewound with simultaneous removal of the coarse faults primarily neps and it led to the improvement in these qualitative parameters after dying. The way of cleaning was proved as insignificant for all qualitative indicators. The diversities among the selected qualitative characteristics from the point of view of way of cleaning is small and in most cases it is hidden in overlapping confidence bounds. As example the dependence of yarn tenacity and elongation on the amount of virgin cotton fibers in raw materials for yarns in gray and dyed form is shown in figure 1.

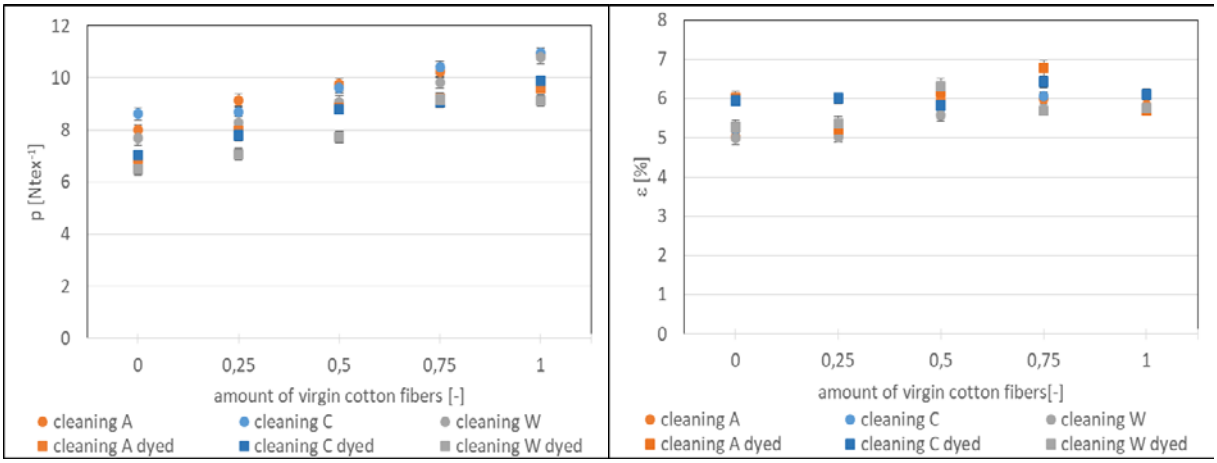

a) b)

Figure 1. The dependence of mechanical characteristics of 29.5 tex yarn in gray and dyed form on amount of virgin cotton fibers in a raw materials for way of cleaning A, C, W

More visible diversity is found when the yarn faults are evaluated. The statistical comparison is limited due to fact that the distribution of faults usually does not follow the normal distribution. The comparison with USTER® STATISTICS [17], where the yarns are prepared from primary original no recycled fibers can be used for verification, whether the way of cleaning influences the quality of yarn significantly or not. The selected qualitative indicators were evaluated as cotton fibers, carded sliver technology, and open-end rotor spun yarn for weaving. Yarn characteristics were compared using a partial qualitative indicator—the relative cumulative frequency—termed "USTER®STATISTICS percentile" (USP^{TM}). In general, the lower the USP^{TM} level is, the better the yarn quality. There are the six qualitative groups, which are used for yarn quality grading (qualitative groups: ≤5, 6–25; 26–50; 51–75; 76–94; ≥95). The

overall USP^{TM} $_{overall}$ can be found by different methods. In this case, the most frequent level of individual USP^{TM} is used to get the USP^{TM} $_{overall}$. The obtained results for selected qualitative yarn indicators of the analysed set of yarns are shown in Table 4. The level of mechanical parameters is not included due to different measurement conditions, especially in terms of testing speed, which could lead to significant underestimation of USP^{TM} for yarn tenacity and elongation. The results show that in most cases the *Trash* and *Dust* deteriorates the quality of analysed gray yarns and for most of yarns is up the USP^{TM} level ≥ 95%. The comparison of yarn quality with USTER® STATISTICS confirmed that the quality of open-end rotor yarn spun from 100% cotton waste can be comparable with the quality of open-end rotor made of 100% virgin cotton, when the appropriate level of twist is used. The way of cleaning allows the processing of input materials with various levels of contamination. The setting of cleaning A, C, W leads to comparable results of yarn quality when the yarns were spun from various portions of cotton waste because simultaneously various levels of twist for a given level of waste portion in raw material were applied. On the other hand it is visible that the way of cleaning W, leads to shifts in individual USP^{TM} to worse levels, see table 4. An example can be dependence of *Neps +200%*, number of *Trash* and *Dust* particles on the amount of virgin cotton fibers in raw input material shown in figure 2. The evaluated yarn characteristics decrease as the amount of cotton waste decreases. The cleaning A and C leads in most cases to very similar results. If the W cleaning is used, the variability of analysed characteristics increases as the amount of waste increases. The quality of open-end rotor spun yarns in dyed form compared to gray yarns show better quality in terms of USP ^{TM} and it is most probably given by partial cleaning during rewinding before the dying process.

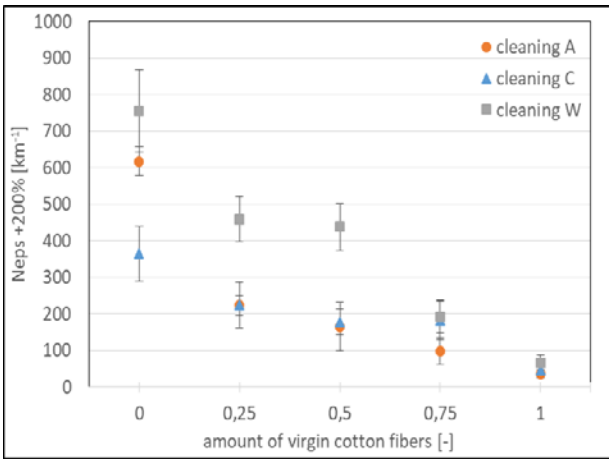

a)

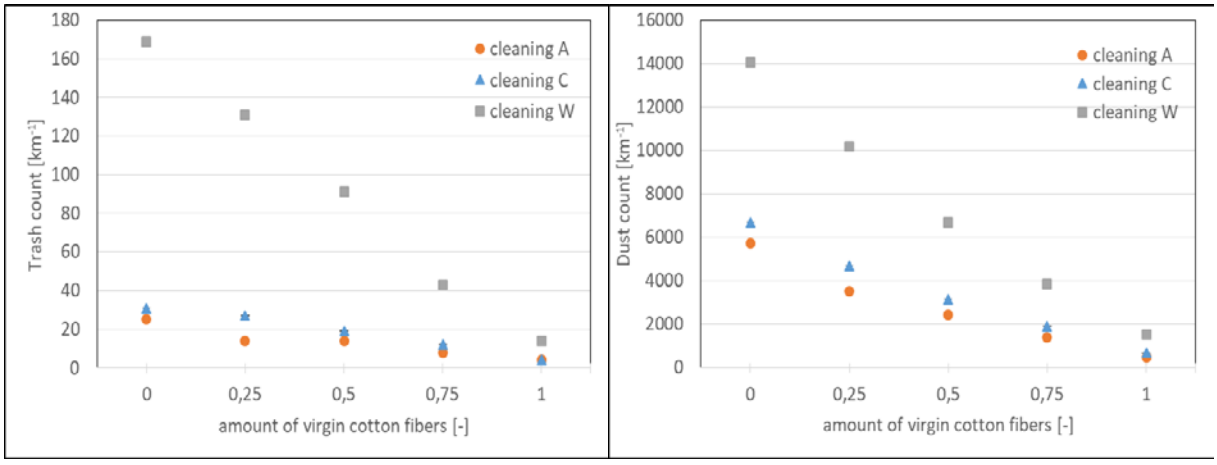

b) c)

Figure 2. The dependence of selected qualitative indicators of 29.5 tex yarn in gray form on amount of virgin cotton fibers in a raw materials for way of cleaning A, C, W

Results of GANOVA and comparison of yarn quality with USTER®STATISTICS are generally in good accordance with earlier experience, where the authors conclude that the amount of waste significantly influences the quality of yarn [6, 7, 18 and 19]. The comparison with earlier studies is limited because most articles define the quality of raw fibrous material for each component, not the quality of prepared blends in slivers to be spun. The crucial is fiber length and its variability in final sliver or roving, because then it can be achieved the similar qualitative results for yarns spun from various portions of waste [19].

4. CONCLUSIONS

Main aim of this study was to verify whether it is possible to optimise the open-end rotor spinning system in terms of cleaning efficiency suitable for given quality of raw fibrous material and obtained yarns which will have expected level of quality for selected end use with minimal variation and with minimal loss of reusable fibres. The innovative way of cleaning, allowing controlled ways of eliminating impurities with a defined possible exclusion of good fibers, is used for the experiment. The analysis of selected yarn qualitative indicators were done for a set of 29.5tex open-end rotor spun yarns. Results and its statistical processing prove, that the open-end rotor spun yarn 29.5tex can be produced from the mixture of cotton waste with or without addition of virgin cotton fibers via selection of spinning strategy (way of cleaning) and suitable level of twist and get yarns with optimal quality for selected final end use in gray state. The use of cleaning method W deteriorates some partial yarn quality indicators, but in our case the shift is mostly within the USP™ level for given quality groups. Thus, no significant deterioration is indicated, even when the yarn is made from 100% cotton waste. In these days, the possible application for middle and lower quality yarns spun from cotton fibers recovered from waste is limited but it can be extended via changes of customer quality perception. We believe that the responsible approach to yarn production, efforts to reduce waste generation and its possible further processing into yarn again is a part of adaptation of the circular economy to the practice.

ACKNOWLEDGEMENTS

This work was supported by the Czech Ministry of Industry and Trade under Grant No. FV40025 Processing of recycled and waste textile fibers.

References

1. ČSN 80 0706 (1992) *Evaluation of material irregularity of threads, rovings and slivers*.
2. EN 12751 (2000) *Textiles - Sampling of fibres, yarns and fabrics for testing*.
3. EN ISO 139 (2005) *Textiles - Standard atmospheres for conditioning and testing.*
4. EN ISO 2060 (1996) *Determination of linear density (mass per unit length) by the skein method.*
5. EN ISO 2062 (2010) *Textiles – Yarns from packages – Determination of single-end breaking force and elongation at break using constant rate of extension (CRE) tester*.
6. Halimi M. T., Azzouz B. A., Hassen B. M., Sakli F. (2009) Influence of spinning parameters and recovered fibers from cotton waste on the uniformity and hairiness of rotor spun yarn. *Journal of Engineered Fibers and Fabrics* 4(3).
7. Halimi M. T., Hassen M. B., Azzouz B., Sakli F. (2007) Effect of cotton waste and spinning parameters on rotor yarn quality. *Journal of the Textile Institute* 98(5) 437.
8. Hassani H., Tabatabaei S. A. (2011) Optimizing spinning variables to reduce the hairiness of rotor yarns produced from waste fibers collected from the ginning process. *Fibers & Textile in Eastern Europe* 19 3(86).
9. Hassani H., Tabatabaei S. A., Semnani D. (2010) Determining the optimum spinning conditions to produce the rotor yarns from cotton wastes. *Industria Textila* 6.
10. IN 32-102-01/01 (2009) *Evaluation of yarn abrasion resistance*, FT TUL.
11. Klein W. (1987) *Practical guide to opening and carding.* Textile Institute, (Manchester).
12. Klein W. (2014) *The Rieter manual of spinning 2 – Blowroom & Carding*. Rieter Machine Works Ltd. (Wintherthur).
13. Lawson Hemphill (2004). *CTT constant tension transport*: User manual, Swansea, USA.
14. Schwippl H. (12/2020) *The Increasing importance of Recycling in the Staple-Fibrer spinning Process*. Rieter Machine Works Ltd: Winterthur, Switzerland.

15. Spatafora J., Schwippl H. (6/2020) *The ideal rotor spinning process for a high short-fiber content*. Technology and Process Analytics Rieter Machines and Systems. Rieter Machine Works Ltd: Winterthur, Switzerland.
16. TriloByte (2010). *The Interactive Data Analysis in Quality Control*, QC Expert: User manual, version 3.2, Pardubice, Czech Republic.
17. Uster® Statistics: (retrieved 06/2020) https://www.uster.com/en/service/uster-statistics/accessed 2020-04-02.
18. Ute T. B., Celik P., Uzumcu M. B. (2019) Utilization of cotton spinning mill wastes in yarn production. *Textile Industry and Environment*. DOI: 10.5772/intechopen.85127 [online]. https://www.intechopen.com/books/textile-industry-and-environment/utilization-of-cotton-spinning-mill-wastes-in-yarn-production.
19. Yilmaz D., Yelkovan S., Tirak Y. (2017) Comparison of the effects of different cotton fibre wastes on different yarn types. *Fibres and Textiles in Eastern Europe* 25 4(124).

Table 4. *USTER STATISTICS 2018 USP™* [%] *levels for set of open-end rotor yarns 29.5 tex*

Material	**100% CO waste**						**75%/ 25% CO waste /CO**						**50%/ 50% CO waste/CO**						**25%/ 75% CO waste /CO**						**100% CO**					
State of yarn	**gray**	**dyed**	**gray**	**dyed**	**gray**	**dyed**	**gray**	**dyed**	**gray**	**dyed**	**gray**	**dyed**	**gray**	**dyed**	**gray**	**dyed**	**gray**	**dyed**	**gray**	**dyed**	**gray**	**dyed**	**gray**	**dyed**	**gray**	**dyed**	**gray**	**dyed**	**gray**	**dyed**
Cleaning	**A**		**C**		**W**		**A**		**C**		**W**		**A**		**C**		**W**		**A**		**C**		**W**		**A**		**C**		**W**	
***Z* [m^{-1}]**	**985**		**985**		**985**		**932**		**932**		**901**		**901**		**901**		**901**		**827**		**827**		**827**		**796**		**796**		**796**	
***CV$_m$* [%]**	56	15	31	17	53	23	36	9	27	16	46	20	24	8	22	≤5	34	≤5	21	≤5	25	≤5	24	9	11	8	10	≤5	12	≤5
***Thin - 40%* [km^{-1}]**	69	19	52	27	67	33	53	21	51	24	62	24	41	20	41	10	57	27	44	7	49	7	46	33	39	34	33	21	41	20
***Thin - 50%* [km^{-1}]**	15	≤5	32	≤5	49	≤5	38	≤5	32	15	15	≤5	24	≤5	15	≤5	15	≤5	44	≤5	24	≤5	24	32	≤5	≤5	15	15	32	≤5
***Thick + 35%* [km^{-1}]**	49	≤5	14	≤5	46	9	21	≤5	14	7	41	13	16	≤5	15	≤5	31	≤5	22	≤5	19	≤5	29	≤5	15	≤5	14	≤5	13	≤5
***Thick + 50%* [km^{-1}]**	42	≤5	7	≤5	58	≤5	7	≤5	≤5	≤5	49	≤5	≤5	≤5	≤5	≤5	41	≤5	≤5	≤5	17	≤5	24	≤5	14	≤5	≤5	≤5	≤5	≤5
***Neps + 200%* [km^{-1}]**	90	≤5	69	14	≥95	44	47	≤5	47	≤5	78	33	33	≤5	37	≤5	76	19	14	≤5	37	≤5	40	≤5	≤5	≤5	≤5	≤5	≤5	≤5
***Neps + 280%* [km^{-1}]**	52	≤5	51	5	≥95	24	12	≤5	19	≤5	91	36	19	≤5	12	≤5	81	27	12	≤5	9	≤5	32	9	≤5	≤5	≤5	≤5	≤5	≤5
***H* [-]**	43	58	58	58	58	39	39	43	39	47	43	35	35	51	31	31	39	23	23	19	19	16	27	16	19	23	16	≤5	19	≤5
sh [-]	57	46	46	57	57	46	32	32	32	57	32	57	20	46	20	32	32	32	20	9	20	9	20	9	20	9	9	9	20	9
***S$_{12}$* [1/100m]**	≤5	9	≤5	≤5	≤5	≤5	≤5	≤5	≤5	≤5	5	9	≤5	≤5	≤5	≤5	≤5	≤5	≤5	≤5	≤5	≤5	≤5	≤5	≤5	≤5	≤5	≤5	≤5	9
***S$_3$* [1/100m]**	28	≤5	15	≤5	≤5	≤5	≤5	≤5	≤5	≤5	5	≤5	≤5	≤5	≤5	≤5	≤5	≤5	≤5	≤5	≤5	≤5	≤5	≤5	≤5	12	≤5	≤5	≤5	16
***Trash* [km^{-1}]**	≥95	-	≥95	-	≥95	-	≥95	-	≥95	-	≥95	-	≥95	-	≥95	-	≥95	-	≥95	-	≥95	-	≥95	-	74	-	74	-	≥95	-
***Dust* [km^{-1}]**	≥95	-	≥95	-	≥95	-	≥95	-	≥95	-	≥95	-	≥95	-	≥95	-	≥95	-	≥95	-	≥95	-	≥95	-	35	-	60	-	≥95	-
USP™ *overall**	51-75	≤5	51-75	≤5	51-75	5-50	6-25	≤5	6-25	≤5	26-50	6-25	6-25	≤5	6-25	≤5	26-50	≤5	6-25	≤5	6-25	≤5	6-25	≤5	5-25	≤5	5-25	≤5	5-25	≤5

*USP™ overall** - overall quality according to the most frequent level of partial USTER® *STATISTICS* percentile *USP™*

USING OF THE CT IMAGES FOR YARN FOREIGN MATTER DEFINITION – TWO VARIOUS APPROACHES

Monika Vyšanská

Technical University of Liberec, Department of Technologies and Structures, Liberec, Czech Republic, monika.vysanska@tul.cz, tel.: +420485353120

Abstract:

There exist several approaches how to find out presence of the foreign matter in textile material and consequently define their color and geometrical parameters. Presented work uses image analysis to define and analyze all objects on virtual cross-sections of the yarn. Work is unique in CT scan usage, what allows getting continuous information from whole length of observed sample, analyzing all or selected virtual cross-sections, recognizing and separating objects on cross-sections without user intervention. Two approaches of objects' separation on binary image are presented, then subjective definition of representative fibers follows and finally rest of the objects is divided to four groups according to ITMF [13] definition. Results are compared mutually and additionally with results from AFIS Trash Tester.

Key words:

CT image, image analysis, foreign matter, maximal Feret's diameter

1. Introduction

Worldwide there is global tendency to find new ways to recycle and produce recyclable textiles [1, 2]. It is needed to analyze these products and raw material for foreign matter presence. The USDA (United States Department of Agriculture) is developing high volume instruments (HVI) to estimate among others the quantity of trash by use of video camera [3, 4, 5].

The Shirley Analyzer provides an effective means for both quantitative and qualitative analyses of foreign matter in cotton lint. It works on the principle of buoyancy separation (air flotation principle) by air currents [6]. A study [7] found out a little correlation between Shirley trash analyzer and HVI results for cotton material.

Measurement of the area covered by trash in raw material realized by video scan trashmeters (black and white TV camera) is solved next to also number of trash particles in [8]. The same author presents video scanning measurements on yarn samples to estimate the quantity of visible trash remaining in yarn [9]. The same problem is solved in [10], where authors determine the potential of hyperspectral NIR (near infrared) cameras in reliably predicting the polyester content of natural and man-made cellulose and polyester blends. Authors [11] uses also image analysis of raw cotton to get information about size, size distribution, spatial density of trash particles. They also evaluate influence of trash on colour grading of raw cotton, they trained artificial neural network, which turns out to have a good classifying ability. The same approach can be seen in [12], where authors conducted a research project to develop a new image analysis system for comprehensive, accurate and fast cotton colour and trash analysis (CCTA). They explained new multi-dimension thresholding for trash identification, methods for trash particles size, shape, colour, density characterization.

Almost all described methods analyze foreign matter in raw material, separate particles mechanically, analyze their image or weigh them.

The main aim of the presented work is to determine “standard” cotton fibers’ cross-sections in recycled yarn on CT images (virtual cross-sections), to separate them mutually and from foreign matter, to compare results of two offered approaches and result from HVI – trash tester in raw material.

2. Introduction of the main idea of yarn foreign matter determination by CT image

The idea of the presented approach is to subjectively define representative fibers’ cross-sections directly on one CT image. On a basement of the values of the set parameters of these representatives rest of the particles in the yarn cross-sections will be analyze and categorize into four groups according to ITMF (International Textile Manufacturers Federation) definition [13]. According to ITMF trash is the general term used for larger impurities containing particles from the cotton plant itself and other plants (weeds) contaminating the cotton field. Dust describes smaller particles from the plant and simply dirt from the cotton field that sticks with the plant during harvesting. ITMF divides foreign mater into four categories according to it lateral size (Maximal Feret’s diameter): respirable dust = (0; 15> μm, micro dust = (15; 20> μm, dust = (20; 500> μm, trash > 500 μm.

3. Definition of the “typical” cotton fibers’ cross-sections in a yarn

Several representative cross-sections of cotton fibers are subjectively selected on randomly chosen yarn CT cross-section. Then geometrical parameters – area and elongation (elongation = maximal Feret’s diameter/minimal Feret’s diameter) are measured on them. The combination of these two parameters was chosen to exclude possible foreign matter with for example the same area like representative fibers, but with very different shape.

Figure 1 shows representative six fibers like ROIs, in Table 1 we can see values of their parameters. Contour of fibers were detected by local threshold in image analysis NIS Elements, then on filled objects mentioned parameters were measured, Table 1.

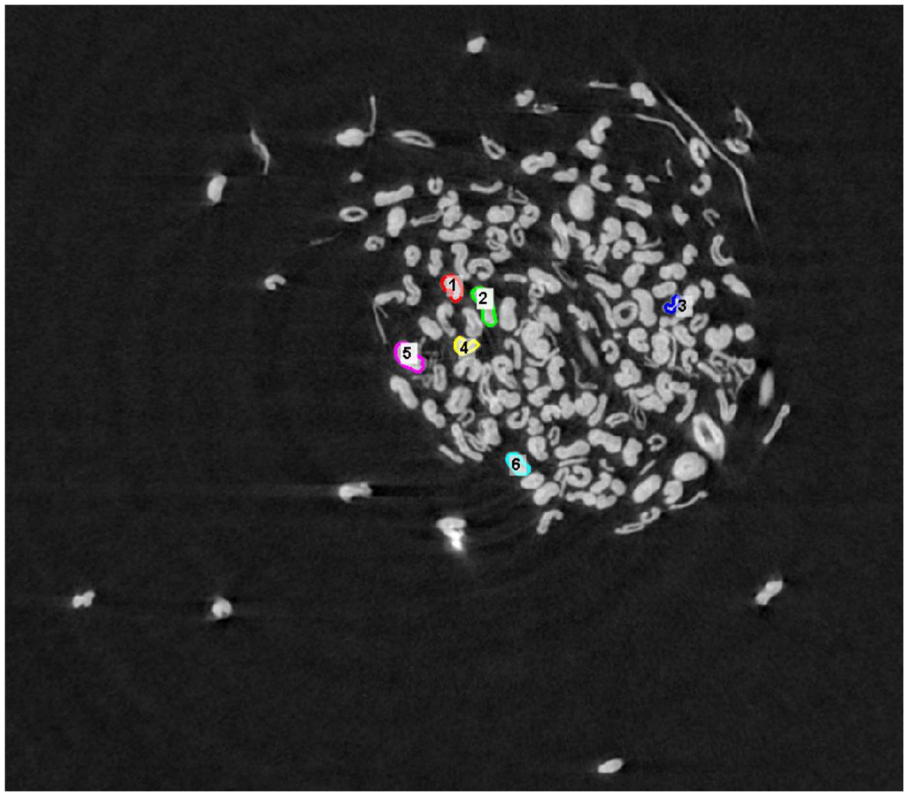

Figure 1. Representative cross-sections of cotton fibers on CT image

Table 1. Specific values of the chosen parameters of representative fibers

ROIs ID	Area [μm²]	Maximal Feret's diameter [μm]	Elongation [-]
1	98.75	14.65	1.56
2	140	21.77	2.35
3	39.75	10.1	1.74
4	65.5	12.76	1.43
5	131	18.7	1.8
6	84.25	14.01	1.77

It was set conditions for fibers definition based on fibers' parameters' values in Table 1: Area of the cross-section of the fibers will be in the interval of <30; 150> μm^2 and at the same time their elongation will be equal or less than 2.5.

4. Two various ways of objects' separation on binary image

Next step to the foreign matter definition and fibers' finding is an elaboration of the calibrated images of the yarn cross-sections with potential foreign matter in the system of image analysis NIS Elements [14]. Two macros were developed to analyze images of yarn cross-sections. They differ just in separation process of binary objects. The first approach uses morphological separation of the objects – Principle01 (Figure 2a), in the second one (Principle02) the fibers' contours are seared and these contours are consequently subtracted from the original binary image (Figure 2b).

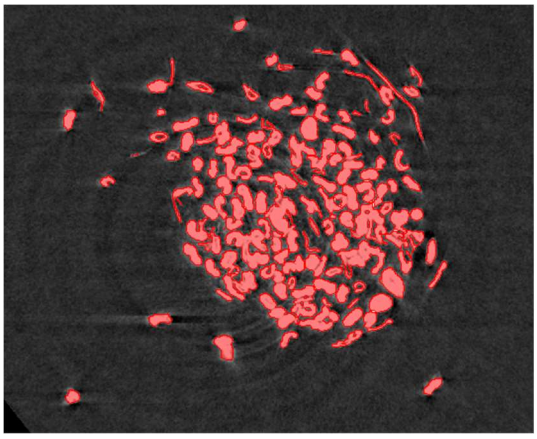

Figure 2a. Morphological separation of the objects – the first approach – Principle01

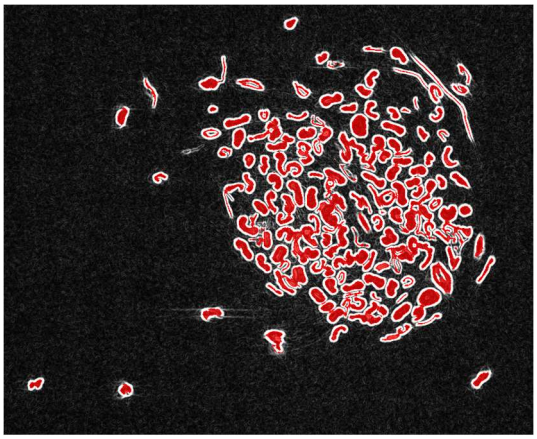

Figure 2b. Subtraction of objects' contours from original image – Principle02

Then the fibers were recognized on the basis of the specified conditions (see capture 3), the rest of objects is set like the foreign matter. The foreign matter was divided according to their maximal Ferets' diameter to four groups (see capture 2).

The Principle01 is explained in the following steps:

1. opening an image/sequence of images
2. image editing – selection of ROI (area of interest in the editor), contrast change if it is necessary,
3. image thresholding – background (background is more clearly defined),
4. inversion of the binary image – obtaining the yarn as an object,

5. morphological separation of objects – user intervention (control) must be considered,
6. selection of object parameters: Area, Elongation, MaxFeret,
7. duplication of the binary layer – creation of the "Fibers" layer (for future definition of the binary image of the fibers),
8. automatic selection of restrictions for selected object parameters,
9. fibers' data are exported to Excel
10. a binary image is created from the restrictions (binary of fibers only),
11. a subtraction is made: the original binary image of the whole yarn - the binary image of the fibers = the binary image of the foreign matter,
12. cancellation of restrictions for set for fibers - Area, Elongation,
13. creation of restrictions for foreign matter, i.e. objects with Maximal Feret's diameter greater than 500 micrometers (MaxFeret value) - defined as trash,
14. Export dirt data to Excel to existing thread data,
15. creation of restrictions for foreign matter with Maximal Feret's diameter smaller than 500 micrometers. For details see capture 2,
16. export foreign matter data to Excel to existing fiber data.

The Principle02 is explained in the following steps:

1. opening an image/sequence of images,
2. image editing - defining the area of interest ROIe using the ROIe editor,
3. a thresholding of the image – in comparison with Principle01 here the objects are thresholded – this binary layer is saved (binary layer is named "Source"),
4. deletion of the binary layer,
5. edge detection on the original monochrome image,
6. thresholding of object edges (binary layer is named "Edges"),
7. arithmetic operation of subtraction of binary images: Final = Source-Edges,

Next process is the same like by Principle01 from point 11.

5. Experiment and Results

Open-end 98 tex fine cotton waste yarn was tested by two described principles (Principle01, Principle02, see capture 4) to examine possible usage of CT images processing for foreign matter (dust and trash) content. Yarn length of 3 mm, with image resolution 0.5 μm/pixel, was analyzed. CT scan was carried out on Rigaku – nano 3DX. For image data minimization every tenth image was selected from whole scan, finally 595 images were processed like image sequence by Principle01 and Principle02 (capture 4).
Graphical interpretation of the comparison of two mentioned approaches can be seen on Figure 3.

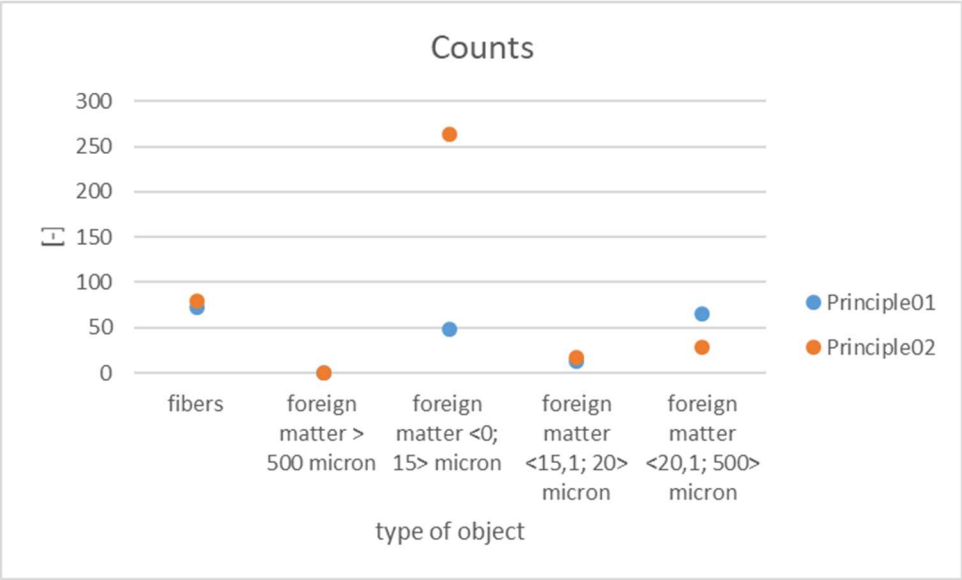

Figure 3. Average counts with interval of confidence (too small for visibility) of various foreign matter

Two data sets of various types of foreign matter count in 3 mm of yarn length were also tested for pairwise comparison and through the ANOVA (analysis of variance), the influence of used objects separation procedure in image analysis on results was analyzed.
On a basement of the pairwise comparison, it was found statistically significant differences (with probability of 100%) for the smallest objects – respirable dust. It is probably caused, because of Principle02 identifies also small objects and Principle01 omits them. Also in case of the dust (20; 500> μm was identified statistically significant differences between Principle01 and Principle02, but with very low probability 1.2 * 10 $^{-21}$ %. Finally ANOVA proved statistically significant effect of the tested factor (used principle of objects 'separation) on objects' data.
The raw material of our waste yarn was tested on Trash Tester (AFIS). These data are graphically compared with results of Principle01 and Principle02 realized on cross-sections' waste yarn CT images, Figure 4.

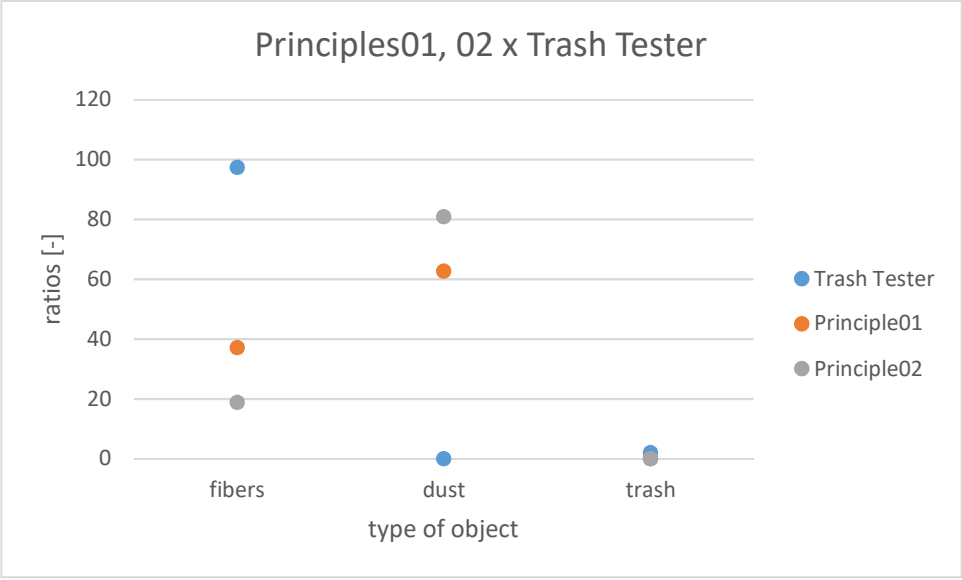

Figure 4. Comparison of ratios (with interval of confidence – not visible) of observed objects in waste yarn cross-section obtained by three approaches

Figure 4 shows statistically significant difference between image principles (Principle01, Principle02) and AFIS – Trash Tester. Reason of this result can be found in different definition of the objects belonging to dust in offered approaches (Principle01, Principle02) from Trash Tester definition. In our case also immature and dead fibers are defined like dust, Trash Tester can recognize them like „Good Fibers“.

6. CONCLUSIONS

Paper tried to find alternative approaches to the definition of fibers and foreign matter in CT images – virtual cross-sections, respectively. CT scan was used to more preciously specify objects on images than on textile branch standardly used soft cross-section [15] images, where objects can be clouded, connected, badly determinable. This approach is unusable in case of request on automatic image processing. Through the CT scan we get continuous information from the observed sample, on the other hand information from soft cross-section image is discontinuous, but can be from for example whole length of the yarn. This method is very time consuming in point of view of laboratory preparation and image processing with inevitable user intervention.
At first two ways of objects‘ separation were presented (Figure 2a, 2b), subsequent processing is almost analogical (capture 4.). The results‘ comparison showed on Figure 3 and analyzed pairwise comparison reflect the biggest differences in the smallest objects counts, so the type of objects’ separation has significant influence on primarily the smallest objects definition.
Secondly, Figure 4 graphically compares counts of the objects detected by Principle01 and Principle02 in 3mm length of the waste yarn with counts of the object detected in raw material by Trash Tester (AFIS). Let us conclude that the results are incomparable. Reason we can find in many possibilities, in different definition of the objects belonging to dust in offered approaches (Principle01, Principle02) from Trash Tester definition, in Principle01, Principle02 yarn cross-sections were analyzed, apparatus Trash Tester analyzes raw material, different methods of objects‘ identification were used in presented approaches.

ACKNOWLEDGEMENTS

This work was supported by the Czech Ministry of Industry and Trade under Grant No. FV40025 Processing of recycled and waste textile fibers.

References

1. *Haslinger, S., Wang, Y., Rissanen, M., Lossa, M.B., Tanttu, M., Ilen, E., Määttänen, M.,Harlin, A., Hummel, M., Sixta, H., 2019a. Recycling of vat and reactive dyed textile waste to new colored man-made cellulose fibers. Green Chem. 21, 5598–5610. https://doi.org/10.1039/c9gc02776a, September 21, 2022.*
2. *Haslinger, S., Hummel, M., Anghelescu-Hakala, A., Määttänen, M., Sixta, H., 2019b. Upcycling of cotton polyester blended textile waste to new man-made cellulose fibers. Waste Manage 97, 88–96. https://doi.org/10.1016/j.wasman.2019.07.040, September 21, 2022.*
3. *Taylor, R. A., Using High Speed Image Analysis to EstimateTrash in Cotton, ASME J. Eng. Ind. 107 (2), 206-219 (1985).*
4. *Taylor, R. A., Estimating the Quantity of Usable Fibers in Baled Cotton, Textile Res. J. 56 (11), 705-711 (1986).*
5. *Taylor, R. A., Grading Cotton Nonlint Content with Television Images, "Proc. Cotton Production Research Conference," 1987, pp. 543-548.*

6. *Matani, A. Shirley Trash Analyser. https://www.textilesphere.com/2019/11/shirley-trash-analyser.html, September 21, 2022.*
7. *Basu Arindam, A comparative study in measuring trash content by using HVI and Shirley trash analyzer, Indian Journal of Fibre and Textile Research, Vol. 24, December 1999, pp. 303-305*
8. *Estimating the Size of Cotton Trash with Video Images R. A. TAYLOR, TRJ, April, 1990, pp. 185 – 193*
9. *R. A. Taylor: Estimating the Nonlint Content of Yarn With Television Images, Journal of Engineering for Industry, AUGUST 1988, Vol. 110/259, pp. 259-262*
10. *Mikko Mäkeläa,b,⁎, Marja Rissanena, Herbert Sixtaa Machine vision estimates the polyester content in recyclable waste textile, Resources, Conservation & Recycling 161 (2020) 105007*
11. *Kang Tae Jin, Kim Soo Chang, Objective Evaluation of the Trash and Color of Raw Cotton by Image Processing and Neural Network, TRJ, 72 (9), 776-782 (2002)*
12. *Bugao Xu and Yu-liang Ting: COTTON TRASH MEASUREMENT USING IMAGE ANALYSIS, Reprinted from the Proceedings of the Beltwide Cotton Conference Volume 2:1701-1705 (1996) National Cotton Council, Memphis TN*
13. *USTER® AFIS PRO – What does the data mean? Common test results in Upland cotton, February 2004*
14. *https://www.nis-elements.cz/en/products, September 21, 2022*
15. *Colective of authors: Internal standard, IS 46-108-01/01 Recommended procedure for preparation of Samples. Soft and Hard cross-sections, Liberec, TUL, 2002*

GEOMETRICAL MODELLING OF INLAID WEFT KNITTED FABRIC

Irena Lenfeldová

A Technical University of Liberec, Department of Technologies and Structures, Studentská 2, 460 17, Liberec, Czech Republic, +420 48 535 3328, +420 48 535 3542,irena.lenfeldova@tul.cz

Abstract:

Loop geometry, structural and mechanical properties of yarn, relaxation process of knitted fabric (or finishing of textiles) affect the final fabric properties. In the time of developing technical application, the weft knitted structures with inlaid yarn could be benefit for expansion of possibilities novel structures. There is described the attempt to analyze and to determine the weft knitted structure with weft-inlaid yarn. The simple geometrical model for the two yarns of the loop structure unit, i.e. an option with the same ground knitted and non-knitted inlaid yarn, which were used for knitting, was carry out. An inlaid yarn assumes a relatively straight configuration between two legs of the loop, which had not any reserve of yarn to distort. Due to fabric construction and friction between the knitted and inlaid yarn the typical properties of knitted structures elasticity and flexibility are reduced. The input parameters for model are yarn diameter, wale and course spacing that can be measure after the knitting and relaxation process. Knitted single-faced fabrics from the different yarn material (but same for knitted and non- knitted yarns) were manufactured with two set of needles from V-bed flat knitting machine. The aim was to produce the more compact structure as is possible, compare the crosswise fabric shrinkage and compare the calculated value of length from loop unit model with experimentally measured.

Key words:

Weft-inlaid yarn, loop unit length, geometrical model, fabric shrinkage

1. Introduction

For special purposes and application of knitted products, it is important to predict their structural and mechanical behavior. Since the 1930s many researches made attempts to design the various geometrical or mechanical loop models – Pierce [1], Dalidovich [2], Leaf and Glaskin [3], Eltahan [4], Kyosev [5] and others to found the mathematical expression of loop length. Some models are for fully compact loop construction, others are elastics or non-elastics and more resent models are based on numerical loop calculation or also applied finite element method for simulation of loop deformations. However, mostly researches express relationships between the size of the loop (sometimes together with the yarn properties) and the loop length with the aim to formulate mathematical equations with different simplify and accuracy, i.e. replacing the loop arc with the circle, ellipse or helix [6].

Peirce's formulas for length of yarn in one loop for single-faced structure was given with expression

$$l = 2c + w + 5,94\, d \quad (1),$$

where *c* is course spacing, *w* the wale spacing and *d* the diameter of the yarn. That model was verified by Fletcher and Roberts [7] based on their experimental work for calculated yarn diameter (multiplier changes to 5,98) and yarn diameter obtained by microscopic measurement (multiplier changes to 4,56).

Assuming the simplifications and the loop geometry of the Dalidovich model for plain weft knitted structure the representation yarn configuration of single-faced structure with weft inlaid were design. In the unit cel is shown in the Figure 1. This element – knitted loops consists of two threads, ground loop length l_I and weft-inlaid length l_{II}.

$$l_I = \frac{\pi}{2} w + \pi\, d + 2\, c. \tag{2}$$

That work is based on Dalidovich [2] model and modified it for the plain structure with weft inlaid yarn (Figure 1). An inlaid yarn is never formed into a knitted loop and is incorporated into the structure [8]. Sometimes, in weft knitted process, that structure is called “hybrid”. That weft knitted fabric was manufactured with V-bed flat knitting machine. Fong, Li and Liu [9] developed the geometric model of lain-in weft-knitted fabrics, but the inlay yarns have different loop intersection points and spatial variations. It consists of tucks and float/miss stitches. The present model of inlay weft knitted unit consists of ground yarn (loop) and weft inlay yarn, which is held between the legs front adjacent loops. That mentioned plain knit structure (jersey) have to be manufactured with two needle beds and needles with clips. After knitting a row with ground yarn some needles transfer loop to the opposite bed and then the weft thread was laying. Receive needles transfer loop back from needle in the opposite needle bed. The knitting the next row with ground yarn is followed. The same yarns were used for both carrier of the V-bed flat knitting machine although usually weft inlay has higher count and rigidity and less flexibility.

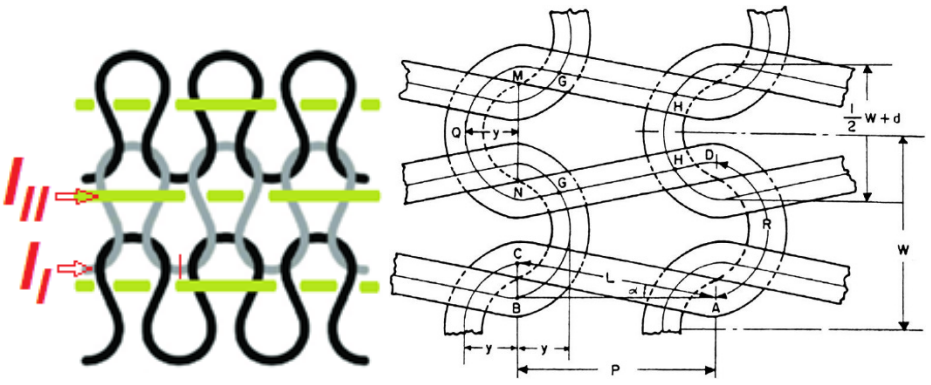

Figure 1. a) Schema of knitted fabric with weft inlaid yarn, b) model of single jersey structure [10]

These aspects have to be taken into account during development the weft inlaid single plain structure:

- Setting the density parameters due to the free (“open”) stitches and due to the space for the other weft thread, which is incorporated into the structure.
- Adjusting the guard cam due to the transferring the loops between the needle beds.
- Greater demands on yarn abrasion due to needle loop transfer.
- The multiple crossing points between weft-inlaid yarns and ground yarn (loop leg).
- Reduction of the wale shrinkage due to the weft inlaid yarn and increasing the friction areas.
- Reduction of the weft-knitted fabric elasticity regards to plain knitted fabric.

Design and characterization of the loop model can be carry out with that geometry (see Figure 1a) assuming the both yarn to have a circular cross-section and the fabric to be theoretically flat [6]. The real multifilament diameter (air texturing) is not constant in the straight shape, let alone after knitting or after relaxation process. During laying the weft-inlaid, the loop presser bed helps to hold that thread, performs the hold-down function and the pull-down roller control the tension. During manufacturing, the knitted structure is stretch, but horizontal shrinkage is not completely prevented in the area between the cast-off and the take-off rollers. Immediately after leaving the take-down system, the shrinkage of the knitted fabric started. The higher number of the binding points together with the compact loop structure affects the fabric's shrinkage. It can be assumed that based on the weft-inlaid yarns it can be better predicted the fabric dimensional properties relative to a single-faced knitted fabric.

The geometric modelling is also used to create a modified model by Dalidovich. It is based on the assumptions that the needle and platinum arcs are circular, equal in size and have centres on the same line. The arcs and leg are connected selectively, the needle and sinker arcs don't have contact. A gap between the arcs are assumed due to the weft-inlaid yarn as is shown in the Figure 2. According that model of weft-inlaid yarn and Euler equation the perimeter *p* of the ellipse is:

$$p = \pi \sqrt{2\,(a^2 + b^2)} \tag{3}.$$

where *a* is the large radius of ellipse, *b* is the small radius of ellipse. The length of the weft-inlaid yarn for one unit (two loop) consists from two halves of the circumferences of the different ellipses and is expressed

$$2 * l_{II} = (\pi/2 \sqrt{2\,(w^2 + b_1^2)} + \pi/2 \sqrt{2\,(w^2 + b_2^2)}\,, \tag{4}$$

were *a* is describes as specified via a major axis and minor axises are described after simplifications together with the wale and course spacing and with the yarn diameter dependences, i.e. *b1= 3/2 d, b2= 5/2 d.*

The final formula for that weft length (*w = 5 d* for loop model) is expressed:

$$l_{II} = 21{,}62(\pi\, d \sqrt{2}\,)/8 \tag{5}.$$

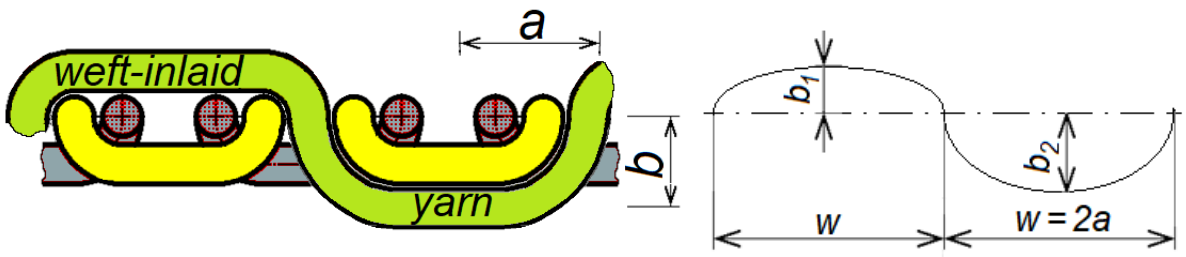

Figure 2. Projections of model knitted structure with weft-inlaid yarn

2. Experimental

The mentioned structure – the single-faces knitted fabric with weft-inlaid yarn (Figure 1a) have been designed with the KnitPaint CAD system of Shima Seiki and for weft-inlaid yarn, the thick type of the carrier was used.

2.1. Materials

Experiment started with material specification for ground and weft-inlaid yarn - polyester multifilament 167dtex x 2, f 36 and polypropylene multifilament 167dtex x 2, f 32. Other selected yarn followed (see Table 1) for comparison the knitability and for different yarn characteristics.

In the Table 1 and Figure 3 the experimental data of input material were shown (measured value of yarn count and values from tensile test of multifilament).The yarn diameter were calculated with the material densities and porosity values *μ= 0,55*.

Table 1. Experimental value of linear density of used materials for knitted samples

	multifilament		yarn	
	polyester	polypropylene	cotton	acrylic
Linear density [tex]	33,42	33,25	70,64	71,94
95 % CI [tex]	<33,19; 33,65>	<33,21; 33,28>	<70,37; 70,91>	<72,78; 72,09>

The tensile tests of textured multifilament were performed by the Instron apparatus (500 mm, 200 mm/min) according to the appropriate standard methods EN ISO 14704-1. The experimental dates of extensibility of both materials differs and the flexibility of polypropylene multifilament causes the loop shape and curvature of weft-inlaid yarn. The relaxed fabrics (see Figure 4) indicates the different fabric shrinkage too.

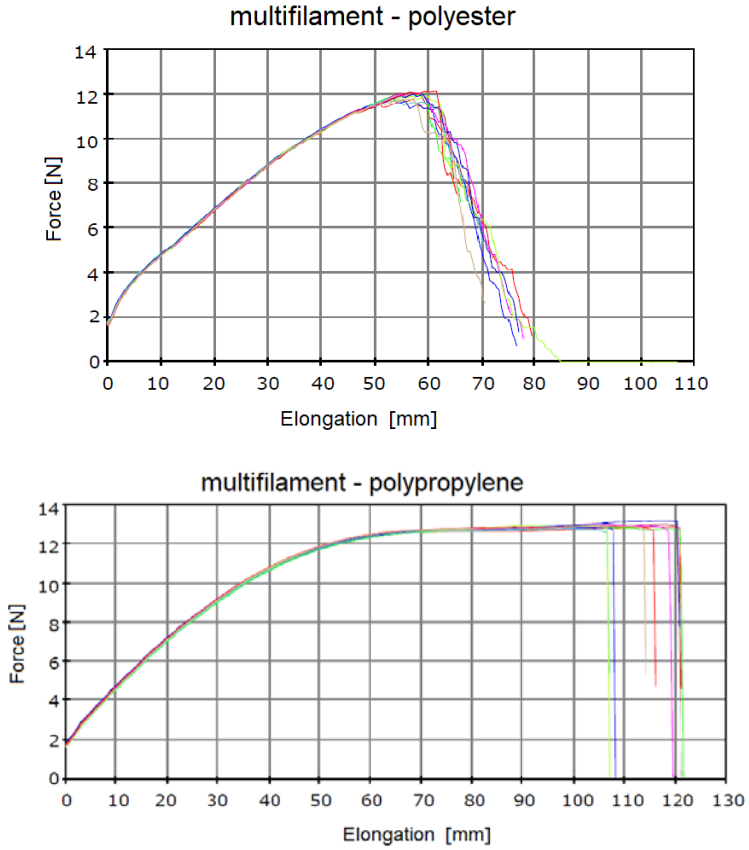

Figure 3. Tensile properties of multifilament (polyester - 167 dtex, f 36, polypropylene 167 dtex, f 32)

2.2. Methods

These structures have been manufactured by the Shima Seiki V-bed flat knitting machine - gauge14G. The use of a loop presser bed achieves a stable hold-down of loops when producing structure with inlaid yarn. Figure 4 shows the weft knitted structure with weft-inlaid yarn (technical face and back). The stitch cam controls the depth to which the needles descend, i.e. controls the amount of the ground thread drawn into the needle loop. For the experiment, the setting the stitch cam was the same for all the samples with the aim to achieve the more compact structure and manufacturing the samples without damage and the faults.

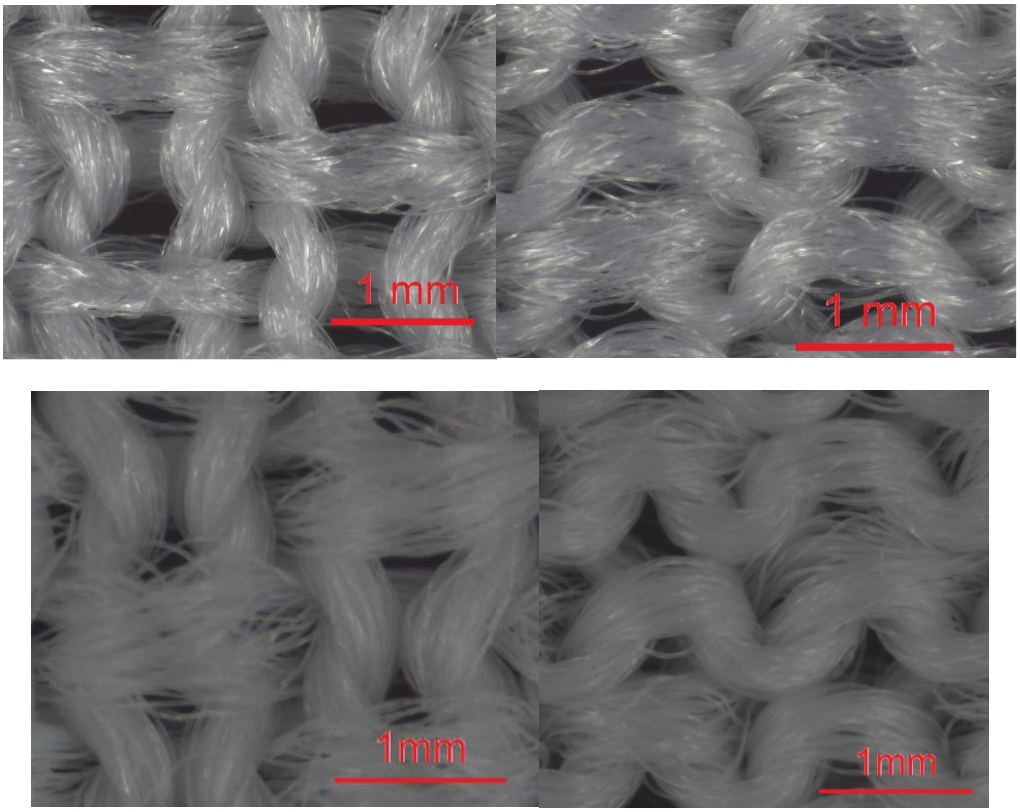

Figure 4. Technical front and back of produced weft knitted fabrics with weft-inlaid yarn (1 mm scale) – polyester (top), polypropylene (bottom)

Basic characteristics of real knitted fabric have been tested under standard conditions after dry fabric relaxation. Number of wales per 10 cm of both multifilament significantly differs (Figure 5) although the linear densities are the same and number of fibres are similar. Therefore, the friction between the weft-inlaid yarn and leg of the loop causes opposite crosswise shrinkage together with the increasing the number of crossing points, which are higher comparing the single jersey structure. In the Figure 5 we can compare the stitch densities of the single jersey structures from polyester and polypropylene. The fabric shrinkage in fabric width are different too.

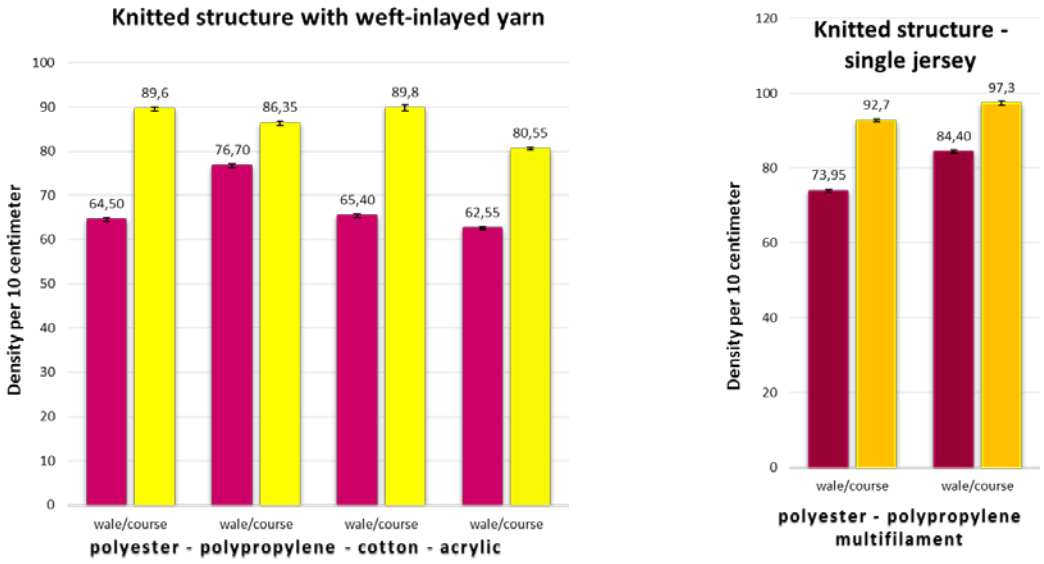

Figure 5. Wale/course density of weft knitted fabrics (with or without weft-inlaid yarn)

With the same stitch cam setting, yarn input tension and take-down tension the single jersey structures were produced, see the Figure 6. The loops are loose and the inclination of the loops from polyester multifilament after relaxation process appears.

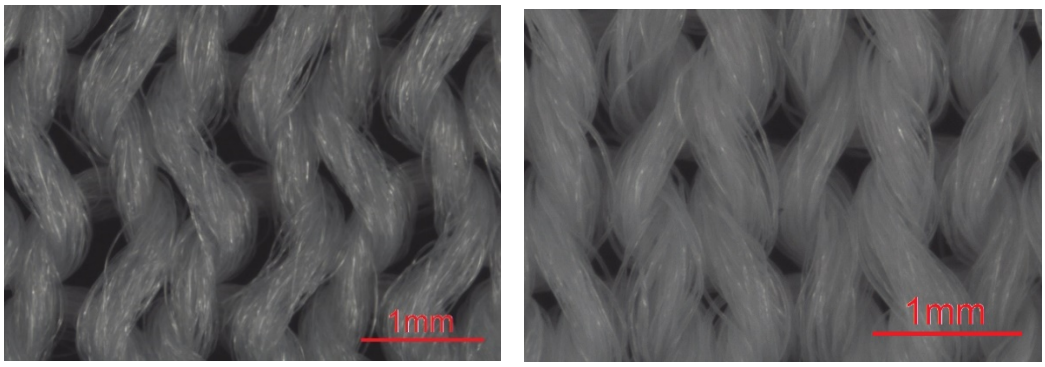

Figure 6. Technical front of produced plain knitted fabrics – single jersey

3. Results and discussion

Bending rigidity or other properties of textured yarn that could influenced the fabric shrinkage are not specified. That fabric behaviour could not expected or predicted. For better understanding the crosswise shrinkage between knitting setting and relaxation the wale spacing changes are plotted in the Figure 7.

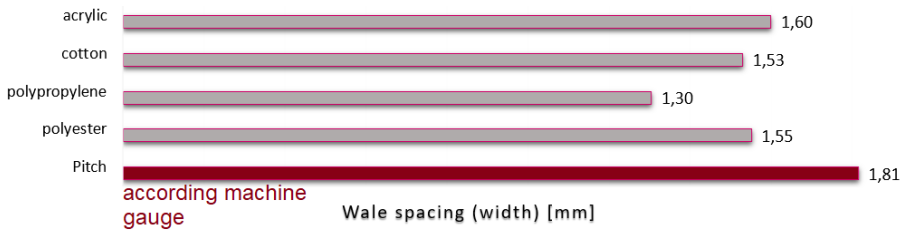

Figure 7. Wale spacing of loops during knitting and after relaxation

Munden's constant takes into considering the course and wale spacing. So if the ratio of single jersey fabric is greater than 1.3, then it indicates higher shrinkage and consequently higher stretch property in width direction. It seams, that the stretching of the polypropylene fabric in the longitudinal and crosswise direction will not be so anisotropic compared to other tested fabrics. The expected effect of the weft on the reduction of the shrinkage value in the crosswise direction in polypropylene fabric was not evident. It seams, that behavior of these fabric does not change.

Table 2. Experimental value of yarn parameters for knitted samples

	Munden's constant = course/wale spacing [1]			
	polyester	polypropylene	cotton	acrylic
Structure with weft-inlayed yarn	1,39	1,13	1,37	1,29
Plain knitted structure	1,25	1,15	X	X

The experimental and calculated values of loop length and weft-inlaid length for weft knitted fabrics are written in Table 3. The experimental data were find out from a weight of 10 threads, which were unrove (separated) from the 100 wales of knitted fabric according the standard ČSN EN 14970. Calculated values of these parameters are obtain from the input data yarn diameter, wale and course spacing that

is expressed for compact structures as a dependence of yarn parameters only. In case of cotton and acrylic yarn the developed model does not suitable.

Table 3. Calculated and experimental value of loop length and weft-inlaid length for knitted fabrics with inlaid yarn

multifilament /yarn	polyester		polypropylene		cotton		acrylic	
	loop	weft	loop	weft	loop	weft	loop	weft
measured values								
length [mm]	5,61	2,08	5,26	2,03	4,88	2,05	4,99	2,01
95 % CI [mm]	<5,59; 5,63>	<2,06; 2,1>	<5,22; 5,3>	<2,01; 2,05>	<4,87; 4,89>	<2,03; 2,07>	<4,97; 5,01>	<2,00; 2,02>
CV [%]	0,53	1,44	1,14	1,48	0,29	1,38	0,56	0,69
calculated values								
length mm]	5,20	2,12	5,97	2,59	6,46	2,92	7,24	3,40

4. CONCLUSIONS

An approach was made to theoretically develop on the base of existing loop model a new geometric model for the unit length determination of single-faced structure with inlaid weft yarn. The simplified equations for unit of adjacent needle and case study when loop and sinker arc are not in contact due to the interlacing the weft yarn.

It was shown that the calculated values of length in unit of samples which were manufactured are very near to the experimental value; so the developed equations are acceptable.

The first experiments show that the differences of the experimentally determined values of unit yarn lengths in the unit and these values theoretically calculated are close to each other. The differences between the fabric shrinkage from polyester and polypropylene with the same linear densities (167 dtex x 2) in crosswise direction was not expected, therefore the aim was to manufacture the compact structure without loose loops (Due to the transfer loops from and to the back needle bed the loop size could not be smaller). It has been confirmed that a weft-inlay threads in knit fabrics modify construction, fabric shrinkage after knitting depends on the mechanical properties of the input material even if we produce the compact structure.

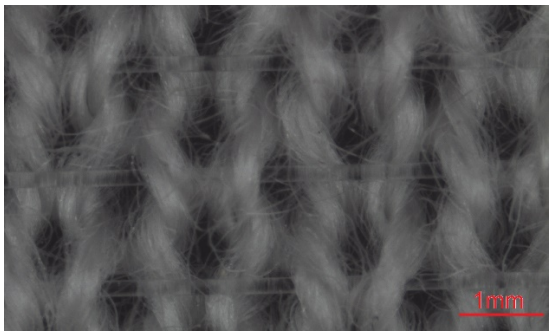

Figure 8. Knitted single jersey fabric with weft-inlaid yarn (ground yarn - acrylic and weft – monofilament)

Whether the developed model - this simplification of the knitted fabric structure - will be suitable as a basis for calculations of porosity, air permeability, abrasion, tension properties or other structure-related properties it remains to be seen. Further follow-up work will be the manufacture sample from monofilament and verification of the proposed model. So far it has been possible to use monofilament only for weft insertion (see Figure 8). Application the monofilament for loops made problems in stitch cam setting, yarn input tension and take-down tension too.

References

1. *Peirce, F.T. (1947) Geometrical Principles Applicable to the Design of Functional Fabrics, Textile Research Journal, Vol.* 17, 123 - 147.
2. *Dalidovich, A.S. (1948) Osnovy teorii vjazanija. Gizleprom, Moskva (in Russian).*
3. *Leaf, G.A.V.; Glaskin.(1955) A. Geometry of a plain-knitted loop. J. Text. Inst. 46, 587–605.*
4. *Eltahan, E., Sultan, M., Mito, A.(2016) Determination of loop length, tightness factor and porosity of single jersey knitted fabric, Alexandria Engineering Journal Vol. 55.*
5. *KYOSEV, Y. (2019) Topology-based modeling of textile structures and their joint assemblies: principles, algorithms and limitations. Cham, Switzerland: Springer, ISBN 978-3-030-02540-3*
6. *Koci, V. (1980), Vlastnosti osnovních jednolícních pletenin, in Vazby pletenin, SNTL, Praha, (In Czech)* ISBN: 04-825-8, 74 -86.
7. *Fletcher, H.M., Roberts, S. H.(1952) The geometry of knit fabrics made of staple rayon and nylon and its relationship to shrinkage in laundering, Textile Research Journal, 446-471*
8. *Spencer, D. (2001). Knitting technology a comprehensive handbook and practical guide. Third edition 2001. Woodhead Publishing Limited and Technomic Publishing Company Inc. (Cambridge). ISBN 1855733331.*
9. *Fong, K.W., Li, S.Q and Liu, R. (2021) A New Geometric Model of Lain-id Weft-Knitted Fabrics, Textile Research Journal, Vol 91(17-18) , 2087-2105.*
10. *Benltoufa, S., Fayala, F., Cheikhrouhou, M., Nasrallah, S.B. (2007); Porosity determination of jersey structure; AUTEX Research Journal, 7 (1).*
11. *Liu, R.L., Lao, TT., Wang, S.X. (2013) Impact of Weft Laid-in Structural Knitting Design on Fabric Tension Behavior and Interfacial Pressure Performance of Circular Knits, Journal of Engineered Fibers and Fabrics, Vol 8, Issue 4, 96 – 107.*

ON THE DEVELOPMENT OF A ONE-LAYER MULTISCALE UNIT CELL MODEL OF 3D WOVEN FABRIC TEXTILE

Johnson Ugochukwu Ezenwankwo, Josef Zak and Iva Petrikova

Studentská 1402/2, 461 17 Liberec 1, Applied Mechanics, Technical University of Liberec, Liberec, Czech Republic, johnson.ezenwankwo@tul.cz

Abstract:

In this work, a representative volume element (RVE) of a 3D woven fabric is generated at mesoscale level with the aid of TexGen, commercial textile fabric generating software. Specifications such as yarn spacing, thickness and width are input directly into the software to generate a simple weave in this case. The output file is exported as a Step file and loaded in Ansys for analysis. Contact information between neighbouring and touching yarns are automatically embedded in the model, and modified to suit the simulation. To accommodate for geometrical nonlinearities, large defection is turned on from the analysis settings. Symmetry is created in two different planes to form 3 different models cases. Plots of prescribed displacement in x andequivalent stresses and equivalent strains are developed for the 3 cases together. The strain energy is plotted against the prescribed displacement and also against step-time to show its maximum value of 0.6mJ. A simplified compression simulation was done on a dual-symmetry model of fibre-alone RVE in Marc-Mentat, and displacement –time, equivalent stress-strain plots were given.

Key words:

Representative Volume Element (RVE), Fabric, Contact, Meso-scale, Symmetry, Analysis.

1. Introduction

Fabric reinforced polymer composites have found remarkable application in materials science and technology. Engineering fieldssuch as aviation, automobile and aerospace industries that rely greatly on material, have found fibre-reinforcedcomposites as a beacon of hope.Thus, natural fibres have presented a silver liningin the challenges associated with synthetic fibres. Understanding the FE results of this material by using the RVEs gives a reasonably reliable and accurate result to predict the real behaviour of the material at a macro (fabric) level. Dixit *et al*[1]performedparametric sweeps to compare the effect of geometric parameter of the unit cell. Lin et al. [2] used described in detail the building of 3D woven fabric models using TexGen. This study seeks to expound on the idea of 3D model generation and design using geometric specification of yarn. The work further describes the export of modelstoa software for analysis and compares the effect of type of plane of symmetry as it affects the structural behavoiur of the model. A comparison is also made of these two symmetry models created with the original full model. Plots of key parameters were obtained and discussed.

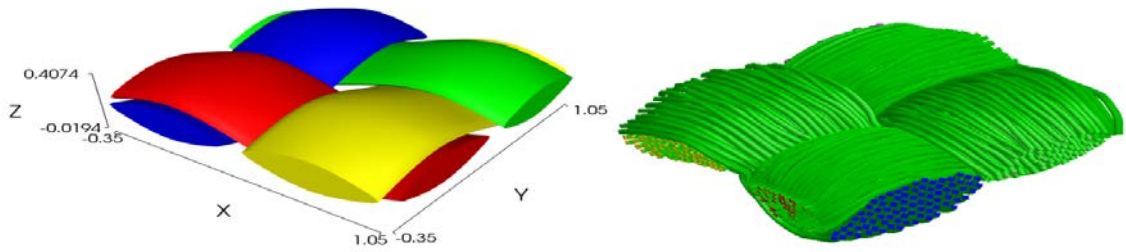

Figure 1. Simple weave unit cell model *(a)*TexGen (mesoscale) *(b)* DFCA (81-fibre microscale)

2. Modelling the Geometry

Wang et al [3] used asoftware, DFCA, to generate fabric models at micro (fibre) level. The software utilizes the direct element approach (DEA) which relies on the idea of considering a fabric as a collection or family of unit cells which is an assembly of yarns formed from a bundle or an organized systemic pack of rod-like elements called digital filaments which are basically at the fibre level.Creating a model for the geometry involves specifying the geometric properties of the model in TexGen which automatically generates the model using its inbuilt algorithm to also assign a 10% clearance on all sides in forming the bounding matrix box. This matrix box can be switched off when exporting the materials so that only the material exported for analysis in a chosen FEA tool. One of the high points of TexGen and DFMA is that one is able to easily adjust the geometric properties of the model. As shown in Fig 1, a 2x2 simple weave model is generated. The material properties and geometric specifications are shown in Table 1 below. The model is further exported in various formats including Abaqus voxel mesh, surface mesh, Abaqus dry fibre or most conveniently, as a Step or IGES file. Abaqus allows for the running python script and inputting * (star) equations and commands making it user-friendly. Fibre-fibre contact interactions between yarns are automatically detected. This depends on the FEM software chosen and the type of export file selected. The type of contact is changed while building the simulation.

A no penetration condition is specified so that the nodes and surfaces are not able to traverse one another. A number of contact types exist including bonded [*glued* in Marc-Mentat], no separation, frictionless and frictional (a friction coefficient value, μ, is specified), this particular taxonomy is found in Ansys, the last three together are referred to as *touching* contact in Marc-Mentat. The frictional behaviour could be set as *Lagrange*, *augmented Lagrange* or *penalty* mode. The contact formulation was set to augment Lagrangian instead of the penalty method. In numerical modelling, it is possible to use both formulations to garner the advantagesin order to reduce the effect of poor representation of the governing equations and to better satisfy the contact constraints with the real penalty parameters. The choice is usually stability, and the idea of not over- or under- constraining the system. More details about constraint type numerical modelling is found in the work of Hirmand *et al.* [4].

Table 1. Specification ofYarn for Plain Weave Fabric

Material Density (Kg/m3)	Fibre Modulus (GPa)	Poisson Ratio	Fabric Thickness	Yarn Width	Yarn Spacing	Yarn Cross-Sectional Area (mm2)
			(mm)			
1520	7.5	0.2	0.388	0.6	0.7	0.084927

Yarn governing equations are given below as:

This is given as $$[K]=\frac{N}{\%\cdot mm} \tag{1}$$

In the same vein, the yarn thickness is given, from the Hookean relation, as

$$[k_1]=\frac{N}{mm},\ k=\frac{cN}{\%\cdot tex} \quad \text{in Uster method} \tag{2}$$

The relationship between k and k_1 in (2) is given in (3)

$$k=k_1\left[\frac{N}{mm}\right]\cdot\frac{L[mm]}{\lambda[tex]}=k_1\cdot\frac{L}{\lambda} \tag{3}$$

The relationship between (1) and (3) is given as $$K=\frac{k\cdot\lambda\cdot d}{10000} \tag{4}$$

Fabric strength is given as $[r_m] = \frac{N}{mm}$. The fabric strength, $f_{\max}$, is given by the relation

$$f_{\max} = 10000 \cdot \frac{r_m}{d} \cdot \tag{5}$$

2.1. Compression of a UC in Marc

This section delves into the compression of a unit cell fabric using Marc-Mentat. The 2020 version of Marc-Mentat FEM tool was used to for the compression analysis. Material properties from the tension test in Ansys were maintained for uniformity and model from TexGen was also used, and the symmetry was performed in Ansys Design Modeller before being exported as a Step file to Marc. Two symmetry operations (boundary conditions) were imposed on the model in the xz and yz planes such that there is no deformation in those planes and also this reduces the full model to a quarter of its original size, this ensures optimization of RAM from reduced solution time without compromising accuracy.

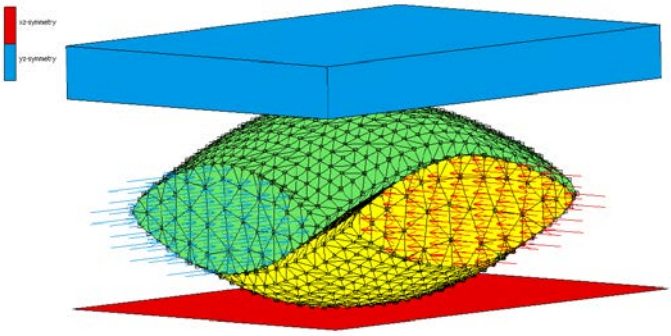

Figure 1. *(c)* Dual-symmetry fibre model in compression

A geometric element is used to model the ground (lower part of the setup) and the compression plate is modelled as a meshed rigid body as well as a 3D geometric element in comparison. It is worthy of note that the user coordinate system for both analysis was set to be the same so that all planes have conforming orientation for the two FEM tools used. Contact information from Ansys was used also in Marc. Self-contact was imposed between the two pieces of macro-fabrics in question with the limit breaking stress specified from experimental data as 244 MPa. When used as a geometric body, even for solids, no meshing or material property is required. On using the second method for the compression plate, the solid is modelled as a meshed rigid body (steel) with material properties of 215GPa and Poisson ratio of 0.28. In all cases, the fibre yarn and ground plate are modelled as meshed deformable bodies and geometric body respectively. The symmetry boundary condition as explained in section 2 above ensures the body experiences no deformation in the direction of planes of symmetry (xz and yz). The model was set to compress upto two-third of the original fabric thickness (0.2592mm) in the downward z direction.

3. Symmetry Effects

Inmechanics of solid,the rule of thumb holds that the displacement vector component orthogonal to the plane of reference is zero. The rotational vector components parallel to the plane is also zero. But in solid modelsthe rotational vector is not active; only the translational vector is considered.

Periodic boundary condition (PBC) can be stated mathematically as,

$$r_i^a - r_i^b = 0, u_i^a = u_i^b + \bar{\varepsilon}_{ij}(x_j^a - x_j^b) \tag{6}$$

where *a*, *b* represent the corresponding surface pairs that describe the RVE, x_j is the distance between the opposite sides, u_i represents the displacement, and ε is the strain homogenous strain across the surface of the RVE [5]. A critical part of the boundary condition is that the nodes along the symmetry

plane for each of the case remained along the plane of symmetry both prior and after loading. For each of the cases of simulation, a full node-node constraint is applied to the symmetry plane so that there is no displacement in the direction perpendicular to the symmetry plane[6]. In applying PBC, it is ensured that there exists equality in values of parameters on opposing edges that are kinematically linked so as to conform to the canonical equation in (6) [7][8][9]. This is typified in the idea that the meshing on each side of the geometry should be indentical and conformal.

4. Results and Discussion

A 4-body single-entity step file is imported into Ansys for simulation. Three independent simulations were performed using the material properties specified in Table 1. The first simulation captures the full completely constrained on the face at the yz-plane. A side control boundary condition is applied on the pair of faces on both sides of the xz-plane to ensure no movement in the y- and the z- directions. A specified displacement of 0.5mm (case 1 and case 3, and 0.25mm for case 2) is applied to the other end of the yz-plane. The displacement is automatically ramped to target by default; beginning from 0 and increasing linearly to 0.5mm.

As shown in Fig 2c below, thereare 4 contact zones with 318 faces apiece in target-contact interaction.Next, the simulation ofmodel with symmetry along the xy-plane is shown in Fig 2a. A total of 90 faces eachwere identified for the contact and the target surfaces for 6 contact zones and 92 contacts, 94 target faces for the remaining contact zones. And finally, the third simulation with symmetry along the zx-plane has 300 target and contact faces each was recorded the 2 contact zones as seen in Fig 2b. As the other simulations, the contact definition behaviour was set to symmetric, so that each side (contact and target) in each contact zone is adjudged to be identical.Contact detection criteria is set to face-to-face and the penetration parameter is program-controlled so that the symmetric contact faces are identified on the surfaces during movement and no penetration occurs; although there may be slips and contact separation which is dependent on material properties, applied force or prescribed displacement.Fig 3 below shows the contour plots of the 3 simulation cases carried out.

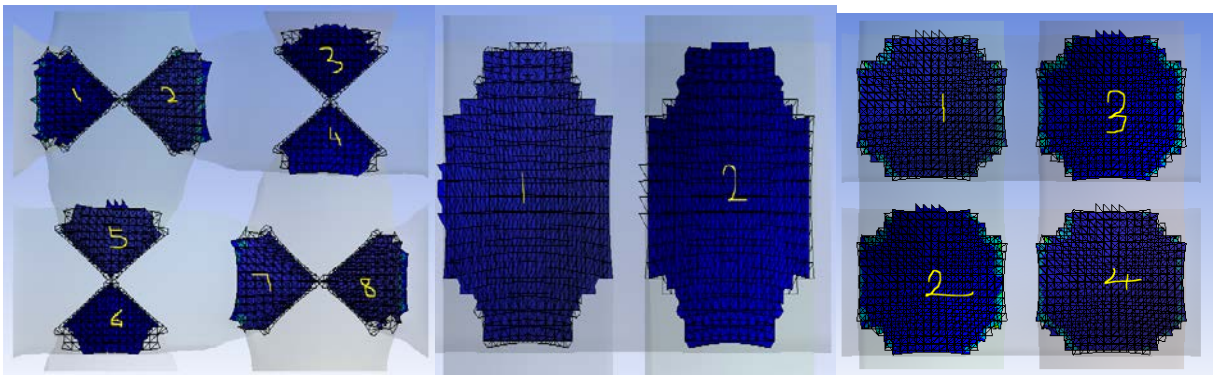

Figure 2. *(a)* 8 contact zones in the xy symmetry plane model *(b)* 2 contact zones in the xz symmetry plane model
(c) 4 contact zones in the complete model

It is clearly seen that as the prescribed displacement is ramped up the material is stretched linearly but the contact regions remain intact and instead deform plasctically. The global coordinate system is captured in Fig 3c.The prescribed displacement applied on the x-face will cause the highest displacement around that region and reaction forces will be appreciable around the bonded contact region.The stresses developed are mainly due to tension in yarn, contact interaction between the touching yarns, shearing forces and yarn bending moment whereas strain energy, as shown in Fig. 5a,b, arises due to bending, shearing forces and tension of yarns.Fig 4a,b shows the relation between directional displacement in x and Equivalent Stress and Equivalent Strain respectively. The geometry of the xy-symmetry plane showed a closer behaviour to the full model than the xz-symmetry plane. Mesh

refinement also played a vital role in both solution time and simulation result. The maximum strain energy as shown in Fig 5a,b is seen to be 0.6mJ. Finally, Fig 6a,b describes the relationship between the prescribed displacement in the x-direction and equivalent stress, maximum shear stress and maximum principal stress and strain. The highest value recorded in principal stress (35000 MPa) and 7.5mm/mm for equivalent strain.

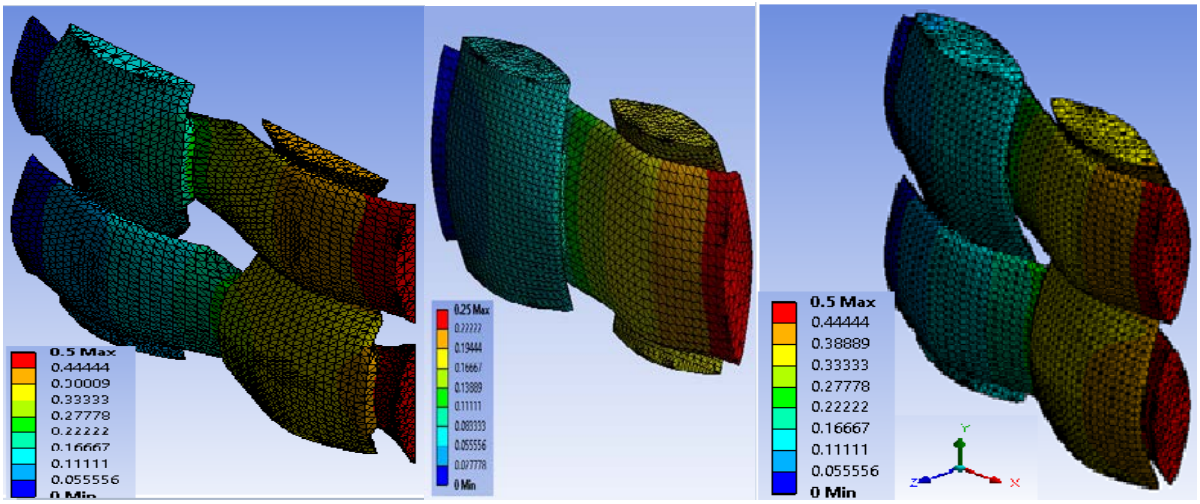

Figure 3. (a) xy-symmetry plane model (b) xz-symmetry plane model (half-loading) (c)full model

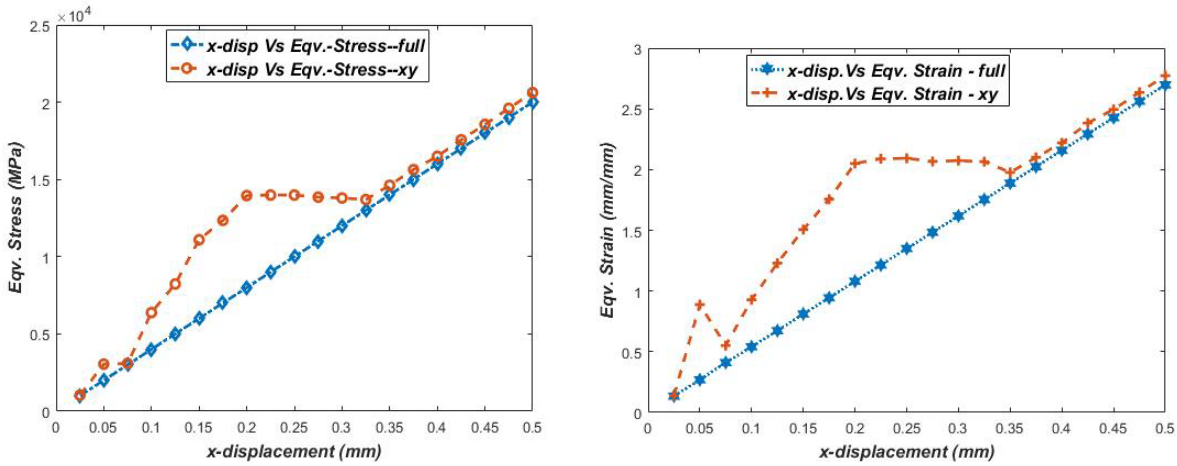

Figure 4. *(a)* displacement in x Vs Eqv.Stress *(b)* displacement in x Vs Eqv. Strain for (-full and –xy)

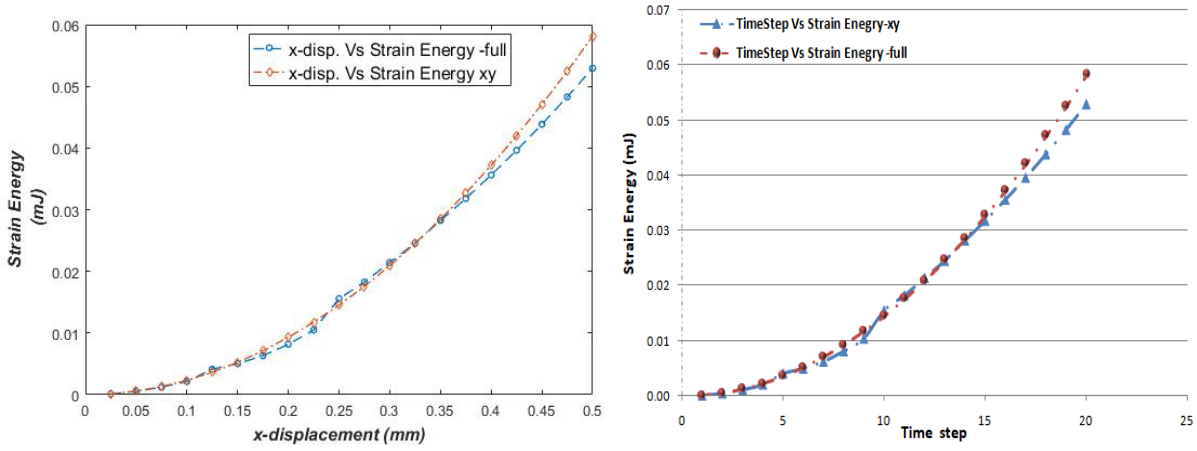

Figure 5. *(a)* displacement in x Vs Strain Energy *(b)* displacement in x TimeStep, (-xy and –full)

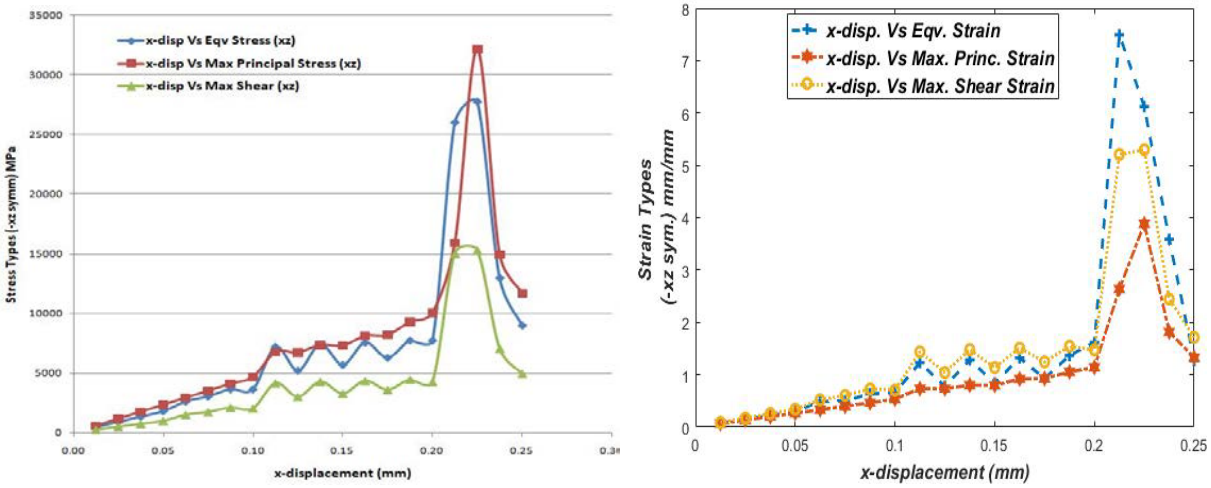

Figure 6. *(a)* displacement in x Vs Stress *(b)* Strain Types (-xzsymm)

4.1. Compression Simulation

Two approximately geographically centralized nodes (847 and 3038) were selected from the faces of the symmetry planes. Deformation in the z-direction was investigated. Two other nodes were also selected from each of the remaining faces (yz_back and xz_back) and the deformation in y- and x-directions were plotted (for nodes 1000 and 3246). Other plots of stress-strain were also obtained. The fibre model is

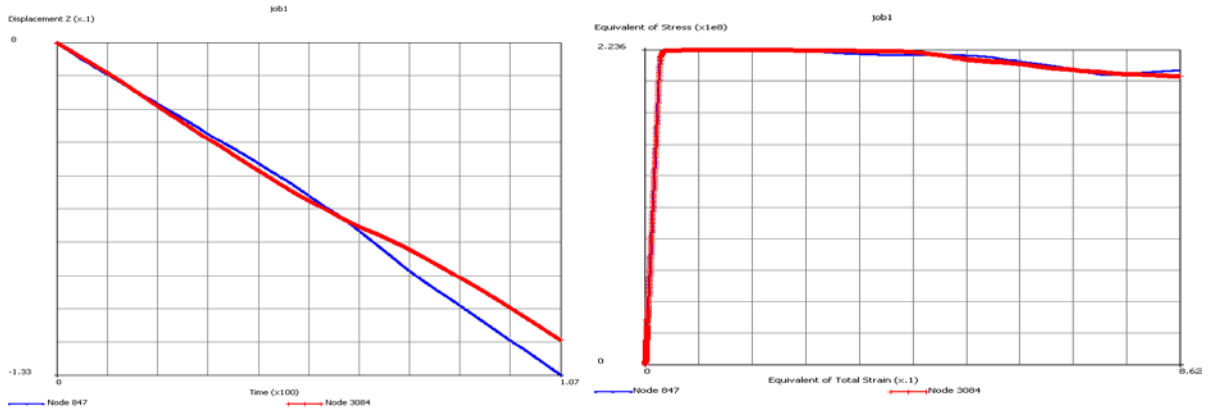

Figure 7. *(a)* Time displacement plot *(b)* Equiv. stress-strain plots (nodes 847 and 3084 – symm. side)

Figure 7a shows the plot of displacement and time in the z-direction, the contact was set to a breaking limit after which the nodes are permitted to begin to shear away and separate from each other. The stress-strain curves are also shown for one node each from the two symmetry plane faces and the free faces. Displacement in the symmetry faces is only tangible in the downward z-direction. The other two faces experienced substantial displacement in all three directions with z direction being the least for both. Figures 8(a,b) and 9(a,b) captures the displacement-time plot for the unconstrained faces which is about 29% more than the displacement in the z direction of the constrained face.

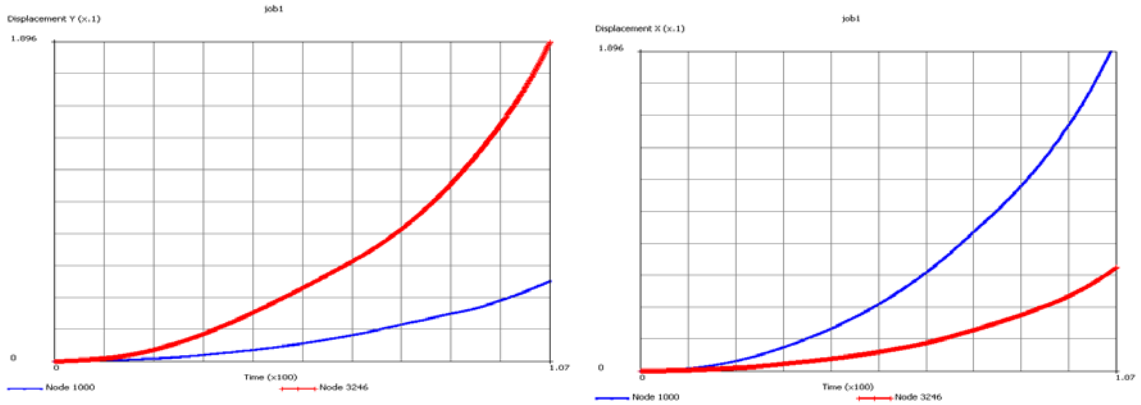

Figure 8. Time-displacement plot (yz_back and xz_back for 2 central nodes) *(a)* x-direction *(b)* y-direction

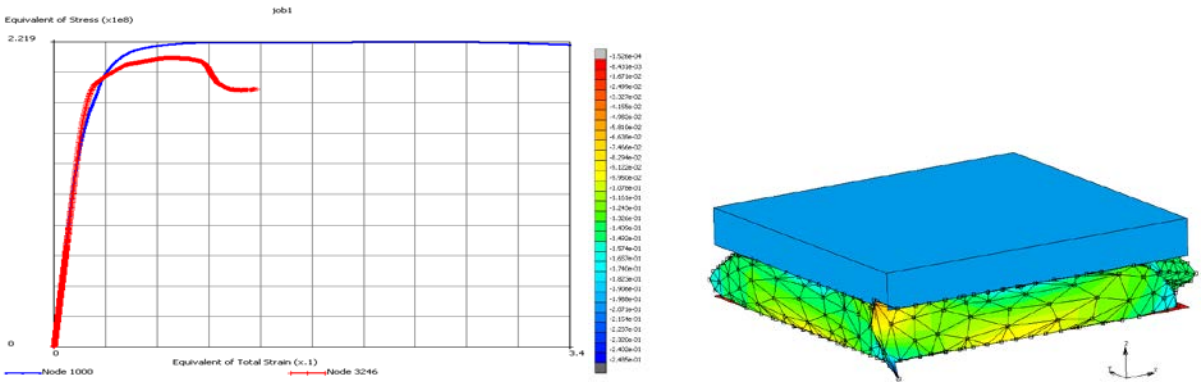

Figure 9. *(a)* Equiv. stress-strain plots (nodes 3246 and 1000 – back sides) *(b)* Fabric Compression in 1000 time step

5. CONCLUSIONS

The results have shown the dynamics and usefulness of modern approaches to developing as-built 3D models that very well captures and exhibits the real behaviour an RVE of a fibre network. By using symmetryand periodic boundary condition, one is able to reduce the processing time required in the calculation as the result from thesmaller model is comfortable and accurately generalized for the whole model. The symmetric model is able capture the key properties that describe the whole model as if it were in full. Also the ability to increase solution steps aids in capturing multiple data points which tend to better characterize the response of the material in simulation. Mechanical properties were found to be greatly influenced by such properties as geometric parameters including yarn spacing, fabric thickness, yarn width, cross-section of yarn, yarn aspect ratio (view/shape factor), loading conditions and mesh refinement. However, the yarns are modelled as solid continuum and the challenges of changes in cross-sectional area and inside deformations are not able to be absolutely correctly predicted during deformation. Further work could be carried out to observe the effect of tied nodes using servolink in Marc-Mentat, and also the effect of weave architecture on fibre mechanical behaviour.

ACKNOWLEDGEMENTS

This publication was written at the Technical University of Liberec as part of the project "Research of advanced materials, and application of machine learning in the area of control and modeling of mechanical systems" nr. SGS-2022-5072 with the support of the Specific University Research Grant, as provided by the Ministry of Education, Youth and Sports of the Czech Republic in the year 2022.

References

1. *Dixit, A., Mali, H. S. &Misra, R. K., (2013)Unit Cell Model of Woven Fabric Textile Composite for Multiscale Analysis.The Mal. Int. Tribloogy Conf. (MITC2013). Proc. Eng. 68 353 - 358.*
2. *Lin, H., Brown, P. L. & Long, C. A. (2011)Modelling and Simulating Textile Structures Using TexGen.Advanced Materials Research, Trans Tech. Publi.Vol. 331, pp 44-47. DOI:10.4028/www.scientific.net/AMR. 331.44.*
3. *Wang, Y., Mazumder, A., Liu, B. &Yen C.F. (2020)Applications of Digital Element Approach in Textile Mechanics and Textile Composite Mechanics. American Soc. for Comp. 35th Tech. Conf., DOI: 10.12783/asc35/34924.*
4. *Hirmand, M., Vahab, M. &Khoei, A.R. (2015)An Augmented Langrangian Contact Formulation for Frictional Discontinuities with the Extended Finite Element Method.Finite Element Analysis and Design, 107, 28—43.*
5. *Xia, W., Galadima, Y. K., Oterkus, E. &Oterkus, S. (2021)Representative Volume Element Homogenization of a Composite Material by Using Bond-based Peridynamics.*
6. *Drach, A., Drach, B., Tsukrov, I., Bayraktar., H. and Goering, J. (2013). Realistic FEA Modelling of 3D Woven Composites on Mesoscale. The 19th Inter. Conf.on Comp. Materials, Montreal, Canada.*
7. *Akoyomare A. I., Okereke M. I. & M.S. Bingley (2016) Enforcing Periodic Boundary Conditions on General Finite Element Discretisation of Heterogeneous Materials. https://www.researchgate.net/publication/309150287. DOI:10.2495/HPSM160121.*
8. *Okereke M. I. &Akoyomare A.I. (2013) Virtual Framework for Prediction of Full-Field Elastic Response of Unidirectional Composites. Computational Material Science, 70(null), pp. 82-99.*
9. *Nguyen V. D., Bechet E., Geuzaine C.&Noels L. (2012) Imposing Periodic Boundary Condition on Arbitrary Meshes by Polynomial Interpolation. Computational Material Science, 55, pp. 390-406.*

IDENTIFYING THE MATERIALS IN ARCHAEOLOGICAL TEXTILES

Helena Březinová[1], Miroslava Pechociaková[2], Jana Grabmüllerová[2]

1 Institute of Archaeology of the Czech Academy of Sciences, Prague, Czech Republic,
brezinova@arup.cas.cz

2 Faculty of Textile Engineering, Technical University of Liberec, Czech Republic

Abstract:

Given their organic origin, textiles rank among the rarest archaeological finds. While the vast majority of these artefacts are preserved as small fragments or mineralised remnants, their detailed textile technology study provides interesting and important information about the use of textile techniques and the quality of processing. The most important information concerns the utilised textile materials, but for degraded textiles, these materials are among the most difficult information to obtain. Image analysis using electron microscopy (SEM) is a significant aide in this pursuit.

Key words:

archaeological textiles, raw material, SEM, image analyses

1. Introduction

Textiles from the prehistoric and medieval periods occur in archaeological contexts mainly as small fragments or mineralised remnants. Their professional evaluation by means of a textile-technological study provides a great deal of important information about the historical development of textile production, with the spectrum of textile raw materials ranking among the basic data produced by this research. The possibility of determining the raw material is directly related to the state of preservation of the textile fibres or the degree of degradation of the characteristic structure of individual types of fibres. In addition to optical microscopy, fibres are identified using various analytical methods connected with fibre sampling and an evaluation employing spectra of standards (e.g., infrared spectroscopy, Raman spectroscopy) [2]. Image analysis using electron microscopy (SEM) produces very good results. The advantage of this method is the possibility to analyse microscopic samples of textile fragments.

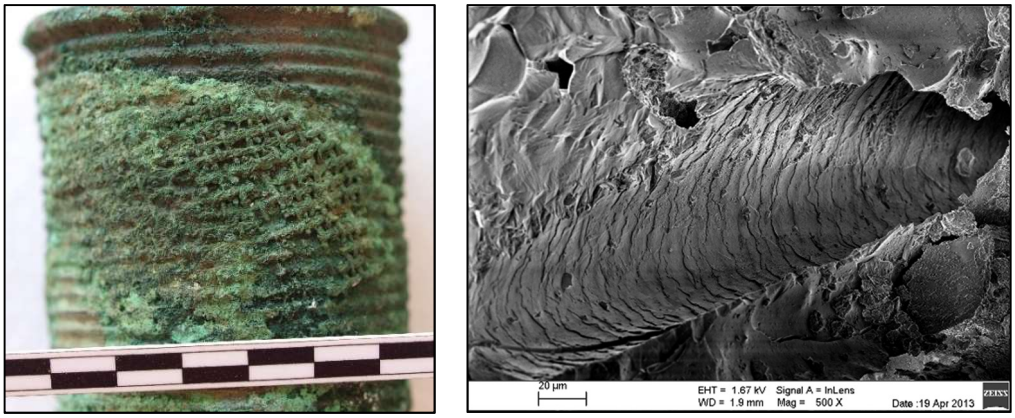

Figure 1. A mineralised fragment of wool fabric preserved on a bronze bracelet; Early Bronze Age Tursko-Těšina; ©Institute of Archaeology of the Czech Academy of Sciences, Prague. Imprint of wool fibre, clearly visible imprints of scales on the surface of the fibre.

2. SEM

SEM analysis was conducted using a TESCAN VEGA3 raster electron microscope. The SEM depicts the studied item by means of a thin electron probe formed and swept by the microscope tube. The majority of the imaging qualities of the microscope depend on the parameters of this electron probe: the size of the electron track, the aperture angle and the current in the probe. The current in the probe is determined by the number of electrons passing throw the probe at a given moment. The microscope tube is an electron optical device that forms and positions the electron probe. A system of magnetic lenses and apertures forms the resulting beam used to display the studied item.

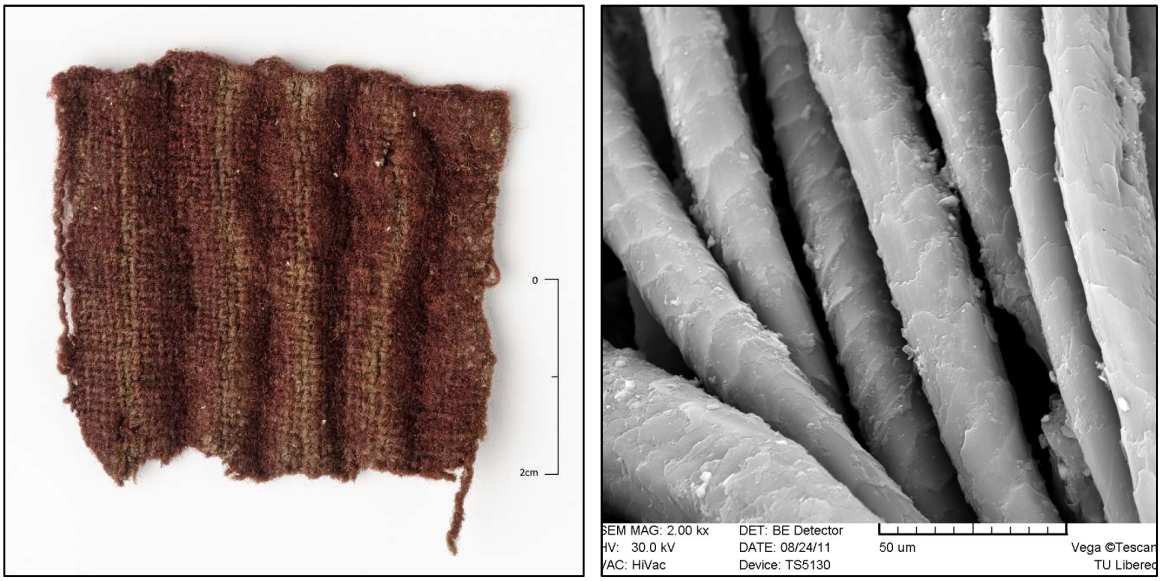

Figure 2. The fragment of wool fabric comes from the archaeological excavation of a medieval dump in the centre of Prague; ©Institute of Archaeology of the Czech Academy of Sciences, Prague. Fibres of "domestic wool" (containing fibres of varying fineness: guard hair, undercoat, intermediate hair).

3. Selected results

A joint project conducted in 2012–2022 by the Institute of Archaeology of the Czech Academy of Sciences, Prague, and the Faculty of Textile Engineering analysed several dozen textile samples from archaeological excavations. The most interesting and important results in the establishment of textile materials – a major contribution to knowledge of the historical development of textile production in this country – came from the following three finds:

- a fragment of wool fabric on a bronze bracelet from the Tursko-Těšina site, which is one of the oldest finds of wool textiles in Europe, dates to the early phase of the Early Bronze Age [4];

- a mineralised remnant of fabric from nettle fibres preserved on an iron artefact from the 9th century from Břeclav-Pohansko, which is the first evidence in the Czech environment of the use of nettle in textile production [3];

- a minute fragment of silk fabric on a small piece of sheet metal from the important Great Moravian site in Mikulčice, which is highly significant and clear confirmation of the presence of luxury silk fabrics imported into the environment of elite society from the Byzantine Empire [1].

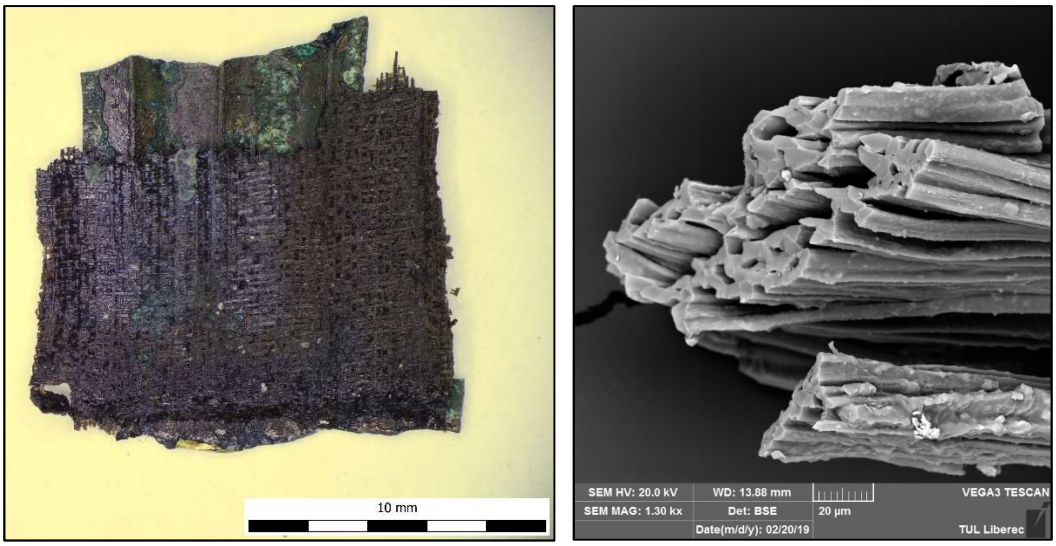

Figure 3. A fragment of silk fabric preserved on a small piece of sheet metal from the Great Moravian agglomeration in Mikulčice; ©Institute of Archaeology of the Czech Academy of Sciences, Brno; silk fibres, with the clearly visible typical shape of the fibre cross-section – a triangle with rounded vertices, also fineness of fibre is very typical.

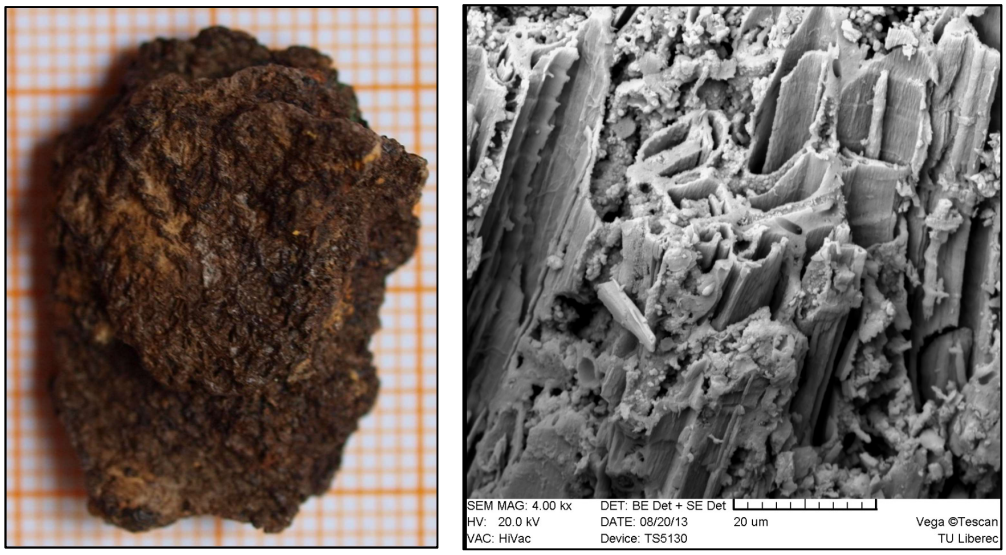

Figure 4. A mineralised fragment of fabric made from nettle fibres; Great Moravian hillfort of Břeclav-Pohansko; ©Department of Archaeology and Museology, Masaryk University Brno. Nettle fibre with the typical traits for bast fibres, which differ from others by the shape of the cross-section and size of the lumen.

4. CONCLUSIONS

The use of scanning electron microscopy is an example of important interdisciplinary and institutional collaboration playing a major role in expanding our knowledge of the history of textile production. Archaeological textile finds document the earliest phase in the development of this craft, which was always a key production activity. The study of textile production using the latest technical equipment is a common practice in archaeology throughout Europe today.

Knowledge of contemporary material engineering can be successfully used to identify fibre fragments. The fibres of natural origin show typical traits (cross-section shape, size and shape of interior “hollows”, the surface pattern, fibre fineness) and are the same for the given fibres. If it is not possible to use other methods for the identification of a find due to its limited amount, contamination by other material, etc., image analysis is the only means of determining the textile material.

Figure 5. A fragment of linen fabric preserved on the surface of a gombík (globular hollow pendant) from the early medieval cemetery in Vinoř.
©Department of Archaeology, Charles University; bundles of elementary flax fibres with the typical nodes and sharp edges of the regular 5–7-side cross-section.

ACKNOWLEDGEMENTS

This work was accomplished with support from the grant project of the Czech Science Foundation GA ČR 19-00166S “Textiles from Archaeological Contexts at Prague Castle – Relics of Czech Rulers, Their Family Members and Church Dignitaries.”

References

1. *Březinová, H. (2013). Finds of textile fragments and evidence of textile production at a major excavation site of the Great Moravia in Mikulčice (South Moravia, Czech Republic). In: Banck-Burges, J., Nübold, C (Eds.). NESAT XI. The North European Symposium for Archaeological Textiles. Verlag Marie Leidorf (Rahden/Westf.), 193–196.*
2. *Březinová, H. – Kohout, D. – Bravermanová, M. – Otavská, V. – Selmi Wallisová, M. (2016). Středověké textilní a barvířské technologie. Soubor textilních fragmentů z odpadních vrstev z Nového Města pražského. (Medieval Textiles and Dyeing Technologies. An Assemblage of Textile Fragments from the Waste Layers of Prague’s New Town). Institute of Archaeology of the Czech Academy of Sciences, Prague.*
3. *Březinová, H. – Přichystalová, R. (2014): Úvahy o textilní výrobě na Pohansku na základě analýzy nálezů textilních fragmentů a předmětů souvisejících se spřádáním a tkaním. (An Examination of Textile Production at Pohansko on the Basis of an Analysis of Textile Fragments and Artefacts Connected with Spinning and Weaving). Památky archeologické, CV, 2014, 155–214.*
4. *Štolcová, T. – Březinová, H. (2018): Textile Fragments from the Bronze Age Site of Tursko-Těšina, Czech Republic (Included in Rast-Eicher, A.: In the Beginning was the Fibre). In: Sofaer, J. (ed.). Considering Creativity. Creativity, Knowledge and Practice in Bronze Age Europe. Archaeopress Archaeology, 121–123.*

STANDARDISING THE SAMPLE PREPARATION FOR ANALYSIS OF FIBRES AND PARTICLES BY STATIC IMAGE ANALYSIS

Holger Fischer[1]; Ina Sigmund[2]; Petra Hartwig[1]; Esther Dederer[1]; Annett Maschinski[2]

[1]Faserinstitut Bremen e.V. FIBRE, Bremen (DE), fischer@faserinstitut.de
[2]Sächsisches Textilforschungsinstitut e.V. STFI, Chemnitz (DE), ina.sigmund@stfi.de

Abstract:

Static image analysis is known as a versatile method, which is in use for characterisation i.e. of fibres, nonwovens, textile recyclates etc. Due to incomplete standardization (esp. in the area of sample preparation) the usage is actually limited. Within the project StaPAFaB two research institutes are engaged to compile a reference manual listing typical classes of materials and optimised methods of sample preparation for each of them. This will be combined with recommendations for reasonable parameters in image acquisition / processing and possible limitations for each type of material. Aim is to enable reproducible and consistent analyses on an inter-laboratory level as well as to reduce the demand of time for the analyses. This article focuses on typical classes of textile materials and adapted methods to enable their quick and reliable sample preparation.

Key words:

image analysis; sample preparation; textile fibres; recycled fibres

1. Introduction

Static image analysis delivers more detailed results than e.g. sieving. Namely there are distributions instead of average values for length, width and several shape factors. As for all analytical methods, standardisation is an essential prerequisite for reproducibility as well as for comparability of the results. Unfortunately, up to now standardisation has taken place only incompletely for static image analysis. ISO 9276–1 to –6 [1] define parameters for evaluation and graphical presentation of the results. Image acquisition and calibration of the experimental setup is only specifically described by the equipment suppliers. This does not cover the way how to prepare samples for the static image analysis.

Consequently this leads to problems in commercial and research laboratories. Static image analysis is a useful method for universal access to parameters like size and shape of a wide range of materials, combined with statistical analysis. This misleads to a frequent use of this method for new questions and single research samples. Finally different ways of sample preparation, combined with various parameters in image acquisition and analysis lead to strongly different results. This guarantees neither a reproducibility of results in one laboratory, nor comparable results between different laboratories. On the other hand it is known from inter-laboratorial round trials, that a well-described procedure can guarantee identical results within a small tolerance [2].

To overcome the problems in the area of sample preparation, the project StaPAFaB has been started, where two research institutes are engaged to compile a reference manual listing typical classes of materials and optimised methods of sample preparation for each of them. The manual will comprise different types of sample preparation as well-documented guideline for scientists and practitioners.

This article presents results for typical ‘easy’ and ‘complicated’ sample materials to give a first insight into the project aims.

2. Definition of Material Classes

Typical sample Materials have been collected during the project and have been classified according to a newly set-up scheme (cf. Figure 1) allowing to find easily adequate methods of preparing samples for analysis. The material classes are:

- **particles with free-flowing property**, e.g. powders, small crystals (minerals), granules, rice husks etc. Main criterion: these particles do not stick together.
- **particles with limited free-flowing property**, e.g. short fibres, shives etc. Main criterion: these particles tend to stick together slightly, but can be separated non-destructively by small mechanical action.
- **single fibres**, which are not short fibres (see above). Main criterion: the length must be smaller than the max. scanner image length.
- **roving snippets**, e.g. cut-offs from processing high performance fibres (glass, carbon, etc.). Main criterion: the snippets are stable enough for either sieving or at least manual separation using tweezers.
- **recyclates** (consisting of several material fractions): depending on structure several options are possible.

Each material class is sub-divided into groups. For each group possible methods of preparation are specified and recommendations are given.

For a correct assignment of a sample to the most relevant group and best fitting preparation method it is essential to know, what the aim of the analysis is and which parameters have to be analysed. Otherwise the preparation time and number of parameters to analyse may exceed your budget and time! In experience of the authors each hour of discussion with the sample supplier can save two or more hours working with the samples.

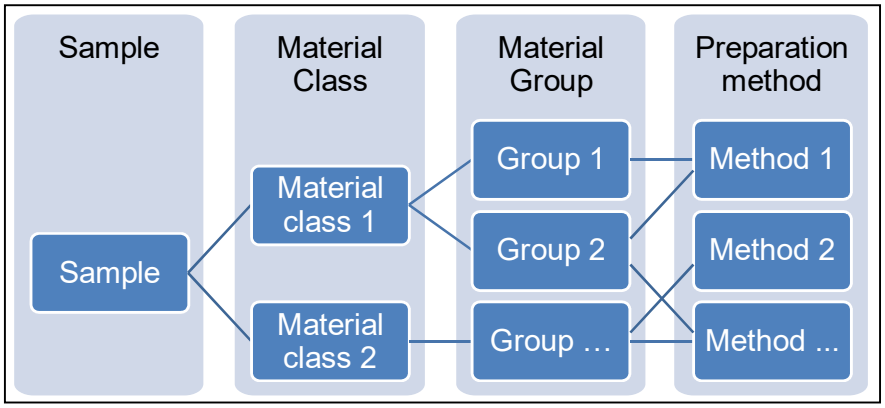

Figure 1. Scheme of material classification to identify adequate method(s) for sample preparation.

Based on this information it is easy to assign each sample material to one of the groups and then to select the preparation method fitting best to analyse the parameters required by the sample supplier. A typical example for saving time and efforts is a fibre sample (class: single fibres). In the worst case there is only manual preparation possible to analyse length and crimp of each fibre. In the best case the fibres can be cut to short fibres and the width distribution can easily be analysed.

3. Examples for sample preparation of different material classes

Within this section typical examples are given for an easy sample preparation using the dispersion by sieving (cf. section 3.1) as well as a quick separation method for complex recyclate mixtures enabling at least access to essential data of composition (cf. section 3.2).

3.1. Example #1: 'easy' sample preparation

As described in the previous section, recommendations for different Materials may end up in the same preparation method. This is the case for e.g.:

- Short cut fibres ('flock fibres') <2 mm length: material class 'single fibres', group short fibres, within the group described as case of 'short enough to exhibit free-flowing property'
- Sand or minerals (Aluminiumtrihydroxide 'ATH', Soda etc.) in dry state: material class 'particles with free-flowing property', group dry powders

For both of them use of a sieve as aid for dispersion is recommended, assisted by shaking or use of a brush. In Figure 2 (a) the experimental setup is shown in brief: a spoon and/or spatula to distribute the sample on the sieve, a brush for additional dispersion, and an analytical sieve in adequate mesh size. To guarantee a reproducibility of the results, the sieve must be certified to a standard like ISO 3310-1 [3]. Some preceding trials are recommended to identify the optimal sieve size: if a sample passes directly through the sieve, the mesh size is too big. If the sample remains (nearly) completely on top of the sieve and does not pass even under vibration, the sieve size is too small. If the sample has a large size distribution, it may be necessary to use two or more sieves to fractionize the sample. In this case the complete sample must be analysed in several images to obtain a valid result representing the sample correctly.

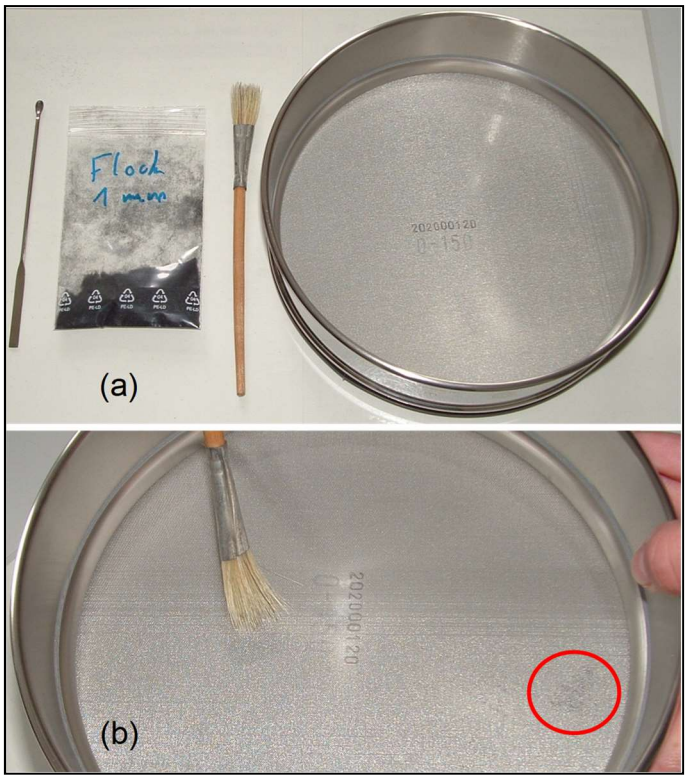

Figure 2. (a) Flock sample, tools and sieve for preparation and
(b) dispersing by brush with flock agglomerate still to disperse in red circle.

For sample preparation mostly it is sufficient to position the sieve above the scanner or a transparent foil, which is later transported into the scanner. Then the sample is distributed over the sieve by the spatula or spoon. Finally the particles can be dispersed by using a brush as shown in Figure 2 (b). Agglomerates of sample particles have to be dispersed carefully in order to achieve a good distribution for scanning. If particles remain on the sieve, they must be transferred to a second transparent foil to be analysed as additional image to guarantee an analysis of the complete sample.

In Figure 3 the greyscale scans of two particle sample are presented as typical examples for the sample types listed above: (a) flock fibres of figure 2 with 1 mm of nominal length representing short fibres and (b) sugar particles as example of crystalline particles.

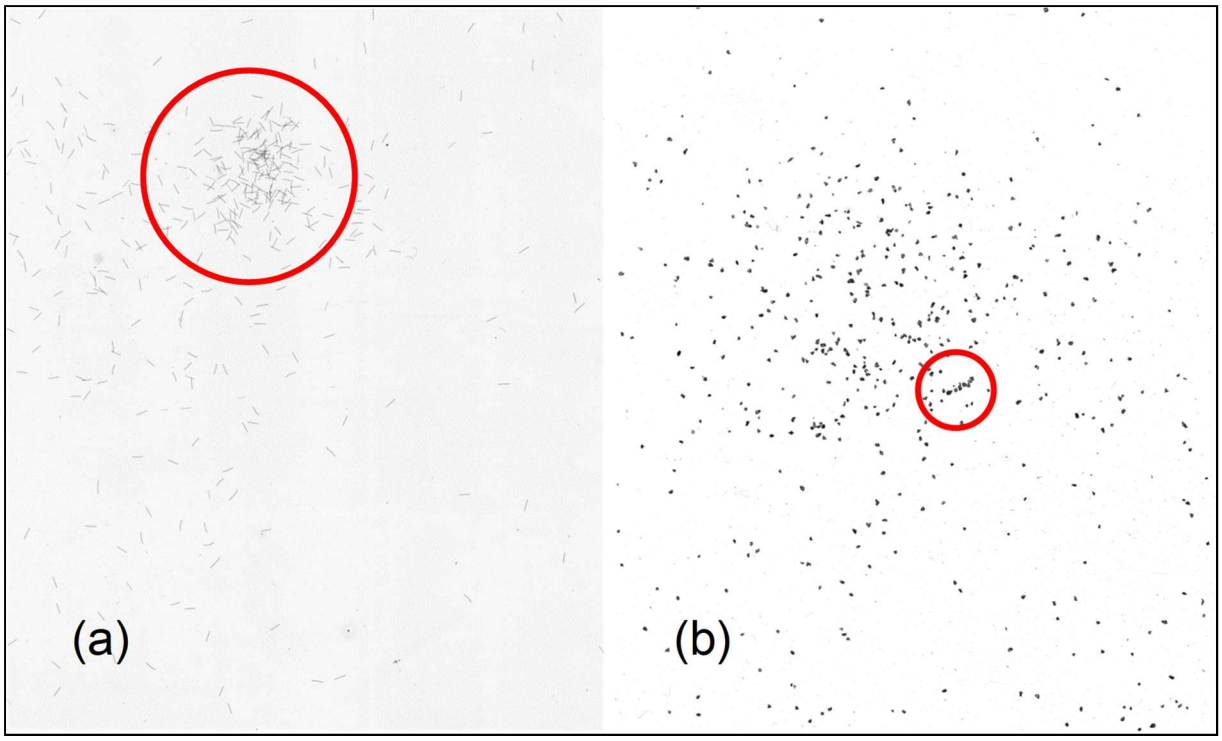

Figure 3. Acquired images of (a) flock fibres of figure 2 and (b) sugar particles.
Red circles indicate remaining agglomerates which should be excluded from analysis.

Both samples exhibit a good dispersion of the particles over the image. But, in both samples there are small regions with insufficient dispersion, indicated by red circles. For the image analysis it is essential, that there are not too much overlapping particles. In general it is not possible to analyse these overlaps correctly, and thus they must be excluded from the analysis. For the sample preparation this means, that either the particles in these regions may be separated manually (only reasonable for large particles), or they must be excluded from the subsequent analysis.

Finally the images can be loaded into the desired image analysis software to perform the analysis of the desired parameters. For short fibres this is typically width and length, while for particles it is typically the grain size, aspect ratio etc.

3.2. Example #2 / complex sample preparation

Textile recyclates often consist of different fractions. Thus there was normally only the time-consuming possibility of manual separation and subsequent analysis of each fraction. Within the project a new approach using compressed air to separate the fractions has been developed. It enables a quick approach to at least rough analysis of the shares.

The experimental setup (cf. Figure 4 a & b) is simply using a sampling bag 42 x 21 cm and a commercial airbrush pistol (a). The sample here is cotton from T-shirts after the tearing process. After separating the agglomerate (b) the bag has to be transported horizontally to a flatbed scanner to acquire a greyscale image (cf. Figure 4 c). The fractions fabrics, yarns and fibres can now be easily identified and quantified by their gray scale values. In this case the fabrics appear black, represented by the greyscale values 0 to 50, while the yarn pieces are dark grey, represented by the greyscale values 51 to 140. The fibres appear light grey, represented by the greyscale values 141 to 200. Values above 200 to 255 represent the background.

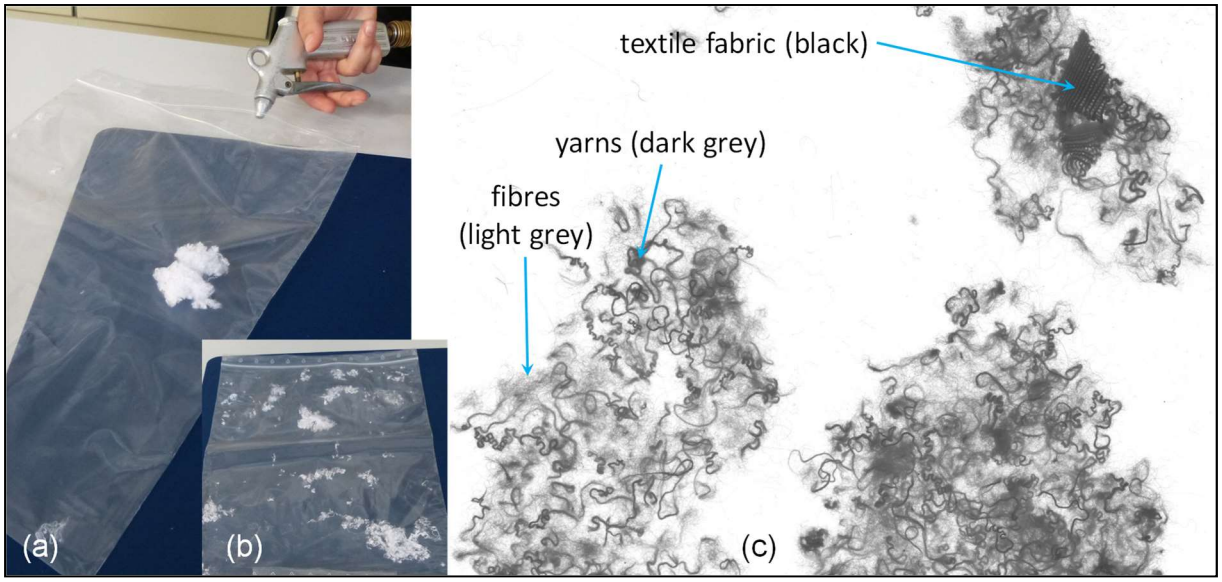

Figure 4. (a) agglomerate of recycled textile in sampling bag, (b) after separation by compressed air and (c) resulting grayscale image in sampling bag with fabrics in black, yarns in dark gray and fibres in light gray.

The exact limits of the different fractions vary for different recyclates depending on structure, colour and degree of disintegration. Thus the greyscale limits for the different fractions should be defined individually. Now it is easy to analyse the greyscale histogram, using e.g. free software like ImageJ [4]. Typically not more than 5 – 10% of the pixels should be particles to avoid too strong overlapping. From these pixels the share of the different fractions can be calculated in %, representing roughly the mass shares.

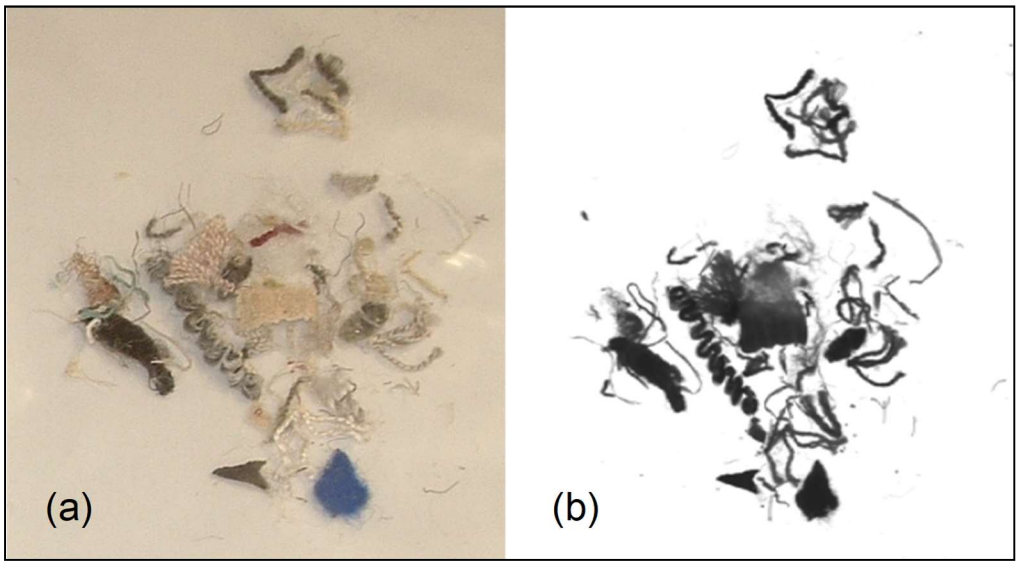

Figure 5. Agglomerate of recycled carpet, (a) photograph and (b) grayscale scan.

As a second example a carpet recyclate after separation in compressed air is shown in Figure 5 with (a) photograph and (b) greyscale scan. For this material the same approach for assessing the shares of different fractions is possible. In this case not only the fabrics (carpet backing), but as well the tufting yarn appear black. For this reason they can only be counted as one fraction. Finer yarns from the backing and fibres are the other fractions evaluatable.

Summing up, by this method of sample preparation it is easily possible to access the share of fractions in textile recyclates. This is important to control the efficiency of the tearing process and gives information necessary to decide, if the degree of disintegration is sufficient.

In principle, some more parameters like size and shape distribution of the fabric fragments or width distribution of the fibres can be analysed.

Other options like length distribution of the yarn pieces and fibres would be only available after manual sample separation.

4. CONCLUSIONS & OUTLOOK

Within the project StaPAFaB a scheme has been set-up for quick and reliable sample preparation for static image analysis. The project work led to progress in sample preparation techniques especially in the field of textile recyclates. At the beginning of the StaPAFaB project the only method to prepare samples from these recyclates was manual separation, demanding up to >1 day per sample. Using the compessed air method described here it is possible to prepare a sample within minutes, which is good enough to assess the parameters important for the tearing process.

In order to disseminate the results to a broad circle of interested scientists as well as practitioners, a public workshop will take place in January 2023 in Bremen / DE for everybody interested in these topics. In addition, the project results will be published in April 2023 as a reference manual listing typical classes of materials and optimised methods of sample preparation for each of them.

ACKNOWLEDGEMENTS

The authors are much indebted to the federal ministry of economic affairs and climate action for funding this research within the programme INNO-KOM (No. 49VF200016 & 49VF200017).

Supported by:

Federal Ministry for Economic Affairs and Climate Action

on the basis of a decision by the German Bundestag

References

1. *International Organization for Standardization ISO (ed.). ISO 9276-1:1998-06: Representation of results of particle size analysis - Part 1: Graphical representation. ISO, Geneva, CH 1998.*
2. *Fischer, H.; Haag, K. & Müssig, J. (2016). Standardisation & Harmonisation of the Length Analysis of Flock Fibres by Scanner-based Image Analysis. Melliand International 22(1), 16 – 18. ISSN 0947-9163.*
3. *International Organization for Standardization ISO (ed.). ISO 3310-1:2016-08: Test sieves - Technical requirements and testing - Part 1: Test sieves of metal wire cloth. ISO, Geneva, CH 2016.*
4. *National Institutes of Health. ImageJ Image Processing and Analysis in Java. https://imagej.nih.gov/ij/download.html . Accessed 2022-10-14.*

ARTISANAL EXFOLIATING SOAPS MADE WITH NATURAL FIBRES AND THEIR POTENTIAL FOR COMMERCIAL APPLICATION

[1]Anagha Vaidya Soocheta; [2]Marie Kelly Sthecy Roman

Department of Applied Sustainability and Enterprise Development, University of Mauritius, Reduit, Mauritius

[1]corresponding author: a.soocheta@uom.ac.mu, mobile: +23057593959
[2] marie.roman@umail.uom.ac.mu

Abstract:

The project investigates the potential of natural fibres from Luffa acutangula, vetiver, banana fibre and pineapple leaf fibre as exfoliating ingredients in bar and liquid soaps. It tests the use of these fibres as an alternative to exfoliating soaps made from synthetic materials. It also explores the prospect of making exfoliating soaps as a viable business opportunity. Soaps are made by saponification of fatty acids. They are sodium or potassium salts of fatty acids used as washing and cleansing agents. The study involved soap making by cold process, hot process and liquid soap making. A combination of olive oil, coconut oil and castor oil was used to make the soap base. Sodium Hydroxide was used for making the bar soap base, while potassium hydroxide was used for making the liquid soap base. The proportions of oils for the soap bases were optimised and their properties were tested for pH, foaming capacity, and degree of cleanliness. The study explores combinations of the soap bars made with blends of Luffa acutangula, vetiver, banana, and pineapple leaf fibre to test their exfoliating properties. Their use as exfoliating ingredients in liquid soap base were also tested and compared. With the focus on developing sustainable and biodegradable product, soap packaging was also created from extraneous waste from the luffa extracts, vetiver leaves, banana and Pineapple leaf fibres. The project provides ideas to start a small business.

Key words:

Exfoliating soaps; Luffa; Vetiver; Banana fibre; Pineapple leaf fibre; Hot process; Cold Process; Liquid soap; Bar soaps; Packaging

1. Introduction

Ecological sustainability has become an important aspect of our society today. The past decades have seen a drastic increase in synthetic materials on the market, which has increased the use of non-biodegradable products. The possibility of manufacturing materials with a reduced production cost can partly explain this rise; it can be profitable for industry and the economy, but it also destroys the environment on a massive scale. Nowadays, numerous people contribute to the protection of the environment by buying and using environmentally friendly and bio-degradable products. The growing concern over the deterioration of the environment has made people more willing to develop eco-friendly and sustainable products, and for good reason we have seen an increase demand in eco-friendly products on the market in recent years. Mauritius Island is surrounded by a wide variety of fibrous natural resources which can be exploited to make artisanal products. Furcraea Foetida [Mauritius hemp], Pandanus Utilis [Vacoas], Ananas comosus [Pineapple], Banana Pseudo stem, Vetiver are some common plants used for the fabrication of crafts products.

1.1. Chemistry of Soap Making

The making of soap involves the hydrolysis of fatty esters (fat or oil) in the form of triglycerides using an alkaline solution, of sodium hydroxide or potassium hydroxide. This chemical process from which fatty acid salts and glycerol are produced is termed as saponification [1].

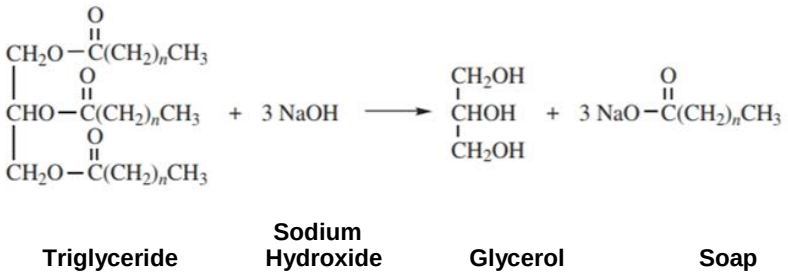

Figure 1. Saponification reaction – Triglyceride and Sodium hydroxide
(Source: Burke, 2005)

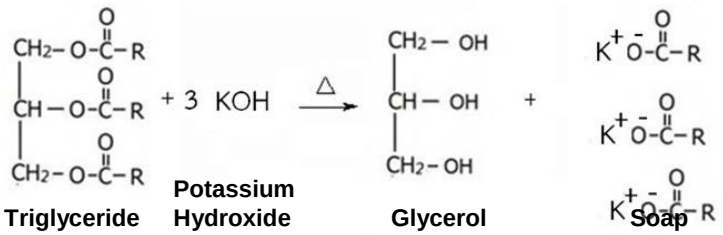

Figure 2. Saponification reaction - Triglyceride and Potassium Hydroxide
(Source: byjus.com)

1.2. Classification of Soap

Soaps are either sodium or potassium salts of fatty acids.
Hard Soap: Sodium hydroxide-based soaps are classified under the generic term of hard soap. Hard soaps are produced through the crystallization of sodium. The crystals bounce the light waves off the bar soaps, giving them an opaque appearance [2]. Also known as soda soap, it can be manufactured by both cold and hot process [3].
Soft Soap: Soaps having potassium hydroxide as alkali based, are termed as soft soaps. Being more soluble than sodium hydroxide, potassium hydroxide tends to form fewer crystals, allowing light to pass through unobstructed [2]. Technically termed as potash soaps, they are known to be more caustic than soda soap [4].

1.3. Natural Exfoliating Ingredients

1.3.1. Luffa

Categorized as a group of the *Cucurbitaceae* family (Cucumber), luffa is cultivated and consumed as a vegetable when it is still an immature fruit, and used mainly as natural fibrous sponge when the fruit has fully matured. Composed predominantly of cellulose/ hemicellulose and lignin, as seen in Table1 and minimally of proteins, amino acids, glycosides and polypeptides [5], luffa fibre is a green renewable resource, valued for its biodegradability, high resistance and natural network [6]. Luffa fibre forms a fibrous vasculature consisting of a bundle of cellulosic fibrils [6]. The structure of the luffa begins with a single 1-millimeter fibre with no fibrous structure, building up to a complex interconnected fibrous pattern of about a hundred millimetres, forming a branched fibre structure, at the end of its growth [5].

Table 1. Chemical Composition of Luffa Fibre

Chemical Composition		
Cellulose (%)	**Hemicellulose (%)**	**Lignin (%)**
55-90%	8-22%	10-23%

(Source: Alhijazi et al. 2020)

Species of Luffa: The luffa acutangula, known as angled luffa, ridged luffa or vegetable gourd, is angled and ridged on the outer layer of the fruit and club-shaped [7]. They tend to be smaller, narrower but more elongate than the luffa aegyptiaca, reaching 70 centimeters in length and 12 centimeters in width [8]. Luffa Aegyptiaca, is believed to be originated from the luffa acutangula, is also known as smooth luffa, luffa cylindrica, Egyptian luffa or gourd luffa. Both species can be distinguished by their morphology and flowering time as seen in figure 3 and 4. The luffa aegyptiaca is found to be more widespread than the luffa acutangula [8]. Egyptian luffa has stronger and rougher fibrous skeleton than the angled luffa, making it more economically important.

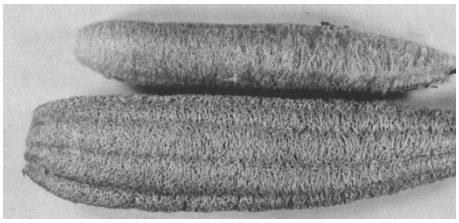

Figure 3. Luffa acutangula (above) and Luffa aegyptiaca (below).

Figure 4. Fibrous vascular system of Luffa acutangula (above) and Luffa aegyptiaca (below).

Mechanical Properties of Luffa: Luffa is a biological cellular material which, despite being inferior to man-made materials, demonstrate great mechanical characteristics at low density and provides long-term durability for the environment. Luffa is made up of an intricate network of fibre bundles bonded together to form an extremely porous three-dimensional network. The luffa is composed of four main parts, as seen in figure 5, the core region, the outer surface, the inner surface and the hoop region, and three main directions, which are the longitudinal direction, the radial direction and the circumferential direction.

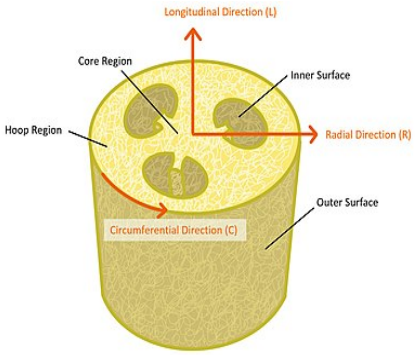

Figure 5. The Structure of the Luffa
Source : https://en.wikipedia.org/wiki/Luffa#Mechanical_properties)

1.3.2. Vetiver

Vetiveria zizanioides, is a graminaceous plant of 0.5 to 1.5 meters high, valued for its morphological, physiological and ecological characteristics which help stabilizing the soil conditions. The root system of the vetiver consists of fibrous roots reaching 3 meters in depth. The aromatic compound obtained after distillation of the roots, is applied for domestic and cosmetic use [9].

Species of Vetiver: Vetiver grass is divided into two main species. *Chrysopogon nigritanus,* known as black vetiver grass, is a specie of the Poaceae family. Native to Africa, this specie grows in seasonally flooded plains, edge of streams, damp places, fresh water. *Chrysopogon zizaniodes,* is a specie of the

Poaceae family, also known as khas-khas or khus grass. Native to India, this specie is known for its rapid growth, and its strong, deeply rooted, extensive fibrous root system [10;11].

Structure of Vetiver: The structure of vetiver can be classified into six significant parts. The vetiver culm is a jointed hollow stem uniting various grasses. The culm has prominent nodes which form the roots, and keep the plant stable in the soil allowing it to rise once buried. Germinating from the bottom of the clumps, are the vetiver leaves 45-100 cm long and 6-12 cm wide. The leaves are long, narrow and coarse, with a parallel angle and a sharp apex. The most valued and useful part are the vetiver roots. They consist of a very dense fibrous system which penetrates vertically deep in the soil, rather than spreading horizontally. The inflorescence of vetiver is erect and in the shape of a panicle. The sessile spikelet which is a hermaphroditic flower generate seeds after pollination. However, not all v*etiveria zizanioides* species produce seeds and propagate as a genuine weed. Clump is considered to be a group of vetivers clustered together. Clumps are formed when plants produce a number of tillers in all directions. 150-200 cm long, the diameter of the clump is of 30 cm [12].

1.3.3. Banana Fibre

Bananas come from the perennial herbaceous group of the Musaceae family [13]. Mauritius is prominent in the cultivation of Banana trees, having an approximate of 8512 tons of its fruit, making an approximate of 550,000 of its pseudo-stem cut down annually. The pseudostems have tightly packed about 25 overlapping leaf sheaths, that yields a strong and resilient fibre [14]. Table 2 shows the chemical composition of the fibres. Being a lignocellulosic natural fibre, banana fibre is valued for its sustainable, renewable, and biodegradable properties. Thin, silk-like banana fibres are obtained from the innermost layers of the stem. Outermost layers contain coarser banana fibres. Banana fibres are found to be white, brownish, and yellowish in colour [13].

Table 2. Chemical Composition of Banana Fibre

Chemical Composition of Banana Fibre			
Cellulose	**Hemicellulose**	**Lignin**	**Pectin**
60-65%	6-19%	5-12%	3-5%

(Source: Eichhorn et al., 2009)

1.3.4. Pineapple Leaf Fibre

Ananas comosus is an herbaceous perennial plant of the Bromeliaceae family. The height and circumference of the plant vary between three to six feet. Yielding both fruit and textile fibre, the ananas comosus is considered to be the most commercially valued crop [15]. The production of pineapple fruit generates a significant amount of agricultural waste, which can be useful in the manufacture of textile [16]. Extracted from the parallel-veined leaves of a monocotyledonous plant, pineapple leaf fibre (PALF) is considered the toughest plant fibre [15]. PALF has high tensile strength and rigidity, and is hydrophilic due to its rich cellulose content [15]. Soft, white in colour, fine and shiny, comparable to silk, the pineapple leaf fibre can be woven without undergoing chemical treatment [18].

Table 3. Chemical Composition of PALF

Chemical Composition of PALF			
Cellulose	**Hemicellulose**	**Lignin**	**Pectin**
70-82%	16-19%	5-12%	2-3%

(Source: Eichhorn et al., 2009)

This project explores the exfoliating properties of the luffa acutangula, widely known in Mauritius as ‘Pipangaye’, to produce unique and environmentally friendly exfoliating soaps, for both local inhabitants and tourists. The luffa acutangula fruit matures into a fibrous mass. The mature luffa fruit can no longer be consumed and is considered as a waste. The dry fibrous skeleton mass has been used as a body scrub luffa since times unknown. The study further explores the exfoliating properties of the vetiver, banana fibre and pineapple leaf fibre in soaps.

2. Experimental Methods

2.1. Extraction of Luffa Fibre

The fibre extraction from luffa acutangula was done in three steps. The green luffa acutangula was air dried in direct sunlight. It loses considerable amount of water as it dries. The skin of the mature luffa hardens and changes from green to yellow-tan or almost brown colour (Figure 6 and Figure 7). Once the rind, or outer layer of the luffa is completely dry, it can be peeled off. The hard ends of the luffa are cut and the seeds are tapped off. It is soaked in hot water for I hour to soften and peel off the outer skin and extraneous matter. This leaves a fibrous skeleton structure of the fruit. The luffa washed dried and cut into several slices, ground or shredded for further use.

Figure 6. Drying of Luffa Acutangula

Figure 7. Dried Luffa

2.2. Extraction of Vetiver Fibre

The fibre extraction from dry Vetiver leaves was carried out manually using simple tools as seen in Figure 8. Dried Vetiver leaves were scrapped with a putty blade by passing it along the length of the

Figure 8. Extraction of Vetiver fibres – Blade and Metallic brush

leaves. The process was repeated a number of times to extract as many fibres as possible from the vetiver. Another technique used a wire metallic brush to scrape off the extraneous material from the leaves. Brushing a bundle of leaves proves to be more efficient technique.

2.3. Extraction of Banana Fibre

The fibres were extracted using the banana fibre extraction machine available in the laboratory as seen in Figure 9.

Figure 9. Banana fibre extraction machine and extracted fibres

One end of the pseudo stem sheet was fed into the extractor machine, between the squeezing roller and the scraper roller. Once the other end reaches the mouth of the feeder it was pulled back. The extracted fibre was thoroughly washed and left to dry.

2.4. Extraction of Pineapple Fibre

Pineapple fibres were sources from the planters. The extraction of pineapple was done using the extractor machine available in the laboratory as seen in Figure 10. Leaves were fed into the extractor machine, between the squeezing roller and the scraper roller till they reach the mouth of the feeder and was pulled back. Fibres were also extracted manually by scrapping the leaves with a blunt blade. The extracted fibre was thoroughly washed and left to dry.

Figure 10. Fibre extraction machine

2.5. Saponification

Cold Process: Required amount of oil, sodium hydroxide and distilled water was measured accurately, as in table 4 table 5 and table 6. The lye solution was prepared by adding sodium hydroxide gradually to the distilled water and stirred constantly till it dissolved. The lye solution was allowed to cool to 37-43 ℃. It was then added to the oil. A stick blender was used to thoroughly stir the mixture to until it reached the trace stage. At this stage fibres, colours, or any other additives can be added. The soap mixture is then poured into moulds, insulated with towels and allowed to set for 48 hours to allow for complete saponification. After the 48 hours, the soaps were unmoulded, cut to desired size, and allowed to cure for 4-6 weeks [19].

Hot Process: Hot process soap making is an extension of the cold process soap making. Required amount of oil, sodium hydroxide and distilled water was measured accurately, as in table 4 table 5 and table 6. The lye solution was prepared by adding sodium hydroxide gradually to the distilled water and stirred constantly till it dissolved. The lye solution was allowed to cool to 37-43 ℃. It was then added to the oil. The mixture is cooked in a double boiler. The soap mixture is constantly as it is gradually heated on the double boiler. The soap paste goes through the “gel phase” until it reaches the “applesauce phase”. The soap is ready when it has a translucent and glossy appearance. At this stage fibres, colours, or any other additives can be added. The soap mixture can be poured into moulds, tapping it down to release any trapped air bubbles from the mixture. The soap is allowed to set and harden for 24-48 hours. The soaps can be unmoulded, cut to desired size, and allowed to cure for 1 week [2; 20].

Liquid Soap Making: The paste method is an extension of the saponification by hot process. The soap paste is diluted in distilled water once it has been neutralized during the cooking stage. The alkali used for liquid soap making is potassium hydroxide. The process is similar to hot process, till the moulding process. Instead of moulding the soap, the mixture is diluted to obtain liquid soap. After cooking, a pH test is done using a digital pH meter to know whether the soap paste has been completely neutralized. A pot is filled with distilled water and bring to boil. The soap paste is added to the pot and stirred periodically with a whisk or spatula to break up the mass and cause it to totally dissolve. The soap is heated at high temperature for 3 hours. The water to soap ratio for the dilution of the soap was 3:1. Once the soap has cooled, pour it into bottles and let it sit for 1-2 weeks in a cool place [2; 20].

Table 4. Coconut Oil Soap recipe

	Grams
Coconut Oil	500
Sodium Hydroxide	110.2
Distilled Water	257.13

Table 5. Olive Oil, Coconut Oil Soap recipe

	Grams
Olive Oil	250
Coconut Oil	250
Sodium Hydroxide	87.16
Distilled Water	203.37

Table 6. Olive Oil, Coconut Oil, Castor Oil Soap recipe

	Grams
Olive Oil	300
Coconut Oil	150
Castor Oil	50
Sodium Hydroxide	77.62
Distilled Water	181.11

Soaps were experimented using the recipes as in table 4, table 5 and table 6 with cold process, hot process and liquid soap technique. The olive, coconut and castor oil recipe were used to produce exfoliating soaps by cold, hot and liquid soap making process. Two grams of fibres were added to 100 g the soap recipe at trace stage. Sliced and shredded Luffa fibre was incorporated to the soap mixture. Similarly, vetiver banana and pineapple leaf fibres were also cut and ground finely.

2.6. Exfoliating Soap Testing

Table 7. Soap testing procedures

Test	Procedures
Determination of pH	0.5 g soap shavings or liquid soap were measured and dissolved in 10 ml of distilled water. The pH readings of the soap solution were tested and recorded using a pH meter [22].
Foam Capacity	The following test is carried out to compare the foaming capacity of the different soaps. • 3 g of soap shavings or liquid soap were mixed with 50 ml distilled water in a measuring cylinder. The soap is stirred to dissolve the soap samples. • 2 ml of the soap solution is poured in a measuring cylinder and 10 ml distilled water is added to it. The solution is shaken for a minute to generate foam. The measuring cylinder is allowed to stand for 10 minutes, the height of foam is then measured and recorded [23].
Exfoliating Capacity	A survey has been carried out with 20 people whereby the different soaps combinations were tested and compared. The standard for the test was: • The soaps should be rubbed 5 times on the palms of the hand. Rotational rubbing, back and forth with clasped fingers of right hand in left palm and vice versa.

2.7. Packaging

The waste material after extraction was used for paper making and developed into to packaging for the soaps. Eco-friendly and biodegradable packaging using various techniques such as basketry, knitting was also made for the soap with the extracted fibres. It recommends resources that will be required and help get started with the venture.

3. Results and Discussion

3.1. Saponification with Coconut Oil

The saponification carried out with coconut oil, yield a hard, white soap, with a stable lather and gentle cleansing action as seen in Figure 11. Results in Table 8 show that as the processing time for cold process is less however it take more time to cure as compared with hot process.

Table 8. Evaluation of Coconut Oil Soap

Coconut Oil	Saponification by Cold Process	Saponification by Hot Process
Processing time (Minutes)	1	15
Time taken to cure (Weeks)	6	1

Figure 11. Coconut oil soap by cold process (left) and hot process (right)

Figure 12. Olive and Coconut oil soap by cold process (left) and hot process (right) soap making

3.2. Saponification with Olive and Coconut Oil

A softer, light cream-colored soap, is obtained (Figure12). As seen in Table 9 the mixture takes more time to trace. The tracing time was 4 minutes for cold process and 35 minutes for hot process.

Table 9. Evaluation of Olive and Coconut oil soap

	Saponification by Cold Process	Saponification by Hot Process
Processing time (Minutes)	4	35
Time taken to cure (Weeks)	6	1

3.3. Saponification with Olive Coconut and Castor Oil

The addition of castor oil in the soap recipe creates a yellowish soap compared to the coconut and olive oil soap. Castor oil also imparts a dense and creamy lather to the soaps. The tracing time of both cold and hot process soap making was 5 minutes as seen in Table 10.

Table 10. Evaluation of Coconut, Olive and Castor oil soap

	Saponification by Cold Process	Saponification by Hot Process
Processing time (minutes)	5	5
Time taken to cure (Weeks)	6	1

It is found that hot process soap making is the most effective technique. It is noted that although the processing time is longer, the curing time is much shorter.

3.4. Exfoliating Soaps

The olive, coconut and castor oil recipe were used to conduct the following experiments. Cold, hot and liquid soap making process were used. Two grams of fibres have been added to 100 g of soap. Table 11 shows the combinations of fibres experimented. The luffa, vetiver, banana, and pineapple leaf fibres impart natural exfoliating properties to the soaps. The soaps produced have proved to have a moderate to excellent exfoliating capacities, restoring and smoothing the skin, by removing dead skin cells. Table 12 shows the soaps developed with fibres. The soaps produced have proved to have a moderate to excellent exfoliating capacities, restoring and smoothing the skin, by removing dead skin cells.

Table 11. Combinations of fibres

	Fibre Combinations	% of fibre 1	Amount of fibre	% of fibre 2	Amount of fibre
1	**Luffa fibre soap**	100	2		
2	**Vetiver fibre soap**	100	2		
3	**Pineapple fibre soap**	100	2		
4	**Banana fibre soap**	100	2		
5	**Luffa & Vetiver fibre soap**	50	1	50	1
6	**Luffa & Pineapple fibre soap**	50	1	50	1
7	**Luffa & Banana fibre soap**	50	1	50	1
8	**Vetiver & Pineapple fibre soap**	50	1	50	1
9	**Vetiver & Banana fibre soap**	50	1	50	1

Table 12. Range of Soaps

 100% Luffa soap – Hot process (left), liquid soap (middle), cold process (right)	 100% Vetiver soap – Hot process (left), liquid soap (middle), cold process (right)	 100% PALF soap – Hot process (left), liquid soap (middle), cold process (right)
 100% Banana soap – Hot process (left), liquid soap (middle), cold process (right)	 50% Luffa, 50% Vetiver soap Hot process (left), liquid soap (middle), cold process (right)	 50% Luffa, 50% PALF soap – Hot process (left), liquid soap (middle), cold process (right)
 . 50% Luffa, 50% Banana soap – Hot process (left), liquid soap (middle), cold process (right)	 50% Vetiver, 50% PALF soap – Hot process (left), liquid soap (middle), cold process (right)	 50% Vetiver, 50% Banana soap – Hot process (left), liquid soap (middle), cold process (right)

3.5. pH Test Exfoliating Soaps

3.5.1. pH of Cold Process Exfoliating Soaps

The pH of the exfoliating soaps before curing was within 11.51 to 12.01. With curing, the pH was between 10.71 to 10.90 (Figure 13).

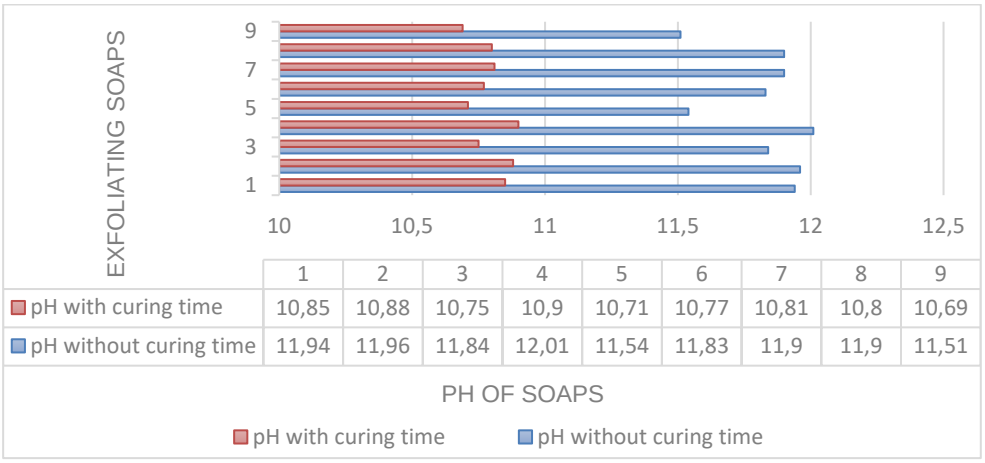

	1	2	3	4	5	6	7	8	9
pH with curing time	10,85	10,88	10,75	10,9	10,71	10,77	10,81	10,8	10,69
pH without curing time	11,94	11,96	11,84	12,01	11,54	11,83	11,9	11,9	11,51

Figure 13. pH of Cold process Exfoliating Soap

3.5.2. pH of Hot Process Exfoliating Soaps

The pH of the exfoliating soaps of hot processed soap was within 10.80 to 11.00. With curing the pH was within the range 9.46 to 10.12 (Figure 14).

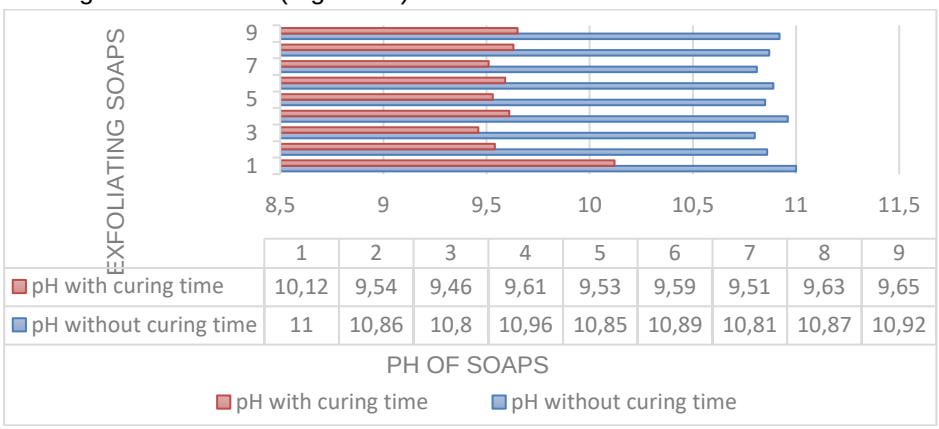

	1	2	3	4	5	6	7	8	9
pH with curing time	10,12	9,54	9,46	9,61	9,53	9,59	9,51	9,63	9,65
pH without curing time	11	10,86	10,8	10,96	10,85	10,89	10,81	10,87	10,92

Figure 14. pH of hot process Exfoliating soaps

3.5.3. pH of Liquid Soap

Before sequestering, the pH liquid soap was 10.80. After sequestering, the pH was found to be 9.73 (Figure 15).

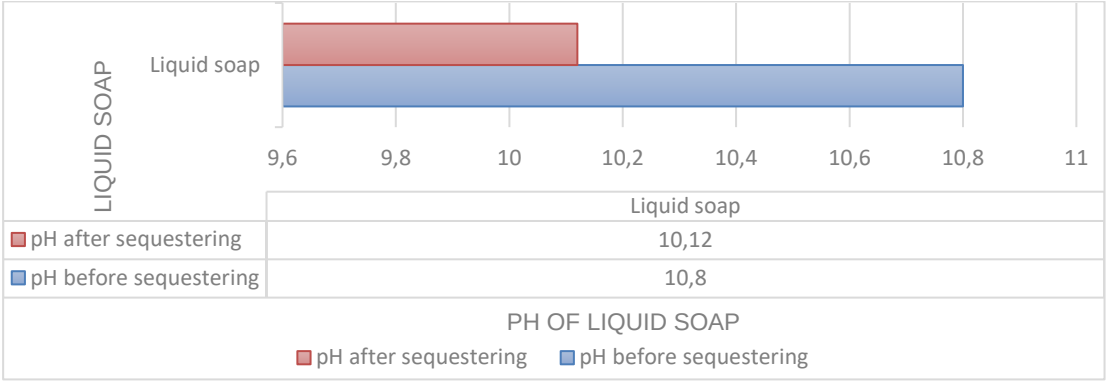

	Liquid soap
pH after sequestering	10,12
pH before sequestering	10,8

Figure 15. pH of liquid soaps

3.6. Test on Exfoliating Soaps – Foaming Capacity

Performance of the foaming capacity test is seen in Figure 16 for cold process, Figure 17 for hot process soaps and Figure 18 for liquid soaps. The soap was agitated and allowed to stand for 5 minutes. The height of the foam was recorded after the 5 minutes. it was ranging from 4-7 cm for both hot and cold process. The height of foam recorded for liquid soap was within the range of 3-7 cm. It can be observed that the height of foam is somewhat similar for the three processes. This can be due to the fact that the optimal amount of NaOH and KOH has been used in the recipe.

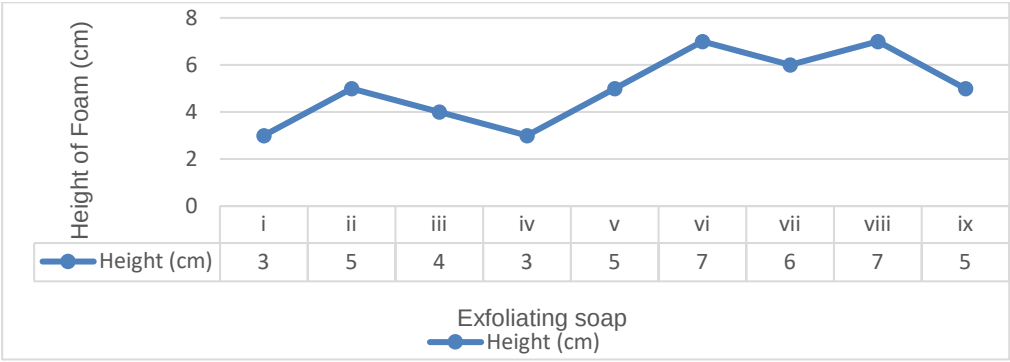

Figure 16. Foam Height Cold Process Exfoliating soaps

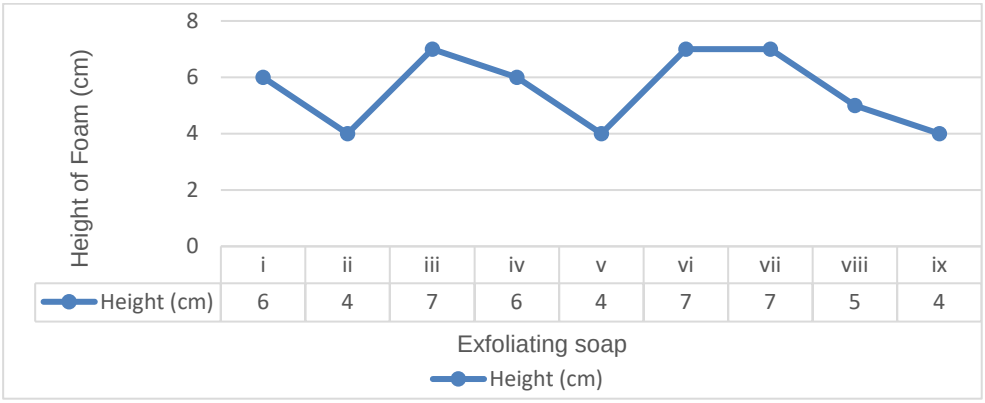

Figure 17. Foam Height Hot Process Exfoliating soaps

3.7. Survey Analysis

Two surveys were conducted for this study to have a better understanding of the performance of the nine exfoliating soaps with 20 subjects. Almost all participants were satisfied with the performance the soaps. They remarked that the soaps had a gently exfoliating feel on the skin without being too rough, and gave a healthy, smooth and glowing skin.

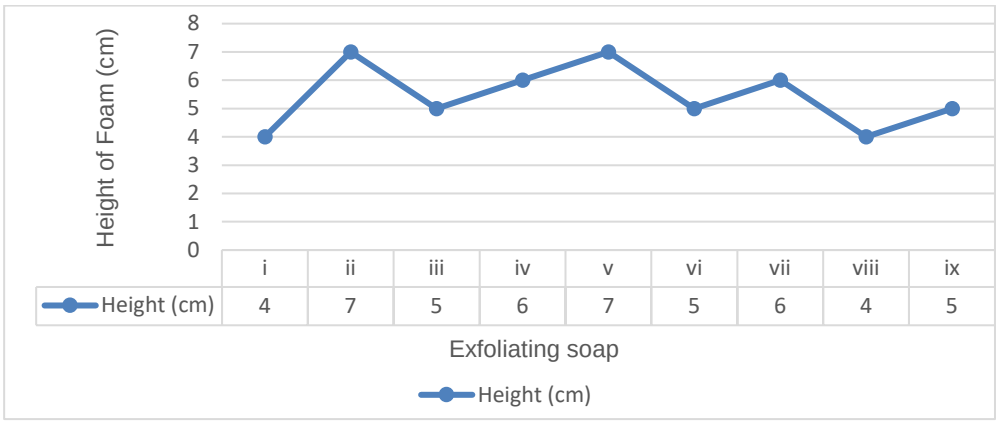

Figure 18. Foam Height Liquid Exfoliating soaps

3.8. Packaging

Figure 19 shows a collage of artisanal soaps that were developed along with their packaging. The packaging were made using various techniques such as basketry, knitting and paper making.

Figure 19. Packaging and Assorted Artisanal Soaps

4. CONCLUSIONS

The study presents the potential of using natural fibres extracted from Luffa acutangula, vetiver, banana fibre and pineapple leaf fibre as exfoliating ingredients in bar and liquid soaps. Luffa acutangula, commonly known as 'pipangaille', is an edible ridged gourd found in abundance all around Mauritius. The fibrous vasculature of the mature, luffa acutangula valued for its high tensile strength and resistance to deterioration by water is used as exfoliating ingredient. It is obtained by drying the vegetable, peeling and removing the extraneous materials. It was impregnated with the soap base for its use as a natural exfoliating soap bar. Vetiver fibres, banana fibres and pineapple leaf were also extracted by mechanical decortication. The extracted fibres were dried and finely chopped and ground and incorporated in the soap base. The liquid soap base was sequestered, to stand for 1-2 weeks so as to clarify the solution and allow any sediments to fall to the bottom of the container. The cut, shredded and ground fibres were added in the liquid base. The cold process exfoliating soap bars required 48 hours to set and 6 weeks for curing. The pH of these soaps without curing ranged from 12.01 to 11.51 and on curing the pH ranged between 10 to 8 making it safe to use on skin. The hot process exfoliating soap bars required 24 hours to set and 1 week to cure. The pH value of the hot process soaps was found to be within the normal range for soaps. It ranged within the pH value of 11.00 to 10.80 without curing, and 10.12 to 9.46 with curing for a week. Liquid soaps also required a week to sequester. Its pH value was 10.80 without sequestering, and 9.73 with a week of sequestering time. The foaming height of the soaps lies between 3 to 7 cm. All soap types showed good cleansing results. The advantages of using these natural resources are that manufacturing of artisanal products do not require advanced technology investments and can be manufactured at a lower cost. They can be hand crafted are biodegradable and create a niche product.

References

1. *Michael R. Burke, 2005. Bailey's Industrial Oil and Fat Products. John Wiley & Sons, 6th Edition.*
2. *Catherine Failor, 2000. Making Natural Liquid Soaps.*
3. *Campbell Morfit, 1856. A treatise on chemistry applied to the manufacture of soap and candle.*
4. *Adolph Ott, 1867. The Art of Manufacturing Soap and Candles.*
5. *Waltraud M. Kriven, Jingyang Wang, Dongming Zhu, Thomas Fischer, 2016. Developments in Strategic Ceramic Materials: A Collection of Papers Presented at the 39th International Conference on Advanced Ceramics and Composites, January 25-30, 2015, Daytona Beach, Florida, Volume 36 Issue 8.*

6. *Sudhir Kumar Saw, Raghwendra Purwar, Sourabh Nandy, Joyjeet Ghose, and Gautam Sarkhel, 2013. Fabrication, Characterization, and Evaluation of Luffa cylindrica fiber Reinforced Epoxy Composites.*
7. *Charles B. Heiser, 2016. The Gourd Book.*
8. *Science and Education Administration, U.S. Department of Agriculture, 1977. Vegetables for the Hot, Humid Tropics: Sponge and bottle gourds, Luffa and Lagenaria.*
9. *Alexia Strokes, Ioannis Spano, Joanne E. Norris, Erik Cammeraat, 2007. Eco- and Ground Bio-Engineering: The Use of Vegetation to Improve Slope Stability.*
10. *Umberto Quattrocchi, 2016. CRC World Dictionary of Medicinal and Poisonous Plants: Common Names, Scientific Names, Eponyms, Synonyms, and Etymology.*
11. *T. K. Lim, 2016. Edible Medicinal and Non-Medicinal Plants: Volume 11 Modified Stems, Roots, Bulbs.*
12. *Alemu Mekonnen, 2000. Hand Book on Vetiver grass technology: From Propagation to utilisation. For Ethiopia.*
13. *Subramanian Senthilkannan Muthu, 2022. Sustainable Approaches in Textiles and Fashion: Fibre, Raw Materials and Product Development.*
14. *C. Picq, E. Fouré, E. A. Frison, 1999. Bananas and Food Security. Les productions bananières: un enjeu économique majeur pour la sécurité alimentaire.*
15. *Mohammad Jawaid, Mohammad Asim, Paridah Md. Tahir, Mohammed Nasir, 2020. Pineapple Leaf Fibers: Processing, Properties and Applications.*
16. *Asril Senoaji Soekoco, Karlina Somantri, Valentinus Galih Vidia Putra, 2019. Proceeding Book of Proceeding Indonesian Textile Conference: Textile 4.0 Clothing & Beyond. 3th Edition, Volume 1.*
17. *J. Gordon Cook, 1984. Handbook of Textile Fibres.*
18. *Garth M. Sanewski, Duane P. Bartholomew, Robert E. Paull, 2018. The Pineapple: Botany, Production and Uses. 2nd Edition.*
19. *Michelle Gaboya, 2012. Soap Making Made Easy (2nd edition).*
20. *Sally Hornsey, 2014. How to Make Your Own Soap in Bars, Liquid and Cream.*
21. *O. G. Tod, 1977. The Joy of Hand Weaving.*
22. *D. L. Pavia, G. S. Kriz, G. M. Lampman, R. G. Engel, 2016. A Microscale Approach to Organic Laboratory Techniques.*
23. *Dr. S. C. Rastogi and Er. Meera Goyal, 2020. Practical/Laboratory Manual Chemistry Class XI based on NCERT guidelines by Dr. S. C. Rastogi & Er. Meera Goyal: SBPD Publications.*
24. *Lawrence A. Schachner, Ronald C. Hansen, 2011. Pediatric Dermatology.*

BACTERIAL CELLULOSE FOR TEXTILE APPLICATIONS

Jaroslava Frajova, Astha Vishwakarma, Jakub Wiener

Technical university in Liberec, Faculty of Textile, Department of Material Engineering, Liberec, Czechia, Husova 1202, Staré Město, 460 01, jaroslava.frajova@tul.cz

Technical university in Liberec, Faculty of Textile, Department of Nonwovens and Nanofibrous Materials Liberec, Czechia, Husova 1202, Staré Město, 460 01

Technical university in Liberec, Faculty of Textile, Department of Material Engineering, Liberec, Czechia, Husova 1202, Staré Město, 460 01

Abstract:

This article focuses on the properties and possible applications of bacterial cellulose. Bacterial cellulose is chemically identical to cotton fibre cellulose but differs significantly from it in its fine fibre structure. Bacterial cellulose is composed of nanofibres of practically pure cellulose, which spontaneously form a compact layer with relatively low porosity and a structure corresponding to non-woven textiles. The bacterial cellulose layer is mechanically highly resistant and flexible at the same time. In the context of this study, the bacterial cellulose layer is basically characterized. Moreover, there is a possibility of improving its properties by combining it with common fibre structures. Possible applications of bacterial cellulose are discussed.

Key words:

Bacterial cellulose, membrane, nanofibres, porosity, application

1. Introduction

Currently, the climate and energy crisis emphasize saving energy in the production of materials and the use of ecological materials that can easily be recycled. This study deals with the biological material bacterial cellulose (BC), which is an ecological material because it consists of cellulose fibers, and its production can also be considered ecological and energy-efficient, since its growth requires a natural fermentation process. BC is characterized by good utility properties, which are studied and described here with combinations with other fibrous flat textiles. Thus, we create BC composites with non-woven textiles, knitted fabrics in various structures and compositions, and it is determined how these combinations affect the visual and functional properties of this investigated material.

Bacterial cellulose is a material that occurs in nature. Bacterial cellulose bacteria are fed by fermentation and create a cellulose structure called fungus. This process is energy-efficient. The fungus shows good properties resembling animal skin. See Figure 1. Currently, this material is the subject of basic research in the fields of medicine, electrical engineering, material engineering, and as a skin substitute.

Bacterial cellulose is an organic polysaccharide compound (-C6H10O5-) Figure 1. Bacterial cellulose creates gel-like fungi on the surface of the culture fluid based on the bacterial growth of yeasts and bacteria called SCOBYs (yeasts from the genus Acetobacter, Sarcina ventriculi, Agrobacterium grow in symbiosis with bacteria, especially Acetobacter Xulinum), which excel in the highest productivity of cellulose and are also bacteria Azotobacter, Rhizobium, Pseudomonas, Salmonella, Alcaligenes) using

a fermentation process. This is a material for future use of the circular economy, for example in filtering, acoustic and clothing applications (1), possible application of BC can also be expected in the electrotechnical industry, medicine, etc. See Figure 2.

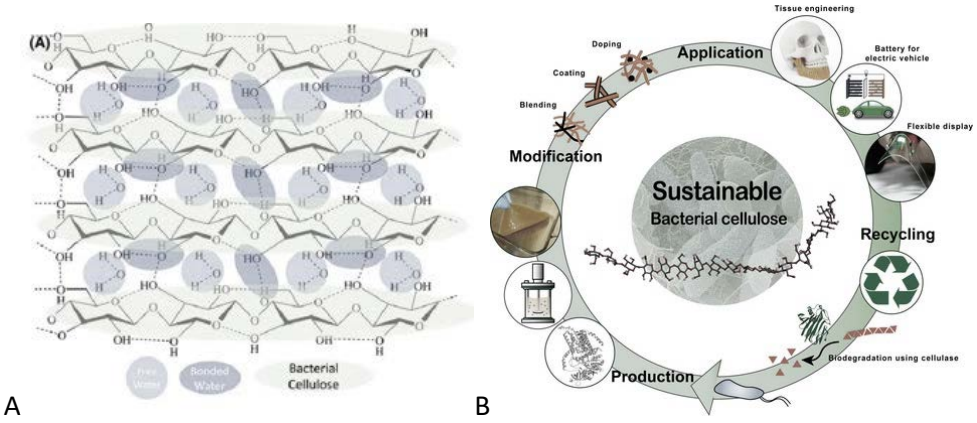

A B

Figure 1., 2. Bacterial cellulose A) Molecular structure of hydrated BC. B) graphic description of basic BC production and its possible modifications and applications. (2)

BC is a biological material that can be easily modified both during the actual production of BC and subsequently using physical and chemical procedures (e.g. using plasma, nanoparticles, etc.). This potential is at the beginning of exploration, and applications are so far sought rather than realised. It is therefore a great challenge to develop this material and its properties into practice for the wider public. The application of bacterial cellulose in the textile and clothing industry is promising due to the simplicity of the technology with minimal demands on the production process. - See Figure 3.

2. Materials and methods

2.1. Materials

Based material is bacterial cellulose (BC) grown by fermentation system by Bacteria Acetobacter Xilium. By standard environment 23°C, humidity 40%, growing process 14 days.

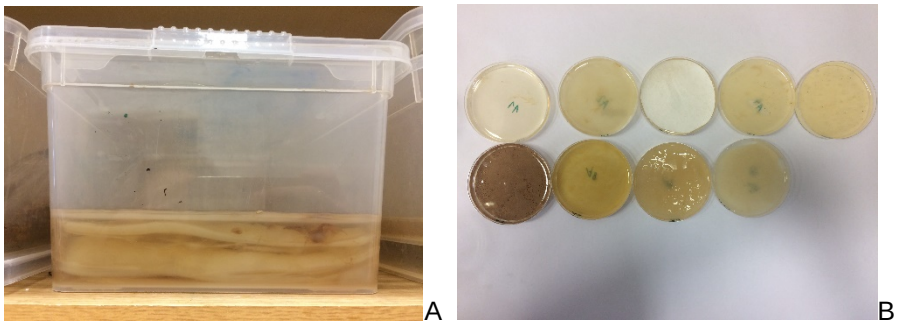

A B

Figure 4. Growing process A, B of BC (bacterial cellulose) by fermentation formula

2.2. Input materials in this study

In this study was used non-woven textile PP, PES, POP and weave structure cotton and warp knitted fabric PES put into the growing system which produce cellulose nanofibres and obtain the textile structures by fermentation process into the textile structure.

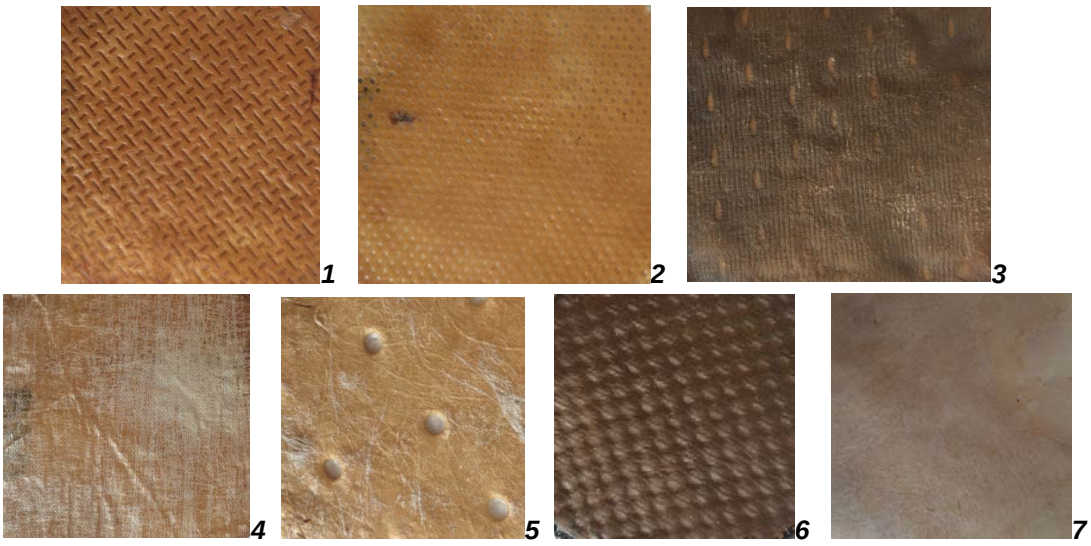

Figure 5. Composites with textile structures Non-woven textiles Milife PES 4, PP filtration Ecotextile 5, non-woven medical structures 1, 2, warp knitting fabric with special porose structures 3, 6, sample without textile addition 7

2.3. Methods

2.3.1 Microscopy SEM

The morphology of electrospun PET fibers and the average diameter of fibers were observed by scanning electron microscopy (SEM), JSM Jeol 6610 microscope at accelerated voltage 15 kV. The samples were sputtered with a thin layer of gold. Images (Figure 6-9) software was utilized to measure the average diameters of the fibers. To ensure accuracy of the calculation; the average diameters of the fibers and their distributions were estimated statistically from 100 measured values.

2.3.2 Mechanical properties

Mechanical properties were tested by Tira Test 2300, device with testing speed 100 mm/min. Analysis was performed according to the EN ISO 13934-1 (EN ISO 6892-1). Tensile properties of nonwoven fabrics at maximum strength and ductility using the Strip method. The samples with dimensions 2 x 15 cm were teste.

2.3.3 Measurement of water vapour permeability (WVP) and air permeability (AP)

The vapour permeability was measured using the PERMETEST Sensora Skin Model. The device provides measurements required in the ISO Standard 11092. The measurements were carried out at laboratory temperature 20–22°C, and the laboratory water vapour concentration (humidity) of the parallel airflow 45–60% was applied. The samples with dimensions 12x12cm were used. For the measurement of breathability, FX3300 air permeability tester III was used for analyses. The measurement pressure was set to 100 Pa, and the test samples dimension was 20x20 cm. The results were evaluated according to EN ISO 9237.

2.3.4 Water column

Hydrostatic pressure or water column value measured on SDL Atlas Hydrostatic Head Tester devices and a device from the Czech manufacturer Řezáč with a clamp for durable materials. The resistance of the material against water penetration under the pressure determined at the height of the water column is determined.

2.3.5 Thickness (mm) and flat weight (g/m2)

Samples was measured by digital thickness machine in scale 0-10 mm (0,005mm) and weight by analytic weight Sartorius.

3. Results and discussion

The overall results show that BC has favorable properties for membrane technologies (Table1). The dependent parameter is the weight of BC, which is influenced by the length of growth and the quality of the fermentation solution. The BC membrane affects the properties of the composite material, especially in the area of vapor permeability. Composites are created by partial growth into a textile membrane, so the material can be used for visual applications. The limitation of the practical application of BC is the low growth rate of fungi and consumption of primary raw materials for bacterial growth (saccharides, possibly polysaccharides). Microscopy shows that bacterial growing process keep the layer with fibres on surface on textile structure. The bacterial fibres grow only on tiny surface of the textile structure. Generally bacterial cellulose grow effectively and deeply into the composite structure on nonwoven porous materials.

We see that Composite weight is positively correlated with Water column and Strength and negatively correlated with air permeability. Increase in air permeability leads to decrease in water column. (Graph1-4)

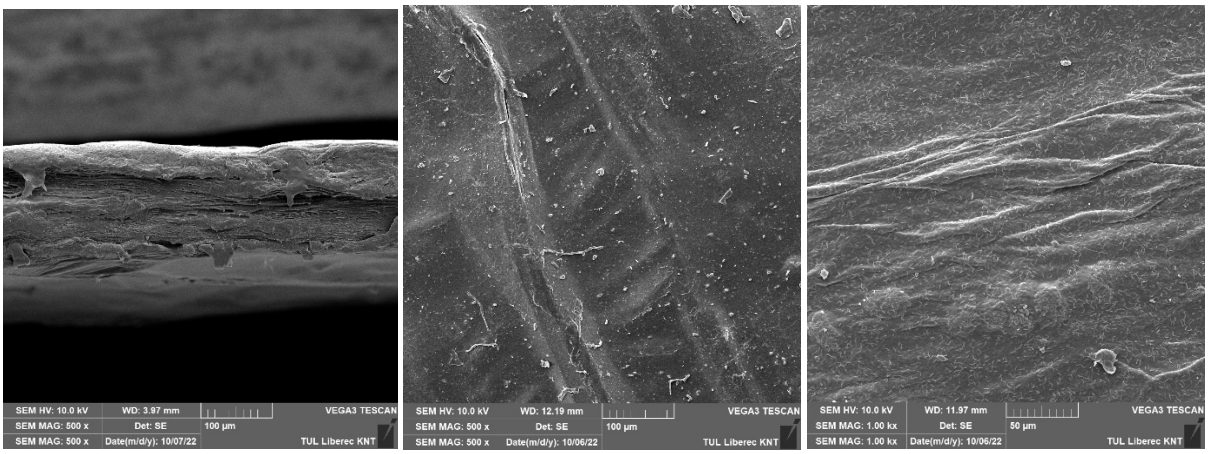

Figure 6., 7. Composite of nano-BC with PES non-woven textile (milife), cut, Microsopy SEM cut, back side, face side, sample 4

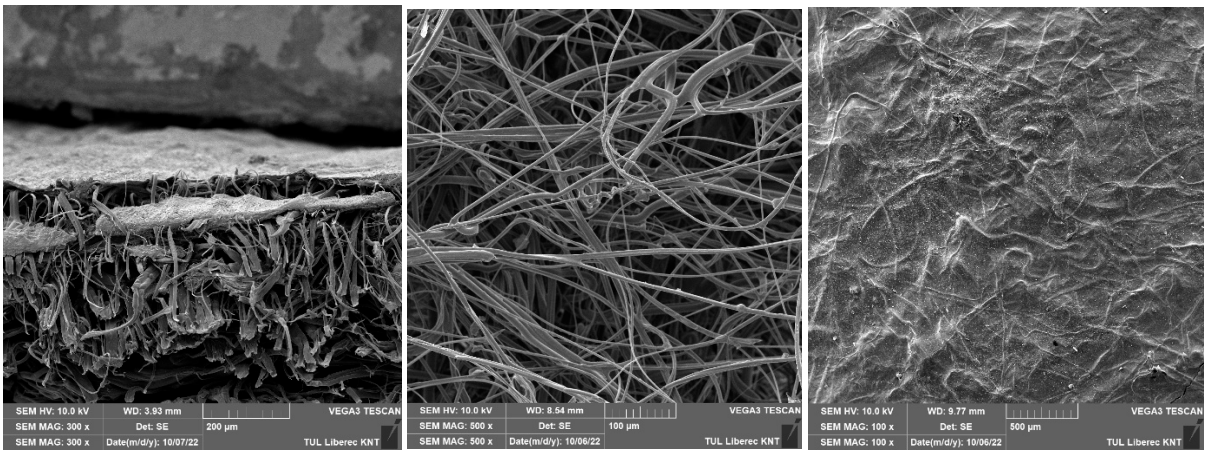

Figure 8., 9. Microscopy SEM of structure of composite BC with Eco-tex non-woven textile, cut, back side, face side sample, number 5

Table 1. Properties of textile composite with bacterial cellulose for membrane applications

Number	Thickness composit (mm)	Thickness of Fabric (mm)	Thickness of BC	Weight (g/m2)	Air permeability (100ml/s)	Permetest (%)	Water column (cm)	Strenght
1	1.42	0.42	1.00	720	0.06	25	5	400
2	0.45	0.37	0.08	210	0.11	62	2.3	180
3	1.19	0.34	0.85	363	0.15	50	2.1	350
4	1.33	0.08	1.25	165	0.16	60	2	175
5	2.61	0.44	2.17	188	0.15	45	2.1	150
6	1.92	1.16	0.76	945	0.08	27	4.5	450
7	0.25		0.25	115	0.16	29	2.5	233

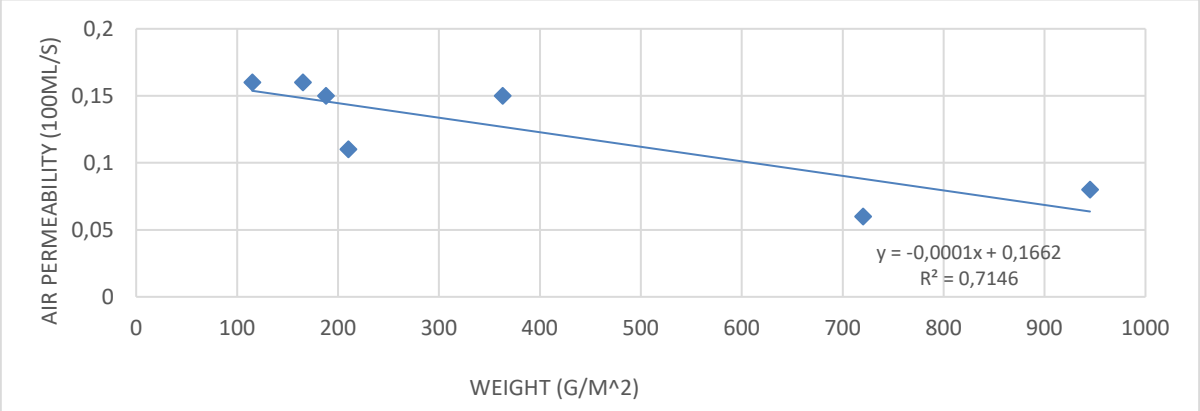

Graph 1. Properties of Bacterial cellulose correlated- Air permeability and weight of composite.

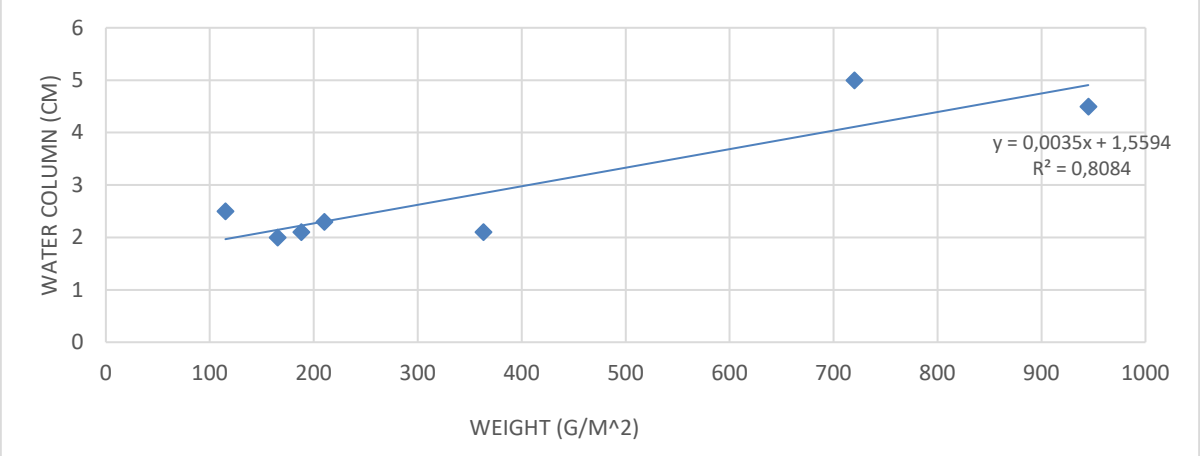

Graph 2. Correlation weight of bacterial cellulose composite with water column

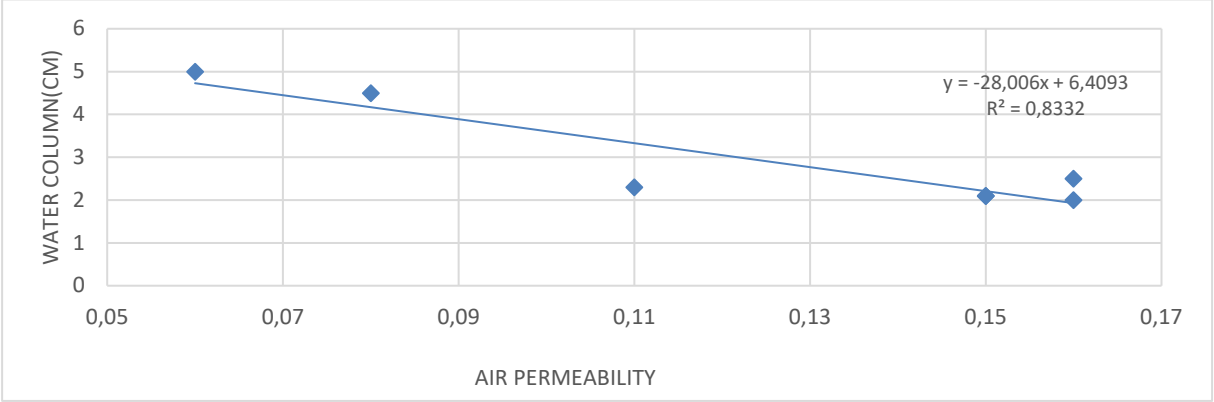

Graph 3. Air Permeability of bacterial cellulose is correlated with water column

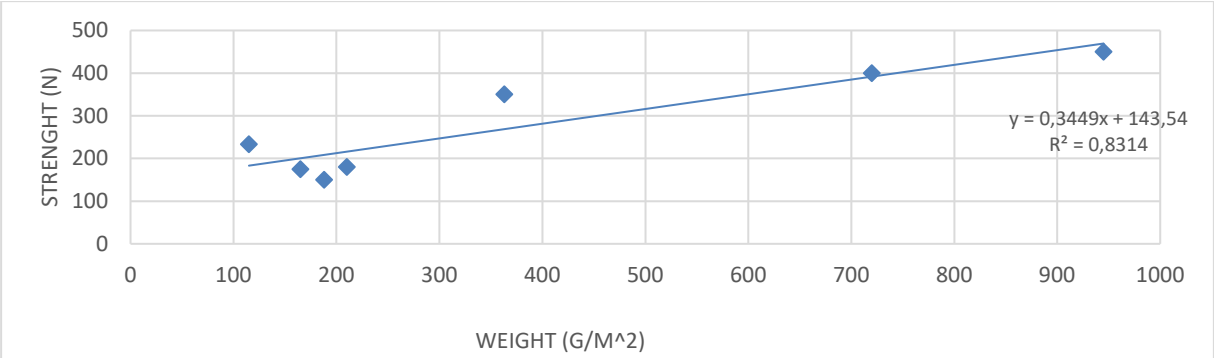

Graph 4. Weight of bacterial cellulose is correlated with strength

4. CONCLUSIONS

Seven membranes were prepared using the fermentation system for the production of bacterial cellulose, which show high potential for use in membrane technology. The advantage is that its porous surface can be combined with composite materials and thus improve the filtering and visual designing properties of the material itself, especially with highly porous non-woven textiles. Individual fibers (1-100nm) in the structure of the bacterial structure move in units of nanomaterials. The thickness of the produced bacterial membrane affects the mechanical properties and breathability of air and steam.

ACKNOWLEDGEMENTS

This work was supported by the Student Grant Competition of the Technical University of Liberec under the project No. SGS-2022-60-69.

Thanks of Department of Nonwovens and Nanofibrous Materials doc. Ing. Jiří Chvojka PhD. and Ing. Zdeňka Hodková for measure of SEM microsopy.

References

1. *Escoto-Palacios, M. J., Pérez-Limiñana, M. A., Arán-Ais F. From leather waste to functional leather. INESCOP. Instituto Tecnológico del Calzado y Conexas, 2016. ISBN 978-84-934261-9-4.*
2. *Embracing Bacterial Cellulose as a Catalyst for Sustainable Fashion Senior Honors Thesis [online].*
3. *Santos, R. J., Agostini D. L. S, Cabrera F. C., Budemberg E. R., Job A. E. Recycling leather waste: Preparing and studying on the microstructure, mechanical, and rheological properties of leather waste/rubber composite. Brazil: Universidade Estadual Paulista, 2015.*
4. *S. Gorgieva, J. Trček, Bacterial cellulose: Production, modification and perspectives in biomedical applications, Nanomaterials. 9 (2019) 1352.*

THE PERFORMANCE OF TEXTILE BASED ELECTRODES DURING DIFFERENT DAILY ACTIVATES FOR CONTINUOUS ECG MONITORING

Roya Aghadavood* , Zahra Shahbaz, Tahereh Kheiri**, Mohsen Shanbeh** , Radek Martinek*,**

*Department of Cybernetics and Biomedical Engineering, VSB - Technical University of Ostrava, 17.listopadu 2172/15, 708 00 Ostrava-Poruba, Czech Republic, +420774812276, roya.aghadavod.marnani.st@vsb.cz.

*Department of Cybernetics and Biomedical Engineering, VSB - Technical University of Ostrava, 17.listopadu 2172/15, 708 00 Ostrava-Poruba, Czech Republic,. radek.martinek@vsb.cz.

**Department of Textile Engineering, Isfahan University of Technology, Isfahan 84156-83111, Iran, +98-(0)31-33912425 , +98-(0)31-33912718444, a.ebadi@tx.iut.ac.ir , r.shakeri@tx.iut.ac.ir mshanbeh@iut.ac.ir .

Abstract:

Long-term vital signs monitoring is essential in order to obtain reliable data on human health. Among all vital signs, electrocardiogram (ECG) has a significant importance, since it includes meaningful information about the person's heart and performance. However, paste of Ag/AgCl electrodes irritate the skin, led to skin rashes and allergies on prolonged use, textile based electrodes are cost-effective, no skin preparation is allowed, easy to integrate, need no special care from the user and perform well, inexpensive, and simple. The aim of this paper is to offer textile-based electrodes, comparing the performance of textile-based electrodes and Ag/AgCl electrodes and assessing the performance of textile-based electrodes during sitting, running, walking and laughing.

In this study, we developed textile-based electrodes (7cmx7cm) with 3 different conductivities. To produce textile-based electrodes, stainless steel/ polyester blend staple fiber yarns with different percentage of stainless-steel fiber (28, 40, and 100%) was used. Textile-based electrodes, containing 28 and 40 percentage of stainless steel fiber were knitted using single jersey Falmace circular knitting machine. However, textile-based electrodes with 100 % conductivity were swan by hand.

Results showed that the ECG signals collected using textile electrodes had a comparable waveform and accuracy to those acquired using Ag/AgCl electrodes. The results show that 100% textile-based electrodes performed well throughout the 4 mentioned status as it has the highest conductivity, however 40 and 28% electrodes performed well during sitting and laughing and had noisy signal in walking and jumping. Therefore, according to the result increasing the conductivity will lead to improved electrode performance and better signal recording. Furthermore, Ag/AgCl electrodes performed well during all status as the ECG signal was observed clearly.

Key words:

Textile based ECG electrode; Vital signs; Ag/AgCl electrode; Wearable electronics;

1. Introduction

Cardiovascular diseases are the main cause of death, therefore continuous vital and behavioral sign monitoring of the patient would be necessary for preventive risk of death[1]. Electrocardiogram (ECG) is a bio potential signal [3]. Nowadays, a new generation of long-term monitoring devices based on the smart textile area is become increasingly widespread which enables the detection of electrical ECG

signals, for earlier detection of heart malfunctioning[4,8]. Textile electrodes are particularly suitable for some long-term ECG monitoring, low weight, and high elasticity for users, soft, flexible, reusable and allowing the wearer to feel more comfortable than Ag/AgCl electrodes[7]. Previuos studies have been done on textile electrodes which are prepared with different methods such as using conductive yarns which include stainless steel fibers and silver printed from knitted cotton and polyester fabric for ECG monitoring [5,6].

Boehm et al developed a garment with the aim og long term ECG monitoring. Ten textile patches with the size of (4 cm × 4 cm)were made using conductive fabric from Shieldex company as textile electrodes and then were sewn into the garment [2].

Weder et al. developed embroidered textile electrode through polyethylene terephthalate yarnwhich is plasma coated with silver in order to monitor ECG countinously [9].

Xiao et al. produced 4 conductive weave electrodes in plain and honeycomb weave patterns. All the electrodes were sewn into the belt in order to monitor ECG signals. Then the signals were compared with the Ag/AgCl electrodes [10].

The purpose of this work is to assess the usefulness of textile-based electrodes for ECG recording in different daily condition as a smart garment, present the performance of textile electrodes and considering the conductivity of the yarn used to produce textile electrodes and comparing the performance of textile electrodes with Ag/AgCl electrodes.

2. Experimental

2.1. Materials

In this study, we developed textile-based electrodes (7cmx7cm) with conductive yarns containing 3 percentages of stailess steal fiber of spun yarn. We also used 5 channel electronic board and ECG leads. Conductive yarns containing 28 and 40% stainless steel fibers were used to knit electrodes using Falmac single jersey circuar machine with 24 gauge. However, textile electrodes which include 100 % stailess steel fibers were swan by hand. The surface resistance of prepared electrodes containing differrent percentage of conductive fiber in yarn structure i.e. 28,40 and 100 percentage of stainless steel fiber was 146.3(Ω⁄square), 77.2(Ω⁄square) and 4.21(Ω⁄square), respectivly. Moreover,in this study, Ag/AgCl electrodes were used in order to asses the performance of the textile electrodes. Figure 1 illustrate the produced textile-based electrodes.

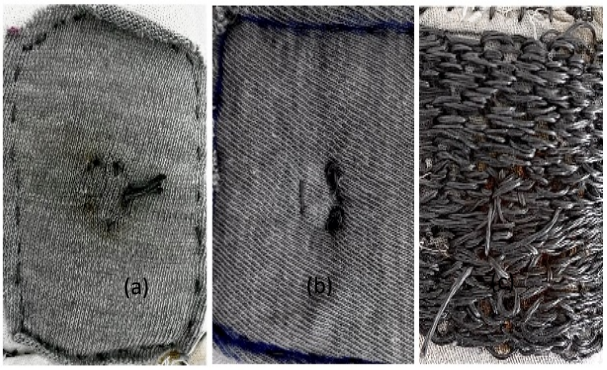

Figure 1.The textile-based electrodes prepared by (a) conductive yarns with 28% stainless steel fiber, (b) 40% stainless steel fiber, (c) 100% stainless steel fibers

2.2. Methods

To record ECG signals during running, seating, jumping, and walking in 5 valentiers, Ag/AgCl and textile-based electrodes were placed on the valentier`s body accordig to the Figure2.The experiment for each test of every valentier took one minute.

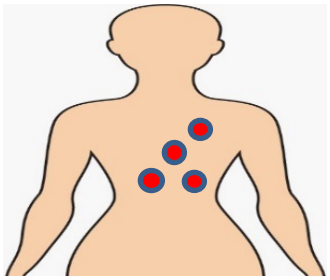

Figure 2. Position of electrodes

3. Results and discussion

In our experiments we compared ECG signals which obtained using Ag/AgCl and textile-based electrodes during 4 mentioned statuses and the electrical properties of the textile electrodes were studied as well.

3.1. Sitting

An example of the signal obtained using two types of electrodes while the user was sitting, is shown in Fig 3. As it can be observed, all electrodes performed well and showed clear R-peaks. According to the all Figures of the recorded signals, the shown A,B,C,D traces are related to the textile electrodes contain 100 %,40% , 28% satinless steel fibers and Ag/AgCl electrodes respectively.

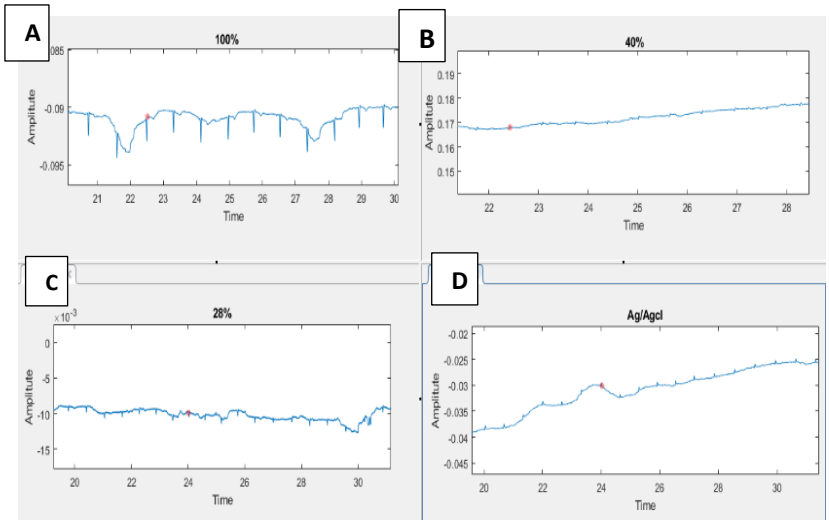

Figure 3. Different ECG traces in sitting position.

3.2. Laughing

As it can be seen in Figure4 all textile electrodes showed relatively better signal quality compared to Ag/AgCl electrode. There is clear difference in the quality of waveform between the signals collected from 100% and Ag/AgCl electrodes.

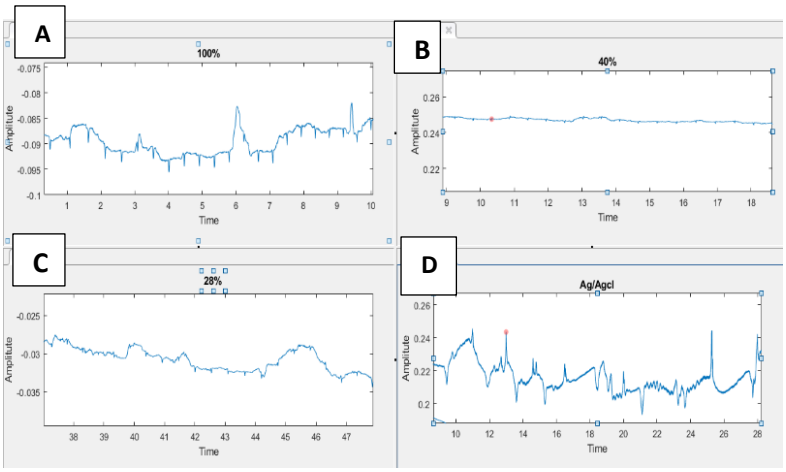

Figure 4. Different ECG traces while laughing,(a)28% conductive yarn

3.3. Walking

As it can be seen in Figure5, the quality of the textile electrodes signal decreased while jumping. The signal to noise ratio (SAR) was larger in the 100% textile electrodes than the Ag/AgCl electrodes. Signals acquired using the 28%textile electrodes were not clear enough.while , 40% electrodes had better signal quality while.

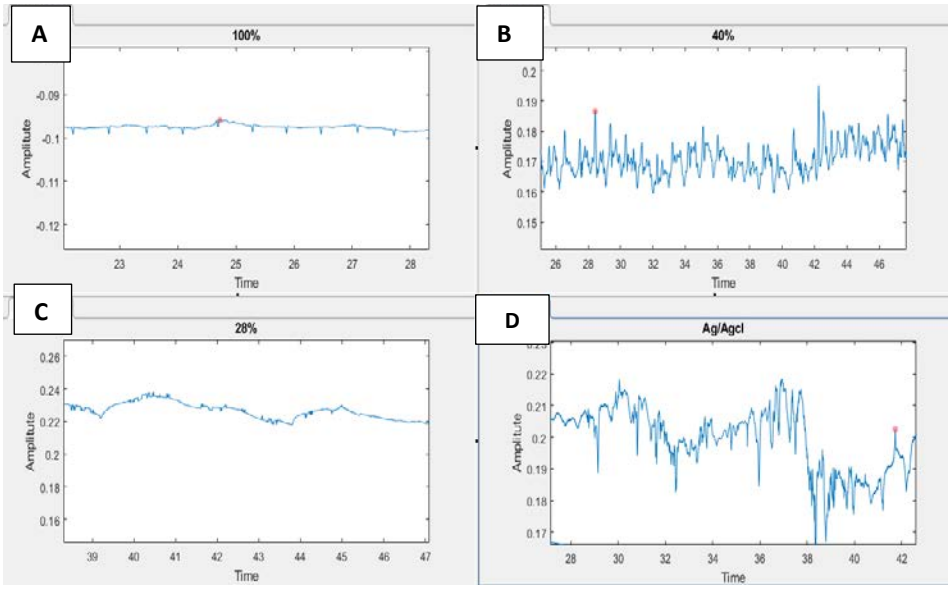

Figure 5.ECG traces while walking

3.4. Jumping

Figure 6 depict the recorded signal while jumping. As we can understand from the signals, Ag/AgCl electrodes had better signal qulity rather than 100% electrodes while jumping and it is due to the better connecting with the body. 100% electrodes showed the ECG signal but not as well as Ag/AgCl electrodes during jumping. 28% electrode didnt show any clear signal. However, R wave of the signal from 40% electrodes is visible in the recorded signal.

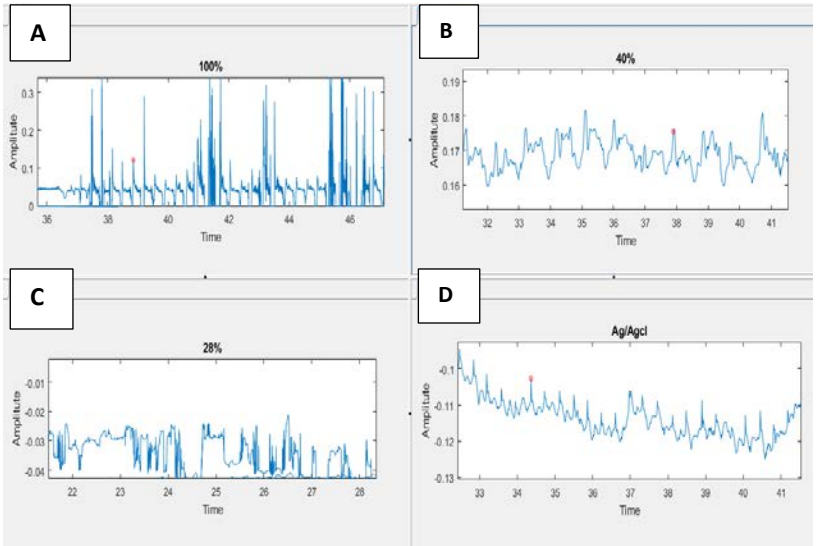

Figure 6.ECG traces while jumping

4. CONCLUSIONS

In this study the prepared textile electrodes could enable applications extending even beyond the clinical area. During the test no skin irritation was seen. The prepared textile-based electrodes showed very good performance for ECG monitoring which is very beneficial for both home and telemonitoring. Compare to Ag/AgCl electrodes prepared textile electrodes are washable and reusable. According to the results 100% stainless steel fibers electrodes performed well throughout the 4 mentioned status as it had the highest conductivity and comparable results with Ag/AgCl electrodes not only in the laughing and sitting but also during walking statuses, however 28% and 40% stainless steel electrodes had acceptable efficiency during sitting and laughing and had noisy signal in walking and jumping. Therefore, increasing the conductivity will lead to improved electrode performance and better signal quality. There are several main factors which can affect the result and the recorded ECG signal while using textile-based electrodes. The most important factor is the skin impedance impact and also other ambient noises.

References

1. *Acar, G., Ozturk, O., Golparvar, A. J., Elboshra, T. A., Böhringer, K., & Yapici, M. K. (2019). Wearable and flexible textile electrodes for biopotential signal monitoring: A review. Electronics, 8(5), 479*
2. *Boehm, A., Yu, X., Neu, W., Leonhardt, S., & Teichmann, D. (2016). A novel 12-lead ECG T-shirt with active electrodes. Electronics, 5(4), 75.*
3. *Gruetzmann, A., Hansen, S., & Müller, J. (2007). Novel dry electrodes for ECG monitoring. Physiological measurement, 28(11), 1375.*
4. *Lee, S. H., Jung, S. M., Lee, C. K., Jeong, K. S., Cho, G., & Yoo, S. K. (2009, July). Wearable ECG monitoring system using conductive fabrics and active electrodes. In International Conference on Human-Computer Interaction (pp. 778-783). Springer, Berlin, Heidelberg.*
5. *Nigusse, A. B., Malengier, B., Mengistie, D. A., Tseghai, G. B., & Van Langenhove, L. (2020). Development of washable silver printed textile electrodes for long-term ECG monitoring. Sensors, 20(21), 6233.*

6. *Rattfält, L., Lindén, M., Hult, P., Berglin, L., & Ask, P. (2007). Electrical characteristics of conductive yarns and textile electrodes for medical applications. Medical & biological engineering & computing, 45(12), 1251-1257.*
7. *Scilingo, E. P., Gemignani, A., Paradiso, R., Taccini, N., Ghelarducci, B., & De Rossi, D. (2005). Performance evaluation of sensing fabrics for monitoring physiological and biomechanical variables. IEEE Transactions on information technology in biomedicine, 9(3), 345-352.*
8. *Tsukada, Y. T., Tokita, M., Murata, H., Hirasawa, Y., Yodogawa, K., Iwasaki, Y. K., ... & Tsukada, S. (2019). Validation of wearable textile electrodes for ECG monitoring. Heart and vessels, 34(7), 1203-121*
9. *Weder, M., Hegemann, D., Amberg, M., Hess, M., Boesel, L. F., Abächerli, R., ... & Rossi, R. M. (2015). Embroidered electrode with silver/titanium coating for long-term ECG monitoring. Sensors, 15(1), 1750-1759.*
10. *Xiao, X., Pirbhulal, S., Dong, K., Wu, W., & Mei, X. (2017). Performance evaluation of plain weave and honeycomb weave electrodes for human ECG monitoring. Journal of Sensors, 2017.*

APPROACH TO THE VISIBILITY INCREASING OF PEOPLE IN ROAD TRAFFIC AT NIGHT

Antonín Havelka[1], Katarina Zelova[1], Viera Glombikova[1], Petra Komarkova[1], Michal Vik[2], Miroslav Tichy[3], Marie Pilikova[3], Marie Vrbova[3]

[1] Technical University of Liberec, Faculty of Textile Engineering, Department of Clothing, Studentská 2, 461 17 Liberec 1, The Czech Republic, Telephone: +420485353390, katarina.zelova@tul.cz

[2] Technical University of Liberec, Faculty of Textile Engineering, Department of Material Engineering, Studentská 2, 461 17 Liberec 1, The Czech Republic,

[3] VÚB a. s., Na Ostrově 1165, 562 01 Ústí nad Orlicí

Abstract:

This paper is focused on the visibility increasing of professional driver's clothing. Passive and active elements were applied to ten clothing, especially polo shirts. A combination of photoluminescent, retroreflective elements and LED light was used in different types of topology and with respect to the principle of biomotion. Moreover, new photoluminescent knitted fabrics were developed in cooperation with the company VÚB, a.s. The high visibility of mentioned fabrics significantly increases the safety of road users, especially under conditions without a light source. In summary, the suggested polo shirt models show high visibility, a high level of physiological comfort, and meet standard ČSN EN ISO 20471 (83 2820).

Key words:

visibility, photoluminescence, retroreflection, knitted fabric

1. Introduction

Reduced visibility is a mutual cause of many tragic road traffic accidents. Pedestrians and cyclists are the weakest participants in road traffic and the most vulnerable ones.[1] At dawn and night, pedestrians are more at risk than in full sunlight. Research has suggested that pedestrians' apparel and poor visibility are likely to contribute to these accidents significantly.[2] European Commission statistics present that vulnerable road users (pedestrians, cyclists and powered two-wheelers) account for 70% of road deaths in urban areas.[3] In 2019, pedestrians in the Czech Republic were involved in a traffic accidents in 3,265 cases (of which 87 people were killed, 427 were seriously hurt, and 2,687 were slightly injured). In the case of the participation of cyclists, there were 4,034 traffic accidents, with 3,594 seriously and slightly injured and 35 people killed.[4] It has been observed that these tragedies most often occur at night.[4] In the case of passive elements, visibility can be increased by a suitable colour of clothing and accessories made of fluorescent, phosphorescent and reflective materials, increasing the light contrast to the background and extending the distance in which a driver can see a pedestrian or a cyclist.[1]. Further, there are LED elements within sophisticated clothes that support visibility in the dark when light from some light sources is missing. Expert studies often solve biomotion to increase the visibility of pedestrians and cyclists at night. Reflective markings on a pedestrian's major joints to facilitate biological motion perception has been proven to significantly enhance pedestrian conspicuity at night. Ankle and knee markings are a simple and very effective way of

strengthening bicyclist conspicuity at night.[5] [7] It has been concluded that adding retroreflective strips in the biomotion configuration can significantly improve road worker conspicuity regardless of the road worker's orientation and the driver's age.[6]

The research in this paper is focused on application possibilities of passive (retroreflective, photoluminescent) and active elements (LED) to support the high visibility of professional workers, especially drivers, to protect them within the public transport.

2. Experimental

2.1. Materials

Polo shirts for professional drivers were tested in this study. These polo shirts were made of newly developed knitted fabrics, two of which prove high physiological comfort and three are equipped with photoluminescent properties. Knitted fabrics VX3 and VX9 achieved the best values of breathability (R), vapour resistance (Ret) and thermal resistance (Rct) according to the TNI standard CEN / TR 16422 Classification of thermoregulatory properties, See Table 1.

Table 1. Basic parameters of knitted fabric

	Materials	Weave	Weight [$g.m^{-2}$]	Rct [$m^2.K.W^{-1}$]	Ret [$m^2.Pa.W^{-1}$]	R [$mm.s^{-1}$]
VX3	52 % Micromodal 13 % Viscose Crabyon 35 % Polypropylene Ag+	interlock double-faced	183	0.042	4.087	43
VX9	face: 52 % Micromodal 13 % Viscose Crabyon back: 35 % Polypropylen Body fresh	double piqué	199	0.032	3.660	70

Photoluminescent knitted fabrics Lum 1, and Lum 2 are single-faced plated knitted fabrics. One row of a polyester luminescent multifilament with a fineness of 167 dtex, f36 and one row of spin viscose fibres (blend of micromodal fibres plus Crabyon fibres contained chitosan). See Table 2. Luminescent knitwear Lum 1 is white, and Lum 2 is green. See Figure 1.

The photoluminescent knitted fabric Lum 3 is a single-faced plated knitted fabric. 1 cm wide stripes are combined (alternating) in the knitted pattern, namely polyester luminescent multifilament (green colour) with a fineness of 167 dtex, f36 and spin viscose fibres (blend of micromodal fibres plus Crabyon fibres contained chitosan). See Fig. 2.

Table 2. Characteristik of photoluminescent knitted fabric

	Materials	Weave	Density [dm^{-1}]		Weight [$g.m^{-2}$]	Thickness [mm]
			courses	wales		
Lum 1	50 % PES lum, multifil / 50 % MicroModal Viscose Crabyon, 1/1, lum - white color	single face plated knit	130	220	246	0.68
Lum 2	50 % PES lum, multifil / 50 % MicroModal Viscose Crabyon, 1/1, lum - green color	single face plated knit	130	220	213	0.60
Lum 3	50 % PES lum, multifil / 50 % MicroModal Viscose Crabyon,1cm/1cm, lum - green color	single face plated knit	130	220	236	0.65

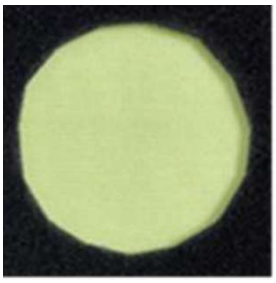
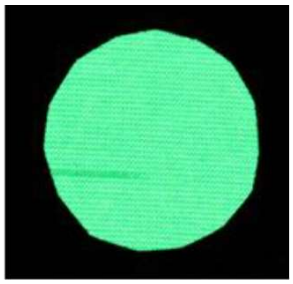

Figure 1. Photoluminescent knitted fabric Lum 2


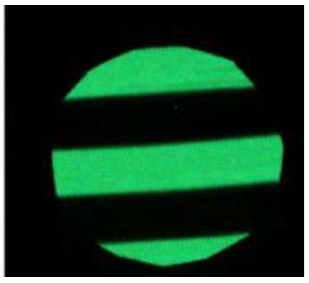

Figure 2. Photoluminescent knitted fabric Lum 3

Passive and active elements increasing visibility were used to make a polo shirt for a professional driver such as:

- retroreflective hatched strip, 5 cm wide, value of Reflectivity: 300cd / lx / m², see Figure 3
- photoluminescent iron-on transfers, 0.2 mm thick, see Figure 4
- photoluminescent sewing thread, two-fold (2 x 220 dtex / f24 PESh luminis), with a fineness of 51 tex; this thread was used as a cover thread for a stitch of class 604, see Figure 5
- 12 pieces of micro LEDs

Figure 3. Segmented reflective heat transfer vinyl

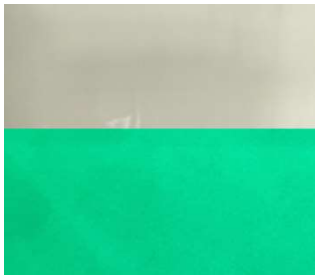

Figure 4. Heat transfer photoluminescent foils

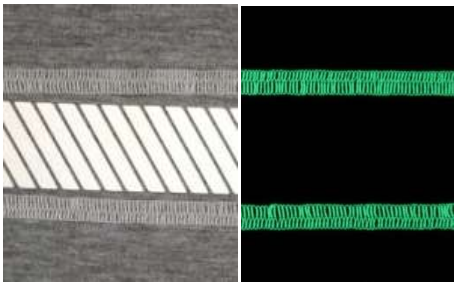

Figure 5. Photoluminescent sewing thread cover-seam chain stitches 604

2.2. Methods

The design of the topology of retroreflective elements on polo shirts for professional drivers was based on the standard ČSN EN ISO 20471 (83 2820) [8], Clothing with high visibility - Test methods and requirements from 2013. In the Czech Republic, there are recommendations for clothing classes according to the minimum area of conspicuous materials; for professional drivers - class 1, for work on existing roads (repairs, maintenance) - class 3, for work on utilities - class 3, surveying and work on new roads - class 2, etc.

The proposed variants of polo shirts for professional drivers meet the requirements of class 1, namely: the minimum required area of the visible (conspicuous) base material is 0.14 m², and the area of retroreflective material is 0.10 m², and the area of material with combined properties is 0.20 m². At least 50% of the minimum area of the visible (conspicuous) base material is (and must be according to the standard) on the front of the garment. Factors related to the risk of clothing for class 1 are described in Table 3.

Table 3. Factors related to the risk level for a professional driver

Risk level	Factors related to the risk level		Risk level	
	Vehicle speed	Type of road user		
High risk ISO20471 class1	≤ 30km/h	passive	High visibility	- day and night visibility - 360° (visibility from all sides) - design for form recognition - quantity and quality for day and night

No standard applies to the placement of post-luminescent elements. However, the rules applicable to retroreflective materials were respected when designing a photoluminescent film topology (1 cm, 2 cm strip width) and luminescent cover stitch.

The use of retroreflective and luminescent elements on clothing was evaluated in natural conditions in the dark. Visibility was assessed at distances of 50 m, 100 m, 150 m and 200 m.

3. Results and discussion

The designs of the topology of passive and active elements for men's polo shirts differed both in the location of the elements and in their area. Retroreflective stripes were placed in both the horizontal and vertical planes, in the chest area, or below the waist. Vertically positioned elements provide the advantage of user visibility also in the forward bend. The retroreflective stripes are bounded by strips of photoluminescent foil (1 cm and 2 cm) and a photoluminescent cover stitch. The length / the area of retroreflective and photoluminescent materials used for each polo shirt design is given in Table 4.

Table 4. Material usage of both passive and active elements for driver's polo shirt - size L

Design	Passive elements				Active elements
	Retroreflective elements		Luminescent elements		LEDs
	Length [m]	Area [m^2]	Length [m]	Area [m^2]	Quantity [pieces]
Design 1	3,04	0.152	3.04	0.030	X
Design 2	3.04	0.152	58.4 m cover thread	0.036	X
Design 3	1.96	0.098	3.84	0.076	X
Design 4	3.12	0.156	3.12	0.031	X
Design 5	1.12	0.029	1.12	0.011	X
Design 6	3.04	0.152	-	0.428	X
Design 7	1.96	0.098	-	0.303	X
Design 8	3.04	0.152	3.04	0.030	12

The combination of three mutually supportive mechanisms has increased driver visibility: passive retroreflective elements, luminescent surfaces, and active LED elements. A suitable topology of retroreflective and luminescent materials can be seen on the realized prototypes of a men's polo shirt for a professional driver (Figure 6). It is advisable to place the photoluminescent tape next to the retroreflective tape (Designs 1, 3, 4, 5). Similarly, it is advisable to sew a covering stitch with luminescent thread along the edge of the retroreflective tape (Design 2).

The clothing mentioned above for drivers meets the ČSN EN ISO 20471 (83 2820) [8] standard for retroreflective material and, in addition, with the use of luminescent material and LEDs, they also exceed safety. The visibility of this clothing in the dark due to LEDs is ≥ 200m. The clothing is seen even under conditions without a car light source or headlight due to the use of luminescent material.

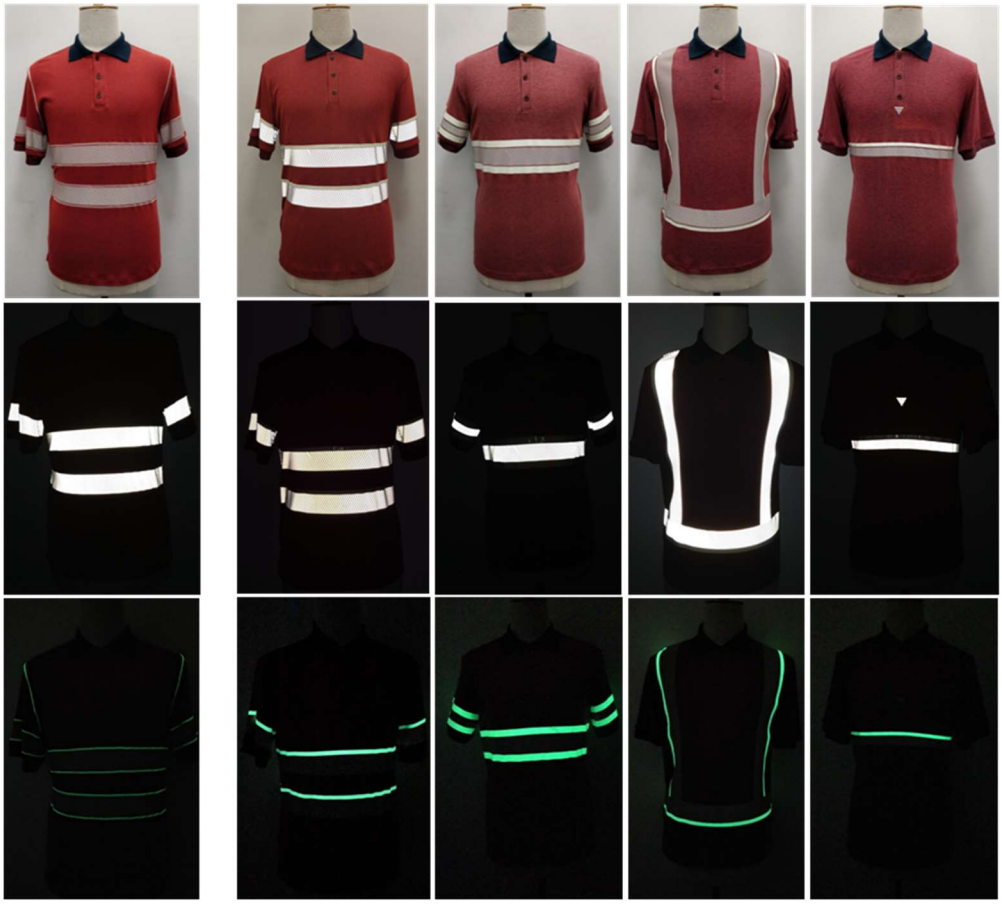

Figure 6. Topology of retroreflective and photoluminescent elements on clothing

Figure 7 (designs 6 and 7) shows the possibilities of applying the developed photoluminescent knitted fabrics Lum 1, Lum 2 and Lum 3 in garment parts such as sleeves, collar, yoke, cuffs and pocket. It is also possible to use these photoluminescent knitted fabrics to produce the whole garment.

The design of the 9 polo shirt combines retroreflective and photoluminescent stripes, as well as elements of active signalling. Micro LEDs were implemented in the retroreflective strip and located on the polo shirt's front and back. The electronic unit is located in the pocket, in the side seams of the polo shirt. It is advisable to attach the electronic unit to the trouser strap while wearing the garment.

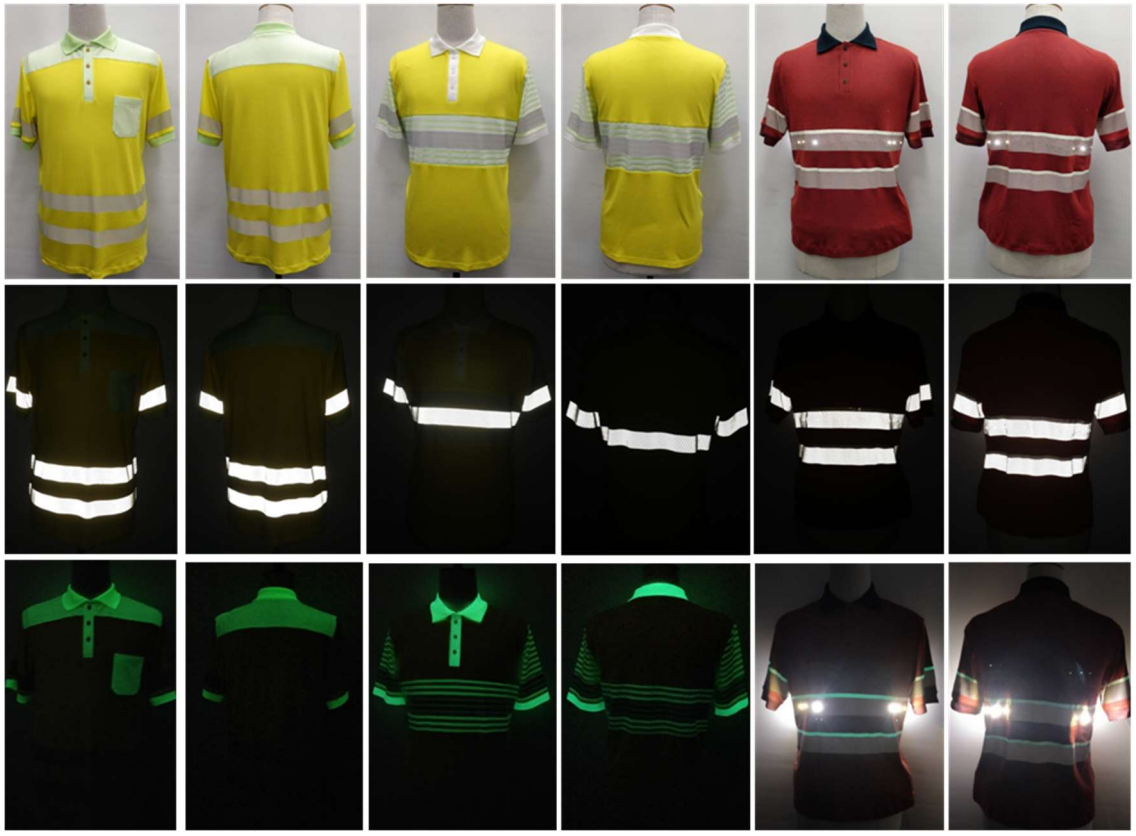

Figure 7. Polo shirt for a professional driver with photoluminescent knitted fabrics and LEDs

The use of developed photoluminescent knitwear with physiological comfort also offers several other uses in areas where it is necessary to increase safety, such as children's clothing, hats, sportswear and accessories, backpacks, etc. (Figure 8).

Figure 8. Other possibilities of using the developer photoluminescent knitted fabrics

Using suitable reflective materials can increase visibility with reduced visibility or in the dark. These elements reflect the light to the source, and the object is sufficiently visible after illumination (for example, car headlights) up to 200 meters, see Figure 9. This distance is sufficient for the driver to analyze and react to the dangerous situation correctly. As the picture shows, a suitable topology and the demarcation of the human body shape make a person more visible on the road. It is suitable to place the elements on the upper limbs and retroreflective stripes in the vertical direction.

It can be seen from the real experiment that in the case of using a photoluminescent iron-on foil, the luminescent elements were sufficiently visible at 200 m. In the case of a photoluminescent cover stitch, it was a distance of up to 50 m.

Figure 9. Visibility of retroreflective and luminescent elements for a night under conditions a car light source for distances from 25m up to 200m [9]

4. CONCLUSIONS

In conclusion, it can be stated that photoluminescent materials appear to be a suitable security element. These materials do not need a power supply or light source from the car headlight. After drawing on the energy they absorb, the elements have a long light emission ability. The emission then begins to fade until it finally goes out completely. Depending on the specific material, this process takes a few minutes to hours. Then it is necessary to re-expose the photoluminescent materials to the energy source. However, the photoluminescent materials again charge and emit light when passing through a place with a light source. It is, therefore, necessary to choose the correct location and amount of these materials and elements when used on clothing. A combination of retroreflective and photoluminescent materials can be recommended. The photoluminescent knitted fabrics show new possibilities for increasing road traffic and transport safety.

ACKNOWLEDGEMENTS

The authors acknowledge with thanks the funding support by the Ministry of Industry and Trade Czech Republic (MPO ČR), Project No. FV40323.

References

1. *Haskova, E., (2020). Viditelnost na silnicích. Policie České republiky. Retriewed 2/12/2021. Web site: https://www.policie.cz/clanek/uzemni-odbor-praha-venkov-vychod-zpravodajstvi-viditelnost-na-silnicich.aspx*
2. *Lin, S., (2019). Reflective Light Sport Suit. International Textile and Apparel Association Annual Conference Proceedings, 76 (1), DOI: https://doi.org/10.31274/itaa.8461*
3. *De Keermsmaecker, S., Meder, S., 2020. 2019 road safety statistics: What is behind the figures? European Commission. Retriewed 1/15/2021. Web site: https://ec.europa.eu/commission/presscorner/detail/en/qanda_20_1004*
4. *Straka, J., Pelešková, J., 2020. Ročenka nehodovosti na pozemních komunikacích v České republice v roce 2019. Ředitelství služby dopravní policie Policejního prezidia České republiky. Retriewed 12/25/2020. Web site: https://www.policie.cz/clanek/statistika-nehodovosti-900835.aspx?q=Y2hudW09Mg%3d%3d*
5. *Wood, J.M., Tyrrell, R.A., Marszalek, R., Lacherez, P., Carberry, T.P., Chu, B.S., (2012). Using reflective clothing to enhance the conspicuity of bicyclists at night. Accident Analysis & Prevention, 45, 726-730*
6. *Wood, J.M., Marszalek, R., Lacherez, P., Tyrrell, R.A., 2014. Configuring retroreflective markings to enhance the night-time conspicuity of road workers. Accident Analysis & Prevention, 70, 209-214, DOI: 10.1016/j.aap.2014.03.018.*
7. *Balk, S.A., Graving, J.S., Chanko, R.G., Tyrrell, R.A., 2007. Effects of Retroreflector Placement on the Night-time Conspicuity of Pedestrians: An Open-Road Study. Proceedings of the human factors and ergonomics society 51st annual meeting, 51(24), 1565-1568. DOI: 10.1177/154193120705102411.*
8. *ČSN EN ISO 20471 (83 2820) - High visibility clothing – Test methods and requirements (2013).*
9. *Mejsnarová, K., (2021) Schopnost vyhasínání luminiscence fotoluminiscenčních šicích nití. Bakalářská práce, Technical University of Liberec.*

PREPARATION AND BASIC PROSPERITIES OF LAMINATED POLYURETHANE MEMBRANES

Sajida Perveen[1], Jakub Wiener[2], Tereza Šubrová[3]

[1]M.Sc. Sajida Perveen; Technical University of Liberec, Faculty of textile Studenská 2, Liberec 46117, Czech Republic, sajida.perveen@tul.cz
[2]prof. Ing. Jakub Wiener, Ph.D.; Technical University of Liberec, Faculty of textile Studenská 2, Liberec 46117, Czech Republic, jakub.wiener@tul.cz
[3]Ing. Tereza Šubrová; Technical University of Liberec, Faculty of textile Studenská 2, Liberec 46117, Czech Republic, tereza.subrova@tul.cz

Abstract:

Currently, polytetrafluoroethylene polymer is mainly used for clothing membranes, which is environmentally problematic and is currently restricted by legislation. An alternative are membranes based on polyurethane. In this study, a series of polyurethane-based membranes are prepared and these membranes are laminated to a conventional fiber substrate. The prepared membranes are extremely thin. The basic mechanical and comfort properties of the prepared laminates are quantified. The results are widely discussed with respect to the possible practical application of the prepared membranes for clothing purposes.

Key words:

Polyurethanes, laminated composites, polyurethanes membranes, membrane process, textile coatings, adhesives

1. Introduction

Polyurethanes are elastomeric, thermoplastic and thermoset in their behavior depending on their morphological chains. Relatively lightweight structures are becoming more and more necessary as resources and energy optimization needs rise. Polyurethanes potentially address this purpose via functioning as stretchable sealants or matrix components for composites [1]. The phenomenal growth of polyurethane into multiple applications is becoming a cause of new horizons in the world of today. Although the use of various polymers in nanofiber technologies is gaining popularity as a positive step toward protecting the environment, some polymers, such as polytetrafluorethylene, which is frequently used in textiles, are still not completely eco-friendly [2]. The unique concept can be strengthened by using different methods, such as polyurethane treatment of nanofiber membranes, to modify the characteristics and attain the desired adaptability. However, the concern of polyurethane is linked to number of fields including; building materials, elastic foams, bags, footwear, leather, rubber, paper and the most important in textiles like cotton, silk, wool etc. in their novel forms. The use of polymers in advanced technology is producing millions of incomes every year [3].

These broad-spectrum applications owe to good chemical and solvent resistance, specific flexibility, toughness, abrasion resistance, weathering and low temperature implementations of polyurethanes which makes it a best suitable candidate for incorporating it into the novel ideas [4]. Polyurethanes laminates are good than vinyl laminates because of many reasons. There are many technical or aesthetic reasons which make polyurethanes characteristics important like the need of producing soft and even more flexible laminates beyond plasticizers. So, no need of extra cost of using any oils or the

fear to get them washed away by the solvents or the problem of contamination of laminations when used with other materials like adhesives [5] or sometimes leathers, resultantly it gives dry and clean polyurethanes laminated membranes [6].

On the other hand, polyurethanes composites as compeered to those of other polymers like PVC (textiles, stiffer and more uncomfortable) are more resistant to low temperatures and gives a soothing feel even in winters. Another property makes it an excellent application in textiles and footwear and upholstery is less cracking at low temperatures [7], [8].

Polyurethanes laminates are very thin layered [12], low weight and resistant to abrasion. Laminated polyurethanes are permeable to water vapors [13] but to achieve this they are tailor made through specified structural techniques. For the reason of polyurethanes being tailormade in nature they are employed in a number of immerging novel ideas with desirable technical and useful properties. They offer immensely dynamic as well as ecological professionals for the contemporary challenges that community is coping with, several of them pose particular requirements on materials [2].

2. Experimentation

The polyurethanes copolymer in order to make their laminates was prepared by using different monomers with different mole ratios. The present paper work was designed to synthesize laminated polyurethanes copolymers using polycaprolactone and methylen bis 4-cyclohexyldiisocyanate with different nanofibers. The resultant copolymer samples were characterized by sophisticated techniques like, FT-IR and the samples were applied to fabrics and tested for their different characteristics which included, tensile strength.

2.1 Materials

Methylene bis(4-cyclohexyldiisocyante) (H_{12}MDI), Polycaprolactone CAPA2200A (Mn=2000g/mol), Propanediol, Nano fiber membrane materials were used in this work.

2.2 Monomers

2.2.1 Isocyanates

Diisocyanates includes aromatic, aliphatic and cycloaliphatic diisocyanates, they have ben used for various polymeric synthesis. Among these diisocyanates the aromatic diisocyanates are very reactive and show much excellant properties as compared to the aliphatic and cycloaliphatic diisocyanates. Methylene bis (4-cyclohexyldiisocyanate) (H_{12}MDI) is very important diisocyanate used for synthesis of polyurethane elastomers [14] and other applications. Such type of H_{12}MDI based polyurethane produts show good thermal, biodegradable [15] and tensil strength properties. These polyuretane materials have been reported to be excellant biomaterials used in various engineering and animation purposes [8], [16].

2.2.2 Polyol

Polycaprolactone CAPA2200A (Mn=2000g/mol) of analytical grade used in the formulation, it imparts less rigidity and flexibility to the final product because of its low molecular weight. They imparts good hydrolytic stability to the products. When it is reacted with isocyanate chain extender they roduce thermoplastc polyurethanes [8].

3. Methodology

3.2 Synthesis of polyurethane prepolymer

The main reaction involved in the preparation of laminated polyurethanes is the reaction of isocyante with the OH bearing polyols which furnishes urethane. It is basically an exothermic reaction. Polyols are the major portion of polymer molecules. The synthesis of PU prepolymers was carried out according to a recommended procedure [8]. Following the procedurer diisocyanate was reacted with macrodiol (3:1) to obtain isocyanate terminated polyurethane prepolymers. For this purpose into a four-necked reaction kettle equipped with mechanical stirrer, heating oil bath, reflux condenser, dropping funnel and N_2 inlet and outlet polyol will be placed. The temperature of the oil bath will be increased to 60°C. Then

diisocyanate will be added and the temperature will then be increased to 60-70°C. It will almost take 1.0 hours to obtain NCO terminated PU prepolymer. The NCO contents in the PU prepolymer will be determined by titration with n-butylamine following ASTM D 2572-80 [ASTM, 2004].

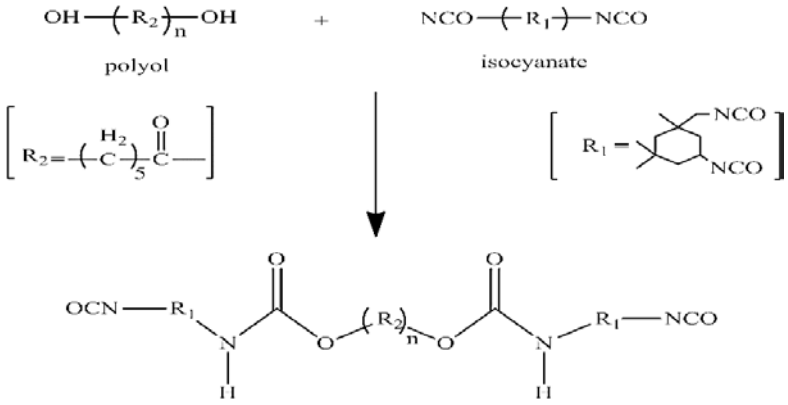

Scheme 1. Synthesis of NCO terminated PU prepolymer

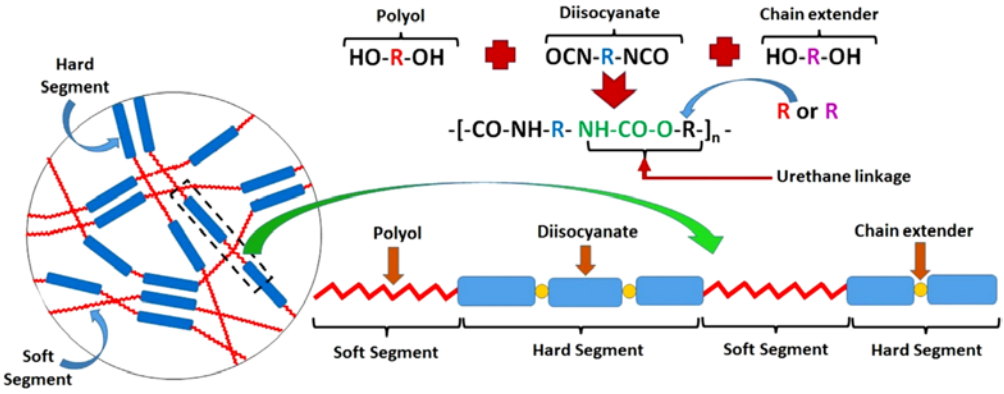

Figure 1. Schemaic diagram of overall reaction showing soft and hard segments [8]

The present figure making the formatin of PU more clear and its structure with the blocks soft and hard portions, while “R” denotes the variable chemical in order to get variety in the nature of polyurethanes. Branching or cross linking developed in polyurethanes depending on the starting cemicals which may have three or more number of functional groups in them [17]. Polyurtehanes are called tailor made polymers but the proper selection of di or polyol an di or polyisocyantes alongwith the chain extender is necessary for this. Aromatc isocyanates are more reactive than aliphatic or cycloalphatic diisocyanates. It depends on the selection of diisocantes that which diisocyantes has been used in the reaction it will imparts the same properties to the fnal product depending on its nature [8].

3.3 Copolymerization

For the preparation of the laminated polyurethane, the last step was to introduce the layer of PU to membrane. In order to meet the set requirements for target applications, the structure property relationship of polyurethanes is very important. The nature of other reactive factors must have to be in count while deciding the morphology [18], structure and properties of laminations, films or coatings. It can basically be figured out by the selection of raw materials, reaction conditions and stochiometric ratios [19].

3.4 Lamination process

After synthesizing polyurethanes copolymer, they are further introduced the reaction media for which they have to be prepared. This process is simple but its practical application is quite complicated. The

main process involves the spreading of prepared polymer onto the target space with an even speed so that it must be free from any kind of blisters or rough surface. One of the main factors defining the fineness of laminating surface is the pressure applied during the application of laminating nip, it is quite critical and can determine the final properties of product. Another factor to keep in check is the solvent media which must be carefully selected so that it cannot produce any wrinkle or crease on the finished surface [20] [21].

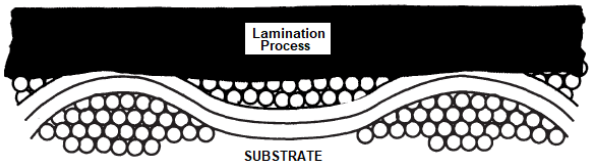

Figure 2. Cross section of coated/laminated surface

Laminated surfaces have some major advantages over the non-laminated ones especially with polyurethanes; they can show more tensile strength, tear resistance, they can give better liquid or gas resistance characteristics with more flexibility and non-affinity of most of other chemicals so that it can remain intact for longer times [20].

3.5 Factors defining the morphology of laminated polyurethane membranes

1 Molecular weight and chemical makeup of the basic ingredients
2 Ratio of hard to soft segments [22]
3 Crystallinity
4 Cross-linking intensity
5 Proprties of the surface
6 Glass transition temperature (Tg)

4. Applications of laminated Polyurethanes membranes

Polyurehtanes laminated membranes are employed in various types of applications including gas barier films and coatings, in platelet-shaped fillers in polyurhetane matrix, in permeability of small gas molecules [23], in textiles for ecological and bioegradable applicaions [24]. Polyurethane laminates are used in as envelop in lighter than air (For example, hot air baloons, airships and aerostat etc), automotive industry, textile industry [25], in biomedical applications membranes encapsulations [26], flame retadrdency, anticorrosion coatings and many more [27]–[29].

5. Result and discussion

5.1 Characteristics

5.1.1 Fourier Transform Infrared (FT-IR) spectroscopy

The FT-IR spectrum of H_{12}MDI (Fig. 3.1) produced a strong characteristic stretching vibration of –NCO at 2259 cm^{-1}. In the spectrum of H_{12}MDI other bands in functional group region of spectrum observed as asymmetric and symmetric stretching vibrations bands of CH_2 at 2929 cm^{-1} and 2853 cm^{-1}, correspondingly. While in the lower frequency region (Fig. 3.1) a strong narrow band at 1449 cm^{-1} (aliphatic CH bending vibration) and a less intense absorption at 1151 cm^{-1} (CH in CH_2, twisting vibration) have also been noticed. was assigned asymmetric, symmetric stretching vibrations bands of CH_2 at 2955 cm^{-1} and 2876 cm^{-1}[30], respectively during structural, composition study of the acrylic urethane latex films composite, such observations were also obtained in Figure 3.2. It was noticed a bending vibration of aliphatic CH groups at 1465 cm^{-1} and twisting vibration of CH in CH_2 groups at 1165 cm^{-1} in FT-IR analysis of the hyper-branched polyurethane acrylates [31].

The bands for polycaprolactone diol (CAPA 2000) (Fig: 3.2) were observed as: 3736 cm^{-1} (vibration of OH stretching): 2941 cm^{-1} (anti-symmetric –CH_2 stretching): 1724 cm^{-1} (C=O) stretching due to oxidation of C=C): 1465 cm^{-1} (C-O-H bending): 1365 cm^{-1} (OH-deformation out of plane): 1165 cm^{-1} (C-O and C-C stretching in the amorphous phase). It was assigned a broad band around 3400-3500 cm^{-1} to OH

groups of soft segments and at 1727 cm^{-1} to C=O groups in a structural study of polyurethane acrylate films by FT-IR technique [32]. In the reaction of –NCO groups of $H_{12}MDI$ with OH groups of PCL, –NCO terminated polyurethane prepolymer obtained at the first step of synthesis. The FT-IR spectrum of –NCO [33] terminated polyurethane prepolymer shown in (Fig: 3.3) which indicate a change i.e., vibrations for the OH-groups of PCL (Fig. 3.2) completely disappeared and intensity of isocyanate (–NCO) groups (Fig.3.3) decreased to some extent. Such changes suggest that OH groups of soft segments of PCL completely reacted with isocyanate (–NCO) groups of $H_{12}MDI$ and a vibration for newly synthesized –NH units emerged out at 3374 cm^{-1} with the increase of the intensity of C=O stretching vibration on the wavenumber of 1724 cm^{-1} confirming the synthesis of PU prepolymer. The disappearance of intense band at 2255 cm^{-1} (–NCO) and emergence of less intense band at 2258 cm^{-1} (–NCO) indicating that the –NCO group have a reaction with OH-groups of PCL but not completely, which provided the proof for the synthesis of isocyanate terminated PU prepolymer.

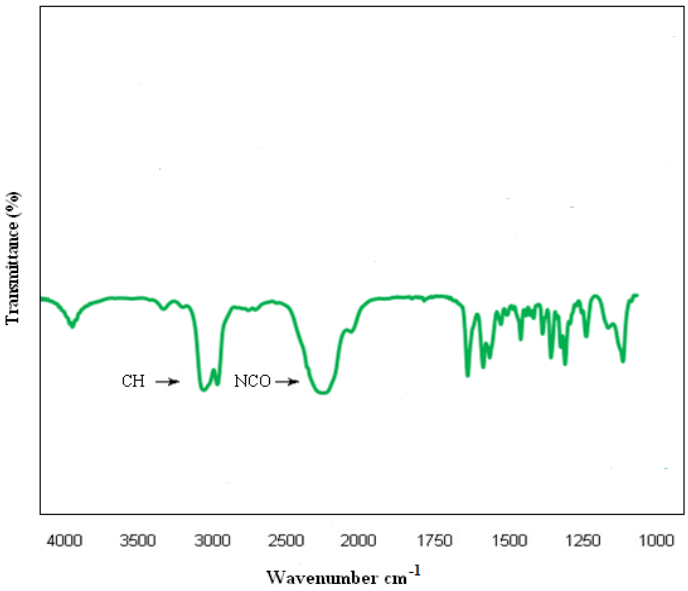

Figure 3.1. FTIR spectrum of $H_{12}MDI$

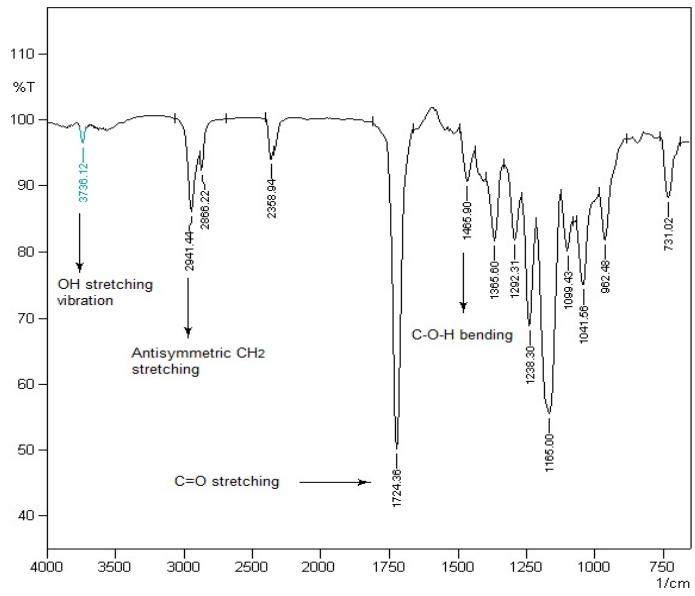

Figure 3.2. FTIR spectrum of CAPA 2000

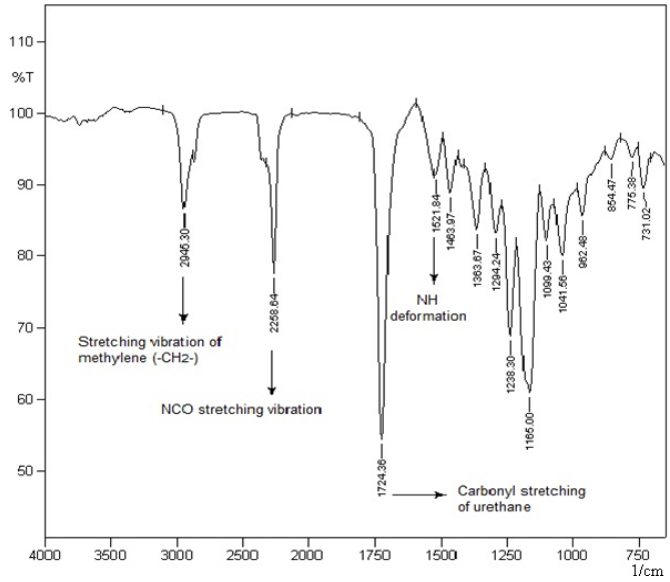

Figure 3.3. FTIR spectrum of NCO terminated polyurethane prepolymer

5.1.2 Textile performance

The prepared of polyurethane copolymer were applied to different fabrics in order to access and determine the performance of the copolymer mixture. The parameters of assessing its quality like tensile strength and TGA sorted out according AATCC8-2005.

5.1.3 Tensile strength

During this work, different thickness layers of prepared samples were tested on the different industrial fabrics. The sample size used “20” wide x “20” long. Table. 1 shows the enhancement of warp and weft wise tensile strength of various coated fabrics. This was noticed that in sample series of SPL2-12, SPL6-12 and SPL4-12 having low molecular weight of polycaprolacton improved the tensile strength warp and weft wise.

Table 1. Tensile Strength (warp side of fabric)

Sample Code	Strength of applied solution (g/L)	% Total elongation at maximum force	Load at maximum load (N)
SPL2-2	20	11.22	319.25
	30	12.6	284.31
	40	12.92	261.72
SPL4-2	20	13.76	330.46
	30	12.92	319.62
	40	11.65	287.79
SPL6-2	20	14.07	330.43
	30	13.62	327.88
	40	10.67	288.91
SPL8-2	20	14.89	309.52
	30	13.67	269.57
	40	15.22	259.41
SPL2-12	20	13.33	337.93
	30	13.73	329.22
	40	15.2	304.61
SPL4-12	20	14.77	317.22
	30	11.31	310.33
	40	10.97	298.85
SPL6-12	20	13.37	312.29
	30	12.89	306.10
	40	10.36	299.65
Untreated	0	05.89	108.56

This is because of the fact that smaller sized particles possess more penetration ability inside the fabrics more effectively. This is how the tensile strength is improved. Similarly, it was also examined that among these series the prominent importance goes to the solution at lower concentrations of polymer mixture because it is able to show better dispersibility and adhesion properties on the fabrics. In these series the fact is very clear that only at low concentration they withstand a high force which is expressed in Newton. However, at the high concentrations not only in these series but also in other series the trend of load bearing capacity of the fabric being laminated with polymer mixture show different behaviors. They withstand a load but not to the larger extent as that observed in the lower concentrations. On the contrary, using high concentration polymer mixture de-stability lowered and adhesion capacity also reduced so tensile strength reduced.

5.1.4 Thermogravimetric analysis

It was done a thermogravimetric analysis on a PerkinElmer TGA (model Pyris 1). The samples first heated up from room temperature to 700°C under nitrogen at a rate of 10°C/min [15].

5.1.5 Differential scanning calorimetry

Differential scanning calorimetry carried out on a Perkin Elmer differential scanning calorimetry. Aluminum pans with a perforated top served as containers for the samples [15]. The scans (-50-50°C) were conducted with nitrogen purging while being heated at a rate of 10°C/min. The midpoints of the regions of significant drop in the observed trends have been designated as the glass transition temperatures (Tg). In the subsequent scanning, the melting points have been determined as that of the peak maxima of the endothermic transition.

6. CONCLUSIONS

Polyurethane is the most versatile and suitable material for thousands of applications in all the fields of life because of their good mechanical properties. Polyurethane belongs to a family of block copolymers with soft segments based on polyether or polyester and hard segments from isocyanates and chain extenders. Polyurethane laminates produced by two component system with a variety of drape qualities as a final product can be made accessible with a selection of proper polyol, isocyanate type, and their quantities. Generally, one component system produces top skin allowing immediate release while two component system is used for laminate coats. In this way the crosslinking structures are capable to produce laminating coats but in case of polyurethanes some special requirements in the form of reaction conditions are required to produce laminating membranes. Polyurethane laminated membranes have also become the part of processes where a very large variety of separation is needed because they can separate the molecules ranging from large scale to a level where particles can actually be observed. Most often it is considered that polyurethane membranes are hydrophobic (make them able to be used in lightweight waterproofing) but they can be made hydrophilic with high selectivity of the molecules to be treated with. Moreover, they are acid, chemical and solvent resistant which make them more suitable to be employed in future prospects.

ACKNOWLEDGEMENTS

This work was supported by research project SGS-2022-6069 of Czech Ministry of Industry.

References

1. *N. M. Zain, E. N. Roslin, and S. Ahmad, "Preliminary study on bio-based polyurethane adhesive/aluminum laminated composites for automotive applications," Int. J. Adhes. Adhes., vol. 71, pp. 1–9, 2016,*
2. *K. Krishnan, "Hydrophilic urethanes for textiles," J. Coat. Fabr., vol. 23, pp. 54–66, 1993,*
3. *R. Jayakumar and S. Nanjundan, "Synthesis of zinc-containing poly(urethane-ether)s based on zinc salt of mono(hydroxypentyl)phthalate," Eur. Polym. J., vol. 41, no. 7, pp. 1623–1629, 2005,*
4. *L. Johnson and J. Samms, "Thermoplastic polyurethane technologies for the textile industry," J.*

Ind. Text., vol. 27, no. 1, pp. 48–62, 1997,

5. *C. Alia, J. M. Arenas, J. C. Suárez, and P. Pinilla, "Mechanical behavior of polyurethane adhesive joints used in laminated materials for marine structures," Ocean Eng., vol. 113, pp. 64–74, 2016,*
6. *J. Lin et al., "Synthesis and properties of epoxy-polyurethane/silica nanocomposites by a novel sol method and in-situ solution polymerization route," Appl. Surf. Sci., vol. 303, pp. 67–75, 2014,*
7. *A. C. Aznar, O. R. Pardini, and J. I. Amalvy, "Glossy topcoat exterior paint formulations using water-based polyurethane/acrylic hybrid binders," Prog. Org. Coatings, vol. 55, no. 1, pp. 43–49, 2006,*
8. *M. Joshi, B. Adak, and B. S. Butola, "Polyurethane nanocomposite based gas barrier films, membranes and coatings: A review on synthesis, characterization and potential applications," Prog. Mater. Sci., vol. 97, no. May, pp. 230–282, 2018.*
9. *F. J. Gasparrini, "Formulation requirements for urethane fabric coatings," J. Ind. Text., vol. 9, no. 3, pp. 195–209, 1980,*
10. *H. W. Engels et al., "Polyurethanes: Versatile materials and sustainable problem solvers for today's challenges," Angew. Chemie - Int. Ed., vol. 52, no. 36, pp. 9422–9441, 2013,*
11. *M. Ovsik, D. Manas, M. Manas, M. Stanek, and M. Reznicek, "The effect of cross-linking on nano-mechanical properties of polyamide," Key Eng. Mater., vol. 699, pp. 37–42, 2016,*
12. *M. S. Škoc, J. Macan, and E. Pezelj, "Modification of polyurethane-coated fabrics by sol-gel thin films," J. Appl. Polym. Sci., vol. 131, no. 4, pp. 1–13, 2014,*
13. *S. Mondal and J. L. Hu, "Water vapor permeability of cotton fabrics coated with shape memory polyurethane," Carbohydr. Polym., vol. 67, no. 3, pp. 282–287, 2007,*
14. *H. Honarkar, "Waterborne polyurethanes: A review," J. Dispers. Sci. Technol., vol. 39, no. 4, pp. 507–516, 2018,*
15. *C. L. Wu, S. H. Chiu, H. T. Lee, and M. C. Suen, "Synthesis and properties of biodegradable polycaprolactone/polyurethanes using fluoro chain extenders," Polym. Adv. Technol., vol. 27, no. 5, pp. 665–676, 2016,*
16. *J. David, L. Vojtová, K. Bednařík, J. Kučerík, M. Vávrová, and J. Jančář, "Development of novel environmental friendly polyurethane foams," Environ. Chem. Lett., vol. 8, no. 4, pp. 381–385, 2010,*
17. *Y. Qian, C. I. Lindsay, C. MacOsko, and A. Stein, "Synthesis and properties of vermiculite-reinforced polyurethane nanocomposites," ACS Appl. Mater. Interfaces, vol. 3, no. 9, pp. 3709–3717, 2011,*
18. *G. Shamini and K. Yusoh, "Gas Permeability Properties of Thermoplastic Polyurethane Modified Clay Nanocomposites," Int. J. Chem. Eng. Appl., vol. 5, no. 1, pp. 64–68, 2014,*
19. *K. Bagdi, K. Molnár, I. Sajó, and B. Pukánszky, "Specific interactions, structure and properties in segmented polyurethane elastomers," Express Polym. Lett., vol. 5, no. 5, pp. 417–427, 2011,*
20. *R.A.Scott, "Coated and laminated fabrics," in Chemistry of the Textiles Industry, Springer, Dordrecht, 1995, pp. 210–248.*
21. *E. Shim, Coating and laminating processes and techniques for textiles. Elsevier Ltd, 2018.*
22. *J. Foks and H. Janik, "Different Hard Segment Con tent," vol. 29, no. 2, pp. 113–119, 1989.*
23. *C. Giordano and N. Ishikawa, "High Moisture Permeability Polyurethane for Textile Applications," J. Ind. Text., vol. 23, no. 1, pp. 74–83, 1993,*
24. *A. Giwa, "The Applications of Membrane Operations in the Textile Industry: A Review," Br. J. Appl. Sci. Technol., vol. 2, no. 3, pp. 296–310, 2012,*
25. *B. Van der Bruggen, E. Curcio, and E. Drioli, "Process intensification in the textile industry: The role of membrane technology," J. Environ. Manage., vol. 73, no. 3, pp. 267–274, 2004,*
26. *F. Salaün, Microencapsulation technology for smart textile coatings. 2016.*
27. *J. N. Gavgani, H. Adelnia, and M. M. Gudarzi, "Intumescent flame retardant polyurethane/reduced graphene oxide composites with improved mechanical, thermal, and barrier properties," J. Mater. Sci., vol. 49, no. 1, pp. 243–254, 2014,*
28. *R. Xu, E. Manias, A. J. Snyder, and J. Runt, "Low permeability biomedical polyurethane nanocomposites," J. Biomed. Mater. Res. - Part A, vol. 64, no. 1, pp. 114–119, 2003,*
29. *U. Chatterjee, B. S. Butola, and M. Joshi, "Optimal designing of polyurethane-based*

nanocomposite system for aerostat envelope," J. Appl. Polym. Sci., vol. 133, no. 24, pp. 1–9, 2016,

30. *L. Wu, H. Yu, J. Yan, and B. You, "Structure and composition of the surface of urethane/acrylic composite latex films," Polym. Int., vol. 50, no. 12, pp. 1288–1293, 2001,*
31. *G. Xu and W. Shi, "Synthesis and characterization of hyperbranched polyurethane acrylates used as UV curable oligomers for coatings," Prog. Org. Coatings, vol. 52, no. 2, pp. 110–117, 2005,*
32. *F. Wang, J. Q. Hu, and W. P. Tu, "Study on microstructure of UV-curable polyurethane acrylate films," Prog. Org. Coatings, vol. 62, no. 3, pp. 245–250, 2008,*
33. *M. Choi et al., "Functionalized Polyurethane-Coated Fabric with High Breathability, Durability, Reusability, and Protection Ability," Adv. Funct. Mater., vol. 31, no. 24, pp. 1–9, 2021,*

EVALUATION OF CUT RESISTANCE OF COATED TEXTILE MATERIALS WITH INORGANIC FILLERS – PRELIMINARY STUDIES

Paulina Kropidłowska, Emilia Irzmańska

Central Institute for Labour Protection – National Research Insitute,
Department of Personal Protective Equipment, 48 Wierzbowa Street, Lodz, Poland,
pakro@ciop.lodz.pl, emirz@ciop.lodz.pl, +48 (42) 678 19 63

Abstract:

The purpose of the study was to compare the cut resistance of a polymer-coated material, whose properties were modified by fillers. In the study, calcium carbonate ($CaCO_3$) and silicon oxide (SiO_2) with size from 1 to 6 µm were used. Testing materials were made using knitted fabric, which were subsequently coated with latex, containing different variants of concentrations of inorganic fillers. The materials were assessed in terms of cut resistance using methods for evaluation of personal protective equipment and glove materials. Variants containing from 0.5 to 2.0 % fillers showed cut resistances ranging from 18.1 to 21.9 N, which placed them at performance level D. The highest cut resistance values were found for variants containing 2.5% silicon oxide. In the presented study it was found, that latex coating with incorporated fillers constituted a layer protecting the fibers against blade action, increasing cut resistance.

Key words:

coated textile materials, cut-resistant properties, inorganic fillers, calcium carbonate, silicon oxide

1. Introduction

Nowadays, development of a new solutions to ensure the high properties of the materials is observed [1]. The protective gloves are commonly used and mainly include knitted fabrics, non-woven fabrics, three-dimensional fabrics and composite fabrics [2-3]. To effectively prevent mechanical injury, protective gloves need to meet the requirements imposed by Regulation (EU) 2016/425 of the European Parliament. In terms of mechanical hazards, a particularly salient protective parameter is cut resistance [4]. Materials claimed to exhibit high cut resistance are tested pursuant to EN ISO 13997 [EN ISO 13997:1999], for the evaluation of lower cut-resistant materials, a method based on EN 388 is applied [5]. The literature indicates, that cut resistance depends, in particular, on the type and structure of the fibers [6], as well as on the use of polymeric materials to increase the mechanical resistance of textiles [7]. In order to increase the mechanical resistance of the materials, a polymer layers can be applied, such as polyvinyl chloride, polyurethane, silicone, nitrile rubber or natural rubber [8]. For this purpose, polymer coatings can be used in the form of continuous or dotted applications [8-9]. The physical and chemical properties of polymers may be modified by the introduction of fillers, whose size, shape, and chemical structure may significantly affect the process of creating structure, which translates into modified mechanical properties [4,10-11]. Fillers also influence the rheological properties of polymers, including viscosity, which also affects the strength properties of polymeric materials, as a result of filler-polymer surface interaction [12]. The size of the fillers used is important, as it can affect the strong cross-linking of the particles and lead to aggregation due to the large specific surface area and high free energy of the particle surface [13]. The most commonly used fillers are mainly calcium carbonate ($CaCO_3$) and silicon oxide (SiO_2) with an amorphous structure [14-15]. Calcium carbonate is used to improve mechanical properties, taking advantage of its compatibility with polymers due to uniform

dispersion on the polymer surface in the case of inorganic matrices [16]. Silicon oxide is widely used in the production of latex and associated materials. The superiority of silicon oxide over calcium carbonate is evident in terms of its effect on mechanical properties, particularly in terms of increased tear and abrasion resistance of material, containing SiO_2 fillers [12,17]. It should be emphasized that these types of materials were not evaluated for cut resistance. Due to novel applications that have not been fully recognized, it is important to evaluate the effectiveness of usage of inorganic fillers in the coating layer, to increase the protection against cutting of textile materials. Due to novel applications that have not been fully recognized, it is important to evaluate the effectiveness of using inorganic fillers, which affect strength properties, in the coating layer to enhance the anti-cutting properties of textile materials.

2. Experimental

2.1. Materials

The testing material were made using knitted fabric (Table 1.), which was subsequently coated with latex, containing different variants of concentrations of inorganic fillers (Fig. 1).

Textile carrier

The study materials was prepared using a textile carrier made of a knitted para-aramid fabric (S.I. ZGODA, Poland) with the following parameters (Table 1).

Table 1. Properties of the textile carrier (knitted para-aramid fabric)

Image of knitted para-aramid fabric	Metric count [Nm]	Pattern	Surface density [g/m2]	Thickness [mm]
	28/2	Plain-stitch	234.1	0.23

Coating of textile carrier

The coating layer was made of a latex (Thorex Sp. J., Poland) reinforced with various fillers concentration, from 0.5 to 2.5 % by weight. Fillers were combined with the polymeric material using a laboratory stirrer (1200 rpm). The textile carrier was placed in the designed experimental stand for the surface application of the resulting polymer paste. The paste was spread evenly by passing the trowel twice over the textile carrier. Next, the surface layer was cured in a laboratory dryer (POL-EKO, Poland) at 120°C for 10 min. to fix the polymer coating on the textile carrier.

a) 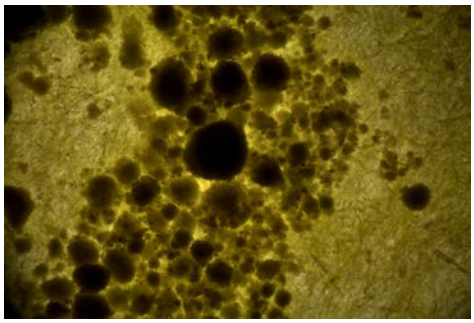 b) 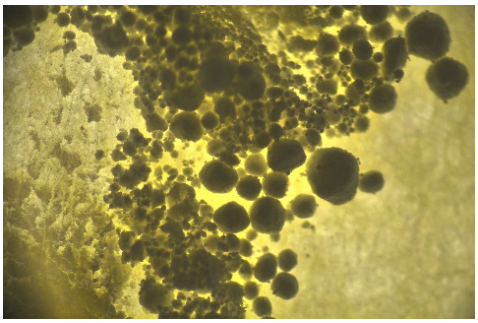

Figure 1. Microscopic image of the inorganic fillers with size 1-6 µm
using stereoscopic microscope (OPTA-TECH, Poland) – magnification x15
(a) calcium carbonate (b) silicon oxide

2.2. Methods

The materials were assessed in terms of cut resistance using methods for evaluation of personal protective equipment and glove materials. The dynamic cut resistance test method were developed using International standard EN ISO 13997. Prior to testing, samples were acclimatized at (23±2)°C and a relative air humidity of (50±5)% for 24 h. Dynamic cut resistance testing under variable load applied to the blade was conducted on the basis of EN ISO 13997:1999 (P.I. Kontech, Poland). Samples were mounted on a metal cylinder with a radius of (38±0.5) mm and a straight blade was drawn across the curvature of the cylinder with the plane of the blade at an angle of (90±2)° to the long axis of the cylinder. During the test, a variable force was applied to the blade. The cutting rate was (2.5±0.5) cm/s. Performance levels were assigned to different cutting force levels according to Table 2.

Table 2. Performance levels of materials tested with variable cutting force [18]

Performance levels	Level A	Level B	Level C	Level D	Level E	Level F
Cutting force [N]	2	5	10	15	22	30

3. Results and discussion

The tests results allowed to compare influence of various concentration of calcium carbonate and silicon oxide fillers on the properties of the coating layer applied to textile carrier. Figure 2 presents the results, as well as an interpretation of cut resistance tests (with standard deviations) for the coated textile carrier. The tests evaluated the effects of fillers on the level of cut resistance offered by the materials.

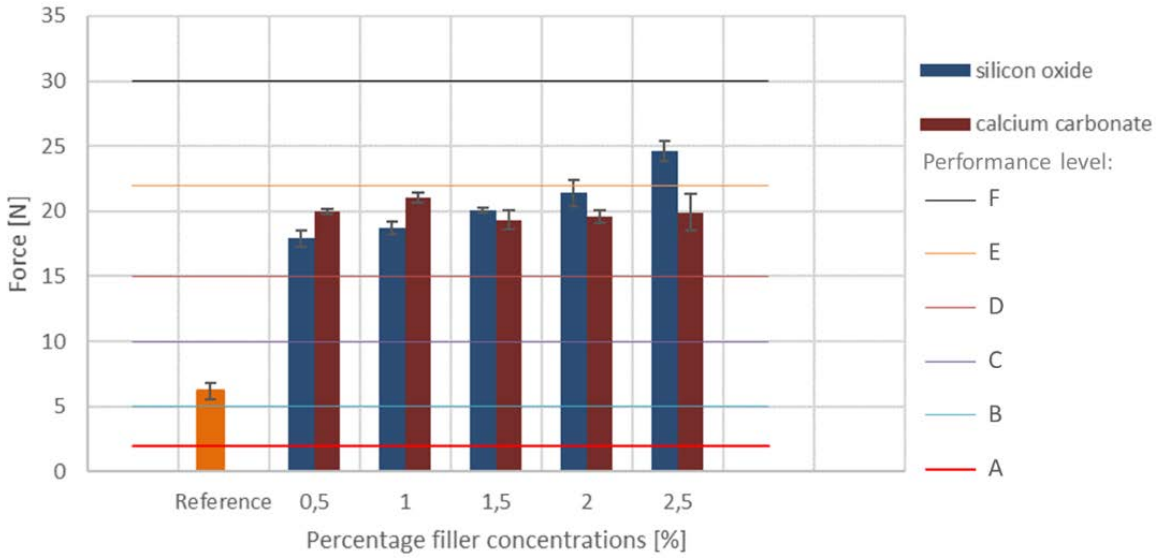

Figure 2. Cut resistance test results with interpretation expressed in performance levels

The studied variants of coated textile carrier with exhibited cut resistance corresponding to performance levels D and E. The highest cut resistance values were found for variants containing 2.5% silicon oxide. The cutting forces determined for those variant (24.6 N) placed them at performance level E. Variants containing from 0.5 to 2.0 % fillers showed cut resistances ranging from 18.1 to 21.9 N, which placed them at performance level D. All the coated textile carriers with polymeric material with fillers, provided higher cut resistance than the reference sample (6,2 N). In addition, it is important to emphasize that the use of silicon oxide allowed to obtain a linear dependence of the cut resistance.

4. CONCLUSIONS

Application of silicon oxide and calcium carbonate allowed to achieve cut resistance corresponding to performance levels D and E.

The highest performance level was observed for variants containing 2.5% of silicon oxide (cutting force = 24.6 N). A threefold increase in the cut resistance of materials containing 2.5% of silicon oxide in comparison with the reference material was confirmed. Application of calcium carbonate showed lower cut resistance tests results, and provided performance level D (cutting force=21.4 N).

In presented study it was found, that latex coating incorporating fillers constituted a layer protecting the fibers against blade action, increasing cut resistance. Preliminary studies confirm the validity of using inorganic fillers in the coating layer of textiles to increase the cut resistance of materials. The higher cut resistance obtained by using silicon oxide is due to the higher adhesion of the filler in the polymer matrix. Based on the results of the study it can be concluded that using silicon oxygen can improve the cut resistance of materials dedicated to use in protective gloves construction.

ACKNOWLEDGEMENTS

This research was funded in whole or in part by National Science Centre, Poland, Grant number: 2021/41/N/ST8/04281. For the purpose of Open Access, the author has applied a CC-BY public copyright licence to any Author Accepted Manuscript (AAM) version arising from this submission.

References

1. *Zhai Y., Mao L., Shen Y., et al.(2021). Research Progress of Cut-Resistant Textile Materials. Frontiers in Chemistry, Vol.9, 745467, DOI=10.3389/fchem.2021.745467.*
2. *Kropidłowska P., Irzmańska E., Sawicki J. (2021). Preliminary Experimental Investigation of Cut-Resistant Materials: A Biomimetic Perspective. Autex Research Journal, vol.0, no.0, DOI: doi.org/10.2478/aut-2021-0006.*
3. *Roda-Sales, A., Sancho-Bru, J.L., Vergara, M., et al. (2020). Effect on manual skills of wearing instrumented gloves during manipulation. Journal of Biomechanics, 98, 109512.*
4. *Kropidłowska P., Jurczyk-Kowalska M., Irzmańska E., et al. (2021) Effects of Composite Coatings Functionalized with Material Additives Applied on Textile Materials for Cut Resistant Protective Gloves. Materials, 14(22):6876. https://doi.org/10.3390/ma14226876.*
5. *Irzmańska, E., Stefko, A. (2012). Comparative Evaluation of Test Methods for Cut Resistance of Protective Gloves According to Polish Standards. Fibres &Textiles in Eastern Europe, 5, 99–103.*
6. *Mayo JB., Wetzel ED. (2014). Cut resistance and failure of high-performance single fibers. Text Res J, 84(12): 1233- 1246.*
7. *Tennebroek R., Casteren H., Swaans R. et al. (2019). Water-based polyurethane dispersions. Polymer International, 68(5): 832-842.*
8. *Harrabi L., Dolez P., Vu-Khanh T.(2008). Evaluation of the Flexibility of Protective Gloves. International Journal of Occupational Safety and Ergonomics, Vol. 14, No. 1, 61–68.*
9. *Thilagavathi G, Rajendrakumar K, Kannaian T. (2010). Development of Textile Laminates for Improved Cut Resistance. Journal of Engineered Fibers and Fabrics, 5(2):40-44.*
10. *Galvin C.J.; Genzer J. (2012). Applications of surface-grafted macromolecules derived from postpolymerization modification reactions. Progres in Polymer Science, 37, 871–906; 19.*
11. *Boguń, M.; Mikołajczyk, T.; Szparaga G, et al. (2008). Comparative Analysis of the Influence of the Kind and Amount of Two Ferromagnetic Nanoadditives on the Structural Properties of Precursor Polyacrylonitrile. Fibres &Textiles in Eastern Europe, 5, 48–53.*

12. *Wijesinghe H., Gamage W., Ariyananda P., et al. (2016). Optimization of calcium carbonate (CaCO3) loading in Natural rubber latex based disposable gloves. International Journal of Scientific and Research Publications, 6(3):266-269.*
13. *MitchelM., Link R., Thabet A., et al. (2010). Rubber-Filler Interactions and Its Effect in Rheological and Mechanical Properties of Filled Compounds. Journal of Testing and Evaluation, 2010, 38(3):101942.*
14. *Yu Y., Zhang J., Wang H., et al. (2020). Silanized Silica-Encapsulated Calcium Carbonate Natural Rubber Composites Prepared by One-Pot Reaction. Polymers, 12(11):2668.*
15. *Lohakul A., Kaesaman A., Rungvichaniwat A., et al. (2007). Rheological Properties of Calcium Carbonate-Epoxidized Natural Rubber Composites Prepared In Latex State. ePolymers, No. 008.*
16. *Chafidz A., Kaavessina M., Al-Zahrani A., et al.(2014). Rheological and mechanical properties of polypropylene/calcium carbonate nanocomposites prepared from masterbatch. Journal of Thermoplastic Composite Materials, 29(5):53-622.*
17. *Ren X., Geng Y., Soboyejo A., et al. (2019). Reinforced mechanical properties of functionalized silica and eggshell filled guayule natural rubber composites. Materials Science, Engineering Rubber Chemistry and Technology, 92(4).*
18. *EN ISO 13997:1999 Protective Clothing - Mechanical Properties - Determination of Resistance to Cutting by Sharp Objects*

COPPER AND SILVER COATED COTTON FABRICS

[1]Azam Ali, [1]Jiri Militky, [1]Sundaramoorthy Palanisamy, [1]Blanka Tomkova, [2]Shaukat Ali

[1]Department of Material Engineering, Faculty of Textile Engineering, Technical University of Liberec
[2]Department of pharmaceutics, Government College University Faisalabad
Studentska 2, Liberec 46117, Czech Republic
Corresponding author Email: - mehr_azam91@yahoo.com

Abstract:

In the current research work, we have fabricated highly durable electrically conductive multifunctional textiles through deposition of copper and silver nanoparticles. For this purpose, the fabric was pre-treated with citric acid followed by the direct growth of the nanoparticles on the fabric surface. The successful pre-treatment of the fabric was confirmed through FTIR analysis. The structural and morphological characteristics of deposited silver and copper nanoparticles were elucidated through XRD, dynamic light scattering, and SEM. The potential of developed conductive fabric for electromagnetic shielding application was assessed within a frequency range of 30 MHz- 1.5 GHz. Moreover, the effect of deposited nanoparticles on the antibacterial effectiveness was also evaluated towards Gram-negative (Escherichia coli) and Gram-positive (Staphylococcus aureus) pathogenic microbes. In the end, the washing durability of the developed conductive fabric for electrical and comfort properties was assessed after multiple launderings. The fabric exhibited significant retention of nanoparticles as confirmed by SEM results and insignificant loss in conductivity after multiple laundry cycles.

Key words:

Multifunctional textiles, electrical conductivity, Silver and copper particles, Durability, Electromagnetic shielding, Antibacterial

1. Introduction

The market for metallized textiles is steadily growing and is becoming more popular in commercial, technical, and high-tech, applications. Anti-bacterial properties, electromagnetic shielding, radar reflectivity, UV radiation screen, energy harvesting, anti-static, and some significant medical applications, such as the fabrication of electrodes for EMG, TENs, and ECG machines, etc., are the applications that are most frequently used [1][2]. In this scenario, selecting a textile made of natural fibres is preferable because environmental pollution is currently a critical threat with the production as well as post-disposal procedures of synthetic fibres. Researchers are therefore fully aware of the need to develop innovative and smart textiles using natural fibre sources to address this challenge. [3][4]. Cotton is well-known for being sustainable and having environmentally favourable qualities including biodegradability. It is patently obvious that pure cotton lacks intrinsic conductivity. A variety of conductive materials are typically added to insulators to make them conductive [5]. There are many ways to metallize the surface of textiles, but the metallic fabric created using these conventional procedures has flaws such weight, rigidity, and poor air permeability. In the current study, in-situ deposition of Cu and Ag nanoparticles to produce electrically conductive and multifunctional cotton fabric is reported.

2. Experimental

2.1. Materials and Methods

The cotton fabric with a 150 GSM plain weave structure was used throughout the study. The fabric was procured from from Licolor,A,S,. All the chemicals being used during the surface metallization process were of Reagent grade. The substrate was pre-treated with 20 g/L citric acid solution for two hours at 90°C prior to the deposition of Cu and Ag nanoparticles. In the start, distilled water was used to dissolve copper sulphate at various concentrations, including 6g/200ml, 4g/200ml, and 2g/200ml. The cotton fabric was then soaked in the solution followed by drying for three minutes at 100 °C. 15 rounds of this continuous dipping and drying process were completed. The treated fabrics were then added to a solution of 6g/200ml sodium hydrosulphite. For the next 20 minutes, the reduction was maintained. Similar to this, varying concentrations of silver nitrate (AgNO3) i.e., 0.30 M, 0.20 M, and 0.10 M were dissolved in distilled water for the deposition of Ag nanoparticles. A transparent solution of [Ag(NH3)2]+ was formed after the aqua ammonia (28wt %) was gradually added to an aqueous solution of silver nitrate. The alkaline cotton fabric was immersed in this solution for 3 mins followed by three minutes of drying at 100°C. The dip and dry procedure was carried out repeatedly to deposit the highest concentration of [Ag(NH3)2]+ on the fabric. 15 rounds of this continuous dipping and drying process were completed. The treated textiles were then added to a stock solution of 0.1M glucose. The reaction was continued for 15 minutes. The fabrics were then air dried after being rinsed with water. The microstructure of textiles coated with Cu and Ag nanoparticles was examined on a scanning electron microscope operating at an accelerated voltage of 15 kV. The electromagnetic shielding effectiveness and electrical resistivity were assessed according to the ASTM D4935-10 and ASTM D257-07 standard testing protocols. The antibacterial activity was evaluated according to the AATCC-147 disc-diffusion method. The washing durability of the developed the fabric was evaluated according to the ISO 105-C01 standard method.

3. Results and discussion

3.1. Electrical conductivity of coated cotton fabrics

The effect of silver nitrate ($AgNO_3$) and copper sulphate ($CuSO_4$) concentration as well as the number of dip cycles for the enhancement of conductivity of the textiles were studied. Figure 1 illustrates the resistivity of the samples as the average of three measurements.

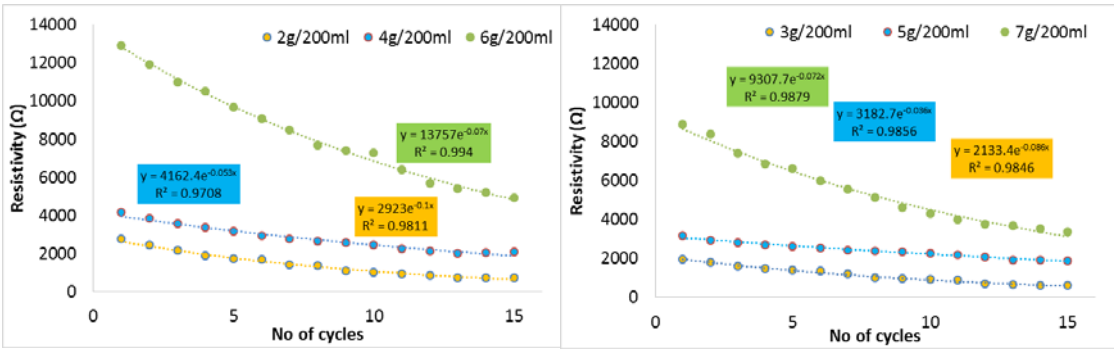

Figure 1. Electrical resistivity behavior of copper and silver coated fabric

The results exhibited a significnat decrease in resistivity i.e., increase in electrical conductivity. This behavior could well be attributed to the formation of relatively large sized Cu nanoparticles at higher concentrations of Cu and Ag salt solution. The lower concentrations of salt produced fabrics with enhanced conductivity due to the development of percolated network through the formation of continuous connectivity between the small sized metallic nanoparticles.

3.2. Morphology of fabric surfaces

3.2.1 FTIR Spectra of pretreated cotton

Figure 2 represents the FTIR spectrum of untreated and treated cotton fabric.A broad band occured at 3300 cm^{-1} is a characteristic strech of O-H group. Additionally, we noted a sharp peak for C-H stretching in the 3000–2800 cm^{-1} range. The adsorbed water molecules cause a peak at about 1640 cm-1. The occurrence of aromatic rings could be explained by the C=C stretching vibrations. The carboxylic group absorption band is clearly visible for the citric acid-grafted cotton at 1732 cm^{-1} [1].

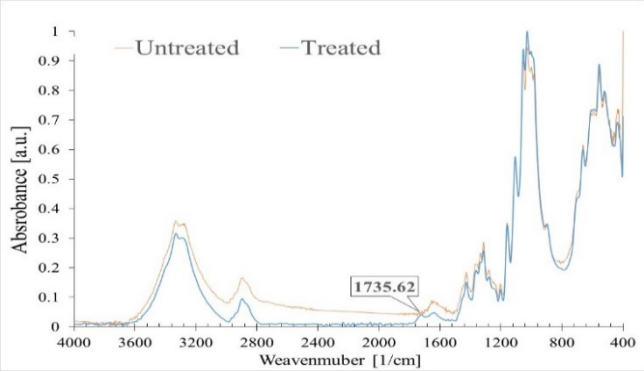

Figure 2. FT-IR spectra of treated and untreated cotton fabric

3.2.2 SEM Structures

The deposition of nanoparticles on the surface of cotton fabric was seen using scanning electron microscopy. The microscopic scale of Cu and Ag nanoparticles coated on fabric surface was shown by the SEM images provided in Figures 3 and 4. The deposition of nanoparticles was observed to be more uniform and thick as the number of dips increased.This further demonstrated that with the increase in the number of dipping cycles, there was a higher probability for a percolated network of nanoparticles to form. The increase in Ag and Cu metal concentrations with further dips was easily noticeable.

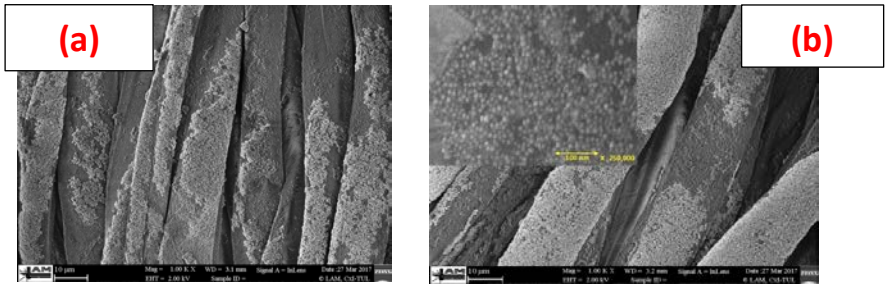

Figure 3. SEM images (a) after 10 cycles (b) after 15 cycles

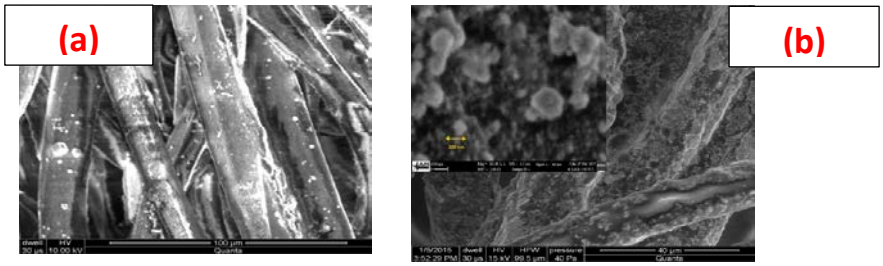

Figure 4. SEM images (a) after 10 cycles (b) after 15 cycles

3.2.3 XRD Analysis

The XRD patterns of treated fabrics for the 2 range of 20 to 80 degrees with a 0.02-degree step are shown in Figure 5(a). The precise indexing of all the diffraction signals to the Ag structure clearly demonstrates the phase purity of the produced silver particles. Four new peaks at 2 values of 38.1°, 44.3°, 64.5°, and 77.5°, that could be ascribed to the diffraction signals of the (1 1 1), (2 0 0), (2 2 0), and (3 1 1) planes of Ag, were found for Ag-coated fabric compared to the untreated fabric. The XRD patterns of fabric for Cu nanoparticle are shown in Figure 5(b). The copper (1 1 1), (2 0 0), and (2 2 0) planes, respectively, were represented by the diffraction signals that occurred at 2θ of 43.3°, 50.5°, and 74.2° [3]. The sharp peak of the Cu nanoparticles indicated their crystallinity, and as a result, no other typical impurity peaks were found besides the signal of Cu2O at 2θ of 38° [4].

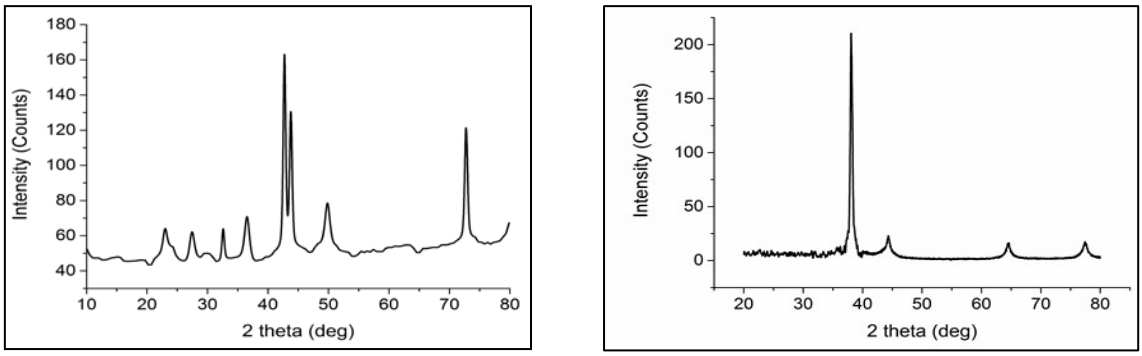

(a) **(b)**

Figure 5. XRD patterns for (a) silver (b) copper coated fabrics

3.3. Electromagnetic Shielding

Figure 6 illustrates the electromagnetic shielding (EMI SE) effect for fabric samples as a function of frequency. According to the data, significant changes in EMI SE occur when electrical conductivity increases, which means resistivity decreases. This leads us to believe that, in addition to electrical conductivity, the close packing of conductive network also affects EMI SE. In comparison to Cu-coated fabric, the highest EMI SH values at 5, 10, and 15 cycles for Ag-coated fabric were 5.8, 9.5, 14.96, and 12.65 dB, respectively. The graph also clearly demonstrates that the EMI SE of fabric samples suddenly increased up to the frequency range between 300 and 400 MG Hz and then it became stable. This indicates that fabric samples can produce strong EMI at low frequencies, and that EMI values are steady up to 1500 MG Hz. Since these samples have the maximum electrical conductivity (low resistivity) of all the samples, they also have the highest value of EMI shielding.

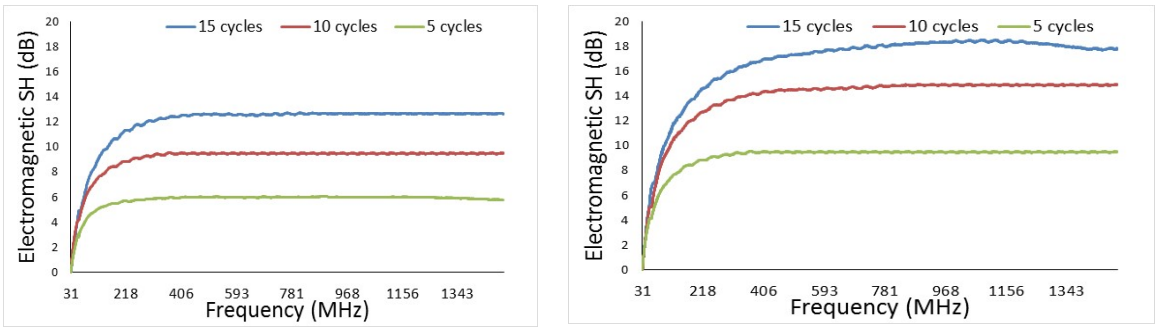

(a) **(b)**

Figure 6. Electromagnetic shielding effectiveness of (a) silver (b) copper coated textile

3.4. Antibacterial Properties

The antibacterial properties of Ag and Cu coated fabrics was evelauted towards Gram-negative (E. coli) and Gram-positive (*S. aureus*) bacterial strains. The coated samples exhibit the zones of inhibition (ZOI) around the fabric samples after 24 hours of incubation at 37 °C in the dark.The experiment was performed in triplicate and the average value for the average zone of inhibition value is shown. The sample of pristine fabric without Ag or Cu coating exhibited no antibacterial properties. However, after the Ag and Cu coating, the zone of inhibitions was demonstrated against both types of bacteria, S. aureus and E. coli. Furthermore, when compared to Staphylococcus aureus, Escherichia coli showed the highest level of resistance.With more dipping cycles, the zone of inhibition for S. aureus increased from 8.5 to 13.43 mm for Ag-coating fabric and from 9.5 to 15.5 mm for Cu-coated fabric, whereas it increased from 7 to 11.78 mm for Ag-coated and from 7.5 to 12 mm for Cu-coated for E.coli bacterial strain.

3.5. Durability in Electrical Conductivity

The durability to washing and rubbing for the conductive fabrics have been a critical challenge. The electrical resistivity of the coated fabric samples was assessed both before and after launderings to investigate these characteristics. The samples were washed as per standard procedure. For the washed samples, the conductivity was examined again, and the results are shown in Table 6.

Table 1. Electrical conductivity of conductive fabrics before and after washing

Fabric samples	Electrical Resistivity Ω	
	Before washing	After washing
Copper treated 5 cycles	1734	1757
Copper treated 10 cycles	1024	1039
Copper treated 15 cycles	756	762
Silver treated 5 cycles	1403	1422
Silver treated 10 cycles	972	960
Silver treated 15 cycles	650	643

It was observed that there is no noticebale decrease in the resistivity of the coated fabrics before and after multiple laundry cycles. It is clear that even after washing, there is barely a difference in the conductivity of these samples. It indicates that nanoparticles are firmly bonded to the surface of fibres. The SEM analysis of the samples of conductive fabrics before and after washing provided further confirmation for this.

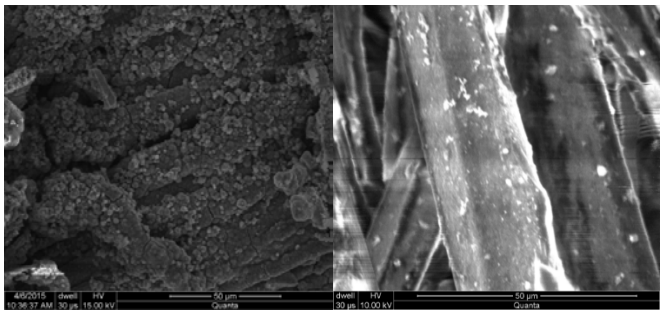

Figure 7. SEM image of silver and copper coated fabric after washing

4. CONCLUSIONS

The successful deposition of silver and copper nanoparticles established their potential applications in the domain of smart textiles. Additionally, it was concluded that the uptake of nanoparticle can be enhanced with the increase in the number of dips for excellent coating of the nanoparticles on the surface of cotton fabric. Furthermore, the morphological and structural characteristics of the silver and copper coated fabrics and particles was evaluated through XRD, dynamic light scattering, and SEM techniques. The potential of conductive fabrics for electromagnetic shielding ability was analyzed over frequency range of 30 MHz-1.5 GHz through coaxial transmission line approach. The sample developed from 5 dip cycles exhibited the minimum electromagnetic shielding effectiveness of about 6.10 dB for Cu and 9.55 dB for Ag-coated fabric samples in frequency range of 600 MHz to 1.5 GHz. On the other hand, the sample produced from 80 dip cycles revealed the shielding effectiveness of 18.54 dB for Ag and 12.65 dB for Cu-coated fabric samples for respective frequency 1.5 GHz. For multifunctional behavior, the developed conductive fabric samples were further evaluated for antibacterial properties towards S. aureus and E. coli bacterial strains. The zone of inhibitions (ZOI) for S. aureus and E. coli significantly increased with the increase in number of dips. In the end, the washing durability of developed conductive fabrics was assessed after multiple launderings. The samples exhibited excellent retention of the nanoparticles, further supported by SEM microstructures and insignificant loss in the conductivity of the fabric after laundry. Therefore, the scientific outcomes of current research work could provide an alternative inexpensive and easier ways to obtain highly durable electrically conductive and multifunctional textiles.

References

1. *Chung, C.,Lee, M.,Choe, MK. (2004) .Characterization of cotton fabric scouring by FT-IR ATR spectroscopy. Carbohydr Polym, 58:417–420*
2. *Shateri-Khalilabad MEY,M.(2017). Fabricating multifunctional silver nanoparticles-coated cotton fabric. Arab J Chem, 10:1016*
3. *Gan, X., Wu, Y., Liu, L., et al. (2008). Electroless plating of Cu-Ni-P alloy on PET fabrics and effect of plating parameters on the properties of conductive fabrics. J Alloys Compd, 455. 313*
4. *Zhao ,Y., Cai, Z., Fu, X., et al. (2013). Electrochemical deposition and characterization of copper crystals on polyaniline/poly(ethylene terephthalate) conductive textiles. Synth Met, 175:1–8.*
5. *Studer, A.M., Limbach, L.K., van Duc., et al. (2010) Nanoparticle cytotoxicity depends on intracellular solubility: Comparison of stabilized copper metal and degradable copper oxide nanoparticles. Toxicol Lett 197:169–174*
6. *Chattopadhyay, Patel BH (2010) Effect of nanosized colloidal copper on cotton fabric. J Eng Fabr Fibers 5:1–6*

SURFACE ROUGHNESS OF POLYAMIDE KNITTED FABRICS

Elena Tomovska, Lubos Hes

University “Ss. Cyril and Methodius”, Faculty of Technology and Metallurgy, Department of Textile Engineering, Skopje, N. Macedonia, Ruger Boskovic 16, 1000 Skopje, tel./fax. + 389 2 3088 201

Technical University of Liberec, Faculty of Textile Engineering, Department of Textile Evaluation, Liberec, Czech Republic, Studentská 2, 461 17 Liberec, tel.+420 48 535 3274, fax. +420 48 535 3542

etomovska@tmf.ukim.edu.mk

Abstract:

Fabrics are never ideally smooth. Their texture varies between fine and coarse, quantified through the surface’s vertical deviation. Fabric roughness, or its opposite smoothness, is employed as measure of the surface texture of fabrics. In general, texture depends upon fiber properties, yarn count, yarn twist, and fabric structure and fabric design). This research aims to determine the limitations in visual perception of surface roughness in comparison to objective surface roughness measurements of low weight polyamide fabrics. Subjective evaluation is used for the visual assessment, while instrumental measurement of the properties was conducted using a noncontact laser profilometer. Subjective evaluation was conducted by a panel of forty untrained evaluators on a sample of seven polyamide knitted fabrics with different yarn count and composition. The roughness profile parameters were measured using Talysurf CLI 500 according to ISO 4827. Although the surface roughness measured as arithmetic mean deviation (Ra) and roughness through visual inspection of the fabric are correlated, instrumental measurements of roughness are more precise. Differences in the surface roughness arising from significantly different yarn structures will be observed, while those due to the knitted fabric structure are negligible in visual inspection.

Key words:

texture, surface roughness, knitted fabrics, visual inspection

1. Introduction

Surface roughness is a tactile property of fabrics that has been widely investigated by many researchers for both woven and knitted fabrics. The research application is mainly dedicated to defining the sensorial or tactile comfort. Tactile comfort properties are complex concepts which include dimensional changes at small forces such as tensile, shear, compression, and bending, surface properties (friction and roughness) and warm/cool feeling evaluate via the Kawabata evaluation system [5]. Numerous research works [1,2,3,4,6] have studied the effect of different fiber materials, fiber blended ratios, fiber morphology, yarn properties, finishing treatments, and fabric constructions on the hand feel properties of knitted fabrics. Furthermore, surface roughness has been used to distinguish between various types of structures [7].

This research aims to investigate the visually perceived surface roughness and luster of pantyhose fabrics. Subjective evaluation is used for the visual assessment, while instrumental measurements of the properties was used to obtain objective fabric parameters.

2. Experimental

2.1. Materials

Samples were knitted from commercially available yarns on industrial circular knitting machine with four systems, diameter of four inches and 400 needles. The physical and structural properties of the samples are presented in Table 1. The pure polyamide knits single jersey, while the addition of elastane was through knitted hopsack structure. Sample S22T was with increased luster, in a plated knit from a covered elastane yarn and a trilobal increased luster filament. The samples are made of fine filaments, with low weight and high cover factor. Figure 1 shows the microscopic images of selected samples, taken on Olympus BX51 microscope at a magnification of 5×.

Table 1. Sample structure

Sample		S5E	S17P	S17E	S22PP	S44CE	S78CE	S22T
Yarn count (dtex)		5.5/2	17/3	17/3	22/5	44/13	78/24	22/5
Density	**Wales (cm-1)**	28.6	42.9	33.3	23.8	23.8	28.6	23.8
	Courses (cm-1)	28.1	24.6	28.1	31.6	21.1	24.6	35.1
Sample code: Number-yarn count, P- polyamide 6.6, PP- polyamide 6, E-polyamide-bare elastane blend, CE-polyamide-covered elastane blend								

S5E S17P S17E S22T S22PP S44CE S78CE

Figure 1. Microscopy of samples

2.2. Methods

Subjective evaluation was conducted on a knee-height leg model. To standardize the evaluation, evaluators were asked to describe the shin part of the leg. The model was placed in a black viewing cabinet (length 60cm, height 50m, depth 45cm), with a D-65 light source, illuminating the leg surface under a 15^{o} angle. Samples were evaluated from a distance of 1.5m. The evaluators were 40 women aged 20 to 60, with normal visual acuity. A semantic differential method in a five-scoring system was used to assess texture, evaluated by bipolar opposites of rough-smooth and uneven-even.

To evaluate surface roughness, Talysurf CLI 500 a noncontact laser profilometer was used. Roughness profile parameters were measured according to ISO 4827. For global evaluation of the roughness amplitude profile the arithmetic mean deviation (Ra, μm) in wales and courses direction on a length of 5±0.05mm was used. This measurement quantifies the absolute values of the profile variations (peaks and valleys) from the mean line in the evaluation length. However, Ra does not give information on the shape of the profile. Therefore, a pseudo-color map was used to assess the reasons for variation of the surface.

3. Results and discussion

The results of the subjective and objective evaluation of pantyhose are presented on Figures 2 and 3. A Pearson correlation coefficient of 0.79 was found between the visually perceived roughness(VR) and the instrumentally measured roughness (Ra) in the wales direction, while a lower correlation (Pr=0.69) was found in the course direction. This points out two important differences between the visual and haptic assessment of fabric. Firstly, the correlation between visual assessment and roughness

measurements is not strong. Small differences in roughness that may be instrumentally measured will escape the human eye. Secondly, the direction of viewing will influence the surface roughness visual perception, as lower correlation was found in the courses direction. As roughness is a three-dimensional property assessment of the fabrics can be made despite directionality.

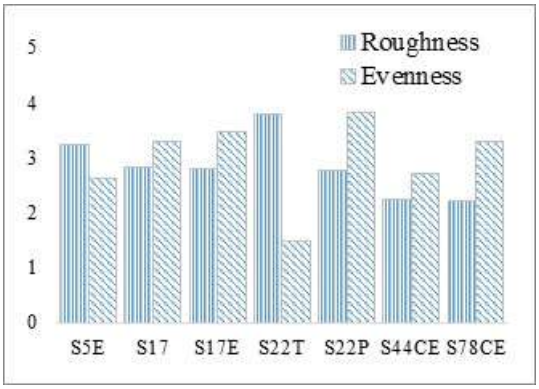

Figure 2. Visual assessment of pantyhose roughness and evenness

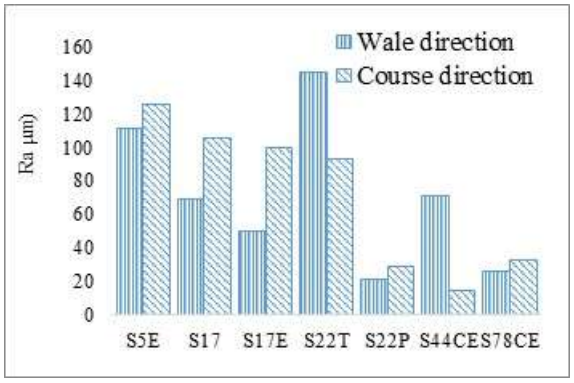

Figure 3. Arithmetic mean deviation of the roughness profile

When examining the values presented in figure 3 S22T is a clear outlier. Unlike the rest of the series which is knit of smooth multifilament yarns, this sample was made of a single covered yarn with an addition of a profiled trilobal filament, thus the uneven structure of the yarn contributes to surface roughness. However, in the objective assessment of the surface roughness an additional outlier was found with sample S44CE. To examine the differences in the surface roughness figure 4 a) and b) presents a pseudo-color map of the two samples. The map the roughness profile of the sample to a color spectrum, with peaks shown as red-white and valleys shown as red green. As can be seen on the representation of the pseudo-color map for sample S22T the roughness in the sample is due to the uneven distribution of peaks and valleys in the sample, caused by the covered yarn, as well as the protrusions of the trilobal filament. On the other hand, the sample S44CE has a fairly even structure with deep valleys occurring periodically, consistent with the knitted structure and the loop shapes within it. The roughness of knitted fabrics comes from the applied yarn, as well as the structure of the fabric, with the former having greater influence on the visual perception of fabrics.

When the outlier sample S22T is removed from the analysis a correlation coefficient of 0.9 is obtained between visually assessed surface roughness and yarn count. However, low correlation (0.54) existed between objectively measured Ra and the yarn count. To illustrate this difference pseudo-color maps of fine filament pantyhose of 17dtex (S17P and S17E) and coarse filament pantyhose (S78CE) are presented on figure 4 c), d) and e). As can be seen from the figure increased yarn count contributes to less differences in height along the roughness profile of a surface, creating a closed, smooth surface. This is due to the even packing of filaments within the loop structure when the yarn count increases. The presence of elastane yarns in the knit (S17E) stabilizes the loop structure, leading to a more even distribution of the peaks and valleys on the fabric surface compared to a sample with no elastane (S17P). Even though these differences in surface can be seen via instrumental analysis, they are not perceivable visually in real conditions of wear.

Furthermore, during visual assessment of pantyhose yarn count is a more important parameter compared to fiber composition, as can be seen by the assessment of sample S22PP made of PA6 in 22dtex. In the visual assessment of the set this sample is seen to have similar roughness to samples with fine yarn count of 17dtex. However, due to the fiber composition the roughness Ra of the sample are closer to those of coarser yarns. Although the difference in roughness caused by different fiber composition will influence the general surface related properties, such as comfort it will not be immediately visually perceivable.

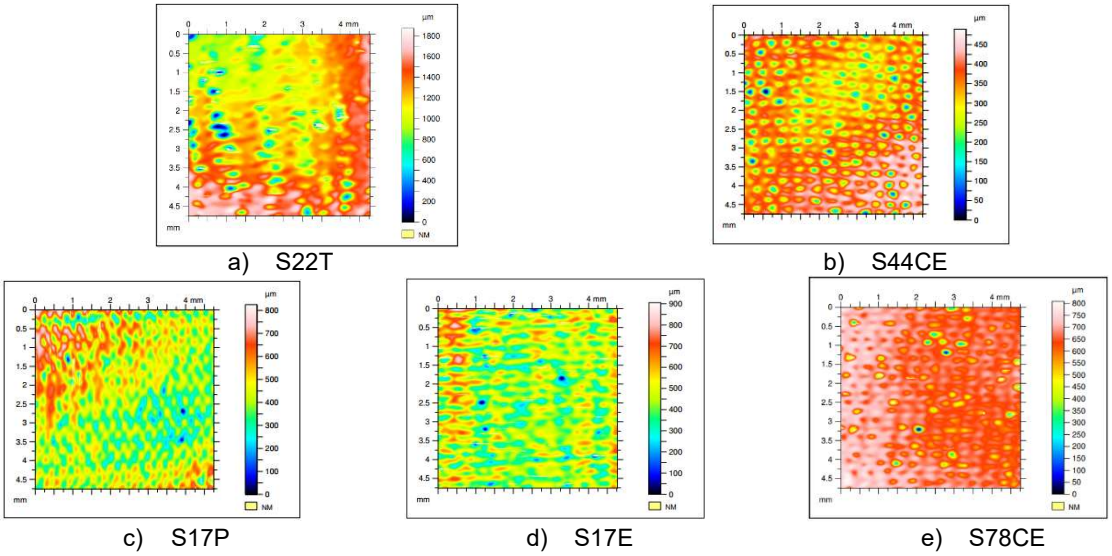

a) S22T b) S44CE

c) S17P d) S17E e) S78CE

Figure 4. Pseudo color maps of samples

4. CONCLUSIONS

This study investigated roughness as a property of knitted fabrics. Although the measured arithmetic mean deviation (Ra) the surface roughness and roughness through visual inspection of the fabric are correlated, instrumental measurements of roughness are more precise. Differences in the surface roughness arising from significantly different yarn structures will be observed, while those due to the knitted fabric structure are negligible in visual inspection.

ACKNOWLEDGEMENTS

The authors would like to thank the Vishegrad Fund for providing a mobility grant for this research.

References

1. *Atalie, D., Gideon, R. K., Ferede, A., Tesinova, P., Lenfeldova, I. (2021): Tactile Comfort and Low-Stress Mechanical Properties of Half-Bleached Knitted Fabrics Made from Cotton Yarns with Different Parameters, Journal of Natural Fibers, 18(11), 1699-171.1*
2. *Balci Kilic, G,, Okur, A. (2018). Effect of yarn characteristics on surface properties of knitted fabrics. Textile Research Journal, 89 (12).*
3. *Demiryürek, O., D. Uysaltürk. (2013). Thermal comfort properties of Viloft/cotton and Viloft/polyester blended knitted fabrics. Textile Research Journal 83 (16):1740-53.*
4. *Mahar, T.J., Wang, H., Postle R. (2013). A review of fabric tactile properties and their subjective assessment for next-to-skin knitted fabrics. The Journal of The Textile Institute, 104:6, 572-589.*
5. *Mooneghi, S. A., S. Saharkhiz, and S. M. H. Varkiani. 2014. Surface roughness evaluation of textile fabrics: A literature review. Journal of Engineered Fibers and Fabrics 9 (2):1-18.*
6. *Vasile, S., Malengier, B., De Raeve, A.,Deruyck, F., (2017). Influence of selected production parameters on the hand of mattress knitted fabrics assessed by the Fabric Touch Tester. Textile Research Journal, 89(1).*
7. *Vassiliadis, S.G. and Provatidis, C.G. (2004), "Structural characterization of textile fabrics using surface roughness data", International Journal of Clothing Science and Technology, Vol. 16 No. 5, pp. 445-457.*

PULLULAN/PVA/ DOXORUBICIN CORE-SHELL ELECTROSPUN NANOFIBERS DRUG DELIVERY SYSTEM FOR THE CHEMOTHERAPY AGAINST CANCER

Tören Elçin, Mazari Adnan Ahmed, Mazari Büyük Funda

Department of Clothing, Faculty of Textile Engineering, Technical University of Liberec
Studenstká 2, 461 17 Liberec, Czech Republic
elcin.toren@tul.cz

Abstract:

Cancer is one of the foremost dangerous illnesses encountered by human beings for the last several decades. In 2022, 1,918,030 new cancer cases and 609,360 cancer deaths are predicted to occur in the Czech Republic, with the Czech Republic among the highest worldwide, with the rate constantly growing. Each year in the Czech Republic (with a total population of over 10.5 million), over 82,000 people are diagnosed with cancer, and over 27,000 patients die from it. Nanotechnology has played a critical part in nearly every field of life, counting restorative sciences. Controlled and assisted release of drugs is much more preferable and beneficial when cancer treatment is required because such drugs also prevent damage to normal cells. Common anticancer drugs used in chemotherapy have extreme side effects due to long measurement requirements. With the assistance of nanotechnology, extraordinary results for occurrence, anticancer sedate-loaded nanofibers, have been accomplished in cancer treatment requiring less drug as the drug is preserved in these nanofibers for a prolonged time. Electrospun nanofibers have a large surface area, controllable pore sizes and tunable drug controls, making these nanofibers promising candidates in the therapeutic field. Doxorubicin may be a sort of chemotherapy drug called an anthracycline. It moderates or stops the development of cancer cells by blocking an enzyme. Cancer cells need enzymes to multiply. PVA is used as a carrier polymer. Poly (vinyl alcohol) (PVA) may be a semi-crystalline hydrophilic compound with sensible chemical and thermal stability. It is a highly biocompatible and non-toxic polymer, and it will be processed and has high water permeability. Advancing the synthesis of nanofibers using biodegradable polymers should successfully utilise water as a soluble rather than toxic chemicals and reduce the environmental burden. This green approach to nanofibers manufacture contains a great potential to be used in regenerative pharmaceuticals, including cancer treatment, since its ecologically friendly characteristics.

Key words:

electrospinning, polysaccharides, membrane antibacterial, antimicrobial, anticarcinogenic.

1. Introduction

Electrospun nanofibers are being utilised in numerous applications, including but not restricted to tissue engineering (bone and skin), wound healing, and potential applications of these nanofibers, including the achievability to treat and analyse cancer cells [1]. After surgery, local recurrence of tumour cells can be a significant concern, which also requires chemotherapy. [2]. The low specificity of drugs utilised for cancer treatment could be a significant major hurdle that kills cancer cells and devastates normal cells. To decrease this toxicity to typical cells, an appropriate concentration of anticancer drugs should be kept up in the local area after surgery. It can be implanted directly to attract the tumour cells for treatment [3]. On the other hand, nanofibers can be inserted directly into the tumour. In this way, it can be said that nanofibers are better for cancer treatment when compared with nanoparticles.

1.1. Drug Dependent Realise

The release of drugs from polymeric nanofiber highly depends on various drug attributes [4]. The amount of loaded drug inside nanofibers plays a crucial role in the final release. High drug loading has been detailed to be one of the most reasons for initial burst release besides the water solubility of the drug since over the basic dissolvability limit, the drug gets stored on the surface of fibres [5]. The increase in molecular mass and interaction between drug and polymer trigger and slow down the drug release [6]. In cancer treatment, nanofibers have numerous advantages, such as obtaining filaments at low ages, allowing surface modification and arrangement variation, and drug encapsulation due to their diameter from nanometres. Anticancer medicate loaded electro spun nanofiber gives controlled and sustained anaesthetise discharge at the desired activity site with progressed efficacy. Electrospun nanofibers can also be utilised as an implant into the post-operative tumour cavity to repress tumour recurrence, and prolong medicate release at the tumour location [8]. Electrospun nanofibers have benefits that are a kind of opportunity to construct cell environments which can mimic the Vivo tumour microenvironment [7].

2. Manufacturing techniques of nanofibers

Many ways are utilised for nanofiber generation: bicomponent extrusion, phase separation, template synthesis, drawing, melt blowing, electrospinning, and centrifugal spinning. Nanofiber materials have a range of uses in these zones; energy exchange devices, composites for zone structures, drug delivery and tissue engineering appreciate batteries and fuel cells, condensers, transistors, and diodes [8].

By electrospinning and non-electrospinning, different materials (metal, metal oxides, ceramics, polymers, and carbon) are created into nanofibers.

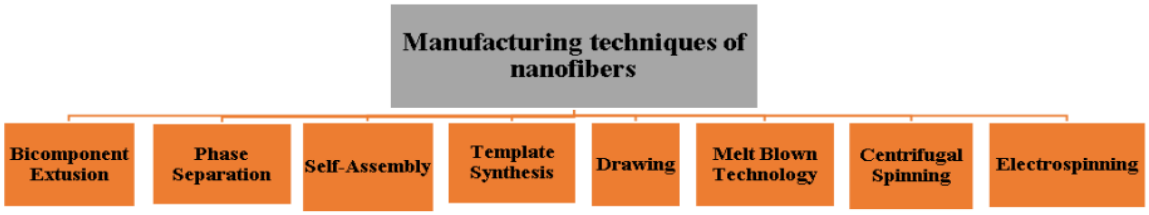

Figure 2.1. Manufacturing techniques for nanofibers [9]

2.1. Coaxial Electrospun Nanofibers

The coaxial electrospinning method can be characterised as modifying the conventional electrospinning apparatus. According to the traditional electrospinning system, the polymer solution is replaced by two needles with two coaxial capillaries, which is associated with feeding. The coaxial arrangement of nozzles can provide different pathways for internal and external structures. Understanding the coaxial electrospinning phenomena and basic material science is best to prepare and control the required coaxial electrospun fibres. In many cases, when using electro spraying, electro spraying can present some handling difficulties, such as arranging monolithic fibre or clogging the nozzle. Unlike electro-spraying, the arrangement of electrospinning remains a continuous jet, which is dominated by viscoelasticity and bending instability. At the exit of coaxial spouts, centre arrangements are trapped in sheath solution forming a droplet with a comparative prolate shape to the Taylor cone. Nanofibers are created by the solid tensile tension of the electrostatic force between the liquid jet, the nozzle and the collector. The spray is directed straight at first and becomes unstable due to bending instability after

travelling a brief distance. Numerical simulations showed that electric charges move to the surface of the jet quickly during electrospinning.

For this reason, the improvement of core arrangement is possibly entrained only by thick traction. Besides the electrostatic force, this bending instability comes about within the quick evaporation of the solvent and significantly stretches the jet into core-shell nanofibers [10]. The coaxial spinning schema was given in Fig.2.2.

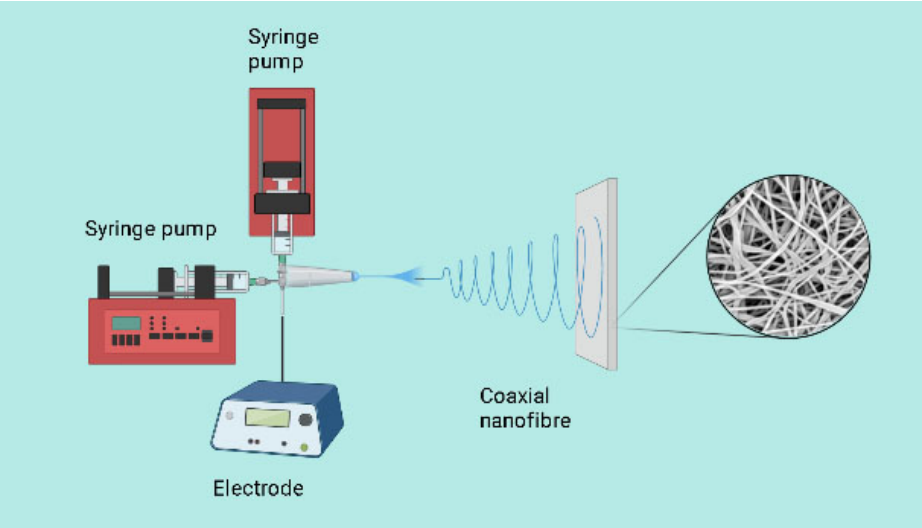

Figure 2.2. Coaxial Spinning schema [11]

Coaxial electrospinning can prepare hollow nanofibers as well. Tubular nanofibers are considered valuable in various applications, including drug delivery and tissue building. Compared to other methods, electrospinning is preferred in preparing long continuous nanoscale hollow fibres, as template-directed approaches only work for short-length threads.

3. Experiment

Materials such as Pullulan, PVA, and DOX (were obtained from Sigma Aldrich, Czech Republic). Nanofibers were prepared using 4SPIN™ (Contipro, Czech Republic).

3.1. ***Formation of PVA/Pullulan Core-Shell Nanofibers***

Pullulan 10 weight rate (wt. %) and PVA 10 wt. % in distilled water with the help of heating and magnetic blending was utilised. The arrangement was prepared independently and blended into a weight ratio (Pullulan/PVA). PVA (Sigma Aldrich, 87%-89% hydrolysed) 10 weight rate (%wt.) refined water we break up at 80 ° C.

Electrospinning equipment was used with two coaxial injectors. The needle of the injector was associated with the emitting electrode of positive polarity, and a collector with aluminium foil was associated with the negative polarity. A voltage of 22 kV was connected to the polymer syringe. The needle tip was put 20 cm. The flow ratio between core and shell solutions (PVA/PULLULAN) was 0.5:0.5.

DOX was chosen to be the demonstrated drug. The Pullulan/PVA/DOX nanofibres were arranged by coaxial electrospinning, and the preparation process was given in Fig.3.1. The mass ratio of DOX to PVA was 1:100.Pullulan/PVA/DOX nanofibers were immersed in 5 mL, and it was shaken at 37 ℃ in temperature.

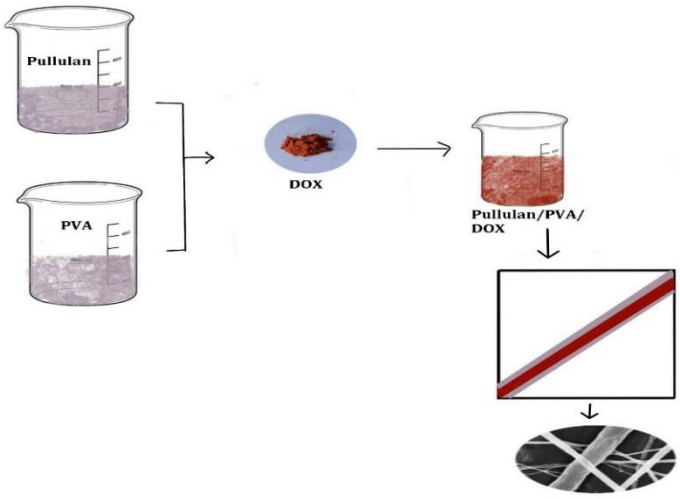

Figure 3.1. Schema of the preparation process

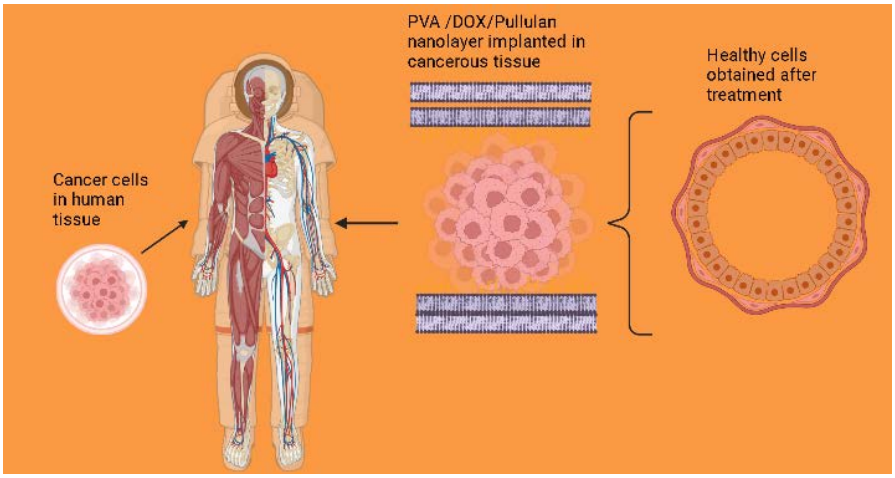

Figure 3.2. Main target of study [11]

4. Results and analysis

4.1. ***Surface Morphology***

A scanning microscope (SEM) is used to determine electrons to scan the sample surface to form a high-resolution image. SEM produces pictures that will show data on a surface of material composition and topography. Membrane morphology was tested using SEM images.

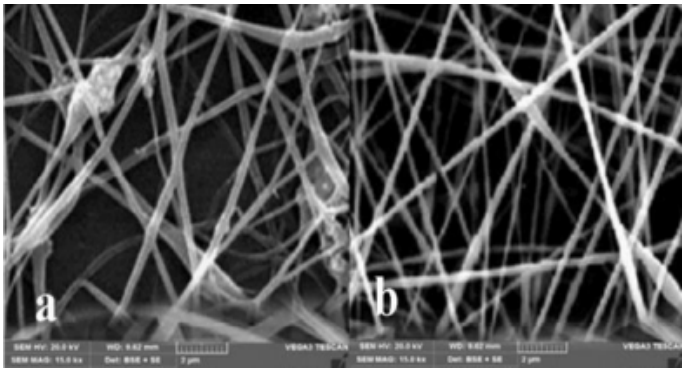

Figure 4.1. SEM images of Pullulan (a), PVA (b).

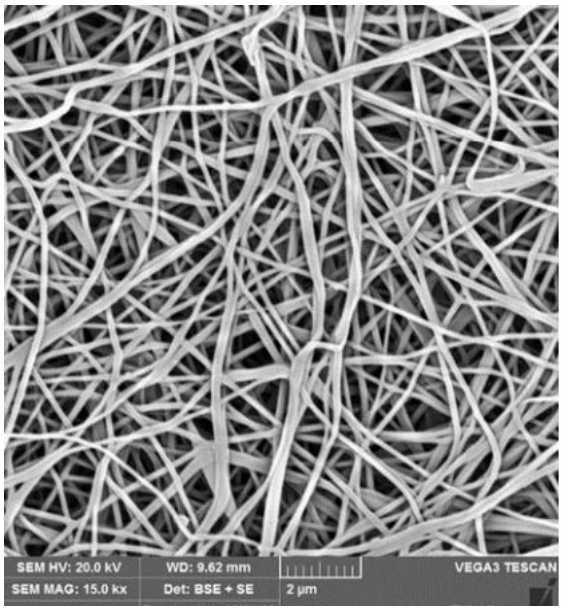

Figure 4.2. SEM images of Pullulan/PVA blend nanofibers

Figure 4.3. PVA/PULLULAN/DOX nanofibers

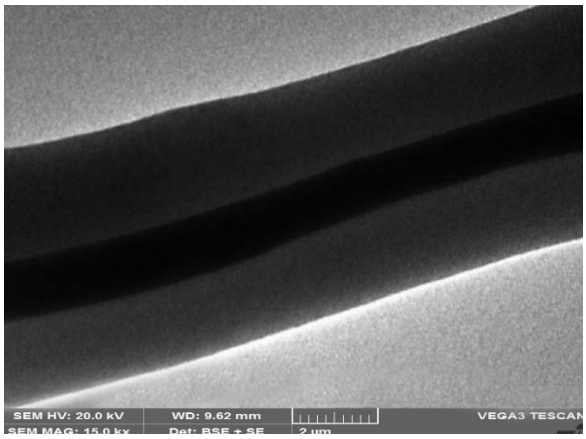

Figure 4.4. PVA/PULLULAN/DOX core shell structure

4.2. *BET Analysis*

This analysis was analysed according to ČSN P CEN ISO/TS 80004-6 standard. The samples were previously saturated for 2 hours at vacuum 160 °C. The parameters were analysed in triplicates and expressed as average ± standard S.D.

Table 4.1.BET analysis for nanofibers

Electrospun Nanofibre	Average Pore Radius (Å) ± SD	Average Total Pore Volume (cc/g) ± SD	Middle Surface area (m^2/g) ± SD
Pullulan	15.80 ± 0,855497	0.1390 ± 0.002	182.60 ± 5.5
PVA	17.40 ± 3,021175	1.1322 ± 0.009	1302 ± 32
Pullulan/PVA/DOX	15.61 ± 1,846691	0.1176 ± 0.0024	150.68 ± 4.5

4.3. *FITR Analysis*

This analysis was examined according to ČSN ISO 19702:2015. FTIR analysis demonstrated that there was no chemical interaction between PVA and Pullulan. The PVA/Pullulan core-shell nanofibers can be degraded effectively in either an acidic or impartial environment. Furthermore, the resulting fibres can be utilised as a carrier for anticancer specialist DOX. The drug-loaded nanofibers played an essential role in not allowing the Hela cell to attach and multiply. In summary, the as-prepared coaxial nanofibrous may have a powerful potential to be a safe and environment-friendly drug carrier against cervical cancer and other solid malignant tumours.

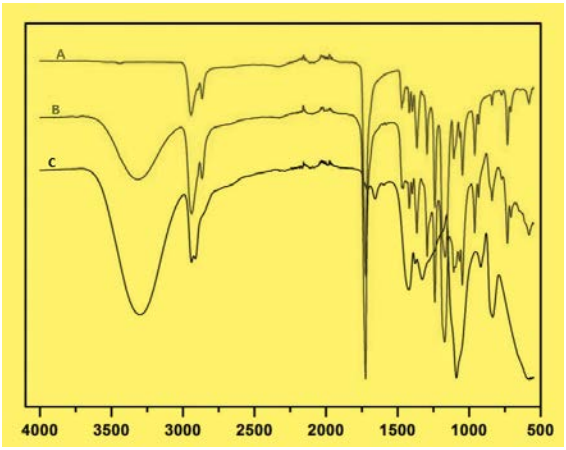

Figure 4.5. FTIR spectra of PVA nanofibers (A), Pullulan nanofibers (B), and Pullulan/PVA core-shell nanofibers with a flow ratio of 0.5:0.5 (C).

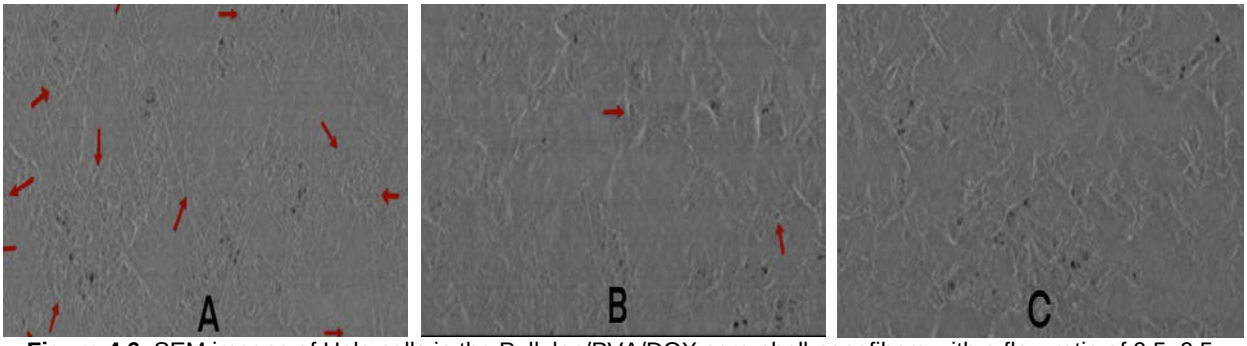

Figure 4.6. SEM images of Hela cells in the Pullulan/PVA/DOX core-shell nanofibers with a flow ratio of 0.5: 0.5 (A 1 day, B 4 days, C 7 days.)

Pullulan/PVA/DOX nanofibers in a ratio of 0.5:0.5 when in contact with cells for one day (in Fig.4.6. *A*), the Hela cells protected their typical morphology, which the shape of fibres can be observed. This occurred because of the high surface area accessible for cell connection due to the three-dimensional features and high surface area to volume ratio of the fibres. After seeding for four days (in Fig.4.6. *B*), a few of the cell states changed overall. Their shape changed from fusiform to round, indicating the apoptosis of cells. The fibres disappeared from the images, revealing that degradation of the fibres happened. As a result of the degradation of the polymers, DOX was released from the fibres, which killed the cancer cells. After being refined for 7 days (in Fig.4.6. *C*), the morphology of the cells cannot be identified, suggesting that the drug killed the Hela cells.

4. CONCLUSIONS

Utilise common polymers in biomedical applications because they are promptly accessible, non-toxic, and biocompatible. In expansion, low cost, and functionalisation of properties by chemical alteration of functional groups, their desired property. One such biocompatible polymer is the scaly one that finds utilise in a unique variety of biomedicals. Doxorubicin (DOX) could be a normal antimicrobial with antineoplastic activity. It has been used for over 30 years and remains one of the foremost utilised drugs in chemotherapy for various cancers. In any case, cardiotoxicity limits its utility for long periods. To overcome this limitation, encapsulation in drug delivery systems offers advantages over free drug organisation. The coaxial electrospinning technology successfully arranged PVA/Pullulan core-shell nanofibers. PVA has been used as a carrier polymer because it is relatively inexpensive, chemically and thermally stable. Additionally, pullulan contains a beaded structure within the nano-surface obtained by the electrospinning method alone, whereas the nanofiber structure obtained by blending with PVA is more uniform and the fibres obtained with electrospinning. DOX is utilised as an anticancer drug that restrains the synthesis of DNA in cancer cells. Pullulan can be used as a drug carrier due to its biocompatibility and non-immunogenicity. Pullulan has several user groups, which can be a helpful feature in drug delivery. DOX shows toxic effects on typical cells that the encapsulation of DOX can decrease. The drug-loaded nanofibers may have a practical potential to be a safe and environment-friendly drug carrier against cervical cancer and other solid and dangerous tumours.

References

1. *SRIDHAR, Radhakrishnan, Subramanian SUNDARRAJAN, Jayarama Reddy VENUGOPAL, Rajeswari RAVICHANDRAN a Seeram RAMAKRISHNA. Electrospun inorganic and polymer composite nanofibers for biomedical applications. Journal of Biomaterials Science, Polymer Edition [online]. 2013, 24(4), 365–385. ISSN 0920-5063, 1568-5624. Dostupné z: doi:10.1080/09205063.2012.690711*
2. *LUO, Xiaoming, Chengying XIE, Huan WANG, Chaoyu LIU, Shili YAN a Xiaohong LI. Antitumor activities of emulsion electrospun fibers with core loading of hydroxycamptothecin via intratumoral implantation. International Journal of Pharmaceutics [online]. 2012, 425(1–2), 19–28. ISSN 03785173. Dostupné z: doi:10.1016/j.ijpharm.2012.01.012*
3. *WEINBERG, Brent D., Elvin BLANCO a Jinming GAO. Polymer Implants for Intratumoral Drug Delivery and Cancer Therapy. Journal of Pharmaceutical Sciences [online]. 2008, 97(5), 1681–1702. ISSN 00223549. Dostupné z: doi:10.1002/jps.21038*
4. *WANG, Yazhou, Weili QIAO, Bochu WANG, Yiqiong ZHANG, Pengyu SHAO a Tieying YIN. Electrospun composite nanofibers containing nanoparticles for the programmable release of dual drugs. Polymer Journal [online]. 2011, 43(5), 478–483. ISSN 0032-3896, 1349-0540. Dostupné z: doi:10.1038/pj.2011.11*
5. *NATU, Mădălina V., Hermínio C. DE SOUSA a M.H. GIL. Effects of drug solubility, state and loading on controlled release in bicomponent electrospun fibers. International Journal of*

Pharmaceutics [online]. 2010, 397(1–2), 50–58. ISSN 03785173. Dostupné z: doi:10.1016/j.ijpharm.2010.06.045

6. *TAEPAIBOON, Pattama, Uracha RUNGSARDTHONG a Pitt SUPAPHOL. Drug-loaded electrospun mats of poly(vinyl alcohol) fibres and their release characteristics of four model drugs. Nanotechnology [online]. 2006, 17(9), 2317–2329. ISSN 0957-4484, 1361-6528. Dostupné z: doi:10.1088/0957-4484/17/9/041*
7. *KENNEDY, Kelsey M., Archana BHAW-LUXIMON a Dhanjay JHURRY. Cell-matrix mechanical interaction in electrospun polymeric scaffolds for tissue engineering: Implications for scaffold design and performance. Acta Biomaterialia [online]. 2017, 50, 41–55. ISSN 17427061. Dostupné z: doi:10.1016/j.actbio.2016.12.034*
8. *jirsak.pdf*
9. *Nanofibers - Production, Properties and Functional Applications | IntechOpen [online]. [vid. 2022-05-03]. Dostupné z: https://www.intechopen.com/books/397*
10. *LU, Yang, Jiangnan HUANG, Guoqiang YU, Romel CARDENAS, Suying WEI, Evan K. WUJCIK a Zhanhu GUO. Coaxial electrospun fibers: applications in drug delivery and tissue engineering. WIREs Nanomedicine and Nanobiotechnology [online]. 2016, 8(5), 654–677. ISSN 1939-5116, 1939-0041. Dostupné z: doi:10.1002/wnan.1391*
11. *BioRender [online]. [vid. 2022-07-03]. Dostupné z: https://app.biorender.com/*

ERASMUS+ PROJECT IN COOPERATION PARTNERSHIPS IN HIGHER EDUCATION GREENTEX – SUSTAINABLE DESIGN AND PROCESS IN TEXTILES FOR HIGHER EDUCATION

Pavla Těšinová

Technical University of Liberec, Faculty of Textile Engineering, Department of Textile Evaluation, Studentská 2, Liberec, Czech Republic, pavla.tesinova@tul.cz

Abstract:

Circular economy introduces the system of behavior and dealing with the sources limited in the world when overwhelmed consumption will cause serious problems as it is possible to see around us already. A lot of movements and organizations are working to help the environment, recycle more and use waste on one side as a material source to the other products. Among the other processes and good practice education is still necessary to show options to the public of students who will be employed in the industry later. The project GREENTEX - Sustainable Design and Process in Textiles for Higher Education aims to undertake various types of educational activities in the area of Sustainable Design and Process in Textile to promote and educate students in the conscious creation of the future products in all the industry they will be working. Teachers will have possibility to use the information sources prepared during the project solving and implement in their courses. The course will be prepared for the bachelor level of university study for the students who have basic knowledge in the textile and clothing.

Key words:

Erasmus+ project, circular economy in textile, sustainability, textile education

1. Introduction

The early definitions state that circular economy is an economy which can regenerate itself. This is done using either organic or renewable materials which are meant to be reused or re-entered into the ecosystem when their life cycle ends or technical materials that switch from production to consumption in cycles losing as little value or quality as possible [1], [2]. The well known and recognized definition says that the circular economy is a systems solution framework that tackles global challenges like climate change, biodiversity loss, waste, and pollution. The circular economy is based on three principles, driven by design [2], see Figure 1.

Figure 1. The 3 main principles of the circular economy [2] Created in Canva

It is underpinned by a transition to renewable energy and materials. A circular economy decouples economic activity from the consumption of finite resources. It is a resilient system that is good for business, people and the environment [3].

It is a high priority to be taken to reduce the amount of waste generated and improve overall waste management processes and programs. The popular prefix re- is used to expand the possibilities as repair, rewear, resold, repurposed, and remake in circular economy behavior. Providing proper and approved information is a task nowadays when information is attacking us and our emotions, for the EU acts The European Environment Agency (EEA) an agency of the European Union, whose task is to provide sound, independent information on the environment [4], [5].

Figure 2. The 3 main points in the hierarchy of the overall waste management processes and programs. Created in Canva

"Only better knowledge about the design and production processes of textile products and the awareness of the negative effects on the environment will make both business and consumers begin to see the real costs of this industry and look for possible solutions [6]."

2. Project GREENTEX aims

Project GREENTEX was built on the cooperation between the partners based on the classical Erasmus+ mobility. Leading organization is the Technical University of Lodz (Poland) with partners from the Faculty of Textile Engineering of the Technical University of Liberec (Czech Republic), University of Zagreb (Croatia), Technical University Kaunas (Lithuania), University of Aveiro (Portugal).

"The aim of the project is to undertake various types of educational activities in the area of Sustainable Design and Process in Textile. It is necessary to change the awareness and approach to this important topic. Future textile designers who in the future will create new products and solutions not only for the textile and clothing industry, but also for others that use textile products, e.g. medicine, transport, hygiene industry, protective equipment) must have full knowledge and awareness of how to create new solutions in line with the goals of sustainable development [6]*."*

"The intention of the project implementers is to fill the knowledge gap in the area of Sustainable Design and Process in Textiles for Higher Education. The condition of the textile and clothing industry and related industries does not look optimistic in the context of care for the natural environment. Therefore, it is necessary to raise awareness of the environmental effects of this industry. But most importantly, innovative solutions and directions of action will be developed so that this industry becomes less carcinogenic for the industry and the end user receives a safe product of high quality. The project beneficiary will be guided through the most important issues helpful in understanding the complexity of the textile and clothing industry. The implementation of the project will allow for the implementation of this goal by expanding knowledge in this field and the use of innovative didactic methods, e.g. such as Design Thinking and Human Centered Design, but also the use of concepts derived from the design strategy for excellence in teaching (design for excelence, DfX) e.g. design for recycling, design for remanufacture, design for repairability, design for disassembly and design for reverse logistics. A broader concept, encompassing all of the above-mentioned elements, is design for circularity, and even broader – design for sustainability. [6]*."*

3. Project GREENTEX upcoming results

Based on the Circular Economy frame the project GREENTEX will create modern research and study materials for the students and teachers who are interested to learn more in sustainable processes in textile available on the online platform. Teachers will have opportunity to implement single topics or use the whole study course as a complete program for a one semester. The course will be prepared for the bachelor level of university study for the students who have basic knowledge in the textile and clothing. Study materials will include a book as a base knowledge summary for those who would like to read continuous text, but it will be prepared also case studies based on the real situation, schematic descriptions and links will spread the reader to the real companies, movements and associations with the experience, special view or strategy to work with sustainability.

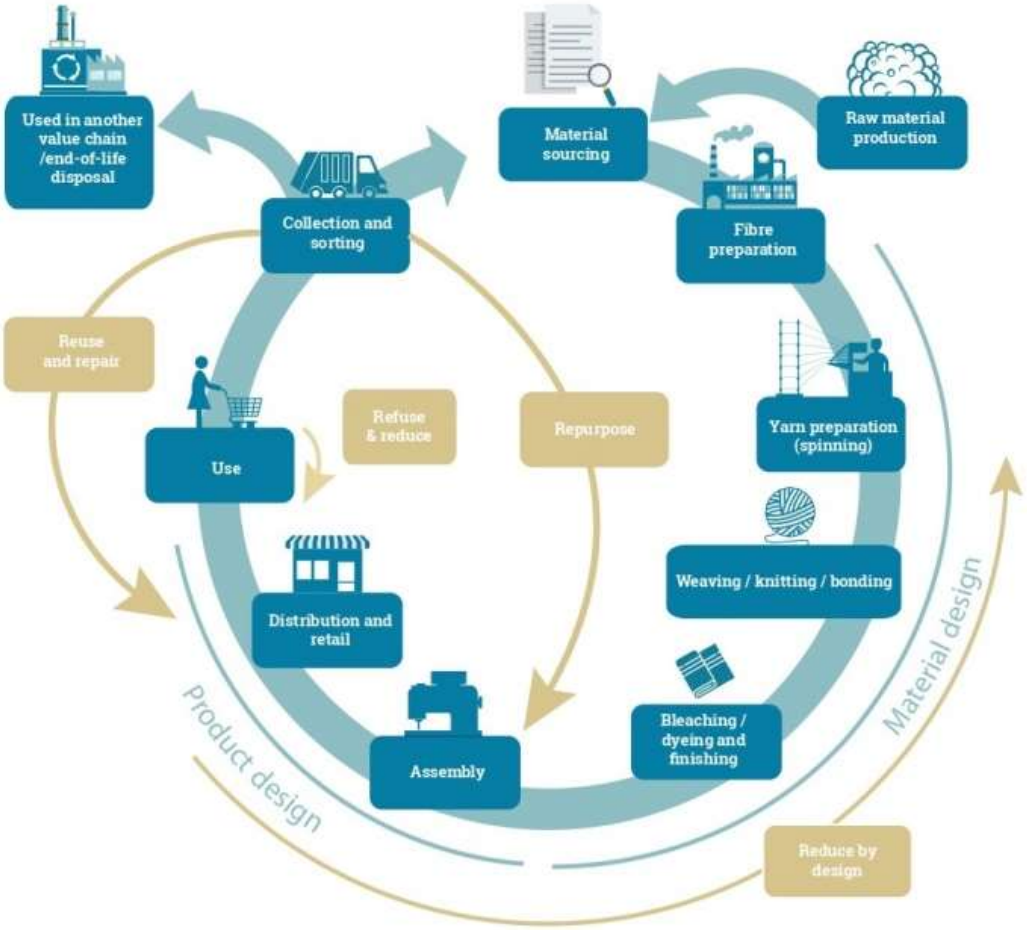

Figure 3. Circular Economy in Textile and Clothing as a frame for the collected knowledge [7]

The General Idea of Circular Economy and Sustainable Development applied to the Textile Industry has got its own specifics and steps on the circle, illustration on Figure 3. Sustainable materials as raw materials can be chosen from the various point of view as ecological production; possibility of recycling when second material is in the relatively same good quality; ecological disposal etc. Green Design is not just about reusing after the first life of the apparel but also cut when no more waste is produced. Sustainable textile processes are necessary to be invented effectively to be ready for mass production with economical aspects too. Sustainable approach to smart textiles is giving another way to give an extra value to the products which is against the fast fashion principles of the speed changing of the clothing. Distribution ways are crucial for saving money for transport and keeping money for production and material themselves. Consumption and market are manly about education of the consumers and end sellers who should be interested in their products through the financial and

marketing analysis. Reusing is giving chance to involve charity. Waste management is not only landfilling but also costly and labor burden activity which needs to be effective. Only after proper sorting recycling can be done in larger volume to the current state.

Program planned for the study course will be applied in the Green Summer School planned for the year 2023 in Portugal. Outputs from the summer school will be supplemented with the green design products to create Green Exhibition. Although exhibition will be virtual, exposed objects will have real format in the world. Project will address also the companies to take part in the good practice presentation. Mainly companies and associations from the countries of involved universities will be visible the most, project will bring the general knowledge from the EU experience and the world.

4. CONCLUSIONS

This paper is introducing Erasmus+ project related to the cooperation between the Technical University of Lodz (Poland), the Faculty of Textile Engineering of the Technical University of Liberec (Czech Republic), University of Zagreb (Croatia), Technical University Kaunas (Lithuania) and University of Aveiro (Portugal). The intention of the project is to fill the knowledge gap in the area of Sustainable Design and Process in Textiles for Higher Education. Based on the Circular Economy frame the project GREENTEX will create modern research and study materials ready to implement into the university courses by teachers or for self-study of individuals with the basic knowledge in textile and clothing in virtual area to effectively disseminate to the public.

ACKNOWLEDGEMENTS

This work was supported by the Project financed under the Erasmus+ Programme from Call 2021 Round 1 KA2, KA220-HED - Cooperation partnerships in higher education, Project No.: 2021-1-PL01-KA220-HED-000032201, Coordinator: Lodz University of Technology.

References

1. *I. Loiske, 'Circular Economy in Textile and Apparel Industry', Univ. Vaasa Sch. Mark. Commun., p. 83.*
2. *Commoner Barry. (1971). The Closing Circle : Nature Man and Technology First ed. New York: Alfred A. Knopf.*
3. *'Circular economy introduction'. https://ellenmacarthurfoundation.org/topics/circular-economy-introduction/overview (accessed Aug. 25, 2022).*
4. *Rinkesh, 'The Three R's: "Reduce, Reuse, Recycle" Waste Hierarchy To Enjoy Trash Free Life - Conserve Energy Future', Conserve Energy Future. Be Green. Stay Green, Sep. 06, 2014. https://www.conserve-energy-future.com/reduce-reuse-recycle.php (accessed Aug. 24, 2022).*
5. *'Data and maps — European Environment Agency'. https://www.eea.europa.eu/data-and-maps (accessed Aug. 24, 2022).*
6. *'Application in Call 2021 Round 1 KA2 KA220-HED - Cooperation partnerships in higher education. Sustainable Design and Process in Textiles for Higher Education'. Politechnika Lodzka, Technicka Univerzita v Liberci, Sveuciliste u Zagrebu, Kauno Technologijos Universitetas, Universidade de Aveiro, May 20, 2021.*
7. *U. N. Environment, 'Sustainable and circular textiles', UNEP - UN Environment Programme, Oct. 29, 2021. http://www.unep.org/explore-topics/resource-efficiency/what-we-do/sustainable-and-circular-textiles (accessed Aug. 25, 2022).*

EFFECT OF ANTI-WASH TREATMENT ON THE WEARING COMFORT PROPERTIES OF THE EMI SHIELDING MATERIAL

Dan Wang[1], Shi Hu[1], Dana Kremenakova[1], Jiri Militky[1]

[1]Department of Material Engineering, Faculty of Textile engineering, Technical university of Liberec, Studentska 1402/2, Liberec, Czech Republic, dan.wang@tul.cz

Abstract

The wearing comfort of metal coated EMI shielding clothing has been studied in recent years. One of the key issues is to balance the washability and wearing comfort properties. This paper uses ultrathin nonwoven polyester with copper-coated fabric as EMI shielding material. After parylene treatment, the washability is increased significantly without blocking all the apertures of the fabric. In this paper, the wearing comfort of this developed EMI shielding textile is analyzed and compared with the untreated fabric. The test result showed optimized washability and decent wearing comfort properties.

Keywords:

EMI shielding material, parylene coating, air permeability, water vapor permeability

1. Introduction

The continuous development of science and technology has also led to the popularization of electronic products. As a carrier of information transmission, electromagnetic waves are used in various fields such as household products and aerospace equipment[1]. While electromagnetic waves provide us with convenience, there is also a potential threat to our bodies[2]. Since people realized the harm of electromagnetic radiation, the related research on the harm of electromagnetic radiation has never stopped. Some electromagnetic shielding products have been produced one after another at present, among which textile shielding materials are mostly used in protective clothing for pregnant women or work clothing[3]. Although these shielding suits cannot completely eliminate the harm of electromagnetic waves, they can reduce the harm of electromagnetic waves to people in normal life and work[4]. But there are several issues that need to be solved for the EMI shielding material, except for improving the EMI shielding effectiveness. The focus of this paper is to study EMI shielding materials that can improve washability and maintain the original comfort performance. In this paper, a kind of ultrathin nonwoven polyester with copper and nickel coated fabric is used and the comfort properties of the samples will be tested, including air permeability and water vapor permeability. Then the fabric samples will be the parylene encapsulation process, there will be a thin protection layer coated on the fiber surface from this anti-wash treatment[5]. After the ensure the protection layer coating process is effective, the comfortable properties will be investigated again. A comparison of the results of the two-time experiments can provide the changes in the wearing comfort properties of the fabric material after anti-

wash treatment, and offer a theoretical basis for the continuous optimization of the anti-wash process in the later stage. This paper could achieve a facile and effective method to fabricate highly comfortable, and durable copper-coated fabric, guaranteeing the reliability for long-term wearable application and showing the great possibility for technical clothing application.

2. Materials and Methods

2.1. Materials

Meftex 10**:** Meftex 10 is a kind of ultrathin nonwoven polyester with copper and nickel coated fabric and it comes from a Czech Republic company named “Bochemie”. This company has succeeded in developing unique patented technology for the chemical deposition of metals on the surface of textile materials, and this kind of material is mainly used for EMI shielding function. In addition, Meftex 10 also has good breathability, antimicrobial, and anticorrosive[6].

Figure 1. The appearance of Meftex 10

Meftex 10 with parylene coating: Parylene is a generic name for a thermoplastic polymer synthesized from p-dimethylbenzene. There are now 3 types of parylene materials on the market, including C-type, D-type, and N-type. C-type was chosen in this paper, mainly because this type of material is very environmentally friendly[7]. It can obtain thin film materials by vapor deposition at room temperature and can generate thin films with any thickness within hundreds of microns. If using the vacuum deposition technology, the film thickness can be controlled more precision. In addition, the vacuum deposited parylene has excellent characteristics such as uniformity, shape retention, no micropores and no defects, and chemical inactivity. Therefore, parylene films are ideal for use as electrical insulating layers, chemical shielding layers, protective layers, and sealing layers[8]. Therefore, the "SCS Parylene Deposition System" is chosen by this paper and it is using vacuum deposition technology. In addition, this paper also selected different parylene contents for treatment and comparison, including 2 grams, 6 grams, and 10 grams.

Figure 2. SCS Parylene Deposition System (left) and the appearance of Meftex 10 with parylene treatment (right)

2.2. Methods

Fabric physical properties and porosity: A measure of the distance between the upper and lower surfaces of fabric under a certain pressure is called fabric thickness, and the common unit is mm. In this paper, the standard for thickness testing is EN ISO5084. The machine tested will apply a pressure of 1.0 kPa on the fabric and use a 50mm diameter presser foot to measure the thickness. In addition, the length, width, and weight of the fabric samples will be measured according to ISO 3801 and aim to calculate the area density of the fabric samples. In the textile industry, the area density is generally expressed by grammage. The grammage refers to the grams per square meter, and the commonly used unit is $g \cdot m^{-29}$. Porosity is also an important indicator for characterizing fabrics and it is the fraction of pore volume in the total volume of the fabric. It is between 0 and 1, or between 0% and 100%. Porosity is always divided into optical porosity and volume porosity, and there are several ways to test the porosity of fabrics. In this paper, the optical porosity will be measured by the microscope, the light, and image analysis software[10].

Electromagnetic shielding effectiveness: All samples are tested from 30 MHz to 3 GHz by the different waves that according to the ASTM D4935-10 standard. This sort of measurement standard calculates the electromagnetic shielding effectiveness of the samples by the insertion loss method. The test machine is built up with the sample holders and network analyzer produced by Rohde & Schwarz company. The network analyzer is an important part of the machine and is used to get and receive electromagnetic signals. In this paper, the fabric samples are measured 5 times at different places, and calculated the average as the result[11].

Air permeability: Air permeability of fabric refers to the performance of gas molecules passing through the fabric, which mainly affects the wearing comfort of the fabric. And the air permeability of the fabric refers to the volume of air flowing through the unit area of the fabric per unit time under a certain pressure difference. Generally, there are two ways for the air to pass through the fabric, including the interweaving gap and the gap between the fibers, and the interweaving gap is the main channel. The FX3300 air permeability meter is used as the test instrument in this paper, and the air permeability of the fabric samples is characterized in accordance with the ISO 923729 test standard. The size of the test fabric

sample is 20cm×20cm, the pressure difference of the measuring instrument is 200Pa, and the measurement unit is l/m^2/s. The measurement time of each sample is 10sec, and it is tested 5 times at different points[12].

Water vapor permeability: Water vapor permeability refers to the ability of fabrics to absorb and diffuse water vapor and is one of the important indicators to identify the comfort and hygiene of fabrics. Permetest is used as the measuring instrument for the water vapor permeability, it is a fast response measuring instrument for the non-destructive determination of relative water vapor permeability (RWVP %) and water vapor resistance (Ret m^2. Pa/W) of textile fabrics and so on. The test requirements for this measuring instrument and the evaluation of its measurement results are based on the ISO 11092 standard. In the measurement process, the fabric samples were exposed to a parallel airflow of 1 m/s and were placed on a water vapor permeable membrane that is on the heated perforated plate. The size of the test fabric sample is 20cm×20cm, and it is tested 5 times at different points. The test conditions should be set to around 20°C and 35% relative humidity[13].

3. Results and Discussion

3.1. Fabric physical properties and porosity

From the table 1, the basic information of the samples that with and without parylene coating can be seen. The original material "Meftex 10" own the lightest areal density of 11.8g/m^2, the thinnest thickness of 0.042mm, and the largest optical porosity of 33.71% in all samples. As the mass of parylene coating increases, it can be seen that the areal density and thickness of samples 1, 2, and 3 also show a positive correlation increase. On the contrary, as the quality of parylene coating increases, the optical porosity of the samples shows a significant decrease trend. The main reason why the optical porosity tends to decrease may be that as the amount of parylene coating on the fabric surface increases, more and more parylene ions cover the surface pores.

Table 1. Basic information of samples

Sample name	Sample description	Areal density [g/m^2]	Thickness [mm]	Optical porosity [%]
Sample reference	Meftex 10	11.8	0.042	33.71
Sample 1	Meftex 10 with 2g parylene coating	16.5	0.057	30.85
Sample 2	Meftex 10 with 6g parylene coating	27.2	0.076	23.19
Sample 3	Meftex 10 with 10g parylene coating	38.1	0.092	19.39

3.2. Electromagnetic shielding effectiveness

The data of all samples' electromagnetic shielding effectiveness at 1.5 GHz after different times washing cycles are presented in Table 2. For the reference sample, its electromagnetic shielding effectiveness dropped directly from 46.8dB to 0.24 dB after ten times washing cycles. This set of data fully demonstrates the poor washability of this kind of electromagnetic shielding material. The electromagnetic shielding performance of the samples was not affected after parylene coating, which can be confirmed by the no washing cycle data in Table 2. Their electromagnetic shielding effectiveness is still maintained above 40dB, but there is a big difference in the effect after washing cycles. Sample 1 has the same situation as the sample reference, and the electromagnetic shielding effectiveness is directly reduced to 1.97dB after ten times washing cycles and it shows that the parylene coating given by 2 grams is not enough to improve its washability. Relatively speaking, sample 2 and sample 3 showed better performance in washability. After ten times washing cycles, the electromagnetic shielding effectiveness of sample 2 decreased to 12.8dB and that of sample 3 only decreased to 23dB. From the above sets of data, it can be concluded that the washability is significantly improved after parylene coating and the parylene coating amount of 10 grams shows the best effect.

Table 2. Electromagnetic shielding effectiveness at 1.5 GHz of all samples after different times washing cycle

	Electromagnetic shielding effectiveness at 1.5 GHz [dB]				
Sample name	**No washing cycle**	**1 time washing cycle**	**2 times washing cycle**	**6 times washing cycle**	**10 times washing cycle**
Sample reference	46.8 ± 1.43	22.8±2.4	6.69±1.28	4.67±1.73	0.24±0.3
Sample 1	47.4±0.17	24.6±1.65	13.4±3.7	3.31±1.3	1.97±1.4
Sample 2	41.7±1.9	40.7±0.06	33.73±1.4	21.2±2.7	12.8±3.3
Sample 3	49.5±1.22	44.2±0.85	38.9±1.5	26.7±1.6	23±3.1

3.3. Air permeability

Meftex10 is a very breathable material, and it can be seen from the figure 3 (left) that its air permeability value can reach more than 6000 l/m^2/s. As the content of the parylene coating increases, more and more of the parylene ions are covered on the fabric. Therefore, the fibers may become slightly thicker, the areal density increases, and the direct air holes become smaller. Table 1 and Figure 3 (right) also demonstrate this. So, the resistance of gas passing through the fabric becomes larger and the air permeability of the fabric decreases. The three samples all showed the phenomenon that the air permeability decreased with the increase of the parylene coating content. Especially sample 2 and sample 3 showed a huge downward trend, they dropped from 6036 l/m^2/s to 3384 l/m^2/s and 2068 l/m^2/s respectively. Although air permeability has dropped a lot, it is still satisfactory for technical clothing

applications.

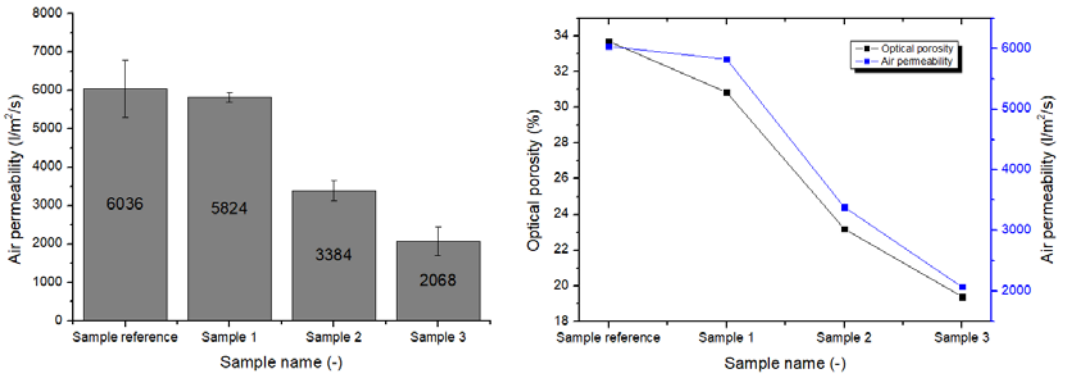

Figure 3. Air permeability of samples (left) and relationship between optical porosity and air permeability (right)

3.4. Water vapor permeability

Water vapor permeability, that is the transfer speed of water vapor in the fabric, depends on the sum of the water vapor transfer speed through the pores between fibers and yarns and the water vapor transfer speed inside the fibers. It can be seen from Figure 4 that the change law of the water vapor permeability of the fabric after the parylene coating is very close to the air permeability. Following the content of parylene coating increases, the value of relative water vapor permeability decreases, and the value of water vapor resistance increases. However, it can be seen from the two sets of data that the magnitude of the change in water vapor permeability is relatively low. Meftex 10, which has the highest relative water vapor permeability and lowest water vapor resistance, is 97.9% and 0.13 Pa.m^2/W. However, sample 3 has the lowest relative water vapor permeability and highest water vapor resistance, the value is 83.7% and 2.17 Pa.m2/W respectively. The main reason for this phenomenon is that the increase in the amount of parylene coating reduces the optical porosity of the samples from Figure 5, resulting in a decrease in water vapor permeability.

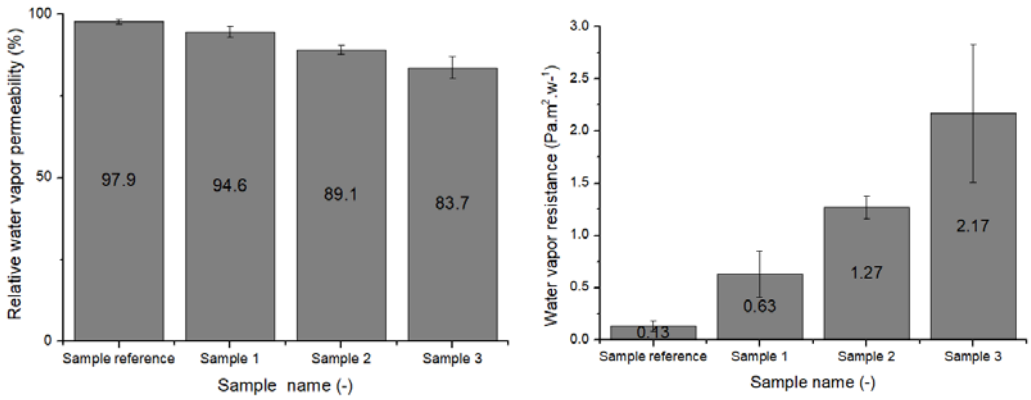

Figure 4. Relative water vapor permeability (left) and water vapor resistance (right) of samples

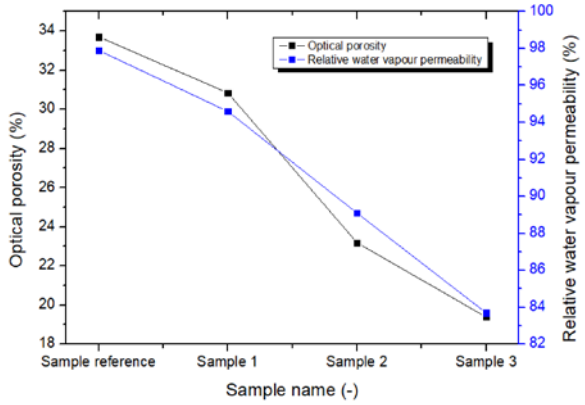

Figure 5. Relationship between optical porosity and relative water vapor permeability

4. CONCLUSION

According to the above experimental results, the following conclusions can be drawn. After coating 6 grams and 10 grams of parylene, the sample washing ability is improved significantly compared to the sample reference and sample 1. After ten times of washing cycles, the electromagnetic shielding effectiveness still remains around 30%-50%. For the air permeability and water vapor permeability, both of them decrease after parylene coating. The reason is coating layer closed part of the pores, which led to a decrease in optical porosity. Since Meftex 10 itself has excellent air permeability and water vapor permeability, even if the performance of these two aspects is reduced after parylene coating and it still meets the comfort requirements of technical clothing.

Acknowledgements

The authors are grateful for the financial support by the student research project 2022 No. SGS-2022-6012 supported by the Czech Ministry of Education and Faculty of Textile, Technical University of Liberec.

References

1. *Munalli D, Dimitrakis G, Chronopoulos D, et al. Electromagnetic shielding effectiveness of carbon fibre reinforced composites. Composites Part B: Engineering 2019; 173: 106906.*
2. *Benefits and hazards of electromagnetic waves, telecommunication, physical and biomedical: a review. European Review, https://www.europeanreview.org/article/17596 (2019, accessed 13 July 2022).*
3. *Yin J, Ma W, Gao Z, et al. A Review of Electromagnetic Shielding Fabric, Wave-Absorbing Fabric and Wave-Transparent Fabric. Polymers 2022; 14: 377.*
4. *Gye MC, Park CJ. Effect of electromagnetic field exposure on the reproductive system. Clin Exp Reprod Med 2012; 39: 1–9.*
5. *Parylene Deposition Process. Specialty Coating Systems, https://scscoatings.com/parylene-*

coatings/parylene-deposition/ (accessed 13 July 2022).

6. *Hu S, Wang D, Periyasamy AP, et al. Ultrathin Multilayer Textile Structure with Enhanced EMI Shielding and Air-Permeable Properties. Polymers 2021; 13: 4176.*
7. *Chang JH-C, Lu B, Tai Y-C. Adhesion-enhancing surface treatments for parylene deposition. In: 2011 16th International Solid-State Sensors, Actuators and Microsystems Conference. 2011, pp. 390–393.*
8. *SCS Parylene Deposition – Cleanroom Research Laboratory, https://cleanroom.utdallas.edu/manuals/scs-parylene-deposition/ (accessed 13 July 2022).*
9. *Cimilli S, Nergis BU, Candan C, et al. A Comparative Study of Some Comfort-related Properties of Socks of Different Fiber Types. Textile Research Journal 2010; 80: 948–957.*
10. *Peckham J, Andrews GT. Simple optical method to determine the porosity of porous silicon films. Thin Solid Films; 520. Epub ahead of print 31 January 2012. DOI: 10.1016/j.tsf.2011.10.146.*
11. *Militký J, Křemenáková D, Venkataraman M, et al. Exceptional Electromagnetic Shielding Properties of Lightweight and Porous Multifunctional Layers. ACS Appl Electron Mater 2020; 2: 1138–1144.*
12. *Hes L. Heat, Moisture and Air Transfer Properties of Selected Woven Fabrics in Wet State. d-wok. Epub ahead of print 2008. DOI: 10.3993/tbis2008157.*
13. *Sabantina L, Hes L, Rodríguez-Mirasol J, et al. Water Vapor Permeability through PAN Nanofiber Mat with Varying Membrane-Like Areas. Fibres and Textiles in Eastern Europe 2019; 133: 12–15.*

POTENTIAL OF NANOFIBROUS MEMBRANES IN MULTI-LAYER FABRICS TO STORE PCMS

Kai Yang[1],*, Xiuling Zhang[1], Jakub Wiener[1], Mohanapriya Venkataraman[1], Yuanfeng Wang[1], Guocheng Zhu[2,5], Juming Yao[3,4,5], Jiri Militky[1]

[1] Department of Material Engineering, Faculty of Textile Engineering, Technical University of Liberec, Liberec, Czech Republic, kai.yang@tul.cz

[2] College of Textiles and Engineering, Zhejiang Sci-tech University, Xiasha Education Park, P.R. China

[3] School of Materials and Engineering, Zhejiang Sci-tech University, Xiasha Education Park, P.R. China

[4] School of Materials Science and Chemical Engineering, Ningbo University, Ningbo City, P.R. China

[5] Zhejiang-Czech Joint Laboratory of Advanced Fiber Materials, Zhejiang Sci-tech University, Xiasha Education Park, P.R. China

Abstract:

Incorporating phase change materials (PCMs) into textiles is one facial method to realize personal thermal management (PTM). Despite the significant progress of PCM-incorporated textiles, the incorporation of PCMs into textiles remains an outstanding challenge. In this work, we described a sandwich-like multi-layer PCM fabric, which consisted of nanofibrous membranes as barrier layers and PCM-loaded viscose fabric as a PCM-loaded layer. Three common organic PCMs including polyethylene glycol (PEG), paraffin wax (PW) and myristic acid (MA), and the polyurethane (PU) nanofibrous membranes was used. As a result, we achieved that weak interfacial adhesion between melting PCMs and PU nanofibrous membranes accounted for leakage phenomena. Only the sample (UPWV) with PU nanofibrous membranes as barrier layers and paraffin wax (PW) as PCMs had no leakage. Besides, thermal energy storage and phase transition of UPWV supported its application in various applications.

Keywords: PCM, nanofibrous membrane, leakage, thermal buffering effect

1. Introduction

Personal thermal management (PTM) has been studied for decades [1]. Incorporation of organic phase change materials (PCMs) (e.g., paraffin wax, fatty acid, polyethylene glycol, etc.) into textiles is one facial method for PTM [2]. During the phase transition of the PCMs over a certain temperature, the

thermal resistance of the PCMs is changeable and the thermal energy is absorbed or released. However, the leakage of the PCMs is the main problem for the practical applications. To avoid leakage, microencapsulated PCMs (MPCMs) and form-stable PCMs (FSPCMs) have been proposed [3]. MPCMs have been the most industrial technology and its application in textiles has been studied for decades [4]. The MPCMs consist of supporting materials as shell and PCMs as core, where stability of thermal energy storage and phase transition of MPCMs is enhanced [5]. However, the encapsulation efficiency of MPCMs required modification [6]. FSPCMs are usually prepared by filling PCMs into porous materials (e.g., zeolite, aerogel, foam etc.) [3,7–9]. Although the leakage of melting PCMs can be avoided, thermal energy storage and phase transition of final FSPCMs is significantly affected by pores. In addition, PCMs are usually coated on fabrics or incorporated into fibers for PTM. For PCM-incorporated fabrics, various methods have been proposed to apply MPCMs or FSPCMs on fabrics, including coating, padding, laminating, printing etc. However, loss of MPCMs or FSPCMs possibly happens because of mechanical movement (e.g., washing, abrasion). For PCM fibers, the incorporation of the pure PCMs, MPCMs or FSPCMs into fibers is the alternative [10,11]. However, the final thermal energy storage and mechanical property of PCM fibers are affected by PCM contents.

It is noticed that the leakage of PCMs from its coated fabric during heating/cooling cycles is governed by viscosity of melting PCMs and adhesion between melting PCMs and fabrics if the pure PCMs are coated on fabrics directly. From this point of view, the multi-layer fabric structure by using barrier layers covering the PCM-loaded layer (PCM-coated fabrics) is possible to avoid leakage [12]. Especially for the selection of the barrier layers, the nanofibrous membranes are alternative. By controlling porosity and surficial chemistry to obtain hydrophilicity or hydrophobicity or oleophobic property, various nanofibrous membranes have been applied for oil/water separation, air filtration etc. [13–15]. Besides, the high resistance against mass transfer of nanofibrous membrane-coated fabrics have been proposed [16]. From this point of view, it is an alternative to use the nanofibrous membranes can be used as barrier layer to resist against the penetration of melting PCMs by adjusting their interfacial adhesion.

In this work, we first tried to construct a multi-layer fabric structure consisting of PCM-loaded layer and barrier layers. Three common PCMs sharing similar phase transition points were used, including polyethylene glycol (PEG) (M_w=6,000), myristic acid (MA) and paraffin wax (PW). The polyurethane (PU) nanofibrous membranes as barrier layers and nonwoven viscose fabric was used to load PCMs. After determining on the suitable nanofibrous membranes and PCMs according to leakage test, the thermal energy storage and phase transition of the multi-layer PCM fabrics as well as their thermal buffering effect were investigated.

2. Experimental

2.1 Materials

Three PCMs including polyethylene glycol (PEG) (M_w=6,000), myristic acid (MA) and paraffin wax (PW) were purchased from Sigma Aldrich. The polyurethane (PU) nanofibrous membranes (3g/m^2) were

provided from Institute for Nanomaterials, Advanced Technology and Innovation, Technical University of Liberec. Viscose fabric (47g/m^2) was provided from Department of Material Engineering, Faculty of Textile Engineering, Technical University of Liberec.

2.2 Preparation of multi-layer fabrics

The preparation of nanofibrous membrane-incorporated multi-layer PCM fabrics followed the diagram of **Figure 1.**, including two barrier layers and one PCM-loaded layer. The preparation of PCM-loaded layer followed the same process of published work [17]. As a result, three PCM-loaded layers were prepared, including MA-coated viscose fabric, PW-coated viscose fabric and PEG-coated viscose fabric. After having their mass, the weight percentage (p_{PCM}) of PCMs for MA-coated viscose fabric, PW-coated viscose fabric and PEG-coated viscose fabric was 80wt%, 86wt% and 88wt%, respectively. Correspondingly, the multi-layer fabrics with MA-coated viscose fabric, PW-coated viscose fabric or PEG-coated viscose fabric as the PCM-loaded layer were labeled as UMAV, UPWV and UPEGV, respectively.

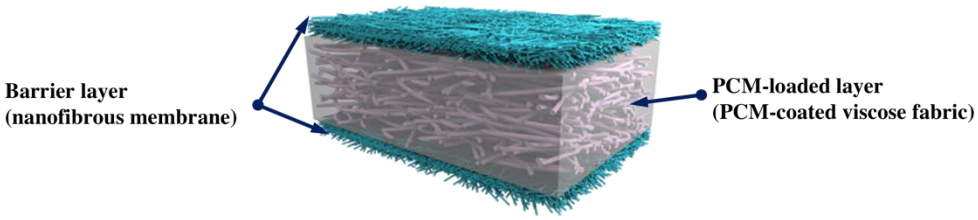

Figure 1. Diagram of nanofibrous membrane-incorporated multi-layer PCM fabrics

2.3 Tests and methods

2.3.1 Characterization of leakage of melting PCMs from PCM-loaded layer and multi-layer fabrics

Before leakage test, all the samples were taken a photo as the reference. Then, the leakage test was to put all the samples on the surface of commercial fabrics on the stable plate heater with temperature of 80^{o}C. The usage of commercial polyester fabrics was to avoid possible quick thermal shrinkage of nanofibrous membranes because the high heating temperature was used. After 30 min, the samples were taken a photo, which was compared with reference photo.

2.3.2 Characterization of contact angle (CA) values of melting PCMs on PU nanofibrous membranes

The CA values of melting PCMs on PU nanofibrous membranes were measured by using a custom setup. All the solid PCMs were firstly put in the breaker. Then, the breakers with solid PCMs were placed on the stable plate heater with temperature of 80^{o}C till all the PCMs became liquid. Then, the nanofibrous membrane was attached on the stable plate heater with temperature of 80^{o}C for 5 min to obtain heat transfer balance. To have a homogenous nanofibrous membrane, the adhesive tape was used to avoid deformation of nanofibrous membranes during measurement. Then, the melting PCMs droplets with

volume of 25 uL were taken from the breaker and then placed on the surface of the nanofibrous membrane. At the same time, the optical camera (DINO) was used to record the shape of droplets of melting PCMs. As a result, the videos that CA values change with time were obtained.

2.3.3 Characterization of thermal energy storage and phase transition measurement

Differential scanning calorimetry (DSC) (METTLER TOLEDO, Swiss) was used to characterize the thermal energy storage and phase transition of samples. The samples were kept ranging from 5.00 to 10.00 mg for the DSC measurement, and the nitrogen (N_2) gas rate was kept as 50 mL/min during the whole DSC measurement. The temperature range was from 25 ^{o}C to 80 ^{o}C. As a result, the parameters related to phase transition and thermal energy storage were obtained, including onset melting/solidifying temperature (T_{om}/T_{oc}), peak melting/solidifying temperature (T_{pm}/T_{pc}), endset melting/solidifying temperature (T_{em}/T_{ec}) and melting/solidifying enthalpy (ΔH_m/ΔH_c). Besides, the supercooling degree was obtained, which was the difference between T_{om} and T_{oc}.

3. Results and discussion

3.1 Determination on the suitable multi-layer fabric structure

The leakage test results of the PCM-loaded layer and the multi-layer PCM fabrics were shown in **Figure 2**. Obviously, the leakage of the PCM-loaded layers was found. During heating process, the solid PCMs melt, and porous structure of viscose fabric did not support to hold the melting PCMs. For the multi-layer PCM fabrics, it was found that only sample consisting of PU nanofibrous membrane as barrier layers and PW-coated viscose fabric as PCM-loaded layer had no leakage while other samples had leakage. We propose that the interfacial adhesion between melting PCMs and nanofibrous membranes accounted for the leakage phenomena. The wetting behavior of melting PCMs on nanofibrous membranes characterized by change of contact angle (CA) values of molten PCM droplets on PU nanofibrous membranes with time was shown in **Figure 3**. In details, the CA values of melting PW on PU nanofibrous membranes were almost constant about 110^{o}, which suggested the stable weak adhesion between melting PW and PU nanofibrous membranes. The CA values of melting PEG or melting MA on PU nanofibrous membranes tended to continuously decrease with time. It took 10s for the melting PEG on PU nanofibrous membranes to have CA values of 90^{o} and took 20s for the melting MA on PU nanofibrous membranes to have 90^{o}. Besides, the porosity of PU nanofibrous membranes also accounted for the leakage. By using IMAGE J software, the surface porosity of PU nanofibrous membrane was measured as 5.07%, and pore size was measured as 356$\pm$147nm. Therefore, the combination of weak adhesion, lower porosity and small pore size of PU nanofibrous membranes increased the difficult for melting PW to penetrate. So, only the sample consisting of PU nanofibrous membranes as barrier layers and PW-coated viscose fabric as PCM-loaded layer was further investigated in the following analysis and labeled as UPWV.

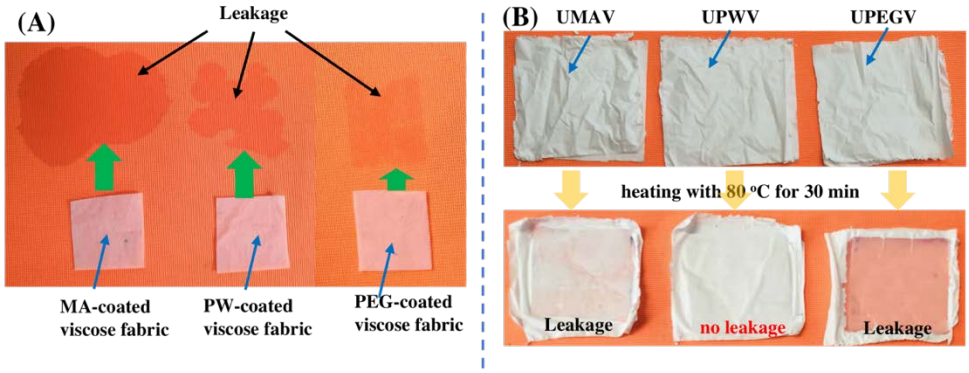

Figure 2. Leakage test results

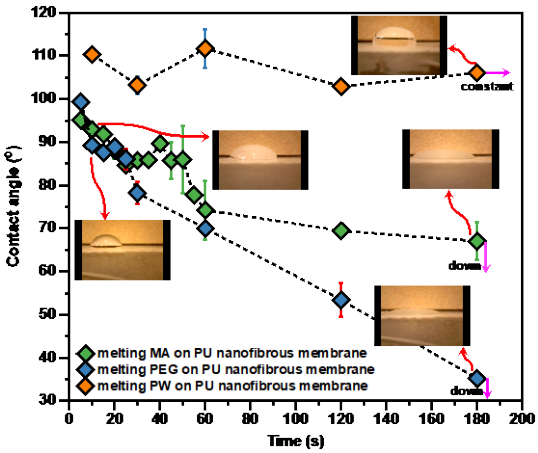

Figure 3. CA values of molten PCMs on surface of nanofibrous membranes

3.2 Phase transition and thermal energy storage of the suitable multi-layer PCM fabric (UPWV sample)

To investigate the thermal energy storage and phase transition of UPWV, DSC measurement of UPWV was performed. It was noticed that UPWV contained viscose fabric and PU nanofibrous membrane, and both thermal property and crystallization behavior of PW in the UPWV may be altered when compared with PW. Therefore, the thermal energy storage and phase transition of PW-coated viscose fabric (labeled as PWV) and the pure PW were also evaluated. All the DSC curves of PW, PWV and UPWV were shown in **Figure 4**. Two peaks including *peak 1* and *peak 2* were observed for PW, PWV and UPWV. The *peak 1* ranging from 30 °C to 40 °C was caused by solid-solid (SS) phase transition in PW, which generally implicates a rotational motion at the molecular level from the rotator phase α to the non-rotating phase β. The *peak 2* ranging from 50 °C to 60 °C was caused by solid-liquid (SL) phase transition in PW during heating/cooling cycles. The details related to phase transition and thermal energy storage were given in shown in **Table 1** and **Table 2**.

For both SS phase transition, PW, PWV and UPWV had similar T_{pm} and T_{pc} values, which suggested that both viscose fabric and PU nanofibrous membrane little affected α phase and β phase of PW. In

addition, it was found that the SS phase transition from α phase to β phase of UPWV and PW started slightly earlier than PW while SS phase transition from β phase to α phase of UPWV and PW started slightly later than PW. Correspondingly, supercooling degree (ΔT_{SS}) was changed, and the order of ΔT values was found as PW>PWV>UPWV. The stable SS phase transition behavior of PW, PWV and UPWV were found. As a result, the PW, PWV and UPWV had ΔH_m values of 31 J/g, 26 J/g and 25 J/g, and ΔH_c of 28 J/g, 23 J/g, 22 J/g, respectively.

For SL phase transition, both viscose fabric and PU nanofibrous membrane little affected major crystalline structure of PW after observing T_{pm} and T_{pc} values. Besides, UPWV and PW started melt slightly later than PW while crystalline earlier than PW, which was opposite against SS phase transition. Both viscose fabric and PU nanofibrous membrane altered the crystallization mechanism and α-β phase transition mechanism. Correspondingly, the supercooling degree (ΔT_{SL}) for SL phase transition was changed, and the order of ΔT_{SL} values was found as PW>PWV>UPWV. By combining with ΔT_{SS}, the higher thermal energy storage efficiency was found in UPWV when compared with PW and PWV. Besides, the PW, PWV and UPWV had ΔH_m values of 132 J/g, 113 J/g and 105 J/g, and ΔH_c values of 133 J/g, 113J/g and 108 J/g, respectively.

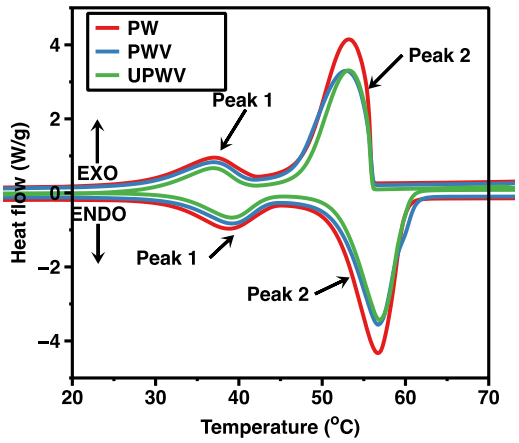

Figure 4. DSC curves for PW, PWV and UPWV

Table 1. Phase transition and thermal energy storage of *peak 1* (solid-solid phase transition)

Sample code	T_{om} (°C)	T_{pm} (°C)	T_{em} (°C)	ΔH_m (J/g)	T_{oc} (°C)	T_{pc} (°C)	T_{ec} (°C)	ΔH_c (J/g)	$\lvert\Delta T\rvert$ (°C)
PW	31.59	38.51	43.84	31.23	41.49	36.82	29.23	28.05	9.9
PWV	32.33	39.06	43.43	25.74	40.88	36.61	29.37	22.69	8.55
UPWV	32.62	39.12	43.32	24.14	40.67	36.71	29.74	21.03	8.05

Table 2. Phase transition and thermal energy storage of *peak 2* (solid-liquid phase transition)

Sample code	T_{om} (°C)	T_{pm} (°C)	T_{em} (°C)	ΔH_m (J/g)	T_{oc} (°C)	T_{pc} (°C)	T_{ec} (°C)	ΔH_c (J/g)	$\lvert\Delta T\rvert$ (°C)
PW	51.27	56.73	59.97	132.33	56.11	53.22	47.5	133.07	4.84
PWV	51.62	56.65	60.2	113.45	56.25	52.97	46.64	115.00	4.63
UPWV	52.05	56.91	60.12	105.39	56.19	53.24	47.67	108.11	4.14

4. CONCLUSION

In conclusion, the possibility of nanofibrous membranes as barrier layers in multi-layer PCM fabrics has been systematically investigated. The control of interfacial adhesion between nanofibrous membranes and melting PCMs was significant for leakage results. As a result, the PU nanofibrous membranes successfully resisted against the penetration of melting PW and corresponding multi-layer PCM fabric without leakage was obtained. The final multi-layer PCM fabric had also high thermal energy storage and stable phase transition. The work not only benefits the textile industrial but also support other fields which requires PCMs.

ACKNOWLEDGEMENTS

This work was supported by the project 'Advanced structures for thermal insulation in extreme conditions' (Reg. No. 21- 32510M) granted by the Czech Science Foundation (GACR).

References

1. *Hu, R., Liu, Y., Shin, S., Huang, S., Ren, X., Shu, W., Cheng, J., Tao, G., Xu, W., Chen, R., and Luo, X. (2020) Emerging Materials and Strategies for Personal Thermal Management. Adv Energy Mater, 10 (17), 1903921.*
2. *Yang, K., Venkataraman, M., Zhang, X., Wiener, J., Zhu, G., Yao, J., and Militky, J. (2022) Review: incorporation of organic PCMs into textiles. J Mater Sci, 1–50.*
3. *Yang, K., Venkataraman, M., Karpiskova, J., Suzuki, Y., Ullah, S., Kim, I.-S., Militky, J., Wang, Y., Yang, T., Wiener, J., Zhu, G., and Yao, J. (2021) Structural analysis of embedding polyethylene glycol in silica aerogel. Micropor Mesopor Mat, 310, 110636.*
4. *Reyez-Araiza, J.L., Pineda-Piñón, J., López-Romero, J.M., Gasca-Tirado, J.R., Contreras, M.A., Correa, J.C.J., Apátiga-Castro, L.M., Rivera-Muñoz, E.M., Velazquez-Castillo, R.R., Bueno, J. de J.P., and Manzano-Ramirez, A. (2021) Thermal Energy Storage by the Encapsulation of Phase Change Materials in Building Elements—A Review. Materials, 14 (6), 1420.*

5. Zhang, L., Yang, W., Jiang, Z., He, F., Zhang, K., Fan, J., and Wu, J. (2017) Graphene oxide-modified microencapsulated phase change materials with high encapsulation capacity and enhanced leakage-prevention performance. Appl Energ, 197, 354–363.
6. Liu, H., Wang, X., and Wu, D. (2019) Innovative design of microencapsulated phase change materials for thermal energy storage and versatile applications: a review. Sustain Energy Fuels, 3 (5), 1091–1149.
7. Tas, C.E., Karaoglu, O., Tas, B.A., Ertas, E., Unal, H., and Bildirir, H. (2020) Improved latent heat storage properties through mesopore enrichment of a zeolitic shape stabilizer. Sol Energ Mat Sol C, 216, 110677.
8. Baruah, J.S., Athawale, V., Rath, P., and Bhattacharya, A. (2022) Melting and energy storage characteristics of macro-encapsulated PCM-metal foam system. Int J Heat Mass Tran, 182, 121993.
9. Su, H., Lin, P., Lu, H., Zhao, X., Sheng, X., and Chen, Y. (2022) Janus-Type Hydroxyapatite-Incorporated Kevlar Aerogel@Kevlar Aerogel Supported Phase-Change Material Gel toward Wearable Personal Thermal Management. Acs Appl Mater Inter, 14 (10), 12617–12629.
10. Niu, Z., and Yuan, W. (2021) Smart nanocomposite nonwoven wearable fabrics embedding phase change materials for highly efficient energy conversion-storage and use as a stretchable conductor. Acs Appl Mater Inter, 13 (3), 4508–4518.
11. Yang, A., Cai, L., Zhang, R., Wang, J., Hsu, P.-C., Wang, H., Zhou, G., Xu, J., and Cui, Y. (2017) Thermal Management in Nanofiber-Based Face Mask. Nano Lett, 17 (6), 3506–3510.
12. Yang, K., Venkataraman, M., Wang, Y.-F., Xiong, X.-M., Yang, T., Wiener, J., Militky, J., Mishra, R., Marek, J., Zhu, G.-C., and Yao, J.-M. (2019) Thermal behaviour of multi-layer composite containing PEG and laponite as PCM. 671–676.
13. Ma, W., Jiang, Z., Lu, T., Xiong, R., and Huang, C. (2022) Lightweight, elastic and superhydrophobic multifunctional nanofibrous aerogel for self-cleaning, oil/water separation and pressure sensing. Chem Eng J, 430, 132989.
14. Xiang, B., Shi, G., Mu, P., and Li, J. (2022) Eco-friendly WBF/PAN nanofiber composite membrane for efficient separation various surfactant-stabilized oil-in-water emulsions. Colloids Surfaces Physicochem Eng Aspects, 645, 128917.
15. Chu, Z., Li, Y., Zhou, A., Zhang, L., Zhang, X., Yang, Y., and Yang, Z. (2022) Polydimethylsiloxane-decorated magnetic cellulose nanofiber composite for highly efficient oil-water separation. Carbohyd Polym, 277, 118787.
16. Knížek, R., Karhánková, D., Bajzík, V., and Jirsák, O. (2019) Lamination of Nanofibre Layers for Clothing Applications. Fibres Text East Europe, 27 (1(133)), 16–22.
17. Yang, K., Wiener, J., Venkataraman, M., Wang, Y., Yang, T., Zhang, G., Zhu, G., Yao, J., and Militky, J. (2021) Thermal analysis of PEG/Metal particle-coated viscose fabric. Polym Test, 100, 107231.

BI-AXIAL STRETCHING OF RIB KNITTED FABRIC AND ITS EMI SHIELDING

Sundaramoorthy Palanisamy[1], Jana Ornstova[2], Veronika Tunakova[1], Monika Vysanska[2], Jiri Militky[1]

[1]Department of Material Engineering,[2]Department of Technologies and Structures
Faculty of Textile Engineering, Technical University of Liberec, Studentska 1402/2, 461 17 Liberec, Czechia.
Corresponding author email: sundaramoorthy.palanisamy@tul.cz; sundar2026@gmail.com

Abstract:

The electrically conductive textiles market expands every year because of its broader applications. Especially in electromagnetic shielding applications, textile materials are widely used. Many studies are on the development and manufacturing of conductive textiles, but very few studies are related to their deformation performance. In this work, the rib knitted fabric sample is developed with silver-coated polyamide yarn and stretched using the biaxial device. While biaxial extension, the sample is tested for electromagnetic shielding, electrical resistance, and porosity as per the standards. There is a significant change in electromagnetic shielding effectiveness during fabric stretching. Also, the fabric's electrical resistance and porosity were changed against the fabric stretching. The deformation performance knowledge of the conductive fabric is essential for developing the samples for wireless strain sensing and motion-detecting applications.

Keywords:

Electromagnetic shielding; Rib-knit; Silver-coated yarn; Biaxial elongation; Porosity.

1. Introduction

The universe is filled with an electromagnetic (EM) field everywhere; naturally and artificially. The natural source of the EM fields are the earth's magnetic fields and lightning, and the artificial or man-made sources of EM fields are all electronic devices and electric power transmission lines [1]. EM ionized radiation is divided into four categories: static fields, extremely low-frequency EM fields, intermediate frequency EM fields, and radiofrequency EM fields [2]. EM radiation of intermediated and radio frequency ranges may be harmful to live beings and electronic devices and travels at the speed of light. It is discussed that living beings exposed to an extreme level of EM radiation may cause cancer, tissue damage, lymphoma, leukemia, etc. [3]. Electronic devices can be damaged by EM radiation because it creates electromagnetic interference (EMI) [4]. Due to the usage of electronic devices at the workplace, the cause of electromagnetic hypersensitivity for humans working in EM radiation environments is increasing [5]. Electronic devices and living beings' shielding is essential to protect from EM radiation and its interferences.

Electrically conductive metals are the best material for EM shielding applications: silver, copper, stainless steel, iron, gold, nickel, brass, etc., are good conductors of electricity and reflect and absorb most of the EM radiations [6]. Metals have some drawbacks, like being heavier, able to corrode, not flexible, etc. Using metal-coated textile materials, these disadvantages can be overcome, i.e., it becomes flexible, less weight, and porous. Different techniques are used in textile materials to convert conventional textile materials to conductive textile materials. The main methods used are coatings by conductive polymers [7-8], metal coatings of fiber, yarn & fabric [9-10], metal fibers blending [11-12], metalcore wires [13-14], and carbonization of fabric, yarn & fibers [15].

Three mechanisms to shield the EM radiation are: reflection is primary, absorption is secondary, and multiple reflections are tertiary. Beyond these mechanisms, the area covered by the shielding material

plays the leading role in shielding. The gap or space, also called an aperture in the textile structure, has the drawback of penetration of the radiations. Study [16] modeled the measured and calculated EM shielding of conductive yarn woven fabric. The difference between the measured and calculated EM shielding is in dB, of which the ASTM D 4935 has a random error of ±5 dB. In study [17], the silver and copper coated cotton single jersey fabric along with spandex is stretched until 100 percent and tested for EM shielding effectiveness (SE). The SE decreases with an increase in the fabric elongation, and the electrical resistivity is increased. The stretching process mainly changes the fabric properties and geometry (porosity), but the reason behind the changes is not reported. The length-related resistance of the knitted fabric was modeled in work [18]. The electrical resistance of the conductive knitted fabric is directly proportional to its length and indirectly proportional to its cross-section. The modeled and measured values are close, proving that the length-related resistance changes with fabric extension. In study [19], the EeonTex (conductive nonwoven microfibril) sample was mounted on a stretching device to measure its electrical resistance. While stretching the fabric sample, the electrical resistance was increased with an increase in elongation. The silver-coated and elastomeric yarn were knitted alternatively with an interlocking design developed in mentioned work. The developed fabric sample was stretched to 200 percent and measured its resistance. The fabric's resistance was increased with an increase in elongation, which is explained by decrease in contact points between conductive loops. Also, the tightness factor of the fabric can influence the SE results [20]. There are many studies on fabric's electrical conductivity during stretching, but very few on EM shielding.

In this work, the silver-plated yarn was procured and used to develop simple rib knitted fabric. The rib fabric was stretched using a biaxial device to measure its EM SE, electrical resistance, and porosity. The change in all studied properties against the stretching of fabric at uni- as well as bi-directional was found. The reasons for this change are also discussed in the results.

2. Materials and Methods

2.1 Materials

The silver-coated polyamide (AgPA) yarn with a linear density of 60 tex was procured from Statex Inc., Breman, Germany. Conductive silver AgPA yarn was used to knit rib stitch on a 14 gauge flat needle bed knitting machine (Shima Seiki Ltd., Japan, and Model SRY 123LP). The typical structure of the knitted fabric is shown in Figure 1 (a). The basic parameters of knitted fabric are shown in Table 1. The knitted fabric was used to examine electrical resistance and electromagnetic shielding during uniaxial and biaxial extensions.

Table 1. Fabric parameters and their results

Fabric parameters	Results
Type	Weft knit (Flat)
Structure	1x1 Rib
Areal density [gram per sq. meter]	442
Thickness [mm]	1.52
Courses per [cm]	9.4
Wales per [cm]	7.5
Loop length [cm]	0.537

2.2 Biaxial device

Figure 1(b) shows the experimental setup of the biaxial device attached to the developed fabric sample. This device contains four separate clamps for the fabric, which function independently and can operate in horizontal and vertical directions separately and together. During horizontal or vertical stretching of the sample, the two clamps placed opposite to each other will extend, and the remaining

two clamps will be idle. In both stretching processes, the fabric, clamps operate simultaneously in four directions. For this experiment, the clamp speed is fixed at 3.5 mm/sec and the maximum elongation length is 30% with a break of 30 seconds at each 7 mm for the measurement. The biaxial device is designed especially for fabric elongation studies.

(a) (b)

Figure 1. Photographic image of (a) fabric sample and (b) fabric attached in biaxial device for the experiment.

2.3 Electromagnetic shielding effectiveness

SE of the sample set was measured according to the ASTM D4935-10 [21] for the planar materials using a plane wave, the far-field EM wave at the temperature T = 21°C, and the relative humidity RH = 54 %. SE of the samples was measured over the frequency range from 30 MHz to 1.5 GHz. The setup consisted of a sample holder with its input and output connected to the network analyzer. A shielding effectiveness test fixture (Electro-Metrics, Inc., model EM-2107A) was used to hold the sample. The design and dimension of the sample holder follow the ASTM method mentioned above. A vector analyzer, Rohde & Schwarz ZN3, was used to generate and receive electromagnetic signals. The standard mentioned above determines the shielding effectiveness of the fabric using the insertion-loss method. The shielding effectiveness assessment required a reference measurement for the empty cell. A “through” calibration with the help of the reference sample was made first. A load measurement was performed on a solid disk shape sample subsequently. The reference and load specimens must be of the same material and thickness. The reference and load samples geometries are according to the ASTM D 4935-10. The subsequent statistical analysis performed the measurements at five different places of the samples.

According to the requirements of EM shielding textiles, depending on professional or general use, textiles can be classified into five grades from a fair grade to an excellent grade (see Tables 2 and 3) [22]. Professional use comprises professional protective uniforms for electronic manufacturers, shielding of medical equipment, etc. In contrast, general use is represented by casual wear, maternity clothes, aprons, shielding of consumptive electronic products and communication-related products, etc.

Table 2. Classification of EM SE textiles for professional use.

Grade	Excellent	Very good	Good	Moderate	Fair
Range [dB]	SE >60	60 ≥ SE >50	50 ≥ SE >40	40 ≥SE >30	30 ≥ SE >20

Table 3. Classification of EM SE textiles for general use.

Grade	Excellent	Very good	Good	Moderate	Fair
Range [dB]	SE >30	30 ≥ SE >20	20 ≥ SE >10	10 ≥ SE >7	7≥ SE >5

2.4 Electrical resistance measurement

The continuous measurement of the electrical resistance of the knitted fabric sample was done using an Arduino resistance meter designed for this experiment. The edges of the fabric samples were connected with two probes from the resistance circuit board at a distance of 14 cm. The sample was stretched at a 3.5 mm/sec speed to measure electrical resistance until 30 percent fabric elongation. While uniaxial stretching, the probes are connected to the stretching direction for a measurement. During biaxial extension, the probes are connected in the vertical direction of the sample, and only wale way resistance is measured. The resistance readings were recorded online using MATLAB software and then saved in a file for further analysis.

2.5 Porosity measurement

The porosity of the fabric sample during the biaxial stretching process was measured using the Nikon camera and NIS element software as per internal standard number 23-107-01/01. Fabric porosity means the ratio between the area of all pores on the image and the area of fabric on the image. The binary image was created using the image analysis, pores were defined as an object for measurement, and the rest was considered as background.

3. Results and discussions

3.1 Frequency versus EM shielding effectiveness

The dependence of SE on frequency from 30 MHz to 1.5 GHz of rib knitted fabric stretched at horizontal, vertical, and both ways are shown in Figure 2.
Figure 2(a) shows that the SE decreases with the increasing frequency of the horizontal way elongated fabric. At 0% elongation, the SE at 1.5 GHz frequency of fabric is reduced up to 5 dB compared with SE at 30 MHz frequency. The increase in extension creates more significant variations on SE, and the deviation was up to 15 dB approximately. While stretching rib fabric in a horizontal way or course way, the inter-loop of yarn between the course directions is relaxing initially and then tightens. At 0% elongation of the fabric, the SE at 30MHz is 61 dB, and SE at 1.5 GHz is 56 dB. After 5 % elongation, the SE decreases drastically with an increase in frequency. At 30 MHz frequency, the SE is about 59 dB, but at 1.5 GHz, the SE is 46 dB for 5% elongation; the difference is almost 13 dB compared with a 5 dB difference in 0%.

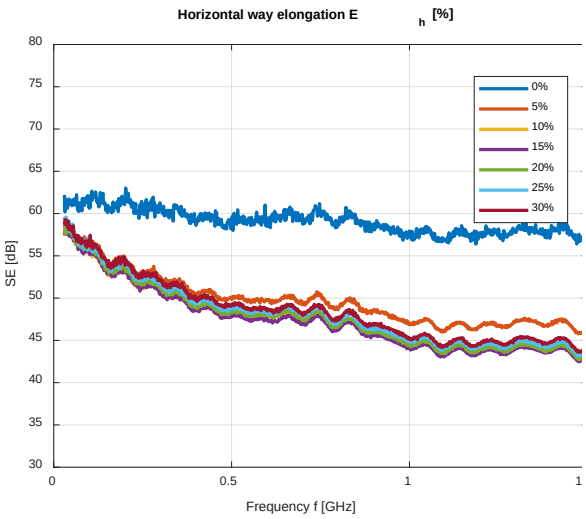

(a)

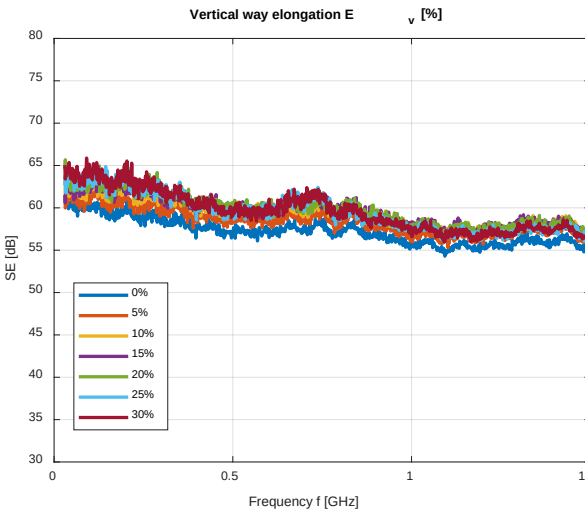

(b)

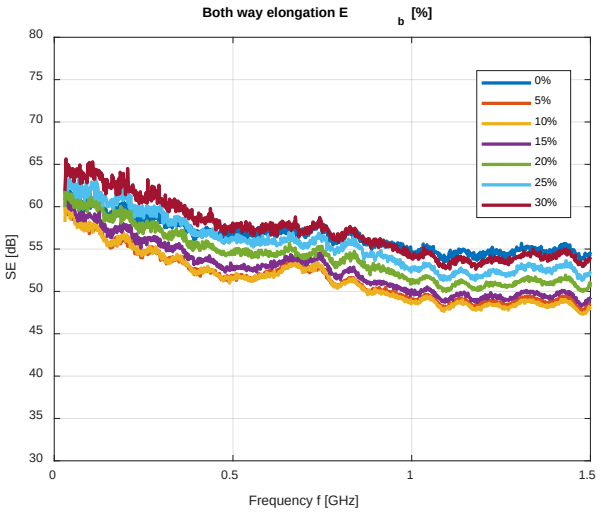

(c)

Figure 2. Frequency, *f* (30 MHz ~ 1.5 GHz) versus electromagnetic shielding effectiveness, SE [dB] during knitted sample elongation *E*, at (a) horizontal way E_h, (b) vertical way E_v, and (c) both ways E_b.

3.2 Effect of biaxial stretching of the fabric on chosen properties

The results of the fabric elongation versus SE, electrical resistance, and porosity are summarized in Figure 3. From 10% to 30% elongation, the fabric has a difference in SE between 16 to 17 dB. The SE change from initial to final frequency is about 28% after the horizontal way elongation. The interloop between the wales gets tightened during the vertical or wale way of the fabric stretching. Figure 2(b) shows the frequency versus SE graph of vertical way stretched rib fabric up to 30% elongation. At an initial frequency of 30MHz, the change in SE against extension is wider than the final frequency of 1.5 GHz, which gets narrower. At 0% elongation, the difference between the initial to final frequency is 5 dB, and a decrease in SE with an increase in frequency is noticed. After 5% elongation, the difference from initial to final SE is about 3 dB, and the maximum change in SE of 8 dB is recorded at 30% elongation. Almost a 12% deviation in SE was noticed at vertical way extension of the rib fabric. Both ways stretching of the fabric samples for frequency versus SE results is shown in Figure 2(c). SE decreases with an increase in frequency, and at 5% both ways elongation of the samples, the initial SE is 60 dB, and the final SE is 48 dB. A maximum of 20% deviation in SE was noticed between the initial and final frequency range.

The maximum deviation in SE results from initial frequency to final frequency is 12%, 20%, and 28% for horizontal, both ways, and vertical ways, respectively. More deviation was noticed in a horizontal way stretching of the fabric.

3.3 *Effect of biaxial stretching of the fabric on chosen properties*

The results of the fabric elongation versus SE, electrical resistance, and porosity are summarized in Figure 3.

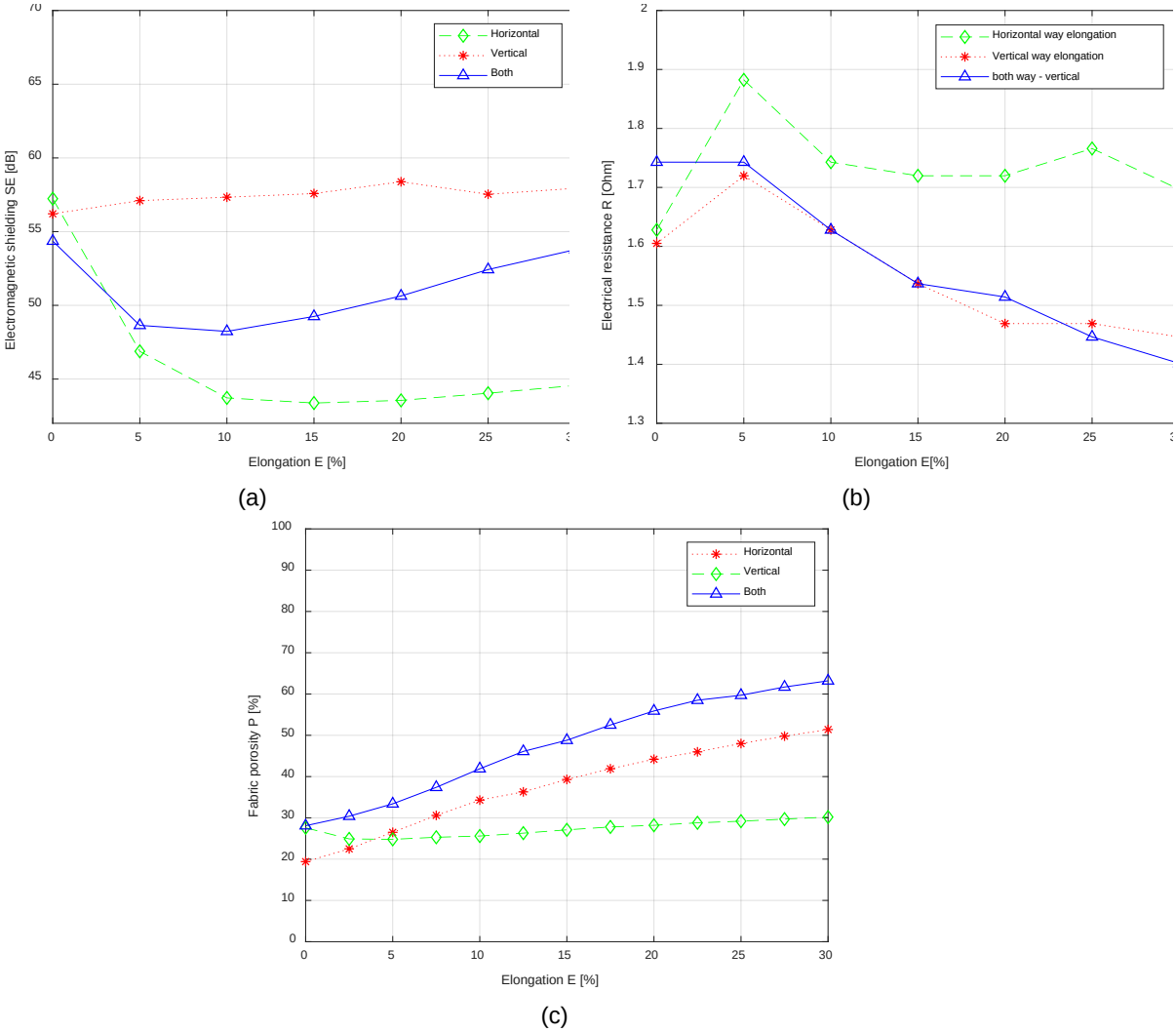

Figure 3. Results of the horizontal way, vertical way, and both ways elongation *E* [%] of the fabric versus (a) electromagnetic shielding effectiveness SE [dB] at 1.5 GHz frequency, (b) electrical resistance *R* [Ω], and (c) fabric porosity *P* [%].

Figure 3(a) shows the graphical results of rib fabric elongation versus SE at 1.5 GHz frequency. Horizontal way elongation of the fabric sample increases, then the SE value decreases until 15% sample elongation after that a slight increase was noticed. In vertical way fabric extension, the SE is increasing slightly with an increase in elongation percentage, and maximum SE was recorded at 20% elongation. In both ways extension of the fabric, the SE values decrease until 10% elongation and then and then there is a drastic increase up to the initial value. The change in SE on fabric elongation is due to the change in contact resistance of the loop yarns and yarn length resistance. The fabric porosity also affects transmitting the radiation through pores, as discussed below. Still, this study noticed that the horizontal way elongation makes the course loops elongate more at the initial stretch to create more contact between the loop yarns. The wale loops are already constructed tightly, but during vertical way stretching, the wale loops are tightened more to make a stronger contact point; which helps to increase electrical conductive paths to increase EM shielding. At both ways elongation, the course loops are loosened to create less contact between the yarns. After more extension, both wale and course loops are pulled from each other to create more contact pressure, causing increasing electrical conductivity. These results are reflected in the elongation versus electrical resistance graph

shown Figure 3(b). The electrical conductivity and shielding effectiveness are directly proportional to each other, and resistance is indirectly proportional. Another reason for the increase or decrease in SE is the fabric porosity in the fabric structure. Elongation versus fabric porosity results of the fabric is shown in figure 3(c). It was noticed that the fabric porosity is almost neutral at vertical way elongation. The open area increases with increasing extension at the horizontal, and both way stretching of the fabric. That is why the horizontal way elongation of fabric transmits more radiation through an open pore and SE decreases with increasing elongation. The interesting thing noticed in both ways elongation of the fabric is that the fabric porosity increases, but the SE decreases initially and then increases. In this case, the open pore and loosening in loops decrease the SE until 10% elongation. After that, the contact pressure increases to increase the SE value. But in both ways, the maximum SE is lesser than the vertical way due to more open area affecting the SE value.

4. CONCLUSIONS

The 1x1 rib structure was fabricated using a silver-coated polyamide yarn of 60 tex with a flat knitting machine. Biaxial stretching of the sample was precisely done using the in-house biaxial device at the step of 5% elongation of the fabric until 30%. The sample damage was noticed at a stretch greater than 30%.

The horizontal way stretching of fabric has a wider deviation in electromagnetic shielding effectiveness value and nearly 12% change in SE at 0 to 5% elongation. The second most deviation in shielding effectiveness is noticed in both ways of stretching fabric, 10% change in SE at 0 to 5% elongation. The least deviation in shielding effectiveness was recorded at a vertical way of stretching, from 0 to 5% elongation has a 2% deviation in SE. The shielding effectiveness decreases with an increase in elongation for the horizontal way. SE decreases until 10% elongation and then increases in both ways. SE increases with an increase in elongation in a vertical way. The change in SE values concerning stretch directions is related to structural changes in knitted loops. Vertical way stretching creates consequent tension on wale loops to increase contact between yarns, and it tends to increase electrical resistance, as shown in Figure 3(b). In a horizontal way stretching, the fabric loosens its loops initially because course loops relax; after that, the loops get tightened to increase the SE value slightly. Both ways stretching have different behavior. The SE decreases initially because of course loops relaxation; both course loops and wale loops are tightened to create more electrical conductance, but the SE value does not increase like the vertical way. In this case, the fabric porosity plays an important role; due to both ways stretching, the porosity is higher than during one-way stretch, so the electromagnetic waves are transmitted more through the open pore area. Hence, it is concluded that the deformation in fabric tends to have statistically significant effect on electromagnetic shielding and electrical conductance values. Designing the conductive fabric for EMI shielding application needs attention to a preparatory process where stretch or elongation can occur.

Acknowledgement

I acknowledge Mrs. Jana Stránská and Mrs. Šárka Řezníčková for their extended support throughout this work.

References

1. *Barnes FS, Greenebaum B (eds). Bioengineering and Biophysical Aspects of Electromagnetic Fields. Third. Boca Raton, Florida, USA.: Taylor & Francis Group, 2006.*
2. *Martin R (ed). Epidemiology of Electromagnetic Fields. Second. Boca Raton, Florida, USA.: Taylor & Francis Group, 2008.*
3. *Lin JC (ed). Electromagnetic Fields in Biological Systems. Boca Raton, Florida, USA.: Taylor & Francis Group, 2012.*
4. *Ott HW. Electromagnetic Compatibility Engineering. Hoboken, NJ, USA: John Wiley & Sons, Inc. Epub ahead of print 12 August 2009. DOI: 10.1002/9780470508510.*

5. *Stein Y, Udasin IG. Electromagnetic hypersensitivity (EHS, microwave syndrome) – Review of mechanisms. Environ Res 2020; 186: 109445.*
6. *Geetha S, Kumar KKS, Rao CRK, et al. EMI shielding: Methods and materials-A review. J Appl Polym Sci 2009; 112: 2073–2086.*
7. *Kaynak A, Håkansson E. Characterization of conducting polymer coated fabrics at microwave frequencies. Int J Cloth Sci Technol 2009; 21: 117–126.*
8. *Yanılmaz M, Sarac AS. A review: Effect of conductive polymers on the conductivities of electrospun mats. Text Res J 2014; 84: 1325–1342.*
9. *Uzun S, Han M, Strobel CJ, et al. Highly conductive and scalable Ti3C2T -coated fabrics for efficient electromagnetic interference shielding. Carbon N Y 2021; 174: 382–389.*
10. *Wu X, Chen Y, Liang K, et al. Fe2O3 Nanowire Arrays on Ni-Coated Yarns as excellent electrodes for High Performance Wearable Yarn-Supercapacitor. J Alloys Compd 2020; 158156.*
11. *Liang R, Cheng W, Xiao H, et al. A calculating method for the electromagnetic shielding effectiveness of metal fiber blended fabric. Text Res J 2018; 88: 973–986.*
12. *Šafářová V, Militký J. Electromagnetic shielding properties of woven fabrics made from high-performance fibers. Text Res J 2014; 84: 1255–1267.*
13. *Ortlek HG, Alpyildiz T, Kilic G. Determination of electromagnetic shielding performance of hybrid yarn knitted fabrics with anechoic chamber method. Text Res J 2013; 83: 90–99.*
14. *Perumalraj R, Nalankilli G, Balasaravanan TR, et al. Electromagnetic shielding tester for conductive textile materials. Indian J Fibre Text Res 2010; 35: 361–365.*
15. *Li TT, Wang R, Lou CW, et al. Manufacture and effectiveness evaluations of high-modulus electromagnetic interference shielding/puncture resisting composites. Text Res J 2013; 83: 1796–1807.*
16. *Neruda M, Vojtech L. Electromagnetic shielding effectiveness of woven fabrics with high electrical conductivity: Complete derivation and verification of analytical model. Materials (Basel) 2018; 11: 1657.*
17. *Ali A, Baheti V, Militky J, et al. Comparative Performance of Copper and Silver Coated Stretchable Fabrics. Fibers Polym 2018; 19: 607–619.*
18. *Li L, Wai Man au, Wan KM, et al. A Resistive Network Model for Conductive Knitting Stitches. Text Res J 2010; 80: 935–947.*
19. *Teyeme Y, Malengier B, Tesfaye T, et al. A fabric-based textile stretch sensor for optimized measurement of strain in clothing. Sensors (Switzerland) 2020; 20: 7323.*
20. *Atalay O, Kennon WR, Husain MD. Textile-Based Weft Knitted Strain Sensors: Effect of Fabric Parameters on Sensor Properties. Sensors 2013; 13: 11114–11127.*
21. *ASTM D4935-10. Standard Test Method for Measuring the Electromagnetic Shielding Effectiveness of Planar Materials. West Conshohocken, PA. Epub ahead of print 2010. DOI: 10.1520/D4935-10.*
22. *FTTS-FA-003. Specified Requirements of Electromagnetic Shielding Textiles. New Taipei City, Taiwan, https://www.ftts.org.tw/images/fa003E.pdf (2005).*

SONOCHEMICAL ROUTE TO DEVELOP FLAME RETARDANT AND ANTIBACTERIAL TEXTILES

Asif Javed[1], Jakub Wiener[1] and Jana Saskova[1]

[1]Department of Material Engineering, Faculty of Textile Engineering, Technical University of Liberec, Studentska 1402/2, 46117, Liberec 1, Czech Republic

Abstract:

In this research work, zinc oxide nanoparticles (ZnO NPs) were grown onto the 100 % cotton fabric by sonochemical method. Zinc acetate dihydrate ($Zn(CH_3COO)_2.2H_2O$) and sodium hydroxide (NaOH) were used as precursors. After ZnO NPs growth N-Methylol dimethylphosphonopropionamide (MDPA) flame retardant was applied in the presence of 1, 2, 3, 4-butanetetracarboxylic acid (BTCA) as cross linker by conventional pad dry cure method. Induced couple plasma atomic emission spectroscopy (ICP-AES) was used to determine the deposited amount of Zn contents and phosphorous (P) contents. Scanning electron microscopy (SEM), and X-ray powder diffraction (XRD) were employed to determine the surface morphology and characterization of developed samples. Furthermore, the vertical flame retardant test, and antibacterial activity of samples were examined. The developed samples showed excellent results for flame retardancy (i.e. 39 mm char length, 0 second after flame time, 0 second after glow time), and 100 % antibacterial activity.

Key words:

Flame retardants, Ultrasonics, Antibacterial, ZnO, Nano particles, Work wear. Metal oxides

1. Introduction

Flame retardant treatment on textile fabrics has gained significant importance because flame retardant fabrics can be used as safety work wear in industry, firefighting wears, in hospitals, and as in household upholstery [1]. Various chemical applications are involved in producing flame retardant fabrics, but most of the flame retardant chemicals contain halogen compounds that are not environmentally friendly[2,3]. Phosphorous based durable flame retardant chemicals are alternative to halogen compounds. These phosphorous based compounds are environmentally friendly and economical for cotton textile application [4]. N-methylol dimethyl phosphonopropion amide (MDPA) is one of the most promising flame retardant compounds due to its durability, low toxicity, environmentally friendly nature and convenient application. When it is applied along with a cross linker onto the cotton fabric, it makes the covalent bond with a hydroxyl group of cotton cellulose, hence enhancing its durability[5,6].

Nanotechnology is another most important field that has been utilized successfully and efficiently in the industry to achieve desired fruitful results. Nanomaterials in the textile industry have earned great importance due to their multipurpose uses [7]. Nanomaterials in the form of nanoparticles are being used in textile industry for antibacterial textile [8], UV protection, to increase flame retardancy etc.[9–11]. Zinc Oxide (ZnO) is one of the most versatile inorganic metal oxides. It is n-type semiconductor white in color, having a high refractive index with wide band gap of 3.37 ev [12,13]. Along with UV protection, antibacterial, and self-cleaning properties, Zinc Oxide nanoparticles (ZnO NPs) are being used in flame retardant coating [14,15]. The main challenges in the flame retardant/ZnO NPs system are the use of formaldehyde free cross linker, homogeneous, even, and stable deposition of ZnO NPs. BTCA is a formaldehyde free cross linker that can be used for cotton flame retardant systems[16,17]. For ZnO NPs Javed et al reported that sonochemical is an advance and economical method for the in-situ synthesis of ZnO NPs onto the cotton fabric. This technique controls the

nanoparticle size without affecting the strength of the fabric. As well as ultrasonic waves disperse and deposit the nanoparticles onto the fabric more stably, homogeneously and evenly [18].

In this research study, ZnO NPs were in-situ synthesized onto the cotton fabric by ultrasonic irradiation method. After that, MDPA flame retardant in the presence of formaldehyde free cross linker BTCA were applied onto the cotton fabric by pad dry cure method. The main goal of the present work is to find out the optimized parameters for in-situ sonochemical synthesis of ZnO NPs, and investigate the role of ZnO NPs in flame retardant finishing and influence on the antibaterial properties.

2. Experimental

2.1. Materials

The 100% percent cotton fabric with plain weave texture, 155 g/m^2 density, 52 ends/inch, 28 picks/inch, and 20 tex warp count, 20 tex filling count was acquired from the Technical University of Liberec, Czech Republic. Zinc acetate dihydrate ($Zn(CH_3COO)_2.2H_2O$), sodium hydroxide (NaOH), sodium hypophosphite (SHP), and 1, 2, 3, 4-butanetetracarboxylic acid (BTCA) chemical reagents were procured from Merk, Prague, Czech Republic. N-Methylol dimethylphosphonopropionamide (MDPA) was obtained from Huntsman Corporation. Acramin SW acrylic based binder was obtained from Tanatex Chemicals Netherlands. All the obtained chemical reagents were of analytical grade and utilized as purchased without further purification.

2.2. Methods

ZnO NPs were synthesized and stabilized onto the cotton fabric concomitantly by hydrolysis of Zinc acetate dihydrate ($Zn(CH_3COO)_2.2H_2O$) and sodium hydroxide (NaOH) in deionized water. The precursors Zinc acetate dihydrate ($Zn(CH_3COO)_2.2H_2O$) (0.05 M, 0.1 M, 0.15 M) and sodium hydroxide (NaOH) (0.1 M, 0.2 M, 0.3 M) with different molar concentrations were dissolved separately in deionized water under vigorous magnetic stirring (300 rpm) condition. After that the cotton fabric piece was dipped into the Zinc acetate dihydrate solution for 10 minutes under vigorous magnetic stirring (300 rpm). After 10 minutes NaOH solution was poured drop wise into that solution at ambient temperature and under vigorous magnetic stirring (300 rpm). For absolute completion of reaction mechanism, the obtained solution containing immersed cotton fabric piece was sonicated for different sonication times (30 min, 60 min, 90 min, and 120 min). The Branson sonication probe (20 kHz, 50 % efficiency, 150 W) was utilized in this experimental procedure. The reaction temperature was maintained at 80 °C by utilizing hot plate. Then the treated fabric pieces were washed thoroughly with deionized water to remove any impurities. Eventually the obtained fabric pieces were dried in air oven at 90 °C for 120 minutes. In order to compare the sonochemical process and to accentuate the critical influence of ultrasound irradiation waves, one sample was developed by conventional magnetic stirring method using same precursor's concentrations (0.1 M $Zn(CH_3COO)_2.2H_2O$, 0.3 M NaOH) and temperature (80 °C) as optimized sample, under vigorous magnetic stirring (300 rpm) for 90 minutes. In this research work this sample is named as sample A.

MDPA application was performed with the help of a laboratory padder (Werner Mathis AG Switzerland) at 80% wet pick up. The bath formulation used 300 g/l MDPA, 60 g/l BTCA crosslinker, 50 g/l SHP catalyst, and 5 g/l acramin SW binder. Various preliminary trials were done to find the best compatible concentrations of MDPA and BTCA with optimized ZnO NPs loaded samples. ZnO NPs loaded samples were impregnated in MDPA and BTCA solution, padded and dried at 110 °C for 3 minutes and cured at 150 °C for 2 minutes. In order to find out the crucial role of ZnO NPs in flame retardancy, a cotton fabric sample was treated with MDPA and BTCA without ZnO NPs treatment. In this research work, that sample is named sample B.
Table 1 shows the complete experimental design for in-situ synthesis of ZnO NPs on the cotton fabric.

Table 1 Molar concentrations of the precursors, sonication time, MDPA, resulting Zn contents, P contents, Experimental results for flammability test, bacterial reduction %

Sample	Zinc Acetate	NaOH	Sonication Time	MDPA	Zn Contents	P contents	Flammability Test			Bacterial Reduction %	
							After Flame Time (s)	After Glow Time (s)	Char Length (mm)	S. areus	E.coli
Untreated	-	-	-	-	-	-	19.34	9.62	Completely burned	-	-
1	0.05	0.1	30	300	1.69	3.88	7.42	3.25	103	41.78	30.34
2	0.05	0.1	60	300	1.84	3.86	7.02	3.11	99	43.29	34.67
3	0.05	0.1	90	300	2.13	3.83	6.,24	2.94	95	47.86	40.45
4	0.05	0.1	120	300	1.91	3.84	6.74	3.03	96	45.76	37.47
5	0.05	0.2	30	300	2.83	3.81	5.83	2.72	92	49.97	41.23
6	0.05	0.2	60	300	3.19	3.79	5.26	2.33	90	51.79	45.57
7	0.05	0.2	90	300	3.34	3.78	4.19	2.04	89	59.93	50.78
8	0.05	0.2	120	300	3.27	3.79	4.84	2.17	89	52.79	45.91
9	0.05	0.3	30	300	4.64	3.75	3.87	1.91	83	69.86	59.92
10	0.05	0.3	60	300	4.86	3.73	3.58	1.62	78	73.32	65.76
11	0.05	0.3	90	300	5.09	3.72	2.82	1.06	76	78.84	74.65
12	0.05	0.3	120	300	5.01	3.72	3.12	1.34	76	75.54	71.78
13	0.1	0.1	30	300	5.34	3.71	2.09	0.78	73	81.45	77.87
14	0.1	0.1	60	300	5.47	3.70	1.56	0.27	71	85.42	82.98
15	0.1	0.1	90	300	5.65	3.70	0.59	0	68	94.43	91.46
16	0.1	0.1	120	300	5.53	3.70	1.17	0	70	89.95	84.56
17	0.1	0.2	30	300	8.78	3.63	0	0	55	100	98.64
18	0.1	0.2	60	300	9.07	3.61	0	0	53	100	100
19	0.1	0.2	90	300	9.31	3.58	0	0	51	100	100
20	0.1	0.2	120	300	9.17	3.60	0	0	52	100	100
21	0.1	0.3	30	300	11.23	3.50	0	0	42	100	100
22	0.1	0.3	60	300	12.09	3.47	0	0	40	100	100
23	0.1	0.3	90	300	13.14	3.44	0	0	39	100	100
24	0.1	0.3	120	300	12.54	3.46	0	0	40	100	100
25	0.15	0.1	30	300	5.39	3.72	1.97	0.53	73	84.49	80.54
26	0.15	0.1	60	300	5.61	3.69	0.92	0	69	93.23	87.76
27	0.15	0.1	90	300	5.73	3.69	0.42	0	65	95.67	92.51
28	0.15	0.1	120	300	5.57	3.70	1.02	0	70	90.42	85.78
29	0.15	0.2	30	300	8.89	3.62	0	0	55	100	100
30	0.15	0.2	60	300	9.21	3.59	0	0	51	100	100
31	0.15	0.2	90	300	9.43	3.55	0	0	50	100	100
32	0.15	0.2	120	300	9.29	3.58	0	0	51	100	100
33	0.15	0.3	30	300	9.63	3.54	0	0	49	100	100
34	0.15	0.3	60	300	9.91	3.53	0	0	47	100	100
35	0.15	0.3	90	300	10.13	3.52	0	0	44	100	100
36	0.15	0.3	120	300	9.97	3.53	0	0	47	100	100
A	0.1	0.3	90 (magnetic stirring)	300	7.83	3.67	2.13	0	76	96.27	93.52
B	-	-	-	300	-	3.92	8.04	5.21	127	-	-

The induced coupled plasma atomic emission spectrometer (ICP AES, Optima7300 DV, Perkin-Elmer Corporation, Waltham, MA, USA) was utilized to analyze the Zinc (Zn) contents and phosphorous (P)

contents. The surface of the pristine cotton and developed samples was visualized using Quanta 200 FEG scanning electron microscope (SEM) (FEI Company, Hillsboro, OR USA). The particle size of the synthesized ZnO NPs was examined by employing dynamic light scattering (DLS) technology using the Malvern zeta sizer (Malvern Panalytical Ltd United Kingdom). The XRD patterns were measured using an X-ray diffraction system (Powder X-ray diffraction system, ARL, X,TRA, Thermo scientific USA). To evaluate the flammability of untreated cotton samples and developed samples, vertical flame test (ASTM 6413-2015) was employed. The quantitative method AATCC 100-2012 was used to analyze the antibacterial performances of the samples. The home laundering washing durability of the treated samples was examined as per ISO 105-CO6 standard.

3. Results and discussion

3.1. SEM Analysis

It can be seen from Figure 1 (a) and Figure 1 (b) that pristine cotton has a clean and smooth surface. Figure 1 (c) and Figure 1 (d) show the SEM images for optimized sample 23, which reveals that after optimized sonochemical treatment ZnO NPs are spread onto the cotton fabric surface homogeneously, finely, and evenly. Figure 1 (c) and Figure 1 (d) show that the surface of the fabric is entirely covered by the ZnO NPs. Figure 2 (f) SEM image for sample A shows that there is a deposition of ZnO NPs onto the cotton fabric surface after the conventional magnetic stirring method but as compared to the snochemical method, the ZnO NPs are not spread smoothly, finely and homogeneously. Figure 1 (e) shows the SEM image for optimized sample 23 at high resolution, showing that ZnO particles are deposited onto the cotton surface at nano scale with narrow size distribution.

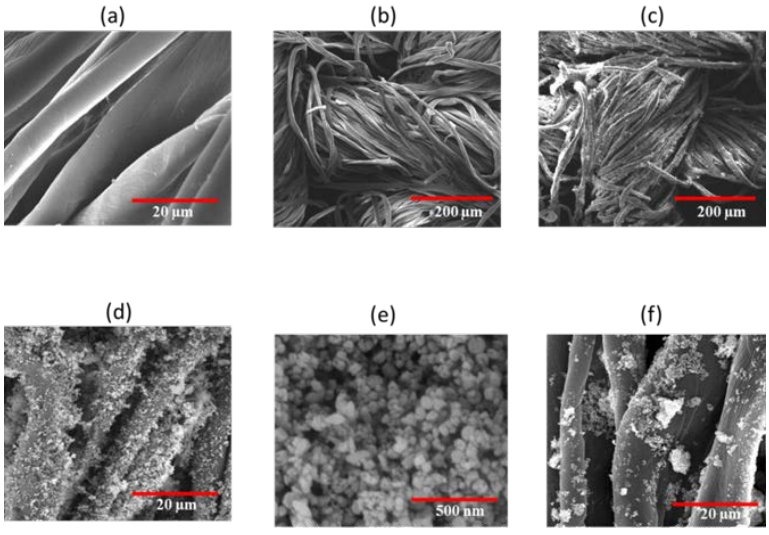

Figure 1. SEM images (a,b) pristine cotton, (c,d,e) sample 23 and (f) sample A

3.2. Particle size

Figure 2 shows the particle size distribution of sonochemical in-situ synthesized ZnO NPs (optimized sample 23). It can be seen from the figure that nanoparticle size distribution is uni-modal with an average particle size of 30.89 nm. At the nano scale the particles have increased surface areas, allowing the nanoparticles to be utilized in many technical applications [19,20].

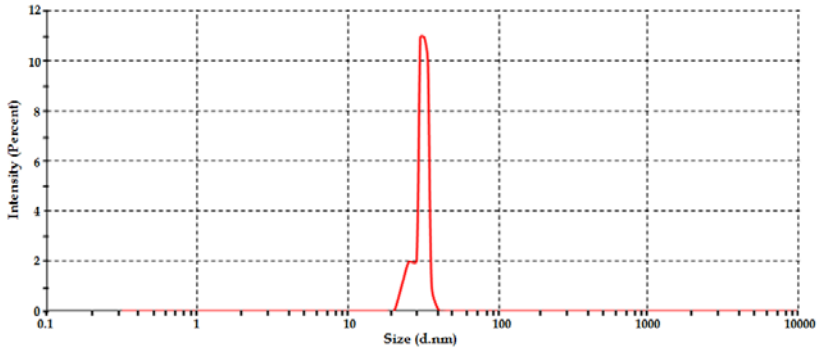

Figure 2. Particle size distribution Sample 23

3.3. XRD Analysis

XRD diffractogram of pristine cotton fabric and optimized sonochemically treated sample 23 are presented in Figure 3. It is obvious from Figure 3 that the pristine cotton fabric has only the characteristic peaks of cellulose (at 2Θ= 14.8, 16.5 and 22.7) (JCDPS No.03-0226) [21]. While the sample 23 has some additional peaks (at 2Θ= 32.1, 34.7, 36.5, 47.8, 56.7, 63.1, 68.1, 69.2) in the diffraction planes (100), (002), (101), (102), (110), (103), (200), and (112). These are characteristic peaks of ZnO NPs (as per diffraction standard No.36-1451 defined by the Joint Committee on powder diffraction standard (JCDPS)) [22]. The additional peaks are evidence of the presence of crystalline hexagonal wurtzite structure of ZnO NPs [23–25]. Moreover, in case of sample 23, the peaks intensity of the cellulose has decreased due to ZnO NPs loading

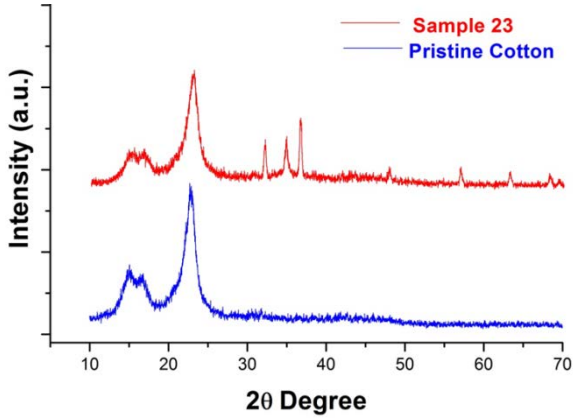

Figure 3. XRD diffractogram of pristine cotton and sample 23.

3.4. Vertical Flame Test

The measurements of the vertical flame test of untreated and developed samples are shown in Table 1 and Figure 4. It can be seen from Table 1 and Figure 4 that MDPA has a good effect on the flame retardancy of the cotton fabric, which further improved by the deposition of ZnO NPs. It is evident from the results that flame retardant properties (i.e. after flame time, after glow time, char length) improved with increased deposition of ZnO NPs. The untreated sample burned intensely in contact with flame. After detaching the flame source, the burning process of the untreated sample remained continue until it completely burned out without any char formation. On the other hand, all the treated samples (MDPA treated and MDPA + ZnO NPs treated) were self-extinguished. Furthermore, char formation was observed in the case of treated samples (MDPA treated and MDPA + ZnO NPs treated). Moreover, it was observed that after flame time, after glow time, and char length of the treated samples decreased with an increased amount of Zn contents. The best flame retardant results were observed in the case of sonochemically optimized Sample 23. Sample 23 self-extinguished immediately after removal of

combustion source and had zero second after flame time, zero second after glow time, and 39 mm char length. Sample A developed by conventional magnetic stirring method had 2.13 seconds after flame time, zero second after glow time, and 76 mm char length, while sample B only treated with MDPA had 8.04 seconds after flame time, 5.21 seconds after glow time, and 127 mm char length. The char formation in the case of MDPA and MDPA + ZnO NPs treated samples was because of water removal from the fabric, which created the insulating layer and protected the fabric after flame removal, hence increasing the flame retardancy [26]. Furthermore, ZnO NPs acted as co-catalyst and decreased the flame spread rate; therefore, improved flame retardancy was achieved [27].

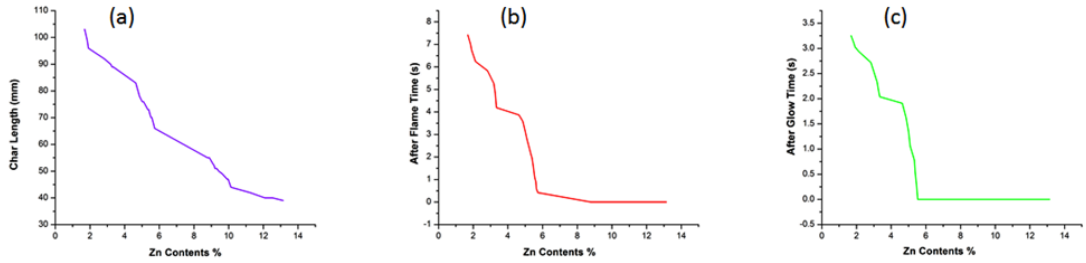

Figure 4. Flammability behavior (a) char length against Zn contents (b) after flame time against Zn contents (c) afterglow time against Zn contents.

3.5. Antibacterial activity

Antibacterial activity of developed samples was investigated according to the colony count test procedure and shown in Table 1 and Figure 5. The results show that treated fabrics exhibit excellent bacterial reduction for both E.coli and S.aureus bacteria. From Table 1 and Figure 5, it is evident that with an increased loaded amount of ZnO NPs, the antibacterial activity of the treated samples also increased for both E.coli and S.aureus bacteria. 100 % S.aureus reduction was achieved with 8.78 % loaded concentration of Zn contents (sample 17). While 100 % E.coli reduction was achieved with 9.07 % loaded concentration of Zn contents (sample 18). As the ZnO NPs interact with bacteria, they generate reactive oxygen species, such as H_2O_2, $\bullet OH^-$, $\bullet O^{2-}$. These reactive oxygen species damage the protein and DNA of the bacterial cell, resulting in the death of a bacterial cell. Furthermore, ZnO NPs deactivate the various necessary enzymes present in a bacterial cell; it is done by the interaction between the ZnO NPs and the thiol group present in bacterial cell. Moreover, the attachment of ZnO NPs onto the cell wall of the bacteria increase the Zn^{2+} cations concentration in cytoplasm, which results in the death of bacteria [28–30].

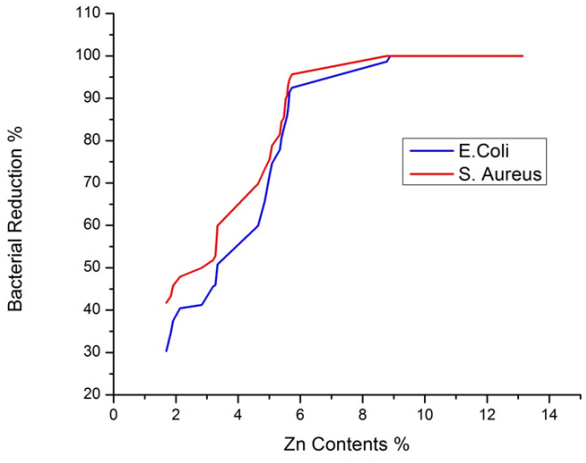

Figure 5 Bacterial reduction % vs Zn contents.

3.6. Wash Durability

Table 2 shows the results after 5, 10 and 20 wash cycles for Sample A, Sample B and Sample 23. The results show that there is a gradual decrease in Zn contents, P contents, flame retardancy, and antibacterial properties of the sample after each wash cycle. However, in the case of ultrasonically optimized Sample 23, there is enough Zn and P contents even after 20 wash cycles. Although char length increased to 52 mm after 20 wash cycles for Sample 23, however, these values are excellent for flame retardancy. Sample 23 retained enough amounts of Zn contents after 20 wash cycles and showed 100 % bacterial reduction for both S.aureus and E.coli bacteria.

Table 2 Results of Zn contents, P contents, flammability test, and bacterial reduction after different wash cycles.

Sample	Zn Contents (%)	P Contents (%)	Flammability Test			Bacterial Reduction (%)	
			After flame Time (s)	After Glow Time (s)	Char Length (mm)	S. aureus	E.coli
After 5 wash cycles							
Sample A	5.76	3.30	5.94	3.15	89	72.43	70.28
Sample B	-	3.48	10.32	5.19	134	-	-
Sample 23	11.38	3.11	0	0	46	100	100
After 10 wash cycles							
Sample A	4.74	3.13	7.03	3.52	93	63.23	60.96
Sample B	-	3.32	10.72	5.89	145	-	-
Sample 23	10.61	2.99	0	0	49	100	100
After 20 wash cycles							
Sample A	3.97	3.04	7.82	4.23	96	54.47	50.52
Sample B	-	3.24	11.29	6.08	149	-	-
Sample 23	10.17	2.93	0	0	52	100	100

4. CONCLUSIONS

In this research study, cotton fabric was modified by the ultrasonically assisted in-situ synthesis of ZnO NPs and MDPA application by the conventional pad dry cure method. The study revealed that MDPA greatly affects flame retardant performance of the cotton fabric, which further increases by the deposition of ZnO NPs. For the deposition of ZnO NPs onto the cotton fabric, sonication time and concentrations of the chemical reagents were varied. The optimized conditions at 0.1 M zinc acetate, 0.3 M of NaOH, and 90 minutes of sonication time produced 13.14 % Zn contents. The pure hexagonal wurtzite crystalline structure of ZnO NPs was confirmed by XRD. The presence of ZnO NPs was confirmed by ICP AES, and SEM. While the presence of phosphorous contents was confirmed by ICP AES. This research work disclosed that the concentration of ZnO NPs deposited onto the fabric has direct correlation with flame retardancy and antibacterial properties. The optimized sample 23 showed excellent performance for flame retardancy before and after washing. 100 % bacterial reduction for both S. aureus and E. coli bacteria was observed even after 20 wash cycles.

References

1. *Zhang, K.K.; Zong, L.; Tan, Y.; Ji, Q.; Yun, W.; Shi, R.; Xia, Y. Improve the Flame Retardancy of Cellulose Fibers by Grafting Zinc Ion. Carbohydr. Polym.* ***2016****, 136, 121–127, doi:10.1016/j.carbpol.2015.09.026.*
2. *Yang, S.; Hu, Y.; Zhang, Q. Synthesis of a Phosphorus–Nitrogen-Containing Flame Retardant and Its Application in Epoxy Resin. High Perform. Polym.* ***2019****, 31, 186–196, doi:10.1177/0954008318756496.*
3. *Rao, T.N.; Naidu, T.M.; Kim, M.S.; Parvatamma, B.; Prashanthi, Y.; Koo, B.H. Influence of Zinc*

*Oxide Nanoparticles and Char Forming Agent Polymer on Flame Retardancy of Intumescent Flame Retardant Coatings. Nanomaterials **2020**, 10, doi:10.3390/nano10010042.*

4. *Nguyen, T.M.; Chang, S.; Condon, B.; Slopek, R.; Graves, E.; Yoshioka-Tarver, M. Structural Effect of Phosphoramidate Derivatives on the Thermal and Flame Retardant Behaviors of Treated Cotton Cellulose. Ind. Eng. Chem. Res. **2013**, 52, 4715–4724, doi:10.1021/ie400180f.*
5. *Huong, N.T.; Khanh, V.T.H.; Linh, N.P.D. Optimizing Content of Pyrovatex CP New and Knittex FFRC in Flame Retardant Treatment for Cotton Fabric. Ind. Textila **2021**, 72, 315–323, doi:10.35530/IT.072.03.1648.*
6. *van der Veen, I.; de Boer, J. Phosphorus Flame Retardants: Properties, Production, Environmental Occurrence, Toxicity and Analysis. Chemosphere **2012**, 88, 1119–1153, doi:10.1016/j.chemosphere.2012.03.067.*
7. *Yaqoob, Asim ALI Parveen, Tabassum Umar, Khalid Nasir, Mohammad Nasir, I. Role of Nanomaterials in the Treatment of Waste Water. Water 2020, **2020**, 12, 495.*
8. *Yaqoob, A.A.; Ahmad, H.; Parveen, T.; Ahmad, A.; Oves, M.; Ismail, I.M.I.; Qari, H.A.; Umar, K.; Mohamad Ibrahim, M.N. Recent Advances in Metal Decorated Nanomaterials and Their Various Biological Applications: A Review. Front. Chem. **2020**, 8, 1–23, doi:10.3389/fchem.2020.00341.*
9. *Galaly, A.R.; Dawood, N. Non-Thermal Plasma Treatment Coupled with a Photocatalyst for Antimicrobial Performance of Ihram Cotton Fabric. Nanomaterials **2022**, 12, 1–14, doi:10.3390/nano12061004.*
10. *Javed, A.; Wiener, J.; Tamulevičienė, A.; Tamulevičius, T.; Lazauskas, A.; Saskova, J.; Račkauskas, S. One Step In-Situ Synthesis of Zinc Oxide Nanoparticles for Multifunctional Cotton Fabrics. Materials (Basel). **2021**, 14, 3956.*
11. *Abramova, A. V.; Abramov, V.O.; Fedulov, I.S.; Baranchikov, A.E.; Kozlov, D.A.; Veselova, V.O.; Kameneva, S. V.; Ivanov, V.K.; Cravotto, G. Strong Antibacterial Properties of Cotton Fabrics Coated with Ceria Nanoparticles under High-Power Ultrasound. Nanomaterials **2021**, 11, doi:10.3390/nano11102704.*
12. *Tănase, M.A.; Soare, A.C.; Oancea, P.; Răducan, A.; Mihăescu, C.I.; Alexandrescu, E.; Petcu, C.; Diţu, L.M.; Ferbinţeanu, M.; Cojocaru, B.; et al. Facile in Situ Synthesis of Zno Flower-like Hierarchical Nanostructures by the Microwave Irradiation Method for Multifunctional Textile Coatings. Nanomaterials **2021**, 11, doi:10.3390/nano11102574.*
13. *Nguyen, H.T.P.; Nguyen, T.M.T.; Hoang, C.N.; Le, T.K.; Lund, T.; Nguyen, H.K.H.; Huynh, T.K.X. Characterization and Photocatalytic Activity of New Photocatalysts Based on Ag, F-Modified ZnO Nanoparticles Prepared by Thermal Shock Method. Arab. J. Chem. **2020**, 13, 1837–1847, doi:10.1016/j.arabjc.2018.01.018.*
14. *Espitia, P.J.P.; Soares, N. de F.F.; Coimbra, J.S. dos R.; de Andrade, N.J.; Cruz, R.S.; Medeiros, E.A.A. Zinc Oxide Nanoparticles: Synthesis, Antimicrobial Activity and Food Packaging Applications. Food Bioprocess Technol. **2012**, 5, 1447–1464, doi:10.1007/s11947-012-0797-6.*
15. *Moezzi, A.; McDonagh, A.M.; Cortie, M.B. Zinc Oxide Particles: Synthesis, Properties and Applications. Chem. Eng. J. **2012**, 185–186, 1–22, doi:10.1016/j.cej.2012.01.076.*
16. *Magovac, E.; Vončina, B.; Jordanov, I.; Grunlan, J.C.; Bischof, S. Layer-by-Layer Deposition: A Promising Environmentally Benign Flame-Retardant Treatment for Cotton, Polyester, Polyamide and Blended Textiles. Materials (Basel). **2022**, 15, doi:10.3390/ma15020432.*
17. *Akhavan Sadr, F.; Montazer, M. In Situ Sonosynthesis of Nano TiO2 on Cotton Fabric. Ultrason. Sonochem. **2014**, 21, 681–691, doi:10.1016/j.ultsonch.2013.09.018.*
18. *Javed, A.; Azeem, M.; Wiener, J.; Thukkaram, M.; Saskova, J.; Mansoor, T. Ultrasonically Assisted In Situ Deposition of ZnO Nano Particles on Cotton Fabrics for Multifunctional Textiles. Fibers Polym. **2021**, doi:10.1007/s12221-021-0051-9.*
19. *Wojnarowicz, J.; Chudoba, T.; Lojkowski, W. A Review of Microwave Synthesis of Zinc Oxide Nanomaterials : Reactants , Process Parameters and Morphologies. **2020**.*
20. *Mohajerani, A.; Burnett, L.; Smith, J. V; Kurmus, H.; Milas, J.; Arulrajah, A.; Horpibulsuk, S.; Abdul Kadir, A. Nanoparticles in Construction Materials and Other Applications, and*

*Implications of Nanoparticle Use. Materials (Basel). **2019**, 12, 3052.*

21. *Jiao, L.; Ma, J.; Dai, H. Preparation and Characterization of Self-Reinforced Antibacterial and Oil-Resistant Paper Using a NaOH/Urea/ZnO Solution. PLoS One **2015**, 10, 1–16, doi:10.1371/journal.pone.0140603.*
22. *Sun, X.Z.; Bremner, D.H.; Wan, N.; Wang, X. Development of Antibacterial ZnO-Loaded Cotton Fabric Based on in Situ Fabrication. Appl. Phys. A Mater. Sci. Process. **2016**, 122, 1–9, doi:10.1007/s00339-016-0482-0.*
23. *Thi, V.H.T.; Lee, B.-K. Development of Multifunctional Self-Cleaning and UV Blocking Cotton Fabric with Modification of Photoactive ZnO Coating via Microwave Method. J. Photochem. Photobiol. A Chem. **2017**, 338, 13–22.*
24. *Shao, D.; Gao, Y.; Cao, K.; Wei, Q. Rapid Surface Functionalization of Cotton Fabrics by Modified Hydrothermal Synthesis of ZnO. J. Text. Inst. **2017**, 108, 1391–1397.*
25. *Li, Y.; Zou, Y.; An, D.; Hou, Y.; Zhou, Q.; Zhang, L. Investigation of Antibacterial Properties of Nano-ZnO Assembled Cotton Fibers. Fibers Polym. **2013**, 14, 990–995.*
26. *Siriviriyanun, A.; O'Rear, E.A.; Yanumet, N. Self-Extinguishing Cotton Fabric with Minimal Phosphorus Deposition. Cellulose **2008**, 15, 731–737, doi:10.1007/s10570-008-9223-7.*
27. *Lam, Y.L.; Kan, C.W.; Yuen, C.W.M. Effect of Zinc Oxide on Flame Retardant Finishing of Plasma Pre-Treated Cotton Fabric. Cellulose **2011**, 18, 151–165, doi:10.1007/s10570-010-9466-y.*
28. *Wang, L.; Hu, C.; Shao, L. The Antimicrobial Activity of Nanoparticles: Present Situation and Prospects for the Future. Int. J. Nanomedicine **2017**, 12, 1227–1249, doi:10.2147/IJN.S121956.*
29. *Sirelkhatim, A.; Mahmud, S.; Seeni, A.; Kaus, N.H.M.; Ann, L.C.; Bakhori, S.K.M.; Hasan, H.; Mohamad, D. Review on Zinc Oxide Nanoparticles: Antibacterial Activity and Toxicity Mechanism. Nano-Micro Lett. **2015**, 7, 219–242, doi:10.1007/s40820-015-0040-x.*
30. *Shaikh, S.; Nazam, N.; Rizvi, S.M.D.; Ahmad, K.; Baig, M.H.; Lee, E.J.; Choi, I. Mechanistic Insights into the Antimicrobial Actions of Metallic Nanoparticles and Their Implications for Multidrug Resistance. Int. J. Mol. Sci. **2019**, 20, 1–15, doi:10.3390/ijms20102468.*

DEVELOPMENT OF CARBON FELTS FOR RESPIRATORY FILTRATION

Yuanfeng Wang, Tereza Šubrová, Dana Křemenáková, Mohanapriya Venkataraman, Jakub Wiener, Jiří Militký

Department of Material Engineering, Technical University of Liberec, Studentská 1402/2, Liberec 1, 461 17 Czech Republic

Corresponding author e-mail: yuanfeng.wang@tul.cz

Abstract:

The increase in environmental pollutants and the pandemic of infectious diseases have drawn attention to respiratory filtration materials. In the present work, we developed carbon felt breathable filtration materials by carbonizing PAN mats at different temperatures. The fiber diameter distribution, air permeability and breathability, electrical heating properties, and antimicrobial properties of the resulting carbon felts were investigated. The results showed that carbon felt as a filtration material can ensure smooth breathing when worn during resting and walking activities. By varying the carbonization temperature, the carbon felt resistance heating performance can be tuned. Finally, the carbon felt exhibits good antibacterial properties at room temperature. Therefore, the carbon felts in this work have great potential for respiratory filtration applications due to their excellent performance and inherent antimicrobial properties.

Key words:

Carbon felt, Respiratory filter, Resistive heating, Antimicrobial

1. Introduction

In the face of an airborne infectious disease pandemic, health care workers working in hospitals are at greater risk of contracting the virus. Currently, the primary means of avoiding infection for all health care workers in hospitals is the use of respirators, such as the N95 respirator. This inevitably leads to a high demand for respirators[1]. Therefore, researchers have been searching for alternative filtration materials for respiratory protection, which has triggered an interest in different filtration materials[2]. Among others, carbon fibers are starting to gain interest as an alternative adsorbent for gaseous pollutants[3]. Carbon fiber filter materials are obtained by carbonizing and activating fiber assemblies. The small diameter homogeneous micropores give the activated carbon fibers a large surface area and high absorption capacity. On the other hand, the characteristic flexibility of the fibers lends the activated carbon fiber filter to be easily applied to a variety of conditions. In addition, the activated carbon fiber filter can be recycled by electric heating, extending its service life[4].

In the present work, we developed carbon felt breathable filtration materials by carbonizing PAN mats at different temperatures. The fiber diameter distribution, air permeability and breathability, electrical heating properties, and antimicrobial properties of the resulting carbon felts were investigated.

2. Experimental

2.1. Materials

The needle-punched PAN felt with PTFE film was purchased from Zhejiang Hengze Filter Material Co.,Ltd, China. The density of the felt is 500g/m2 and the thickness is 2.0- 2.1 mm, where the PAN fibers have a diameter of about 12-16 μm.

2.2. Methods

Preparation of carbon felt

PAN felts used as the precursor to prepare carbon felts were cut into square pieces. First, the felt was oxidized and stabilized in an air atmosphere using a muffle furnace at a temperature of 200°C for 2 hours. During the oxidation process, the sample was placed between two metal plates to maintain its original flat shape. Subsequently, the carbonization of the oxidized PAN felts was carried out in a muffle furnace under nitrogen atmosphere. The sample was carbonized at a temperature of 800-1100 degrees C for 30 min with a heating rate of 10°C/min. The samples were labeled as PAN_x, where x is the carbonized temperature.

It is well known that fibers inevitably shrink during the carbonization process and the usual solution is to apply appropriate tension to the fibers. Here, during the carbonization process, the tension was applied to the fibers by simply placing cylindrical blocks weighing 66g at each of the four corners of the sample. On the one hand, the loading of the four corners ensures that the sample remained flat during the carbonization process. On the other hand, the proper weight of the cylindrical block enables its movement with the shrinkage of the sample, continuously applying tension to the fibers during the shrinkage of the sample without breaking the sample.

Characterization

The TS5130-Tescan scanning electron microscope(SEM) was used to observe the surface of obtained carbon felt at 10 kV acceleration voltage. A metal layer was deposited on the surface of the sample prior to the SEM test. The diameter of the fibers was measured by SEM images of the samples using Image J software. FX3300 Textech Air Permeability Tester was used to test the air permeability of the prepared carbon felt at pressure from 60 to 260 pa. The breathability of the sample was calculated according to the permeability values at different pressures. The resistive heating behavior of the carbon felt was studied by applied voltages of 0–8 V using a test setup consisting of power supply and infrared camera (FLIR E6, USA). The power supply was connected to carbon felt at two edges of the sample using curved electrodes. The infrared camera was placed 10 cm above the surface of the sample and the center temperature was recorded during the heating process. For antimicrobial testing of the samples, the felt was contaminated using environmental microbial contact, and then the environmental microbial-contaminated felt was printed on the agar plates. Subsequently, the antimicrobial properties of the samples were examined by observing the growth of microbes on the agar plates after placed in an incubator at 37 ℃ for 24 hours.

3. Results and discussion

3.1. Morphology

The SEM images of the obtained carbon felts are shown in Figure 1(a-c). It can be seen that the fineness of the resulting carbon fibers changed compared to the PAN fibers used as precursors, and the carbon fibers became finer as the carbonization temperature increased. This is due to the loss of hydrogen and nitrogen in PAN as the degree of carbonization increased, resulting in shrinkage of the fiber. In addition, significant wrinkles appeared on the surface of the fibers carbonized at 1100℃, with the increased specific surface area of the obtained wrinkles providing a potential possibility to improve the adsorption performance of the felt. Figure1 (d) presents the photograph of the obtained carbon felt, where the good flexibility and morphological recovery can be seen.

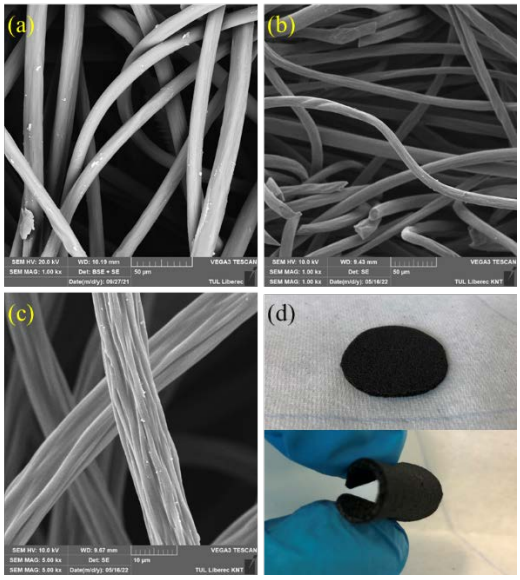

Figure 1. SEM images of (a) precursor PAN fiber, (b) PAN_800, and (c)PAN_1100; (d) Photograph of the obtained carbon felt.

3.2. Fiber diameter distribution

The fineness of the fibers is considered to be a key indicator of the filtration performance of the fiber aggregates. The distribution of carbon fiber diameters obtained in this work is shown in Figure 2. The average diameter of the fibers decreased from 12.74 to 9.2μm, with the increase in carbonization temperature from 800 to 1100℃. As the temperature increased, the fiber diameter distribution tended to be more normal, indicating that the increased carbonization temperature contributed to the optimization of the fiber fineness distribution. The research showed that the PM2.5 filtration efficiency of fiber filter materials was negatively correlated with the fiber diameter[5]. From this, we can assume that a higher carbonization temperature will improve the respiratory filtration efficiency of the carbon felt.

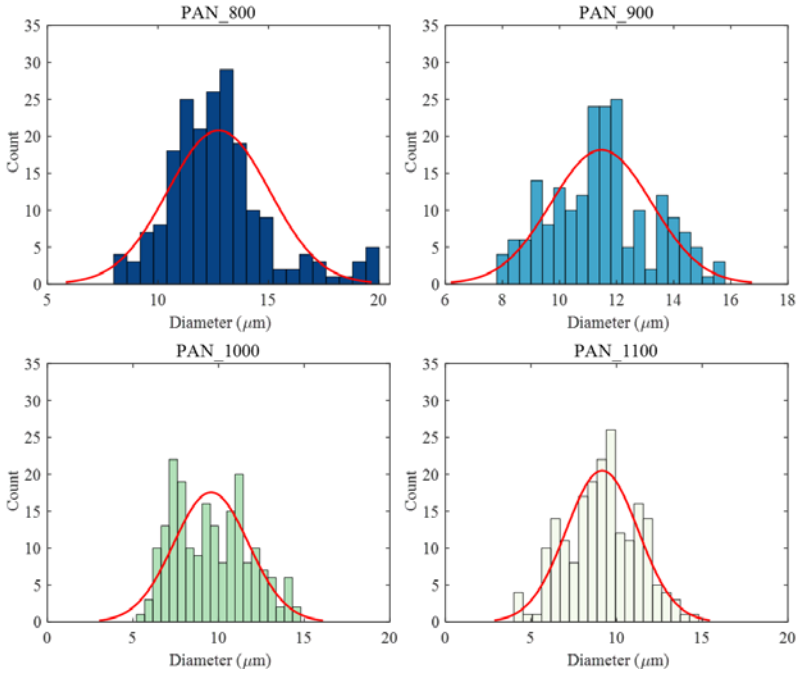

Figure 2. Fiber diameter distribution of carbon felts at different carbonization temperatures.

3.3. Air permeability and breathability

Air permeability and breathability are essential properties of respiratory filter materials. Figure 3 shows the permeability of the carbon felt at different pressures. It is clear that the permeability correlated positively with pressure and carbonization temperature. The previous results of fiber fineness distribution can well explain the phenomenon that the permeability increased with the carbonization temperature. The decrease in fiber fineness has created more space within the fiber assembly, which facilitated the air flow and thereby improved air permeability. Later, the breathability was calculated from the values of permeability at different pressures and the exact area of the respiratory filter. In our design, the area of respiratory filter is 35cm^2. First, with the determination of the filter area, the volume of air per minute that can pass through the filter media at different pressures can be obtained. Subsequently, a linear relationship between air permeability and pressure can be established. By using this linear relationship, we can assume the pressure required to achieve different air flows. The resulting breathability properties are listed in Table 1. Here, we assume that 100 Pa is critical value for breathing, which means that it can breathe smoothly when the value is below 100 Pa. From the data in the table, it can be noted that the samples PAN_800 and 900 can satisfy the peace and walk human activity. While samples PAN_1000 and 1100 can further ensure smooth breathing during accelerated movement. This respiratory filter material is designed for use in hospitals, bacteriological laboratories, etc., where resting and walking would be the main human activities of the wearer. Therefore, all four carbon felts prepared in this work can provide breathing performance that ensures basic human activities.

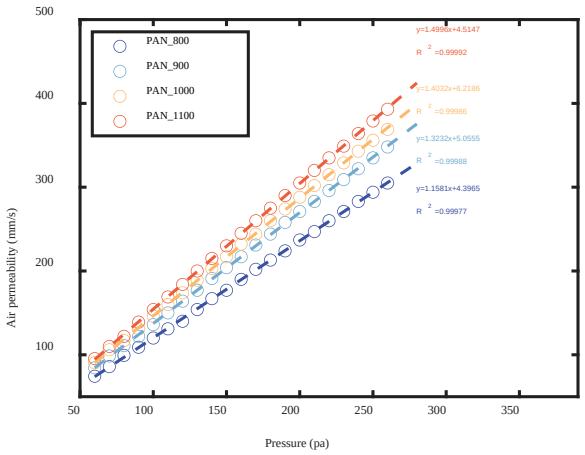

Figure 3. Air permeability of carbon felts at different pressures.

Table 1. Breathability (Pa) of the carbon felt.

Air volume during various human activities	PAN_800	PAN_900	PAN_1000	PAN_1100
Peace 8 – 10 l/min	32-40	28-35	27-33	25-31
Walk 15 – 20 l/min	60-81	53-70	50-66	47-62
Accelerated movement 20 – 30 l/min	81-121	70-106	66-99	62-94
Medium work 30 – 40 l/min	121-161	106-141	99-133	94-125
Hard work 40 – 50 l/min	161-201	141-176	133-166	125-156
Extreme stress 50 – 120 l/min	201-483	176-423	166-398	156-375

3.4. Resistive heating

The temperature variation as a function of applied voltage and electrical power for different carbon felt samples is presented in Figure 4. The temperature was found to increase quadratically with the applied

voltage, which can be explained by Joule's first law, where the heat generated by Joule heating is proportional to the square of the applied voltage. The electrothermal conversion efficiency of the samples increased with increasing carbonization temperature, which can be attributed to the higher carbonization temperature reducing the resistance of the carbon felt. The inset in the voltage temperature dependence graph shows the IR camera screen at different heating temperatures. Uniform heat distribution under different heating conditions can be observed in the circular samples indicating that the samples prepared in this work were homogeneous in texture and electrodes were connected in an appropriate mode. Later, the relationship between the heating power and the achieved temperature was analyzed by linear regression. It can be noted that for all samples, the power and temperature showed a linear relationship. Except for the PAN_800 sample, the slope of the fitted curve became larger with increasing carbonization temperature, indicating that samples with higher carbonization temperatures require less electrical power consumption to reach the target heating temperature.

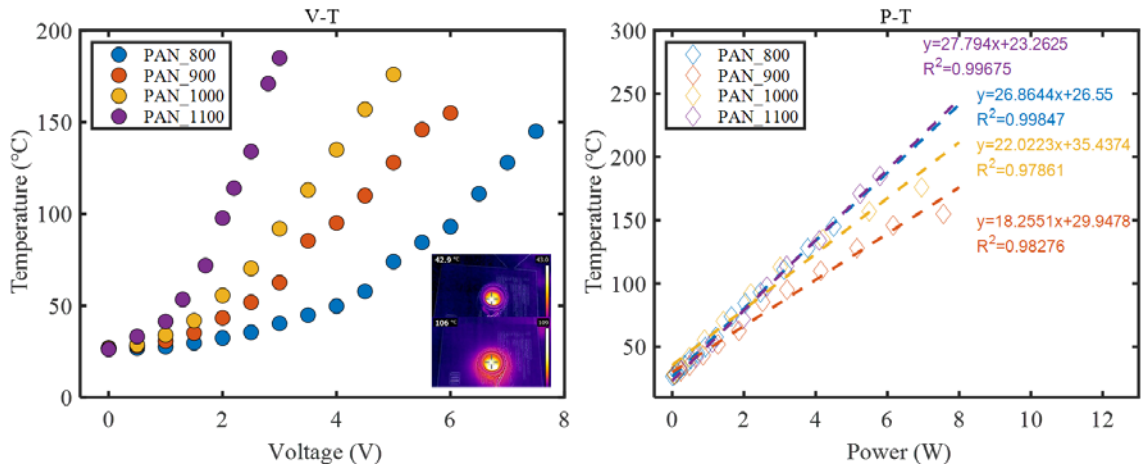

Figure 4. Resistive heating performance of the carbon felt.

3.5. Antimicrobial property

In the face of infectious disease pandemics, the demand for antimicrobial properties in respiratory filtration materials is rising. In the present work, we simply collected environmental microorganisms and contaminated carbon felts with them as well as control samples of cotton cloth, and subsequently blotted the contaminated samples on agar plates to visualize the growth of bacteria. In addition, considering the feasibility of electrical heating of carbon felts, contaminated samples were also heated and heated to 80℃ with hot plates, and the same tests were subsequently repeated on the agar plates. Figure 5 exhibits the growth of the bacterial colonies on the agar plates. For the samples at room temperature, the plates printed by carbon felt (Figure5 b) displayed significantly less bacteria than those of the control samples (Figure5 a). After both sets of samples were heated, a very small amount of bacteria were found on the control sample plates(Figure5 c), while the carbon felt sample plates(Figure5 d) were completely clean. The bactericidal effect of high temperatures was expected, whereas the antimicrobial properties of carbon felts at room temperature were more interesting. It has been noted in the literature that the antimicrobial activity of carbon nanomaterials depends on their composition, surface modification, target microorganisms and the reaction environment. The main antimicrobial mechanism is based on the induction of microbial cell wall/membrane invasion and structural damage, and the physical mechanism of biological separation of microbial cells from their supporting environment[6]. However, the carbon fibers obtained in this work did not reach the nanoscale, so the specific antibacterial mechanism needs to be further explored.

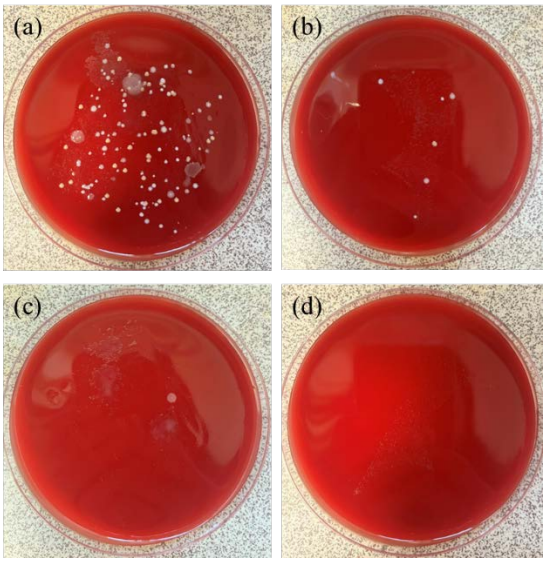

Figure 5. Antimicrobial property of the control sample(a,c) and the carbon felt(b,d).

4. CONCLUSIONS

The current work has reported the development of PAN-derived carbon felt respiratory filtration materials. Carbon felts were prepared using a muffle furnace in the temperature range 800-1100℃ under an inert gas atmosphere. The fiber diameter of the resulting carbon felts decreased with increasing carbonization temperature, while wrinkles were formed on the fiber surface. The breathability of the carbon felt was calculated by linearly fitting the permeability results measured under different pressure conditions, indicating that the carbon felt as a filtration material can ensure human breathing under resting and walking activities. Later, the resistance heating performance of carbon felt at different voltages was studied, and the relationship between electrical power and heating temperature was examined. Finally, the carbon felt performed well in antimicrobial tests, providing antimicrobial properties at room temperature and completely killing microorganisms under heated conditions. Therefore, these carbon felts have great potential for respiratory filtration applications because of their attractiveness as heatable respiratory filters due to their excellent heating efficiency and their inherent antimicrobial properties.

ACKNOWLEDGEMENTS

The authors acknowledge the project 'Advanced structures for thermal insulation in extreme conditions' (Reg. No. 21–32510 M) granted by the Czech Science Foundation (GACR).

References

1. Wang W, Chen T, Li Z, Tan Q, Meng Z, Qiu H, et al. Comparison of filtration efficiency and respiratory resistance of COVID-19 protective masks by multi-national standards. Am J Infect Control 2022;50:516–24. https://doi.org/10.1016/j.ajic.2022.02.009.
2. Sousan S, Garcia N, White A, Balanay JA. Filtration efficiency of surgical sterilization fabric for respiratory protection during COVID-19 pandemic. Am J Infect Control 2021;49:1–7. https://doi.org/10.1016/j.ajic.2020.11.005.

3. Sim KM, Kim KH, Hwang GB, Seo S, Bae G-N, Jung JH. Development and evaluation of antimicrobial activated carbon fiber filters using Sophora flavescens nanoparticles. Sci Total Environ 2014;493:291–7. https://doi.org/10.1016/j.scitotenv.2014.06.002.
4. Kim M, Lim G-T, Kim Y-J, Han B, Woo CG, Kim H-J. A novel electrostatic precipitator-type small air purifier with a carbon fiber ionizer and an activated carbon fiber filter. J Aerosol Sci 2018;117:63–73. https://doi.org/10.1016/j.jaerosci.2017.12.014.
5. ian Y, Wang S, Zhang L, Chen C. Influence of fiber diameter, filter thickness, and packing density on PM2.5 removal efficiency of electrospun nanofiber air filters for indoor applications. Build Environ 2020;170:106628. https://doi.org/10.1016/j.buildenv.2019.106628.
6. Azizi-Lalabadi M, Hashemi H, Feng J, Jafari SM. Carbon nanomaterials against pathogens; the antimicrobial activity of carbon nanotubes, graphene/graphene oxide, fullerenes, and their nanocomposites. Adv Colloid Interface Sci 2020;284:102250. https://doi.org/10.1016/j.cis.2020.102250.

ELECTROMAGNETIC INTERFERENCE SHIELDING SIMULATION OF COPPER COATED POLYESTER NON-WOVEN FABRIC AND PORE SIZE ADJUSTING

Shi Hu[1*] , Dan Wang[1], Dana Kremenakova[1], Jiri Militky[1]

Department of Material Engineering, Faculty of Textile Engineering, Technical University of Liberec, Studentska 1402/2, Liberec, Czech Republic

Abstract:

The development of simulation technology motivated EMI shielding simulation research. However, EMI shielding simulation for textile-based material is problematic for complicated textile geometrical models due to the complex meshing process and limited calculation power. This paper presents one method using the optimized textile model replacing the original textile geometrical model then imported for EMI shielding simulation. The environment constructed from the waveguide model. The simulated result shows good compatibility with measured shielding effectiveness (SE). The adjusting of the pore morphology in the optimized textile model suggested less pore number and same pore size were recommended for this type of EMI simulation model.

Key words:

EMI shielding simulation, textile model, electroless copper coating, porosity

1. Introduction

With the fast development of information technology and the running innovation of electronic equipment, electromagnetic waves, as an essential carrier of information transmission, have become inseparable from our daily life and further drive economic development and social production[1]. However, the intricately connected electromagnetic network brings us convenience and invisibly dramatically affects the living environment of human beings, which becoming the fourth most significant source of pollution after water pollution, air pollution, and noise pollution[2] In terms of human health, exposure to electromagnetic waves for a long time will seriously affect the human visual system, central nervous system, and reproductive system and cause a series of clinical symptoms such as blindness, neurasthenia, and hereditary diseases[3,4] In this case, the extra electromagnetic interference shielding(EMI shielding) is essential not only for the daily life but also for the working applications[5].

Electromagnetic shielding materials can achieve protective effects by reflecting and absorbing electromagnetic waves[6]. Flexible electromagnetic protective textiles are widely used in civil electromagnetic protection due to their excellent wearability, electromagnetic interference protection performance, and low cost[7]. With the metallization of fibers and fabrics, the maturity of metallization technology, and the rapid development of conductive polymer doped polymerization technology, new functions can be given to textiles, making them both soft, lightweight, and electromagnetic[8,9,10]

EMI shielding simulation is widely accepted as one of the practical solutions to develop and predict the shielding effectiveness of the sample[11]. However, for metal-coated textiles, there is few reseach about the EMI shielding simulation. One of the main resaon is due to the textile geometrical model is too complex for the simulation software. In this cacse, during the meshing process, the system can be crashed, otherwise the simulation will costs a lot of time. In this case, it's very hard to change the textiles parameter for the simulation run.

Many researchers have already studied the different parameters that impact the EMI shielding performance of textile-based material[12,13,14]. The main factors are porosity, thickness, and material. The advantage of simulation run is to apply the different parameters of textile-based material for optimization the EMI shielding performance[15,16,17]. In this paper we present the simulation process with optimized model which matching good to the real measured result. The optimized model is suitable to change different parameters for EMI shielding performance optimization.

2. Experimental

2.1. Materials

In this research, polyester nonwoven fabric is purchased from Kordárna Plus, a.s. Czech Republic. The coating process is realized by the electroless plating method. All chemicals used for copper coating are supplied from Sigma Aldrich Czech Republic. The copper coating process is listed in the Table 1. The coated fabric information is listed in Table 2.

Table 1. Electroless plating procedure for PET woven fabrics

Process	Chemicals and Processing	
1. Surface treatment	2.5% NaOH	40℃ 10min
2. Activation	1 g/100mL SnCl2	Room temperature10min
	0.05g/100mL PdCl2	Room temperature 10min
3. Deposition	6.5g/500mL CuSO4.5H2O	Sample- Solution ratio: 5g/500mL, PH 12.75 (NaOH 2.5g) ,45℃ 20min
	10g/500mL EDTA.2Na	
	10g/500mL KNaC4H4O6.4H2O	
	0.04g/500mL K4[Fe (CN)6].3H2O	
	0.005g/500m 2'-2'-Bipyridine	
	7.5mL/500mL CH2O	

Table 2. Geometrical information of copper coated woven fabrics

Sample Number	Mass per unit area (g/m2)	Sample thickness (mm)	Optical Porosity (%)
PET	10	0.068	56.81
PETCu1	12.725	0.07	55.81
PETCu2	15.951	0.072	48.56
PETCu3	17.025	0.074	42.93

2.2. Methods

The optimized textile geometrical modeling is presented in Figure 1(a). In this model, the porosity remains exactly same as the original sample. The porosity of the optimized model can be changed via the different pore size adjustment. The coating material and greige fabric also set as sample as original sample. The coated metal was continuous on the surface of the sample, it's reasonable to assume that the coated copper particles as copper layer attached on the surface of polyester.

To analyze the influence of different textile parameters on the shielding effectiveness, the ANSYS HFSS 15.0 software was used to simulate different scenarios. The simulation environment is constructed according to the waveguide model(Figure 1b). Using the finite element method, these simulated results of the shielding effectiveness in the form of transmittance coefficients were performed in the ANSYS HFFS software environment. In Figure 1b, a virtual measuring environment was constructed in Ansys HFSS by creating the geometry of the actual measuring stand consisting of the following waveguides: WR-2100, WR1500, WR975, WR-650 in the TE10 mode and the appropriate frequency ranges from 0.5GHz-1.5GHz. Regarding comparing the simulation environment accuracy, a real EMI shielding test is performed using the coaxial transmission method according to the standard ASTM 4935-10, which is designed to evaluate flat materials. This standard assumes a plane wave's impact on a shielding barrier in the near zone of the electromagnetic field at a frequency of 30 MHz to 1.5 GHz. We use the SE value from 0.5GHz – 1.5GHz to compare with the results from the simulation environment

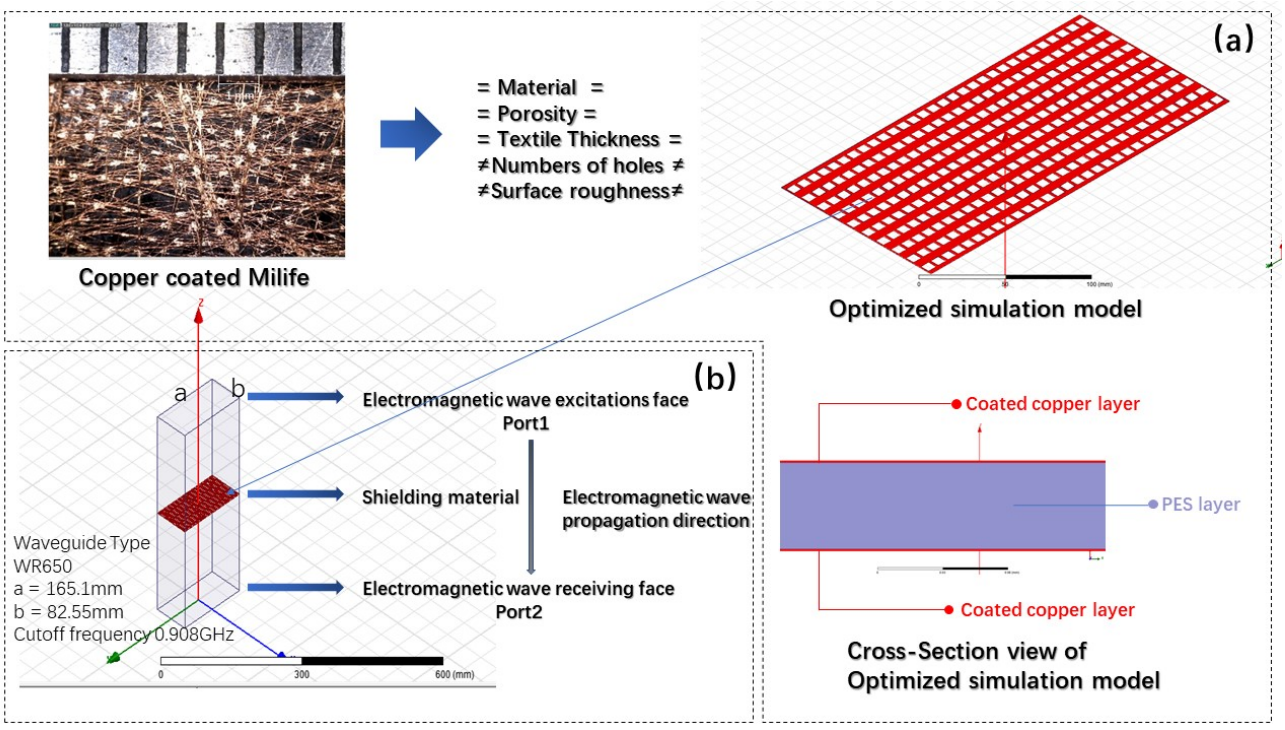

Figure 1. Waveguide model building in ANSYS HFSS (a) Optimized textile model for the simulation environment and cross-section view of this model (b) WR650 Waveguide mode for EMI shielding simulation

3. Results and discussion

3.1 EMI shielding simulation

Figures 2 show the copper-coated samples' measured and simulated EMI shielding effectiveness. The measured results from 0.5GHz to 1.5GHz are constantly exported from the network analyzer. The simulated result presents inconstantly due to the results were combined three types of the waveguide. Obviously, with the increased copper content from PETCu1 to PETCu3, the SE performance is improved

from both measured and simulated results. The average SE of three kinds of samples (Table 3), according to the classification in the document, is evaluated in the "excellent" category for Class II general use. For Class I Professional use, PETCu1 and PETCu2 fulfill the SE requirements of grade "AA" (Moderate), and PETCu3 fulfills the SE requirements of grade "AAA" (Good).

The MAPE error means the percentage measure of the distance between the simulated and measured curves within each measurement frequency point together determined by three types of waveguides. The result is present in Figures 2(d) in the entire measuring range from 0.5 to 1.5 GHz. The result shows that the average error of fitting the simulated and measured SE does not exceed 10%. For SE simulation, the MAPE of sample PETCu3 is even lower than 4%.

Due to the limitation of the waveguide model, the simulated value performs discontinuity at the boundary frequency point. The simulated results perform relatively good arrangement with the measured value. When the sample's SE is over 35dB, this mode faithfully represents the measured results in the frequency ranges from 0.5GHz to 1.5GHz. The compatibility is slightly worse for the sample's SE, around 30dB, but the error does not exceed 5 dB.

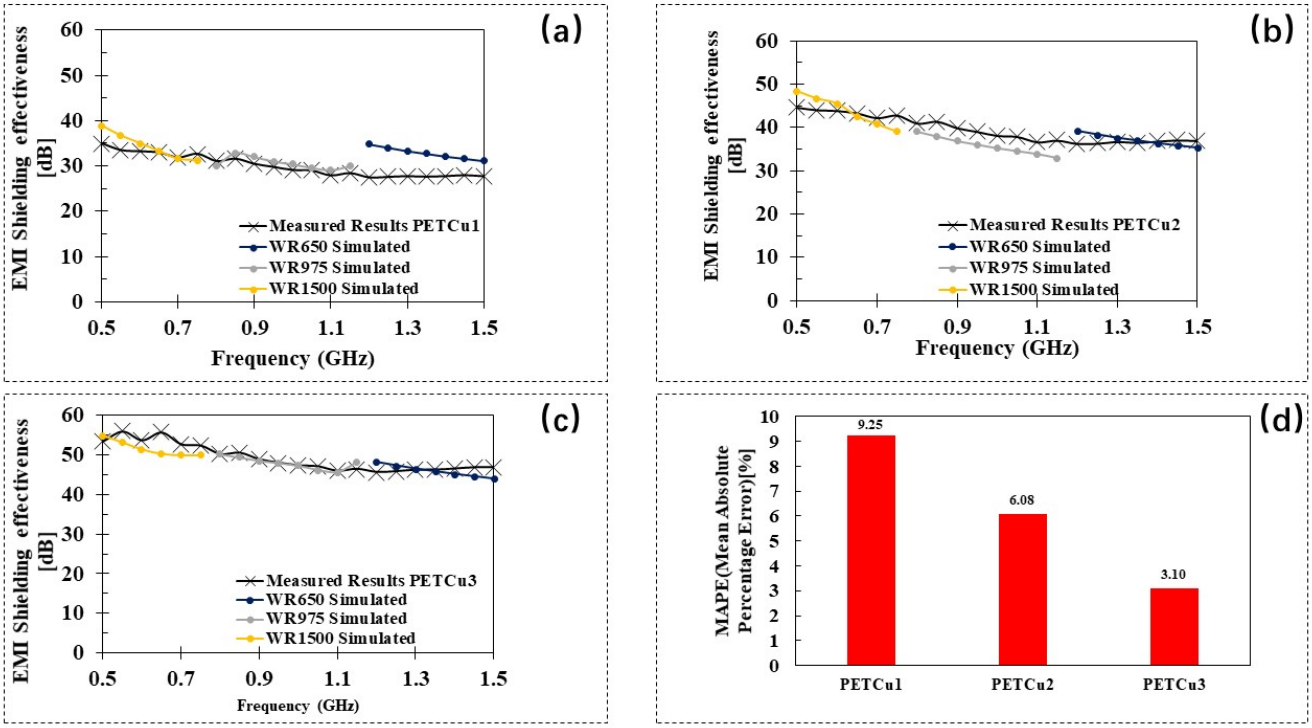

Figure 2. Results of measurements and simulated SE in the tested frequency range from0.5 to 1.5 GHz for textile samples (a) PETCu1 (b) PETCu2 (c) PETCu3 (d) MEAP error between measured and simulated results

Table 3. Measured and simulated average SE from 0.5GHz to 1.5GHz

	PETCu1	PETCu2	PETCu3
Measured average SE from 0.5GHz to 1.5GHz	30.03dB	39.46dB	49.15dB
Simulated average SE from 0.5GHz to 1.5GHz	32.44dB	39.04dB	48.31dB

3.2 Pore morphology and determine the numbers and shape of apertures for the optimized textile module

It's obviously that the pore size of nonwoven fabrics is different. Even the porosity of optimized sample and original sample are same, but the shape and size of the pore are totally different.

The first situation is different size of all the pores in the model but keep the same porosity. As we know the porosity will be increased which lead to a decrease of EMI shielding effectiveness. When the same porosity maintained but different pore size, the numbers of pores will be different, which means more numbers of pores, the less size of the pore. This case is presented in Figure 3(a). With less pore size (even more numbers of pores), the EMI shielding effectiveness is increased.

Another situation is in one model, the pore size is distributed differently. The problem is how to define the "difference"? For example how many pores should be in size A and how many pores should in size B. To define the different pore sizes in the model we can follow the distribution of pore size from the real sample to check the percentage of one pore size(Figure 4(c)), with the consideration of porosity and numbers of pores, we can define the different pore size in one model. By using this method, we defined the different pore size distributions in the new model as shown in the following Table 4. In this model, the percentage of pores size are distributed as same as the real sample from the image analysis and the porosity for both case are same as the real sample.

The simulated result is presented as follows. As the result(Figure 5), it obvious to see that even though the porosity is the same for both cases, but with the same pore size, the simulated result is more closed to the real test result.

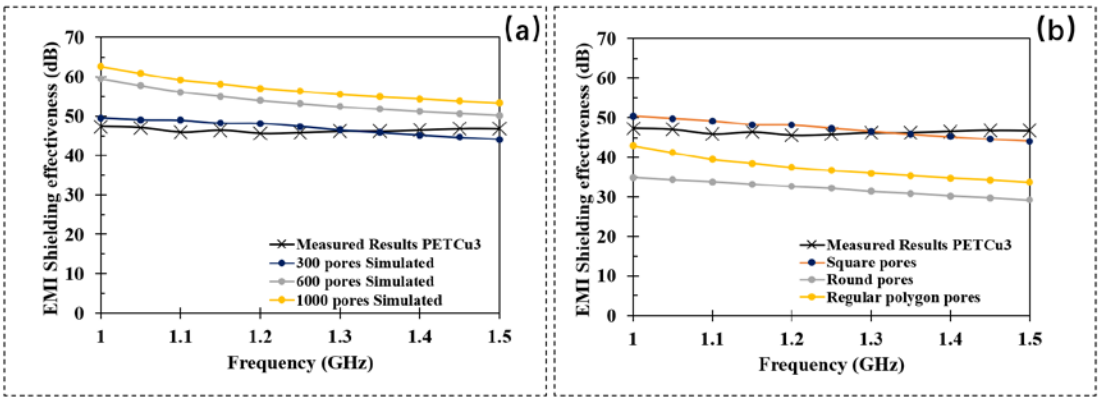

Figure 3. Pores numbers and shape impact the shielding effectiveness (a) Same porosity different numbers of pores (b) Same porosity different shape of pores

Table 4. Same and different pore size distribution

Porosity=42.93%	Pore Size A(mm2)	Numbers of pores in Size A	Pore Size B(mm2)	Numbers of pores in Size B	Pore Size C (mm2)	Numbers of pores in Size C	Pore Size D (mm2)	Numbers of pores in Size D
Sample with same pore size	19.36	300	-	-	-	-	-	-
Sample with different pore size	17.64	280	35.28	12	52.92	6	70.56	2

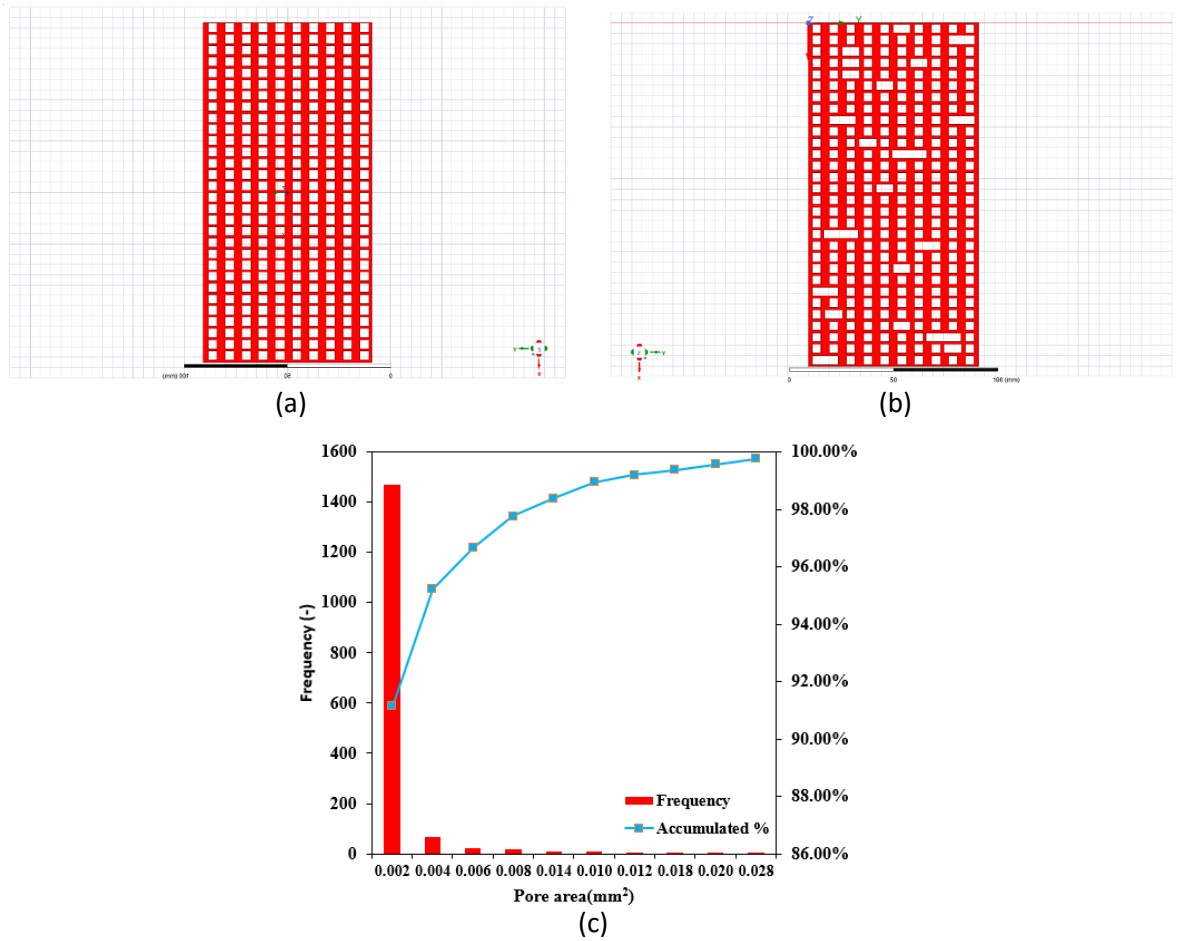

Figure 4. Optimized model with (a) Same size pore distribution (b) Different size of pore randomly distribution. (c) Pore size distribution of the real sample

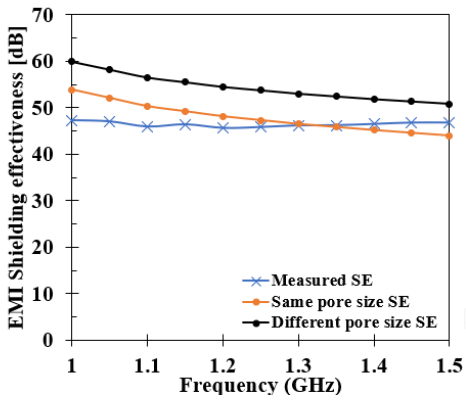

Figure 5. Simulated SE with the same and different pore size compared with the measured SE

For the optimized model, due to the certain numbers of the pore (300), the size of the pore is much larger than the pore size in the real sample. Even though the calculation is based on the same distribution, the difference between two grades of pore size is still large compared to the real sample. For real sample, the different grades of pore size in 0.002mm^2, but for the optimized model set the different grades as 17.64mm^2, this big difference may cause the increased error of simulated results.

Regarding the time calculation power cost and time cost, one of the advantages or novelty of this work is using the simplified model to simulate nonwoven-based EMI shielding material to get a relatively accurate result within a shorter simulation calculation time, which means with the consideration of porosity and numbers of pores, using one defined pore size instead of different pore size in one model is more efficient for the simulation run.

4. CONCLUSIONS

This paper introduced the new method for EMI shielding simulation of copper coated nonwoven fabric. By importing the optimized textile module, the simulated results presented good compatibility to the real tested results. Regarding to the pore morphology adjusting in the optimized module, after investigating the pore size distribution, the same pore size and less numbers of pore was suggested for the EMI shielding simulation run regarding to the simulated result.

ACKNOWLEDGEMENTS

The authors are grateful for the financial support from the project of the Ministry of Education, Youth and Sports of the Czech Republic and the European Structural and Investment Funds – Hybrid Materials for Hierarchical Structures (HyHi, Reg. No. CZ.02.1.01/0.0/0.0/16_019/0000843).

References

1. *I. F. Akyildiz, A. Kak, and S. Nie. 6G and Beyond: The Future of Wireless Communications Systems. IEEE Access 2020; 8: 133995–134030.*
2. *G. Redlarski .The influence of electromagnetic pollution on living organisms: Historical trends and forecasting changes. Biomed Res Int 2015;2015: 1-18.*
3. *J. R. Jauchem. Effects of low-level radio-frequency (3 kHz to 300 GHz) energy on human cardiovascular, reproductive, immune, and other systems: A review of the recent literature. Int J Hyg Environ Health 2008; 211 : 1–29.*
4. *T. Hughes-Riley, T. Dias, and C. Cork. A Historical Review of the Development of Electronic Textiles. Fibers 2018; 6:34 .*
5. *V. Rubežienė and S. Varnaitė-Žuravliova. EMI shielding textile materials. Mater Potential EMI Shield Appl. 2020;22: 357–378.*
6. *A. L. Apreutesei, A. Curteza, V. David, I. Nica, M. Rau, and O. Baltag. Investigation of the textile structures with different design used in electromagnetic shielding 2014; 2014: 596–601.*
7. *X. Ding, W. Wang, Y. Wang, R. Xu, and D. Yu. High-performance flexible electromagnetic shielding polyimide fabric prepared by nickel-tungsten-phosphorus electroless plating. J Alloys Compd 2019: 1265–1273*
8. *X. Gan, Y. Wu, L. Liu, B. Shen, and W. Hu. Electroless copper plating on PET fabrics using hypophosphite as reducing agent. Surf Coatings Technol 2007; 201: 7018–7023.*
9. *Y. Tai, C. Xu, and H. Chen. Silver-coated glass fabric composites prepared by electroless plating. Mater Lett 2016;180: 144–147.*
10. *Wei Q, Yu L, Wu N. Preparation and characterization of copper nanocomposite textiles. Journal of Industrial Textiles 2008; 37(3): 275-283.*
11. *T. Rybicki, Z. Stempien, and I. Karbownik. EMI Shielding and Absorption of Electroconductive Textiles with PANI and PPy Conductive Polymers and Numerical Model Approach. Energies 2021;14, 7746.*
12. *S. Palanisamy. Electromagnetic Interference Shielding of Metal Coated Ultrathin Nonwoven Fabrics and Their Factorial Design. Polym 2021;13:484.*

13. *S. Hu, D. Wang, A. P. Periyasamy, D. Kremenakova, J. Militky, and M. Tunak. Ultrathin Multilayer Textile Structure with Enhanced EMI Shielding and Air-Permeable Properties. Polym 2021; 13; 4176.*
14. *[Periyasamy, A. P., Yang, K., Xiong, X., Venkataraman, M., Militky, J., Mishra, R., Kremenakova, D.Effect of silanization on copper coated milife fabric with improved EMI shielding effectiveness. Materials Chemistry and Physics 2020, 239: 122008.*
15. *Jia, Li‐Chuan. Highly conductive and machine‐washable textiles for efficient electromagnetic interference shielding. Advanced Materials Technologies 2019;4.2: 1800503.*
16. *Zong, J. Y., Zhou, X. J., Hu, Y. F., Yang, T. B., Yan, D. X., Lin, H., ... & Li, Z. M.. A wearable multifunctional fabric with excellent electromagnetic interference shielding and passive radiation heating performance. Composites Part B: Engineering 2021;225:109299.*
17. *Pakdel, E., Wang, J., Kashi, S., Sun, L., & Wang, X. Advances in photocatalytic self-cleaning, superhydrophobic and electromagnetic interference shielding textile treatments. Advances in Colloid and Interface Science 2020;277:102116.*

Název/Title	23. konference STRUTEX (sborník) 23rd conference STRUTEX (Proceedings)
Autor/Author	Kolektiv autorů/Team of Authors
Vydavatel/Publisher	Technická univerzita v Liberci Technical University of Liberec Studentská 1402/2, Liberec
Schváleno/Authorized	Rektorátem TUL dne 26. 9. 2022, čj. RE 39/22
Vyšlo/Date of issue	Prosinec / December 2022
Vydání/Edition	první/first
ISBN	978-80-7494-621-9
Číslo publikace/Publication number	55-039-22

ISBN 978-80-7494-621-9

ISBN 978-80-7494-621-9